AWARD NUMBER: W81XWH-14-1-0149

TITLE: Glyphosate Vedotin for Treatment of Bone Metastatic Castration-Resistant Prostate Cancer

PRINCIPAL INVESTIGATOR: Zongbing You

CONTRACTING ORGANIZATION: Tulane University, New Orleans, LA 70112

REPORT DATE: July 2015

TYPE OF REPORT: Annual

PREPARED FOR: U.S. Army Medical Research and Materiel Command
Fort Detrick, Maryland 21702-5012

DISTRIBUTION STATEMENT: Approved for Public Release;
Distribution Unlimited

The views, opinions and/or findings contained in this report are those of the author(s) and should not be construed as an official Department of the Army position, policy or decision unless so designated by other documentation.

# REPORT DOCUMENTATION PAGE

*Form Approved*
*OMB No. 0704-0188*

Public reporting burden for this collection of information is estimated to average 1 hour per response, including the time for reviewing instructions, searching existing data sources, gathering and maintaining the data needed, and completing and reviewing this collection of information. Send comments regarding this burden estimate or any other aspect of this collection of information, including suggestions for reducing this burden to Department of Defense, Washington Headquarters Services, Directorate for Information Operations and Reports (0704-0188), 1215 Jefferson Davis Highway, Suite 1204, Arlington, VA 22202-4302. Respondents should be aware that notwithstanding any other provision of law, no person shall be subject to any penalty for failing to comply with a collection of information if it does not display a currently valid OMB control number. **PLEASE DO NOT RETURN YOUR FORM TO THE ABOVE ADDRESS.**

| 1. REPORT DATE : | 2. REPORT TYPE: | 3. DATES COVERED |
|---|---|---|
| July 2015 | Annual | 1 JUN 2014-31 May 2015 |

**4. TITLE AND SUBTITLE**
Glyphosate Vedotin for Treatment of Bone Metastatic Castration-Resistant Prostate Cancer

**5a. CONTRACT NUMBER**
W81XWH-14-1-0149

**5b. GRANT NUMBER**

**5c. PROGRAM ELEMENT NUMBER**

**6. AUTHOR(S)**
Zongbing You

E-Mail: zyou@tulane.edu

**5d. PROJECT NUMBER**

**5e. TASK NUMBER**

**5f. WORK UNIT NUMBER**

**7. PERFORMING ORGANIZATION NAME(S) AND ADDRESS(ES)**
The Administrators of the Tulane Educational Fund
6823 SAINT CHARLES AVE
NEW ORLEANS, LA 70118-5665

**8. PERFORMING ORGANIZATION REPORT NUMBER**

**9. SPONSORING / MONITORING AGENCY NAME(S) AND ADDRESS(ES)**
U.S. Army Medical Research and Materiel Command
Fort Detrick, Maryland 21702-5012

**10. SPONSOR/MONITOR'S ACRONYM(S)**

**11. SPONSOR/MONITOR'S REPORT NUMBER(S)**

**12. DISTRIBUTION / AVAILABILITY STATEMENT**
Approved for Public Release; Distribution Unlimited

**13. SUPPLEMENTARY NOTES**

**14. ABSTRACT**

When prostate cancer is confined within the prostate, surgery or radiation therapy will cure almost all of them. When prostate cancer spreads to the lymph nodes or other organs, it is treated by androgen ablative therapy including drugs or surgery. However, the tumors eventually re-grow and become so called castration-resistant prostate cancer (CRPC) in about 2 years. Bone metastatic CRPC causes severe pain, pathologic fracture, spinal cord compression and paralysis, impairment of the quality of life, and eventual death. However, there is no effective treatment available for bone metastatic CRPC. In this project, we propose to create a new drug and test its selective anti-cancer effects in the cultured prostate cancer cell lines (Specific Aim 1) and in the bone tumor animal models that mimic human bone metastatic CRPC (Specific Aim 2). This drug is a conjugation of glyphosate (with a phosphate group that we predict will bind to calcium in the bone matrix, thus enriching the compound in the bone) and a toxin Vedotin (chemical name is monomethyl auristatin E, MMAE).

**15. SUBJECT TERMS**
Prostate cancer, bone metastasis, Vedotin, MMAE, MMAEp, cell death, apoptosis, tumor growth, Castration-resistant prostate cancer (CRPC).

| 16. SECURITY CLASSIFICATION OF: | | | 17. LIMITATION OF ABSTRACT | 18. NUMBER OF PAGES | 19a. NAME OF RESPONSIBLE PERSON |
|---|---|---|---|---|---|
| a. REPORT | b. ABSTRACT | c. THIS PAGE | | | USAMRMC |
| Unclassified | Unclassified | Unclassified | Unclassified | 182 | 19b. TELEPHONE NUMBER *(include area code)* |

**Standard Form 298 (Rev. 8-98)**
**Prescribed by ANSI Std. Z39.18**

## Table of Contents

**Page**


1. **Introduction…….4**
2. **Keywords…….5**
3. **Accomplishments……..……...6**
4. **Impact……...……12**
5. **Changes/Problems...…..……13**
6. **Products……..……..…..…….14**
7. **Participants & Other Collaborating Organizations……16**
8. **Special Reporting Requirements……18**
9. **Appendices……18**

## 1. INTRODUCTION

When prostate cancer is confined within the prostate, surgery or radiation therapy will cure almost all of them. When prostate cancer spreads to the lymph nodes or other organs (called metastasis, about 85% to bone), it is treated by androgen ablative therapy including drugs or surgery (commonly called castration). Initially, most prostate cancers respond to castration, evidenced by regression of tumor and decrease of blood prostate-specific antigen (PSA) level. However, the tumors eventually re-grow and become so called castration-resistant prostate cancer (CRPC) in about 2 years and the patients succumb to uncontrollable widespread metastases within the next year. Bone metastatic CRPC causes severe pain, pathologic fracture, spinal cord compression and paralysis, impairment of the quality of life, and eventual death. Therefore, bone metastatic CRPC is the killer of prostate cancer patients. However, there is no effective treatment available for bone metastatic CRPC. The existing FDA-approved therapies only extend patient's life by about 2.4 to 4.8 months, including Docetaxel + prednisone, Cabazitaxel + prednisone, Sipuleucel-T, Abiraterone + prednisone, MDV3100, and Radium-223. There is an urgent need to design and test new drugs that can extend patient's life longer, and ideally, eliminate death caused by bone metastatic CRPC. In this project, we propose to design a new drug, named Glyphosate Vedotin, based on the unique properties of glyphosate (that provide a phosphate group to bind to calcium in the bone matrix) and a strong toxin Vedotin (chemical name is monomethyl auristatin E, MMAE). Vedotin has been linked to other molecules such as anti-CD30 antibodies (Brentuximab), so that it can be delivered to lymphoma cells that express CD30 (*1*). This approach has been successfully used to create a new FDA-approved drug named Brentuximab Vedotin for the treatment of human lymphomas. Our hypothesis is that, based on glyphosate's enrichment in the bone, glyphosate will bring Vedotin to the bone with bone metastatic CRPC; once the bone metastatic prostate cancer cells take up Glyphosate Vedotin, they will be killed. The objectives of this project are to complete two specific aims: Aim 1. To determine selective anti-cancer effects of Glyphosate Vedotin in CRPC cells in vitro. Aim 2. To determine selective anti-cancer effects of Glyphosate Vedotin in a bone tumor model in vivo.

## 2. KEYWORDS:

Prostate cancer, bone metastasis, Vedotin, MMAE, MMAEp, cell death, apoptosis, tumor growth, Castration-resistant prostate cancer (CRPC).

## 3. ACCOMPLISHMENTS:

- **What were the major goals of the project: see Table 1.**

Table 1. List of major goals, milestones/target dates, and actual completion dates

| Specific Aim 1(specified in proposal) | Timeline | Actual completion date |
|---|---|---|
| **Major Task 1:**<br>**To determine selective anti-cancer effects of Glyphosate Vedotin in CRPC cells in vitro** | Months | |
| DoD HRPO approval | 1-3 | 2/26/2014 |
| Local IACUC Approval | 1-2 | 1/31/2014 |
| ACURO Approval | 1-2 | *2/24/2014* |
| Milestone(s) Achieved: determine that Glyphosate Vedotin selectively acts on CRPC cells | 6 | *Mostly completed, published as an abstract on 3/25-26/2015* |
| **Specific Aim 2** | | |
| **Major Task 2:**<br>**To determine selective anti-cancer effects of Glyphosate Vedotin in a bone tumor model in vivo** | | |
| Milestone(s) Achieved:<br>obtain data to support that Glyphosate Vedotin selectively inhibits bone tumors | 12 | Partially completed, published as an abstract on 3/25-26/2015 |

- **What was accomplished under these goals:**

1) **Major activities:**

First, we purchased MMAE compound from Concortis Biosystems (San Diego, CA);

Second, we explored the possibility of conjugating glyphosate with MMAE. After consulting with a collaborator and chemical engineers at Concortis Biosystems, we realized that there were multiple technical obstacles in conjugating glyphosate with MMAE. Because glyphosate mainly provides a phosphate group to deliver the conjugated compound to the bone through phosphate-calcium interaction in the bone matrix, we decided to directly synthesize MMAE with a phosphate group attached, resulting in a compound called MMAE-phosphate (MMAEp);

Third, we assessed the in vitro binding of MMAE and MMAEp to mouse bone matrix;

Fourth, we compared the effects of MMAE and MMAEp on PC-3 and C4-2B cells in vitro;

Fifth, we established intratibial xenograft prostate tumor model by injecting PC-3-LacZ-luc cells into the tibia of athymic nude mice;

Sixth, we assessed effects of MMAE and MMAEp on intratibial xenograft prostate tumor model in vivo.

**2) Specific objectives:**

Our specific objectives were to complete two specific aims:

Aim 1. To determine selective anti-cancer effects of Glyphosate Vedotin in CRPC cells in vitro.

Aim 2. To determine selective anti-cancer effects of Glyphosate Vedotin in a bone tumor model in vivo.

**3) Significant results:**

a) We successfully synthesized a new chemical compound MMAEp (see Figure 1). The molecular weight of MMAEp was 797.47 Daltons and the purity of MMAEp was > 95% based on high performance liquid chromatography (HPLC) analysis. The molecular weight of MMAE was 717.98 Daltons and the purity of MMAE was > 95% based on high performance liquid chromatography (HPLC) analysis. Both MMAE and MMAEp were dissolved in dimethylsulfoxide (DMSO) and stored at -80 °C before use.

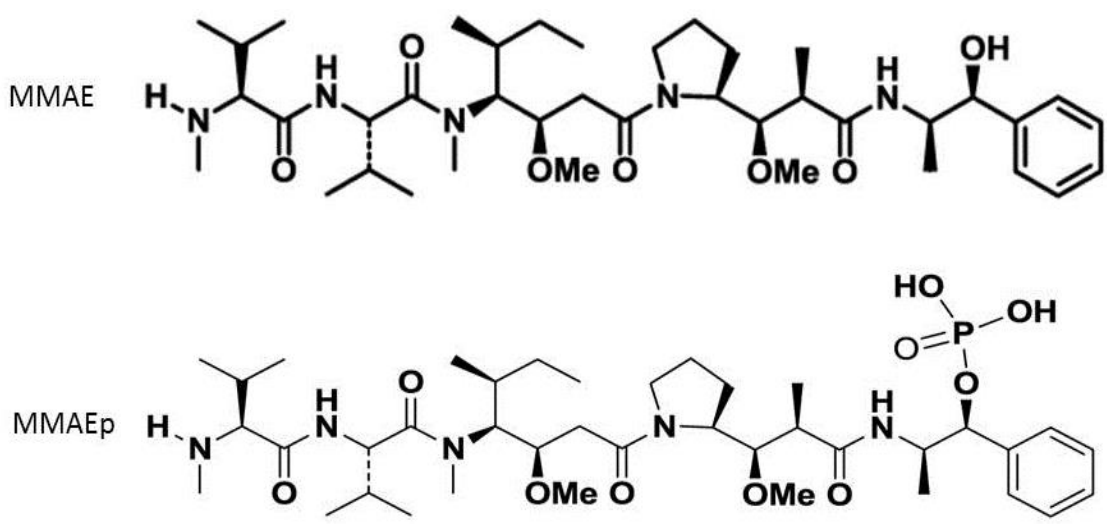



**Figure 1. Chemical structures of MMAE and MMAEp.** A phosphate group was added directly on MMAE to form MMAEp.

b) We found that MMAEp bound to the bone matrix while MMAE did not bind to the bone matrix (Table1).

| Drug | Initial (nM) | Measured (nM) | Drop (nM) | Observed Molecular Weight (Daltons) | Nanogram Bound per Milligram bone |
|---|---|---|---|---|---|
| **MMAE** | 100 | 105.8* | N/A | 718.0 | 0 |
| **MMAEp** | 100 | 4.5 | 95.5 | 798.7 | 1 |

**Table 1.** *Ex vivo* bone matrix binding assay. Both MMAEp and MMAE (control group) were incubated with fresh mouse tibia bone pieces at indicated initial concentrations in 500 µl in miniprep spin columns. The chemicals passed through the columns filled with mouse bone pieces five times. The pass-through samples (eluates) were then measured with mass spectrometry (MS) which indicated > 95% of MMAEp had been chelated out of the solution by the bone matrix, while MMAE did not bind to the bone matrix. Using the observed molecular weight provided by the manufacturer and the mass of the tibia bone sample, we calculated that approximately 1 ng of MMAEp bound to each mg of bone matrix. *Note, the increased concentration in the MMAE eluate might be due to the variation of the measurement (that is, a measurement error).

c) We found that both MMAEp and MMAE dose-dependently inhibited growth of PC-3 and C4-2B cells in in-vitro studies (Figure 2). The half maximal inhibitory concentration (IC50) values of MMAEp were 47.28 nM for PC3 cells and 48.17 nM for C4-2B cells. The IC50 values of MMAE were 2.43 nM for PC3 cells and 1.65 nM for C4-2B cells. At low concentrations (less than 50 nM), MMAEp was less toxic to the cells than MMAE. At a high concentration (100 nM), MMAEp was equally toxic to MMAE.

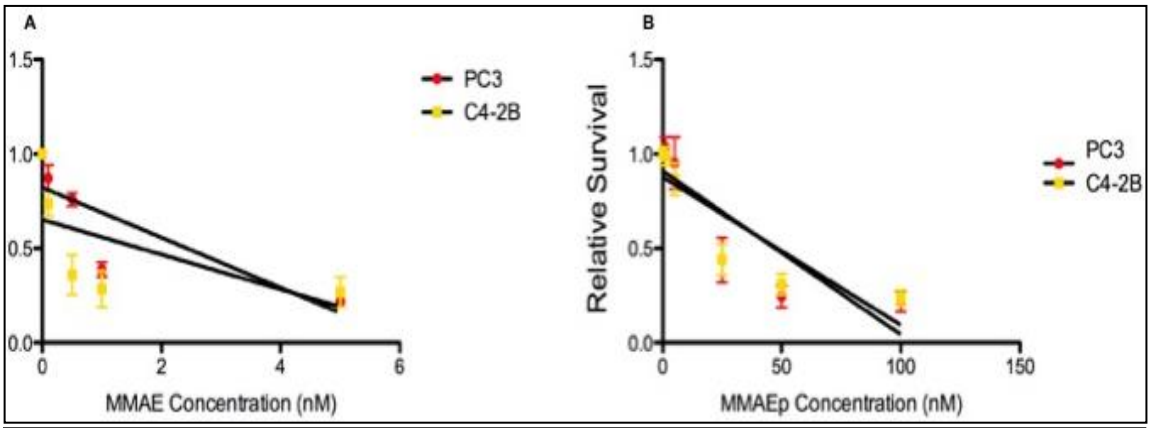



**Figure 2. In-vitro half maximal inhibitory concentration (IC50) values of MMAEp and MMAE**. PC3 and C4-2B cells were incubated with indicated concentrations of MMAE and MMAEp for 3 days. Viable cell number was determined using the CellTiter-Glo® Luminescence Cell Viability Assay (ProMega, Madison, WI) and measurement on a FLUOstar Optima® plate reader (BMG Labtech, Cary, NC). The results were normalized to the mock DMSO treatment (control group, arbitrarily assigned a number "1" for 100% viability. **(A)** Linear regression analysis of MMAE data showed IC50 values of 2.43 nM for PC3 cells and 1.65 nM for C4-2B cells. **(B)** Linear regression analysis of MMAEp data showed IC50 values of 47.28 nM for PC3 cells and 48.17 nM for C4-2B cells. The date represent mean ± standard error of the mean (SEM) (n = 3 independent experiments).

d) We established intratibial xenograft prostate tumor model by injecting PC-3-LacZ-luc cells into the tibia of athymic nude mice (see Figure 3).

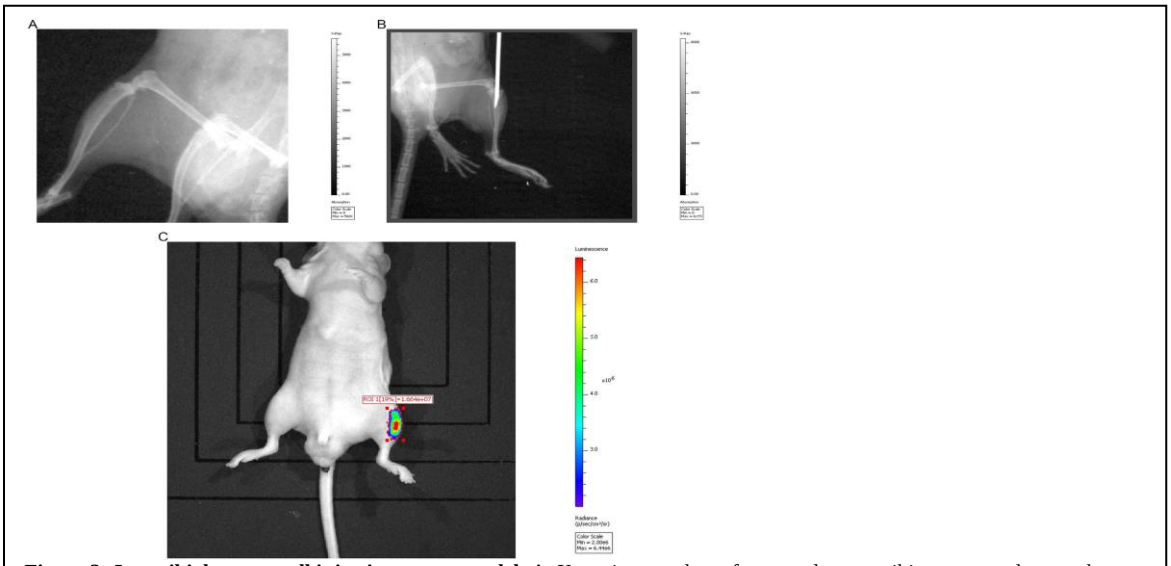



**Figure 3. Intratibial cancer cell injection mouse model.** A. X-ray image taken of a normal mouse tibia pre-procedure on the contralateral side with the radiolucent bone marrow cavity visible on the proximal end of the bone. B. X-ray image of a mouse tibia with a 21-gauge needle inserted into the proximal bone marrow cavity. C. Results of successful injection of PC3-LacZ-luc cells expressing luciferase (and an injection of D-luciferin) using an IVIS (IVIS® Lumina XRMS Series III, PerkinElmer, Waltham, MA, USA).

e) We found that at a dose of 1 mg/Kg animal body weight, MMAE was very toxic to the animals, so as to cause animal deaths after two injections of MMAE in a pilot study of five animals (Figure 4). In contrast, MMAEp was well tolerated at 1 mg/Kg body weight and all animals survived except one animal died of lung metastasis (Figure 4). However, at 1 mg/kg dose, MMAEp did not show any effects on bone tumor growth (Figure 5). These pilot results forced us to amend our original protocol by deleting MMAE group (as it was too toxic) and to increase MMAEp dose up to 2 mg/Kg. We obtained the final approval of our amendment on April 27, 2015.

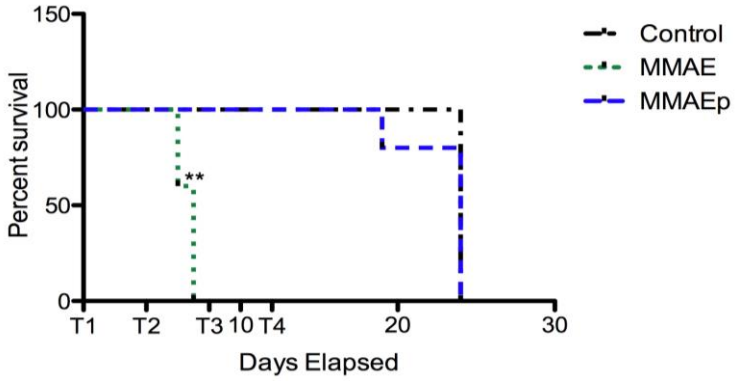



**Figure 4. Kaplan-Meier survival curves of mice.** PC3-LacZ-luc cells were injected into the tibias of athymic nude mice. Mice were randomized the following day based on a coin flip with n = 5 in control (vehicle PBS treatment) and treatment groups. Treatments were given at days 0, 4, 8, and 12 with 1 mg/Kg of MMAE or MMAEp intraperitoneally. T1 –T4, indicate the time of treatment. Animals of the control and MMAEp groups were euthanized at day 24 due to large tumor sizes.

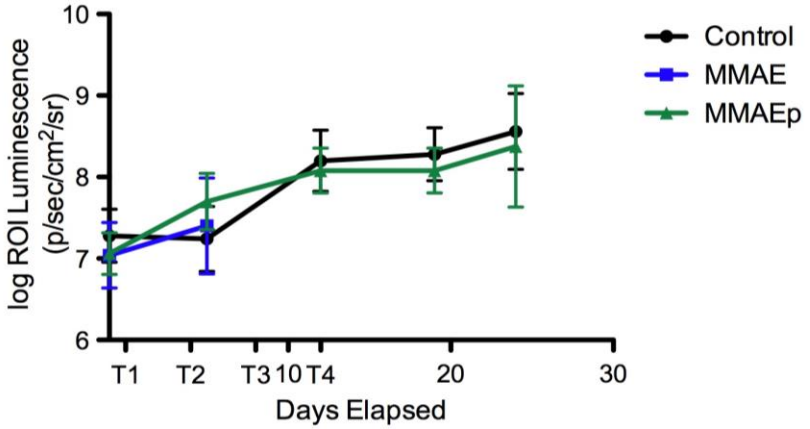



**Figure 5. Tumor size of animals over the treatment period.** T1-T4, indicate the time of treatment (similar to Figure 4). Tumors were imaged non-invasively utilizing luciferase expression in the tumor cells and a subcutaneous administration of D-luciferin. Signal is acquired through the use of an in vivo imaging system (IVIS) (IVIS® Lumina XRMS Series III). Y-axis uses log of the region of interest (ROI) luminescence to represent tumor sizes. $P > 0.05$ among the groups using analysis of variance (ANOVA) statistical analysis. The control and MMAEp groups were euthanized at day 24 due to large tumor sizes.

f) After obtaining the approval for increasing MMAEp dose to up to 2 mg/Kg, we tested if this higher dose was effective. According to the approved amendment protocol, we injected $2x10^5$ PC-3-LacZ-luc cells in 5 µl of PBS mixed with 5 µl of Matrigel. On the next day, MMAEp at 2 mg/Kg was injected intraperitoneally and repeated every four days for a total of six doses. We found that the tibia bone tumor growth was inhibited in the MMAEp group compared to the control group (Figure 6). However, this study needs to be repeated for further validation, thus we have applied for and obtained the approval for a no-cost-extension to extend the performance period by 12 months.

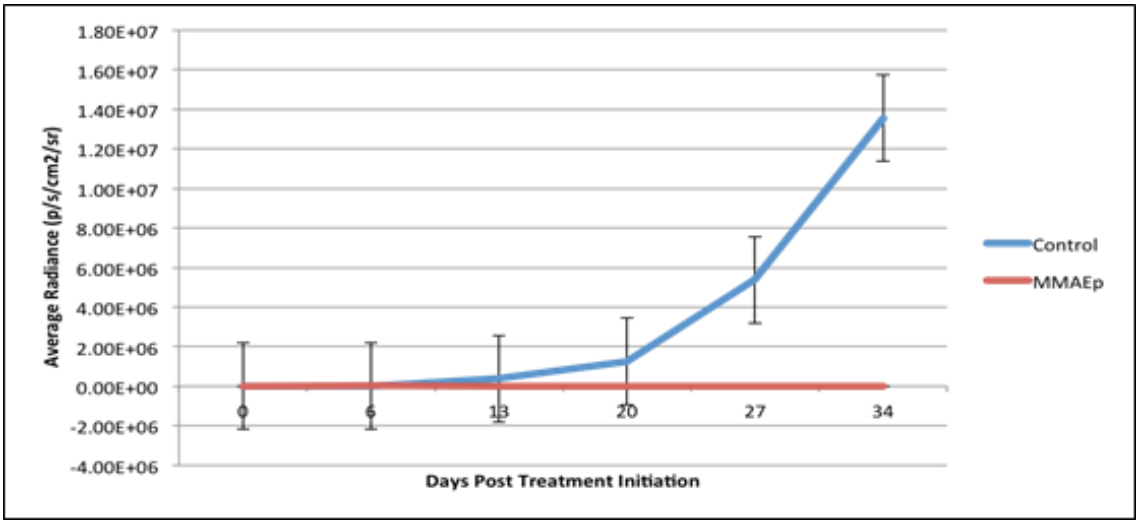



**Figure 6. Tumor size of animals over the treatment period.** PC3- LacZ-luc cells were injected into the tibias of athymic nude mice. Mice were randomized the following day based on a coin flip with n = 7 in control (PBS treatment) and n = 8 in the MMAEp treatment group. The treatments were given intraperitoneally at days 0, 4, 8, 12, 16, and 20. Tumors were imaged non-invasively utilizing luciferase expression in the tumor cells and a subcutaneous administration of D-luciferin. Signal is acquired through the use of an in vivo imaging system (IVIS) (IVIS® Lumina XRMS Series III). Tumor luminescence values below the linear range are treated as zero. Treatment group is compared to DMSO control treated mice.

- **Interpretation and Discussion of the findings**: we found that MMAEp, but not MMAE, binds to the bone matrix (Table 1), which suggests that this phosphate-modified form of MMAE is able to enrich the compound in the bone. We found that MMAEp is less toxic to the cancer cells than MMAE at low concentrations in in-vitro studies, which may be due to the changes of cellular permeability because of the negative-charged phosphate group. However, at high concentrations, MMAEp is equally toxic to the cancer cells compared to MMAE. The in-vivo studies show that MMAE is too toxic to be administrated to the animals (Figure 4). This is a surprise as the previous study reported that the maximal tolerable dose of free MMAE in severe combined immunodeficient (SCID) mice was between 0.5 and 1 mg/Kg (*1*). We speculate that the intolerable 1 mg/Kg dose may be partly due to the difference in mouse strains (athymic nude mice in our study versus SCID mice in the previous study). However, MMAEp is much less toxic to the animals. We think that this may be due to 1) MMAEp is less toxic to the cells than MMAE; and 2) MMAEp is enriched to the bone thus causing less general toxicity. Nonetheless, MMAEp at 1 mg/Kg dose is not effective in inhibiting bone tumor growth (Figure 5). Therefore, we amended our animal protocol to increase MMAEp dose up to 2 mg/Kg. A single study using 2 mg/Kg MMAEp

shows that MMAEp at the increased dose is able to inhibit bone tumor growth. Therefore, we have obtained approval of a 12-month no-cost-extension to repeat this study.

**4) Other achievements:**

Besides the above work that is directly related to the funded project, we have performed other studies. Because the PI's effort was partially funded by this award, we acknowledged this award in our following publications based on these studies:

(1) Parajuli KR, Zhang Q, Liu S, Patel NK, Lu H, Zeng SX, Wang G, Zhang C, You Z*. Methoxyacetic acid suppresses prostate cancer cell growth by inducing growth arrest and apoptosis. Am J Clin Exp Urol 2014;2(4):300-312. PMCID: PMC4297326 (***Corresponding author**). Status of publication: published; acknowledgement of federal support: Yes.

(2) Parajuli KR, Zhang Q, Liu S, You Z*. Aminomethylphosphonic Acid and methoxyacetic Acid induce apoptosis in prostate cancer cells. Int J Mol Sci. 2015 May 22;16(5):11750-65. doi: 10.3390/ijms160511750. PMID: 26006246; PMCID: PMC4463728 (***Corresponding author**). Status of publication: published; acknowledgement of federal support: Yes.

(3) Qiuyang Zhang, Sen Liu, Qingsong Zhang, Zhenggang Xiong, Alun R. Wang, Leann Myers, Jonathan Melamed, Wendell W. Tang, and **Zongbing You***. Interleukin-17 promotes development of castration-resistant prostate cancer potentially through creating an immunotolerant and pro-angiogenic tumor microenvironment. The Prostate 2014 Jun;74(8):869-79. doi: 10.1002/pros.22805. PMID: 24691769; PMCID: PMC4063299 **(*Corresponding author).** Status of publication: published; acknowledgement of federal support: Yes.

(4) Ge D, Zhang QS, Zabaleta J, Zhang Q, Liu S, Reiser B, Bunnell BA, Braun SE, O'Brien MJ, Savoie FH, **You Z***. Doublecortin may play a role in defining chondrocyte phenotype. Int J Mol Sci. 2014 Apr 22;15(4):6941-60. doi: 10.3390/ijms15046941. PMID: 24758934; PMCID: PMC4013671 **(*Corresponding author).** Status of publication: published; acknowledgement of federal support: Yes.

(5) Xu B, Guenther JF, Pociask DA, Wang Y, Kolls JK, **You Z**, Chandrasekar B, Shan B, Sullivan DE, Morris GF. Promotion of lung tumor growth by interleukin-17. Am J Physiol Lung Cell Mol Physiol 2014;307(6):L497-508. PMID: 25038189; PMCID: PMC4166785. Status of publication: published; acknowledgement of federal support: Yes.

(6) Fuqiang Ren, Mingyu Fan, Jiandong Mei, Yongqiang Wu, Chengwu Liu, Qiang Pu, **Zongbing You*,** and Lunxu Liu*. Interferon-γ and celecoxib inhibit lung tumor growth through modulating M2/M1 macrophage ratio in the tumor microenvironment. Drug Design, Development and Therapy. 2014 Sep 23;8:1527-38. doi: 10.2147/DDDT.S66302. eCollection 2014. **(*Correspondence author)** PMID: 25284985; PMCID: PMC4181549. Status of publication: published; acknowledgement of federal support: Yes.

(7) Mark Lambrechts, Behrooz Nazari, Arash Dini, Michael J. O'Brien, Wendell M. R. Heard, Felix H. Savoie, **Zongbing You***. Comparison of the cheese-wiring effects among three sutures used in rotator cuff repair. International Journal of Shoulder Surgery 2014, 8:81-5 PMID: 25258499; PMCID: PMC4168657 **(*Correspondence author)**. Status of publication: published; acknowledgement of federal support: Yes.

(8) Chong Chen, Qiuyang Zhang, Sen Liu, Mark Lambrechts, Yine Qu, and **Zongbing You***. AZD5363 inhibits inflammatory synergy between interleukin-17 and insulin/insulin-like growth factor 1. Front Oncol. 2014 Dec 1;4:343. doi: 10.3389/fonc.2014.00343. eCollection 2014. PMID: 25520943 [PubMed] PMCID: PMC4249256 **(*Correspondence author).** Status of publication: published; acknowledgement of federal support: Yes.

(9) Chen C, Zhang Q, Liu S, Parajuli KR, Qu Y, Mei J, Chen Z, Zhang H, Khismatullin DB, **You Z*.** IL-17 and insulin/IGF1 enhance adhesion of prostate cancer cells to vascular endothelial cells through CD44-VCAM-1 interaction. Prostate. 2015 Feb 14. 75(8):883-95. doi: 10.1002/pros.22971. PMID: 25683512; PMCID: PMC4405436 **(*Corresponding author)**. Status of publication: published; acknowledgement of federal support: Yes.

(10) Chen RY, Fan YM*, Zhang Q, Liu S, Li Q, Ke GL, Li C, **You Z***. Estradiol Inhibits Th17 Cell Differentiation through Inhibition of RORgammaT Transcription by Recruiting the ERalpha/REA Complex to Estrogen Response Elements of the RORgammaT Promoter. J Immunol. 2015 Apr 15;194(8):4019-28. doi: 10.4049/jimmunol.1400806. PMID: 25769926; PMCID: PMC4390502 **(*Corresponding author)**. Status of publication: published; acknowledgement of federal support: Yes.

**(11)** David Cunningham, **Zongbing You***. In vitro and in vivo model systems used in prostate cancer research. J Biol Methods 2015, 2(1):e17; Published online 2015-06-04 doi: 10.14440/jbm.2015.63 (Invited review article); NIHMS: 698295 **(*Corresponding author).** Status of publication: published; acknowledgement of federal support: Yes.

**Summary and Discussion of the Accomplishments:**

We have performed most of the research work that was originally proposed in our application. We have almost achieved the two major goals and determined that 1) MMAEp inhibits CRPC cell growth in vitro; and 2) MMAEp may inhibit bone tumor growth in vivo. The in-vitro effects of MMAEp are confirmed, which is a positive outcome. The in-vivo effects of MMAEp await further tests in the no-cost-extension performance period. The reason for not able to complete the entire project during the proposed one-year performance period is because the proposed drug dosage (1 mg/Kg) was not as effective as we previously expected, thus we had to amend the animal protocol, which took some time to get the local IACUC and DoD ACURO approval. However, the initial results from the study with increased drug dosage (2 mg/Kg) appear promising. Overall, we remain positive that MMAEp may show a positive outcome in the ongoing in-vivo studies.

- **What opportunities for training and professional development has the project provided:**
  Nothing to Report.

- **How were the results disseminated to communities of interest:**
  Nothing to Report.

- **What do you plan to do during the next reporting period to accomplish the goals:**
  During the 12-month no-cost-extension, we plan to accomplish the following goals: 1) optimize the drug dose and determine if the drug is effective in inhibiting bone tumor growth (Specific Aim 2 of the original proposal); and 2) test the drug's effects on cell cycle, apoptosis, migration and invasion of prostate cancer cells in vitro (Specific Aim 1 of the original proposal).

**4. IMPACT:**

- **What was the impact on the development of the principal discipline(s) of the project?**
  The findings from this project demonstrate that MMAEp has potentials to be developed into ant-cancer drugs. Publication of these findings may stimulate the cancer research field to perform studies to further verify and improve the anti-cancer actions of MMAEp. Thus, the results of this project advance our knowledge in targeting CRPC bone metastasis, which opens a new window in the cancer research field. In theory, the results demonstrate that MMAEp can become a new drug in the treatment of bone metastatic CRPC.

- **What was the impact on other disciplines**
  Nothing to Report.

- **What was the impact on technology transfer?**
  Nothing to Report.

- **What was the impact on society beyond science and technology?**
  Nothing to Report.

## 5. CHANGES/PROBLEMS:

- **Changes in approach and reasons for change:**
  The animal study protocol was amended. The changes are: 1) MMAE group was cancelled; the reason was that MMAE at 1 mg/Kg dose was too toxic to be tolerated by the animals; during the initial pilot study, five animals died after two doses of MMAE. In addition, we did not intend to develop MMAE as a drug, as our intention was to develop its modified form MMAEp into a drug. Therefore, without MMAE group, it will not affect our overall goal. 2) The dosage of MMAEp was increased from 1 mg/Kg up to 2 mg/Kg; the reason was that MMAEp at 1 mg/Kg was well tolerated by the animals, but the bone tumor growth was not inhibited at this low dose. Our initial experiment with 2 mg/Kg MMAEp showed that the animals could tolerate this increased dosage and the bone tumor growth was inhibited at this high dosage. The amendment was approved by both local IACUC and DoD ACURO.

- **Actual or anticipated problems or delays and actions or plans to resolve them:**
  Three problems were encountered: 1) Conjugation of glyphosate to MMAE was technically difficult to achieve based on consultation with a collaborator Dr. Noshir Pesika (Assistant Professor of Chemical & Biomolecular Engineering) and chemical engineers at Concortis Biosystems. Instead, a phosphate group could be added directly to MMAE during chemical synthesis, thus forming MMAEp that is functionally equal to a conjugate of glyphosate and MMAE. Our in vitro bone matrix binding assay showed that MMAEp bound to the mouse bone matrix, a property that is expected of the glyphosate and MMAE conjugate. Because the pharmaceutic pipeline for synthesis of MMAEp did not allow contamination with radioactive isotope, we could not generate isotope-labelled MMAEp to do autoradiographical tracing of the compound in the animals in vivo. However, we have developed a mass spectrometry assay to measure MMAEp in solution, which can be used to measure the concentration of MMAEp bound to the bone matrix. 2) In animal studies, MMAE group was cancelled; the reason was that MMAE at 1 mg/Kg dose was too toxic to be tolerated by the animals; during the initial pilot study, five animals died after two doses of MMAE. In addition, we did not intend to develop MMAE as a drug, as our intention was to develop its modified form MMAEp into a drug. Therefore, without MMAE group, it will not affect our overall goal. 2) In animal studies, the dosage of MMAEp was increased from 1 mg/Kg up to 2 mg/Kg; the reason was that MMAEp at 1 mg/Kg was well tolerated by the animals, but the bone tumor growth was not inhibited at this low dose. Our initial experiment with 2 mg/Kg MMAEp showed that the animals could tolerate this increased dosage and the bone tumor growth was inhibited at this high dosage. The amendment was approved by both local IACUC and DoD ACURO. Because it took some time to obtain the approvals, we could not complete the proposed work in the one-year performance

period. Therefore, I have applied for a 12-month no-cost-extension, which has been approved by DoD. During the 12-month no-cost-extension, we plan to accomplish the following goals: 1) optimize the drug dose and determine if the drug is effective in inhibiting bone tumor growth (Specific Aim 2 of the original proposal); and 2) test the drug's effects on cell cycle, apoptosis, migration and invasion of prostate cancer cells in vitro (Specific Aim 1 of the original proposal).

- **Changes that had a significant impact on expenditures:**
  Nothing to Report.

- **Significant changes in use or care of human subjects:**
  Nothing to Report.

- **Significant changes in use or care of vertebrate animals.**
  We used fewer animals than proposed, because we were only able to use one cell line PC-3-LacZ-luc, instead of three cell lines. We were unable to generate DU-145-LacZ-luc cell line, and the C4-2B-LacZ-luc cell line was not able to form tumors in animals. Given the proof-of-principle nature of this project, we plan to focus on PC-3-LacZ-luc cell line in in-vivo studies to generate solid data to prove or disprove MMAEp's efficacy.

- **Significant changes in use of biohazards and/or select agents:**
  Nothing to Report.

## 6. PRODUCTS:

- **Publications, conference papers, and presentations:**

  - **Journal publications:**

    The foll**o**wing publications are directly funded by this award or closely related:

    (1) David Cunningham, **Zongbing You***. In vitro and in vivo model systems used in prostate cancer research. J Biol Methods 2015, 2(1):e17; Published online 2015-06-04 doi: 10.14440/jbm.2015.63 (Invited review article); NIHMS: 698295 **(*Corresponding author)**. Status of publication: published; acknowledgement of federal support: Yes.

    The following publications are not directly funded by this award, but this award was acknowledged because the PI's effort was partially supported by this award:

    (2) Parajuli KR, Zhang Q, Liu S, Patel NK, Lu H, Zeng SX, Wang G, Zhang C, You Z*. Methoxyacetic acid suppresses prostate cancer cell growth by inducing growth arrest and apoptosis. Am J Clin Exp Urol 2014;2(4):300-312. PMCID: PMC4297326 (***Corresponding author**). Status of publication: published; acknowledgement of federal support: Yes.

    (3) Parajuli KR, Zhang Q, Liu S, You Z*. Aminomethylphosphonic Acid and methoxyacetic Acid induce apoptosis in prostate cancer cells. Int J Mol Sci. 2015 May 22;16(5):11750-65. doi: 10.3390/ijms160511750. PMID: 26006246; PMCID: PMC4463728 (***Corresponding author**). Status of publication: published; acknowledgement of federal support: Yes.

    (4) Qiuyang Zhang, Sen Liu, Qingsong Zhang, Zhenggang Xiong, Alun R. Wang, Leann Myers, Jonathan Melamed, Wendell W. Tang, and **Zongbing You***. Interleukin-17 promotes development of castration-resistant prostate cancer potentially through creating an

immunotolerant and pro-angiogenic tumor microenvironment. The Prostate 2014 Jun;74(8):869-79. doi: 10.1002/pros.22805. PMID: 24691769; PMCID: PMC4063299 **(*Corresponding author).** Status of publication: published; acknowledgement of federal support: Yes.

(5) Ge D, Zhang QS, Zabaleta J, Zhang Q, Liu S, Reiser B, Bunnell BA, Braun SE, O'Brien MJ, Savoie FH, **You Z***. Doublecortin may play a role in defining chondrocyte phenotype. Int J Mol Sci. 2014 Apr 22;15(4):6941-60. doi: 10.3390/ijms15046941. PMID: 24758934; PMCID: PMC4013671 **(*Corresponding author).** Status of publication: published; acknowledgement of federal support: Yes.

(6) Xu B, Guenther JF, Pociask DA, Wang Y, Kolls JK, **You Z**, Chandrasekar B, Shan B, Sullivan DE, Morris GF. Promotion of lung tumor growth by interleukin-17. Am J Physiol Lung Cell Mol Physiol 2014;307(6):L497-508. PMID: 25038189; PMCID: PMC4166785. Status of publication: published; acknowledgement of federal support: Yes.

(7) Fuqiang Ren, Mingyu Fan, Jiandong Mei, Yongqiang Wu, Chengwu Liu, Qiang Pu, **Zongbing You*,** and Lunxu Liu*. Interferon-γ and celecoxib inhibit lung tumor growth through modulating M2/M1 macrophage ratio in the tumor microenvironment. Drug Design, Development and Therapy. 2014 Sep 23;8:1527-38. doi: 10.2147/DDDT.S66302. eCollection 2014. **(*Correspondence author)** PMID: 25284985; PMCID: PMC4181549. Status of publication: published; acknowledgement of federal support: Yes.

(8) Mark Lambrechts, Behrooz Nazari, Arash Dini, Michael J. O'Brien, Wendell M. R. Heard, Felix H. Savoie, **Zongbing You***. Comparison of the cheese-wiring effects among three sutures used in rotator cuff repair. International Journal of Shoulder Surgery 2014, 8:81-5 PMID: 25258499; PMCID: PMC4168657 **(*Correspondence author)**. Status of publication: published; acknowledgement of federal support: Yes.

(9) Chong Chen, Qiuyang Zhang, Sen Liu, Mark Lambrechts, Yine Qu, and **Zongbing You***. AZD5363 inhibits inflammatory synergy between interleukin-17 and insulin/insulin-like growth factor 1. Front Oncol. 2014 Dec 1;4:343. doi: 10.3389/fonc.2014.00343. eCollection 2014. PMID: 25520943 [PubMed] PMCID: PMC4249256 **(*Correspondence author).** Status of publication: published; acknowledgement of federal support: Yes.

(10) Chen C, Zhang Q, Liu S, Parajuli KR, Qu Y, Mei J, Chen Z, Zhang H, Khismatullin DB, **You Z*.** IL-17 and insulin/IGF1 enhance adhesion of prostate cancer cells to vascular endothelial cells through CD44-VCAM-1 interaction. Prostate. 2015 Feb 14. 75(8):883-95. doi: 10.1002/pros.22971. PMID: 25683512; PMCID: PMC4405436 **(*Corresponding author)**. Status of publication: published; acknowledgement of federal support: Yes.

(11) Chen RY, Fan YM*, Zhang Q, Liu S, Li Q, Ke GL, Li C, **You Z***. Estradiol Inhibits Th17 Cell Differentiation through Inhibition of RORgammaT Transcription by Recruiting the ERalpha/REA Complex to Estrogen Response Elements of the RORgammaT Promoter. J Immunol. 2015 Apr 15;194(8):4019-28. doi: 10.4049/jimmunol.1400806. PMID: 25769926; PMCID: PMC4390502 **(*Corresponding author)**. Status of publication: published; acknowledgement of federal support: Yes.

- **Books or other non-periodical, one-time publications:**
  Nothing to Report.

- **Other publications, conference papers, and presentations:**

1) Cunningham D, Parajuli K, Zhang C, Wang G, Zhang Q, Liu S, Mei J, You Z. MONOMETHYL AURISTATIN E PHOSPHATE: A MODIFIED MONOMETHYL AURISTATIN E WITH POTENTIAL ANTI-TUMOR ACTIVITY. The Tulane University Health Sciences Research Days, March 25-26, 2015, New Orleans, LA. Status of publication: published; acknowledgement of federal support: Yes.

2) Keshab R. Parajuli, Qiuyang Zhang, Sen Liu, Neil K. Patel, Zongbing You. Methoxyacetic acid inhibits prostate cancer cell growth. 2014 SBUR Fall Symposium, Nov 13-16, 2014, Dallas, TX. Status of publication: published; acknowledgement of federal support: Yes.

3) Parajuli KR, Zhang Q, Liu S, Patel NK, You Z. METHOXYACETIC ACID SUPPRESSES PROSTATE CANCER CELL GROWTH BY INDUCING GROWTH ARREST AND APOPTOSIS. The Tulane University Health Sciences Research Days, March 25-26, 2015, New Orleans, LA. Status of publication: published; acknowledgement of federal support: Yes.

4) Keshab R. Parajuli, Qiuyang Zhang, Sen Liu, and Zongbing You. Aminomethylphosphonic acid inhibits human prostate xenograft tumor growth through interfering glycine synthesis in the cancer cells. 2015 Metabolism and Cancer, American Association of Cancer Research, June 7-10, 2015, Hyatt Regency Bellevue, Bellevue, WA. Status of publication: published; acknowledgement of federal support: Yes.

5) Zhang Q., Liu S., Parajuli K., Qu Y. Mei J. Chen Z. Zhang H., and You Z. MMP7 promotes the invasion and progression of prostate cancer adenocarcinoma in mouse models. Louisiana Cancer Research Consortium Annual Scientific Retreat, April 10, 2015, New Orleans, LA. Status of publication: published; acknowledgement of federal support: Yes.

- **Website(s) or other Internet site(s):**
  Nothing to Report.

- **Technologies or techniques:**
  Nothing to Report.

- **Inventions, patent applications, and/or licenses:**
  A provisional patent application has been filed to the United States Patent and Trademark Office (USPTO) on March 24, 2015. Application number: 62137691; EFS ID: 21867552; Title: Monomethyl auristatin E phosphate as a treatment for cancer and other diseases; First Named Inventor: Zongbing You. The receipt and application documents are enclosed in the Appendices of this report.

- **Other Products:**
  Models: PC3-LacZ-luc cell line, which is a good cell model for prostate cancer research, especially for in vivo animal studies.

## 7. PARTICIPANTS & OTHER COLLABORATING ORGANIZATIONS

- **What individuals have worked on the project?**

| | |
|---|---|
| Name: | *Zongbing You* |
| Project Role: | *PD/PI* |

| | |
|---|---|
| Researcher Identifier (e.g. ORCID ID): | *0000-0001-5048-2229* |
| Nearest person month worked: | *1* |
| Contribution to Project: | *Dr. You was responsible for the overall direction, administration, supervision of laboratory staff, coordination and completion of the project, preparation of publications and annual report/final report. Dr. You performed in vitro studies and assisted Dr. Chong Chen in performing in vitro and in vivo studies.* |
| Funding Support: | Not Applicable |
| Name: | *Chong Chen* |
| Project Role: | *Postdoctoral Fellow* |
| Researcher Identifier (e.g. ORCID ID): | *0000-0002-4464-5797* |
| Nearest person month worked: | *5* |
| Contribution to Project: | *Dr. Chen performed part of the in-vitro and in-vivo studies.* |
| Funding Support: | *Not Applicable* |
| Name: | *Keshab Parajuli* |
| Project Role: | *Postdoctoral Fellow* |
| Researcher Identifier (e.g. ORCID ID): | *0000-0003-3799-6991* |
| Nearest person month worked: | *4* |
| Contribution to Project: | *Dr. Parajuli performed part of the in-vitro and in-vivo studies.* |
| Funding Support: | *Not Applicable* |
| Name: | *David Cunningham* |
| Project Role: | *PhD student* |
| Researcher Identifier (e.g. ORCID ID): | *0000-0002-8857-779X* |
| Nearest person month worked: | *8* |
| Contribution to | *Mr. Cunningham performed part of the in-vitro and in-vivo studies with* |

| | |
|---|---|
| Project: | *assistances of Dr. Chen and Dr. Parajuli.* |
| Funding Support: | *Not Applicable* |

- **What other organizations were involved as partners?**
  Nothing to Report.

## 8. SPECIAL REPORTING REQUIREMENTS

Nothing to Report (not applicable).

## 9. APPENDICES:

The 11 articles and 5 meeting abstracts are enclosed in Appendices in the order shown under 6. Products. The provisional patent application documents are also enclosed in the Appendices.

### References Cited in this report:


1. **J. A. Francisco *et al.*, cAC10-vcMMAE, an anti-CD30-monomethyl auristatin E conjugate with potent and selective antitumor activity. *Blood* 102, 1458-1465 (2003).**

Am J Clin Exp Urol 2014;2(4):300-312
www.ajceu.us /ISSN:2330-1910/AJCEU0003630

*Original Article*

# Methoxyacetic acid suppresses prostate cancer cell growth by inducing growth arrest and apoptosis

Keshab R Parajuli[1], Qiuyang Zhang[1], Sen Liu[1], Neil K Patel[1], Hua Lu[2,3], Shelya X Zeng[2,3], Guangdi Wang[4], Changde Zhang[4], Zongbing You[1,3,5,6,7]

*[1]Department of Structural & Cellular Biology, Tulane University, New Orleans, LA, USA; [2]Department of Biochemistry and Molecular Biology, Tulane University, New Orleans, LA, USA; [3]Tulane Cancer Center and Louisiana Cancer Research Consortium, Tulane University, New Orleans, LA, USA; [4]Department of Chemistry and RCMI Cancer Research Center, Xavier University of Louisiana, New Orleans, LA, USA; [5]Department of Orthopaedic Surgery, Tulane University, New Orleans, LA, USA; [6]Tulane Center for Stem Cell Research and Regenerative Medicine, Tulane University, New Orleans, LA, USA; [7]Tulane Center for Aging, Tulane University, New Orleans, LA, USA*

Received November 5, 2014; December 9, 2014; Epub December 25, 2014; Published December 31, 2014

**Abstract:** Methoxyacetic acid (MAA) is a primary metabolite of ester phthalates that are used in production of consumer products and pharmaceutical products. MAA causes embryo malformation and spermatocyte death through inhibition of histone deacetylases (HDACs). Little is known about MAA's effects on cancer cells. In this study, two immortalized human normal prostatic epithelial cell lines (RWPE-1 and pRNS-1-1) and four human prostate cancer cell lines (LNCaP, C4-2B, PC-3, and DU-145) were treated with MAA at different doses and for different time periods. Cell viability, apoptosis, and cell cycle analysis were performed using flow cytometry and chemical assays. Gene expression and binding to DNA were assessed using real-time PCR, Western blot, and chromatin immunoprecipitation analyses. We found that MAA dose-dependently inhibited prostate cancer cell growth through induction of apoptosis and cell cycle arrest at G1 phase. MAA-induced apoptosis was due to down-regulation of the anti-apoptotic gene baculoviral inhibitor of apoptosis protein repeat containing 2 (BIRC2, also named cIAP1), leading to activation of caspases 7 and 3 and turning on the downstream apoptotic events. MAA-induced cell cycle arrest (mainly G1 arrest) was due to up-regulation of p21 expression at the early time and down-regulation of cyclin-dependent kinase 4 (CDK4) and CDK2 expression at the late time. MAA up-regulated p21 expression through inhibition of HDAC activities, independently of p53/p63/p73. These findings demonstrate that MAA suppresses prostate cancer cell growth by inducing growth arrest and apoptosis, which suggests that MAA could be used as a potential therapeutic drug for prostate cancer.

**Keywords:** Prostate cancer, cell death, cell cycle, apoptosis, p21

## Introduction

Methoxyacetic acid (MAA, linear chemical formula: $CH_3OCH_2COOH$) is a primary metabolite of ester phthalates widely used in the manufacture of household products (building materials, plastics, textiles, adhesives, paints, and deodorants), food and personal care products (agricultural adjuvants, pesticides, cosmetics, and perfumes), electronics (coatings, stabilizers, and surfactants), and pharmaceutical products (oral pill coatings, viscosity control agents, surfactants, and stabilizers) [1]. Over 18 billion pounds of ester phthalates are used globally each year. Ingestion, inhalation, intravenous injection, and dermal exposure of ester phthalates may lead to toxicities through their metabolite MAA [1]. MAA is converted from ethylene glycol monomethyl ether (also called 2-methoxyethanol) by alcohol dehydrogenase. In a workplace with daily 2-methoxyethanol exposure of 4.5 μg/ml (within the permissible exposure limit), urine MAA concentrations reached up to 0.6 millimoles/liter (mM) [2], which could be accumulated to higher concentrations due to the long elimination half-life of 77 hours [3]. Exposure to 2-methoxyethanol increases risks of spontaneous abortion and subfertility in women [4] and decreases sperm counts in men [5]. In pregnant mice, single i.v. injection of 250-325 mg/kg 2-methoxyethanol created peak plasma concentrations of 5-8 mM MAA, which led to embryo malformation and lethality [6].

MAA causes toxicities through multiple mechanisms. In normal human fibroblasts, MAA treatment induces production of radical oxygen species, resulting in DNA damage and loss of mitochondrial membrane potential [1]. MAA treatment down-regulates expression of estrogen receptor α (ERα) and estradiol-induced gene expression in human breast cancer cell line MCF-7 and mouse uterus [7]. In contrast, it has been reported that MAA exposure increases ERβ expression in pachytene spermatocytes, which may be associated with MAA-induced apoptosis of pachytene spermatocytes in rats [8]. In rat seminiferous tubules, MAA treatment alters the expression of androgen receptor (AR) and androgen-binding protein (ABP) in a stage-specific manner. On one hand, MAA treatment up-regulates AR expression in the early and late stages, but down-regulates AR expression in the middle stage [9]; on the other hand, this same treatment down-regulates ABP expression in the late stage, but up-regulates ABP expression in the middle stage [9]. Spermatogenesis requires normal functions of AR [10, 11], ERα [12], and ERβ [13] and their disruption leads to testicular degradation after MAA exposure. In addition, MAA has been found to activate the tyrosine kinase – PI3K pathway and other pathways to enhance or antagonize androgen-induced gene expression [14-16]. Similarly, MAA can enhance the transcriptional activities of ERα and ERβ by activating MAPK and inhibiting histone deacetylases (HDACs) [17]. MAA can inhibit HDAC1, HDAC2, and HDAC3, thus increasing the levels of acetylated histone H4, like the other well-known HDAC inhibitors such as trichostatin, valproic acid, and butyric acid [17]. In fact, it has been reported that MAA-induced hyperacetylation of histones H3 and H4 is associated with rapid spermatocyte death following MAA exposure [18].

These previous studies on MAA largely focused on its toxic effects on the reproductive system. Some HDAC inhibitors such as suberanilohydroxamic acid (SAHA) and romidepsin have been approved for the treatment of cutaneous T cell lymphoma, and panobinostat and valproic acid are being tested in the treatment of prostate cancer, breast cancer, cervical cancer, ovarian cancer, and lymphomas [19]. We speculated that MAA might also possess anti-cancer activity. In the present study, we tested this idea and found that MAA can indeed induce apoptosis and growth arrest of prostate cancer cells. MAA-induced apoptosis was highly associated with decreased protein expression of baculoviral inhibitor of apoptosis protein repeat containing 2 (BIRC2, also named cIAP1), whereas MAA-caused G1 arrest was closely associated with induction of p21 level and reduction of cyclin-dependent kinase 4 (CDK4) and CDK2 levels. The MAA-induced p21 level was likely due to the inhibition of HDAC activities by this compound, leading to increased association of acetylated histone H3 and H4 with the specificity protein 1 (Sp1) binding sites-rich DNA element on the p21 promoter, independently of p53/p63/p73 proteins. Thus, these results suggest that MAA might possess a potential anti-cancer activity by inhibiting anti-apoptotic protein and inducing apoptosis as well as inducing cell growth arrest via induction of p21.

## Materials and methods

### *Cell culture*

The sources and cell culture conditions of two immortalized human normal prostatic epithelial cell lines (RWPE-1 and pRNS-1-1) and four human prostate cancer cell lines (LNCaP, C4-2B, PC-3, and DU-145) were described previously [20]. Cells were cultured in a 5% $CO_2$ humidified incubator at 37°C.

### *Cell viability assay*

The number of live cells was determined using the CellTiter-Glo® Luminescent Cell Viability Assay (Promega Corp, Fitchburg, WI, USA) as described previously [20]. Cell viability was calculated as (luminescence of the treatment group – background luminescence) ÷ (luminescence of the control group – background luminescence) × 100%. The data are presented as the mean and standard error of the mean (SEM) of three independent experiments.

### *Detection of apoptotic nucleosomes*

Cells were seeded on 12-well plates with 1 × $10^5$ cells/well in triplicate per group in the complete culture medium with FBS. After overnight incubation, cells were treated with 5 mM MAA for 24 hours (h); a control group was treated with PBS. Apoptotic nucleosomes were detected using Cell Death Detection ELISA kit (Roche Diagnostics Corporation, Indianapolis, IN, USA) according to the manufacturer's instructions [21]. Absorbance was measured at 405 nm (A405) with a reference wavelength at 490 nm (A490) using a plate reader (Bio-Tek U.S.,

**Table 1.** PCR primers

| Primer | | Sequence |
|---|---|---|
| p21 | Forward | 5'-ACCCATGCGGCAGCAA-3' |
| | Reverse | 5'-CGCCATTAGCGCATCACA-3' |
| GAPDH | Forward | 5'-TAAAAGCAGCCCTGGTGACC-3' |
| | Reverse | 5'-CCACATCGCTCAGACACCAT-3' |
| Sp1-rich region | Forward | 5'-CAGCGCACCAACGCAGGCG-3' |
| | Reverse | 5'-CAGCTCCGGCTCCACAAGGA-3' |
| Adjacent region | Forward | 5'-GGTGTCTAGGTGCTCCAGGT-3' |
| | Reverse | 5'-GCACTCTCCAGGAGGACACA-3' |

Winooski, VT, USA). The amount of apoptotic nucleosomes was represented by A405-A490.

*Cell cycle analysis*

Cells were treated without or with 5 mM or 20 mM MAA for 24 h. The percentage of cells at G1/G0, S, and G2/M phases was determined by flow cytometry analysis as described previously [20].

*Western blot analysis*

Cells were treated without or with MAA at concentrations of 5 mM or 20 mM for 0, 12, 24, 48, and 72 h. Proteins were extracted for Western blot analysis as described previously [20]. Rabbit anti-caspase 7, rabbit anti-caspase 6, and rabbit anti-caspase 9 antibodies were purchased from Cell Signaling Technology (Danvers, MA, USA). Mouse anti-p53, mouse anti-p63, rabbit anti-p73, rabbit anti-caspase 10, mouse anti-caspase 8, rabbit anti-BIRC2, and rabbit anti-BIRC3 antibodies were obtained from Santa Cruz Biotechnology (Dallas, TX, USA). Mouse anti-GAPDH, mouse anti-caspase 3, and rabbit anti-cleaved poly (ADP-ribose) polymerase (PARP) antibodies were purchased from EMD Millipore Corp (Billerica, MA, USA). Rabbit anti-CDK2 and mouse anti-CDK4 antibodies were purchased from GeneTex, Inc., Irvine, CA, USA. Rabbit anti-cyclin D1 antibodies were bought from Abcam, Cambridge, MA, USA.

*Reverse transcription (RT) and quantitative (q) PCR analysis*

Cells were treated with 20 mM MAA for 0, 12, 24, 48, and 72 h. Total RNAs were extracted for RT and qPCR analysis as described previously [22]. Results were normalized against GAPDH levels using the formula ΔCt (Cycle threshold) = Ct of target gene – Ct of GAPDH. The mRNA level of a control group was used as the baseline; therefore, ΔΔCt was calculated using the formula ΔΔCt = ΔCt of target gene – ΔCt of the baseline. The fold change of mRNA level was calculated as fold = $2^{-\Delta\Delta Ct}$. PCR primers used are shown in **Table 1**.

*Chromatin immunoprecipitation (ChIP) assay*

Cells were plated at a density of $2 \times 10^6$ cells per dish in four 100-mm dishes in each group and incubated overnight. Cells were treated without or with 20 mM MAA for 24 h and fixed in 1% formaldehyde for 10 minutes. ChIP assays were performed using Magna ChIP™ G Chromatin Immunoprecipitation Kit (EMD Millipore Corp, Billerica, MA, USA) according to the manufacturer's instructions. Briefly, 1 mL of 10x glycine was added to the cells to quench formaldehyde; after washing with ice-cold PBS containing protease inhibitor cocktail II, the cells were resuspended in 0.5 mL of SDS lysis buffer with protease inhibitor cocktail II; after centrifugation, cell pellets were resuspended in 0.5 mL nuclear lysis buffer; the lysates were sonicated for about 10-15 seconds on ice; after centrifugation, an aliquot of 5 microliter (μL) of the supernatant chromatin preparation was set aside as the Input fraction; then, 50 μL chromatin preparations were diluted with 450 μL ChIP dilution buffer and added with 5 μg of rabbit anti-acetyl-histone H3, rabbit anti-acetyl-histone H4 (EMD Millipore Corp), or rabbit IgG (Santa Cruz Biotechnology) for overnight incubation at 4°C; protein G magnetic beads (20 μL) were added for 1 h incubation; next, protein G magnetic bead complexes were separated with magnetic separator and washed with washing buffers; immune complex samples and inputs were eluted with 100 μL of ChIP elution buffer and digested with proteinase K at 62°C for 2 h; immunoprecipitated DNA samples and Inputs were purified with DNA purification spin column and analyzed by PCR with the products analyzed by 2% agarose/ethidium bromide gel electrophoresis. PCR primers used for ChIP assays are shown in **Table 1**.

*Statistical analysis*

Results from this study were presented as the mean ± SEM. Statistical analysis was performed using two-tailed Student's *t* test. A *p*-value < 0.05 was considered statistically significant.

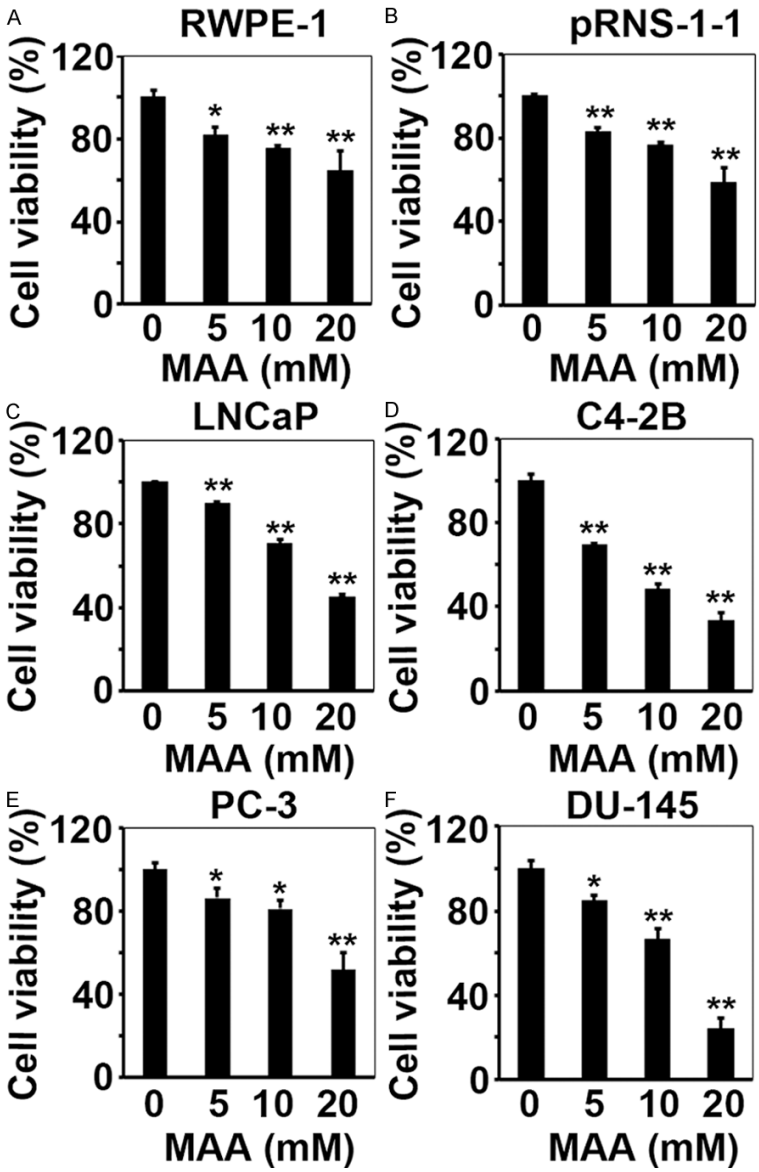



**Figure 1.** MAA inhibits prostate cancer cell growth. A-F: Normal prostatic epithelial cells and prostate cancer cells were plated in 96-well plates in triplicate per group and were treated with 0, 5, 10, and 20 mM MAA for 72 h. The live cell numbers were determined using the CellTiter-Glo® Luminescent Cell Viability Assay. The data are presented as the mean ± SEM of three independent experiments. *$p < 0.05$; **$p < 0.01$.

## Results

*MAA inhibits prostate cancer cell growth*

To study the effects of MAA on prostate cancer cell growth, we treated two immortalized human normal prostatic epithelial cell lines RWPE-1 and pRNS-1-1 and four prostate cancer cell lines LNCaP, C4-2B, PC-3, and DU-145, with 5, 10, and 20 mM of MAA. We chose to start with 5 mM MAA because a previous study showed that the $IC_{50}$ was 5.6 mM for MAA to inhibit cell growth of human leukemia cell line HL60 [23]. We found that MAA inhibited cell growth in all of the six cell lines in a dose dependent fashion (**Figure 1A-F**). Interestingly, four prostate cancer cell lines (LNCaP, C4-2B, PC-3, and DU-145) were more sensitive to MAA than were two normal prostatic epithelial cell lines (RWPE-1 and pRNS-1-1), as the number of viable cells was decreased by approximately 50% to 75% in the four prostate cancer cell lines (**Figure 1C-F**), whereas it was only reduced by 40% in RWPE-1 and pRNS-1-1 cells, when these cell lines were individually treated with 20 mM MAA (**Figure 1A**, **1B**).

*MAA induces apoptosis of prostate cancer cells*

To test if MAA induces apoptosis of prostate cancer cells, we measured apoptotic nucleosomes in untreated and MAA-treated cells. We found that 5mM MAA treatment for 24 h significantly increased the amounts of apoptotic nucleosomes in LNCaP, C4-2B, PC-3, and DU-145 cells, compared to the untreated control groups (**Figure 2A-D**, $p < 0.05$ or 0.01). Consistently, PARP cleavage in all four prostate cancer cell lines was induced by MAA in a dose- and time-dependent manner (**Figure 2E**, **2F**). Since PARP cleavage has been widely used as an indicator of apoptosis [24, 25], these results indicate that MAA induces apoptosis of four prostate cancer cell lines.

*MAA blocks G1/S transition of prostate cancer cell cycle*

To assess if MAA induces cell cycle arrest, we analyzed the percentages of cells in the G1

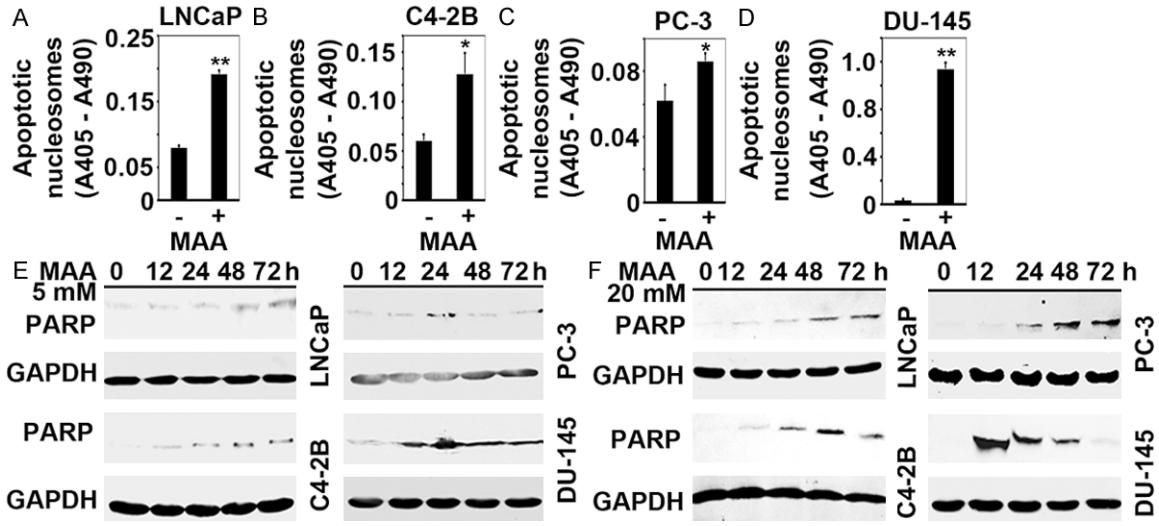



**Figure 2.** MAA induces apoptosis of prostate cancer cells. (A-D) Prostate cancer cells were plated in 12-well plates in triplicate per group and treated with 5 mM MAA for 24 h; the control group was treated with PBS. Apoptotic nucleosomes were detected using Cell Death Detection ELISA kit, which were calculated as absorbance at 405 nm (A405) – absorbance at 490 nm (A490). The data are presented as the mean ± SEM of three independent experiments. *$p < 0.05$; **$p < 0.01$. (E, F) Prostate cancer cells were treated with 5 mM (E) or 20 mM (F) MAA for up to 72 h. Protein extracts were used for Western blot analysis of cleaved PARP. For the loading control, the blots were probed for GAPDH.

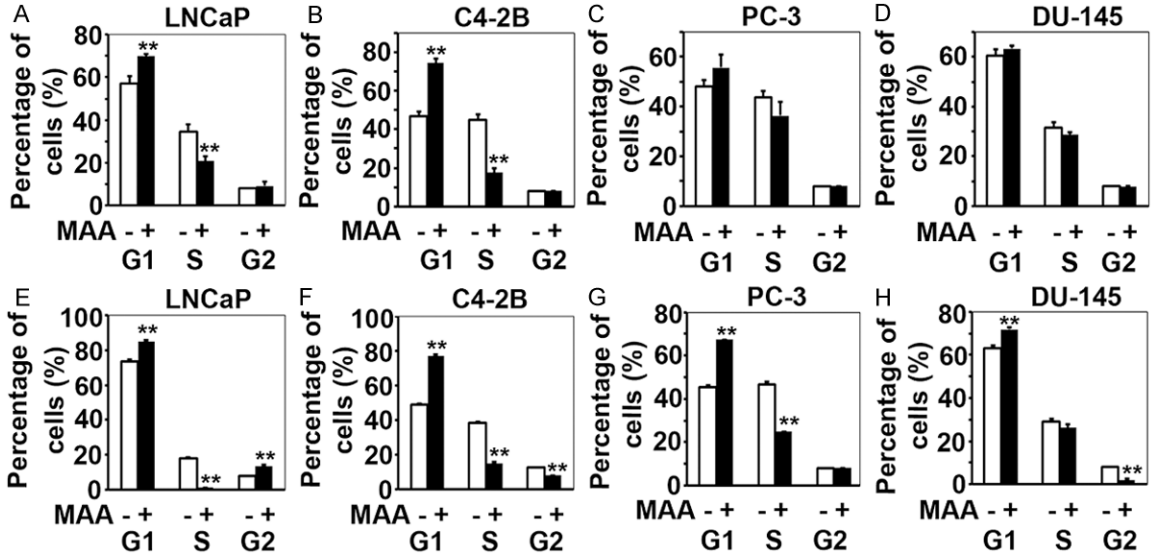



**Figure 3.** MAA blocks G1/S transition of prostate cancer cell cycle. (A-H) Prostate cancer cells were plated in 60-mm dishes in triplicate per group and treated with 5 mM (A-D) or 20 mM (E-H) MAA for 24 h; the control group was treated with PBS. The percentages of cells at G1 (and G0), S, and G2 (and M) phases were determined by flow cytometry analysis. The data are presented as the mean ± SEM, n = 3. **$p < 0.01$.

(and G0), S, and G2 (and M) phases of the cell cycle using flow cytometry analysis. We found that 5 mM MAA treatment significantly increased the percentage of LNCaP and C4-2B cells at the G1/G0 phase, but significantly decreased the percentage of cells at the S phase (**Figure 3A**, **3B**, $p < 0.01$). However, although some effects were found in PC-3 and DU-145 cells, the differences were not statistically significant at the low dosage of MAA (**Figure 3C**, **3D**, $p > 0.05$). At a high dose such as 20 mM, MAA treatment significantly

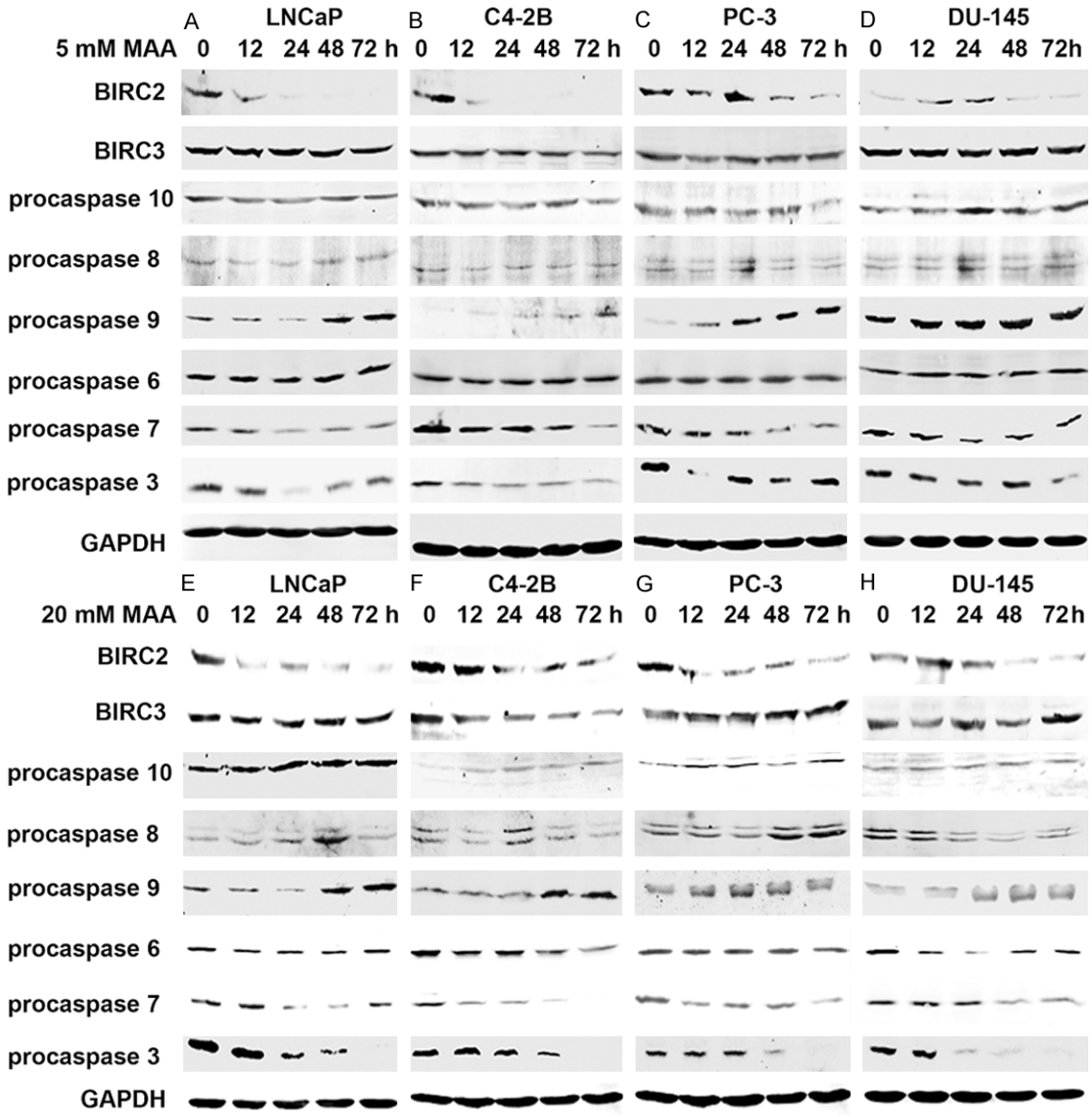



**Figure 4.** MAA decreases protein expression of BIRC2 and activates caspases 7 and 3. (A-H) Prostate cancer cells were treated with 5 mM (A-D) or 20 mM (E-H) MAA for up to 72 h. Protein extracts were used for Western blot analysis of the indicated proteins. For the loading control, the blots were probed for GAPDH.

increased the percentage of cells at the G1/G0 phase with the corresponding decrease of cells at the S phase in all four prostate cancer cell lines (**Figure 3E-H**). These results imply that MAA treatment blocks the G1/S transition, and thus inhibits cell proliferation.

*MAA decreases protein expression of BIRC2 and activates caspases 7 and 3*

To illustrate the mechanisms underlying MAA-induced apoptosis of prostate cancer cells, we examined the expression of a panel of anti-apoptotic and pro-apoptotic genes, using Western blot analysis. Although there was not any detectable expression or any change upon MAA treatment for B-cell CLL/lymphoma 2 (BCL2), BCL2-associated X protein (BAX), BCL2-like 1 (BCL2L1), BCL2-associated agonist of cell death (BAD), BH3 interacting domain death agonist (BID), myeloid cell leukemia 1 (MCL1), and CASP8 and FADD-like apoptosis regulator (CFLAR) (data not shown), we found that MAA treatment decreased the protein level of BIRC2 in all four prostate cancer cell lines (**Figure**

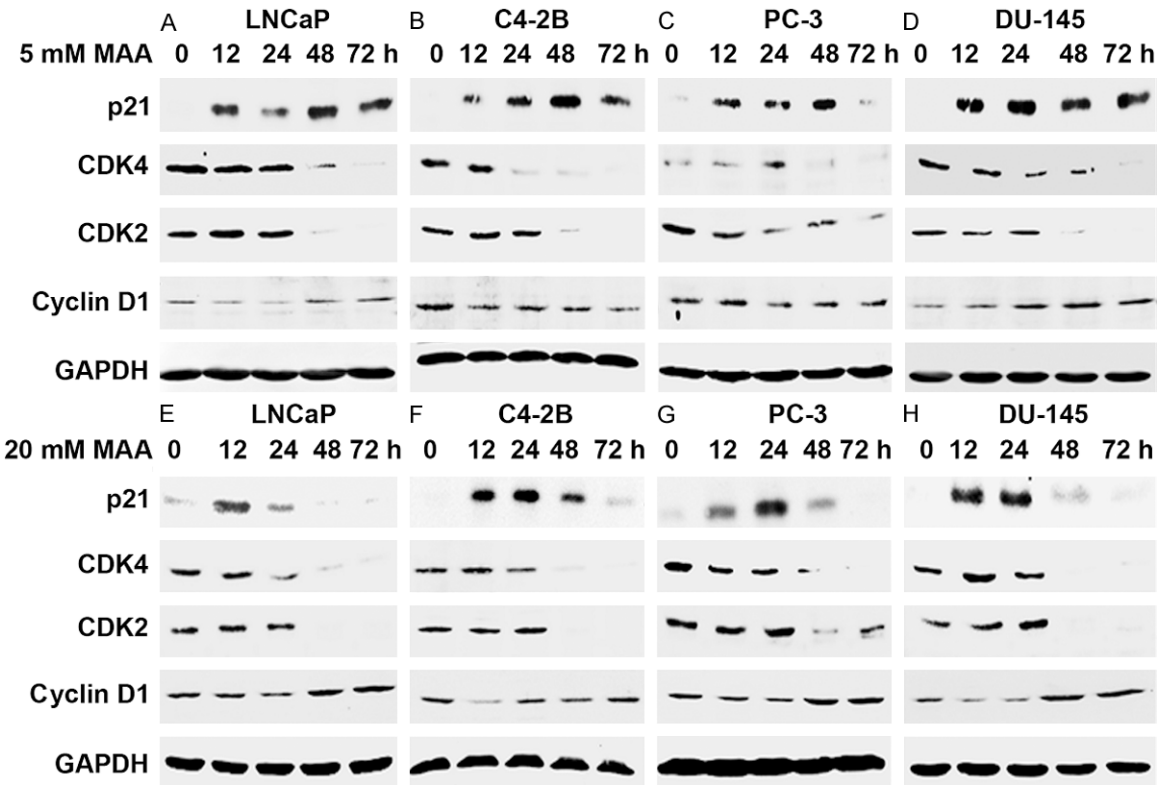



**Figure 5.** MAA induces p21 level but reduces CDK4 and CDK2 levels. (A-H) Prostate cancer cells were treated with 5 mM (A-D) or 20 mM (E-H) MAA for up to 72 h. Protein extracts were used for Western blot analysis of the indicated proteins. For the loading control, the blots were probed for GAPDH.

**4A-H**). This decrease was specific to BIRC2, as there were not any obvious changes in the protein levels of BIRC3, another member of the inhibitors of apoptosis protein (IAP) family [26]. It has been shown that proteasome-mediated and/or HTRA2 serine protease-mediated degradation of BIRC2 can relieve BIRC2's inhibitory function on caspases, thus activating caspases-mediated apoptosis [27, 28]. Therefore, we examined a panel of key caspases in both extrinsic and intrinsic apoptosis pathways. Caspases are endoproteases that are initially produced as inactive monomeric procaspases, which require dimerization and often cleavage for activation [29]. Among the apoptosis-relevant caspases, the level of procaspase 9 in all four prostate cancer cell lines was induced by MAA treatment at both 5 mM (**Figure 4A-D**) and 20 mM (**Figure 4E-H**), whereas little change of the level of procaspases 10, 8 and 6 was observed with the same treatment (**Figure 4A-H**). By contrast, the level of procaspases 7 and 3 was decreased by MAA treatment at both 5 mM (**Figure 4A-D**) and 20 mM (**Figure 4E-H**). Decrease of the procaspases indicates cleavage of the proenzymes and activation of caspases 7 and 3, two key executioner caspases [29].

*MAA induces p21 level but reduces CDK4 and CDK2 levels*

To determine which protein molecules might be responsible for MAA-induced G1 arrest, we first examined the levels of several cell cycle-regulated proteins during the G1/S transition. It has been shown that in the late G1 phase, the cyclin D-CDK4/6 kinase complex initiates phosphorylation of retinoblastoma protein (pRb), and this phosphorylation dissociates pRb from E2F transcription factors, thus allowing them to be functional and transactivate expression of the genes necessary for G1/S transition. This process is enhanced by the cyclin E-CDK2 complex, but inhibited by p21 [30]. We found that the level of p21 protein was increased as early as 12 h after cells were treated with 5 mM MAA (**Figure 5A-D**). However, surprisingly and interestingly, at 20 mM, MAA-induced p21 level reached a peak at 12 to 24 h, and then started

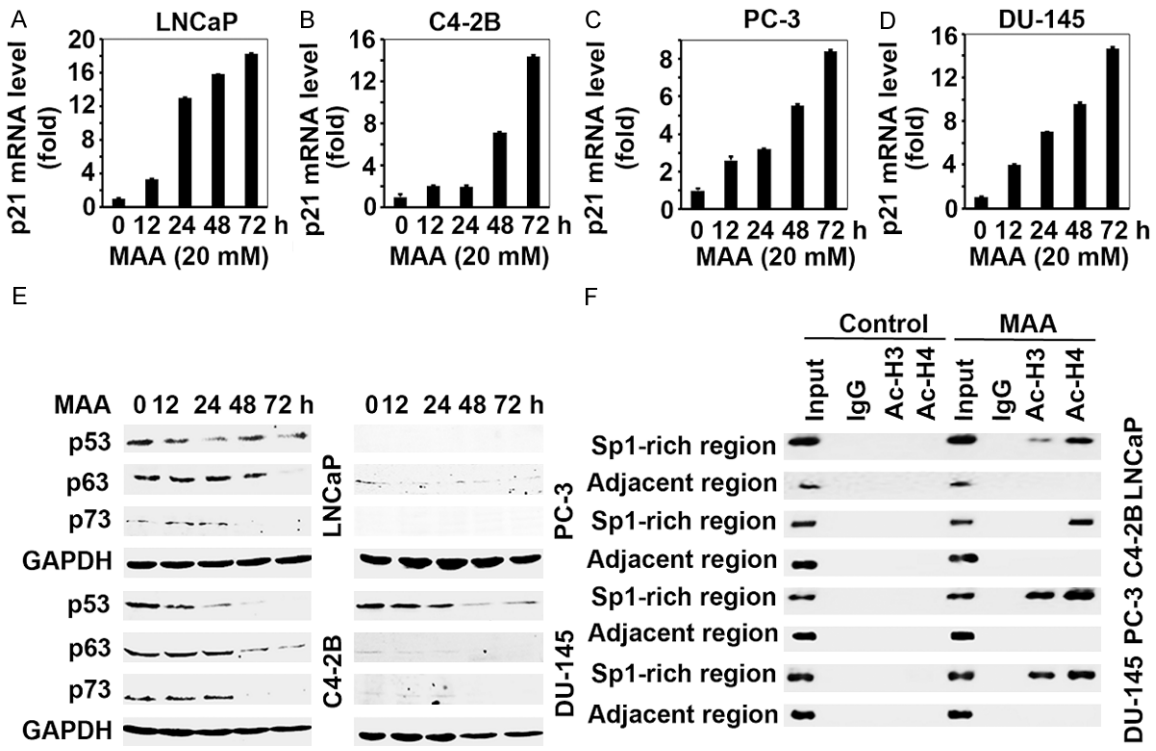



**Figure 6.** MAA enhances p21 transcription by inhibiting HDACs, independently of p53/p63/p73. A-D: Prostate cancer cells were treated with 20 mM MAA for up to 72 h. RNAs were analyzed with reverse transcription and quantitative PCR. Fold changes were calculated based on normalization to GAPDH levels and using the untreated control group as base line. The data are presented as the mean ± SEM, n = 3. E: Prostate cancer cells were treated with 20 mM MAA for up to 72 h. Protein extracts were used for Western blot analysis of the indicated proteins. For the loading control, the blots were probed for GAPDH. F: Prostate cancer cells were treated with 20 mM MAA for 24 h and fixed in 1% formaldehyde. The chromatin preparations were immunoprecipitated with anti-acetyl-histone H3 (Ac-H3), anti-acetyl-histone H4 (Ac-H4), or control IgG, plus protein G magnetic beads. The purified DNAs were analyzed by PCR using primers specific for the Sp1 binding sites-rich region (Sp1-rich region) or the adjacent upstream region without Sp1 binding sites (Adjacent region). An aliquot of the chromatin preparations was used as Input control. PCR products were run on 2% agarose/ethidium bromide gel electrophoresis.

to drop down to the basal level from 48 h post treatment (**Figure 5E-H**). By contrast, CDK4 and CDK2 levels started to decrease in most of the four tested cell lines at 48 and 72 h after MAA treatment at 5 and 20 mM, whereas cyclin D1 levels were not dramatically altered after MAA treatment of all of the cell lines (**Figure 5A-H**). These results suggest that MAA may induce G1 arrest by increasing p21 level and decreasing the levels of CDK2 and CDK4.

*MAA enhances p21 transcription by inhibiting HDACs*

To further illustrate possible molecular mechanisms underlying p21 up-regulation by MAA, we first performed qPCR and found that MAA increased p21 mRNA levels as early as 12 h after its treatment at 20 mM, and p21 mRNA levels continued to rise over the 72 h treatment period (**Figure 6A-D**). Since p21 transcription is often activated by the p53 family of genes [31, 32], we examined the levels of p53, p63, and p73 proteins. It is known that LNCaP and its derivative C4-2B cells harbor a wild-type TP53 gene, while DU-145 cells have a mutant TP53 gene, but PC-3 cells have a truncation mutation in the TP53 gene hence do not express p53 protein [33]. We found that none of p53, p63, and p73 protein expression was induced by MAA treatment; instead, they were decreased after 48 or 72 h in some cells, such as LNCaP, C4-2B and DU-145 (**Figure 6E**). Also, expression of p53 or p73 proteins was not detected in PC-3 cells, while a low level of p63 protein was present, but decreased during the treatment period (**Figure 6E**). Since it has been reported that p21 expression is repressed by HDAC1 and HDAC4 in a p53-independent mechanism

[34, 35], we examined whether MAA as an HDAC inhibitor could enhance binding of acetylated histone H3 and H4 to the Sp1 binding sites-rich region within the p21 promoter. We adopted the PCR primers spanning the Sp1 binding sites-rich region (abbreviated as Sp1-rich region) and the Sp1 binding sites-deficient adjacent region (abbreviated as adjacent region) used in a previous study [35]. We also used the same anti-acetylated histone H3 and H4 antibodies to perform ChIP analysis as previously described [34]. As shown in **Figure 6F**, MAA treatment increased binding of acetylated histone H3 and/or H4 to the Sp1-rich region of the p21 promoter, which was specific to this region as there was no increase in binding to the adjacent region (**Figure 6F**), suggesting that MAA might induce histone H3 and H4 acetylation at the p21 promoter region and thus open up the Sp1-binding DNA element to Sp1 that in turn activates the expression of p21 at the transcriptional level. Taken together, these results indicate that MAA induces p21 transcription by inhibiting HDAC activity and consequently leading to hyperacetylation of histone H3 and H4 and opening the promoter region of the p21 gene, in a p53 family independent manner.

## Discussion

Prostate cancer, particularly castration-resistant prostate cancer, is lethal to the patients, as the currently available treatments can only extend patient's survival by 2.4 to 4.8 months [36]. Thus, new therapeutics are urgently needed for this type of malignancy. HDAC inhibitors can promote growth arrest, differentiation, and apoptosis of cancer cells, with minimal effects on normal tissues, thus HDAC inhibitors are emerging as promising anti-cancer drugs which possess tumor-selective cytotoxicity [37]. MAA has been demonstrated to be an HDAC inhibitor [17, 18], yet its anti-cancer potential has never been assessed. In the present study, we demonstrated that MAA suppressed the survival of four prostate cancer cell lines (LNCaP, C4-2B, PC-3, and DU-145) in a dose-dependent manner by inducing apoptosis and G1 arrest. Although MAA has been shown to cause apoptosis of spermatocytes (5), this cellular toxicity would be acceptable or minimal to most of the prostate cancer patients because the majority of the patients are 60 years or older who have passed their reproductive age [38]. MAA has been shown to be responsible for immunosuppression in rats, but it does not suppress humoral immunity in mice [39]. In humans, only a few cases were reported to have mild anemia and leukopenia in individuals exposed to ethylene glycol monomethyl ether [40]. Therefore, MAA is a promising chemical candidate for the treatment of prostate cancer.

MAA induces apoptosis of rat germ cells through release of mitochondrial cytochrome c, thus activating caspase 9 and caspase 3 [41]. Cytochrome c release from mitochondria is controlled by the antagonistic actions of pro-apoptotic and anti-apoptotic genes of the BCL2 family [42], which is true in rat germ cells [43]. However, we did not find any MAA-induced changes of BCL2, BAX, BCL2L1, BAD, BID, MCL1, and CFLAR in the four prostate cancer cell lines. Instead, we found that BIRC2 (also called cIAP1) protein expression was consistently decreased by MAA treatment in all four prostate cancer cell lines, which was specific to BIRC2 as BIRC3 (also called cIAP2) expression was not affected. BIRC2, like other IAP family proteins, has ubiquitin protein ligase (E3) activity [28]. BIRC2 binds to tumor necrosis factor receptor associated factor 2 (TRAF2) and becomes activated to initiate ubiquitination of receptor-interacting protein 1 (RIP1), subsequently inhibiting activation of caspase 8 [26]. However, we did not observe any MAA-induced activation of caspase 8 or other initiator caspases such as caspase 10, in the decrease of BIRC2 protein levels. On the other hand, we found activation of caspase 7 and caspase 3. Previously, it was found that although BIRC2 can bind to caspases 7 and 9, it is a weak inhibitor of caspases 9, 7, and 3 [44]. But later on, it was found that BIRC2 potently inhibited activation of procaspase 3 by the cytochrome c-dependent apoptotic protease activating factor 1 (APAF1)·caspase 9 apoptosome complex [45]. This finding explains the observed activation of caspases 3 and 7 when MAA treatment decreased BIRC2 protein levels in our study. Of note, MAA treatment consistently increased the procaspase 9 protein level, though the mechanism of this action is not known. We and other investigators have previously noticed that some apoptosis-inducing chemicals can up-regulate procaspase 9 expression [20, 46]. Our speculation is that the increased procaspase 9 levels might be involved in activation of caspases 7 and 3, which awaits further verification.

Also, we showed that MAA causes G1 arrest in all of the four prostate cancer cell lines regardless of the status of p53. It is known that cyclin D-CDK4/6 complex phosphorylates pRb, leading to separation of pRb from E2F transcription factors, thus transactivating genes needed for the G1/S transition and S phase, including cyclin E. Then, activation of cyclin E-CDK2 complex further phosphorylates and completely releases pRb from interacting with E2Fs. However, association of p21 with cyclin D-CDK4/6 inhibits pRb phosphorylation and induces cell cycle arrest in G1 phase [30]. We found that MAA treatment induced up-regulation of p21 mRNA expression and protein expression. At the earlier time points, such as 12 and 24 h, p21 mRNA transcription could be responsible for the increase of its protein level by MAA. However, the protein level of p21 decreased after 24 h of MAA treatment at 20 mM (**Figure 5E-H**), which was inconsistent with the increase of its mRNA level (**Figure 6A-D**). The mechanism for this difference at later time points remains unclear, which is possibly caused by rapid degradation of p21 protein by caspase 3-mediated cleavage as shown in a previous study [47]. p21 is well known for its role in cell cycle arrest, yet p21 can also inhibit apoptosis by interacting with and inhibiting caspase 3 [48, 49]. On the other hand, active caspase 3 can cleave p21 protein, thus converting the cells from cell cycle arrest to apoptosis [47, 50]. This is consistent to our findings that procaspase 3 was dramatically cleaved hence activated at 48 to 72 h (**Figure 4E-H**), which then cleaved and degraded p21 protein (**Figure 5E-H**). Further, we found that at the high dose of 20 mM, MAA treatment also reduced the percentage of C4-2B and DU-145 cells in G2 phase (**Figure 3F**, **3H**). This is possibly due to inhibition of cyclin A-CDK1/2 by p21, as it has been reported that p21 can induce G2 arrest [51], or due to loss of CDK2. On the other hand, we consistently found that 20 mM MAA treatment increased the percentage of LNCaP cells in G2 phase, but there were only few cells left in S phase (**Figure 3E**). We do not have a good explanation for this observation, which is unique only to LNCaP cell line at this 20 mM dose of MAA treatment. It is worthy notice that MAA-induced p21 up-regulation was independent of p53/p63/p73, as we did not find any induction of the p53 family proteins by MAA treatment, rather than seeing a slight decrease of their expression (**Figure 6E**). Nevertheless, we found that MAA treatment increased binding of acetylated histone H3 and H4 to the Sp1 binding sites-rich region of p21 promoter, suggesting that MAA inhibits HDAC activities that repress p21 expression. Our findings are consistent with two previous studies showing that HDAC inhibitors up-regulate p21 expression through a Sp1-dependent, p53-independent mechanism [34, 35].

In addition, we also found that protein levels of CDK4 and CDK2, but not cyclin D1, were decreased by MAA treatment at 48 to 72 h. It has been demonstrated that CDK4 and CDK2 cooperate to phosphorylate pRb and drive G1/S transition, thus loss of both CDK4 and CDK2 leads to G1 arrest [52]. The timing of loss of CDK4 and CDK2 couples with reduction of p21 protein levels, particularly with 20 mM MAA treatment (**Figure 5E-H**), suggesting that in the absence of p21, loss of CDK4 and CDK2 becomes the main reason for G1 arrest. However, the mechanisms of how MAA treatment leads to loss of CDK4 and CDK2 are not clear, which requires further investigation.

In summary, the results as presented here demonstrate that MAA, as an HDAC inhibitor, can inhibit prostate cancer cell growth through induction of apoptosis and cell cycle arrest. MAA-induced apoptosis is likely due to down-regulation of the anti-apoptotic gene BIRC2, leading to activation of caspases 7 and 3 and turning on the downstream apoptotic events. MAA-induced G1 arrest is due to up-regulation of p21 expression at the early time and down-regulation of CDK4 and CDK2 expression at the late time post its treatment. MAA up-regulates p21 expression through inhibition of HDAC activities, independently of the p53 family members. Thus, our results strongly suggest that MAA could be developed into a potential therapy for prostate cancer.

**Acknowledgements**

The authors thank Mary Price from Tulane Cancer Center and Louisiana Cancer Research Consortium FACS Core for flow cytometry analysis. This work was supported in whole or in part by Department of Defense Health Program through the Prostate Cancer Research Program (W81XWH-14-1-0050, W81XWH-14-1-0149, and W81XWH-14-1-0458; the U.S. Army

Medical Research Acquisition Activity, 820 Chandler Street, Fort Detrick MD 21702-5014 is the awarding and administering acquisition office) and by National Institutes of Health (P20GM103518 and R01CA174714 to Z. Y.; 2G12MD007595 to G. W.). The content of this article is solely the responsibility of the authors and does not necessarily represent the official views of the National Institutes of Health or the Department of Defense.

## Disclosure of conflicts of interest

The authors disclose no conflicts of interest.

**Address correspondence to:** Dr. Zongbing You, Department of Structural & Cellular Biology, Tulane University School of Medicine, 1430 Tulane Ave mailbox 8649, New Orleans, LA 70112, USA. Tel: 504-988-0467; Fax: 504-988-1687; E-mail: zyou@tulane.edu (Zongbing You); kparajuli55@gmail.com (Keshab R Parajuli)

## References

[1] Priyandoko D, Ishii T, Kaul SC and Wadhwa R. Ashwagandha leaf derived withanone protects normal human cells against the toxicity of methoxyacetic acid, a major industrial metabolite. PLoS One 2011; 6: e19552.

[2] Shih TS, Liou SH, Chen CY and Smith TJ. Urinary 2-methoxy acetic acid accumulation in response to 2-methoxy ethanol exposure. Arch Environ Health 2001; 56: 20-25.

[3] Groeseneken D, Veulemans H, Masschelein R and Van Vlem E. Experimental human exposure to ethylene glycol monomethyl ether. Int Arch Occup Environ Health 1989; 61: 243-247.

[4] Correa A, Gray RH, Cohen R, Rothman N, Shah F, Seacat H and Corn M. Ethylene glycol ethers and risks of spontaneous abortion and subfertility. Am J Epidemiol 1996; 143: 707-717.

[5] Welch LS, Schrader SM, Turner TW and Cullen MR. Effects of exposure to ethylene glycol ethers on shipyard painters: II. Male reproduction. Am J Ind Med 1988; 14: 509-526.

[6] Terry KK, Elswick BA, Stedman DB and Welsch F. Developmental phase alters dosimetry-teratogenicity relationship for 2-methoxyethanol in CD-1 mice. Teratology 1994; 49: 218-227.

[7] Henley DV, Mueller S and Korach KS. The short-chain fatty acid methoxyacetic acid disrupts endogenous estrogen receptor-alpha-mediated signaling. Environ Health Perspect 2009; 117: 1702-1706.

[8] Tirado OM, Selva DM, Toran N, Suarez-Quian CA, Jansen M, McDonnell DP, Reventos J and Munell F. Increased expression of estrogen receptor beta in pachytene spermatocytes after short-term methoxyacetic acid administration. J Androl 2004; 25: 84-94.

[9] Tirado OM, Martinez ED, Rodriguez OC, Danielsen M, Selva DM, Reventos J, Munell F and Suarez-Quian CA. Methoxyacetic acid disregulation of androgen receptor and androgen-binding protein expression in adult rat testis. Biol Reprod 2003; 68: 1437-1446.

[10] De Gendt K, Swinnen JV, Saunders PT, Schoonjans L, Dewerchin M, Devos A, Tan K, Atanassova N, Claessens F, Lecureuil C, Heyns W, Carmeliet P, Guillou F, Sharpe RM and Verhoeven G. A Sertoli cell-selective knockout of the androgen receptor causes spermatogenic arrest in meiosis. Proc Natl Acad Sci U S A 2004; 101: 1327-1332.

[11] Roberts KP and Zirkin BR. Androgen regulation of spermatogenesis in the rat. Ann N Y Acad Sci 1991; 637: 90-106.

[12] Abney TO. The potential roles of estrogens in regulating Leydig cell development and function: a review. Steroids 1999; 64: 610-617.

[13] O'Donnell L, Robertson KM, Jones ME and Simpson ER. Estrogen and spermatogenesis. Endocr Rev 2001; 22: 289-318.

[14] Bagchi G, Hurst CH and Waxman DJ. Interactions of methoxyacetic acid with androgen receptor. Toxicol Appl Pharmacol 2009; 238: 101-110.

[15] Bagchi G, Zhang Y, Stanley KA and Waxman DJ. Complex modulation of androgen responsive gene expression by methoxyacetic acid. Reprod Biol Endocrinol 2011; 9: 42.

[16] Bagchi G, Zhang Y and Waxman DJ. Impact of methoxyacetic acid on mouse Leydig cell gene expression. Reprod Biol Endocrinol 2010; 8: 65.

[17] Jansen MS, Nagel SC, Miranda PJ, Lobenhofer EK, Afshari CA and McDonnell DP. Short-chain fatty acids enhance nuclear receptor activity through mitogen-activated protein kinase activation and histone deacetylase inhibition. Proc Natl Acad Sci U S A 2004; 101: 7199-7204.

[18] Wade MG, Kawata A, Williams A and Yauk C. Methoxyacetic acid-induced spermatocyte death is associated with histone hyperacetylation in rats. Biol Reprod 2008; 78: 822-831.

[19] Li X, Zhang J, Xie Y, Jiang Y, Yingjie Z and Xu W. Progress of HDAC inhibitor panobinostat in the treatment of cancer. Curr Drug Targets 2014; 15: 622-634.

[20] Li Q, Lambrechts MJ, Zhang Q, Liu S, Ge D, Yin R, Xi M and You Z. Glyphosate and AMPA inhibit cancer cell growth through inhibiting intracellular glycine synthesis. Drug Des Devel Ther 2013; 7: 635-643.

[21] You Z, Saims D, Chen S, Zhang Z, Guttridge DC, Guan KI, MacDougald OA, Brown AMC, Evan G,

Kitajewski J and Wang CY. Wnt signaling promotes oncogenic transformation by inhibiting c-Myc-induced apoptosis. J Cell Biol 2002; 157: 429-440.
[22] Ge D, Dauchy RT, Liu S, Zhang Q, Mao L, Dauchy EM, Blask DE, Hill SM, Rowan BG, Brainard GC, Hanifin JP, Cecil KS, Xiong Z, Myers L and You Z. Insulin and IGF1 enhance IL-17-induced chemokine expression through a GSK3B-dependent mechanism: a new target for melatonin's anti-inflammatory action. J Pineal Res 2013; 55: 377-387.
[23] Takagi A, Yamada T, Hayashi K, Nakade Y, Kojima T, Takamatsu J, Shibata E, Ichihara G, Takeuchi Y and Murate T. Involvement of caspase 3 mediated apoptosis in hematopoietic cytotoxicity of metabolites of ethylene glycol monomethyl ether. Ind Health 2002; 40: 371-374.
[24] You Z, Shi XB, DuRaine G, Haudenschild D, Tepper CG, Lo SH, Gandour-Edwards R, de Vere White RW and Reddi AH. Interleukin-17 receptor-like gene is a novel antiapoptotic gene highly expressed in androgen-independent prostate cancer. Cancer Res 2006; 66: 175-183.
[25] Fang EF, Scheibye-Knudsen M, Brace LE, Kassahun H, SenGupta T, Nilsen H, Mitchell JR, Croteau DL and Bohr VA. Defective mitophagy in XPA via PARP-1 hyperactivation and NAD(+)/SIRT1 reduction. Cell 2014; 157: 882-896.
[26] de Almagro MC and Vucic D. The inhibitor of apoptosis (IAP) proteins are critical regulators of signaling pathways and targets for anti-cancer therapy. Exp Oncol 2012; 34: 200-211.
[27] Jin S, Kalkum M, Overholtzer M, Stoffel A, Chait BT and Levine AJ. CIAP1 and the serine protease HTRA2 are involved in a novel p53-dependent apoptosis pathway in mammals. Genes Dev 2003; 17: 359-367.
[28] Yang Y, Fang S, Jensen JP, Weissman AM and Ashwell JD. Ubiquitin protein ligase activity of IAPs and their degradation in proteasomes in response to apoptotic stimuli. Science 2000; 288: 874-877.
[29] McIlwain DR, Berger T and Mak TW. Caspase functions in cell death and disease. Cold Spring Harb Perspect Biol 2013; 5: a008656.
[30] Jung YS, Qian Y and Chen X. Examination of the expanding pathways for the regulation of p21 expression and activity. Cell Signal 2010; 22: 1003-1012.
[31] Lane D and Levine A. p53 Research: the past thirty years and the next thirty years. Cold Spring Harb Perspect Biol 2010; 2: a000893.
[32] Riley T, Sontag E, Chen P and Levine A. Transcriptional control of human p53-regulated genes. Nat Rev Mol Cell Biol 2008; 9: 402-412.
[33] Isaacs WB, Carter BS and Ewing CM. Wild-type p53 suppresses growth of human prostate cancer cells containing mutant p53 alleles. Cancer Res 1991; 51: 4716-4720.
[34] Gui CY, Ngo L, Xu WS, Richon VM and Marks PA. Histone deacetylase (HDAC) inhibitor activation of p21WAF1 involves changes in promoter-associated proteins, including HDAC1. Proc Natl Acad Sci U S A 2004; 101: 1241-1246.
[35] Mottet D, Pirotte S, Lamour V, Hagedorn M, Javerzat S, Bikfalvi A, Bellahcene A, Verdin E and Castronovo V. HDAC4 represses p21(WAF1/Cip1) expression in human cancer cells through a Sp1-dependent, p53-independent mechanism. Oncogene 2009; 28: 243-256.
[36] Sartor O and Gillessen S. Treatment sequencing in metastatic castrate-resistant prostate cancer. Asian J Androl 2014; 16: 426-431.
[37] Zhang L, Lei J, Shan Y, Yang H, Song M and Ma Y. Recent progress in the development of histone deacetylase inhibitors as anti-cancer agents. Mini Rev Med Chem 2013; 13: 1999-2013.
[38] Siegel R, Ma J, Zou Z and Jemal A. Cancer statistics, 2014. CA Cancer J Clin 2014; 64: 9-29.
[39] Riddle MM, Williams WC and Smialowicz RJ. Repeated high dose oral exposure or continuous subcutaneous infusion of 2-methoxyacetic acid does not suppress humoral immunity in the mouse. Toxicology 1996; 109: 67-74.
[40] Larese F, Fiorito A and De Zotti R. The possible haematological effects of glycol monomethyl ether in a frame factory. Br J Ind Med 1992; 49: 131-133.
[41] Rao AV and Shaha C. N-acetylcysteine prevents MAA induced male germ cell apoptosis: role of glutathione and cytochrome c. FEBS Lett 2002; 527: 133-137.
[42] Yang J, Liu X, Bhalla K, Kim CN, Ibrado AM, Cai J, Peng TI, Jones DP and Wang X. Prevention of apoptosis by Bcl-2: release of cytochrome c from mitochondria blocked. Science 1997; 275: 1129-1132.
[43] Yan W, Suominen J, Samson M, Jegou B and Toppari J. Involvement of Bcl-2 family proteins in germ cell apoptosis during testicular development in the rat and pro-survival effect of stem cell factor on germ cells in vitro. Mol Cell Endocrinol 2000; 165: 115-129.
[44] Eckelman BP and Salvesen GS. The human anti-apoptotic proteins cIAP1 and cIAP2 bind but do not inhibit caspases. J Biol Chem 2006; 281: 3254-3260.
[45] Burke SP, Smith L and Smith JB. cIAP1 cooperatively inhibits procaspase-3 activation by the caspase-9 apoptosome. J Biol Chem 2010; 285: 30061-30068.
[46] Wong RP, Tsang WP, Chau PY, Co NN, Tsang TY and Kwok TT. p53-R273H gains new function in induction of drug resistance through down-regulation of procaspase-3. Mol Cancer Ther 2007; 6: 1054-1061.

[47] Zhang Y, Fujita N and Tsuruo T. Caspase-mediated cleavage of p21Waf1/Cip1 converts cancer cells from growth arrest to undergoing apoptosis. Oncogene 1999; 18: 1131-1138.
[48] Suzuki A, Kawano H, Hayashida M, Hayasaki Y, Tsutomi Y and Akahane K. Procaspase 3/p21 complex formation to resist fas-mediated cell death is initiated as a result of the phosphorylation of p21 by protein kinase A. Cell Death Differ 2000; 7: 721-728.
[49] Suzuki A, Tsutomi Y, Miura M and Akahane K. Caspase 3 inactivation to suppress Fas-mediated apoptosis: identification of binding domain with p21 and ILP and inactivation machinery by p21. Oncogene 1999; 18: 1239-1244.
[50] Jin YH, Yoo KJ, Lee YH and Lee SK. Caspase 3-mediated cleavage of p21WAF1/CIP1 associated with the cyclin A-cyclin-dependent kinase 2 complex is a prerequisite for apoptosis in SK-HEP-1 cells. J Biol Chem 2000; 275: 30256-30263.
[51] Niculescu AB 3rd, Chen X, Smeets M, Hengst L, Prives C and Reed SI. Effects of p21(Cip1/Waf1) at both the G1/S and the G2/M cell cycle transitions: pRb is a critical determinant in blocking DNA replication and in preventing endoreduplication. Mol Cell Biol 1998; 18: 629-643.
[52] Berthet C, Klarmann KD, Hilton MB, Suh HC, Keller JR, Kiyokawa H and Kaldis P. Combined loss of Cdk2 and Cdk4 results in embryonic lethality and Rb hypophosphorylation. Dev Cell 2006; 10: 563-573.

*Int. J. Mol. Sci.* **2015**, *16*, 11750-11765; doi:10.3390/ijms160511750

OPEN ACCESS
International Journal of
**Molecular Sciences**
**ISSN 1422-0067**
www.mdpi.com/journal/ijms

*Article*

# Aminomethylphosphonic Acid and Methoxyacetic Acid Induce Apoptosis in Prostate Cancer Cells

**Keshab R. Parajuli, Qiuyang Zhang, Sen Liu and Zongbing You ***

Departments of Structural & Cellular Biology and Orthopaedic Surgery, Tulane Cancer Center and Louisiana Cancer Research Consortium, Tulane Center for Stem Cell Research and Regenerative Medicine, Tulane Center for Aging, Tulane University, New Orleans, LA 70112, USA; E-Mails: kparajuli55@gmail.com (K.R.P.); qzhang3@tulane.edu (Q.Z.); senliu@yahoo.com (S.L.)

* Author to whom correspondence should be addressed; E-Mail: zyou@tulane.edu; Tel.: +1-504-988-0467; Fax: +1-504-988-1687.

Academic Editor: Paul B. Tchounwou

*Received: 13 April 2015 / Accepted: 15 May 2015 / Published: 22 May 2015*

**Abstract:** Aminomethylphosphonic acid (AMPA) and its parent compound herbicide glyphosate are analogs to glycine, which have been reported to inhibit proliferation and promote apoptosis of cancer cells, but not normal cells. Methoxyacetic acid (MAA) is the active metabolite of ester phthalates widely used in industry as gelling, viscosity and stabilizer; its exposure is associated with developmental and reproductive toxicities in both rodents and humans. MAA has been reported to suppress prostate cancer cell growth by inducing growth arrest and apoptosis. However, it is unknown whether AMPA and MAA can inhibit cancer cell growth. In this study, we found that AMPA and MAA inhibited cell growth in prostate cancer cell lines (LNCaP, C4-2B, PC-3 and DU-145) through induction of apoptosis and cell cycle arrest at the G1 phase. Importantly, the AMPA-induced apoptosis was potentiated with the addition of MAA, which was due to downregulation of the anti-apoptotic gene baculoviral inhibitor of apoptosis protein repeat containing 2 (BIRC2), leading to activation of caspases 7 and 3. These results demonstrate that the combination of AMPA and MAA can promote the apoptosis of prostate cancer cells, suggesting that they can be used as potential therapeutic drugs in the treatment of prostate cancer.

**Keywords:** prostate cancer cells; cell death; apoptosis; AMPA; MAA

## 1. Introduction

Aminomethylphosphonic acid (AMPA; linear chemical formula: CH6NO3P) is the primary degradation product of glyphosate (*N*-(phosphonomethyl)glycine), which is a broad-spectrum systemic herbicide used to kill weeds, especially annual broadleaf weeds and grasses known to compete against commercial crops grown around the globe [1]. In the environment, glyphosate can be naturally converted into AMPA [2]. AMPA has no significant toxicity in acute, subchronic and chronic animal studies, nor any genotoxicity, teratogenicity or carcinogenicity [3,4]. When AMPA was administered via gavage at a dose of 6.7 mg/kg in rats, approximately 20% of the AMPA was absorbed, and 74% of the administered dose was excreted in the feces over a five-day period of experimental observation. The absorbed AMPA was not bio-transformed and was excreted rapidly in the urine with approximately 65% of the absorbed dose eliminated in the urine within 12 h and essentially 100% excreted between 24 and 120 h. Only trace residues were detected in various organs, including liver, kidney and skeletal muscle, five days after dosing [3,4]. AMPA and glyphosate are analogs to glycine. Recently, glycine was revealed to play a key role in rapid cancer cell proliferation [5]. In rapidly-proliferating cancer cells, there is an increased reliance on glycine metabolism, a phenotype that was not observed in rapidly-proliferating non-transformed cells [5]. Glycine metabolism may therefore represent a metabolic vulnerability in rapidly-proliferating cancer cells that may be targeted for therapeutic benefits. As analogs to glycine, glyphosate and AMPA were also found to inhibit proliferation and promote apoptosis in cancer cells, but not in normal cells in our previous study [6]. However, higher concentrations of this chemical may affect normal cells and produce adverse side effects. One of the strategies to improve AMPA's inhibitory actions on cancer cells and to reduce its side effects is to find a compound that can potentiate AMPA's efficacy, thus reducing its dosage.

Methoxyacetic acid (MAA) is the primary active metabolite of ester phthalates widely used in industry as gelling, viscosity and stabilizer reagents [7]. MAA exposure is associated with various developmental and reproductive toxicities in both rodents and humans, including neural toxicity, blood and immune disorders, limb degeneration and testicular toxicity [8–10]. The mechanisms of MAA-induced toxicities are multiple. MAA induces the production of reactive oxygen species, resulting in DNA damage and loss of mitochondrial membrane potential in normal human fibroblasts [7]. MAA treatment alters the expression of androgen receptor (AR) and androgen-binding protein (ABP) in a stage-specific manner in rat seminiferous tubules [11]. MAA treatment downregulates the expression of estrogen receptor α (ERα) and estradiol-induced gene expression in human breast cancer cell line MCF-7 and mouse uterus [12], but increases ERβ expression by inducing apoptosis in pachytene spermatocytes in rats [11]. MAA has been found to activate the tyrosine kinase-PI3K pathway and other pathways to enhance or antagonize androgen-induced gene expression [9,10,13]. Similarly, MAA can activate mitogen-activated protein kinase (MAPK) and inhibit histone deacetylases (HDACs), thus increasing the levels of acetylated histone H4, like the other well-known HDAC inhibitors, such as trichostatin, valproic acid and butyric acid [14]. In fact, it has been reported that MAA-induced hyperacetylation of histone H3 and H4 is associated with rapid spermatocyte death [15]. Some HDAC inhibitors (suberanilohydroxamic acid and romidepsin) have been approved for the treatment of cutaneous T-cell lymphoma, while panobinostat and valproic acid are being tested in the treatment of

prostate cancer, breast cancer, cervical cancer, ovarian cancer and lymphomas [16]. We have previously shown that MAA can induce apoptosis and growth arrest of prostate cancer cells [17].

Our rationale was that intracellular glycine is converted from serine, which may be inhibited by AMPA (a glycine analog) [18], and glycine is also converted from sarcosine, which may be inhibited by MAA (a sarcosine analog) [19]. Therefore, we speculated that a combination of AMPA and MAA might inhibit glycine synthesis more effectively, hence potentiating the inhibition of prostate cancer growth. In the present study, we tested the effects of a combination of AMPA and MAA on two immortalized human normal prostatic epithelial cell lines (RWPE-1 and pRNS-1-1) and four human prostate cancer cell lines (LNCaP, C4-2B, PC-3 and DU-145). We found that the combination of AMPA and MAA significantly induced the apoptosis and growth arrest of prostate cancer cells. The apoptosis induced by the combination of AMPA and MAA was highly associated with decreased protein expression of baculoviral inhibitor of apoptosis protein repeat containing 2 (BIRC2), whereas the G1 arrest caused by the combination of AMPA and MAA was closely associated with induction of p21 and reduction of cyclin D3. BIRC2 is also named cellular inhibitor of apoptosis protein (cIAP) 1 [20]. cIAP1 and cIAP2 have an *N*-terminal BIRC domain and a *C*-terminal ring domain that confers E3 ubiquitin ligase activity. CIAP2 also contains a caspase recruitment domain (CARD), which is involved in auto-inhibition of its E3 ligase activity [21]. It is known that BIRC2 inhibits caspases 7 and 3 [22]. Therefore, decreased cIAP1 leads to activation of caspases 7 and 3, thus inducing apoptosis. Our findings suggest that MAA can potentiate AMPA's anti-cancer activities by inhibiting anti-apoptotic protein and activating pro-apoptotic proteins.

## 2. Results and Discussion

### *2.1. The Aminomethylphosphonic Acid (AMPA) and Methoxyacetic Acid (MAA) Combination Inhibits Prostate Cancer Cell Viability*

Therapy for advanced prostate cancer centers on suppressing systemic androgens and blocking activation of the androgen receptor. However, nearly all patients develop castration-resistant prostate cancer (CRPC). The currently available treatments for CRPC can only extend patient's survival by 2.4 to 4.8 months [23]. Thus, new therapeutics is urgently needed for this type of malignancy. Based on our previous study, AMPA and MAA both have inhibitory effects on prostate cancer cells. In order to enhance AMPA's efficacy and reduce its dosage, we investigated the effects of a combination of AMPA and MAA on the growth of prostate cancer cells. Our previous studies showed that 50 mM AMPA and 20 mM MAA can significantly inhibit the growth of prostate cancer cells individually [6,17]. In the present study, we used 15 mM AMPA and 5 mM MAA to treat the two immortalized human normal prostatic epithelial cell lines (RWPE-1 and pRNS-1-1) and four prostate cancer cell lines (LNCaP, C4-2B, PC-3 and DU-145) alone or in combination. We found that the number of viable cells was decreased by approximately 9% to 24% or 15% to 40% in the four prostate cancer cells compared to 4% to 9% or 12% to 14% in normal prostatic epithelial cells, respectively, when treated with AMPA or MAA alone. However, the number of viable cells decreased by 32% to 68% in the four prostate cancer cells, compared to 22% and 31% in RWPE-1 and pRNS-1-1 cells when treated with the combination of AMPA and MAA (Figure 1A–F). Thus, MAA obviously

potentiates the effects of AMPA, especially on the rapidly proliferating prostate cancer cells, but less so on the normal prostatic cells. At these dosages, AMPA has little effect on normal prostatic cells. Although MAA has been reported to be a testicular toxicant in mammals [24,25], this toxicity would be acceptable to most of the prostate cancer patients, since the majority of the patients are old and have passed their reproductive age [15]. Therefore, AMPA and MAA combination appears to be a promising therapy in the treatment of prostate cancer.

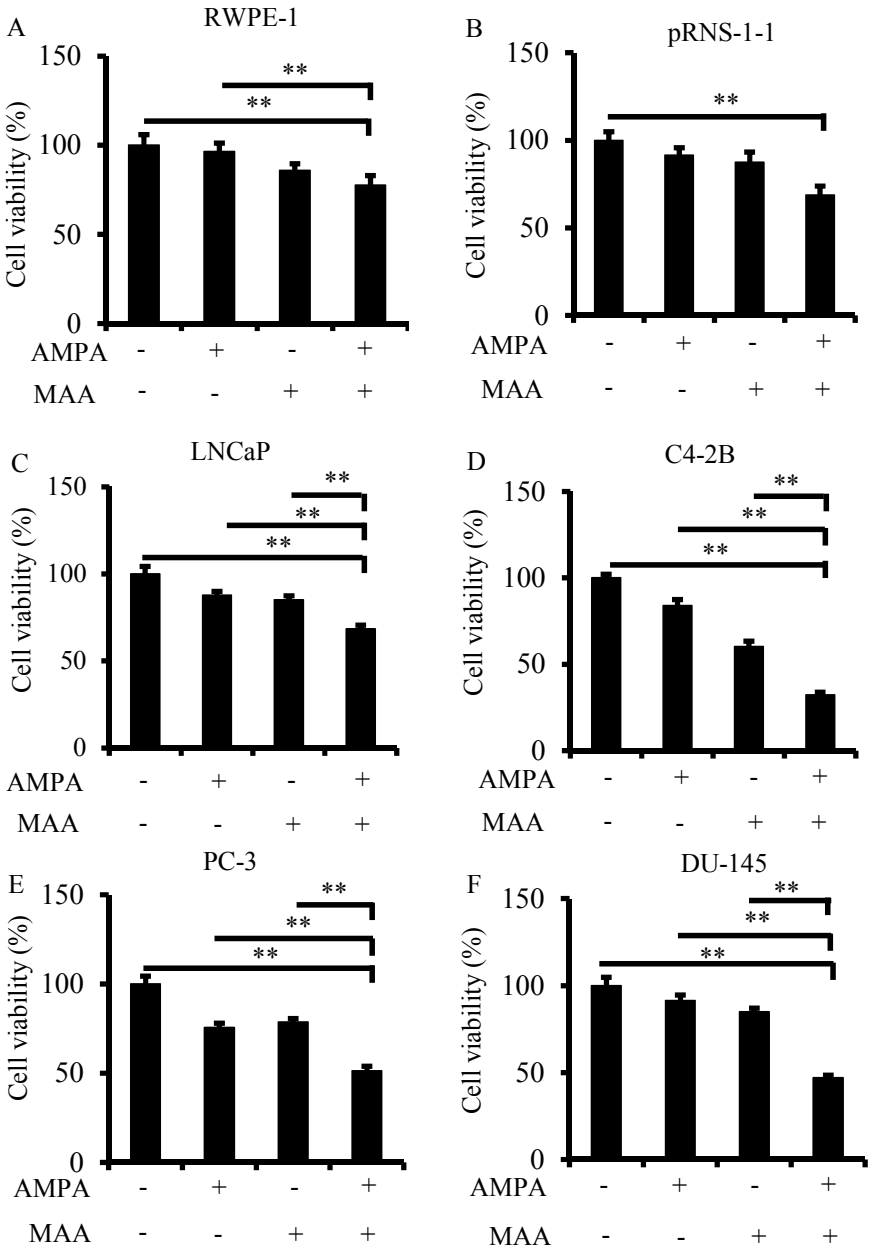



**Figure 1.** The combination of aminomethylphosphonic acid (AMPA) and methoxyacetic acid (MAA) suppresses cancer cell viability. (**A**–**F**) Normal prostate epithelial cells and prostate cancer cells were plated in 96-well plates in triplicate per group and then treated with 15 mM AMPA, 5 mM MAA and a combination of both for 72 h. The viable cells were measured using the CellTiter-Glo® Luminescent Cell Viability Assay. The data are presented as the mean ± standard error of the mean (SEM) of three independent experiments ($n = 3$). ** $p < 0.01$.

### *2.2. The Combination of AMPA and MAA Potentiates Apoptosis in Prostate Cancer Cells*

To know why the combination of AMPA and MAA can inhibit prostate cancer cell growth, we measured the apoptotic nucleosomes in the cells treated with 15 mM AMPA and 5 mM MAA, either alone or in combination for 24 h. Although the induced apoptotic nucleosomes were slightly increased when treated with AMPA or MAA alone compared to the non-treated cells, the combination of AMPA and MAA increased the apoptotic nucleosomes by 4.2- and 2.5-fold in LNCaP cells, by 6.3- and 5.7-fold in C4-2B cells, by 2.1- and two-fold in PC3 cells and by 21.4- and 2.6-fold in DU-145 cells, compared to the treatment with AMPA or MAA alone (Figure 2A–D). These results indicated that AMPA and MAA at low concentrations potentiate the apoptosis of prostate cancer cells.

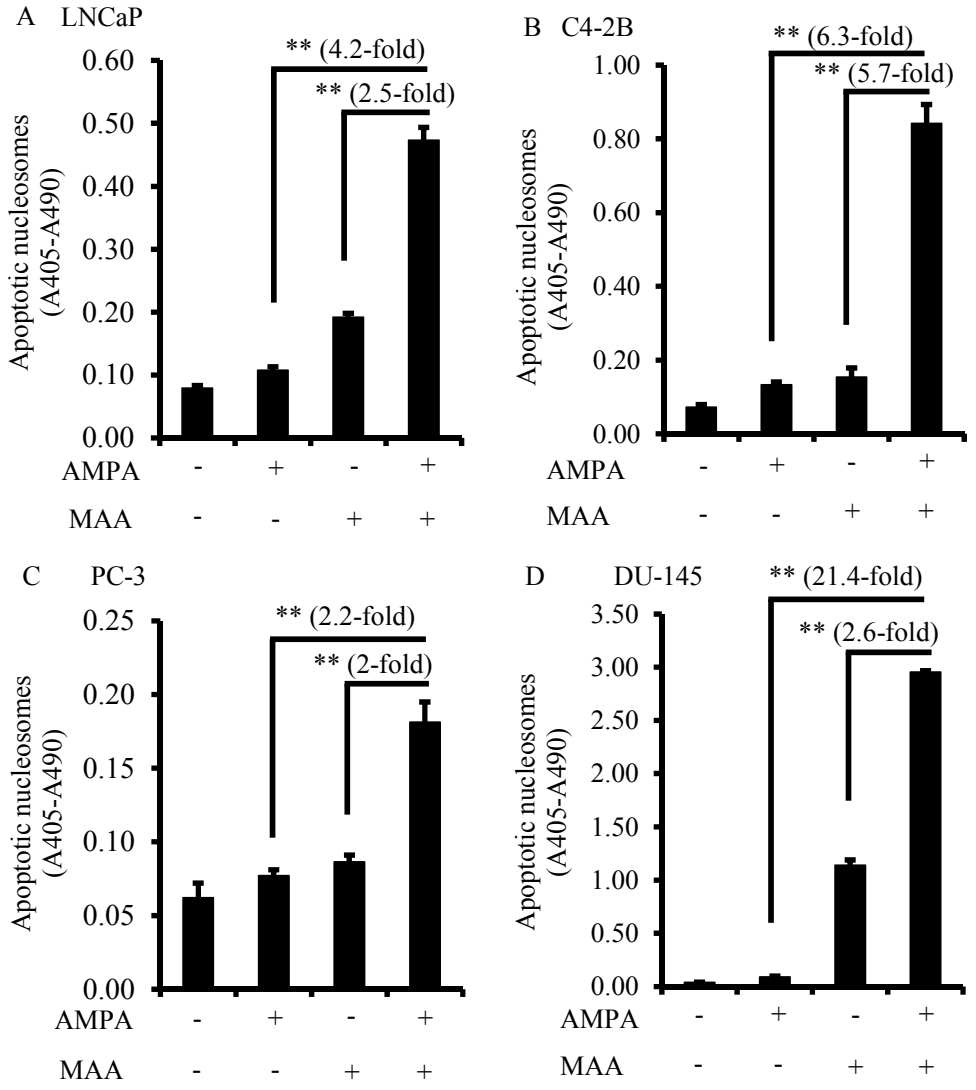



**Figure 2.** The AMPA and MAA combination induces apoptosis in prostate cancer cells. (**A**–**D**) Prostate cancer cells were plated in 12-well plates in triplicate per group and treated with 15 mM AMPA, 5 mM MAA and a combination of AMPA and MAA for 24 h. Apoptotic nucleosomes were measured using the Cell Death Detection ELISA kit. Apoptotic nucleosomes were calculated by absorbance at 405 nm (A405) minus absorbance at 490 nm (A490). The data are presented as the mean ± SEM of three independent experiments ($n = 3$). ** $p < 0.01$.

### *2.3. The Combination of AMPA and MAA Blocks the Entry of Cells from the G1 to S Phase of the Cell Cycle*

To determine if the combination of AMPA and MAA induces cell cycle arrest, we treated four types of prostate cancer cells for 24 h and analyzed the percentage of cells in the G1 (and G0), S and G2 (and M) phase of the cell cycle using flow cytometry analysis. We found that MAA alone increased the percentage of LNCaP and C4-2B cells at the G1/G0 phase and decreased the percentage of cells at the S phase (Figure 3A,B; $p < 0.01$), whereas MAA alone did not have significant effects in PC-3 and DU-145 cells (Figure 3C,D; $p > 0.05$). However, the combination of AMPA and MAA significantly increased the percentage of PC-3 and DU-145 cells at the G1/G0 phase and decreased the percentage of cells at the S phase, whereas the number of cells in the G2/M phase was not affected (Figure 3C,D; $p < 0.05$). In addition, there were not any significant differences in all four cell lines when treated with AMPA alone (Figure 3A–D; $p > 0.05$). These results indicated that the combination of AMPA and MAA blocks the G1/S transition in PC-3 and DU-145 cell lines. Our previous study demonstrated that AMPA at 50 mM can arrest cancer cells in the G1/G0 phase of the cell cycle, thus inhibiting entry into the S phase [6]. MAA has also been demonstrated to be an HDAC inhibitor [14,15], which suppresses the growth of four prostate cancer cell lines (LNCaP, C4-2B, PC-3 and DU-145) in a dose-dependent manner by inducing apoptosis and G1 arrest.

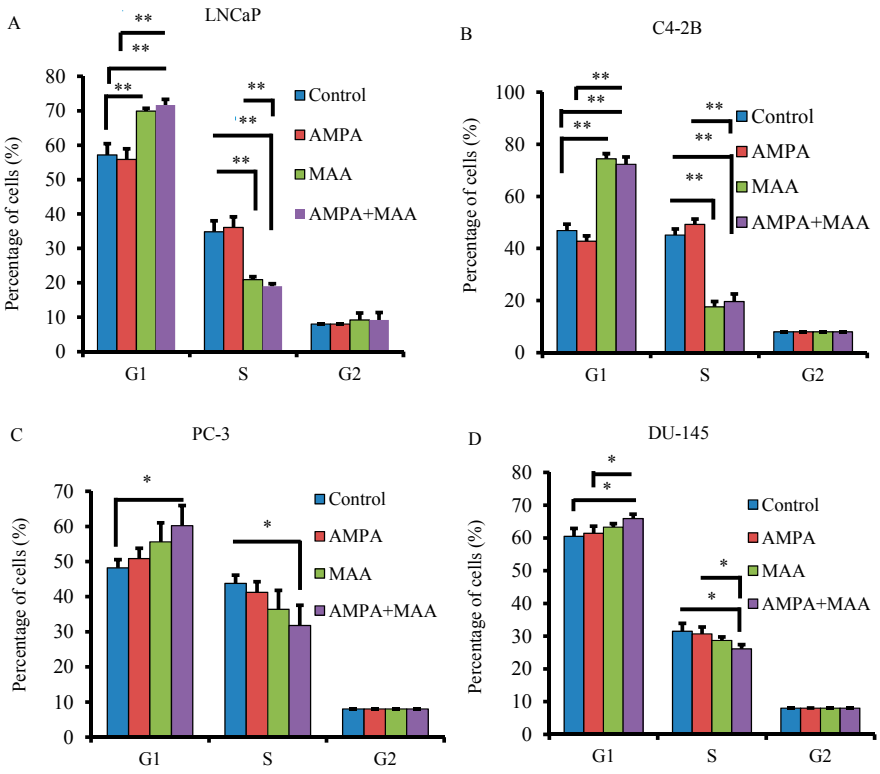



**Figure 3.** AMPA and MAA block the G1/S transition of the prostate cancer cell cycle. (**A**–**D**) Prostate cancer cells were plated in 60-mm dishes in triplicate per group and treated with 15 mM AMPA, 5 mM MAA, alone or in combination, for 24 h. The control groups was treated with phosphate-buffer saline (PBS). The percentages of cells at G1 (and $G_0$), S and G2 (and M) phases were determined by flow cytometry analysis. The data are presented as the mean ± SEM of three independent experiments ($n = 3$). * $p < 0.05$; ** $p < 0.01$.

### *2.4. The AMPA and MAA Combination Induces Changes in the Expression Levels of Genes Involved in the Cell Cycle and Apoptosis*

To study the genes involved in cell cycle arrest and apoptosis in prostate cancer cells treated with the combination of AMPA and MAA, we did Western blot analysis of the protein expression. We found that the combination treatment clearly increased the levels of cleaved poly(ADP-ribose) polymerase (PARP) in C4-2B, PC-3 and DU-145 cell lines in a time-dependent manner compared to the cells treated with AMPA or MAA alone, though there was no obvious increase in the LNCaP cell line (Figures 4–7). PARP cleavage has been widely used as an indicator of apoptosis marker [26,27]. This finding confirmed that the combination of AMPA and MAA induced apoptosis in prostate cancer cells.

We found that the combination treatment clearly decreased the protein levels of BIRC2 in all four prostate cancer cell lines and decreased BIRC3 levels in C4-2B and DU-145 cells at late time points (48 and 72 h) (Figures 4–7). The protein level of BIRC2 was decreased more obviously than that of BIRC3, which is another member of the IAP family [28]. It has been shown that proteasome-mediated degradation of BIRC2 can relieve the inhibitory function of BIRC2 on caspases, thus activating caspase-mediated apoptosis [29,30]. We found that the combination of AMPA and MAA increased the levels of procaspase 9 starting from 24 or 48 h in C4-2B, PC-3 and DU-145 cell lines (Figures 5–7). In contrast, the combination of AMPA and MAA decreased the levels of procaspases 7 and 3 at different time points (12, 24, 48 and 72 h) (Figures 4–7). The increases of procaspase 9 levels and simultaneously decreases of procaspase 3 levels induced by the combination of AMPA and MAA may mediate apoptosis, as shown in a previous study [31]. The decrease of procaspase 3 indicated cleavage of the proenzyme and activation of caspase 3, which is a key executioner caspase [32]. The previous study demonstrated that MAA induces apoptosis of rat germ cells through the release of mitochondrial cytochrome c, which further activates caspases 9 and 3 [33]. BIRC2 has also been reported to be able to bind to caspases 7 and 9, thus serving as a weak inhibitor of caspases 9, 7 and 3 [34]. Later on, it was found that BIRC2 potently inhibited activation of procaspase 3 [35]. Thus, the decreased levels of procaspases 7 and 3 may be due to down-regulation of BIRC2.

We further checked the protein levels of p53 and its downstream gene p21. We found that the combination of AMPA and MAA obviously increased the levels of p21 at 12 h after treatment in LNCaP, C4-2B and DU-145 cells (Figures 4, 5 and 7) and at a later time point in PC-3 cells (Figure 6). However, the levels of p53 protein were decreased slightly in the cells upon the combination treatment. Therefore, the induced expression of p21 in the cells under the combination treatment is independent of p53 protein level. This result is consistent with the previous study showing that MAA induces p21 transcription through inhibition of HDAC activities, in a p53 family-independent manner [17]. In addition, the protein levels of cyclin D3 were decreased in the cells under the combination treatment compared to the cells treated with AMPA or MAA alone (Figures 4–7). The downregulated cyclin D3 may contribute to the cell cycle inhibition [32]. The combination of AMPA and MAA increased p21 and decreased the protein level of cyclin D3, thus inducing G1 arrest.

It is noted that the combination of AMPA and MAA appears to be more effective in the inhibition of PC-3 and DU-145 growth than LNCaP growth (Figure 1). PC-3 and DU-145 cells do not express intracellular androgen receptor (AR) [36,37], while all three cell lines express membrane-associated

AR [38–40]. Activation of the membrane-associated AR may potentiate the anti-proliferative effects of chemotherapeutics [41–43]. Given that MAA alters AR expression in rat seminiferous tubules [11], it is an intriguing question whether MAA acts through affecting AR expression in these cell lines. MAA has been shown to potentiate AR signaling even in the presence of AR antagonists, such as bicalutamide [9]. It may be possible that such a potentiation of AR signaling in LNCaP cells slightly affects MAA's inhibitory function in LNCaP cells, compared to PC-3 and DU-145 cells that lack intracellular AR.

Taken together, the combination of AMPA and MAA at low doses significantly induced apoptosis and, to a lesser extent, cell cycle arrest, in four prostate cancer cell lines in the present *in vitro* study. These findings suggest that a further *in vivo* study is warranted to test if the combined AMPA and MAA treatment may efficaciously inhibit prostate tumor growth in animals. Based on the present *in vitro* study, it appears that the combined AMPA and MAA treatment may be of potential in the treatment of prostate cancer.

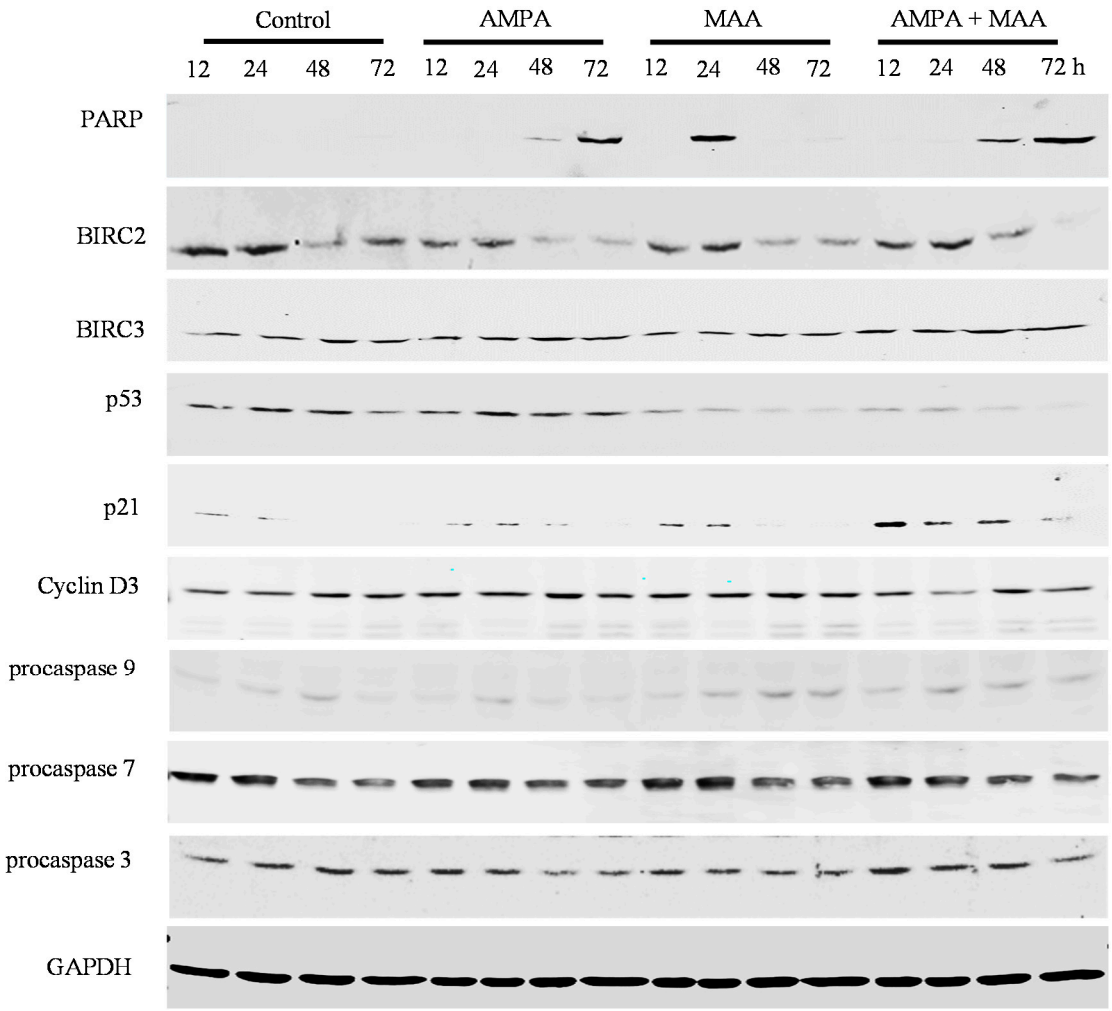



**Figure 4.** AMPA and MAA induce changes in the expression levels of genes involved in cell cycle arrest and apoptosis. LNCaP cells were exposed to 15 mM AMPA, 5 mM MAA or a combination of both AMPA and MAA for different time periods. The protein extracts were analyzed by Western blot to detect the indicated proteins. Glyceraldehyde 3-phosphate dehydrogenase (GAPDH) was probed as the loading control.

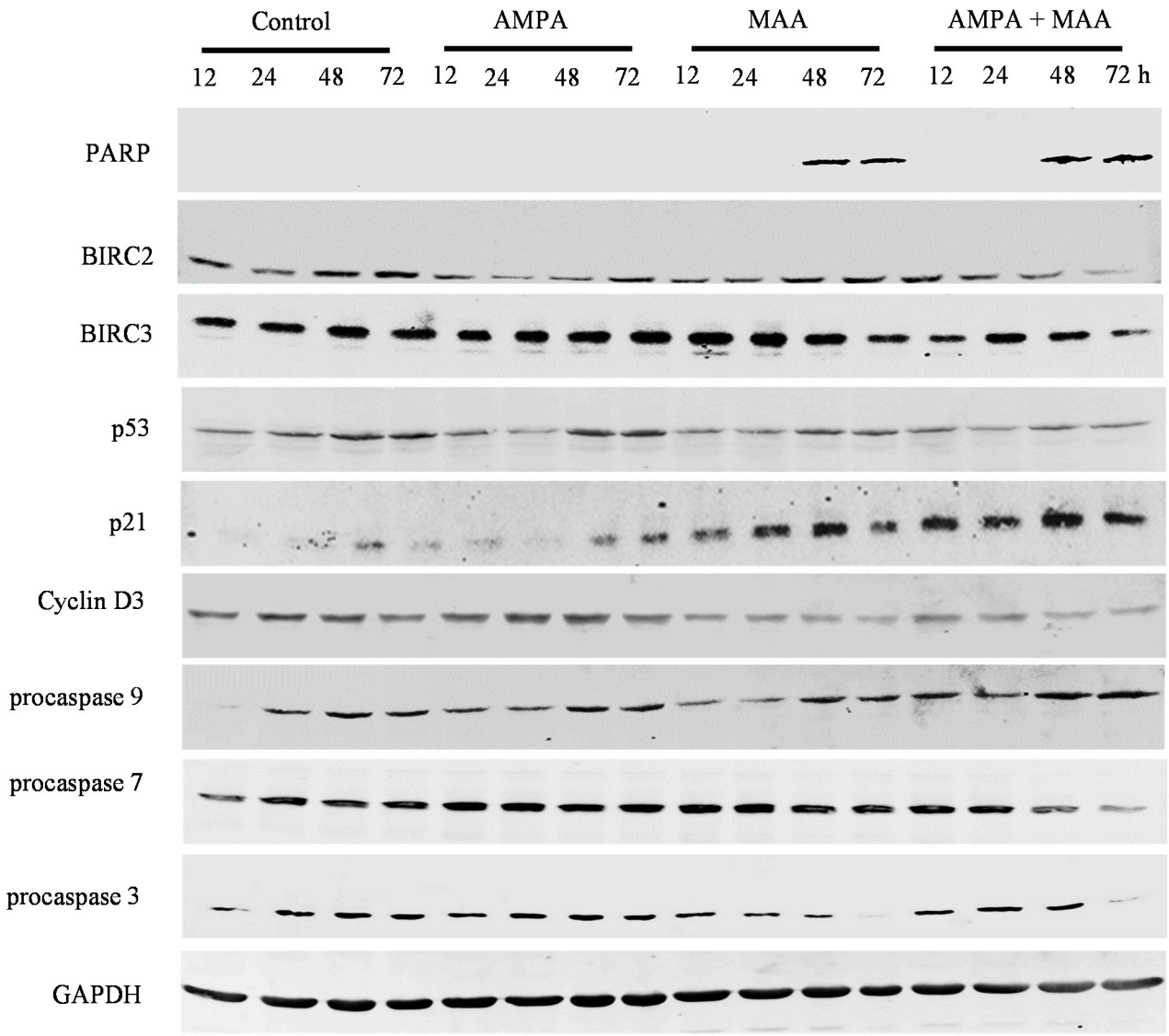



**Figure 5.** AMPA and MAA induce changes in the expression levels of genes involved in cell cycle arrest and apoptosis. C4-2B cells were exposed to 15 mM AMPA, 5 mM MAA or a combination of both AMPA and MAA for different time periods. The protein extracts were analyzed by Western blot to detect the indicated proteins. GAPDH was probed as the loading control.

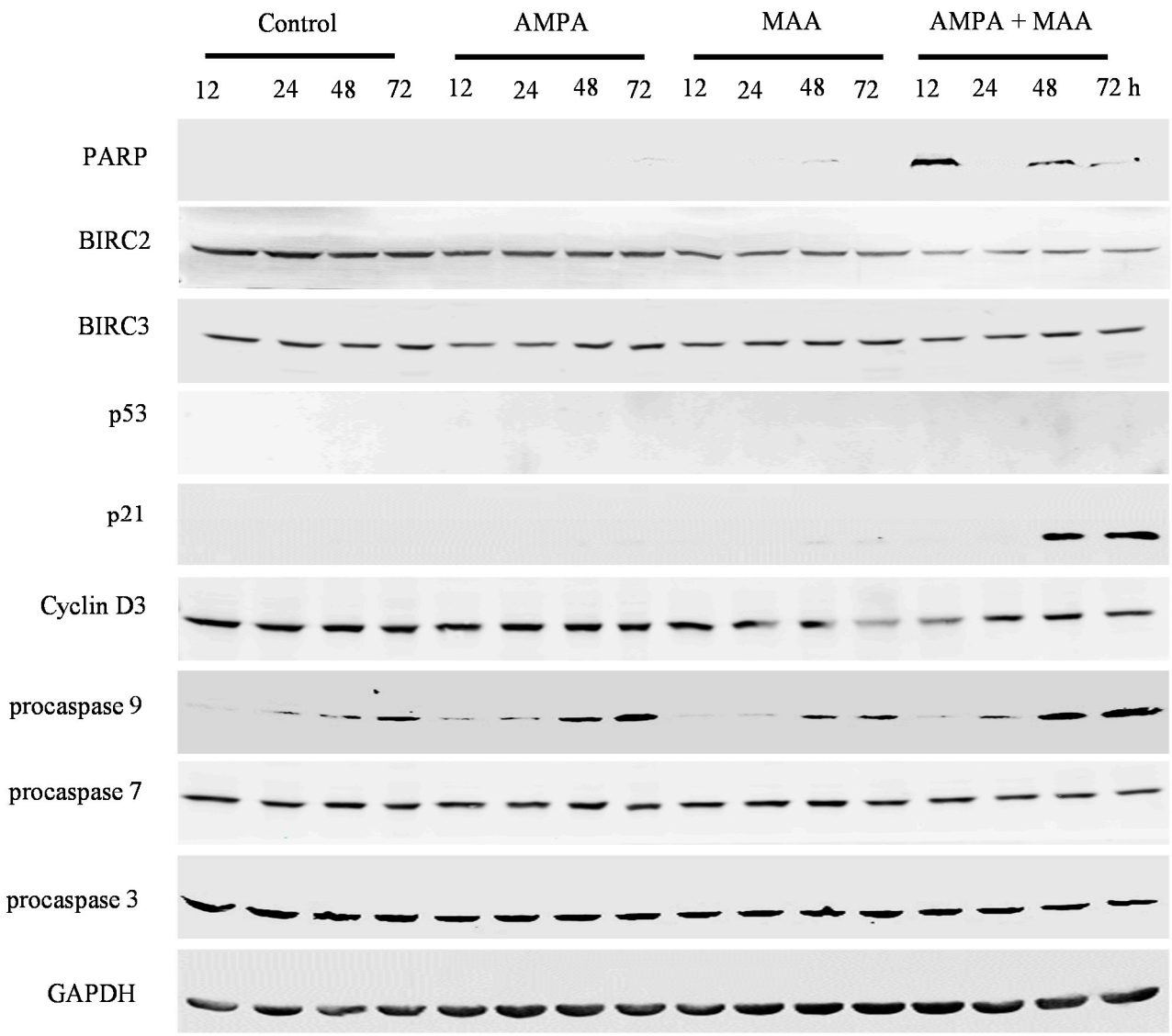



**Figure 6.** AMPA and MAA induce changes in the expression levels of genes involved in cell cycle arrest and apoptosis. PC-3 cells were exposed to 15 mM AMPA, 5 mM MAA or a combination of both AMPA and MAA for different time periods. The protein extracts were analyzed by Western blot to detect the indicated proteins. GAPDH was probed as the loading control.

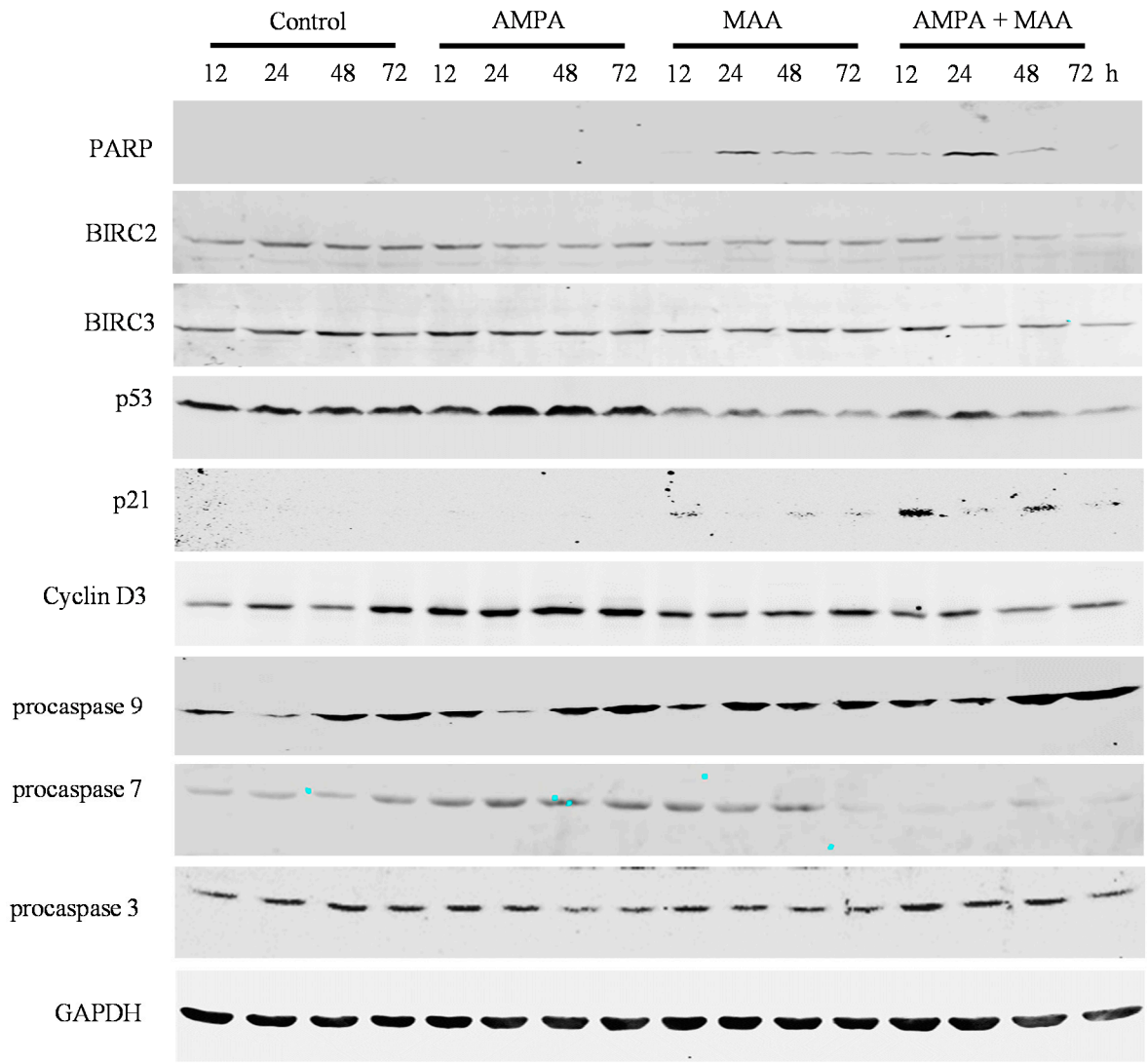



**Figure 7.** AMPA and MAA induce changes in the expression levels of genes involved in cell cycle arrest and apoptosis. DU-145 cells were exposed to 15 mM AMPA, 5 mM MAA or a combination of both AMPA and MAA for different time periods. The protein extracts were analyzed by Western blot to detect the indicated proteins. GAPDH was probed as the loading control.

## 3. Experimental Section

### *3.1. Cell Culture*

The sources and cell culture conditions of two immortalized human normal prostatic epithelial cell lines (RWPE-1 and pRNS-1-1) and four human prostate cancer cell lines (LNCaP, C4-2B, PC-3 and DU-145) were described previously [6]. Cells were cultured in a 5% $CO_2$ humidified incubator at 37 °C.

### *3.2. Cell Viability Assay*

The number of live cells was determined using the CellTiter-Glo® Luminescent Cell Viability Assay (Promega Corp, Fitchburg, WI, USA) as described previously [6]. Cell viability was calculated as (luminescence of the treatment group − background luminescence) ÷ (luminescence of the control

group − background luminescence) × 100%. The data are presented as the mean and standard error of the mean (SEM) of three independent experiments.

### *3.3. Detection of Apoptotic Nucleosomes*

Cells were seeded on 12-well plates with $1 \times 10^5$ cells/well in triplicate per group in the complete culture medium with fetal bovine serum (FBS). After overnight incubation, cells were treated with 15 mM AMPA, 5 mM MAA and the AMPA and MAA combination for 24 h; a control group was treated with phosphate-buffered saline (PBS). Apoptotic nucleosomes were detected using the Cell Death Detection ELISA kit (Roche Diagnostics Corporation, Indianapolis, IN, USA) according to the manufacturer's instructions [44]. Absorbance was measured at 405 nm (A405) with a reference wavelength at 490 nm (A490) using a plate reader (Bio-Tek U.S., Winooski, VT, USA). The amount of apoptotic nucleosomes was represented by A405−A490.

### *3.4. Cell Cycle Analysis*

Cells were treated without or with 15 mM AMPA or 5 mM MAA or AMPA and MAA combination for 24 h. The percentage of cells at G1/G0, S and G2/M phases was determined by flow cytometry analysis as described previously [6].

### *3.5. Western Blot Analysis*

Cells were treated without or with 15 mM AMPA, 5 mM MAA or the AMPA and MAA combination for 0, 12, 24, 48 and 72 h. Proteins were extracted for Western blot analysis as described previously [6]. Rabbit anti-caspase 9, rabbit anti-caspase 7 and mouse anti-cyclin D3 antibodies were purchased from Cell Signaling Technology (Danvers, MA, USA). Mouse anti-p53, rabbit anti-BIRC2 and rabbit anti-BIRC3 antibodies were obtained from Santa Cruz Biotechnology (Dallas, TX, USA). Mouse anti-GAPDH, mouse anti-caspase 3 and rabbit anti-cleaved poly(ADP-ribose) polymerase (PARP) antibodies were purchased from EMD Millipore Corp (Bilerica, MA, USA). Rabbit anti-p21 antibody was bought from Abcam, Cambridge, MA, USA.

### *3.6. Statistical Analysis*

Results from this study were presented as the mean ± SEM. Statistical analysis was performed using two-tailed Student's *t*-test. A $p$-value $<0.05$ was considered statistically significant.

## 4. Conclusions

The present study demonstrated that a combination of AMPA and MAA can inhibit prostate cancer cell growth through inducing apoptosis and cell cycle arrest. Induction of apoptosis may be due to downregulation of BIRC2 (cIAP1), leading to activation of pro-apoptotic factors, such as caspases 7 and 3. Induction of cell cycle arrest may be due to up-regulation of p21 expression at the early time and downregulation of cyclin D3 expression at the late time. These findings suggest that the AMPA and MAA combination may have potential in the treatment of prostate cancer.

**Acknowledgments**

The authors thank Mary Price from Tulane Cancer Center and Louisiana Cancer Research Consortium Fluorescence-activated cell sorting (FACS) Core for flow cytometry analysis. This work was supported in whole or partially by the Department of Defense Health Program through the Prostate Cancer Research Program (W81XWH-14-1-0050, W81XWH-14-1-0149 and W81XWH-14-1-0458; the US Army Medical Research Acquisition Activity, 820 Chandler Street, Fort Detrick MD 21702-5014 is the awarding and administering acquisition office) and by the National Institutes of Health (P20GM103518 and R01CA174714). The content of this article is solely the responsibility of the authors and does not necessarily represent the official views of the National Institutes of Health or the Department of Defense. This work was also partially supported by the Developmental Fund of Tulane Cancer Center and Louisiana Cancer Research Consortium fund.

**Author Contributions**

Keshab R. Parajuli designed the study, performed the experiment, analyzed and interpreted the data and prepared the first draft of the manuscript. Sen Liu contributed to the design and statistical analysis. Qiuyang Zhang contributed to the design, data analysis and revision of the manuscript. Zongbing You developed the concept of the study, performed the data analysis and revised the manuscript. All authors read and approved the final manuscript.

**Conflicts of Interest**

The authors declare no conflict of interest.

**References**

1. Kudzin, Z.H.; Gralak, D.K.; Drabowicz, J.; Luczak, J. Novel approach for the simultaneous analysis of glyphosate and its metabolites. *J. Chromatogr. A* **2002**, *947*, 129–141.
2. Vereecken, H. Mobility and leaching of glyphosate: A review. *Pest Manag. Sci.* **2005**, *61*, 1139–1151.
3. World health organization. Glyphosate and AMPA in drinking-water. Background document for development of who guidelines for drinking-water quality. Available online: http://www.who.int/water_sanitation_health/ (accessed on 18 May 2015).
4. Williams, G.M.; Kroes, R.; Munro, I.C. Safety evaluation and risk assessment of the herbicide roundup and its active ingredient, glyphosate, for humans. *Regul. Toxicol. Pharmacol.* **2000**, *31*, 117–165.
5. Jain, M.; Nilsson, R.; Sharma, S.; Madhusudhan, N.; Kitami, T.; Souza, A.L.; Kafri, R.; Kirschner, M.W.; Clish, C.B.; Mootha, V.K. Metabolite profiling identifies a key role for glycine in rapid cancer cell proliferation. *Science* **2012**, *336*, 1040–1044.
6. Li, Q.; Lambrechts, M.J.; Zhang, Q.; Liu, S.; Ge, D.; Yin, R.; Xi, M.; You, Z. Glyphosate and ampa inhibit cancer cell growth through inhibiting intracellular glycine synthesis. *Drug Des. Dev. Ther.* **2013**, *7*, 635–643.

7. Priyandoko, D.; Ishii, T.; Kaul, S.C.; Wadhwa, R. Ashwagandha leaf derived withanone protects normal human cells against the toxicity of methoxyacetic acid, a major industrial metabolite. *PLoS ONE* **2011**, *6*, e19552.
8. Li, L.H.; Wine, R.N.; Chapin, R.E. 2-Methoxyacetic acid (MAA)-induced spermatocyte apoptosis in human and rat testes: An *in vitro* comparison. *J. Androl.* **1996**, *17*, 538–549.
9. Bagchi, G.; Hurst, C.H.; Waxman, D.J. Interactions of methoxyacetic acid with androgen receptor. *Toxicol. Appl. Pharmacol.* **2009**, *238*, 101–110.
10. Bagchi, G.; Zhang, Y.; Waxman, D.J. Impact of methoxyacetic acid on mouse leydig cell gene expression. *Reprod. Biol. Endocrinol.* **2010**, *8*, 65.
11. Tirado, O.M.; Selva, D.M.; Toràn, N.; Suárez-Quian, C.A.; Jansen, M.; McDonnell, D.P.; Reventós, J.; Munell, F. Increased expression of estrogen receptor β in pachytene spermatocytes after short-term methoxyacetic acid administration. *J. Androl.* **2004**, *25*, 84–94.
12. Henley, D.V.; Mueller, S.; Korach, K.S. The short-chain fatty acid methoxyacetic acid disrupts endogenous estrogen receptor-α-mediated signaling. *Environ. Health Perspect.* **2009**, *117*, 1702–1706.
13. Bagchi, G.; Zhang, Y.; Stanley, K.A.; Waxman, D.J. Complex modulation of androgen responsive gene expression by methoxyacetic acid. *Reprod. Biol. Endocrinol.* **2011**, *9*, 42.
14. Jansen, M.S.; Nagel, S.C.; Miranda, P.J.; Lobenhofer, E.K.; Afshari, C.A.; McDonnell, D.P. Short-chain fatty acids enhance nuclear receptor activity through mitogen-activated protein kinase activation and histone deacetylase inhibition. *Proc. Natl. Acad. Sci. USA* **2004**, *101*, 7199–7204.
15. Wade, M.G.; Kawata, A.; Williams, A.; Yauk, C. Methoxyacetic acid-induced spermatocyte death is associated with histone hyperacetylation in rats. *Biol. Reprod.* **2008**, *78*, 822–831.
16. Li, X.; Zhang, J.; Xie, Y.; Jiang, Y.; Yingjie, Z.; Xu, W. Progress of hdac inhibitor panobinostat in the treatment of cancer. *Curr. Drug Targets* **2014**, *15*, 622–634.
17. Parajuli, K.R.; Zhang, Q.; Liu, S.; Patel, N.K.; Lu, H.; Zeng, S.X.; Wang, G.; Zhang, C.; You, Z. Methoxyacetic acid suppresses prostate cancer cell growth by inducing growth arrest and apoptosis. *Am. J. Clin. Exp. Urol.* **2014**, *2*, 300–312.
18. Anderson, D.D.; Stover, P.J. SHMT1 and SHMT2 are functionally redundant in nuclear *de novo* thymidylate biosynthesis. *PLoS ONE* **2009**, *4*, e5839.
19. Porter, D.H.; Cook, R.J.; Wagner, C. Enzymatic properties of dimethylglycine dehydrogenase and sarcosine dehydrogenase from rat liver. *Arch. Biochem. Biophys.* **1985**, *243*, 396–407.
20. Lorick, K.L.; Jensen, J.P.; Fang, S.; Ong, A.M.; Hatakeyama, S.; Weissman, A.M. Ring fingers mediate ubiquitin-conjugating enzyme (E2)-dependent ubiquitination. *Proc. Natl. Acad. Sci. USA* **1999**, *96*, 11364–11369.
21. Lopez, J.; John, S.W.; Tenev, T.; Rautureau, G.J.; Hinds, M.G.; Francalanci, F.; Wilson, R.; Broemer, M.; Santoro, M.M.; Day, C.L.; *et al.* Card-mediated autoinhibition of cIAP1's E3 ligase activity suppresses cell proliferation and migration. *Mol. Cell* **2011**, *42*, 569–583.
22. Huang, Y.; Park, Y.C.; Rich, R.L.; Segal, D.; Myszka, D.G.; Wu, H. Structural basis of caspase inhibition by XIAP: Differential roles of the linker *versus* the BIR domain. *Cell* **2001**, *104*, 781–790.
23. Sartor, O.; Gillessen, S. Treatment sequencing in metastatic castrate-resistant prostate cancer. *Asian J. Androl.* **2014**, *16*, 426–431.

24. Brinkworth, M.H.; Weinbauer, G.F.; Schlatt, S.; Nieschlag, E. Identification of male germ cells undergoing apoptosis in adult rats. *J. Reprod. Fertil.* **1995**, *105*, 25–33.
25. Li, L.H.; Wine, R.N.; Miller, D.S.; Reece, J.M.; Smith, M.; Chapin, R.E. Protection against methoxyacetic-acid-induced spermatocyte apoptosis with calcium channel blockers in cultured rat seminiferous tubules: Possible mechanisms. *Toxicol. Appl. Pharmacol.* **1997**, *144*, 105–119.
26. You, Z.; Shi, X.B.; DuRaine, G.; Haudenschild, D.; Tepper, C.G.; Lo, S.H.; Gandour-Edwards, R.; de Vere White, R.W.; Reddi, A.H. Interleukin-17 receptor-like gene is a novel antiapoptotic gene highly expressed in androgen-independent prostate cancer. *Cancer Res.* **2006**, *66*, 175–183.
27. Fang, E.F.; Scheibye-Knudsen, M.; Brace, L.E.; Kassahun, H.; SenGupta, T.; Nilsen, H.; Mitchell, J.R.; Croteau, D.L.; Bohr, V.A. Defective mitophagy in XPA via PARP-1 hyperactivation and NAD(+)/SIRT1 reduction. *Cell* **2014**, *157*, 882–896.
28. De Almagro, M.C.; Vucic, D. The inhibitor of apoptosis (IAP) proteins are critical regulators of signaling pathways and targets for anti-cancer therapy. *Exp. Oncol.* **2012**, *34*, 200–211.
29. Jin, S.; Kalkum, M.; Overholtzer, M.; Stoffel, A.; Chait, B.T.; Levine, A.J. cIAP1 and the serine protease HTRA2 are involved in a novel p53-dependent apoptosis pathway in mammals. *Genes Dev.* **2003**, *17*, 359–367.
30. Yang, Y.; Fang, S.; Jensen, J.P.; Weissman, A.M.; Ashwell, J.D. Ubiquitin protein ligase activity of IAPS and their degradation in proteasomes in response to apoptotic stimuli. *Science* **2000**, *288*, 874–877.
31. Sakai, T.; Liu, L.; Teng, X.; Mukai-Sakai, R.; Shimada, H.; Kaji, R.; Mitani, T.; Matsumoto, M.; Toida, K.; Ishimura, K.; *et al.* Nucling recruits APAF-1/pro-caspase-9 complex for the induction of stress-induced apoptosis. *J. Biol. Chem.* **2004**, *279*, 41131–41140.
32. McIlwain, D.R.; Berger, T.; Mak, T.W. Caspase functions in cell death and disease. *Cold Spring Harb. Perspect. Biol.* **2013**, *5*, a008656.
33. Rao, A.V.; Shaha, C. *N*-Acetylcysteine prevents MAA induced male germ cell apoptosis: Role of glutathione and cytochrome c. *FEBS Lett.* **2002**, *527*, 133–137.
34. Eckelman, B.P.; Salvesen, G.S. The human anti-apoptotic proteins cIAP1 and cIAP2 bind but do not inhibit caspases. *J. Biol. Chem.* **2006**, *281*, 3254–3260.
35. Burke, S.P.; Smith, L.; Smith, J.B. cIAP1 cooperatively inhibits procaspase-3 activation by the caspase-9 apoptosome. *J. Biol. Chem.* **2010**, *285*, 30061–30068.
36. Alimirah, F.; Chen, J.; Basrawala, Z.; Xin, H.; Choubey, D. DU-145 and PC-3 human prostate cancer cell lines express androgen receptor: Implications for the androgen receptor functions and regulation. *FEBS Lett.* **2006**, *580*, 2294–2300.
37. Van Bokhoven, A.; Varella-Garcia, M.; Korch, C.; Johannes, W.U.; Smith, E.E.; Miller, H.L.; Nordeen, S.K.; Miller, G.J.; Lucia, M.S. Molecular characterization of human prostate carcinoma cell lines. *Prostate* **2003**, *57*, 205–225.
38. Thomas, P.; Pang, Y.; Dong, J.; Berg, A.H. Identification and characterization of membrane androgen receptors in the ZIP9 zinc transporter subfamily: II. Role of human ZIP9 in testosterone-induced prostate and breast cancer cell apoptosis. *Endocrinology* **2014**, *155*, 4250–4265.

39. Papadopoulou, N.; Charalampopoulos, I.; Anagnostopoulou, V.; Konstantinidis, G.; Föller, M.; Gravanis, A.; Alevizopoulos, K.; Lang, F.; Stournaras, C. Membrane androgen receptor activation triggers down-regulation of PI-3k/Akt/NF-κB activity and induces apoptotic responses via Bad, FasL and caspase-3 in DU145 prostate cancer cells. *Mol. Cancer* **2008**, *7*, 88.
40. Kampa, M.; Papakonstanti, E.A.; Hatzoglou, A.; Stathopoulos, E.N.; Stournaras, C.; Castanas, E. The human prostate cancer cell line lncap bears functional membrane testosterone receptors that increase PSA secretion and modify actin cytoskeleton. *FASEB J.* **2002**, *16*, 1429–1431.
41. Kampa, M.; Kogia, C.; Theodoropoulos, P.A.; Anezinis, P.; Charalampopoulos, I.; Papakonstanti, E.A.; Stathopoulos, E.N.; Hatzoglou, A.; Stournaras, C.; Gravanis, A.; *et al.* Activation of membrane androgen receptors potentiates the antiproliferative effects of paclitaxel on human prostate cancer cells. *Mol. Cancer Ther.* **2006**, *5*, 1342–1351.
42. Papadopoulou, N.; Papakonstanti, E.A.; Kallergi, G.; Alevizopoulos, K.; Stournaras, C. Membrane androgen receptor activation in prostate and breast tumor cells: Molecular signaling and clinical impact. *IUBMB Life* **2009**, *61*, 56–61.
43. Lang, F.; Alevizopoulos, K.; Stournaras, C. Targeting membrane androgen receptors in tumors. *Expert Opin. Ther. Targets* **2013**, *17*, 951–963.
44. You, Z.; Saims, D.; Chen, S.; Zhang, Z.; Guttridge, D.C.; Guan, K.L.; MacDougald, O.A.; Brown, A.M.; Evan, G.; Kitajewski, J.; *et al.* Wnt signaling promotes oncogenic transformation by inhibiting c-Myc-induced apoptosis. *J. Cell Biol.* **2002**, *157*, 429–440.

© 2015 by the authors; licensee MDPI, Basel, Switzerland. This article is an open access article distributed under the terms and conditions of the Creative Commons Attribution license (http://creativecommons.org/licenses/by/4.0/).

# Interleukin-17 Promotes Development of Castration-Resistant Prostate Cancer Potentially Through Creating an Immunotolerant and Pro-Angiogenic Tumor Microenvironment

Qiuyang Zhang,[1] Sen Liu,[1] Qingsong Zhang,[1,2] Zhenggang Xiong,[6] Alun R. Wang,[6] Leann Myers,[7] Jonathan Melamed,[8] Wendell W. Tang,[9] and Zongbing You[1,2,3,4,5]*

[1]*Department of Structural & Cellular Biology, Tulane University, New Orleans, Louisiana*
[2]*Department of Orthopaedic Surgery, Tulane University, New Orleans, Louisiana*
[3]*Tulane Cancer Center and Louisiana Cancer Research Consortium, Tulane University, New Orleans, Louisiana*
[4]*Tulane Center for Stem Cell Research and Regenerative Medicine, Tulane University, New Orleans, Louisiana*
[5]*Tulane Center for Aging, Tulane University, New Orleans, Louisiana*
[6]*Department of Pathology and Laboratory Medicine, School of Medicine, Tulane University, New Orleans, Louisiana*
[7]*Department of Biostatistics and Bioinformatics, School of Public Health and Tropical Medicine, Tulane University, New Orleans, Louisiana*
[8]*Department of Pathology, New York University School of Medicine, New York, New York*
[9]*Department of Pathology, Ochsner Clinic Foundation, New Orleans, Louisiana*

**BACKGROUND.** Interleukin-17 (IL-17) has been demonstrated to promote formation and growth of hormone-naïve prostate adenocarcinoma in mice. IL-17's role in development of castration-resistant prostate cancer is unknown. In the present study, we investigated IL-17's role in castration-resistant prostate cancer in a mouse model.

**METHODS.** IL-17 receptor C (IL-17RC) deficient mice were interbred with *Pten* conditional mutant mice to produce $RC^+$ mice that maintained IL-17RC expression and $RC^-$ mice that were IL-17RC deficient. Male $RC^+$ and $RC^-$ mice were *Pten*-null and were castrated at

Abbreviations: AR, androgen receptor; Bcl-2; B-cell, lymphoma 2; COX-2, cyclooxygenase-2; Cre, Cre recombinase; CRPC, castration-resistant prostate cancer; CXCL, C-X-C motif ligand; GU, genitourinary; Gr-1, granulocyte-differentiation antigen-1; H&E, hematoxylin and eosin; HER-2, human epidermal growth factor receptor 2; HIF, hypoxia inducible factor; IL, interleukin; IL-17RC, IL-17 receptor C; iNOS, inducible nitric oxide synthase; KO, knockout; MDSCs, myeloid-derived suppressor cells; MMP, matrix metalloproteinase; MTA1, metastasis associated 1; PIN, prostatic intraepiethelial neoplasia; Pten, phosphatase and tensin homolog; Ras, rat sarcoma gene; SMA, smooth muscle actin; $T_H17$, T helpher cells expressing IL-17; TMPRSS2-ERG, transmembrane protease, serine 2 - E-twenty six related gene; TUNEL, terminal deoxynucleotidyl transferase-mediated dUTP nick end labeling; UBE2C, ubiquitin-conjugating enzyme E2C; VEGF, vascular endothelial growth factor; YBX1, Y-box binding protein 1.

Grant sponsor: National Institute of General Medical Sciences; Grant number: P20GM103518; Grant sponsor: National Cancer Institute; Grant number: R01CA174714; Grant sponsor: Department of Defense; Grant numbers: PC121647; PC131448; Grant sponsor: The Developmental Fund of Tulane Cancer Center (TCC); Grant sponsor: Louisiana Cancer Research Consortium (LCRC) Fund.

The content of this article is solely the responsibility of the authors and does not necessarily represent the official views of the National Institutes of Health.

*Correspondence to: Zongbing You, Department of Structural & Cellular Biology, Tulane University School of Medicine, 1430 Tulane Ave SL 49, New Orleans, LA 70112. E-mail: zyou@tulane.edu
Received 27 January 2014; Accepted 5 March 2014
DOI 10.1002/pros.22805
Published online 1 April 2014 in Wiley Online Library (wileyonlinelibrary.com).

© 2014 Wiley Periodicals, Inc.

16 weeks of age when invasive prostate cancer had already formed. At 30 weeks of age, all male mice were analyzed for the prostate phenotypes.

**RESULTS.** $RC^-$ mice displayed prostates that were smaller than $RC^+$ mice. Approximately 23% of prostatic glands in $RC^-$ mice, in contrast to 65% of prostatic glands in $RC^+$ mice, developed invasive adenocarcinomas. Compared to castrate $RC^+$ mice, castrate $RC^-$ mouse prostate had lower rates of cellular proliferation and higher rates of apoptosis as well as lower levels of MMP7, YBX1, MTA1, and UBE2C proteins. In addition, castrate $RC^-$ mouse prostate had less angiogenesis, which was associated with decreased levels of COX-2 and VEGF. Moreover, castrate $RC^-$ mouse prostate had fewer inflammatory cells including lymphocytes, myeloid-derived suppressor cells, and macrophages.

**CONCLUSIONS.** Taken together, our findings suggest that IL-17 promotes development of invasive prostate adenocarcinomas under castrate conditions, potentially through creating an immunotolerant and pro-angiogenic tumor microenvironment. *Prostate 74:869–879, 2014.*
© 2014 Wiley Periodicals, Inc.

***KEY WORDS:*** **prostate cancer; castration-resistant; interleukin-17; tumor immunology; tumor microenvironment**

## INTRODUCTION

Locally confined prostate cancer is treated by surgery or radiation. At the advanced stage when metastases occur, prostate cancer is treated with androgen deprivation therapy. However, Castration-induced regression of tumor is typically followed by re-growth with castrate levels of androgens, a status known as castration-resistant prostate cancer (CRPC) [1]. The mechanisms of how hormone-sensitive prostate cancer develops into CRPC remain to be defined. Alterations of androgen receptor (AR) signaling pathways, such as *AR* gene amplification, increase in AR expression, and *AR* gene mutations [2], may cause hypersensitivity of AR to low levels of both endocrine and intracrine androgens [3]. AR splicing variants may constitutively activate AR signaling in ligand-independent manners [4]. AR signaling may also be activated by growth factors in the absence of androgens [5]. Activation of HER-2/neu and Ras/mitogen-activated protein kinase pathways causes androgen-independent AR activities [6]. Transcriptional coactivators may lead to ligand-independent AR activation [7]. Focal neuroendocrine differentiation seems to be a common feature of prostate cancer. By secretion of a number of growth factor-like molecules (such as bombesin, calcitonin, and parathyroid hormone-related peptide), neuroendocrine cells can support the growth and progression of surrounding prostate cancer cells toward the castration-resistant state [8]. Androgen ablation up-regulates expression of the anti-apoptotic *Bcl-2* gene [9] and *clusterin* gene [10], whereas the pro-apoptotic *p53* gene is often mutated [11]. Decreased PTEN or increased Akt activities are linked to castration-resistant progression of prostate cancer [12,13]. Expression of TMPRSS2-ERG (transmembrane protease, serine 2-E26 related gene) fusion protein [14,15] and some microRNAs [16,17] has also been associated with CRPC.

Interleukin-6 (IL-6) and IL-8 have been found to play a role in development of CRPC [18,19]. Both IL-6 and IL-8 are downstream targets of IL-17, a cytokine that is produced by $T_H17$ cells, γδ T cells, and other immune cells [20]. IL-17 acts through a heterodimer of receptors IL-17RA and IL-17RC [21–23], thus, either *Il17ra* knockout (KO) or *Il17rc* KO completely abolishes IL-17 signaling [24,25]. We have previously reported that IL-17RC protein expression as detected by the anti-IL-17RC intracellular domain antibodies is significantly increased in CRPC, compared to hormone-sensitive prostate cancer [26,27]. Recently, we cross-bred *Il17rc* KO ($Il17rc^{-/-}$) mice with *Pten* conditional KO mice ($Pten^{L/L}$;$Cre^+$) and found that, in *Pten*-deficient context, *Il17rc* KO mice developed significantly smaller prostate tumors compared to *Il17rc* wild-type mice [28]. Our findings suggest that IL-17 promotes formation and growth of hormone-naïve prostate adenocarcinoma. However, it is unknown whether IL-17 plays any role in the development of CRPC. In the present study, we castrated the mice at 16 weeks of age and examined them at 30 weeks of age. We found that *Il17rc* KO mice developed significantly smaller prostates compared to *Il17rc* wild-type mice under castrate conditions.

## MATERIALS AND METHODS

### Mice

Animal protocol was approved by the Animal Care and Use Committee of Tulane University. The breeding strategy and genotyping protocols have been described previously, using $Pten^{loxp/loxp}$ ($Pten^{L/L}$) mice, PB-Cre4 mice, and $Il17rc^{-/-}$ mice [28]. Male $RC^+$ (n = 9) and $RC^-$ (n = 9) mice at 16 weeks of age were

castrated. This age was chosen because a majority of $RC^+$ and $RC^-$ mice had already developed invasive adenocarcinomas by this age [28,29]. The castration procedures were as the following: mice were anesthetized with 4% isoflurane; the skin over the scrotum was disinfected by 70% ethanol and Betadine solution; a 0.5-cm incision was made over the scrotum; the testes were exposed by pulling the adipose tissue; a hemostat was applied to curtail blood flow followed by silk ligation of blood vessels; the ductus deferentes were ligated and cut; the testes were excised; and the skin incision was closed with #5–0 nylon suture that was removed 7 days later. All instruments used were sterile. To alleviate pain, Carprofen (2 mg/kg) was injected subcutaneously at the end of surgical procedure and then every 12 hr up to 48 hr.

### Histopathology

Mice were euthanized and weighed at 30 weeks of age. The genitourinary (GU) blocs were photographed, weighed with an empty bladder, and fixed *en bloc* as described previously [28,30]. Twenty-eight consecutive 4-μm sections of each prostate were cut and four sections (from every seventh section) were stained with hematoxylin and eosin (H&E) for histopathologic assessment in a blinded fashion according to the Bar Harbor Classification [30]. The prostatic glands were assessed under low- and high-power magnifications, and approximately 27–94 prostatic glands in each prostate were counted, with a total of over 500 prostatic glands in nine mouse prostates per genotype. The number of inflammatory cells in the connective tissue space between the prostatic glands was counted in ten high-power fields (×400 magnification) of each dorsal prostatic lobe; the average number of inflammatory cells per high-power field in nine mouse prostates per genotype was compared.

### Immunohistochemical and Terminal Deoxynucleotidyl Transferase-Mediated dUTP Nick End Labeling Staining

Immunohistochemical staining and double immunofluorescent staining were performed as described previously [28]. The antibodies used were: rabbit anti-p-Akt (1:100), mouse anti-PTEN (26H9, 1:50), rabbit anti-YB1 (D299, 1:50), and rabbit anti-MTA1 (D40D1, 1:25) from Cell Signaling Technology, Inc., Danvers, MA; rabbit anti-Ki-67 (1:100, EMD Millipore, Billerica, MA); rabbit anti-VEGF (A-20, sc-152, 1:200), goat anti-HIF-1α (Y-15, sc-12542, 1: 50), rabbit anti-NOS2 (iNOS, N-20, sc-651, 1:100), rabbit anti-Integrin αM (CD11b, H-61, sc-28664, 1:100), goat anti-Ly6C (P-12, sc-23080, 1:100), goat anti-Ly6G (Y-11, sc-103603, 1:100), goat anti-arginase I (V-20, sc-18345, 1:100), and goat anti-COX-2 (C-20, sc-1745, 1:200) from Santa Cruz Biotechnology, Inc., Santa Cruz, CA; rabbit anti-CD31 (Ab28364, 1:50, Abcam, PLC., Cambridge, MA); rabbit anti-laminin (1:100, Sigma–Aldrich, St. Louis, MO); rabbit anti-α-smooth muscle actin (1:200, Pierce Biotechnology, Rockford, IL); goat anti-MMP7 (1:200, R&D systems, Minneapolis, MN); rabbit anti-UbcH10/UBE2C (1:200, Boston Biochem, Cambridge, MA); and Cy3-conjugated anti-goat IgG and DyLight 488-conjugated anti-rabbit IgG (Jackson ImmunoResearch Laboratories, Inc., West Grove, PA). Terminal deoxynucleotidyl transferase-mediated dUTP nick end labeling (TUNEL) staining was performed using TACS. XL® Blue Label *In Situ* Apoptosis Detection Kits (Trevigen, Inc., Gaithersburg, MD) according to the manufacturer's instructions [28]. To quantify Ki-67-positive and TUNEL-positive cells, three animals from each genotype group were randomly selected; three representative prostate sections from each animal were stained; approximately 200 cells per field of ten high-power fields (×400 magnification) of each prostate lobe were counted; and the percentages of positive cells were calculated as the number of positive cells divided by the total number of cells. The density of microvessels was evaluated by counting the CD31-positive microvessels in ten high-power fields per lobe; the average number of CD31-positive microvessels per high-power field in three random mouse prostates per genotype was compared. The myeloid-derived suppressor cells (MDSCs) were defined as CD11b/Gr-1 (CD11b/Ly6C and CD11b/Ly6G) double positive cells. The M1 and M2 macrophages were defined as iNOS-positive and arginase I-positive cells, respectively. The numbers of MDSCs, M1 macrophages, and M2 macrophages in the connective tissue space between the prostatic glands were counted in ten high-power fields (×400 magnification) in each dorsal prostatic lobe; the average numbers of MDSCs, M1 and M2 macrophages per high-power field in three random mouse prostates per genotype were compared.

### Statistical Analysis

Comparisons of the GU-bloc weights were analyzed using Student's *t*-test. Kruskal–Wallis test was used to compare the incidences of normal, PIN and invasive adenocarcinoma. Student's *t*-test was used to analyze the remaining data.

## RESULTS

### Castrate $RC^-$ Mice Developed Smaller Prostate Glands Than Castrate $RC^+$ Mice

Previously, we found that there were no significant differences in the expression of *Il17rc* mRNA

and protein, GU-bloc weight, and histopathology between *Il17rc*$^{+/+}$;*Pten*$^{L/L}$;Cre$^{+}$ and *Il17rc*$^{+/-}$;*Pten*$^{L/L}$;Cre$^{+}$ mice [28]. Therefore, we put *Il17rc*$^{+/+}$;*Pten*$^{L/L}$;Cre$^{+}$ mice and *Il17rc*$^{+/-}$;*Pten*$^{L/L}$;Cre$^{+}$ mice into one group, named RC$^{+}$ mice that expressed IL-17RC receptor. Likewise, *Il17rc*$^{-/-}$;*Pten*$^{L/L}$;Cre$^{+}$ mice were named RC$^{-}$ mice that did not express IL-17RC receptor. Both RC$^{+}$ and RC$^{-}$ mice had *Pten* gene conditionally knocked out in the prostatic epithelium due to probasin promoter-driven Cre recombinase [28]. We reported that the GU blocs, including the prostatic glands, were clearly larger in the non-castrate (or intact) RC$^{+}$ mice than in the intact RC$^{-}$ mice at 30 weeks of age (Fig. 1A and B) [28]. In the present study, we found that the GU blocs also appeared larger in the castrate RC$^{+}$ mice than in the castrate RC$^{-}$ mice at 30 weeks of age (Fig. 1C and D). The average GU bloc weight was 946.3 mg in the intact RC$^{+}$ mice compared to 644.7 mg in the intact RC$^{-}$ mice ($P < 0.01$, Fig. 1E). Castration at 16 weeks of age significantly reduced the GU bloc weight at 30 weeks of age in both RC$^{+}$ and RC$^{-}$ mice to an average of 224.1 and 164.3 mg, respectively ($P < 0.01$, Fig. 1E). Yet, the GU bloc weight of castrate RC$^{+}$ mice was still significantly heavier than that of castrate RC$^{-}$ mice ($P < 0.05$, Fig. 1E).

### Castrate RC$^{-}$ Mice Developed Fewer Invasive Adenocarcinomas Than Castrate RC$^{+}$ Mice

It has been reported that intact RC$^{+}$ mice developed invasive adenocarcinomas, that is, the neoplastic cells have invaded through the basement membrane and into the stroma, at 30 weeks of age with 100% penetrance [28,29], whereas intact RC$^{-}$ mice developed invasive adenocarcinomas in about 70% of prostates at 30 weeks of age [28]. In the castrate RC$^{+}$ mice, we found that approximately 65% of prostatic glands presented with invasive adenocarcinomas (Fig. 2A), 33% of prostatic glands had prostatic intraepithelial neoplasia (PIN), and 2% of prostatic glands appeared "normal" as they presented with a single layer of luminal epithelial cells. In contrast, the castrate RC$^{-}$ mice showed approximately 23% of prostatic glands with invasive adenocarcinomas, 64% of prostatic glands with PIN, and 12% of prostatic glands with normal epithelia (Fig. 2B). Under higher magnification, the invasive adenocarcinoma cells presented with atypical hyperchromatic nuclei and invaded into the surrounding stroma (Fig. 2C and D). The rate of invasive adenocarcinomas was 42% lower in RC$^{-}$ mice than in RC$^{+}$ mice ($P < 0.001$, Fig. 2E).

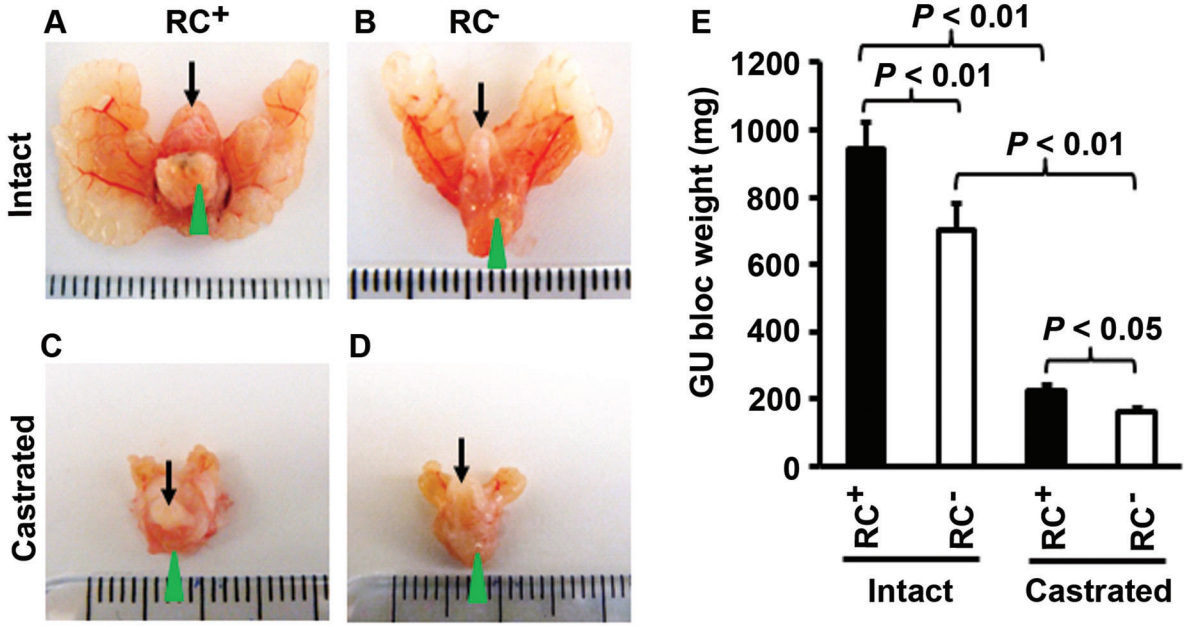



**Fig. 1.** Castrate RC$^{-}$ mice developed smaller prostate glands than castrate RC$^{+}$ mice. **A–D**: Representative photographs of the GU blocs; arrows indicate urinary bladders and arrowheads indicate the ventral prostatic lobes for orientation of the view. **E**: The GU bloc weights at 30 weeks of age; n = 20 for intact RC$^{+}$ mice, n = 12 for intact RC$^{-}$ mice, n = 9 for castrate RC$^{+}$ mice, and n = 9 for castrate RC$^{-}$ mice.

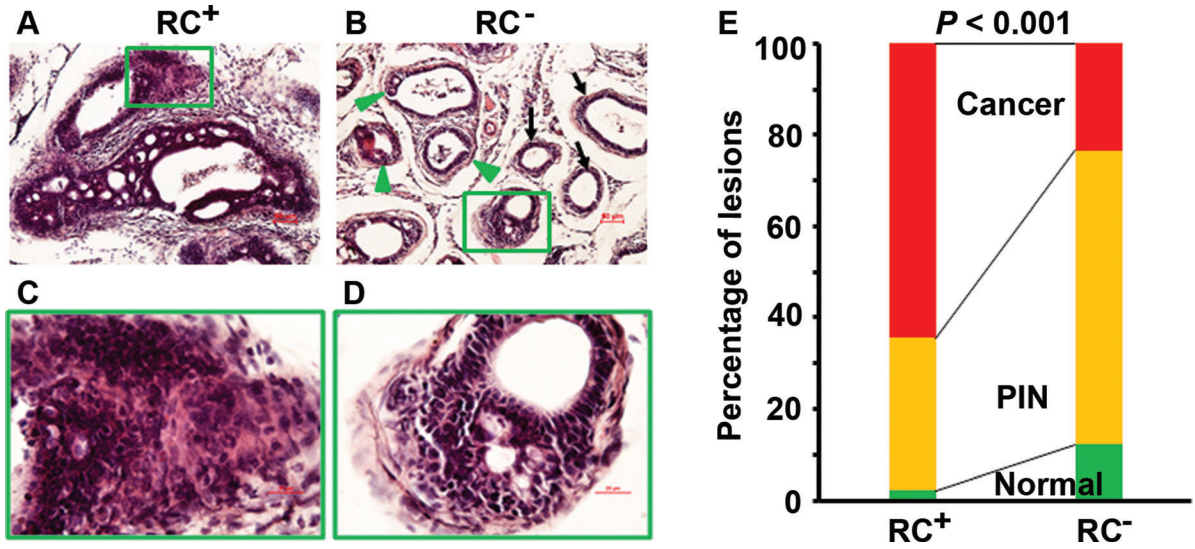



**Fig. 2.** Castrate $RC^-$ mice developed fewer invasive adenocarcinomas than castrate $RC^+$ mice. **A–D**: Representatives of H&E-stained dorsal prostatic lobes; arrows indicate normal glands with a single layer of luminal epithelium, arrowheads indicate PIN lesions, and rectangular frames indicate invasive adenocarcinomas; original magnification, ×100 for (A, B) and ×400 for (C, D). **E**: Percentages of normal, PIN, and invasive cancer in dorsal, lateral, and ventral prostatic lobes.

To verify our diagnosis of invasive adenocarcinoma versus PIN based on H&E-stained tissue sections, consecutive sections were stained with H&E and immunohistochemically stained with anti-laminin or anti-α-smooth muscle actin (α-SMA) antibodies. As shown in Supplementary Figure S1A, invasive adenocarinoma showed lack of staining or discontinuity of staining for laminin. In contrast, PIN lesion presented a continuous layer of laminin staining around the prostatic gland (Supplementary Fig. S1B). Similarly, α-SMA staining showed lack of continuity in invasive adenocarcinoma (Supplementary Fig. S1C), whereas a continuous layer of α-SMA staining was present in the PIN lesion and normal gland (Supplementary Fig. S1D).

### Castrate $RC^-$ Prostate Had Less Cellular Proliferation and More Apoptosis Than Castrate $RC^+$ Prostate

We found that $RC^+$ mouse prostate had clearly more Ki-67-positive neoplastic cells (Fig. 3A) than $RC^-$ mouse prostate (Fig. 3B). The differences between $RC^+$ and $RC^-$ mice were statistically significant in the dorsal prostatic lobes (DP), lateral prostatic lobes (LP), and ventral prostatic lobes (VP) ($P < 0.05$ or $P < 0.01$, Fig. 3C). On the other hand, the number of apoptotic cells as detected by TUNEL staining was fewer in the $RC^+$ mouse prostatic lobes (Fig. 3D) than in the $RC^-$ mouse prostatic lobes (Fig. 3E), which was statistically significant ($P < 0.01$, Fig. 3F).

### Castrate $RC^-$ Prostate Decreased Expression of Invasion-Related Proteins

Previously, we reported that the intact $RC^-$ mice expressed significantly less MMP7 in the prostate than the intact $RC^+$ mice, which partially explained the lower rate of invasive cancer in $RC^-$ mice compared to $RC^+$ mice [28]. In the castrate mice, the level of MMP7 expression was also lower in the $RC^-$ prostate than in the $RC^+$ prostate (Fig. 4A and B).

To search for other proteins that might contribute to the different incidence rates of invasive cancer in our animal models, we tested several candidates that were reportedly involved in prostate carcinogenesis. YBX1 (also known as YB-1) is a Y-box binding protein [31], which has been demonstrated to confer invasiveness to breast cancer cells [32]. YBX1 level is elevated in human PIN and invasive adenocarcinomas [33], similar to the pattern of MMP7 expression [28]. We found that YBX1 expression was clearly decreased in the castrate $RC^-$ prostate compared to the castrate $RC^+$ prostate (Fig. 4C and D). Metastasis associated 1 (MTA1) was originally identified from rat mammary adenocarcinoma cell lines [34] and recently it has been associated with the invasiveness of human prostate cancer cells [35]. We found that MTA1 expression was discernibly decreased in the castrate $RC^-$ prostate compared to the castrate $RC^+$ prostate (Fig. 4E and F). Ubiquitin-conjugating enzyme E2C (UBE2C, also called UBCH10) is needed for degradation of mitotic cyclins [36], which has been associated

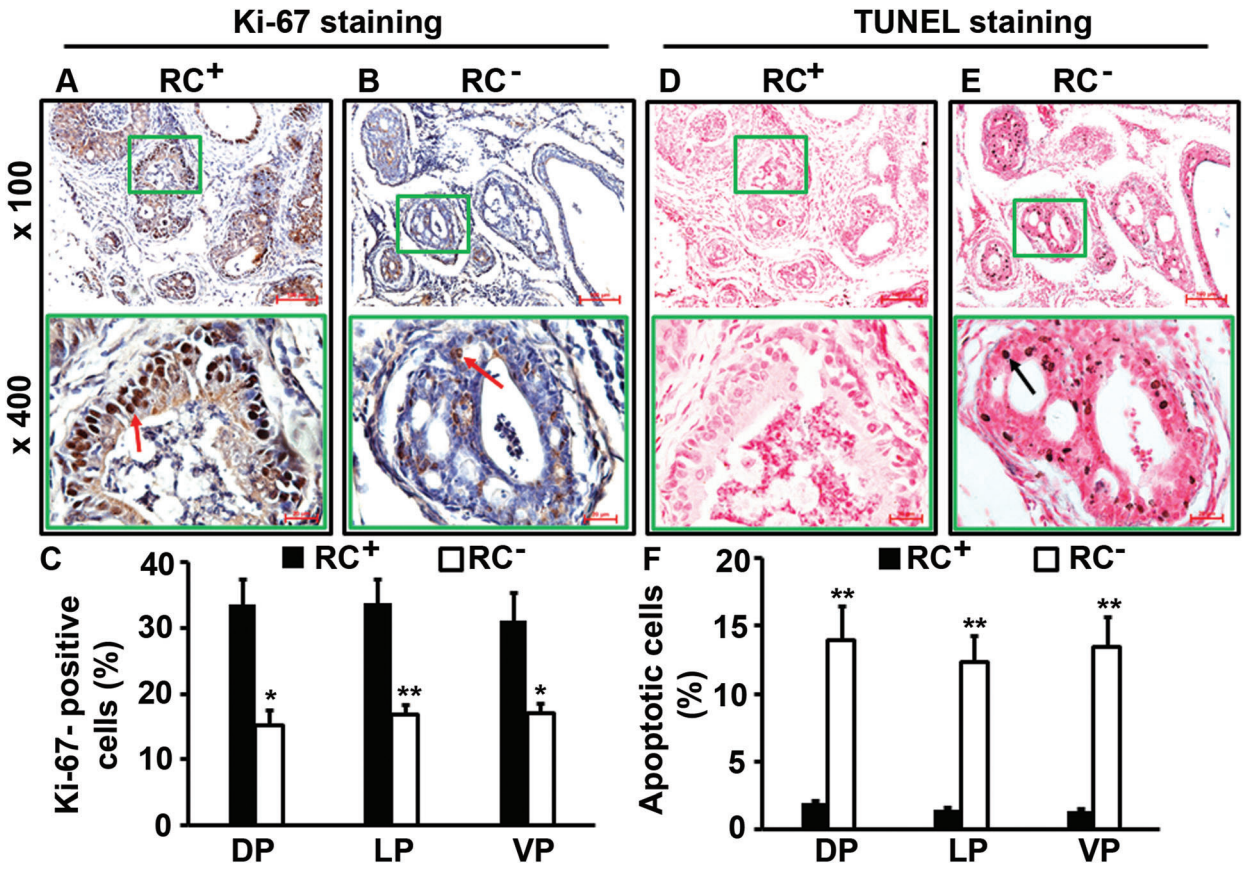



**Fig. 3.** Castrate $RC^-$ prostate had less cellular proliferation and more apoptosis than castrate $RC^+$ prostate. **A**, **B**: Ki-67 staining; arrows indicate the positive cells. **C**: Percentages of Ki-67-positive cells in dorsal (DP), lateral (LP), and ventral (VP) prostatic lobes; $^*P < 0.05$ and $^{**}P < 0.01$. **D**, **E**: TUNEL staining; arrow indicates the positive cells. **F**: Percentages of apoptotic cells in prostatic lobes; $^{**}P < 0.01$.

with malignant transformation and aggressiveness of many tumors [37]. UBE2C level is undetectable in human normal prostate, low in hormone-sensitive prostate cancer and high in CRPC [38]. Again, we found that UBE2C level was obviously higher in the castrate $RC^+$ prostate than the castrate $RC^-$ prostate (Fig. 4G and H).

### Castrate $RC^-$ Prostate Had Less Angiogenesis Than Castrate $RC^+$ Prostate

IL-17 has been found to be able to promote migration and cord formation of vascular endothelial cells through induction of a variety of proangiogenic factors [39], thus IL-17 may enhance in vivo lung cancer growth via promoting angiogenesis [40]. By immunohistochemical staining of CD31, we found that there were clearly more blood vessels in the castrate $RC^+$ prostate than in the castrate $RC^-$ prostate (Fig. 5A and B), which was statistically significant in the prostatic lobes examined ($P < 0.01$, Fig. 5C). We and other investigators have shown that IL-17 can induce angiogenic CXC chemokines including CXCL1, CXCL5, and CXCL8 expression [28,40]. It has been reported that cyclooxygenase-2 (COX-2) is induced by IL-17 in keratinocytes [41]. In the present study, we found that COX-2 level was dramatically lower in $RC^-$ prostate than $RC^+$ prostate (Fig. 5D and E). We also found that hypoxia inducible factor 1-α (HIF1A) level was not discernibly different between $RC^+$ and $RC^-$ prostates (Fig. 5F and G). However, the level of vascular endothelial growth factor A (VEGFA) was clearly higher in $RC^+$ prostate than $RC^-$ prostate (Fig. 5H and I). It has been demonstrated that the COX-2-VEGF pathway is involved in gastric angiogenesis [42]. Our findings suggest that the COX-2-VEGF pathway plays a role in prostatic angiogenesis while HIF1A's role may be very limited.

### Castrate $RC^-$ Prostate Had Less Inflammatory Cell InfiltrationThan Castrate $RC^+$ Prostate

Previously, we reported that the inflammatory cell population was mainly composed of macrophages (or

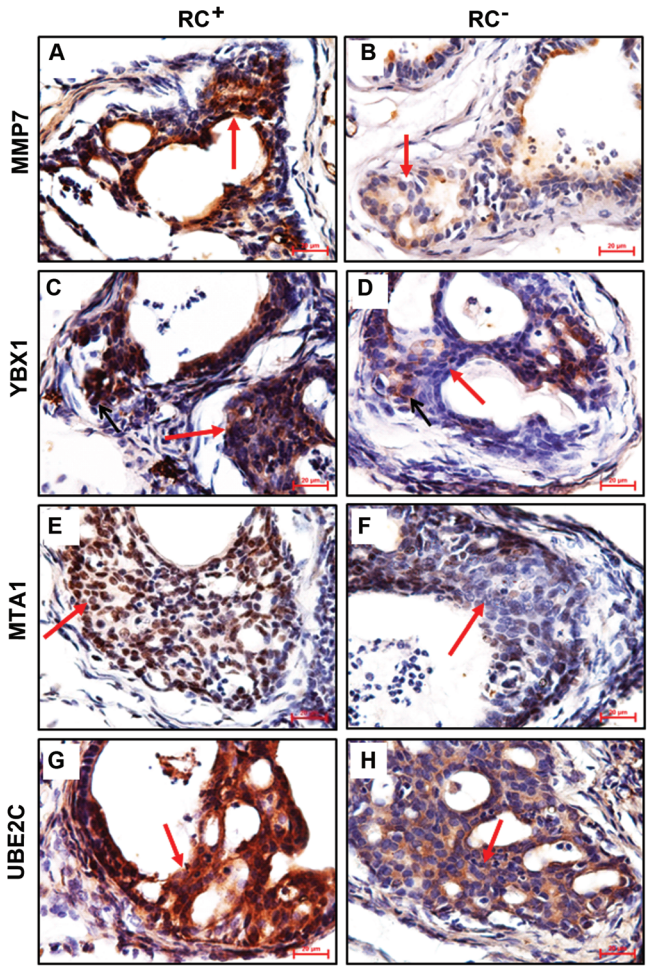



**Fig. 4.** Castrate RC$^-$ prostate decreased expression of invasion-related proteins. **A**–**H**: Representatives of immunohistochemical staining; arrows indicate neoplastic cells; original magnification, ×400.

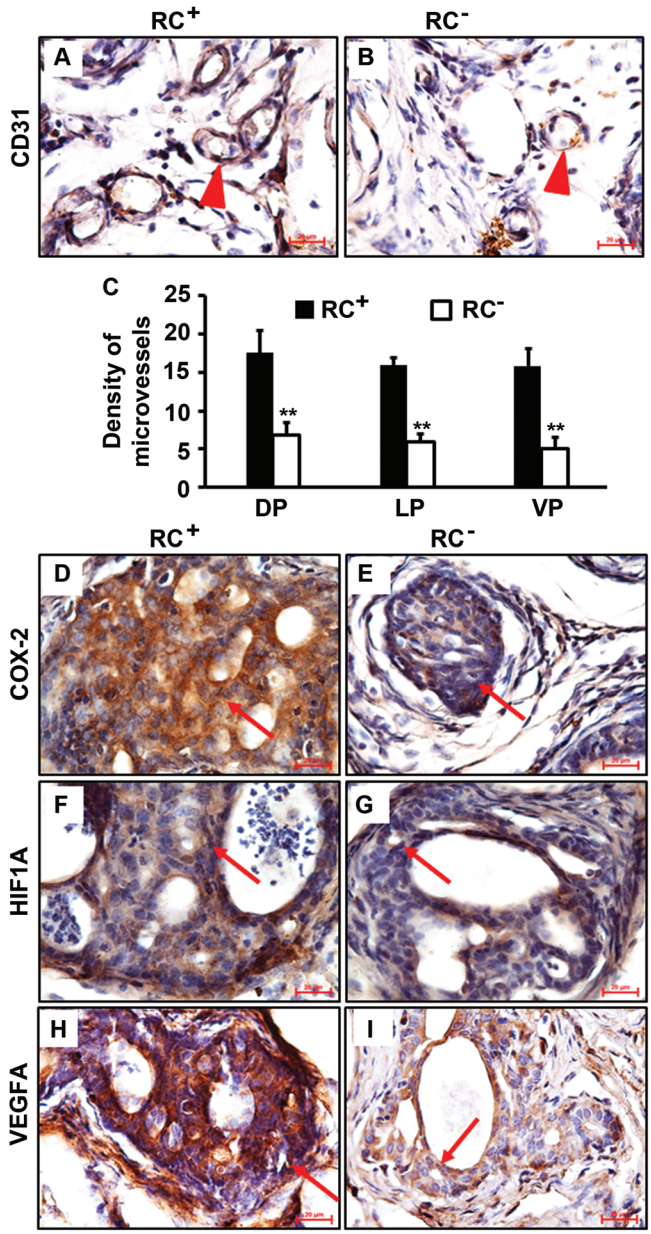



**Fig. 5.** Castrate RC$^-$ prostate had less angiogenesis than castrate RC$^+$ prostate. **A**, **B**: Representatives of CD31 staining; arrowheads indicate microvessels. **C**: Density of microvessels in prostatic lobes; $^{**}P < 0.01$. **D**–**I**: Representatives of immunohistochemical staining; arrows indicate neoplastic cells; original magnification, ×400.

myeloid cells) and lymphocytes in the intact mouse prostate and the number of inflammatory cells was significantly reduced in RC$^-$ prostate compared to RC$^+$ prostate [28]. In the castrate mouse prostate, the inflammatory cell population was mainly composed of lymphocytes (Fig. 6A). Consistent with our observation in the intact mice, we found that the number of inflammatory cells was much fewer in the castrate RC$^-$ prostate than the castrate RC$^+$ prostate (Fig. 6A and B), which was statistically significant ($P < 0.01$, Fig. 6C).

It has been shown that IL-17 induces infiltration of myeloid-derived suppressor cells (MDSCs) to promote prostate tumor growth [43]. MDSCs are considered as immature myeloid cells that are identified as CD11b/granulocyte-differentiation antigen-1 (Gr-1) double-positive cells. Gr-1 antigen consists of two epitopes recognized by anti-Ly6G (lymphocyte antigen 6 complex, locus G) and anti-Ly6C (lymphocyte antigen 6 complex, locus C). Thus, MDSCs consist of two major subsets: cells with granulocytic phenotype marked by CD11b$^+$/Ly6G$^+$ and cells with monocytic phenotype marked by CD11b$^+$/Ly6C$^+$, both subsets having equal suppressive activities against T cell function [44]. Therefore, we examined the infiltration of the two MDSC subsets in mouse prostate. We found that the

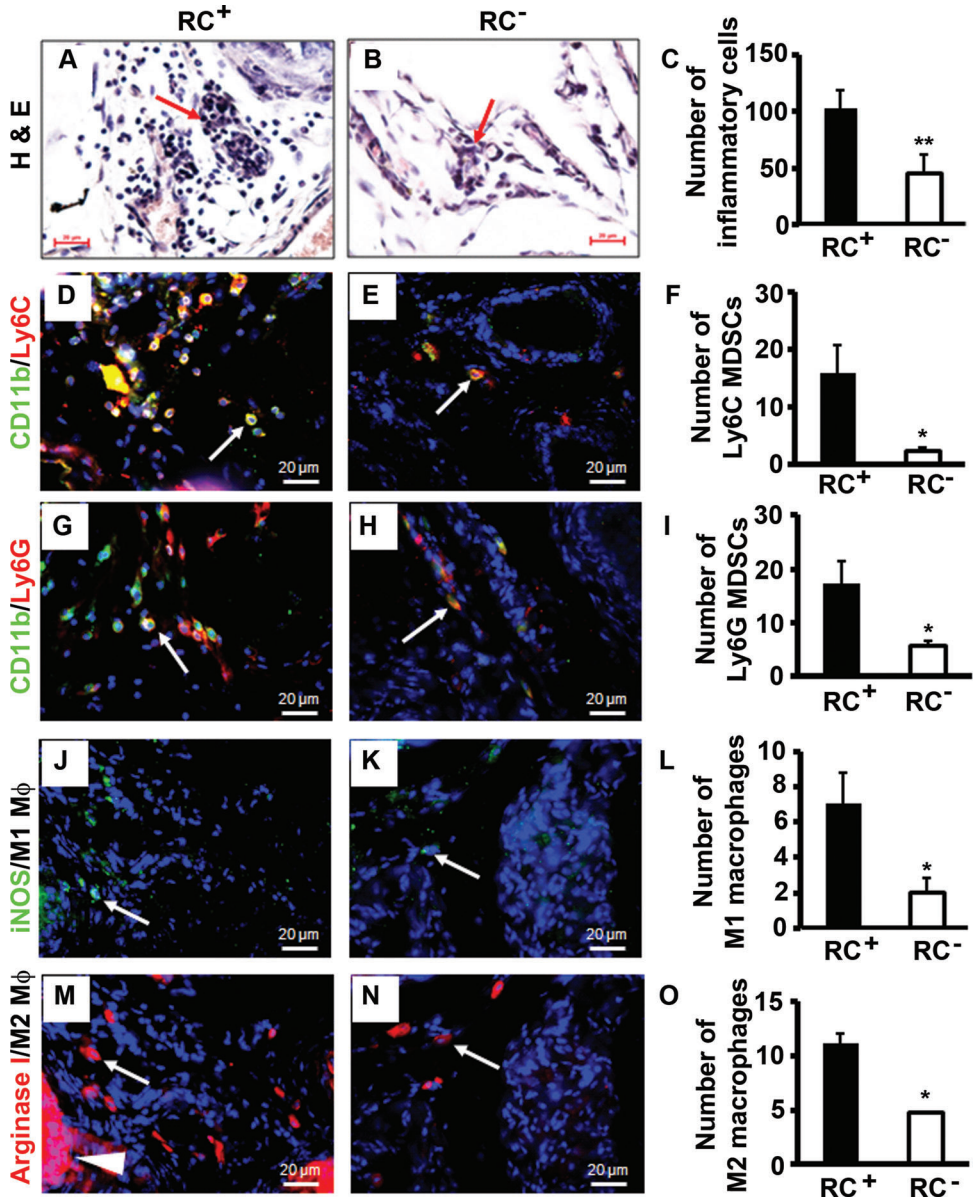



**Fig. 6.** Castrate RC$^-$ prostate had less inflammatory cell infiltration than castrate RC$^+$ prostate. **A**, **B**: H&E staining; arrows indicate lymphocytes. **C**: Number of inflammatory cells counted on H&E-stained sections. **D**, **E**: Double immunofluorescent staining of CD11b and Ly6C. **F**: Number of Ly6C MDSCs. **G**, **H**: Double immunofluorescent staining of CD11b and Ly6G. **I**: Number of Ly6G MDSCs. **J**, **K**: Immunofluorescent staining of iNOS-positive MI macrophages. **L**: Number of MI macrophages. **M**, **N**: Immunofluorescent staining of arginase I-positive M2 macrophages; arrowhead indicates positively stained prostatic epithelium. **O**: Number of M2 macrophages. Original magnification, ×400; arrows indicate positive cells; $^*P < 0.05$ and $^{**}P < 0.01$.

numbers of both MDSC subsets were significantly reduced in RC$^-$ prostate compared to RC$^+$ prostate ($P < 0.05$, Fig. 6D–I).

It has been reported that the inducible nitric oxide synthase (iNOS)-positive M1 macrophages and arginase I-positive M2 macrophages are present in the mouse prostate tumors, where M1 macrophages have anti-tumor functions while M2 macrophages have protumor functions [45]. We found that there were slightly fewer M1 macrophages than M2 macrophages in both RC$^+$ and RC$^-$ prostates (Fig. 6J–O). Yet, the numbers of M1 and M2 macrophages were significantly reduced in RC$^-$ prostate compared to RC$^+$ prostate (Fig. 6L and O).

## DISCUSSION

We previously reported that *Il17rc* knockout inhibited formation and growth of hormone-naïve prostate adenocarcinoma in the *Pten* conditional knockout

mouse model [28]. In the present study, we used the same mouse model and castrated the animals at 16 weeks of age. Fourteen weeks after castration, we found that invasive adenocarcinomas were present in both $RC^+$ and $RC^-$ mouse prostates, albeit at different incidence rates. The GU bloc size, judged by the GU bloc weight, was significantly smaller in the castrate mice than the intact mice (Fig. 1). The remaining invasive adenocarcinomas in the castrate mice presumably are CRPC based on the direct evidence that cellular proliferation was still present 14 weeks after the absence of testicular androgens. Another line of indirect evidence is that UBE2C level was very high in the castrate $RC^+$ mouse prostate as UBE2C was only expressed at high levels in CRPC [38].

The most significant phenotypic difference between the castrate $RC^+$ and $RC^-$ mice is the incidence rate of invasive adenocarcinomas. $RC^+$ mice presented invasive adenocarcinomas in 65% of prostatic glands, in sharp contrast to 23% of prostatic glands in $RC^-$ mice (Fig. 2E). These incidence rates are much lower than the rates in the non-castrate $RC^+$ and $RC^-$ mice (i.e., 100% and 70%, respectively) [28,29]. One possible reason is that the AR-positive prostatic epithelium undergoes increased apoptosis in response to castration. A 10-times increase of apoptotic cells in the *Pten*-null prostate cancer was found compared to the intact mouse prostate cancer, and the apoptotic rate was even higher in the prostate cancer than the normal epithelium 3 days post-castration [29]. Apoptosis may possibly lead to regression of some invasive adenocarcinomas and PIN lesions, resulting in a heterogeneous appearance of normal epithelium, PIN, and invasive adenocarcinomas.

There are several possible reasons to explain the different incidence rates of invasive adenocarcinomas between the castrate $RC^+$ and $RC^-$ mice. First, the cellular proliferation rate is higher in $RC^+$ prostate than $RC^-$ prostate while the apoptotic rate is lower in $RC^+$ prostate than $RC^-$ prostate. These differences confer an advantage to the tumor growth in $RC^+$ mice over $RC^-$ mice. Second, several proteins, namely, MMP7, YBX1, MTA1, and UBE2C, are expressed at higher levels in $RC^+$ prostate than $RC^-$ prostate. These proteins have been associated with the invasiveness and aggressiveness of human prostate cancer cells [28,32,33,35,38]. While we have demonstrated that MMP7 is a direct downstream target of IL-17 signaling pathway [28], it remains to be determined if YBX1, MTA1, and UBE2C are also IL-17 downstream targets. Third, angiogenesis is reduced in $RC^-$ prostate compared to $RC^+$ prostate. Angiogenesis is an integral hallmark of cancer and it has recently been associated with early neoplastic progression besides its well-known role in macroscopic tumors [46]. One mechanism by which IL-17 promotes lung cancer growth is through induction of angiogenesis [40]. The reduced levels of COX-2 and VEGFA in $RC^-$ prostate may be responsible for the decreased angiogenesis, as the COX-2-VEGF pathway has been associated with gastric angiogenesis [42]. COX-2 is an IL-17 downstream target in keratinocytes [41]. And last, inflammatory cell infiltration is reduced in $RC^-$ prostate compared to $RC^+$ prostate. The number of inflammatory cells appears to be more in the prostate of the castrate mice than the intact mice. It has been reported that androgen ablation increased infiltration of CD4+ T cells and macrophages in human prostate tumors [47]. The inflammatory cell population shifts from myeloid cells/lymphocytes in the intact mice to mainly lymphocytes in the castrate mice. This finding is in line with a recent report that castration elicits infiltration of $T_H1$ cells followed by predominantly $T_H17$ cells in rat prostate [48]. The subtypes of lymphocytes in our animal models are the subjects of our ongoing studies. Nevertheless, we have shown that the numbers of two major myeloid cell types, MDSCs and macrophages, are significantly reduced in $RC^-$ mice compared to $RC^+$ mice. We have recently demonstrated that IL-17 is a chemoattractant for monocytes/macrophages [49]. The reduced infiltration of MDSCs and macrophages may be caused by lack of IL-17RC receptor on these cells and/or indirectly by the decreased chemokine levels in the tumor microenvironment of $RC^-$ mice. Since MDSCs and M2 macrophages are pro-tumor inflammatory cells, a decrease in their numbers may partially contribute to the phenotype of reduced incidence rate of invasive adenocarcinomas in $RC^-$ mice.

In summary, the present study demonstrates that IL-17 promotes development of CRPC in the *Pten* conditional knockout mouse model. IL-17 may affect several hallmark capabilities of cancer, including sustaining proliferation, resisting cell death, activating invasion, inducing angiogenesis, and recruiting pro-tumor inflammatory cells [46]. These findings suggest that blocking IL-17 signaling through pharmacological interventions may have potentials in the prevention and treatment of CRPC.

## CONCLUSIONS

IL-17 promotes development of invasive prostate adenocarcinomas in *Pten* conditional knockout mice under castrate conditions, potentially through creating an immunotolerant and pro-angiogenic tumor microenvironment.

## ACKNOWLEDGMENTS

We thank Drs. Prescott L. Deininger, Asim B. Abdel-Mageed, Steven M. Hill, David E. Blask, Brian

G. Rowan, and Oliver Sartor (Tulane University) for their advices and comments on the manuscript. Tulane Cancer Center Core Facilities were used in this study. We thank Dr. Wenjun Ouyang and Genentech for providing the *Il17rc*$^{-/-}$ mice and NCI MMHCC for providing the PB-Cre4 mice.

## REFERENCES

1. Harris WP, Mostaghel EA, Nelson PS, Montgomery B. Androgen deprivation therapy: Progress in understanding mechanisms of resistance and optimizing androgen depletion. Nat Clin Pract Urol 2009;6(2):76–85.
2. Newmark JR, Hardy DO, Tonb DC, Carter BS, Epstein JI, Isaacs WB, Brown TR, Barrack ER. Androgen receptor gene mutations in human prostate cancer. Proc Natl Acad Sci USA 1992;89(14): 6319–6323.
3. Mohler JL, Gregory CW, Ford OH III, Kim D, Weaver CM, Petrusz P, Wilson EM, French FS. The androgen axis in recurrent prostate cancer. Clin Cancer Res 2004;10(2):440–448.
4. Hu R, Dunn TA, Wei S, Isharwal S, Veltri RW, Humphreys E, Han M, Partin AW, Vessella RL, Isaacs WB, Bova GS, Luo J. Ligand-independent androgen receptor variants derived from splicing of cryptic exons signify hormone-refractory prostate cancer. Cancer Res 2009;69(1):16–22.
5. Culig Z, Hobisch A, Cronauer MV, Radmayr C, Trapman J, Hittmair A, Bartsch G, Klocker H. Androgen receptor activation in prostatic tumor cell lines by insulin-like growth factor-I, keratinocyte growth factor, and epidermal growth factor. Cancer Res 1994;54(20):5474–5478.
6. Craft N, Shostak Y, Carey M, Sawyers CL. A mechanism for hormone-independent prostate cancer through modulation of androgen receptor signaling by the HER-2/neu tyrosine kinase. Nat Med 1999;5(3):280–285.
7. Debes JD, Schmidt LJ, Huang H, Tindall DJ. p300 mediates androgen-independent transactivation of the androgen receptor by interleukin 6. Cancer Res 2002;62(20):5632–5636.
8. Jin RJ, Wang Y, Masumori N, Ishii K, Tsukamoto T, Shappell SB, Hayward SW, Kasper S, Matusik RJ. NE-10 neuroendocrine cancer promotes the LNCaP xenograft growth in castrated mice. Cancer Res 2004;64(15):5489–5495.
9. McDonnell TJ, Troncoso P, Brisbay SM, Logothetis C, Chung LW, Hsieh JT, Tu SM, Campbell ML. Expression of the protooncogene bcl-2 in the prostate and its association with emergence of androgen-independent prostate cancer. Cancer Res 1992;52(24): 6940–6944.
10. July LV, Akbari M, Zellweger T, Jones EC, Goldenberg SL, Gleave ME. Clusterin expression is significantly enhanced in prostate cancer cells following androgen withdrawal therapy. Prostate 2002;50(3):179–188.
11. Heidenberg HB, Bauer JJ, McLeod DG, Moul JW, Srivastava S. The role of the p53 tumor suppressor gene in prostate cancer: A possible biomarker? Urology 1996;48(6):971–979.
12. Abate-Shen C, Banach-Petrosky WA, Sun X, Economides KD, Desai N, Gregg JP, Borowsky AD, Cardiff RD, Shen MM. Nkx3.1; Pten mutant mice develop invasive prostate adenocarcinoma and lymph node metastases. Cancer Res 2003;63(14): 3886–3890.
13. Graff JR, Konicek BW, McNulty AM, Wang Z, Houck K, Allen S, Paul JD, Hbaiu A, Goode RG, Sandusky GE, Vessella RL, Neubauer BL. Increased AKT activity contributes to prostate cancer progression by dramatically accelerating prostate tumor growth and diminishing p27Kip1 expression. J Biol Chem 2000;275(32):24500–24505.
14. Cai C, Wang H, Xu Y, Chen S, Balk SP. Reactivation of androgen receptor-regulated TMPRS S2: ERG gene expression in castration-resistant prostate cancer. Cancer Res 2009;69(15):6027–6032.
15. Tomlins SA, Rhodes DR, Perner S, Dhanasekaran SM, Mehra R, Sun XW, Varambally S, Cao X, Tchinda J, Kuefer R, Lee C, Montie JE, Shah RB, Pienta KJ, Rubin MA, Chinnaiyan AM. Recurrent fusion of TMPRSS2 and ETS transcription factor genes in prostate cancer. Science 2005;310(5748):644–648.
16. Shi XB, Tepper CG, White RW. MicroRNAs and prostate cancer. J Cell Mol Med 2008;12(5A):1456–1465.
17. Sun T, Wang Q, Balk S, Brown M, Lee GS, Kantoff P. The role of microRNA-221 and microRNA-222 in androgen-independent prostate cancer cell lines. Cancer Res 2009;69(8):3356–3363.
18. Corcoran NM, Costello AJ. Interleukin-6: Minor player or starring role in the development of hormone-refractory prostate cancer? BJU Int 2003;91(6):545–553.
19. Lee LF, Louie MC, Desai SJ, Yang J, Chen HW, Evans CP, Kung HJ. Interleukin-8 confers androgen-independent growth and migration of LNCaP: Differential effects of tyrosine kinases Src and FAK. Oncogene 2004;23(12):2197–2205.
20. Onishi RM, Gaffen SL. Interleukin-17 and its target genes: Mechanisms of interleukin-17 function in disease. Immunology 2010;129(3):311–321.
21. Toy D, Kugler D, Wolfson M, Vanden Bos T, Gurgel J, Derry J, Tocker J, Peschon J. Cutting edge: Interleukin 17 signals through a heteromeric receptor complex. J Immunol 2006;177(1):36–39.
22. Haudenschild D, Moseley T, Rose L, Reddi AH. Soluble and transmembrane isoforms of novel interleukin-17 receptor-like protein by RNA splicing and expression in prostate cancer. J Biol Chem 2002;277(6):4309–4316.
23. Ely LK, Fischer S, Garcia KC. Structural basis of receptor sharing by interleukin 17 cytokines. Nat Immunol 2009;10(12):1245–1251.
24. Ye P, Rodriguez FH, Kanaly S, Stocking KL, Schurr J, Schwarzenberger P, Oliver P, Huang W, Zhang P, Zhang J, Shellito JE, Bagby GJ, Nelson S, Charrier K, Peschon JJ, Kolls JK. Requirement of interleukin 17 receptor signaling for lung CXC chemokine and granulocyte colony-stimulating factor expression, neutrophil recruitment, and host defense. J Exp Med 2001; 194(4):519–527.
25. Hu Y, Ota N, Peng I, Refino CJ, Danilenko DM, Caplazi P, Ouyang W. IL-17RC is required for IL-17A- and IL-17F-dependent signaling and the pathogenesis of experimental autoimmune encephalomyelitis. J Immunol 2010;184(8):4307–4316.
26. You Z, Dong Y, Kong X, Zhang Y, Vessella RL, Melamed J. Differential expression of IL-17RC isoforms in androgen-dependent and androgen-independent prostate cancers. Neoplasia 2007;9(6):464–470.
27. You Z, Shi XB, DuRaine G, Haudenschild D, Tepper CG, Lo SH, Gandour-Edwards R, de Vere White RW, Reddi AH. Interleukin-17 receptor-like gene is a novel antiapoptotic gene highly expressed in androgen-independent prostate cancer. Cancer Res 2006;66(1):175–183.
28. Zhang Q, Liu S, Ge D, Xue Y, Xiong Z, Abdel-Mageed AB, Myers L, Hill SM, Rowan BG, Sartor O, Melamed J, Chen Z, You Z. Interleukin-17 promotes formation and growth of prostate adenocarcinoma in mouse models. Cancer Res 2012;72(10): 2589–2599.

29. Wang S, Gao J, Lei Q, Rozengurt N, Pritchard C, Jiao J, Thomas GV, Li G, Roy-Burman P, Nelson PS, Liu X. Wu H. Prostate-specific deletion of the murine Pten tumor suppressor gene leads to metastatic prostate cancer. Cancer Cell 2003;4(3):209–221.
30. Shappell SB, Thomas GV, Roberts RL, Herbert R, Ittmann MM, Rubin MA, Humphrey PA, Sundberg JP, Rozengurt N, Barrios R, Ward JM, Cardiff RD. Prostate pathology of genetically engineered mice: Definitions and classification. The consensus report from the Bar Harbor meeting of the Mouse Models of Human Cancer Consortium Prostate Pathology Committee. Cancer Res 2004;64(6):2270–2305.
31. Didier DK, Schiffenbauer J, Woulfe SL, Zacheis M, Schwartz BD. Characterization of the cDNA encoding a protein binding to the major histocompatibility complex class II Y box. Proc Natl Acad Sci USA 1988;85(19):7322–7326.
32. Lovett DH, Cheng S, Cape L, Pollock AS, Mertens PR. YB-1 alters MT1-MMP trafficking and stimulates MCF-7 breast tumor invasion and metastasis. Biochem Biophys Res Commun 2010; 398(3):482–488.
33. Gimenez-Bonafe P, Fedoruk MN, Whitmore TG, Akbari M, Ralph JL, Ettinger S, Gleave ME, Nelson CC. YB-1 is upregulated during prostate cancer tumor progression and increases P-glycoprotein activity. Prostate 2004;59(3):337–349.
34. Toh Y, Pencil SD, Nicolson GL. A novel candidate metastasis-associated gene, mta1, differentially expressed in highly metastatic mammary adenocarcinoma cell lines. cDNA cloning, expression, and protein analyses. J Biol Chem 1994;269(37):22958–22963.
35. Kai L, Wang J, Ivanovic M, Chung YT, Laskin WB, Schulze-Hoepfner F, Mirochnik Y, Satcher RL Jr, Levenson AS. Targeting prostate cancer angiogenesis through metastasis-associated protein 1 (MTA1). Prostate 2011;71(3):268–280.
36. Townsley FM, Aristarkhov A, Beck S, Hershko A, Ruderman JV. Dominant-negative cyclin-selective ubiquitin carrier protein E2-C/UbcH10 blocks cells in metaphase. Proc Natl Acad Sci USA 1997;94(6):2362–2367.
37. Hao Z, Zhang H, Cowell J. Ubiquitin-conjugating enzyme UBE2C: Molecular biology, role in tumorigenesis, and potential as a biomarker. Tumour Biol 2012;33(3):723–730.
38. Wang Q, Li W, Zhang Y, Yuan X, Xu K, Yu J, Chen Z, Beroukhim R, Wang H, Lupien M, Wu T, Regan MM, Meyer CA, Carroll JS, Manrai AK, Janne OA, Balk SP, Mehra R, Han B, Chinnaiyan AM, Rubin MA, True L, Fiorentino M, Fiore C, Loda M, Kantoff PW, Liu XS, Brown M. Androgen receptor regulates a distinct transcription program in androgen-independent prostate cancer. Cell 2009;138(2):245–256.
39. Numasaki M, Fukushi J, Ono M, Narula SK, Zavodny PJ, Kudo T, Robbins PD, Tahara H, Lotze MT. Interleukin-17 promotes angiogenesis and tumor growth. Blood 2003;101(7):2620–2627.
40. Numasaki M, Watanabe M, Suzuki T, Takahashi H, Nakamura A, McAllister F, Hishinuma T, Goto J, Lotze MT, Kolls JK, Sasaki H. IL-17 enhances the net angiogenic activity and in vivo growth of human non-small cell lung cancer in SCID mice through promoting CXCR-2-dependent angiogenesis. J Immunol 2005; 175(9):6177–6189.
41. Kanda N, Koike S, Watanabe S. IL-17 suppresses TNF-alpha-induced CCL27 production through induction of COX-2 in human keratinocytes. J Allergy Clin Immunol 2005;116(5):1144–1150.
42. Miura S, Tatsuguchi A, Wada K, Takeyama H, Shinji Y, Hiratsuka T, Futagami S, Miyake K, Gudis K, Mizokami Y, Matsuoka T, Sakamoto C. Cyclooxygenase-2-regulated vascular endothelial growth factor release in gastric fibroblasts. Am J Physiol Gastrointest Liver Physiol 2004;287(2):G444–G451.
43. He D, Li H, Yusuf N, Elmets CA, Li J, Mountz JD. Xu H. IL-17 promotes tumor development through the induction of tumor promoting microenvironments at tumor sites and myeloid-derived suppressor cells. J Immunol 2010;184(5):2281–2288.
44. Youn JI, Nagaraj S, Collazo M, Gabrilovich DI. Subsets of myeloid-derived suppressor cells in tumor-bearing mice. J Immunol 2008;181(8):5791–5802.
45. Redente EF, Dwyer-Nield LD, Merrick DT, Raina K, Agarwal R, Pao W, Rice PL, Shroyer KR, Malkinson AM. Tumor progression stage and anatomical site regulate tumor-associated macrophage and bone marrow-derived monocyte polarization. Am J Pathol 2010;176(6):2972–2985.
46. Hanahan D, Weinberg RA. Hallmarks of cancer: The next generation. Cell 2011;144(5):646–674.
47. Mercader M, Bodner BK, Moser MT, Kwon PS, Park ES, Manecke RG, Ellis TM, Wojcik EM, Yang D, Flanigan RC, Waters WB, Kast WM, Kwon ED. T cell infiltration of the prostate induced by androgen withdrawal in patients with prostate cancer. Proc Natl Acad Sci USA 2001;98(25):14565–14570.
48. Morse MD, McNeel DG. T cells localized to the androgen-deprived prostate are T(H) 1 and T(H) 17 biased. Prostate 2012;72(11):1239–1247.
49. Liu L, Ge D, Ma L, Mei J, Liu S, Zhang Q, Ren F, Liao H, Pu Q, Wang T, You Z. Interleukin-17 and prostaglandin E2 are involved in formation of an M2 macrophage-dominant microenvironment in lung cancer. J Thorac Oncol 2012;7(7):1091–1100.

## SUPPORTING INFORMATION

Additional supporting information may be found in the online version of this article at the publisher's website.

*Int. J. Mol. Sci.* **2014**, *15*, 6941-6960; doi:10.3390/ijms15046941

OPEN ACCESS
International Journal of
**Molecular Sciences**
**ISSN 1422-0067**
www.mdpi.com/journal/ijms

*Article*

# Doublecortin May Play a Role in Defining Chondrocyte Phenotype

**Dongxia Ge [1,†], Qing-Song Zhang [1,2,†], Jovanny Zabaleta [3], Qiuyang Zhang [1], Sen Liu [1], Brendan Reiser [1], Bruce A. Bunnell [4], Stephen E. Braun [4], Michael J. O'Brien [5], Felix H. Savoie [5] and Zongbing You [1,5,*]**

[1] Department of Structural and Cellular Biology, Tulane Cancer Center, Louisiana Cancer Research Consortium, Tulane Center for Aging and Tulane Center for Stem Cell Research and Regenerative Medicine, Tulane University Health Sciences Center, New Orleans, LA 70112, USA; E-Mails: gedongx@gmail.com (D.G.); qingsong.chang@gmail.com (Q.-S.Z.); qzhang3@tulane.edu (Q.Z.); senliu@yahoo.com (S.L.); brendan.reiser@gmail.com (B.R.)

[2] Department of Orthopaedic Surgery, Pu Ai Hospital of Tongji Medical College, Huazhong University of Science and Technology, Wuhan 430033, China

[3] Department of Pediatrics and Stanley S. Scott Cancer Center, Louisiana State University Health Sciences Center, New Orleans, LA 70112, USA; E-Mail: jzabal@lsuhsc.edu

[4] Department of Pharmacology, Tulane Center for Stem Cell Research and Regenerative Medicine and Division of Regenerative Medicine of Tulane National Primate Research Center, Tulane University Health Sciences Center, New Orleans, LA 70112, USA; E-Mails: bbunnell@tulane.edu (B.A.B); sbraun@tulane.edu (S.E.B.)

[5] Department of Orthopaedic Surgery and Tulane Institute of Sports Medicine, Tulane University School of Medicine, New Orleans, LA 70112, USA; E-Mails: michaelobrien76@gmail.com (M.J.O.); fsavoie@tulane.edu (F.H.S.)

† These authors contributed equally to this work.

* Author to whom correspondence should be addressed; E-Mail: zyou@tulane.edu; Tel.: +1-504-988-0467; Fax: +1-504-988-1687.

*Received: 17 February 2014; in revised form: 3 April 2014 / Accepted: 14 April 2014 / Published: 22 April 2014*

---

**Abstract:** Embryonic development of articular cartilage has not been well understood and the role of doublecortin (*DCX*) in determination of chondrocyte phenotype is unknown. Here, we use a *DCX* promoter-driven *eGFP* reporter mouse model to study the dynamic gene expression profiles in mouse embryonic handplates at E12.5 to E13.5 when the condensed mesenchymal cells differentiate into either endochondral chondrocytes or joint

interzone cells. Illumina microarray analysis identified a variety of genes that were expressed differentially in the different regions of mouse handplate. The unique expression patterns of many genes were revealed. *Cytl1* and *3110032G18RIK* were highly expressed in the proximal region of E12.5 handplate and the carpal region of E13.5 handplate, whereas *Olfr538*, *Kctd15*, and *Cited1* were highly expressed in the distal region of E12.5 and the metacarpal region of E13.5 handplates. There was an increasing gradient of *Hrc* expression in the proximal to distal direction in E13.5 handplate. Furthermore, when human DCX protein was expressed in human adipose stem cells, collagen II was decreased while aggrecan, matrilin 2, and *GDF5* were increased during the 14-day pellet culture. These findings suggest that *DCX* may play a role in defining chondrocyte phenotype.

**Keywords:** articular cartilage; chondrocytes; doublecortin; *DCX*

## 1. Introduction

Diseases of articular joints, such as osteoarthritis, cause pain and impaired mobility. It is estimated that 24.3 million American adults have osteoarthritis [1]. The current clinical treatments, other than total joint replacement, do not change the course of osteoarthritis. Regenerative medicine, including tissue engineering, offers exciting opportunities to restore functional articular cartilage. However, currently the tissue-engineered cartilages behave like physeal or endochondral cartilages that undergo premature hypertrophy, unlike the stable articular cartilage that lasts a lifetime [2]. The current tissue engineering of cartilage follows a paradigm of high-density cell culture such as pellet culture, micromass culture, or high-density culture in certain matrix scaffolds. This paradigm essentially mimics embryonic development of skeletal anlage (*i.e.*, endochondral cartilage), rather than articular cartilage. Although endochondral and articular cartilages are both hyaline cartilages, they differ significantly [3]. Embryonic development of articular cartilage has not been well understood. This lack of complete understanding of articular chondrocyte phenotype establishment is a problem for the field of articular cartilage tissue engineering/regeneration.

It is well recognized that the mechanism of regeneration recapitulates the mechanism of embryonic development [4,5]. Therefore, it is critical to understand the determinants of chondrocyte phenotype during embryonic chondrogenesis. In mouse embryonic limb buds, the mesenchymal cells appear homogeneous at embryonic stages of 9.5 to 11.5 days postcoitus (*i.e.*, E9.5 to E11.5). Mesenchymal condensation occurs in the limb buds at E12.5, without any signs of joint interzones—presumptive sites of articular joints [6]. At E13.5, joint interzones appear in the proximal to distal order [7], and the long bone anlagen intervening between the joint interzones become cartilaginous with endochondral chondrocytes residing within the anlagen [8]. Joint interzone can be recognized by postmortem histologic staining or LacZ staining in mice with *Gdf5-cre*-driven *LacZ* expression [8]. Recently, live imaging of joint interzones became possible when doublecortin reporter mice were developed [9]. Doublecortin (*DCX*) is a gene located on chromosome Xq22.3-Xq23, encoding a microtubule-binding protein that is expressed in migrating and differentiating neurons [10–12]. We originally found that *DCX* is expressed in human and mouse articular chondrocytes, but not in endochondral chondrocytes,

synovium, or cruciate ligaments [13]. Using two reporter mouse strains with *DCX* promoter-driven *LacZ* or enhanced green fluorescence protein (*eGFP*), we found that *DCX* is expressed in the mesenchymal cells in mouse embryonic limb buds, however, a population of mesenchymal cells maintain *DCX* expression when they differentiate into joint interzone cells and articular chondrocytes, whereas the other population of mesenchymal cells that differentiate into endochondral chondrocytes lose *DCX* expression [9]. The *DCX-EGFP* reporter mouse provides a unique tool to investigate the dynamic changes of chondrocyte phenotype *in vivo* or *ex vivo*.

## 2. Results and Discussion

### *2.1. The DCX-Positive Proximal and DCX-Negative Distal Regions of E12.5 Mouse Handplate Express Different Genes*

Limbs develop in the proximal to distal order [7]. The regional differences are obvious morphologically. This study focused on mouse handplates at E12.5 to E13.5, because differentiation of the condensed mesenchymal cells into chondrocytes occurs during this period. Our previous study showed that the proximal region of E12.5 handplate expresses high levels of *DCX* as shown by eGFP signals, whereas the distal region is almost negative for eGFP signals except the faint signals in the digit rays [9]. Thus, we cut mouse handplates into proximal and distal regions based on eGFP signals under an epifluorescence microscope (Figure 1A). RNA was isolated from the proximal and distal tissues and Illumina microarray analysis was performed. Judging by a two-fold difference, we found that there were 34 genes with mRNA expression levels higher in the proximal region than the distal region, while there were 44 genes expressed at higher levels in the distal region than the proximal region (Tables 1 and S1). Many of these genes have never been studied in limb development. Delta-like 1 homolog (*Dlk1*, No. 1 in Table 1) was highly expressed in the proximal region of mouse handplate, where mesenchymal condensation occurs and chondrogenesis is ongoing. However, it has been shown that *Dlk1* inhibits *in vitro* chondrogenesis [14]. We speculate that the increased *Dlk1* level may be needed to antagonize other signals that drive chondrogenesis, so as chondrogenesis occurs in a controlled manner. *Cytokine-like 1* (*Cytl1*, No. 3 in Table 1) was a gene highly expressed in the proximal region of mouse handplate. Cytl1 is a secreted, cytokine-like factor that has chondrogenic effect via stimulation of sex determining region *Y-box 9* (*Sox9*) transcriptional activity [15]. The increased level of *Cytl1* in the proximal region possibly correlates with the earlier start of chondrogenesis in the proximal region than the distal region. However, a recent study showed that deletion of the *Cytl1* gene did not affect chondrogenesis or cartilage development [16]. In that study, *Cytl1*-null mice also showed normal endochondral ossification and long bone development. In addition, the ultrastructural features of matrix organization and chondrocyte morphology in articular cartilage were similar between wild-type and *Cytl1*-null mice. However, *Cytl1*-null mice were more sensitive to osteoarthritic (OA) cartilage destruction upon destabilization of the medial meniscus of mouse knee joints. Furthermore, the expression levels of Cytl1 were markedly decreased in OA cartilage of humans and experimental mice. Therefore, the authors of that study concluded that, rather than regulating cartilage and bone development, Cytl1 is required for the maintenance of cartilage homeostasis, and loss of Cytl1 function is associated with experimental OA cartilage destruction in mice [16]. Another gene,

*paired related homeobox 2* (*Prrx2*, No. 19 in Table 1), was highly expressed in the distal region compared to the proximal region. It has been reported that *Prrx2* is highly expressed in undifferentiated mesenchymal cells and its expression decreases when the mesenchymal cells differentiate into chondrocytes [17]. Given that chondrogenesis proceeds from the proximal region to the distal region, it makes sense that the distal region with more undifferentiated mesenchymal cells expresses higher levels of *Prrx2*. Therefore, our results, at least for *Cytl1* and *Prrx2*, are consistent with the published literature.

**Figure 1.** Illustration of dissection of mouse embryonic handplates. (a) the distal region (DCX-eGFP-negative); (b) the proximal region (DCX-eGFP-positive); (c) the metacarpal-phalange region (DCX-eGFP-positive); (d) the metacarpal region (DCX-eGFP-negative); (e) the carpal region (DCX-eGFP-positive). All photomicrographs were taken under an epifluorescence microscope with 6× (**A**); 1.3× (**B**) and (**C**); and 1× (**D**) original magnification.

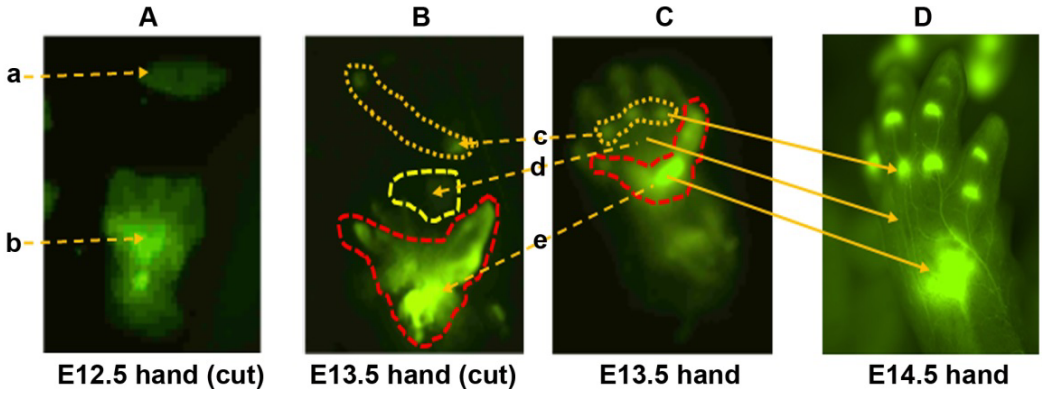



**Table 1.** Differential gene expression between the proximal and distal regions of E12.5 mouse handplate.

| No. | Gene ID | Gene Symbol | Proximal/Distal Ratio of Expression | Gene Name | Function |
|---|---|---|---|---|---|
| 1 | 13386 | *Dlk1* | 14.40 | *Delta-like 1 homolog (Drosophila)* | Inhibitory non-canonical protein ligand for the NOTCH1 receptor |
| 2 | 15464 | *Hrc* | 4.84 | *Histidine rich calcium binding protein* | Interactions with SERCA2 and triadin |
| 3 | 231162 | *Cytl1* | 4.53 | *Cytokine-like 1* | Cytl1-null mice show normal cartilage and bone development but exhibit augmented osteoarthritic cartilage destruction |
| 4 | 53412 | *Ppp1r3c* | 3.19 | *Protein phosphatase 1, regulatory (inhibitor) subunit 3C* | Activates glycogen synthase, reduces glycogen phosphorylase activity and limits glycogen breakdown |
| 5 | 16664 | *Krt14* | 3.15 | *Keratin 14* | Enhances the mechanical properties involved in resilience of keratin intermediate filaments |
| 6 | 74194 | *Rnd3* | 2.90 | *Rho family GTPase 3* | Binds GTP but lacks intrinsic GTPase activity |
| 7 | 12306 | *Anxa2* | 2.39 | *Annexin A2* | Calcium-regulated membrane-binding protein |
| 8 | 14314 | *Fstl* | 2.34 | *Follistatin-like 1* | May modulate the action of some growth factors on cell proliferation and differentiation |

**Table 1.** *Cont.*

| No. | Gene ID | Gene Symbol | Proximal/Distal Ratio of Expression | Gene Name | Function |
|---|---|---|---|---|---|
| 9 | 21847 | *Klf10* | 2.32 | *Kruppel-like factor 10* | Inhibits cell growth |
| 10 | 16002 | *Igf2* | 2.31 | *Insulin-like growth factor 2* | Growth-promoting activity |
| 11 | 17709 | *Mt-co2* | 2.18 | *Cytochrome c oxidase subunit II* | Component of the respiratory chain |
| 12 | 73121 | *3110032G18RIK* | 2.05 | *Family with sequence similarity 101, member A* | Unknown |
| 13 | 15401 | *Hoxa4* | 0.49 | *Homeobox A4* | Sequence-specific transcription factor |
| 14 | 15117 | *Has2* | 0.48 | *Hyaluronan synthase 2* | Hyaluronan/hyaluronic acid (HA) synthesis |
| 15 | 77087 | *3010027A04RIK* | 0.44 | *Ankyrin repeat domain 11* | Bone development |
| 16 | 258201 | *Olfr538* | 0.43 | *Olfactory receptor 538* | Interact with odorant molecules in the nose |
| 17 | 233107 | *Kctd15* | 0.39 | *Potassium channel tetramerisation domain containing 15* | Unknown |
| 18 | 12705 | *Cited1* | 0.36 | *Cbp/p300-interacting transactivator with Glu/Asp-rich carboxy-terminal domain 1* | Transcriptional coactivator of the p300/CBP-mediated trancription complex |
| 19 | 20204 | *Prrx2* | 0.29 | *Paired related homeobox 2* | A developmental protein |

### *2.2. The DCX-Positive and DCX-Negative Regions of E13.5 Mouse Handplate Express Different Genes*

At E13.5 in mouse handplate, the condensed mesenchymal cells already differentiate into endochondral chondrocytes or joint interzone cells. The joint interzones are clearly shown by expression of eGFP signals in the *DCX-EGFP* mice [9]. Based on the principle of proximal to distal development, the joint interzones in the carpal region develop first, followed by the joint interzones between the metacarpal bones and phalangeal bones, and then the joint interzones between the phalangeal bones. Due to the gel-like physical property and small size of mouse handplate at E13.5, it is very difficult to dissect out individual joint interzones and cartilaginous anlagen. Thus, we cut the mouse handplate into three regions, namely, the carpal region (containing *DCX*-positive joint interzones), metacarpal region (containing *DCX*-negative metacarpal cartilaginous anlagen), and metacarpal-phalange region (containing *DCX*-positive joint interzones between the metacarpal bones and phalangeal bones) (Figure 1B,C). These regions are so designated as we previously observed that they correspond to the aforementioned regions at E14.5 when hand morphogenesis becomes very clear (Figure 1D and reference [9]).

Microarray analysis showed that there were only four genes that were expressed at higher levels in the carpal region than the metacarpal region (Tables 2 and S2). One of these genes is *Cytl1* (No. 2 in Table 2). Since *Cytl1* has chondrogenic effect and its expression is high in articular chondrocytes [18], it is reasonably expected that *Cytl1* level should be higher in the joint interzones of the carpal region than the cartilaginous anlagen in the metacarpal region, which is consistent with the expression pattern

at E12.5. Microarray analysis also showed that there were 28 genes that were expressed at higher levels in the metacarpal region than the carpal region (Tables 2 and S2). Most of them have never been associated with chondrogenesis. *Frizzled homolog 10* (*Fzd10*, No. 8 in Table 2) is linked to Wnt signaling, and *Delta-like 2 homolog* (*Dlk2*, No. 10 in Table 2) inhibits NOTCH1 signaling. Both Wnt and NOTCH1 signaling pathways are known to play roles in chondrogenesis [19,20].

**Table 2.** Differential gene expression between the carpal and metacarpal regions of E13.5 mouse handplate.

| No. | Gene ID | Gene Name | Carpal/Metacarpal Ratio of Expression | Gene Name | Function |
|---|---|---|---|---|---|
| 1 | 73121 | *3110032G18rik* | 4.55 | *Family with sequence similarity 101, member A* | A novel gene uniquely expressed in developing forebrain and midbrain, but its null mutant exhibits no obvious phenotype |
| 2 | 231162 | *Cytl1* | 3.54 | *Cytokine-like 1* | Cytl1-null mice show normal cartilage and bone development but exhibit augmented osteoarthritic cartilage destruction |
| 3 | 50781 | *Dkk3* | 3.26 | *Dickkopf homolog 3 (Xenopus laevis)* | Antagonizes canonical Wnt signaling |
| 4 | 77853 | *Msl2* | 2.17 | *Male-specific lethal 2 homolog (Drosophila)* | Promotes Mdm2-independent cytoplasmic localization of p53 |
| 5 | 17709 | *Mt-co2* | 0.46 | *Cytochrome c oxidase subunit II* | Component of the respiratory chain |
| 6 | 21804 | *Tgfb1I1* | 0.46 | *Transforming growth factor beta 1 induced transcript 1* | A molecular adapter coordinating multiple protein-protein interactions |
| 7 | 233107 | *Kctd15* | 0.46 | *Potassium channel tetramerisation domain containing 15* | Unknown |
| 8 | 93897 | *Fzd10* | 0.45 | *Frizzled homolog 10 (Drosophila)* | Receptor for Wnt proteins |
| 9 | 258201 | *Olfr538* | 0.45 | *Olfactory receptor 538* | Interact with odorant molecules in the nose |
| 10 | 106565 | *Dlk2* | 0.42 | *Delta-like 2 homolog (Drosophila)* | Acts as inhibitory non-canonical protein ligands for the NOTCH1 receptor |
| 11 | 12705 | *Cited1* | 0.41 | *Cbp/p300-interacting transactivator with Glu/Asp-rich carboxy-terminal domain 1* | Transcriptional coactivator of the p300/CBP-mediated trancription complex |
| 12 | 15464 | *Hrc* | 0.32 | *Histidine rich calcium binding protein* | May play a key role in the regulation of SR Ca cycling through its direct interactions with SERCA2 and triadin |
| 13 | 54419 | *Cldn6* | 0.29 | *Claudin 6* | Plays a major role in tight junction-specific obliteration of the intercellular space, through calcium-independent cell-adhesion |
| 14 | 16664 | *Krt14* | 0.15 | *keratin 14* | The nonhelical tail domain is involved in promoting KRT5-KRT14 filaments to self-organize into large bundles |

Microarray analysis showed that there were six genes that were expressed at higher levels in the metacarpal region than the metacarpal-phalange region (Table 3). One of them is *Delta-like 1 homolog* (*Dlk1*, No. 1 in Table 3). Dlk1 inhibits NOTCH signaling that inhibits chondrogenesis [20]. In contrast, there were 11 genes that were expressed at higher levels in the metacarpal-phalange region than the metacarpal region (Table 3). It appears that none of these genes has been studied in skeletal development.

**Table 3.** Differential gene expression between the metacarpal and metacarpal-phalange regions of E13.5 mouse handplate.

| No. | Gene ID | Gene Symbol | Metacarpal/Metacarpal-Phalange Ratio of Expression | Gene Name | Function |
|---|---|---|---|---|---|
| 1 | 13386 | *Dlk1* | 2.64 | *Delta-like 1 homolog (Drosophila)* | Acts as inhibitory non-canonical protein ligand for the NOTCH1 receptor |
| 2 | 71706 | *Slc46a3* | 2.35 | *Solute carrier family 46, member 3* | Unknown |
| 3 | 11806 | *Apoa1* | 2.25 | *Apolipoprotein A-I* | Reverse transport of cholesterol from tissues to the liver for excretion |
| 4 | 54419 | *Cldn6* | 2.15 | *Claudin 6* | Role in tight junction-specific obliteration of the intercellular space, through calcium-independent cell-adhesion activity |
| 5 | 21804 | *Tgfb1I1* | 2.12 | *Transforming growth factor beta 1 induced transcript 1* | Functions as a molecular adapter coordinating multiple protein-protein interactions at the focal adhesion complex in nucleus |
| 6 | 12709 | *Ckb* | 2.06 | *Creatine kinase, brain* | Phospholipid biosynthesis |
| 7 | 11472 | *Actn2* | 0.48 | *Actinin alpha 2* | F-actin cross-linking protein which is thought to anchor actin to a variety of intracellular structures |
| 8 | 15464 | *Hrc* | 0.48 | *Histidine rich calcium binding protein* | Regulation of SR Ca cycling through its direct interactions with SERCA2 and triadin |
| 9 | 16876 | *Lhx9* | 0.46 | *LIM homeobox protein 9* | Gonadal development |
| 10 | 56360 | *Acot9* | 0.46 | *Acyl-CoA thioesterase 9* | Catalyze the hydrolysis of acyl-CoAs to the free fatty acid and coenzyme A |
| 11 | 72739 | *Zkscan3* | 0.46 | *Zinc finger with KRAB and SCAN domains 3* | Acts as a transcriptional regulator |
| 12 | 16704 | *Krtap8-2* | 0.45 | *Keratin associated protein 8-2* | Essential for the formation of a rigid and resistant hair shaft through their extensive disulfide bond cross-linking |
| 13 | 68895 | *Rasl11a* | 0.44 | *RAS-like, family 11, member A* | Regulator of rDNA transcription. Acts in cooperation UBF/UBTF and positively regulates RNA polymerase I transcription |
| 14 | 17883 | *Myh3* | 0.39 | *Myosin, heavy polypeptide 3, skeletal muscle, embryonic* | Mutations in this gene have been associated Freeman-Sheldon syndrome and Sheldon-Hall syndrome |

**Table 3.** *Cont.*

| No. | Gene ID | Gene Symbol | Metacarpal/Metacarpal-Phalange Ratio of Expression | Gene Name | Function |
|---|---|---|---|---|---|
| 15 | 17885 | *Myh8* | 0.38 | *Myosin, heavy polypeptide 8, skeletal muscle, perinatal* | Motor protein of muscle thick filaments |
| 16 | 19791 | *Rn18s* | 0.28 | *18S Ribosomal RNA* | A 45S rRNA, which serves as the precursor for the 18S, 5.8S and 28S rRNA, is transcribed from rDNA unit by RNA polymerase I |
| 17 | 226856 | *Lpgat1* | 0.26 | *Lysophosphatidylglycerol acyltransferase 1* | Recognizes various acyl-CoAs and LPGs as substrates but demonstrates a clear preference |

### *2.3. Dynamic Gene Expression Profiles between the DCX-Positive Proximal Region of E12.5 Mouse Handplate and the DCX-Positive Carpal or Metacarpal-Phalange Region of E13.5 Mouse Handplate*

Microarray analysis found that there were 62 genes with expression levels higher in the proximal region of E12.5 mouse handplate than the carpal region of E13.5 mouse handplate (Tables 4 and S3). Among them, *Cytl1* (No. 1 in Table 4), Dickkopf homolog 3 (*Dkk3*, No. 3 in Table 4), and *Dlk1* (No. 6 in Table 4) are known for their roles in chondrogenesis. In contrast, there were 47 genes that were expressed at higher levels in the carpal region of E13.5 mouse handplate than the proximal region of E12.5 mouse handplate (Tables 4 and S3). Most of these genes are not known for their roles in chondrogenesis, except *Fzd10* (No. 15 in Table 4) that may play a role in chondrogenesis through Wnt signaling [19].

**Table 4.** Differential gene expression between the proximal region of E12.5 handplate and the carpal region of E13.5 mouse handplate.

| No. | Gene ID | Gene Symbol | E12.5 Proximal/E13.5 Carpal Ratio of Expression | Gene Name | Function |
|---|---|---|---|---|---|
| 1 | 231162 | *Cytl1* | 18.15 | *Cytokine-like 1* | Cytl1-null mice show normal cartilage and bone development but exhibit augmented osteoarthritic cartilage destruction. |
| 2 | 73121 | *3110032G18rik* | 7.09 | *Family with sequence similarity 101, member A* | A novel gene uniquely expressed in developing forebrain and midbrain |
| 3 | 50781 | *Dkk3* | 6.15 | *Dickkopf homolog 3 (Xenopus laevis)* | Antagonizes canonical Wnt signaling |
| 4 | 19791 | *Rn18s* | 6.07 | *18S ribosomal RNA* | Encodes a 18S rRNA |
| 5 | 319480 | *Itga11* | 3.89 | *Integrin alpha 11* | Regulating Bone morphogenetic protein (BMP)-2 and transforming growth factor (TGF)-beta1 |

**Table 4.** *Cont.*

| No. | Gene ID | Gene Symbol | E12.5 Proximal/E13.5 Carpal Ratio of Expression | Gene Name | Function |
|---|---|---|---|---|---|
| 6 | 13386 | *Dlk1* | 2.93 | *Delta-like 1 homolog (Drosophila)* | Acts as inhibitory non-canonical protein ligand for the NOTCH1 receptor |
| 7 | 15401 | *Hoxa4* | 2.70 | *Homeobox A4* | Sequence-specific transcription factor |
| 8 | 20680 | *Sox7* | 2.29 | *SRY-box containing gene 7* | A member of the SOX (SRY-related HMG-box) family of transcription factors involved in regulation |
| 9 | 67586 | *D4bwg1540e* | 2.29 | *UBX domain protein 11* | May be involved in the reorganization of actin cytoskeleton mediated by RND1, RND2, and RND3 |
| 10 | 26433 | *Plod3* | 2.11 | *Procollagen-lysine, 2-oxoglutarate 5-dioxygenase 3* | Forms hydroxylysine residues in -Xaa-Lys-Gly- sequences in collagens |
| 11 | 100034361 | *Mfap1b* | 0.48 | *Microfibrillar-associated protein 1B* | Component of the elastin-associated microfibrils By similarity |
| 12 | 21371 | *Tbca* | 0.47 | *Tubulin cofactor A* | Tubulin-folding protein; involved in the early step of the tubulin folding pathway |
| 13 | 26941 | *Slc9a3r1* | 0.41 | *Solute carrier family 9 (sodium/hydrogen exchanger), member 3 regulator 1* | Scaffold protein that connects plasma membrane proteins with members of the ezrin/moesin/radixin |
| 14 | 12301 | *Cacybp* | 0.29 | *Calcyclin binding protein* | CacyBP/SIP interacts with tubulin in neuroblastoma NB2a cells and induces formation of globular tubulin assemblies. |
| 15 | 93897 | *Fzd10* | 0.25 | *Frizzled homolog 10 (Drosophila)* | Receptor for Wnt proteins. Most of frizzled receptors are coupled to the beta-catenin canonical signaling pathway |
| 16 | 18590 | *Pdgfa* | 0.24 | *Platelet derived growth factor, alpha* | Growth factor that plays an essential role in the regulation of embryonic development |
| 17 | 66643 | *Lix1* | 0.24 | *Limb expression 1 homolog (chicken)* | Unknown |
| 18 | 16664 | *Krt14* | 0.15 | *Keratin 14* | Involved in resilience of keratin intermediate filaments |

Microarray analysis also showed that there were 79 genes that were expressed at higher levels in the proximal region of E12.5 mouse handplate than the metacarpal-phalange region of E13.5 mouse handplate (Tables 5 and S4). These genes include *Cytl1* (No. 3 in Table 5) and *Dkk3* (No. 9 in Table 5) that are known to play roles in chondrogenesis. However, the other genes have rarely been studied in

chondrogenesis. On the other hand, there were 24 genes with expression levels higher in the metacarpal-phalange region of E13.5 mouse handplate than the proximal region of E12.5 mouse handplate (Tables 5 and S4). However, none of them has been studied in chondrogenesis.

**Table 5.** Differential gene expression between the proximal region of E12.5 handplate and the metacarpal-phalange region of E13.5 mouse handplate.

| No. | Gene ID | Gene Symbol | E12.5 Proximal/E13.5 Metacarpal-Phalange Ratio of Expression | Gene Name | Function |
|---|---|---|---|---|---|
| 1 | 19791 | *Rn18s* | 6.66 | *Rn18s 18S ribosomal RNA* | Encodes a 18S rRNA |
| 2 | 319480 | *Itga11* | 4.54 | *Integrin alpha 11* | Regulating Bone morphogenetic protein (BMP)-2 and transforming growth factor (TGF)-beta1 |
| 3 | 231162 | *Cytl1* | 4.09 | *Cytokine-like 1* | Cytl1-null mice show normal cartilage and bone development but exhibit augmented osteoarthritic cartilage destruction. |
| 4 | 72053 | *2010008E23Rik* | 3.93 | *Transmembrane and ubiquitin-like domain containing 2* | Unknown |
| 5 | 21804 | *Tgfb1i1* | 3.16 | *Transforming growth factor beta 1 induced transcript 1* | A molecular adapter coordinating multiple protein-protein interactions at the focal adhesion complex and in the nucleus |
| 6 | 108903 | *Tbcd* | 2.79 | *Tubulin-specific chaperone d* | Tubulin-folding protein |
| 7 | 67586 | *Ubxn11* | 2.3 | *UBX domain protein 11* | Reorganization of actin cytoskeleton |
| 8 | 20680 | *Sox7* | 2.24 | *SRY-box containing gene 7* | member of the SOX (SRY-related HMG-box) family of transcription factors |
| 9 | 50781 | *Dkk3* | 2.16 | *Dickkopf homolog 3 (Xenopus laevis)* | Inhibit Wnt regulated processes |
| 10 | 258201 | *Olfr538* | 2.06 | *Olfactory receptor 538* | Olfactory receptors interact with odorant molecules in the nose |
| 11 | 100034361 | *Mfap1b* | 0.45 | *Microfibrillar-associated protein 1B* | Component of the elastin-associated microfibrils by similarity |
| 12 | 66643 | *Lix1* | 0.15 | *Limb expression 1 homolog (chicken)* | Little is known about LIX1, except that it is evolutionarily conserved and highly expressed in spinal cord motor neurons |

In a comparison analysis of the above microarray data, we found some patterns of gene expression that are worth discussion. First, *Cytl1* and *3110032G18RIK* (also called *Fam101a*, *i.e.*, family with sequence similarity 101, member A) are consistently highly expressed in the *DCX*-positive proximal region of E12.5 mouse handplate and the *DCX*-positive carpal region of E13.5 mouse handplate, compared to the *DCX*-negative distal region of E12.5 mouse handplate and the *DCX*-negative metacarpal region of E13.5 mouse handplate (Figure 2A,B). On the opposite, Olfactory receptor 538 (*Olfr538*), Potassium channel tetramerisation domain containing 15 (*Kctd15*), and Cbp/p300-interacting transactivator with Glu/Asp-rich carboxy-terminal domain 1 (*Cited1*) are expressed at higher levels in the *DCX*-negative distal region of E12.5 mouse handplate and the *DCX*-negative metacarpal region of E13.5 mouse handplate than the *DCX*-positive proximal region of E12.5 mouse handplate and the *DCX*-positive carpal region of E13.5 mouse handplate (Figure 2A,B). These genes show a consistent expression pattern in the proximal to distal direction through E12.5 to E13.5; Second, several genes present a reverse expression pattern, including *Hrc*, *Krt14*, and *Mt-co2*. These genes are expressed at higher levels in the *DCX*-positive proximal region than the *DCX*-negative distal region of E12.5 mouse handplate (Figure 2A), however, their levels are lower in the *DCX*-positive carpal region than the *DCX*-negative metacarpal region of E13.5 mouse handplate (Figure 2B). Interestingly, the level of *Hrc* is higher in the *DCX*-positive metacarpal-phalange region than the *DCX*-negative metacarpal region of E13.5 mouse handplate (Figure 2B). These findings suggest that at E13.5, *Hrc* gene displays an expression pattern with increasing levels along the proximal-distal axis. *Rasl11a* gene also shows the similar pattern (Figure 2B); Third, *Claudin 6* (*Cldn6*) and *Transforming growth factor beta 1 induced transcript 1* (*Tgfb1I1*) genes are expressed at higher levels in the *DCX*-negative metacarpal region than the *DCX*-positive carpal region or metacarpal-phalange region of E13.5 mouse handplate (Figure 2B). Whether this expression pattern is linked to the difference between cartilaginous anlagen and joint interzone requires further investigation.

### *2.4. DCX Affects Expression of Genes Associated with Chondrocyte Phenotype*

Our previous studies have demonstrated that *DCX* is expressed in the osteo-chondral mesenchymal precursor cells and its expression is maintained in joint interzone cells and articular chondrocytes [9,13]. Other investigators have also shown *DCX* expression in articular chondrocytes [21]. It has been recognized that the permanent cartilage (articular cartilage) expresses *DCX*, *growth differentiation factor 5* (*GDF5*), and versican, whereas the transient cartilage (skeletal anlagen or endochondral cartilage) expresses matrilin 1 [22]. However, the role of *DCX* in chondrogenesis has not been understood. Therefore, we studied whether consistent expression of low level of *DCX* in the mesenchymal stromal/stem cells (MSCs) would affect chondrocyte phenotype during chondrogenesis using a pellet culture model.

We constructed a lentiviral vector (HRST-*DCX-GP-eGFP*) to express human *DCX* in human adipose tissue-derived MSCs, also called adipose stem cells (ASCs). GP stands for glycine and proline within a consensus peptide sequence that automatically self-cleaves to separate DCX and eGFP proteins once *DCX-GP-eGFP* gene is translated based on a previous study [23]. As a control group, HRST-*eGFP* lentiviral vector was used. Human ASCs transduced with either HRST-*eGFP* or HRST-*DCX-GP-eGFP* lentiviruses were sorted out, based on eGFP expression (Figure 3A,B). DCX protein expression was

confirmed by Western blot analysis (Figure 3C). Of note, DCX protein size was approximately 40 KDa, similar to the endogenous DCX protein expressed in mouse brain tissues, which indicates that the DCX-GP-eGFP fusion protein was indeed cleaved into separate DCX and eGFP proteins. DCX protein expression level was much lower in the transduced ASCs than the mouse brain tissues, which is comparable to the physiologic levels where DCX expression level in the limbs is dramatically less than in the brain and spinal cord [9]. Human ASCs with eGFP or DCX-GP-eGFP expression were cultured in pellets with chondrogenic media for 14 days. We found that both groups of human ASCs produced pieces of cartilage-like tissues with similar appearance (Figure 3D,E). Western blot analysis showed that DCX protein was expressed in the cartilage-like tissues derived from HRST-*DCX-GP-eGFP* lentivirus-transduced ASCs, but not in the cartilage-like tissues derived from HRST-*eGFP* lentivirus-transduced ASCs (Figure 3F). We checked a series of genes that are known to be expressed in articular or endochondral chondrocytes. We found that expression of collagen II was significantly decreased in the DCX-expressing pellets, whereas expression of aggrecan, matrilin 2, and *GDF5* was significantly increased in the DCX-expressing pellets (Figure 3G, $p < 0.05$). Superficial zone protein (*SZP*) was not detectable in either group. Collagen I is expressed by human ASCs. Expression of collagen I is expected to be reduced in chondrogenesis, however, we only observed a slight decrease in collagen I expression (Figure 3G). We speculate that this may be caused by an incomplete change from fibroblastic to chondrocytic phenotypes. It is paradoxical to observe that collagen II was reduced by DCX expression. However, we previously found that collagen II is expressed at higher levels in endochondral cartilage than articular cartilage [3], which suggests that less collagen II expression implies more articular chondrocytic phenotype than endochondral chondrocytic phenotype. Matrilin 2 and *GDF5* are restricted to articular chondrocytes [22–25]. DCX expression was decreased by 44-fold when E11.5 mouse limb bud mesenchymal cells were cultured in micromasses from day 3 to day 15 [23]. It is noteworthy that, in monolayer culture of mouse embryonic stem cells, GDF5 induced *DCX* expression on day four but its expression diminished over next eight days [26]. It is possible that *GDF5* and *DCX* provide reciprocal positive feedback in their expression, as both GDF5 and DCX proteins are restricted to articular cartilage. The differences in collagen II, matrilin 2, and *GDF5* between the two groups indicate that the DCX-expressing cartilage-like tissues lean towards expressing more genes that are specific for articular cartilage. Matrilin 1 levels were quite variable during our experiments (Figure 3G). However, since matrilin 1 is specific for endochondral chondrocytes [25], its increased expression in the DCX-expressing cartilage-like tissues argues against the speculation that *DCX* drives ASCs towards articular chondrocyte differentiation. Therefore, it awaits further investigation to clarify what *DCX*'s role is in chondrogenesis.

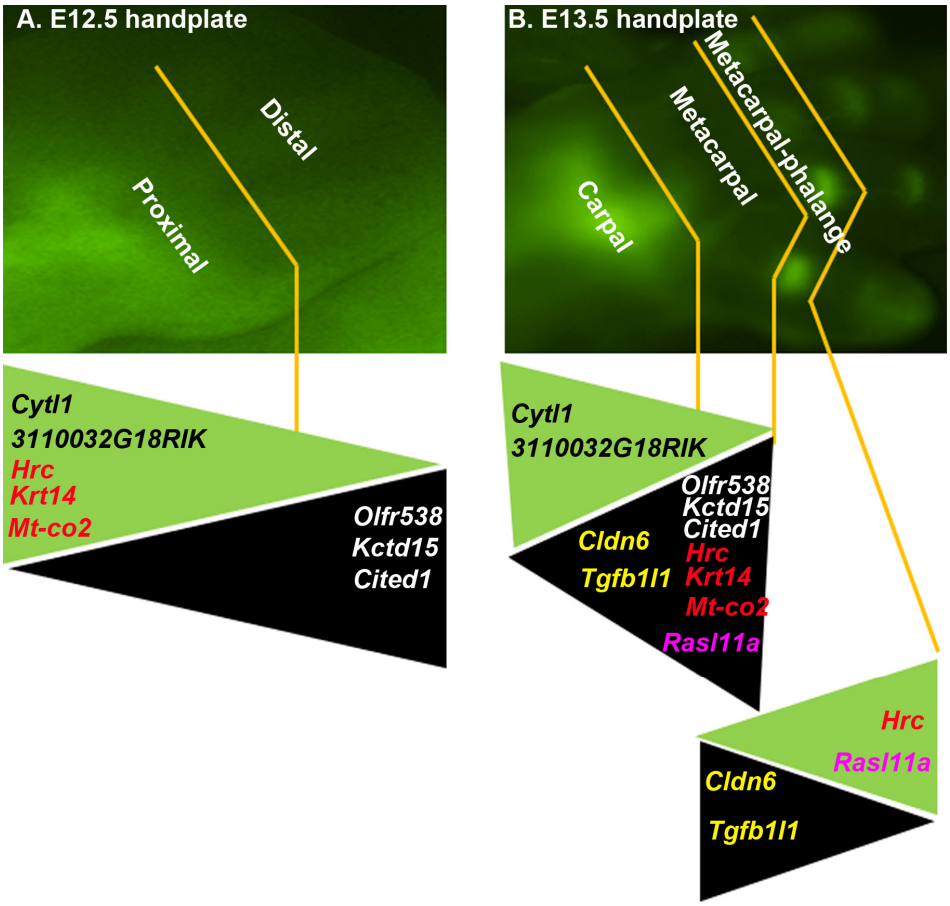
## 3. Experimental Section

### *3.1. Animals*

Animal study was approved by the Institutional Animal Care and Use Committee of Tulane University (Protocol# 4040R, approved on 17 January 2011, valid through 16 January 2014). The *Dcx-EGFP* mice with a strain name of Tg (*Dcx-EGFP*) BJ224Gsat/Mmmh were obtained from the Mutant Mouse Regional Resource Center, University of Missouri, which were characterized previously [9]. Enhanced

green fluorescence protein (eGFP) was expressed in *Dcx*-expressing cells in these mice. E12.5 and E13.5 mouse embryos were obtained through timed pregnancies. Images of mouse handplates were taken with an epifluorescence microscope (Nikon AZ100) equipped with a digital camera (Nikon DS-Qi1Mc) and NIS-Elements Basic 3.0 software (Nikon Instruments Inc., Melville, NY, USA). The handplates were dissected into different regions under the epifluorescence microscope, using VANNAS microdissecting spring scissors (Roboz Surgical, Gaithersburg, MD, USA). Approximately 16 handplates from 8 embryos of a single pregnant mouse each at E12.5 and E13.5 were collected and pooled.

**Figure 2.** Comparison analysis of gene expression patterns between different regions. (**A**) E12.5 mouse handplate (original magnification, 6×); (**B**) E13.5 mouse handplate (original magnification, 1.3×). Selected genes are shown with their gene symbols color-coded and the ones with the same color are in comparison between the different regions. The genes are laid on colored triangles, the base of each triangle indicating higher levels of gene expression with the tip indicating lower levels of gene expression; green triangles indicate higher levels of gene expression in the DCX-eGFP-positive regions, whereas black triangles indicate higher levels of gene expression in the DCX-eGFP-negative regions.

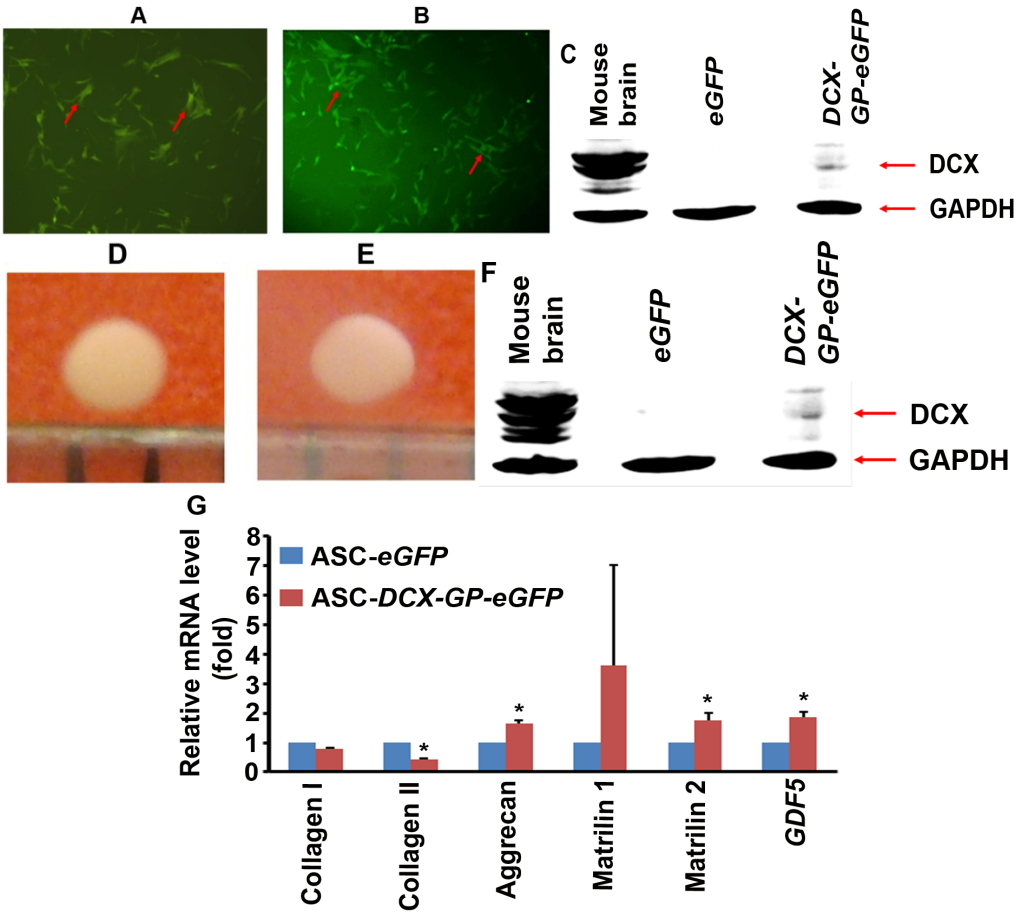



### *3.2. RNA Extraction and Microarray*

The dissected mouse embryonic tissues were homogenized and total RNA was extracted using RNeasy Mini Kit (QIAGEN, Valencia, CA, USA) with DNase I digestion to avoid genomic DNA contamination. RNA was dissolved in DNase/RNase-free water, quantified by a NanoDrop instrument

(NanoDrop Products, part of Thermo Fisher Scientific, Wilmington, DE, USA) and set at a concentration of ~1.0 μg/μL. The quality of the RNA was confirmed by Agilent 2100 Bioanalyzer (Agilent Technologies, Palo Alto, CA, USA). Two hundred ng of RNA were used to make biotinylated cRNA using the Illumina TotalPrep RNA Amplification Kit (Ambion, Austin, TX, USA), and hybridized to the Illumina chips for 14 h at 58 °C. After washing and staining, the arrays were scanned with the BeadArray Reader (Illumina Inc., San Diego, CA, USA) and analyzed with the GenomeStudio software (Illumina Inc.) as described previously [27]. All microarray analysis was done at the LCRC Genomics Facility in New Orleans, LA, USA.

**Figure 3.** The effects of *DCX* expression on chondrocyte differentiation of human ASCs in pellet cultures. (**A**) and (**B**) Human ASCs transduced with HRST-*eGFP* (**A**) and HRST-*DCX-GP-eGFP* (**B**) lentiviruses and sorted by flow cytometry; arrows indicate eGFP-positive cells; original magnification, 200×; (**C**) Western blot analysis of the sorted human ASCs; mouse brain serves as a positive control; (**D**) and (**E**) Representative photomicrographs of the cartilage-like tissues derived from HRST-*eGFP*-transduced ASCs (**D**) and HRST-*DCX-GP-eGFP*-transduced ASCs (**E**); (**F**) Western blot analysis of the proteins extracted from the cartilage-like tissues; (**G**) qRT-PCR analysis of gene expression in the cartilage-like tissues. Data represent mean ± SD (error bars) of three independent experiments; the difference between the ASC-*eGFP* and ASC-*DCX-GP-eGFP* groups was statistically significant (* $p < 0.05$).



### *3.3. Microarray Data Analysis*

After subtracting the background, the samples were normalized using the "cubic spline" algorithm assuming a similar distribution of transcript abundance in all the samples. Gene expression levels were compared to select only those genes with >2-fold differences (up or down-regulated) between the samples in comparison. All sequence data were assigned a gene ID corresponding to the Gene Symbol from the National Center for Biotechnology Information (NCBI) gene database [28]. These genes were then researched using both the NCBI database and the UniProt Protein Knowledgebase database [29] to annotate the corresponding protein function.

### *3.4. Cultures of Human Adipose Tissue-Derived Mesenchymal Stromal/Stem Cells*

Human adipose tissue-derived mesenchymal stromal/stem cells (MSCs), also called adipose stem cells (ASCs), were collected at the Pennington Biomedical Research Center (Baton Rouge, LA, USA) with approval of the Institutional Review Board and all human participants provided written informed consent (PBRC #23040) as previously described [30,31]. The ASCs were provided to the researchers as de-identified materials. The ASCs were cultured in α-minimum essential medium (α-MEM, Mediatech Inc., Herndon, VA, USA) with 20% fetal bovine serum (FBS, Bio-West, Rosenberg, TX, USA) and 1% L-glutamine in a 37 °C, 5% $CO_2$ humidified incubator.

### *3.5. Transduction of Human ASCs*

HRST-eGFP lentiviral expression vector was derived from the original pHR' CMV-lacZ vector [32], which expresses eGFP. Full-length human *DCX* cDNA was subcloned into HRST-*eGFP* vector through BamHI and XhoI sites, upstream to *eGFP*, thus, constructing HRST-*DCX-GP-eGFP* vector. GP stands for glycine and proline within a consensus peptide sequence that automatically self-cleaves to separate DCX and eGFP proteins once *DCX-GP-eGFP* gene was translated based on a previous study [33]. HRST-*eGFP* and HRST-*DCX-GP-eGFP* plasmids were individually packaged into replication-incompetent lentiviruses in 293T cells by co-transfection with packaging plasmids as described previously [34]. The packaging plasmids were pHDM-Hgpm2 (HIV gag-pol expression plasmid), pRC/CMV-Rev 1b (Accessory protein rev), pHDM-Tat 1b (Accessory protein tat), and pHDM.G (env, VSVG pseudotype). Human ASCs (within the first three passages following initial plating) were transduced with either HRST-eGFP or HRST-DCX-GP-eGFP lentiviruses for 16 h, and then thoroughly rinsed with phosphate-buffered saline (PBS) and cultured in complete medium. Forty-eight hours after transduction, the cells were harvested and eGFP-positive cells were sorted with a flow cytometry cell sorter (BD FACSAria, BD Biosciences, San Jose, CA, USA).

### *3.6. Pellet Culture*

Approximately 200,000 eGFP+ or DCX-GP-eGFP+ ASCs were centrifuged in 15-mL conical polypropylene centrifuge tubes [13]. The cell pellets were cultured in chondrogenic media, that is, Dulbecco's modified Eagle's medium (DMEM) supplemented with 10 ng/mL BMP-7 (R&D Systems, Minneapolis, MN, USA), ITS solution (BD Biosciences, San Jose, CA, USA), 50 μg/mL 2-phospho-L-ascorbic acid trisodium salt (Sigma-Aldrich, St. Louis, MO, USA), 100 μg/mL sodium

pyruvate (Invitrogen, Carlsbad, CA, USA), 100 nM dexamethasone (Sigma-Aldrich), 0.1% bovine serum albumin (Sigma-Aldrich). The medium was replaced every 3 days during 14 days of pellet culture.

### *3.7. Real-Time Quantitative Reverse Transcriptase PCR (qRT-PCR)*

Pellets were homogenized and total RNA was extracted using RNeasy Mini Kit (QIAGEN, Valencia, CA, USA) with DNase I digestion to avoid genomic DNA contamination. cDNA was made from total RNA using iScript™ cDNA Synthesis Kit (Bio-Rad Laboratories, Hercules, CA, USA). PCR primers for human collagen I, collagen II, aggrecan, superficial zone protein (*SZP*), matrilin 1, matrilin 2, *GDF5*, and glyceraldehyde-3-phosphate dehydrogenase (*GAPDH*) were obtained from Eurofins MWG Operon (Huntsville, AL, USA) (Table 6). qRT-PCR was done in triplicates with an iQ5® iCycler and iQ™ SYBR® Green Supermix (Bio-Rad Laboratories, Hercules, CA, USA) following the recommended protocols. Results were normalized to *GAPDH* levels using the formula $\Delta C_t$ (Cycle threshold) = $C_t$ of target gene − $C_t$ of *GAPDH*. The mRNA level of the ASCs transduced with HRST-eGFP lentiviruses was used as the baseline; therefore, $\Delta\Delta C_t$ was calculated using the formula $\Delta\Delta C_t = \Delta C_t$ of the target gene − $\Delta C_t$ of the baseline. The fold change of mRNA level was calculated as fold = $2^{-\Delta\Delta Ct}$ [35]. Three independent experiments were conducted and data represent mean ± SD (error bars) of 3 independent experiments.

**Table 6.** Nucleotide sequences of each PCR primer pair.

| Gene | Primer | Nucleotide Sequence (5' to 3') |
|---|---|---|
| *Collagen I* | sense | CACCAATCACCTGCGTACAGAA |
| | antisense | ACAGATCACGTCATCGCACAAC |
| *Collagen II* | sense | GGCAATAGCAGGTTCACGTACA |
| | antisense | CGATAACAGTCTTGCCCCACTT |
| *Aggrecan (core protein)* | sense | AAGTATCATCAGTCCCAGAATCTAGCA |
| | antisense | CGTGGAATGCAGAGGTGGTT |
| *SZP* | sense | TTGCGCAATGGGACATTAGTT |
| | antisense | AGCTGGAGATGGTGGACTGAA |
| *Matrilin 1* | sense | AGGGACTGCGTTTGCATTTTT |
| | antisense | TCAGTAAAGAAATTCACAGCACTCAGA |
| *Matrilin 2* | sense | GACGGACGGGCTCAGGAT |
| | antisense | GATACCATTGGCCTTGGCTTTA |
| *GDF5* | sense | ATTTGTGCCTGGTGACTTCC |
| | antisense | AGCCCTCTCCTCTTCTCTCC |
| *GAPDH* | sense | TAAAAGCAGCCCTGGTGACC |
| | antisense | CCACATCGCTCAGACACCAT |

### *3.8. Western Blot Analysis*

Human ASCs (after flow cytometry sorting) and homogenates of the ASCs pellets were lysed with lysis buffer (50 mM sodium fluoride, 0.5% Igepal CA-630 (NP-40), 10 mM sodium phosphate, 150 mM sodium chloride, 25 mM Tris pH 8.0, 1 mM phenylmethylsulfonyl fluoride, 2 mM ethylenediaminetetraacetic acid (EDTA), 1.2 mM sodium vanadate) supplemented with protease

inhibitor cocktail (Sigma-Aldrich, St. Louis, MO, USA). Equal amount of proteins was subjected to 10% SDS-polyacrylamide gel electrophoresis and transferred to polyvinylidene difluoride membrane. Protein extract from mouse brain tissues was used as a positive control for DCX protein [36]. The membranes were blocked with 5% nonfat dry milk in TBST buffer (25 mM Tris-HCl, 125 mM NaCl, 0.1% Tween 20) for 2 h and incubated with goat anti-DCX antibodies (sc-8066, Santa Cruz Biotechnology, Santa Cruz, CA, USA) overnight and then IRDye®800CW-conjugated donkey anti-goat secondary antibodies (LI-COR Biosciences, Lincoln, NE, USA) for 1 h. The results were visualized by using an Odyssey Infrared Imager (LI-COR Biosciences, Lincoln, NE, USA). For loading control, the membranes were also probed for GAPDH using mouse anti-GAPDH antibodies (MAB374, Millipore Corporation, Billerica, MA, USA).

### *3.9. Statistical Analysis*

Student's *t*-test (two-tailed) was used to analyze the qRT-PCR data and $p$-value $<0.05$ was considered statistically significant.

## 4. Conclusions

The present study used *DCX* promoter-driven *eGFP* expression as a guide to dissect different regions of E12.5 and E13.5 mouse embryonic handplates. Microarray analysis of gene expression profiles identified a variety of genes that were expressed differentially in the different regions of mouse handplate *in vivo*. The unique expression patterns of several genes, e.g., *Cytl1*, are intriguing targets for further investigation. The *in vitro* experiments showed that DCX affected expression of several genes associated with chondrocyte phenotype, such as collagen II, aggrecan, matrilin 2, and *GDF5*. These findings imply that *DCX* may play a role in driving differentiation of articular chondrocyte phenotype, which awaits future studies for further clarification.

## Acknowledgments

This work was partially supported by a National Natural Science Foundation of China (NSFC#81201394: The mechanism of the effect and regulation from the dynamic expression of doublecortin on bone fracture healing, to Q.-S.Z). Z.Y. was partially supported by two grants from the National Institute of General Medical Sciences (P20GM103518) and the National Cancer Institute (R01CA174714) of the National Institutes of Health, four grants from Department of Defense (W81XWH-10-1-0937, W81XWH-14-1-0050, PC131448, and PC130118), the Developmental Fund of Tulane Cancer Center (TCC), Tulane University School of Medicine Pilot Fund, and Louisiana Cancer Research Consortium (LCRC) Fund. J.Z. was partially funded by the Louisiana Cancer Research Consortium and by a grant of the National Institute of General Medical Sciences (P20GM103501). S.E.B was partially funded by the base grant to the Tulane National Primate Research Center (2P51RR000164-52). The content of this article is solely the responsibility of the authors and does not necessarily represent the official views of the National Institutes of Health. TCC/LCRC Flow Cytometry Core Facility was used in this study.

## Author Contributions

D.G. did the pellet culture and isolated RNA from mouse embryos; Q.-S.Z participated in study design, animal husbandry, and manuscript preparation; J.Z. did Illumina microarray analysis; Q.Z. participated in animal husbandry and taking photos of mouse embryos; S.L. did Western blot analysis; B.R. annotated the microarray data; B.A.B. provided human ASCs and participated in study design; S.E.B. constructed the lentiviral vectors; M.J.O. and F.H.S. participated in study design; Z.Y. participated in study design, data analysis, and manuscript preparation. All authors contributed to manuscript preparation, agreed to be listed, and approved the submitted version of the manuscript.

## Conflicts of Interest

The authors declare no conflict of interest.

## References

1. Singh, G.; Miller, J.D.; Lee, F.H.; Pettitt, D.; Russell, M.W. Prevalence of cardiovascular disease risk factors among US adults with self-reported osteoarthritis: Data from the third national health and nutrition examination survey. *Am. J. Manag. Care* **2002**, *8*, S383–S391.
2. Tuan, R.S. Stemming cartilage degeneration: Adult mesenchymal stem cells as a cell source for articular cartilage tissue engineering. *Arthritis Rheumatol.* **2006**, *54*, 3075–3078.
3. Yamane, S.; Cheng, E.; You, Z.; Reddi, A.H. Gene expression profiling of mouse articular and growth plate cartilage. *Tissue Eng.* **2007**, *13*, 2163–2173.
4. Muneoka, K.; Bryant, S.V. Evidence that patterning mechanisms in developing and regenerating limbs are the same. *Nature* **1982**, *298*, 369–371.
5. Reddi, A.H. Cartilage-derived morphogenetic proteins and cartilage morphogenesis. *Microsc. Res. Tech.* **1998**, *43*, 131–136.
6. Martin, P. Tissue patterning in the developing mouse limb. *Int. J. Dev. Biol.* **1990**, *34*, 323–336.
7. Mitrovic, D. Development of the diarthrodial joints in the rat embryo. *Am. J. Anat.* **1978**, *151*, 475–485.
8. Koyama, E.; Shibukawa, Y.; Nagayama, M.; Sugito, H.; Young, B.; Yuasa, T.; Okabe, T.; Ochiai, T.; Kamiya, N.; Rountree, R.B.; *et al.* A distinct cohort of progenitor cells participates in synovial joint and articular cartilage formation during mouse limb skeletogenesis. *Dev. Biol.* **2008**, *316*, 62–73.
9. Zhang, Q.; Cigan, A.D.; Marrero, L.; Lopreore, C.; Liu, S.; Ge, D.; Savoie, F.H.; You, Z. Expression of doublecortin reveals articular chondrocyte lineage in mouse embryonic limbs. *Genesis* **2011**, *49*, 75–82.
10. Bai, J.; Ramos, R.L.; Ackman, J.B.; Thomas, A.M.; Lee, R.V.; LoTurco, J.J. RNAi reveals doublecortin is required for radial migration in rat neocortex. *Nat. Neurosci.* **2003**, *6*, 1277–1283.
11. Gleeson, J.G.; Allen, K.M.; Fox, J.W.; Lamperti, E.D.; Berkovic, S.; Scheffer, I.; Cooper, E.C.; Dobyns, W.B.; Minnerath, S.R.; Ross, M.E.; *et al.* Doublecortin, a brain-specific gene mutated in human X-linked lissencephaly and double cortex syndrome, encodes a putative signaling protein. *Cell* **1998**, *92*, 63–72.

12. Des Portes, V.; Francis, F.; Pinard, J.M.; Desguerre, I.; Moutard, M.L.; Snoeck, I.; Meiners, L.C.; Capron, F.; Cusmai, R.; Ricci, S.; *et al.* Doublecortin is the major gene causing X-linked subcortical laminar heterotopia (SCLH). *Hum. Mol. Genet.* **1998**, *7*, 1063–1070.
13. Zhang, Y.; Ryan, J.A.; di Cesare, P.E.; Liu, J.; Walsh, C.A.; You, Z. Doublecortin is expressed in articular chondrocytes. *Biochem. Biophys. Res. Commun.* **2007**, *363*, 694–700.
14. Chen, L.; Qanie, D.; Jafari, A.; Taipaleenmaki, H.; Jensen, C.H.; Saamanen, A.M.; Sanz, M.L.; Laborda, J.; Abdallah, B.M.; Kassem, M. Delta-like 1/fetal antigen-1 (Dlk1/FA1) is a novel regulator of chondrogenic cell differentiation via inhibition of the Akt kinase-dependent pathway. *J. Biol. Chem.* **2011**, *286*, 32140–32149.
15. Kim, J.S.; Ryoo, Z.Y.; Chun, J.S. Cytokine-like 1 (*Cytl1*) regulates the chondrogenesis of mesenchymal cells. *J. Biol. Chem.* **2007**, *282*, 29359–29367.
16. Jeon, J.; Oh, H.; Lee, G.; Ryu, J.H.; Rhee, J.; Kim, J.H.; Chung, K.H.; Song, W.K.; Chun, C.H.; Chun, J.S. Cytokine-like 1 knock-out mice (*Cytl1*−/−) show normal cartilage and bone development but exhibit augmented osteoarthritic cartilage destruction. *J. Biol. Chem.* **2011**, *286*, 27206–27213.
17. Leussink, B.; Brouwer, A.; el Khattabi, M.; Poelmann, R.E.; Gittenberger-de Groot, A.C.; Meijlink, F. Expression patterns of the paired-related homeobox genes MHox/Prx1 and S8/Prx2 suggest roles in development of the heart and the forebrain. *Mech. Dev.* **1995**, *52*, 51–64.
18. Minogue, B.M.; Richardson, S.M.; Zeef, L.A.; Freemont, A.J.; Hoyland, J.A. Characterization of the human nucleus pulposus cell phenotype and evaluation of novel marker gene expression to define adult stem cell differentiation. *Arthritis Rheumatol.* **2010**, *62*, 3695–3705.
19. Liu, S.; Zhang, E.; Yang, M.; Lu, L. Overexpression of Wnt11 promotes chondrogenic differentiation of bone marrow-derived mesenchymal stem cells in synergism with TGF-β. *Mol. Cell. Biochem.* **2014**, *390*, 123–131.
20. Zanotti, S.; Canalis, E. Notch suppresses nuclear factor of activated T cells (NFAT) transactivation and Nfatc1 expression in chondrocytes. *Endocrinology* **2013**, *154*, 762–772.
21. Yamagami, T.; Molotkov, A.; Zhou, C.J. Canonical Wnt signaling activity during synovial joint development. *J. Mol. Histol.* **2009**, *40*, 311–316.
22. Pitsillides, A.A.; Beier, F. Cartilage biology in osteoarthritis—Lessons from developmental biology. *Nat. Rev. Rheumatol.* **2011**, *7*, 654–663.
23. James, C.G.; Appleton, C.T.; Ulici, V.; Underhill, T.M.; Beier, F. Microarray analyses of gene expression during chondrocyte differentiation identifies novel regulators of hypertrophy. *Mol. Biol. Cell.* **2005**, *16*, 5316–5333.
24. Klatt, A.R.; Paulsson, M.; Wagener, R. Expression of matrilins during maturation of mouse skeletal tissues. *Matrix Biol.* **2002**, *21*, 289–296.
25. Segat, D.; Frie, C.; Nitsche, P.D.; Klatt, A.R.; Piecha, D.; Korpos, E.; Deak, F.; Wagener, R.; Paulsson, M.; Smyth, N. Expression of matrilin-1, -2 and -3 in developing mouse limbs and heart. *Matrix Biol.* **2000**, *19*, 649–655.
26. Craft, A.M.; Ahmed, N.; Rockel, J.S.; Baht, G.S.; Alman, B.A.; Kandel, R.A.; Grigoriadis, A.E.; Keller, G.M. Specification of chondrocytes and cartilage tissues from embryonic stem cells. *Development* **2013**, *140*, 2597–2610.

27. Kim, S.H.; Sierra, R.A.; McGee, D.J.; Zabaleta, J. Transcriptional profiling of gastric epithelial cells infected with wild type or arginase-deficient Helicobacter pylori. *BMC Microbiol.* **2012**, *12*, 175.
28. National Center for Biotechnology Information (NCBI) Gene Database. Available online: http://www.ncbi.nlm.nih.gov/ (accessed on 16 April 2014).
29. UniProt Protein Knowledgebase Database. Available online: http://www.uniprot.org/ (accessed on 16 April 2014).
30. Yu, G.; Wu, X.; Dietrich, M.A.; Polk, P.; Scott, L.K.; Ptitsyn, A.A.; Gimble, J.M. Yield and characterization of subcutaneous human adipose-derived stem cells by flow cytometric and adipogenic mRNA analyzes. *Cytotherapy* **2010**, *12*, 538–546.
31. Strong, A.L.; Strong, T.A.; Rhodes, L.V.; Semon, J.A.; Zhang, X.; Shi, Z.; Zhang, S.; Gimble, J.M.; Burow, M.E.; Bunnell, B.A. Obesity associated alterations in the biology of adipose stem cells mediate enhanced tumorigenesis by estrogen dependent pathways. *Breast Cancer Res.* **2013**, *15*, R102.
32. Naldini, L.; Blomer, U.; Gallay, P.; Ory, D.; Mulligan, R.; Gage, F.H.; Verma, I.M.; Trono, D. *In vivo* gene delivery and stable transduction of nondividing cells by a lentiviral vector. *Science* **1996**, *272*, 263–267.
33. Szymczak, A.L.; Workman, C.J.; Wang, Y.; Vignali, K.M.; Dilioglou, S.; Vanin, E.F.; Vignali, D.A. Correction of multi-gene deficiency *in vivo* using a single 'self-cleaving' 2A peptide-based retroviral vector. *Nat. Biotechnol.* **2004**, *22*, 589–594.
34. Mostoslavsky, G.; Kotton, D.N.; Fabian, A.J.; Gray, J.T.; Lee, J.S.; Mulligan, R.C. Efficiency of transduction of highly purified murine hematopoietic stem cells by lentiviral and oncoretroviral vectors under conditions of minimal *in vitro* manipulation. *Mol. Ther.* **2005**, *11*, 932–940.
35. Ge, D.; Dauchy, R.T.; Liu, S.; Zhang, Q.; Mao, L.; Dauchy, E.M.; Blask, D.E.; Hill, S.M.; Rowan, B.G.; Brainard, G.C.; *et al.* Insulin and IGF1 enhance IL-17-induced chemokine expression through a GSK3B-dependent mechanism: a new target for melatonin's anti-inflammatory action. *J. Pineal Res.* **2013**, *55*, 377–387.
36. Corbo, J.C.; Deuel, T.A.; Long, J.M.; LaPorte, P.; Tsai, E.; Wynshaw-Boris, A.; Walsh, C.A. Doublecortin is required in mice for lamination of the hippocampus but not the neocortex. *J. Neurosci.* **2002**, *22*, 7548–7557.

© 2014 by the authors; licensee MDPI, Basel, Switzerland. This article is an open access article distributed under the terms and conditions of the Creative Commons Attribution license (http://creativecommons.org/licenses/by/3.0/).

*Am J Physiol Lung Cell Mol Physiol* 307: L497–L508, 2014.
First published July 18, 2014; doi:10.1152/ajplung.00125.2014.

# Promotion of lung tumor growth by interleukin-17

**Beibei Xu,[1] James F. Guenther,[1] Derek A. Pociask,[6] Yu Wang,[1] Jay K. Kolls,[6] Zongbing You,[4] Bysani Chandrasekar,[5] Bin Shan,[3] Deborah E. Sullivan,[2] and Gilbert F. Morris[1]**

[1]*Department of Pathology and Laboratory Medicine, Tulane University, New Orleans, Louisiana;* [2]*Department of Microbiology, Tulane University, New Orleans, Louisiana;* [3]*Department of Medicine-Pulmonary Section, Tulane University, New Orleans, Louisiana;* [4]*Department of Structural and Cellular Biology, Tulane University, New Orleans, Louisiana;* [5]*Heart and Vascular Insitute, Tulane University, New Orleans, Louisiana; and* [6]*Children's Hospital of Pittsburgh, University of Pittsburgh, Pittsburgh, Pennsylvania*

Submitted 7 May 2014; accepted in final form 12 July 2014

**Xu B, Guenther JF, Pociask DA, Wang Y, Kolls JK, You Z, Chandrasekar B, Shan B, Sullivan DE, Morris GF.** Promotion of lung tumor growth by interleukin-17. *Am J Physiol Lung Cell Mol Physiol* 307: L497–L508, 2014. First published July 18, 2014; doi:10.1152/ajplung.00125.2014.—Recent findings demonstrate that inhaled cigarette smoke, the predominant lung carcinogen, elicits a T helper 17 (Th17) inflammatory phenotype. Interleukin-17A (IL-17), the hallmark cytokine of Th17 inflammation, displays pro- and antitumorigenic properties in a manner that varies according to tumor type and assay system. To investigate the role of IL-17 in lung tumor growth, we used an autochthonous tumor model (*K-Ras$^{LA1}$* mice) with lung delivery of a recombinant adenovirus that expresses IL-17A. Virus-mediated expression of IL-17A in *K-Ras$^{LA1}$* mice at 8–10 wk of age doubled lung tumor growth in 3 wk relative to littermates that received a green fluorescent protein-expressing control adenovirus. IL-17 induced matrix metalloproteinase-9 (MMP-9) expression in vivo and in vitro. In accord with this finding, selective and specific inhibitors of MMP-9 repressed the increased motility and invasiveness of IL-17-treated lung tumor cells in culture. Knockdown or mutation of p53 promoted the motility of murine lung tumor cells and abrogated the promigratory role of IL-17. Coexpression of siRNA-resistant wild-type, but not mutant, human p53 rescued both IL-17-mediated migration and MMP-9 mRNA induction in p53 knockdown lung tumor cells. IL-17 increased MMP-9 mRNA stability by reducing interaction with the mRNA destabilizing serine/arginine-rich splicing factor 1 (SRSF1). Taken together, our results indicate that IL-17 stimulates lung tumor growth and regulates MMP-9 mRNA levels in a p53- and SRSF1-dependent manner.

IL-17; MMP-9; p53; SRSF1; lung tumor growth

THE INTERLEUKIN-17 FAMILY consists of six members, IL-17A to IL-17F. Although the family members are structurally related, they originate from different cell types and have diverse biological functions (28). IL-17 family members bind to a family of IL-17 receptors (IL-17 receptor A to E) that form hetero- and homodimers with bound ligand to activate downstream signaling (14). Because these IL-17 receptor family members have different ligand-binding specificities and variable tissue distributions, the IL-17 cytokine family associates with multiple inflammatory responses. IL-17A, commonly called IL-17, is the first identified and by far the most well-studied IL-17 family member. T helper 17 (Th17) cells are the primary source of IL-17A and homologous family member IL-17F (56). In both humans and mice, IL-17A and IL-17F bind and activate a heterodimeric receptor formed by IL-17RA and IL-17RC (24, 30). IL-17RA is expressed ubiquitously, whereas IL-17RC is mainly expressed in epithelial cells and fibroblasts (47).

Clinical findings with cancers of the stomach (78), prostate (59), colon (34), and lung (38) demonstrate that elevated levels of IL-17 correlate with a worse prognosis. However, in experimental models, the role of IL-17 in tumor growth depends on context. In many models, particularly in immunodeficient mice, IL-17 promotes tumorigenesis, and enhanced angiogenesis appears to account, in large part, for this protumorigenic effect (52). However, in immunocompetent mice, IL-17 impairs growth of tumor allografts by stimulating antitumor immunity (29, 42). A possible explanation for these disparate findings is that tumor graft models are inadequate in testing the effect of IL-17 in tumorigenesis. In autochthonous models of prostate and lung cancer in immunocompetent mice, IL-17 deficiency impairs tumor growth (3, 79). In an autochthonous model of pancreatic cancer, IL-17 overexpression accelerates tumorigenesis (44).

In lung cancer, dissection of the inflammatory response to lung carcinogens could be used to identify specific inflammatory mediators that promote lung tumor progression. In support of this view, lung inflammation induced by cigarette smoke accelerates progression of lung adenocarcinoma in mice (69). Since cigarette smoke elicits Th17 inflammation (4, 61), tumors arising in the lung must adapt to this inflammatory phenotype. This observation prompted us to determine the consequence of overexpression of IL-17A, the prototypical Th17 cytokine, on progression of mutant *K-Ras*-driven lung adenocarcinoma.

## MATERIALS AND METHODS

*Animal model. K-Ras$^{LA1}$* mice in the C57BL/6 background were provided by Dr. Tyler Jacks through the National Cancer Institute Mouse Repository. Mice were maintained under pathogen-free conditions and experimental protocols were approved by the Tulane University Institutional Animal Care and Use Committee following guidelines of the Association for Assessment and Accreditation of Laboratory Animal Care.

*Plasmids.* Plasmids pCMV-p53-wt (60) and pCMV-p53-R175H express the wild-type human p53 and dominant negative R175H mutant human p53, respectively, from the CMV promoter. The pCMV-p53-R175H plasmid was constructed by digesting the SPC-p53-R175H plasmid (49) with *Bam*HI and adding *Eco*RI linkers after filling in the restricted DNA. After digestion with *Hind*III, the R175H mutant p53 cDNA was subcloned into the pCMV12S.FS plasmid (50) at the *Eco*RI-*Hind*III sites after removal of the EIA cDNA insert.

*Adenovirus administration to mice and assessment of tumor progression.* Lung tumor-bearing *K-Ras$^{LA1}$* mice 8–10 wk of age were anesthetized with isoflurane before being administered $1\times10^8$

Address for reprint requests and other correspondence: G. F. Morris, Dept. of Pathology and Laboratory Medicine, SL-79, Tulane Univ. Medical Center, 1430 Tulane Ave., New Orleans, LA 70112 (e-mail: gmorris2@tulane.edu).

 1040-0605/14 Copyright © 2014 the American Physiological Society 

pfu IL-17-expressing recombinant adenovirus [AdV-IL-17 (58)] by oropharyngeal aspiration (32). Control *K-Ras$^{LA1}$* mice received an identical amount of GFP-expressing adenovirus [AdV-GFP (13)]. Three weeks after treatment the mice were euthanized and the lungs were inflated by perfusion with 10% formalin at 30 cm pressure for 20 min before removal. After overnight fixation, the number of lung tumors on the pleural surface was quantified without knowledge of the sample identity. Tissue sections prepared from paraffin-embedded lung tissue were stained with hematoxylin and eosin (H&E) before evaluation of tumor burden. The tumor burden [defined as the ratio of hyperplastic lesion area to total lung section area on H&E-stained sections (27)] was quantified with an Aperio ScanScope slide scanner.

*Cell culture.* mK-Ras-LE cells, a murine lung cancer epithelial cell line, were established from a lung tumor-bearing *K-Ras$^{LA1}$* mouse (35). The mK-Ras-LE cells form tumors in syngeneic mice and express the lung epithelial cell markers surfactant protein C and E-cadherin but fail to express Clara cell secretory protein or N-cadherin (data not shown). mK-Ras-R172H-LE cells were established from a lung tumor-bearing *K-Ras$^{LA1}$* mouse that was also heterozygous for a R172H knockin mutation of p53 (33). The line had been backcrossed to the C57BL/6 inbred strain for more than 10 generations before the cells were prepared. The mK-Ras-R172H-LE cells are positive for SPC and cytokeratin but negative for E-cadherin and slightly positive for vimentin (our unpublished observation). Both cell lines were cultured in RPMI medium with 10% FBS and 1% penicillin-streptomycin (complete medium) at 37°C with 5% $CO_2$ (35).

*Immunohistochemistry.* Immunohistochemistry was performed as described (17) with some modifications. Lung tissue sections were blocked in PBS with 3% BSA overnight at 4°C before incubation overnight at 4°C with the primary antibody against matrix metalloproteinase-9 (MMP-9; 1:200 dilution) (NBP1–57940; Novus Biologicals, Littleton, CO) diluted in PBS with 3% BSA. The negative control tissue sections were incubated with normal rabbit serum replacing the primary antibody diluted to the same concentration. After one washing with 3% BSA in PBS, the sections were incubated with biotin-conjugated donkey anti-rabbit secondary antibody (1:2,500 dilution) (711-065-152; Jackson ImmunoResearch Laboratories, West Grove, PA) for 1 h at room temperature. After three washes with 3% BSA in PBS, the sections were incubated with streptavidin-conjugated horseradish peroxidase (1:2,000 dilution) (016-030-084; Jackson ImmunoResearch Laboratories) in the same solution for 1 h at room temperature. Visualization with diaminobenzidine and counterstaining were as previously described (17).

*Wound healing assay.* Cells were seeded on 12-well plates with RPMI complete medium. When the cells reached about 80% confluence, the medium was replaced with serum-free RPMI followed by overnight incubation. Then a single artificial wound was made by scratching the center of the monolayer of cells with a 200-μl pipet tip at *time 0*. After wounding, the cells were washed with PBS to remove detached cells and fresh serum-free RPMI was added containing increasing concentrations of mouse IL-17. During the postwounding period, images within the same area of the scratches were taken with a phase-contrast microscope. Ten measurements of wound width were taken for each scratch and were averaged. Percent of wound closure was calculated as the distance (μm) the cells migrated relative to the initial scratch width. In some experiments, a selective inhibitor of MMP-9 or an antibody to MMP-9 was added simultaneously with IL-17. The MMP-9 selective inhibitor (MMP-9 Inhibitor I, CAS 1177749-58-4, Millipore, Billerica, MA) was added at the dose of 10 nM. The MMP-9 antibody (AB19016; Millipore) was added at the dose of 12 μg/ml to inhibit MMP-9 and the same amount of rabbit IgG was used as the negative control. In the migration assay using cells infected with recombinant adenovirus expressing reversion-inducing-cysteine-rich protein with kazal motifs [AdV-RECK (63), a cellular repressor of metalloproteinases, including MMP-9 (2)], or AdV-GFP, cells were infected (MOI = 10) for 24 h before wounding and addition of IL-17. For the migration assays with p53 knockdown experiments, cells growing in 1 ml RPMI containing 10% FBS in 24-well plate were transfected with 5 pm siRNA using Lipofectamine diluted in 50 μl Opti-MEM according to the supplier's (Invitrogen) specifications. For the p53 knockdown-restoration experiments, cells growing in 1 ml RPMI containing 10% FBS in 24-well plate were transfected with 5 pm siRNA plus 150 ng pCMV-p53-wt plasmid or pCMV-p53-R175H plasmid using Lipofectamine diluted in 50 μl Opti-MEM according to the supplier's (Invitrogen) specifications. The protocol for the wound healing assay in p53 knockdown or knockdown-restoration experiments was the same as in untransfected cells, except the treatment incubation time was 30 h. Silencer Select siRNAs specifically targeting mouse p53 (gene ID: s75472) and Silencer Select Negative Control no. 1 siRNA were purchased from Invitrogen.

*Transwell migration assays.* Cells at about 80% confluence were incubated overnight with serum-free RPMI. The next day, the cells were trypsinized and resuspended in serum-free RPMI before seeding $2.5 \times 10^5$ cells in 200 μl in 24-well Transwell migration inserts (8-μm pore, BD Biosciences, San Jose, CA). Serum-free RPMI with or without 10 ng/ml mouse IL-17 was added to the lower chamber. After 24 h, the cells on the upper surface of the insert were removed by scraping with cotton swabs and the cells that migrated to the lower surface were fixed and stained with the HEMA-3 staining kit (Thermo Fisher Scientific, Waltham, MA). After air drying, the inserts were mounted with Permount on glass slides. At least five random images were taken at ×200 magnification under a light microscope. The number of migrated cells were quantified per image and averaged per well.

*Transwell invasion assays.* The invasion assays were performed with 24-well BD BioCoat Matrigel Invasion Chambers as described by the supplier (BD Biosciences). Briefly, cells were seeded in the inserts coated with growth factor reduced Matrigel at a density of $2.5 \times 10^5$ cells/well in 200 μl serum-free RPMI. RPMI containing 0.5% FBS with or without 10 ng/ml mouse IL-17 was added to the lower chamber. After 48 h, the inserts were stained and photographed as described above and the number of cells that invaded through the Matrigel was quantified as described above.

*RNA quantification.* Total RNA was extracted from cultured cells or mouse lung tissue with TriPure Isolation Reagent (Roche Applied Science, Mannheim, Germany) and purified by use of the RNeasy Mini Kit (Qiagen, Valencia, CA), followed by TURBO DNase treatment (Invitrogen, Carlsbad, CA) as described by the supplier. RNA purity and concentration were measured using a NanoDrop Spectrophotometer (Thermo Scientific). First-strand cDNA was generated by reverse transcription using the *iScript* cDNA Synthesis Kit (Bio-Rad, Hercules, CA). Quantitative PCR of the MMP-9 and β-actin cDNAs was performed with primer sets (MMP-9 forward 5′-CAATCCTTGCAATGTGGATG-3′ and MMP-9 reverse 5′-TAAGGAAGGGGCCCTGTAAT-3′, β-actin forward 5′-TCTACGAGGGCTATGCTCTCC-3′, β-actin reverse 5′-GGATGCCACAGGATTCCATAC-3′) by use of iQ SYBR Green Supermix (Bio-Rad). PCR conditions were 95°C for 3 min, followed by 45 cycles at 95°C for 15 s, 60°C for 30 s, and 72°C for 15 s. After PCR, a melting curve validated the specificity of the amplification. Relative expression of the MMP-9 mRNA was normalized against the internal control mouse β-actin mRNA by the $2^{-\Delta\Delta Ct}$ method (39).

*Cell viability assay.* mK-Ras-LE cells were seeded into 96-well plates in RPMI complete medium for 24 h. Then the complete medium was removed and serum-free RPMI was added followed by incubation overnight. The next day the medium was replaced with serum-free RPMI with increasing concentrations of mouse IL-17. After 48 h, the cell viability was determined by using the MTT Cell Proliferation Assay kit (ATCC, Manassas, VA) according to the manufacturer's protocol.

*Bronchoalveolar lavage.* Bronchoalveolar lavage (BAL) was performed after intubation of mice with a 20-gauge 1.25-in. catheter secured in place with a suture (17). Mice were lavaged with 5 × 0.8 ml of ice-cold lavage buffer (0.137 M sodium chloride, 2.7 mM

potassium chloride, 12 mM phosphate buffer, 0.4 mM EDTA, pH 7.4). After removal of the cells from the first lavage by centrifugation at 1,500 *g* for 5 min, the samples were aliquoted and stored at −70°C. The cells from the first lavage were combined with lavages 2–5 and the collected cell pellet was resuspended in 500 μl of ice-cold lavage buffer. The total cell count was recorded by mixing 10 μl of the resuspended cells 1:1 with Trypan blue (MP Biomedicals, Solon, OH) and counted on a Bright-Line Hemacytometer. Then $5 \times 10^4$ cells were cytospun onto slides by using a Shandon Cytospin 3 at 600 RPM for 3 min. The slides were allowed to dry before staining with Hema 3 (Fisher Scientific, Pittsburgh, PA) followed by dehydration with xylene and mounting with Permount (Fisher Scientific). Differential cell counts were performed on 200 cells on randomly selected fields per sample by an investigator who was unaware sample identity. The first aliquot of BAL fluid was analyzed for IL-17 protein expression with a Mouse IL-17A ELISA kit (BioLegend, San Diego, CA) according to the manufacturer's instruction.

*Gelatin zymography.* MMP-9 levels in cell culture media or BAL fluid from mice was determined by gelatin zymography (55). The samples were loaded on a Novex 10% Zymogram (Gelatin) Gel (Invitrogen). The gel was run at constant voltage (~100 V) at 4°C until the bromophenol blue tracking marker reached the bottom. Then the gel was incubated in 1× Zymogram Renaturing Buffer (2.5% Triton X-100 in water) for 30 min at room temperature with gentle agitation and subsequently incubated in 1× Zymogram Developing Buffer (50 mM Tris, 5 mM $CaCl_2$, 0.2 M NaCl) for another 30 min. The gel was incubated in fresh 1× developing buffer overnight at 37°C for maximum sensitivity. Then the gel was stained with 0.5% Coomassie blue in methanol-acetic acid-water, 50:10:40, for 45 min and destained in the same solution without dye to detect the clear area of protease activity.

*mRNA stability assay.* mK-Ras-LE cells were pretreated in serum-free RPMI with or without 10 ng/ml IL-17 for 2 h. At *time 0* total RNA was prepared from the cells with Tripure (Roche) and RNeasy Mini Kit (Qiagen) as described above then the medium was replaced with fresh serum-free RPMI medium containing 10 μg/ml actinomycin D (Sigma-Aldrich, St. Louis, MO) or the same concentration actinomycin D plus 10 ng/ml IL-17 for 8 h before preparation of total RNA. The abundance of mRNA for MMP-9, β-actin, CXCL-1, and CXCL-2 at *time 0* and 8 h was determined by quantitative RT-PCR (CXCL-1 forward 5′-GGGCGCCTATCGCCAAT-3′, CXCL-1 reverse 5′-ACCTTCAAGCTCTGGA TGTTCTTG-3′; CXCL-2 forward 5′-TGTCAATGCCTGAAGACCCTGCC-3′, CXCL-2 reverse 5′-AACTTTTTGACCGCCC TTGAGA-3′). PCR conditions for CXCL-1 and CXCL-2 were 95°C for 3 min followed by 40 cycles at 95°C for 15 s, 60°C for 1 min.

*siRNA transfection.* Cells growing in 2 ml RPMI containing 10% FBS in a six-well plate were transfected with 30 pm siRNA by using Lipofectamine 2000 transfection reagent (Invitrogen) diluted in 500 μl of Opti-MEM I reduced-serum medium (Invitrogen) according to the manufacturer's recommendations. Silencer Select siRNAs specifically targeting serine/arginine-rich splicing factor 1 (SRSF1) (gene ID: s200965) and Silencer Select Negative Control no. 1 siRNA were purchased from Invitrogen. After 48 h, total cellular RNA was prepared and subjected to quantitative RT-PCR as described above.

*RNA immunoprecipitation.* RNA coimmunoprecipitation assays were performed as described previously with some modifications (19). mK-Ras-LE cells were incubated in serum-free RPMI medium overnight and treated with or without 10 ng/ml IL-17 for another 48 h. After treatment, $4 \times 10^6$ cells were harvested by trypsinization and fixed in PBS solution with 0.1% formalin for 15 min. The fixation procedure was quenched by incubating in 10 ml PBS with 0.25 M glycine (pH 7) for 5 min. Then the cells were washed with PBS and resuspended in 1 ml RIPA buffer (50 mM Tris-Cl pH 8, 150 mM NaCl, 1% Nonidet P-40, 0.5% sodium deoxycholate, 0.1% SDS) containing 1× protease inhibitors (Roche), and sonicated (30% power, 12 s; 40% power, 12 s; 50% power, 5 s twice) with a Branson Sonifier. After removal of insoluble material by centrifugation at 16,000 *g* for 15 min, 1 ml of each cell extract was incubated with 5 μg antibody to SRSF1 (Santa Cruz Biotechnology, Santa Cruz, CA) or the same volume of PBS for 1 h. Then 20 μl BSA preblocked protein A/G Plus-Agarose beads (Santa Cruz) were added and incubated on a rotating incubator overnight at 4°C. The next day, the agarose beads were collected by centrifugation at 3,000 *g*, 4°C for 5 min. After being washed three times with 1 ml RIPA buffer, the beads were resuspended in 200 μl elution buffer (50 mM Tris-Cl pH 7, 5 mM EDTA, 10 mM DTT, 1% SDS) and incubated at 70°C for 1 h to reverse formalin cross-linking. RNA was extracted from the eluate by using TriPure (Roche) reagent according to the manufacturer's protocol. cDNA was prepared as described above. The same volume of each cDNA product (1.5 out of 40 μl) was subjected to quantitative RT-PCR for measuring CXCL-2, β-actin, and MMP-9 mRNA levels as described above.

*Statistical analysis.* Data are presented as means ± SE. Data were analyzed by using Student's *t*-test or Mann-Whitney test when appropriate with GraphPad Prism 5 software. *P* values lower than 0.05 were considered as statistically significant.

## RESULTS

*IL-17 overexpression increases lung tumor growth in K-Ras$^{LA1}$ mice.* To overexpress IL-17 in the lungs of mice we administered an IL-17A-expressing recombinant adenovirus (AdV-IL-17) to 8- to 10-wk-old wild-type mice by oropharyngeal aspiration. This route of delivery produces expression of the transduced gene in epithelial cells throughout the lung (17). For control purposes, an equivalent amount of AdV-GFP was delivered to littermates. One week after virus delivery, a 150-fold increase in IL-17 levels (Fig. 1*A*) and a corresponding fivefold increase in lung neutrophilia (Fig. 1*B*) were detected in the BAL fluid from mice treated with AdV-IL-17 compared with that of the AdV-GFP-treated control group.

To evaluate the effect of IL-17A on lung tumor growth, AdV-IL-17 or an equivalent amount of AdV-GFP was delivered to the lungs of tumor-bearing *K-Ras$^{LA1}$* mice at 8 to 10 wk of age. Three weeks after adenovirus treatment, the number of visible tumors on the pleural surface of AdV-IL-17-treated mice doubled relative to that in AdV-GFP-treated littermates (Fig. 2*A*). *K-Ras$^{LA1}$* littermates that did not receive adenovirus had a comparable number of tumors on the pleural surface relative to that of the AdV-GFP-treated control group. To confirm IL-17-mediated acceleration of lung tumor growth, we used a slide scanner to quantify tumor burden on H&E-stained lung tissue sections from the adenovirus-treated animals. Consistent with quantification of tumors on the pleural surface, tumor burden expressed as the ratio of tumor lesion area to total lung area in H&E-stained tissue sections (27) nearly doubled in *K-Ras$^{LA1}$* mice overexpressing IL-17 (AdV-IL-17) relative to the AdV-GFP control group (Fig. 2*B*). These data confirmed that IL-17 overexpression stimulated a rapid increase in lung tumor growth in vivo over a relatively brief 3-wk period. However, IL-17 failed to stimulate proliferation of serum-starved mutant K-Ras-expressing lung tumor cells [prepared from a *K-Ras$^{LA1}$* mouse (35)] in cell culture (Fig. 2*C*).

*IL-17 enhances MMP-9 expression and lung tumor cell motility.* IL-17 can stimulate expression of MMP-9 (1, 18, 36), and this may partially account for the selective stimulation of lung tumor growth in vivo. Consequently, we evaluated gelatinase activity in the BAL fluid from adenovirus-treated mice by zymography. One week after virus delivery, BAL fluid and

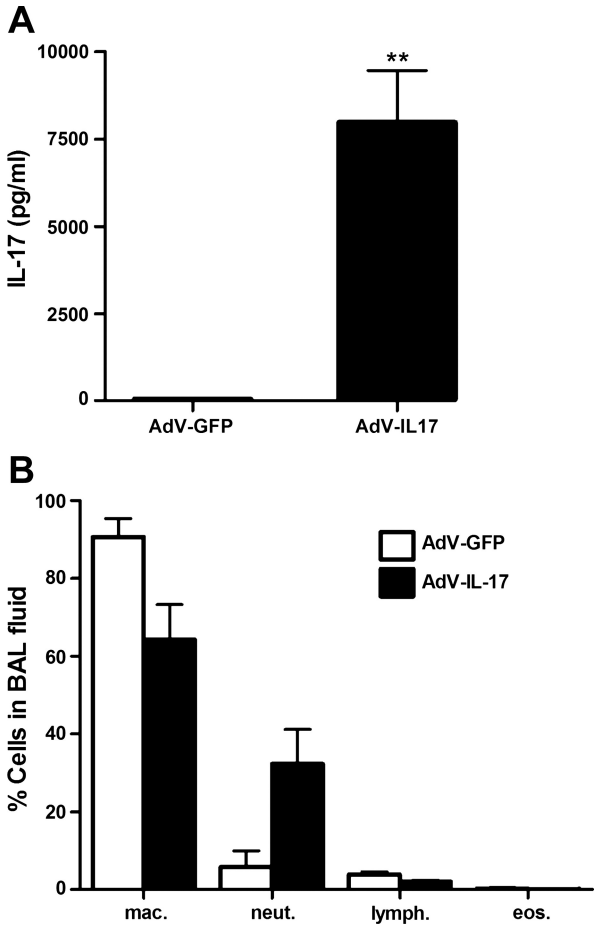



Fig. 1. Expression of IL-17 and lung neutrophilia in IL-17-expressing recombinant adenovirus (AdV-IL-17)-treated mice. *A*: AdV-IL-17 or an equivalent amount ($1\times10^8$ pfu) of green fluorescent protein-expressing recombinant adenovirus (AdV-GFP) was delivered to C57BL/6 mice by oropharyngeal aspiration. One week posttreatment, bronchoalveolar lavage (BAL) was performed. The levels of IL-17 in the BAL fluid were determined by ELISA. Graph shows mean levels ± SE IL-17 in the first 0.8 ml aliquot of BAL fluid (**$P < 0.01$ vs. AdV-GFP group, $n = 5$ per group). *B*: differential cell counts of BAL cells. Cytospin samples of the cells recovered by BAL were stained with Hema 3 (Fisher). Cells were visualized by microscopy, and 200 cells were counted from each sample. Graph shows percentage of the indicated cell type (means ± SE) in the cells recovered from the BAL fluid from mice treated with AdV-IL-17 (solid bars) and AdV-GFP (open bars). $P = 0.07$, percentage neutrophils AdV-GFP vs. AdV-IL-17, $n = 5$ per group.

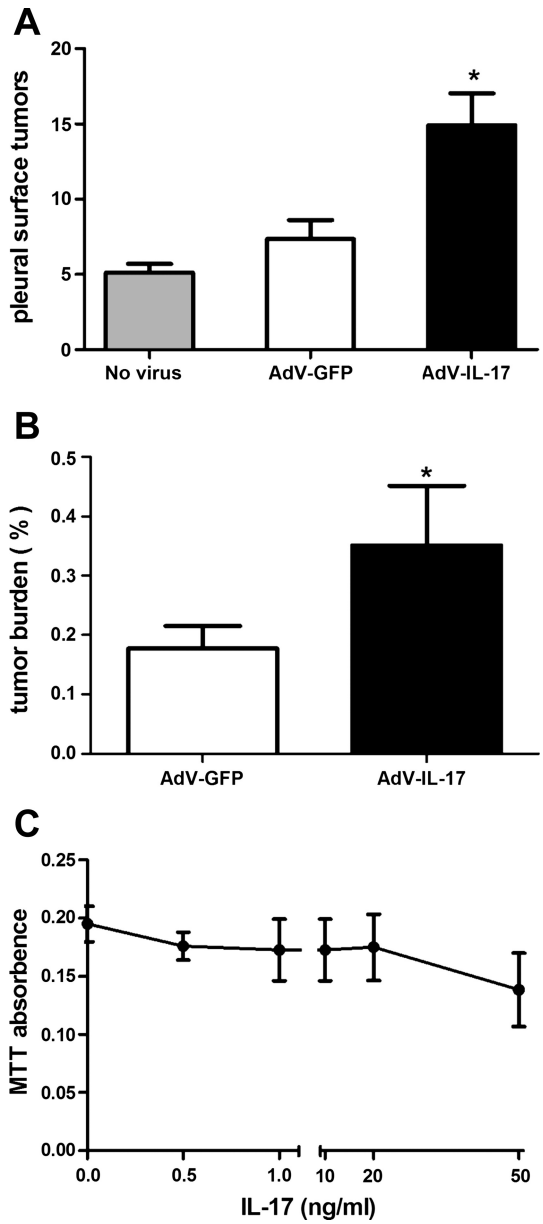



Fig. 2. Overexpression of IL-17 promotes lung tumor growth in *K-Ras*$^{LA1}$ mice. *A*: quantification of tumor nodules on the lung pleural surfaces of *K-Ras*$^{LA1}$ mice after AdV-IL-17 treatment. *K-Ras*$^{LA1}$ mice at 8–10 wk received $1\times10^8$ pfu IL-17-expressing recombinant adenovirus (AdV-IL-17) ($n = 9$), green fluorescent protein expressing adenovirus (AdV-GFP) ($n = 6$), or no virus treatment ($n = 3$) by oropharyngeal aspiration. Three weeks after adenovirus treatment, the mice were evaluated for lung tumor nodules on the pleural surface. Graph shows the mean number (± SE) of tumor modules on the pleural surface of fixed lung tissue from *K-Ras*$^{LA1}$ mice untreated (shaded bar, $n = 3$), or treated with control virus (AdV-GFP, open bar, $n = 6$), or treated with IL-17-expressing adenovirus (AdV-IL-17, solid bar, $n = 9$). *$P <$ 0.05 AdV-IL-17 vs. AdV-GFP. *B*: evaluation of tumor burden. The area of hyperplastic lesions and total area of lung tissue examined was quantified on hematoxylin and eosin (H&E)-stained tissue sections from each mouse. Graph shows the mean lung tumor burden (± SE) as measured by the ratio (percent) of the tumor area vs. total area evaluated. Open bar represents the tumor burden of AdV-GFP treated *K-Ras*$^{LA1}$ mice ($n = 6$) and solid bar represents the tumor burden of AdV-IL-17-treated littermates ($n = 9$). *$P < 0.05$ AdV-IL-17 vs. AdV-GFP. *C*: serum-starved mK-Ras-LE cells were treated with increasing concentrations of mouse IL-17 for 48 h. Relative cell number was assessed by MTT assay. The experiment was repeated twice in triplicate. Data shown are means ± SE.

lung tissue were prepared from wild-type mice treated with AdV-IL-17 or AdV-GFP. Gelatin-zymography revealed a less than twofold increase in MMP-2 and approximately a 30-fold increase in MMP-9 in the BAL fluid from AdV-IL-17-treated mice relative to that from AdV-GFP-treated littermates (Fig. 3*A*). The increased amount of MMP-9 in the BAL fluid correlated with more than a twofold increase in MMP-9 mRNA in total lung RNA (Fig. 3*B*). Immunohistochemistry with tissue sections prepared from *K-Ras*$^{LA1}$ mice 1 wk after AdV-IL-17 administration revealed expression of MMP-9 in a variety of lung cells including both tumor cells and immune cells infiltrating the tumor (Fig. 3*C*). These data are consistent with the possibility that induction of MMP-9 could at least partially account for lung tumor growth mediated by IL-17 overexpression. Since MMP-9 expression correlates with progression of lung adenocarcinoma in a number of studies (6, 7, 26, 43, 70,

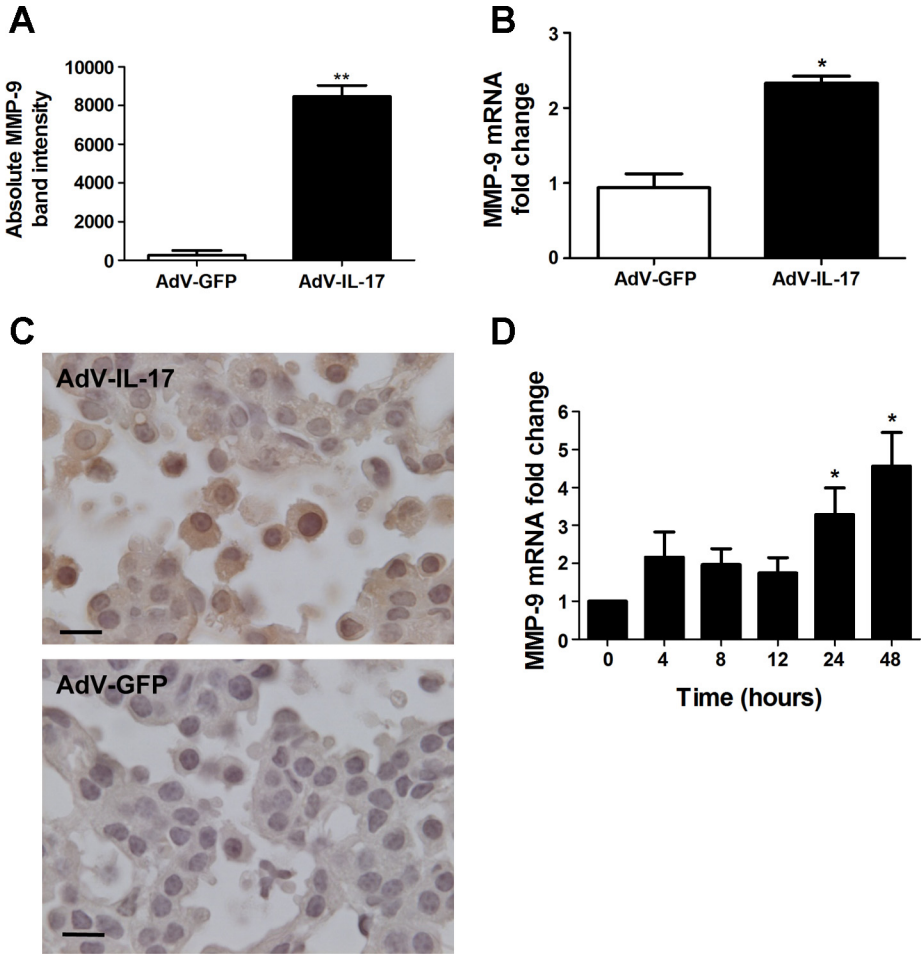



Fig. 3. Induction of MMP-9 by IL-17. *A*: wild-type mice were treated with $1\times10^8$ pfu AdV-IL-17 or AdV-GFP by oropharyngeal aspiration. One week after treatment, the mice were euthanized and evaluated for MMP-9 expression. Equal volumes of BAL fluid from AdV-IL-17- or AdV-GFP-treated mice were assessed by gelatin zymography for MMP activity ($n = 4$ per group). Bands corresponding to MMP-9 on the zymogram were quantified by densitometry. Graph shows the MMP-9 band intensity from the BAL fluid of AdV-GFP- (open bar) or AdV-IL-17-treated (solid bar) mice. Data shown are means ± SE. $^{**}P < 0.01$ AdV-IL-17 vs. AdV-GFP. *B*: total lung RNA prepared from the mice in *A* was assessed by qRT-PCR for MMP-9 mRNA levels with β-actin mRNA as the internal control. Mice treated with AdV-IL-17 (solid bar) showed a 2.3-fold increase ($2^{-\Delta\Delta CT}$ method) in MMP-9 mRNA levels compared with AdV-GFP treated littermates (open bar). Data shown are means ± SE; $n = 3$ per group. $^{*}P < 0.05$ AdV-IL-17 vs. AdV-GFP. *C*: *K-Ras*$^{LA1}$ mice were treated with AdV-IL-17 as described above. One week post-exposure the lungs of the treated mice were fixed and paraffin embedded. Lung tissue sections were immunostained with an antibody to MMP-9 by the diaminobenzidine method. MMP-9-positive (brown) staining tumor and immune cells did not appear in the tumor area on an adjacent section stained with the negative control antibody. *D*: total RNA was prepared from mK-Ras-LE cells at increasing times after treatment with 10 ng/ml IL-17. Graph shows mean levels of MMP-9 mRNA relative to β-actin ($2^{-\Delta\Delta CT}$ method) at the indicated time after addition of IL-17 to the serum-starved cells. The bars represent means ± SE ($n \geq 4$). $^{*}P < 0.05$ relative to the 0 time point.

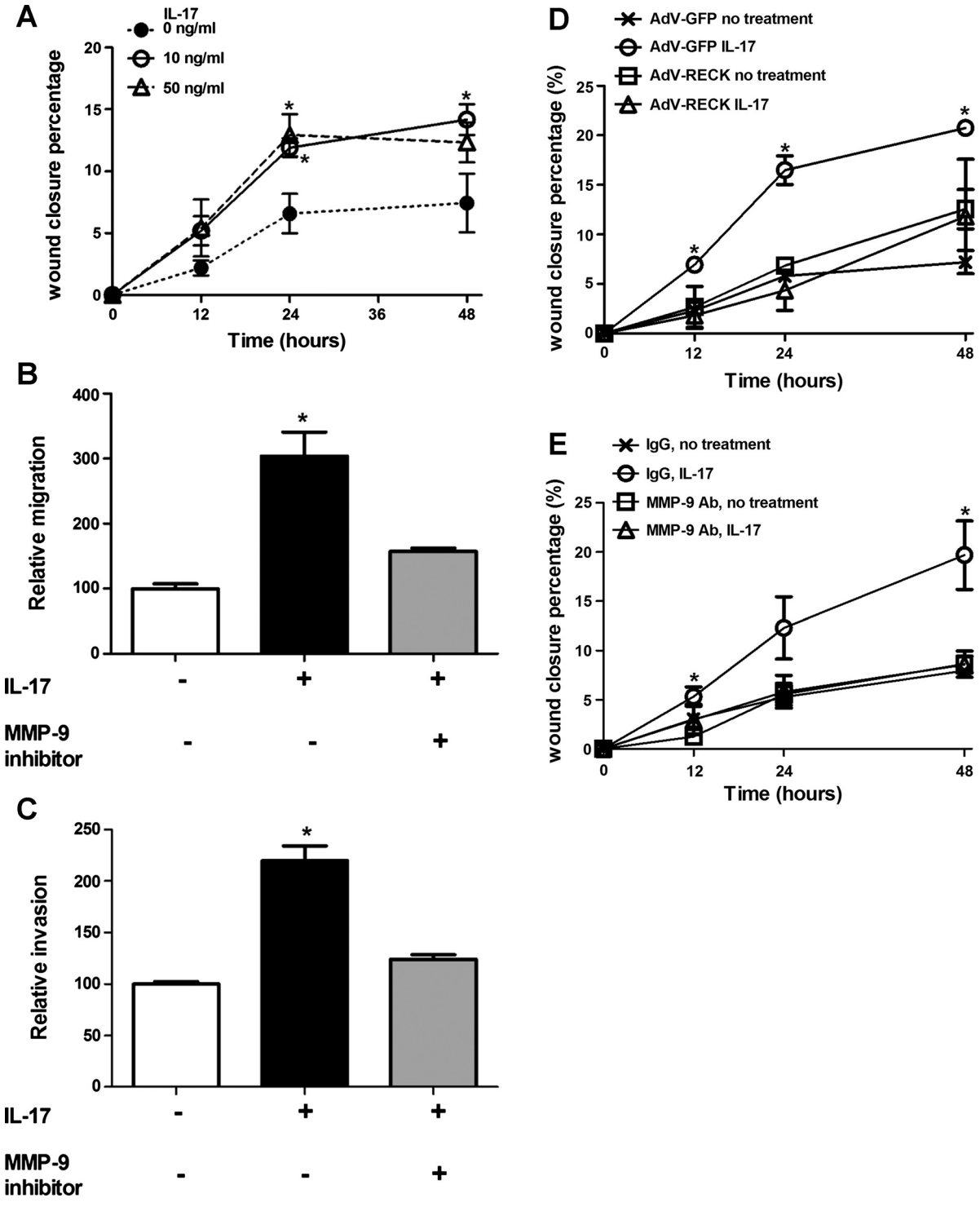
73, 74), we addressed the mechanism of MMP-9 activation by IL-17 in cell culture. Gelatin zymography of the cell culture medium from serum-starved mK-Ras-LE cells treated with IL-17 displayed a time- and concentration-dependent increase in MMP-9 (data not shown). In accord with these findings, IL-17 treatment increased MMP-9 mRNA levels more than fourfold relative to β-actin mRNA in mK-Ras-LE cells (Fig. 3*E*). Thus IL-17 enhanced expression of MMP-9 in murine lung tumor cells.

MMP-9 can increase cell motility and invasion (64). Therefore, we determined whether IL-17 could increase the motility and invasiveness of mK-Ras-LE cells. IL-17 promoted migration of mK-Ras-LE cells in a scratch-wound closure assay (Fig. 4*A*). In agreement with the concept that the enhanced motility and invasion of IL-17-treated mK-Ras-LE cells required MMP-9, a selective MMP-9 inhibitor prevented augmented migration mediated by IL-17 (Fig. 4*B*). In addition, enhanced invasion of IL-17-treated mK-Ras-LE cells through a Matrigel matrix in Transwell invasion assays was also repressed by the MMP-9 inhibitor (Fig. 4*C*). Although these results implicate MMP-9 in the enhanced motility and invasiveness of IL-17-treated mK-Ras-LE cells, the lack of inhibitor specificity precludes the conclusion that the enhanced motility is MMP-9 dependent. Two additional strategies were employed to further test role of MMP-9 in IL-17-mediated motility. In the first approach, mK-Ras-LE cells were infected with a recombinant adenovirus that expresses reversion-inducing-cysteine-rich protein with kazal motifs [RECK, a cellular repressor of MMP-2, MMP-9, and MMP-14 (2, 54)] and the effect of IL-17 on the motility of the RECK-expressing cells was compared with that of IL-17-treated control cells infected with AdV-GFP. As expected, IL-17 increased wound closure of AdV-GFP-infected mK-Ras-LE cells. AdV-RECK infection increased RECK protein expression ~130-fold compared with that in AdV-GFP infected mK-Ras-LE cells and significantly repressed the induction of motility mediated by IL-17 (Fig. 4*D*). Similarly, addition of an antibody that inhibits MMP-9 activity (15) also repressed the increased motility of IL-17-treated mK-Ras-LE cells (Fig. 4*E*). These data demonstrate that induction of lung tumor cell motility by IL-17 is MMP-9 dependent.

*Knockdown or mutation of p53 abrogates promotion of lung tumor cell motility by IL-17.* Lung tumors harboring mutations in both *K-Ras* and the p53 tumor suppressor protein grow more rapidly and metastasize more readily than lung tumors with mutations only in *K-Ras* (25, 33). To test the effect of p53 mutation on the response of lung tumor cells to IL-17, we determined the consequences of p53 knockdown in mK-Ras-LE cells upon promotion of migration by IL-17. Knockdown of p53 (~90% knockdown efficiency confirmed by immunoblotting) enhanced migration of mK-Ras-LE cells and produced no additional effect on enhanced migration mediated by IL-17 (Fig. 5*A*). In contrast, mK-Ras-LE cells transfected with a mock siRNA migrated more slowly than the p53

siRNA-transfected counterparts and retained the response to IL-17. In accord with these findings, IL-17 increased MMP-9 mRNA levels in the mock siRNA-transfected cells, whereas p53 knockdown increased MMP-9 mRNA levels and IL-17 had no additional effect (Fig. 5*B*). Thus the effect of the p53 siRNA on migration and response to IL-17 correlated with a similar effect on MMP-9 expression. Restoration of p53 by cotransfection of the mouse p53 siRNA with a plasmid that expresses a siRNA resistant wild-type human p53 into mK-Ras-LE cells repressed migration and restored the enhanced migratory response to IL-17 (Fig. 5*C*). Furthermore, restoration of wild-type p53 rescued IL-17-mediated induction of MMP-9 mRNA (Fig. 5*D*). These experiments demonstrated that IL-17-mediated induction of MMP-9 and migration is dependent on p53.

Although p53 deletion promotes tumor progression, most tumor-promoting mutations of p53 are missense mutations that lead to expression of a mutant protein (10). To address the



effects of mutant p53 upon lung tumor promotion by IL-17, we prepared a lung tumor cell line, mK-Ras-R172H-LE cells, from *K-Ras*$^{LA1}$ mice that were also heterozygous knockin for the tumor promoting R172H mutation of p53 (33). Treatment of mK-Ras-R172H-LE cells with IL-17 had no effect on migration (Fig. 6*A*) or invasion (Fig. 6*B*) and IL-17 failed to increase MMP-9 mRNA levels in mK-Ras-R172H-LE cells (Fig. 6*C*). To confirm that IL-17 does not promote migration of mutant p53-expressing cells, we attempted a similar p53 rescue experiment like that shown in Fig. 5 with a mutant p53-expressing plasmid. mK-Ras-LE cells cotransfected with the mouse p53 siRNA and a plasmid that expresses a siRNA-resistant mutant human p53 R175H (equivalent to the mouse R172H mutant) failed to display enhanced migration upon IL-17 treatment (Fig. 6*D*). Taken together, these data suggest that IL-17 enhances migration of lung tumor cells through a MMP-9-dependent mechanism and that wild-type, but not mutant, p53 mediates the response to IL-17.

*IL-17 upregulates MMP-9 expression via mRNA stabilization.* A previous report demonstrated that IL-17 enhanced the stability of chemokine mRNAs (67). To test whether induction of MMP-9 by IL-17 also involved stabilization of MMP-9 mRNA, we treated mK-Ras-LE cells with IL-17 for 2 h before inhibiting transcription with 10 μg/ml actinomycin D. The amount of β-actin mRNA remaining appeared similar in mK-Ras-LE cells in the presence and absence of IL-17 after 8 h of actinomycin D treatment (Fig. 7). Consistent with previous findings, IL-17 treatment increased CXCL-1 and CXCL-2 chemokine mRNA levels 8 h after inhibition of mRNA synthesis (Fig. 7). Similarly, IL-17 treatment also stabilized MMP-9 mRNA (Fig. 7). Chemokine mRNA stabilization by IL-17 requires the serine/arginine-rich splicing factor 1, SRSF1 (67). To determine whether SRSF1 altered the stability of MMP-9 mRNA, we transfected mK-Ras-LE cells with a siRNA that targeted SRSF1. After 48 h, Western blots showed ~80% knockdown efficiency of the SRSF1 protein in mK-Ras-LE cells (Fig. 8*A*). The SRSF1-targeting siRNA increased MMP-9 mRNA ~1.4-fold in transfected mK-Ras-LE cells relative to control cells transfected with scrambled siRNA (Fig. 8*B*). To demonstrate IL-17-regulated interaction between SRSF1 and MMP-9 mRNA, we performed RNA coimmunoprecipitation assays followed by mRNA quantification by qRT-PCR. An antibody to SRSF1 coimmunoprecipitated approximately sevenfold more MMP-9 mRNA than the negative control from whole cell extracts of untreated serum-starved mK-Ras-LE cells (Fig. 8*C*). Treatment of the cells with IL-17 reduced the amount of MMP-9 mRNA that coimmunoprecipitated with the antibody to SRSF1 to levels approximating the negative control. Immunoblots confirmed that equal amounts of SRSF1 immunoprecipitated specifically with or without IL-17 treatment (Fig. 8*C*). Additional assays did not show an association between β-actin mRNA with SRSF1 in extracts from untreated or IL-17-treated cells (data not shown). Positive control experiments replicated previous findings (19), demonstrating an IL-17-dependent association between SRSF1 and CXCL-2 mRNA (Fig. 8*D*). These observations support the concept that IL-17 increased MMP-9 mRNA stability by reducing interaction with SRSF1. These data agree with our conclusion that IL-17 increases expression of MMP-9 in lung tumor cells via posttranscriptional stabilization of the MMP-9 mRNA by reducing interaction with SRSF1.

## DISCUSSION

Our data show that IL-17A overexpression promotes rapid growth of mutant *K*-Ras-driven lung cancers. Coincident with stimulation of tumorigenesis in vivo, IL-17 stimulates the expression of MMP-9 in the lung and in lung epithelial cells in culture. Consistently, IL-17-treated mK-Ras-LE cells display enhanced migration and invasiveness that is MMP-9 dependent, as demonstrated by selective (pharmacological inhibitor and RECK overexpression) and specific (antibody) inhibition of MMP-9. A knockdown-restoration strategy demonstrated that IL-17-mediated migration and induction of MMP-9 depend on wild-type p53. In contrast, IL-17 does not enhance MMP-9 expression or consequent motility and invasion of mutant p53-expressing lung tumor cells. IL-17 increases MMP-9 mRNA stability. In accord with posttranscriptional regulation, siRNA-mediated knockdown of SRSF1 increases levels of MMP-9 mRNA. Moreover, MMP-9 mRNA binds to SRSF1 in a manner that is regulated by IL-17. We conclude that IL-17 enhances migration of wild-type p53-expressing lung tumor

Fig. 4. IL-17 promotes MMP-9-dependent migration and invasion of mK-ras-LE cells. *A*: confluent mK-Ras-LE cells in 24-well plates were serum-starved overnight, then a scratch wound was made at *time 0* (0 h) and fresh serum-free medium or serum-free medium supplemented with 10 or 50 ng/ml IL-17 was added before returning the cells to the incubator. Cell motility was measured as the ratio of wound closure relative to initial wound width. Graph shows percentage of wound closure vs. time for cells incubated in 0 (●, dotted line), 10 (○, solid line) and 50 (△, dashed line) ng/ml IL-17. Data shown are means ± SE ($n$ = 4). *$P < 0.05$ vs. negative control group at the same time point. *B*: Transwell migration assays were performed with (solid and shaded bars) or without (open bar) 10 ng/ml IL-17 added to the bottom of the Transwells. The extent of migration is expressed as the number of cells on the underside of the Transwell in the treated group relative to the number of cells on the underside of the Transwell in the negative control group, which was normalized to 100. Enhanced migration mediated by IL-17 (solid bar) was reduced by the inhibitor of MMP-9 (shaded bar). Data shown are means ± SE ($n$ = 4). *$P < 0.05$ vs. negative control or IL-17 and MMP-9 inhibitor cotreatment. *C*: mK-Ras-LE cells were plated onto a Matrigel-coated porous membrane without serum. Transwell invasion assays were performed with (solid and shaded bars) or without (open bar) addition of 10 ng/ml IL-17 added to the bottom of the Transwells. The extent of invasion is expressed as the number of cells on the underside of the Transwell in the treated group relative to the number of cells on the underside of the Transwell in the negative control group, which was normalized to 100. Enhanced invasion mediated by IL-17 (solid bar) was reduced by the inhibitor of MMP-9 (shaded bar). Data shown are means ± SE ($n$ = 4). *$P < 0.05$ vs. negative control or IL-17 and MMP-9 inhibitor cotreatment. *D*: a migration assay was performed as described in *A* except the cells were infected at a MOI of 10 with recombinant adenovirus expressing reversion-inducing-cysteine-rich protein with kazal motifs (AdV-RECK) or AdV-GFP 24 h before wounding and addition of IL-17. Graph shows percentage wound closure at the indicated times in cells infected with AdV-GFP (×) or AdV-RECK (□) in the absence of IL-17 and in cells transfected with AdV-GFP (○) or AdV-RECK (△) in the presence of 10 ng/ml IL-17. Data shown are means ± SE ($n$ = 3). *$P < 0.05$ vs. negative control group at the same time point. *E*: a migration assay was performed as described in *A* except an MMP-9 antibody (12 μg/ml, Millipore AB19016) was used to inhibit MMP-9. In place of the MMP-9 antibody, the same amount of rabbit IgG was used as the negative control. Graph shows percentage wound closure at the indicated times in cells treated with rabbit IgG (×) or MMP-9 antibody (□) in the absence of 10 ng/ml IL-17, and in cells treated with rabbit IgG (○) or MMP-9 antibody (△) in the presence of 10 ng/ml IL-17. Data shown are means ± SE ($n$ = 3). *$P <$ 0.05 vs. negative control group at the same time point.

cells in a MMP-9-dependent manner that includes dissociation of the SRSF1-destabilizing factor from the MMP-9 mRNA.

IL-17A displays dichotomous roles in tumor progression. For example, it has been proposed that IL-17A enhances antitumor immunity in immunocompetent mice but increases tumor growth in the absence of an adaptive immune response (41), but this distinction is not so clear cut (40). Tumor type appears to be an important determinant of the prognostic significance of Th17 inflammation on clinical outcome (12). In addition, our data suggest that p53 status affects IL-17-mediated promotion of lung tumorigenesis. SRSF1 overexpression can induce p53 (11). Consequently, the ability of the activated IL-17 receptor to sequester SRSF1 (67) may be related to the opposing effects of IL-17 and p53 in MMP-9 regulation shown here. Consistent with our findings, prior studies have identified a protumorigenic role for IL-17 in models of lung adenocarcinoma (3, 37, 38, 57). However, with one exception (3), these previous investigations did not examine the effects of IL-17A in an autochthonous lung tumor model and studies with tumor grafts have produced results that were often contradictory (40, 72). Our results agree with, and extend, previous findings demonstrating that Th17 inflammation accelerates lung tumorigenesis in an autochthonous model of mutant K-Ras-expressing lung cancer (3). However, the approach here differs by

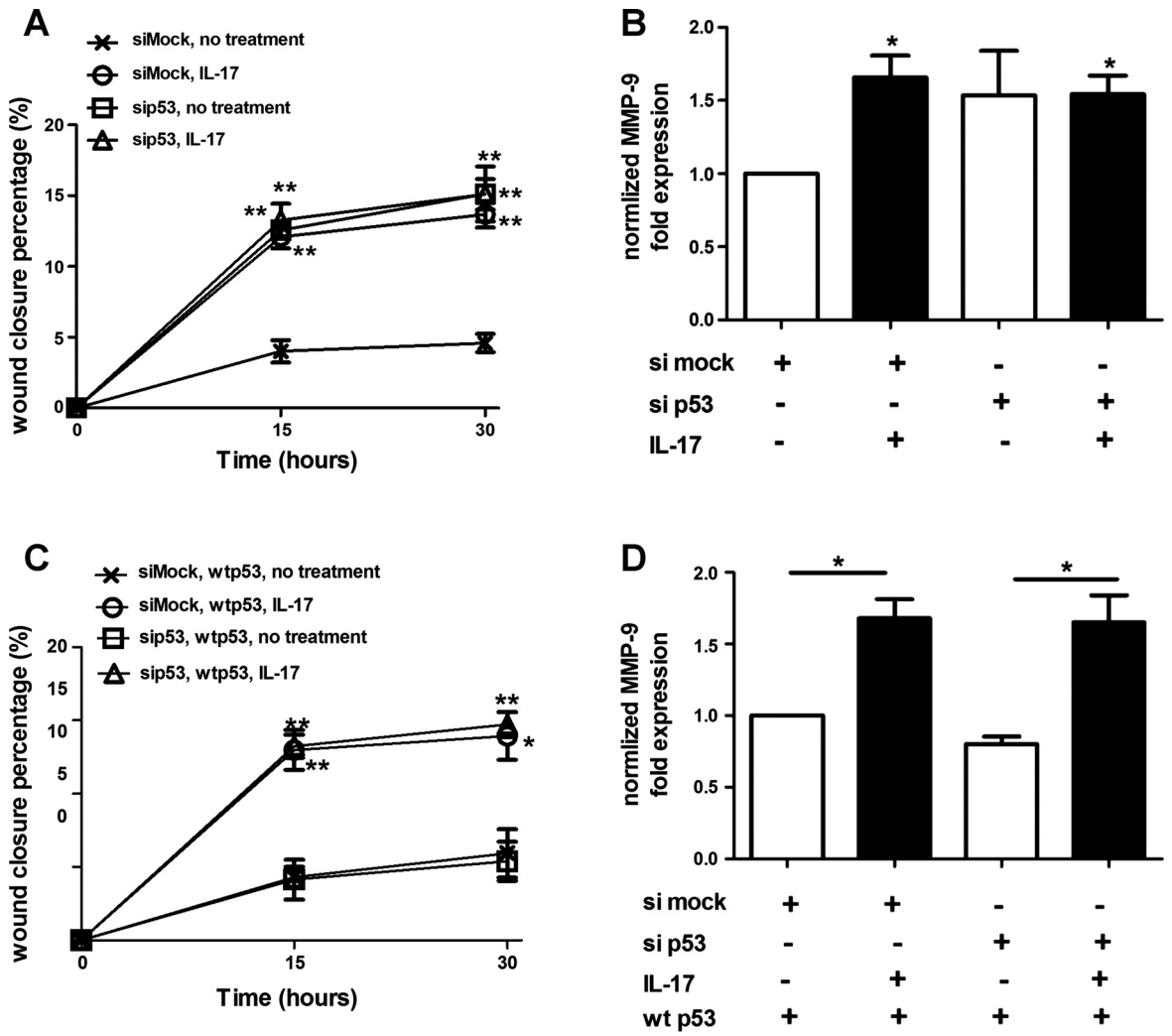



Fig. 5. IL-17 fails to enhance migration and MMP-9 expression in p53-knockdown lung tumor cells. *A*: knockdown of p53 prevents enhanced migration of IL-17-treated cells. mK-Ras-LE cells were transfected with a p53-targeting siRNA (sip53) or a non-targeting control siRNA (siMock) before growth to confluence. A scratch wound was made in the confluent cultures at *time 0* (0 h) and fresh serum-free medium or serum-free medium supplemented with 10 ng/ml IL-17 was added before returning the cells to the incubator. At 15 and 30 h after the addition of IL-17, the percentage of wound closure was assessed for mock- (×) and p53-targeting (□) siRNA-transfected cells incubated without IL-17 or mock- (○) and p53-targeting (△) siRNA-transfected cells incubated with 10 ng/ml IL-17. Data shown are means ± SE ($n = 4$). $^{**}P < 0.01$ vs. negative control at the same time point. *B*: RNA was prepared from the cells at the 30-h time point in *A* and levels of MMP-9 mRNA were determined by qRT-PCR. Graph shows the mean fold change (± SE) of MMP-9 mRNA levels relative to β-actin ($2^{-\Delta\Delta CT}$ method) with (solid bars) or without (open bars) IL-17. For normalization purposes, the MMP-9/β-actin mRNA ratio in siMock-transfected, untreated cells was made equal to 1. $^{*}P < 0.05$ vs. negative control. *C*: restoration of wild-type p53 rescues enhanced motility mediated by IL-17. mK-Ras-LE cells were cotransfected with a p53-targeting siRNA (sip53) or a nontargeting control siRNA (siMock) with a plasmid (pCMV-p53-wt) that expresses wild-type human p53, which is siRNA resistant. Graph shows percentage wound closure at the indicated times after wild-type human p53 expression in cells transfected with mock siRNA (×) or p53 siRNA (□) in the absence of 10 ng/ml IL-17 and in cells transfected with mock siRNA (○) or p53 siRNA (△) in the presence of 10 ng/ml IL-17. Data shown are means ± SE ($n = 4$). $^{*}P < 0.05$, $^{**}P < 0.01$ vs. negative control at the same time point. *D*: restoration of wild-type p53 rescues induction of MMP-9 mRNA by IL-17. Same as *B*, except the levels of MMP-9 mRNA at the 30-h time point from the cells in *C* were determined. $^{*}P < 0.05$.

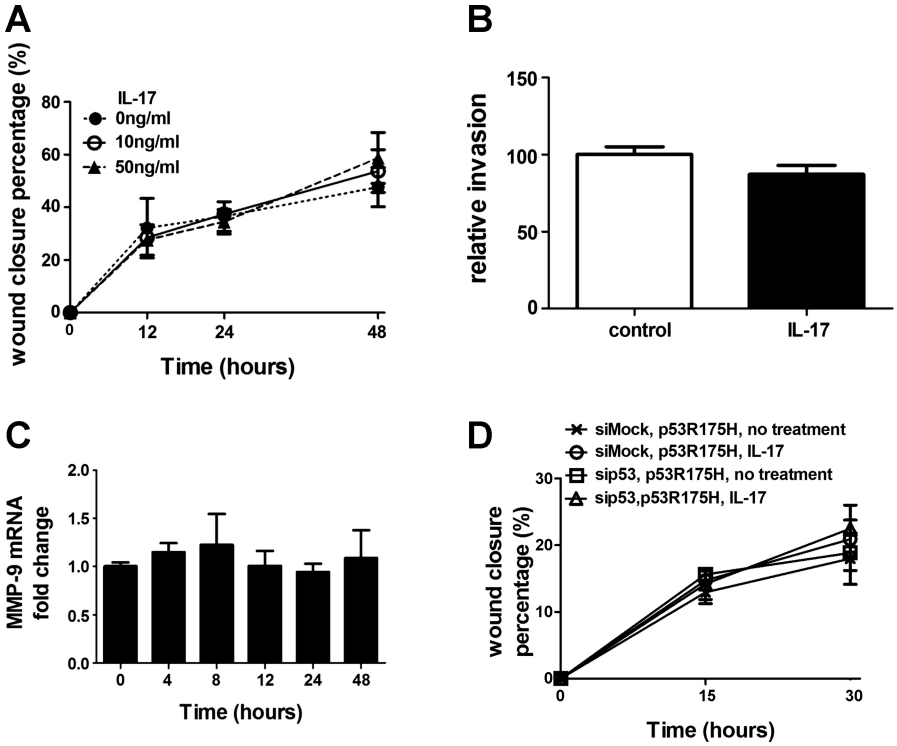



Fig. 6. Mutant p53 alters IL-17-mediated promotion of migration and induction of MMP-9. *A*: effect of IL-17 on migration of mutant p53-expressing cells. Same as Fig. 4*A* except confluent mK-Ras-R172H-LE cells were assessed for migration in serum-free medium (●, dotted line) or serum-free medium supplemented with 10 (○, solid line) or 50 (△, dashed line) ng/ml IL-17. Graph shows percentage of wound closure vs. time. Data shown are means ± SE ($n = 4$). *B*: IL-17 does not promote invasion of mutant p53-expressing cells. Transwell migration assays (see Fig. 4*B*) were performed with mK-Ras-R172H-LE cells in serum-free media with (solid bar) or without (open bar) 10 ng/ml IL-17. Data shown are means ± SE ($n = 4$). *C*: total RNA was prepared from mK-Ras-R172H-LE cells at increasing times after treatment with 10 ng/ml IL-17. Graph shows the mean level of MMP-9 mRNA relative to β-actin ($2^{-\Delta\Delta CT}$ method) at the indicated time after addition of IL-17 to the serum-starved cells. Data shown are means ± SE ($n \geq 5$). *D*: same as Fig. 5*C*, except the cotransfected plasmid (pCMV-p53R175H) expressed the R175H mutant of human p53 in the K-Ras-LE cells with p53 knocked down. Graph shows percentage wound closure at the indicated times with mutant human p53 expression in cells transfected with mock siRNA (×) or p53 siRNA (□) in the absence IL-17 and in cells transfected with mock siRNA (○) or p53 siRNA (△) in the presence of 10 ng/ml IL-17. Data shown are means ± SE ($n = 4$).

overexpressing IL-17 to identify the cytokine-tumor relationship rather than using IL-17-deficient mice, which lack the homeostatic functions of IL-17. Although IL-17 overexpression more accurately reflects the clinical scenario of lung inflammation than the use of genetically deficient mice, the epithelial source of IL-17 overexpression consequent to adenovirus infection does not model the Th17 cell source of IL-17 that occurs in the lung exposed to carcinogens. IL-17-mediated lung neutrophilia likely increases levels of neutrophil elastase, an established inducer of lung tumor growth (23). Indeed, IL-17 recruits Gr-$1^+$-CD$11b^+$ myeloid cells to the lung and their depletion suppresses growth of *K-Ras*-driven lung tumors (3).

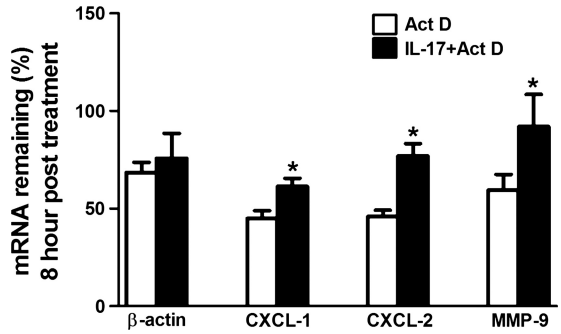



Fig. 7. IL-17 enhanced MMP-9 mRNA stability in mK-Ras-LE cells. Serum-starved mK-Ras-LE cells were untreated (open bars) or treated with 10 ng/ml IL-17 (solid bars) for 2 h. Then 10 μg/ml actinomycin D (Act D) was added to both groups at *time 0* and total RNA was prepared. Equal amounts of total RNA prepared at *time 0* and 8 h from duplicate or triplicate samples were assessed for the target mRNAs (β-actin, CXCL-1, CXCL-2, and MMP-9) by qRT-PCR. Results are presented as percent of the indicated mRNA remaining relative to the amount at *time 0*. The mRNA levels before actinomycin D treatment were set to 1. Data shown are means ± SE ($n \geq 4$). *$P < 0.05$ for IL-17 treated vs. untreated control.

Typically, lung tumors develop in the context of chronic inflammation associated with inhaled carcinogens, primarily cigarette smoke. Consistent with the approach here, cigarette smoke is a Th17 adjuvant (4, 61) and inflammation associated with cigarette smoke promotes progression of mutant *K-Ras*-driven lung tumors (69). Moreover, a bacterial pathogen promotes chronic Th17 lung inflammation and accelerates lung tumorigenesis in mutant *K-Ras*-expressing mice (3, 48). These observations are consistent with the dependence of mutant *K-Ras*-expressing lung tumors on signaling by the proinflammatory transcription factor nuclear factor-κB [NF-κB (45, 75)]. Enhanced tumor progression associated with inflammation occurs in other tumor types driven by mutant *K-Ras* (6, 16). In a model of pancreatic cancer, inflammation initiates an NF-κB-dependent positive feedback loop that amplifies *K-Ras* activity (6). Moreover, tumors harboring mutant *K-Ras* develop in an inflammatory microenvironment fostered by the oncoprotein (44, 65, 68), and this selective pressure likely contributes to adaptation and escape from antitumor immunity.

High serum levels of MMP-9 (76) or immunohistochemical detection of MMP-9 in tumor specimens (80) are poor prognostic indicators in lung cancer. Moreover, increasing serum MMP-9 concentrations correlate with disease severity in chronic obstructive pulmonary disease, COPD (51), a disease that predisposes lung cancer (21). Chemokine-mediated release of MMP-9 stored in tertiary granules of neutrophils infiltrating the lung can exacerbate COPD (71) and lung cancer (22). Indeed, tumor-associated leukocytes appear to be a major source of MMP-9 during stimulation of tumor growth by AdV-IL-17 (Fig. 3*C*). Active MMP-9 can release growth factors, promote angiogenesis, accelerate tumor cell migration into surrounding normal tissue, and prepare the premetastatic niche (8, 20, 66, 77), which likely contributes to the association of MMP-9 expression with increasing lung tumor grade (46).

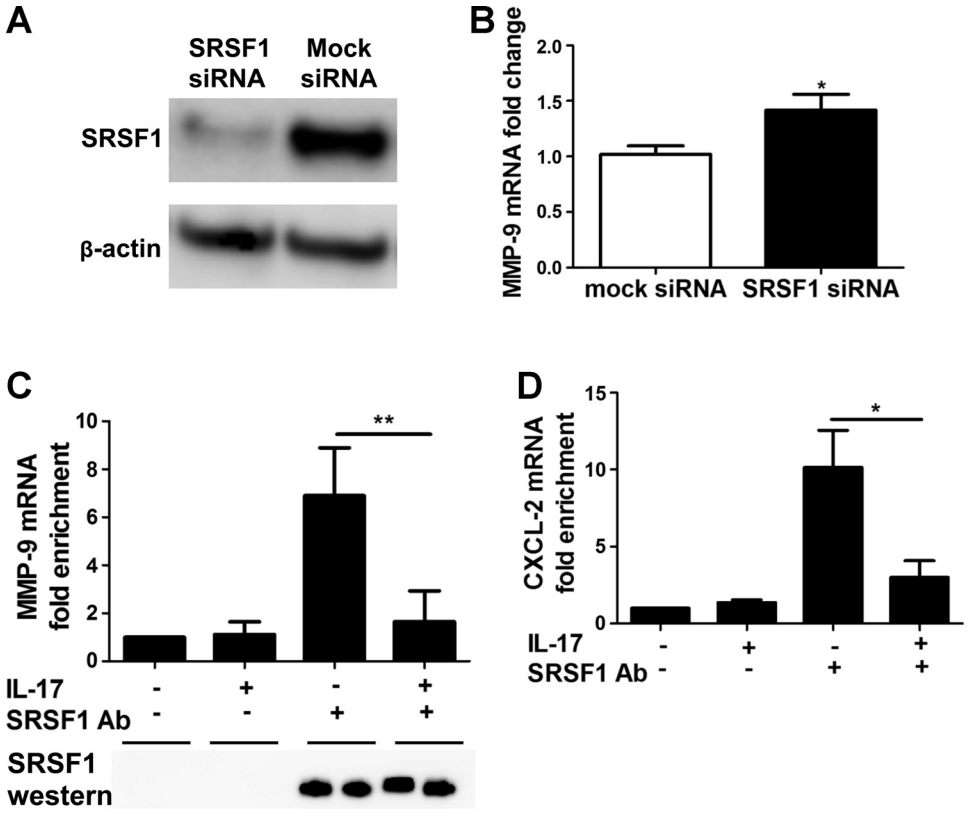



Fig. 8. IL-17 regulates MMP-9 mRNA levels via serine/arginine-rich splicing factor 1 (SRSF1). *A*: mK-Ras-LE cells were transfected with a scrambled siRNA or a siRNA targeted to SRSF1. After 48 h, cell lysates were prepared and subjected to Western blot. Western blots confirmed siRNA knockdown of SRSF1 compared with the level in cells transfected with a Mock siRNA. *B*: same as *A* except total RNA was analyzed for MMP-9 mRNA levels in mK-Ras-LE cells transfected with a siRNA targeting SRSF1. Reduction of SRSF1 with a siRNA increased the MMP-9 mRNA level 1.4-fold (solid bar) relative to that in cells transfected with the control siRNA (open bar). The levels of MMP-9 mRNA were determined by qRT-PCR ($2^{-\Delta\Delta CT}$ method) relative to β-actin mRNA. Results are means ± SE of 3 independent experiments. $^*P < 0.05$ vs. mock siRNA-transfected group. *C*: serum-starved mK-Ras-LE cells were treated with or without 10 ng/ml IL-17 for 48 h. The cells were briefly fixed with formalin prior to preparation of cell lysates as described in MATERIALS AND METHODS. Coimmunoprecipitated RNA was extracted from the protein A/G beads and cross-linking was reversed prior to conversion to cDNA. The amount of MMP-9 cDNA in each sample was quantified by real-time PCR. The results obtained with protein A/G beads alone with extracts from untreated cells were normalized to one. Data are presented as fold enrichment of MMP-9 mRNA compared with the negative control samples. Data shown are means ± SE ($n = 4$). $^{**}P < 0.01$. Treatment of mK-Ras-LE cells with 10 ng/ml IL-17 reduced the amount of MMP-9 mRNA that could be selectively immunoprecipitated with an antibody to SRSF1 to near negative control levels. *Bottom*: immunoblotting showed that equal amounts of SRSF1 were immunoprecipitated from the extracts of IL-17-treated and untreated cells. *D*: same as *C*, except coimmunoprecipitation of CXCL-2 mRNA with an antibody to SRSF1 was assessed. Data are presented as fold enrichment of CXCL-2 mRNA compared with the negative control samples. Data are means ± SE ($n = 4$). $^*P < 0.05$.

Our data demonstrating MMP-9-dependent migration of lung epithelial cells agree with previous findings that addition of active MMP-9 accelerates migration of A549 cells (62) and that MMP-9 expression by alveolar type II cells is essential for wound healing (53). Knockdown or mutation of p53 increases lung tumor cell motility and abrogates IL-17-mediated induction of MMP-9. In addition, IL-17-mediated stabilization of MMP-9 mRNA by disruption of SRSF1 interaction coincides with previous findings demonstrating this mechanism of mRNA regulation for chemokine mRNAs (67).

Improving the survival rates in non-small cell lung cancer (NSCLC) will require the identification of novel therapeutic targets. Our data are consistent with the view that cigarette smoke promotes progression of NSCLC by inducing expression of IL-17. One mechanism that could account for enhanced proliferation in response to IL-17 is induction of MMP-9. Our data also suggest that, once p53 is inactivated by mutation, lung tumor promotion would be independent of IL-17. In NSCLC, serum MMP-9 levels potentially serve as a prognostic marker (31) and an indicator of response to chemotherapy (9). Although inhibitors of matrix metalloproteinases have not improved survival in patients with NSCLC, clinical trial end points and the late stage of disease in study participants have complicated the interpretation of these findings (5). Toward a goal of personalized therapy, our results suggest that MMP-9 inhibition in lung tumors with high levels of IL-17 and wild-type p53 warrants reinvestigation.


## GRANTS

This work was supported by National Institutes of Health Grant CA132603 (B. Shan, D. E. Sullivan, G. F. Morris) and by the Wetmore Foundation. B. Xu received fellowship support from the Foundation in Lung Pathobiology and Matching Funds from the Tulane Cancer Center. Z. You received grants from the National Institutes of Health (P20GM103518 and R01CA174714) and Department of Defense (PC121647, PC13448, and PC130118).


## DISCLOSURES

J. Kolls is employed by Vitae and got grants from Amgen and Constellation Pharmaceuticals.

## AUTHOR CONTRIBUTIONS

B.X., D.A.P., J.K.K., B.C., B.S., D.E.S., and G.F.M. conception and design of research; B.X., J.F.G., Y.W., B.S., D.E.S., and G.F.M. performed experi-

ments; B.X., B.S., D.E.S., and G.F.M. analyzed data; B.X., Z.Y., B.C., B.S., D.E.S., and G.F.M. interpreted results of experiments; B.X. and G.F.M. prepared figures; B.X. and G.F.M. drafted manuscript; B.X., D.A.P., B.S., D.E.S., and G.F.M. edited and revised manuscript; B.X., J.F.G., D.A.P., Y.W., J.K.K., Z.Y., B.C., B.S., D.E.S., and G.F.M. approved final version of manuscript.

## REFERENCES


1. **Benevides L, Cardoso CR, Tiezzi DG, Marana HR, Andrade JM, Silva JS.** Enrichment of regulatory T cells in invasive breast tumor correlates with the upregulation of IL-17A expression and invasiveness of the tumor. *Eur J Immunol* 43: 1518–1528, 2013.
2. **Chang CK, Hung WC, Chang HC.** The Kazal motifs of RECK protein inhibit MMP-9 secretion and activity and reduce metastasis of lung cancer cells in vitro and in vivo. *J Cell Mol Med* 12: 2781–2789, 2008.
3. **Chang SH, Mirabolfathinejad SG, Katta H, Cumpian AM, Gong L, Caetano MS, Moghaddam SJ, Dong C.** T helper 17 cells play a critical pathogenic role in lung cancer. *Proc Natl Acad Sci USA* 111: 5664–5669, 2014.
4. **Chen K, Pociask DA, McAleer JP, Chan YR, Alcorn JF, Kreindler JL, Keyser MR, Shapiro SD, Houghton AM, Kolls JK, Zheng M.** IL-17RA is required for CCL2 expression, macrophage recruitment, and emphysema in response to cigarette smoke. *PLoS One* 6: e20333, 2011.
5. **Coussens LM, Fingleton B, Matrisian LM.** Matrix metalloproteinase inhibitors and cancer: trials and tribulations. *Science* 295: 2387–2392, 2002.
6. **Daniluk J, Liu Y, Deng D, Chu J, Huang H, Gaiser S, Cruz-Monserrate Z, Wang H, Ji B, Logsdon CD.** An NF-kappaB pathway-mediated positive feedback loop amplifies Ras activity to pathological levels in mice. *J Clin Invest* 122: 1519–1528, 2012.
7. **Diament MJ, Peluffo GD, Stillitani I, Cerchietti LC, Navigante A, Ranuncolo SM, Klein SM.** Inhibition of tumor progression and paraneoplastic syndrome development in a murine lung adenocarcinoma by medroxyprogesterone acetate and indomethacin. *Cancer Invest* 24: 126–131, 2006.
8. **Egeblad M, Werb Z.** New functions for the matrix metalloproteinases in cancer progression. *Nat Rev Cancer* 2: 161–174, 2002.
9. **Ertan E, Soydinc H, Yazar A, Ustuner Z, Tas F, Yasasever V.** Matrix metalloproteinase-9 decreased after chemotherapy in patients with non-small cell lung cancer. *Tumori* 97: 286–289, 2011.
10. **Freed-Pastor WA, Prives C.** Mutant p53: one name, many proteins. *Genes Dev* 26: 1268–1286, 2012.
11. **Fregoso OI, Das S, Akerman M, Krainer AR.** Splicing-factor oncoprotein SRSF1 stabilizes p53 via RPL5 and induces cellular senescence. *Mol Cell* 50: 56–66, 2013.
12. **Fridman WH, Pages F, Sautes-Fridman C, Galon J.** The immune contexture in human tumours: impact on clinical outcome. *Nat Rev Cancer* 12: 298–306, 2012.
13. **Friedlander PL, Delaune CL, Abadie JM, Toups M, LaCour J, Marrero L, Zhong Q, Kolls JK.** Efficacy of CD40 ligand gene therapy in malignant mesothelioma. *Am J Respir Cell Mol Biol* 29: 321–330, 2003.
14. **Gaffen SL.** Structure and signalling in the IL-17 receptor family. *Nat Rev Immunol* 9: 556–567, 2009.
15. **Gong Y, Hart E, Shchurin A, Hoover-Plow J.** Inflammatory macrophage migration requires MMP-9 activation by plasminogen in mice. *J Clin Invest* 118: 3012–3024, 2008.
16. **Grivennikov SI, Wang K, Mucida D, Stewart CA, Schnabl B, Jauch D, Taniguchi K, Yu GY, Osterreicher CH, Hung KE, Datz C, Feng Y, Fearon ER, Oukka M, Tessarollo L, Coppola V, Yarovinsky F, Cheroutre H, Eckmann L, Trinchieri G, Karin M.** Adenoma-linked barrier defects and microbial products drive IL-23/IL-17-mediated tumour growth. *Nature* 491: 254–258, 2012.
17. **Guenther JF, Cameron JE, Nguyen HT, Wang Y, Sullivan DE, Shan B, Lasky JA, Flemington EK, Morris GF.** Modulation of lung inflammation by the Epstein-Barr virus protein Zta. *Am J Physiol Lung Cell Mol Physiol* 299: L771–L784, 2010.
18. **Hemdan NY.** Anti-cancer vs. cancer-promoting effects of the interleukin-17-producing T helper cells. *Immunol Lett* 149: 123–133, 2013.
19. **Herjan T, Yao P, Qian W, Li X, Liu C, Bulek K, Sun D, Yang WP, Zhu J, He A, Carman JA, Erzurum SC, Lipshitz HD, Fox PL, Hamilton TA.** HuR is required for IL-17-induced Act1-mediated CXCL1 and CXCL5 mRNA stabilization. *J Immunol* 191: 640–649, 2013.
20. **Hiratsuka S, Nakamura K, Iwai S, Murakami M, Itoh T, Kijima H, Shipley JM, Senior RM, Shibuya M.** MMP9 induction by vascular endothelial growth factor receptor-1 is involved in lung-specific metastasis. *Cancer Cell* 2: 289–300, 2002.
21. **Houghton AM.** Mechanistic links between COPD and lung cancer. *Nat Rev Cancer* 13: 233–245, 2013.
22. **Houghton AM.** The paradox of tumor-associated neutrophils: fueling tumor growth with cytotoxic substances. *Cell Cycle* 9: 1732–1737, 2010.
23. **Houghton AM, Rzymkiewicz DM, Ji H, Gregory AD, Egea EE, Metz HE, Stolz DB, Land SR, Marconcini LA, Kliment CR, Jenkins KM, Beaulieu KA, Mouded M, Frank SJ, Wong KK, Shapiro SD.** Neutrophil elastase-mediated degradation of IRS-1 accelerates lung tumor growth. *Nat Med* 16: 219–223, 2010.
24. **Hu Y, Ota N, Peng I, Refino CJ, Danilenko DM, Caplazi P, Ouyang W.** IL-17RC is required for IL-17A- and IL-17F-dependent signaling and the pathogenesis of experimental autoimmune encephalomyelitis. *J Immunol* 184: 4307–4316, 2010.
25. **Jackson EL, Olive KP, Tuveson DA, Bronson R, Crowley D, Brown M, Jacks T.** The differential effects of mutant p53 alleles on advanced murine lung cancer. *Cancer Res* 65: 10280–10288, 2005.
26. **Kao SJ, Su JL, Chen CK, Yu MC, Bai KJ, Chang JH, Bien MY, Yang SF, Chien MH.** Osthole inhibits the invasive ability of human lung adenocarcinoma cells via suppression of NF-kappaB-mediated matrix metalloproteinase-9 expression. *Toxicol Appl Pharmacol* 261: 105–115, 2012.
27. **Kasinski AL, Slack FJ.** miRNA-34 prevents cancer initiation and progression in a therapeutically resistant K-ras and p53-induced mouse model of lung adenocarcinoma. *Cancer Res* 72: 5576–5587, 2012.
28. **Kolls JK, Linden A.** Interleukin-17 family members and inflammation. *Immunity* 21: 467–476, 2004.
29. **Kryczek I, Wei S, Szeliga W, Vatan L, Zou W.** Endogenous IL-17 contributes to reduced tumor growth and metastasis. *Blood* 114: 357–359, 2009.
30. **Kuestner RE, Taft DW, Haran A, Brandt CS, Brender T, Lum K, Harder B, Okada S, Ostrander CD, Kreindler JL, Aujla SJ, Reardon B, Moore M, Shea P, Schreckhise R, Bukowski TR, Presnell S, Guerra-Lewis P, Parrish-Novak J, Ellsworth JL, Jaspers S, Lewis KE, Appleby M, Kolls JK, Rixon M, West JW, Gao Z, Levin SD.** Identification of the IL-17 receptor related molecule IL-17RC as the receptor for IL-17F. *J Immunol* 179: 5462–5473, 2007.
31. **Laack E, Kohler A, Kugler C, Dierlamm T, Knuffmann C, Vohwinkel G, Niestroy A, Dahlmann N, Peters A, Berger J, Fiedler W, Hossfeld DK.** Pretreatment serum levels of matrix metalloproteinase-9 and vascular endothelial growth factor in non-small-cell lung cancer. *Ann Oncol* 13: 1550–1557, 2002.
32. **Lakatos HF, Burgess HA, Thatcher TH, Redonnet MR, Hernady E, Williams JP, Sime PJ.** Oropharyngeal aspiration of a silica suspension produces a superior model of silicosis in the mouse compared with intratracheal instillation. *Exp Lung Res* 32: 181–199, 2006.
33. **Lang GA, Iwakuma T, Suh YA, Liu G, Rao VA, Parant JM, Valentin-Vega YA, Terzian T, Caldwell LC, Strong LC, El-Naggar AK, Lozano G.** Gain of function of a p53 hot spot mutation in a mouse model of Li-Fraumeni syndrome. *Cell* 119: 861–872, 2004.
34. **Le Gouvello S, Bastuji-Garin S, Aloulou N, Mansour H, Chaumette MT, Berrehar F, Seikour A, Charachon A, Karoui M, Leroy K, Farcet JP, Sobhani I.** High prevalence of Foxp3 and IL17 in MMR-proficient colorectal carcinomas. *Gut* 57: 772–779, 2008.
35. **Li C, Nguyen HT, Zhuang Y, Lin Y, Flemington EK, Guo W, Guenther J, Burow ME, Morris GF, Sullivan D, Shan B.** Post-transcriptional up-regulation of miR-21 by type I collagen. *Mol Carcinog* 50: 563–570, 2011.
36. **Li J, Lau GK, Chen L, Dong SS, Lan HY, Huang XR, Li Y, Luk JM, Yuan YF, Guan XY.** Interleukin 17A promotes hepatocellular carcinoma metastasis via NF-kB induced matrix metalloproteinases 2 and 9 expression. *PLoS One* 6: e21816, 2011.
37. **Li Q, Han Y, Fei G, Guo Z, Ren T, Liu Z.** IL-17 promoted metastasis of non-small-cell lung cancer cells. *Immunol Lett* 148: 144–150, 2012.
38. **Li Y, Cao ZY, Sun B, Wang GY, Fu Z, Liu YM, Kong QF, Wang JH, Zhang Y, Xu XY, Li HL.** Effects of IL-17A on the occurrence of lung adenocarcinoma. *Cancer Biol Ther* 12: 610–616, 2011.
39. **Livak KJ, Schmittgen TD.** Analysis of relative gene expression data using real-time quantitative PCR and the 2(-Delta Delta C(T)) Method. *Methods* 25: 402–408, 2001.
40. **Maniati E, Soper R, Hagemann T.** Up for Mischief? IL-17/Th17 in the tumour microenvironment. *Oncogene* 29: 5653–5662, 2010.
41. **Martin-Orozco N, Dong C.** The IL-17/IL-23 axis of inflammation in cancer: friend or foe? *Curr Opin Investig Drugs* 10: 543–549, 2009.

42. **Martin-Orozco N, Muranski P, Chung Y, Yang XO, Yamazaki T, Lu S, Hwu P, Restifo NP, Overwijk WW, Dong C.** T helper 17 cells promote cytotoxic T cell activation in tumor immunity. *Immunity* 31: 787–798, 2009.
43. **Martins SJ, Takagaki TY, Silva AG, Gallo CP, Silva FB, Capelozzi VL.** Prognostic relevance of TTF-1 and MMP-9 expression in advanced lung adenocarcinoma. *Lung Cancer* 64: 105–109, 2009.
44. **McAllister F, Bailey JM, Alsina J, Nirschl CJ, Sharma R, Fan H, Rattigan Y, Roeser JC, Lankapalli RH, Zhang H, Jaffee EM, Drake CG, Housseau F, Maitra A, Kolls JK, Sears CL, Pardoll DM, Leach SD.** Oncogenic Kras activates a hematopoietic-to-epithelial IL-17 signaling axis in preinvasive pancreatic neoplasia. *Cancer Cell* 25: 621–637, 2014.
45. **Meylan E, Dooley AL, Feldser DM, Shen L, Turk E, Ouyang C, Jacks T.** Requirement for NF-kappaB signalling in a mouse model of lung adenocarcinoma. *Nature* 462: 104–107, 2009.
46. **Minamoto H, Antonangelo L, da Silva AG, Gallo CP, de Andrade e Silva FB, Fenezelian S, Rodrigues OR, Jatene F, Saldiva P, Capelozzi VL.** Tumour cell and stromal features in metastatic and non-metastatic non-small cell lung carcinomas. *Histopathology* 43: 427–443, 2003.
47. **Miossec P, Kolls JK.** Targeting IL-17 and TH17 cells in chronic inflammation. *Nat Rev Drug Discov* 11: 763–776, 2012.
48. **Moghaddam SJ, Li H, Cho SN, Dishop MK, Wistuba II, Ji L, Kurie JM, Dickey BF, Demayo FJ.** Promotion of lung carcinogenesis by chronic obstructive pulmonary disease-like airway inflammation in a K-ras-induced mouse model. *Am J Respir Cell Mol Biol* 40: 443–453, 2009.
49. **Morris GF, Hoyle GW, Athas GB, Lei WH, Xu J, Morris CB, Friedman M.** Lung-specific expression in mice of a dominant negative mutant form of the p53 tumor suppressor protein. *J La State Med Soc* 150: 179–185, 1998.
50. **Morris GF, Labrie C, Mathews MB.** Modulation of transcriptional activation of the proliferating cell nuclear antigen promoter by the adenovirus E1A 243-residue oncoprotein depends on proximal activators. *Mol Cell Biol* 14: 543–553, 1994.
51. **Navratilova Z, Zatloukal J, Kriegova E, Kolek V, Petrek M.** Simultaneous up-regulation of matrix metalloproteinases 1, 2, 3, 7, 8, 9 and tissue inhibitors of metalloproteinases 1, 4 in serum of patients with chronic obstructive pulmonary disease. *Respirology* 17: 1006–1012, 2012.
52. **Numasaki M, Watanabe M, Suzuki T, Takahashi H, Nakamura A, McAllister F, Hishinuma T, Goto J, Lotze MT, Kolls JK, Sasaki H.** IL-17 enhances the net angiogenic activity and in vivo growth of human non-small cell lung cancer in SCID mice through promoting CXCR-2-dependent angiogenesis. *J Immunol* 175: 6177–6189, 2005.
53. **O'Kane CM, McKeown SW, Perkins GD, Bassford CR, Gao F, Thickett DR, McAuley DF.** Salbutamol up-regulates matrix metalloproteinase-9 in the alveolar space in the acute respiratory distress syndrome. *Crit Care Med* 37: 2242–2249, 2009.
54. **Oh J, Takahashi R, Kondo S, Mizoguchi A, Adachi E, Sasahara RM, Nishimura S, Imamura Y, Kitayama H, Alexander DB, Ide C, Horan TP, Arakawa T, Yoshida H, Nishikawa S, Itoh Y, Seiki M, Itohara S, Takahashi C, Noda M.** The membrane-anchored MMP inhibitor RECK is a key regulator of extracellular matrix integrity and angiogenesis. *Cell* 107: 789–800, 2001.
55. **Okamoto T, Valacchi G, Gohil K, Akaike T, van der Vliet A.** S-nitrosothiols inhibit cytokine-mediated induction of matrix metalloproteinase-9 in airway epithelial cells. *Am J Respir Cell Mol Biol* 27: 463–473, 2002.
56. **Park H, Li Z, Yang XO, Chang SH, Nurieva R, Wang YH, Wang Y, Hood L, Zhu Z, Tian Q, Dong C.** A distinct lineage of CD4 T cells regulates tissue inflammation by producing interleukin 17. *Nat Immunol* 6: 1133–1141, 2005.
57. **Reppert S, Boross I, Koslowski M, Tureci O, Koch S, Lehr HA, Finotto S.** A role for T-bet-mediated tumour immune surveillance in anti-IL-17A treatment of lung cancer. *Nat Commun* 2: 600, 2011.
58. **Schwarzenberger P, La Russa V, Miller A, Ye P, Huang W, Zieske A, Nelson S, Bagby GJ, Stoltz D, Mynatt RL, Spriggs M, Kolls JK.** IL-17 stimulates granulopoiesis in mice: use of an alternate, novel gene therapy-derived method for in vivo evaluation of cytokines. *J Immunol* 161: 6383–6389, 1998.
59. **Sfanos KS, Bruno TC, Maris CH, Xu L, Thoburn CJ, DeMarzo AM, Meeker AK, Isaacs WB, Drake CG.** Phenotypic analysis of prostate-infiltrating lymphocytes reveals TH17 and Treg skewing. *Clin Cancer Res* 14: 3254–3261, 2008.
60. **Shan B, Morris GF.** Binding sequence-dependent regulation of the human proliferating cell nuclear antigen promoter by p53. *Exp Cell Res* 305: 10–22, 2005.
61. **Shan M, Yuan X, Song LZ, Roberts L, Zarinkamar N, Seryshev A, Zhang Y, Hilsenbeck S, Chang SH, Dong C, Corry DB, Kheradmand F.** Cigarette smoke induction of osteopontin (SPP1) mediates TH17 inflammation in human and experimental emphysema. *Sci Transl Med* 4: 117ra119, 2012.
62. **Shyamsundar M, McAuley DF, Ingram RJ, Gibson DS, O'Kane D, McKeown ST, Edwards A, Taggart C, Elborn JS, Calfee CS, Matthay MA, O'Kane CM.** Keratinocyte growth-factor promotes epithelial survival and resolution in a human model of lung injury. *Am J Respir Crit Care Med* 189: 1520–1529, 2014.
63. **Siddesha JM, Valente AJ, Sakamuri SS, Yoshida T, Gardner JD, Somanna N, Takahashi C, Noda M, Chandrasekar B.** Angiotensin II stimulates cardiac fibroblast migration via the differential regulation of matrixins and RECK. *J Mol Cell Cardiol* 65: 9–18, 2013.
64. **Sossey-Alaoui K, Ranalli TA, Li X, Bakin AV, Cowell JK.** WAVE3 promotes cell motility and invasion through the regulation of MMP-1, MMP-3, and MMP-9 expression. *Exp Cell Res* 308: 135–145, 2005.
65. **Sparmann A, Bar-Sagi D.** Ras-induced interleukin-8 expression plays a critical role in tumor growth and angiogenesis. *Cancer Cell* 6: 447–458, 2004.
66. **Stamenkovic I.** Extracellular matrix remodelling: the role of matrix metalloproteinases. *J Pathol* 200: 448–464, 2003.
67. **Sun D, Novotny M, Bulek K, Liu C, Li X, Hamilton T.** Treatment with IL-17 prolongs the half-life of chemokine CXCL1 mRNA via the adaptor TRAF5 and the splicing-regulatory factor SF2 (ASF). *Nat Immunol* 12: 853–860, 2011.
68. **Sunaga N, Imai H, Shimizu K, Shames DS, Kakegawa S, Girard L, Sato M, Kaira K, Ishizuka T, Gazdar AF, Minna JD, Mori M.** Oncogenic KRAS-induced interleukin-8 overexpression promotes cell growth and migration and contributes to aggressive phenotypes of non-small cell lung cancer. *Int J Cancer* 130: 1733–1744, 2012.
69. **Takahashi H, Ogata H, Nishigaki R, Broide DH, Karin M.** Tobacco smoke promotes lung tumorigenesis by triggering IKKbeta- and JNK1-dependent inflammation. *Cancer Cell* 17: 89–97, 2010.
70. **To Y, Dohi M, Matsumoto K, Tanaka R, Sato A, Nakagome K, Nakamura T, Yamamoto K.** A two-way interaction between hepatocyte growth factor and interleukin-6 in tissue invasion of lung cancer cell line. *Am J Respir Cell Mol Biol* 27: 220–226, 2002.
71. **Vlahos R, Wark PA, Anderson GP, Bozinovski S.** Glucocorticosteroids differentially regulate MMP-9 and neutrophil elastase in COPD. *PLoS One* 7: e33277, 2012.
72. **Wilke CM, Kryczek I, Wei S, Zhao E, Wu K, Wang G, Zou W.** Th17 cells in cancer: help or hindrance? *Carcinogenesis* 32: 643–649, 2011.
73. **Wu KC, Yang ST, Hsia TC, Yang JS, Chiou SM, Lu CC, Wu RS, Chung JG.** Suppression of cell invasion and migration by propofol are involved in down-regulating matrix metalloproteinase-2 and p38 MAPK signaling in A549 human lung adenocarcinoma epithelial cells. *Anticancer Res* 32: 4833–4842, 2012.
74. **Wu MH, Hong TM, Cheng HW, Pan SH, Liang YR, Hong HC, Chiang WF, Wong TY, Shieh DB, Shiau AL, Jin YT, Chen YL.** Galectin-1-mediated tumor invasion and metastasis, up-regulated matrix metalloproteinase expression, and reorganized actin cytoskeletons. *Mol Cancer Res* 7: 311–318, 2009.
75. **Xue W, Meylan E, Oliver TG, Feldser DM, Winslow MM, Bronson R, Jacks T.** Response and resistance to NF-kappaB inhibitors in mouse models of lung adenocarcinoma. *Cancer Discov* 1: 236–247, 2011.
76. **Ylisirnio S, Hoyhtya M, Turpeenniemi-Hujanen T.** Serum matrix metalloproteinases -2, -9 and tissue inhibitors of metalloproteinases -1, -2 in lung cancer–TIMP-1 as a prognostic marker. *Anticancer Res* 20: 1311–1316, 2000.
77. **Yu Q, Stamenkovic I.** Localization of matrix metalloproteinase 9 to the cell surface provides a mechanism for CD44-mediated tumor invasion. *Genes Dev* 13: 35–48, 1999.
78. **Zhang B, Rong G, Wei H, Zhang M, Bi J, Ma L, Xue X, Wei G, Liu X, Fang G.** The prevalence of Th17 cells in patients with gastric cancer. *Biochem Biophys Res Commun* 374: 533–537, 2008.
79. **Zhang Q, Liu S, Ge D, Xue Y, Xiong Z, Abdel-Mageed AB, Myers L, Hill SM, Rowan BG, Sartor O, Melamed J, Chen Z, You Z.** Interleukin-17 promotes formation and growth of prostate adenocarcinoma in mouse models. *Cancer Res* 72: 2589–2599, 2012.
80. **Zheng S, Chang Y, Hodges KB, Sun Y, Ma X, Xue Y, Williamson SR, Lopez-Beltran A, Montironi R, Cheng L.** Expression of KISS1 and MMP-9 in non-small cell lung cancer and their relations to metastasis and survival. *Anticancer Res* 30: 713–718, 2010.

Drug Design, Development and Therapy

Dovepress
open access to scientific and medical research

Open Access Full Text Article

ORIGINAL RESEARCH

# Interferon-γ and celecoxib inhibit lung-tumor growth through modulating M2/M1 macrophage ratio in the tumor microenvironment

This article was published in the following Dove Press journal:
Drug Design, Development and Therapy
23 September 2014
Number of times this article has been viewed

Fuqiang Ren[1,2,*]
Mingyu Fan[1,2,*]
Jiandong Mei[1,2]
Yongqiang Wu[3]
Chengwu Liu[1,2]
Qiang Pu[1,2]
Zongbing You[4–9]
Lunxu Liu[1,2]

[1]Department of Thoracic Surgery, West China Hospital, [2]Western China Collaborative Innovation Center for Early Diagnosis and Multidisciplinary Therapy of Lung Cancer, [3]Regenerative Medicine Research Center, West China Hospital, Sichuan University, Chengdu, People's Republic of China; [4]Department of Structural and Cellular Biology, [5]Department of Orthopaedic Surgery, [6]Tulane Cancer Center, [7]Louisiana Cancer Research Consortium, [8]Tulane Center for Stem Cell Research and Regenerative Medicine, [9]Tulane Center for Aging, Tulane University Health Sciences Center, New Orleans, LA, USA

*These two authors contributed equally to this study

Correspondence: Zongbing You
Department of Structural and Cellular Biology, Tulane University, 1430 Tulane Avenue – SL49, New Orleans, LA70112, USA
Tel +1 504 988 0467
Fax +1 504 988 1687
Email zyou@tulane.edu

Lunxu Liu
Department of Thoracic Surgery, West China Hospital, Sichuan University, 37 Guoxue Alley, Chengdu, Sichuan 610041, People's Republic of China
Tel +86 28 8542 2494
Fax +86 28 8542 2494
Email lunxu_liu@aliyun.com

**Abstract:** Tumor-associated macrophages play an important role in tumor growth and progression. These macrophages are heterogeneous with diverse functions, eg, M1 macrophages inhibit tumor growth, whereas M2 macrophages promote tumor growth. In this study, we found that IFNγ and/or celecoxib (cyclooxygenase-2 inhibitor) treatment consistently inhibited tumor growth in a mouse lung cancer model. IFNγ alone and celecoxib alone increased the percentage of M1 macrophages but decreased the percentage of M2 macrophages in the tumors, and thus the M2/M1 macrophage ratio was reduced to 1.1 and 1.7 by IFNγ alone and celecoxib alone, respectively, compared to the M2/M1 macrophage ratio of 4.4 in the control group. A combination of IFNγ and celecoxib treatment reduced the M2/M1 macrophage ratio to 0.8. Furthermore, IFNγ and/or celecoxib treatment decreased expression of matrix metalloproteinase (MMP)-2, MMP-9, and VEGF, as well as the density of microvessels in the tumors, compared to the control group. This study provides the proof of principle that IFNγ and/or celecoxib treatment may inhibit lung-tumor growth through modulating the M2/M1 macrophage ratio in the tumor microenvironment, suggesting that IFNγ and celecoxib have potential to be further optimized into a new anticancer therapy.

**Keywords:** tumor-associated macrophages, M1 macrophages, M2 macrophages, lung cancer, interferon-γ, celecoxib

## Introduction

Globally, lung cancer is the most common cause of cancer-related deaths. Currently, surgical resection is the standard of care for most patients with nonmetastatic non-small-cell lung cancer. Other therapeutic approaches are needed to improve the survival of lung cancer patients. Cancer immunotherapy has reappeared as a powerful weapon against cancer recently,[1] since the US Food and Drug Administration approved Provenge® (sipuleucel-T) for the treatment of metastatic castration-resistant prostate cancer and Yervoy® (ipilimumab) for the treatment of metastatic melanoma.[2,3] Inhibitors of PD-1, an immunosuppressive checkpoint protein, and its ligand PD-L1 and PD-L2, have shown promising results in the treatment of cancers, including lung cancer, in clinical trials.[4] A Phase I clinical trial showed that anti-PD-1 antibody produced objective responses in approximately one in four to one in five patients with non-small-cell lung cancer, melanoma, or renal cell cancer; the adverse-event profile did not appear to preclude its use.[5] Another Phase I clinical trial showed that anti-PD-L1 antibody induced objective response rates of 6%–17% and a stabilization of disease at rates of 12%–41% at 24 weeks in patients with advanced cancers, including non-small-cell lung cancer, melanoma, and renal cell cancer.[6] Three patients sustained long-term partial or complete response 16 months to 3 years off therapy.[7]

submit your manuscript | www.dovepress.com
Dovepress
http://dx.doi.org/10.2147/DDDT.S66302



© 2014 Ren et al. This work is published by Dove Medical Press Limited, and licensed under Creative Commons Attribution – Non Commercial (unported, v3.0) License. The full terms of the License are available at http://creativecommons.org/licenses/by-nc/3.0/. Non-commercial uses of the work are permitted without any further permission from Dove Medical Press Limited, provided the work is properly attributed. Permissions beyond the scope of the License are administered by Dove Medical Press Limited. Information on how to request permission may be found at: http://www.dovepress.com/permissions.php

The tumor microenvironment is critical for lung cancer growth and progression. The tumor microenvironment consists of tumor cells, fibroblasts, endothelial cells, and immune cells (including macrophages, dendritic cells, and lymphocytes), as well as these cells' products, such as extracellular matrix, cytokines, chemokines, growth factors, enzymes, and cellular metabolites.[8] Macrophages influence tumor growth, angiogenesis, invasion, and metastasis through producing growth factors, cytokines, chemokines, and enzymes.[9] The tumor-associated macrophages (TAMs) are heterogeneous, with diverse, and even opposite, biological properties, such as the so called M1 (classically activated) and M2 (alternatively activated) macrophages.[10] IFNγ, lipopolysaccharides, TNFα, and GM-CSF induce monocytes to differentiate into M1 macrophages that express high levels of inducible nitric oxide synthase (iNOS), TNFα, IL-1β, IL-6, IL-12, IL-18, IL-23, CXCL10, human leukocyte antigen DR, and reactive oxygen and nitrogen intermediates.[10–14] IL-4, IL-10, IL-13, IL-21, activin A, immune complexes, and glucocorticoids are able to induce monocyte differentiation into M2 macrophages that express high levels of arginase (ARG)-1, IL-1RA, IL-10, CCL22, mannose receptor, galactose receptor, and CD163 antigen.[10,15] M1 macrophages can inhibit tumor growth by producing effector molecules, such as reactive oxygen intermediates, reactive nitrogen intermediates, and TNFα, whereas M2 macrophages promote tumor growth and metastasis by secretion of growth factors, VEGF, matrix metalloproteinases (MMPs), and immunosuppressive cytokines/chemokines.[11] The ratio of M1 and M2 macrophages determines the net anti- or protumor effects of the TAM population in the tumor microenvironment.[16] However, it is very common that M2 macrophages outnumber M1 macrophages in the tumors, so the TAMs provide a protumor microenvironment to support tumor progression.[17]

We previously found that about 70% of TAMs are M2 macrophages and the remaining 30% are M1 macrophages in human non-small-cell lung cancer.[18] We have demonstrated that cyclooxygenase (COX)-2 is expressed at higher levels in human lung tumors than normal lung tissues, leading to increased prostaglandin $E_2$ ($PGE_2$) in lung tumors, which facilitates M2 macrophage differentiation.[19] Given that IFNγ can induce M1 macrophage polarization,[20,21] and celecoxib can inhibit COX-2 enzyme activity,[22] we hypothesized that IFNγ and celecoxib might have a synergistic effect in reversing the M2/M1 macrophage ratio in the tumor microenvironment by promoting M1 macrophage differentiation and inhibiting M2 macrophage differentiation, thus inhibiting tumor growth. In the present study, we designed an in vivo animal study to test this hypothesis. In addition, because zoledronic acid has been shown to deplete TAMs and inhibit tumor progression in a human liver cancer xenograft model,[23] we also tested if zoledronic acid could inhibit lung-tumor growth in a mouse lung cancer model in immunocompetent syngeneic mice. We found that IFNγ alone or celecoxib alone was able to significantly reduce the M2/M1 macrophage ratio in the tumors ($P<0.01$), and thus significantly inhibited tumor growth ($P<0.01$). However, although the combination of IFNγ and celecoxib further reduced the M2/M1 macrophage ratio, the combined treatment did not significantly inhibit tumor growth further, compared to the single-agent treatment. Furthermore, zoledronic acid alone did not show any consistent antitumor effects.

## Materials and methods

### Animal model

The animal study was approved by the Animal Care and Use Committee of West China Hospital, Sichuan University, Chengdu, People's Republic of China (PRC). The mouse Lewis lung carcinoma (LLC)-1 cell line was obtained from the American Type Culture Collection, Manassas, VA, USA. LLC1 was originally derived from C57BL/6 mouse LLC.[24] The cells were cultured in Dulbecco's Modified Eagle's Medium containing 10% fetal bovine serum (HyClone, Logan, UT, USA) and 100 IU/mL penicillin/streptomycin, in a 5% $CO_2$ humidified incubator at 37°C. A total of 115 8-week-old female C57BL/6 mice were purchased from the West China Laboratory Animal Center, Sichuan University, and were housed at this facility in a specific pathogen-free condition. The mice were used in two independent experiments. The first experiment used 75 mice (n=15 mice per group), and the second experiment used 40 mice (n=8 mice per group). In each experiment, 50 μL (containing $1\times10^6$ cells) LLC1 cell suspension was mixed with 50 μL of Matrigel® (BD Biosciences, San Jose, CA, USA), which was injected subcutaneously in the left axilla of each mouse, using a 20-gauge needle and 1 cc tuberculin syringe.

### Experimental groups and treatment

One day after tumor-cell implantation, each mouse was randomly assigned to the following five groups (n=15 and n=8 per group, in the first and second independent experiments, respectively) and treated accordingly: a) treated with saline as a placebo control group; b) treated with recombinant human IFNγ (Shanghai Chemo Wanbang Biopharm, Shanghai, PRC), at a dose of 10,000 IU in 200 μL saline by intraperitoneal injection once a day for 5 consecutive days,

then discontinued for 2 days, and followed by another 5 days (Figure 1A); c) treated with celecoxib (Pfizer China, Shanghai, PRC), at a dose of 60 mg/kg in 200 μL saline, administered by gavage on every other day (Figure 1A); d) treated with a combination of IFNγ and celecoxib at the same dose and schedule described earlier (Figure 1A); and e) treated with zoledronic acid (China National Medicines Guorui Pharmaceutical, Beijing, PRC), at a dose of 0.4 mg/kg in 100 μL saline intraperitoneally twice a week (Figure 1A). Animal body weight was weighed on days 1, 4, 7, 10, and 14.

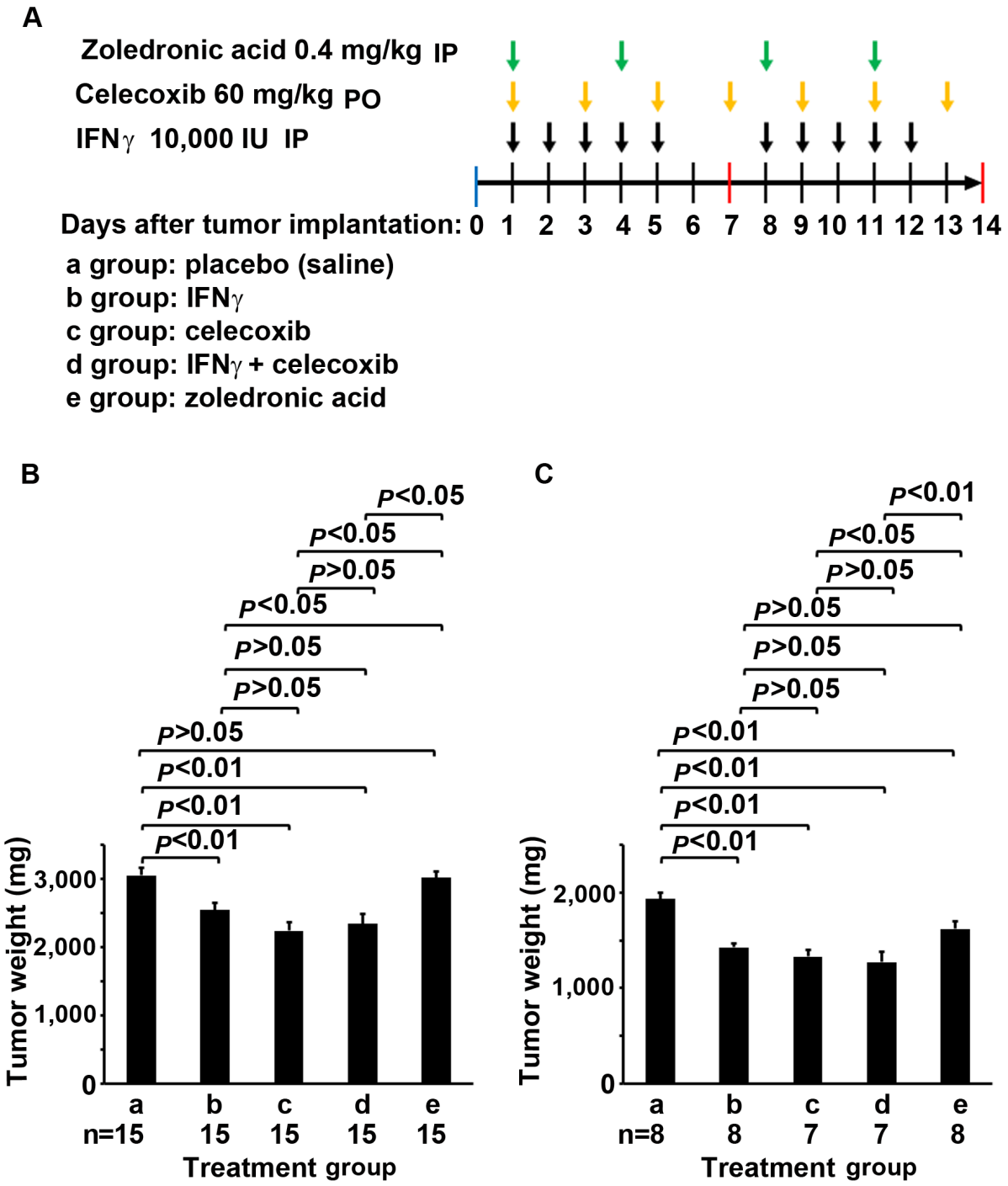



**Figure 1** Experimental design and outcome.

**Notes:** (**A**) Mouse Lewis lung carcinoma LLC1 cells ($1\times10^6$) mixed with Matrigel were injected subcutaneously in C57BL/6 mice on day 0. The mice were randomly assigned into five treatment groups (a–e). Treatment started on day 1, with the doses and schedules indicated by arrows along the time course. (**B**, **C**) The results (tumor weight) of the first and second experiments, respectively. Data represent means ± SEM (error bars). The number of animals per group is indicated under each group.

**Abbreviations:** IP, intraperitoneally; PO, per os (by mouth); IU, international unit; SEM, standard error of the mean.

Animals were killed on day 14, when the largest tumors reached about 1.5 cm in diameter.

## Histopathology

The subcutaneous tumors were dissected out en bloc and weighed for wet weight. In the first experiment, all tumor tissues were fixed with 10% formalin and embedded in paraffin. Five-micrometer sections were cut for histopathologic examination and immunohistochemical (IHC) staining. In the second experiment, approximately 10% of each tumor was fixed and paraffin-sectioned for histopathologic examination, and the rest was used for flow-cytometry analysis.

## Immunohistochemical staining

IHC staining was performed as described previously.[25,26] The primary antibodies used were: rabbit anti-MMP-2 (1:50 dilution), rabbit anti-MMP-9 (1:150 dilution), rabbit anti-VEGF (1:100 dilution), and rabbit anti-factor VIII (1:200). All primary antibodies were purchased from Beijing Biosynthesis Biotechnology (Beijing, PRC). Tissue sections previously stained positively were used as positive controls, while tissue sections with primary antibodies replaced by phosphate-buffered saline (PBS) served as negative controls. Streptavidin peroxidase-conjugated secondary antibodies (SP-9002) and a diaminobenzidine substrate kit were obtained from Zhongshan Golden Bridge Biotechnology (Beijing, PRC). The staining was performed according to the kit manufacturer's instructions. Sections were then counterstained with hematoxylin and mounted in an aqueous mounting medium. Positive cells showed brown particles on the cellular membrane and/or in the cytoplasm. The stained sections were evaluated in a blinded manner (ie, the examiner did not know which group the sections belonged to). Staining of MMP-2, MMP-9, and VEGF was graded in a two-score system according to a previous report.[27] The proportion score represented the estimated fraction of positive staining: 0= no staining, 1=1%–25%, 2=26%–50%, 3=51%–75%, 4=76%–100%. The intensity score represented the estimated average staining intensity of the positive staining: 0= no staining, 1= weak, 2= intermediate, 3= strong. The overall score of staining is the sum of the proportion score and the intensity score (range 0–7). The average score from five high-power fields (magnification 200×) represented the staining score of each tumor. The density of microvessels was assessed according to a previous study.[28] The number of factor VIII-positive microvessels was counted under five high-power fields (magnification 200×), and the average number per high-power field represented the density of microvessels in each tumor. The data represent means ± standard error of the mean of 15 tumors per group (n=15).

## Flow-cytometry analysis

Fresh tumors were cut into approximately 1 $mm^3$ pieces and digested with 0.5 mg/mL collagenase IV in Dulbecco's Modified Eagle's Medium at 37°C with shaking at 100 rounds per minute for 2 hours. The cells were filtered through a 70 μm filter and subjected to red cell-lysis buffer. Then, the cells were fixed with 4% paraformaldehyde and permeabilized with 0.5% Triton X-100. After being washed twice with PBS, the cells were aliquoted into $1\times10^6$ cells in 100 μL PBS in 1.5 mL microcentrifuge tubes for staining. To each test tube was added three antibodies conjugated with different fluorophores: rat antimouse CD68-phycoerythrin (PE) (1:100 dilution; BioLegend, San Diego, CA, USA), rat antimouse iNOS-Alexa Fluor® 488 (1:50 dilution; eBioscience, San Diego, CA, USA), and sheep antimouse arginase 1-allophycocyanin (APC) (1:50 dilution, R&D Systems, Minneapolis, MN, USA). As negative control, three isotype control antibodies were used: rat $IgG_{2\alpha}$, κ-PE (1:100 dilution, BioLegend), rat $IgG_{2\alpha}$, κ-Alexa Fluor 488 (1:50 dilution; eBioscience), and sheep IgG-APC (1:50 dilution; R&D Systems). The cells were stained for 1 hour at 4°C, with gentle shaking every 10 minutes. After being washed twice with PBS, the cells were suspended in 0.5 mL PBS and analyzed with Cytomics FC500 flow cytometry and its software (Beckman Coulter, Brea, CA, USA). Unstained and single antibody-stained samples were used to adjust color compensation and gating of the positively stained population. The CD68-PE-positive cells (macrophages) were gated first, from which population the iNOS-Alexa Fluor 488-positive cells ($CD68^+iNOS^+$ M1 macrophages) and ARG1-APC-positive cells ($CD68^+ARG1^+$ M2 macrophages) were gated. Data represent the means ± standard error of the mean of seven or eight tumors (n=7 for groups c and d, in which one mouse each died due to injuries caused by gavage, and thus only seven mice per group survived to the end point; n=8 for groups a, b, and e, as originally planned).

## Statistical analysis

Statistical analysis was carried out using the SPSS version 19.0 for Windows (SPSS, Chicago, IL, USA). Comparison among multiple groups was analyzed with analysis of variance. $P$-values $<0.05$ were considered statistically significant.

# Results

## IFNγ and celecoxib inhibit mouse lung-tumor growth

We implanted mouse LLC1 cells subcutaneously into syngeneic C57BL/6 mice. The mice were randomly assigned into five groups: a) treated with saline as the placebo control group, b) treated with IFNγ, c) treated with celecoxib (COX-2 inhibitor), d) treated with a combination of IFNγ and celecoxib, and e) treated with zoledronic acid that can kill macrophages (Figure 1A). In the first experiment, we found that IFNγ alone reduced tumor weight by 17% compared to the control group ($P<0.01$, Figure 1B). Celecoxib alone reduced tumor weight by 27% compared to the control group ($P<0.01$, Figure 1B). The combination of IFNγ and celecoxib reduced tumor weight by 23% compared to the control group ($P<0.01$, Figure 1B). However, there was no statistically significant difference between the combined-treatment group and IFNγ-alone or the celecoxib-alone groups ($P>0.05$, Figure 1B). Zoledronic acid did not significantly reduce tumor weight compared to the control group ($P>0.05$, Figure 1B). In the second experiment, we found that IFNγ alone reduced tumor weight by 26% compared to the control group ($P<0.01$, Figure 1C). Celecoxib alone reduced tumor weight by 31% compared to the control group ($P<0.01$, Figure 1C). The combination of IFNγ and celecoxib reduced tumor weight by 34% compared to the control group ($P<0.01$, Figure 1C). Like the first experiment, there was no statistically significant difference between the combined-treatment group and IFNγ-alone or celecoxib alone groups ($P>0.05$, Figure 1C). Unlike the first experiment, zoledronic acid reduced tumor weight by 16% compared to the control group ($P<0.01$, Figure 1C). Of note, we found that all animals gained body weight during the treatment, and there was no statistically significant difference among the five groups (data not shown).

## IFNγ and celecoxib modulate the M2/M1 macrophage ratio in the tumors

We examined the percentage of macrophages in the cellular population of the tumors by staining with anti-CD68 antibodies and analyzing with flow cytometry. The CD68-positive macrophages were gated in window C of the histograms (Figure 2, A–E, left panels). From the CD68-positive population, iNOS-positive ($CD68^+iNOS^+$) cells and ARG1-positive ($CD68^+ARG1^+$) cells were separately gated out, representing M1 and M2 macrophages, respectively (Figure 2, A–E, right panels). Isotype antibody controls are shown in Figure 2F. We found that IFNγ or celecoxib alone did not change the percentage of macrophages, while the combination of IFNγ and celecoxib increased the proportion of macrophages by approximately 11% ($P<0.05$, Figure 2G). In contrast, zoledronic acid decreased the proportion of macrophages by approximately 30% ($P<0.01$, Figure 2G). Both IFNγ alone and celecoxib alone increased the proportion of M1 macrophages by 116% compared to the control group ($P<0.01$, Figure 2H). The combination of IFNγ and celecoxib increased the proportion of M1 macrophages by 158% compared to the control group ($P<0.01$, Figure 2H), the increase of which was also significantly higher than IFNγ alone or celecoxib alone ($P<0.01$). In contrast, zoledronic acid did not change the proportion of M1 macrophages ($P>0.05$, Figure 2H). On the other hand, IFNγ decreased the proportion of M2 macrophages by 48% compared to the control group ($P<0.01$, Figure 2I). Celecoxib decreased the proportion of M2 macrophages by 19% compared to the control group ($P<0.01$, Figure 2I). The combination of IFNγ and celecoxib decreased the proportion of M2 macrophages by 52% compared to the control group ($P<0.01$, Figure 2I), the decrease of which was significantly more than celecoxib alone ($P<0.01$), but not significantly more than IFNγ alone ($P>0.05$). In contrast, zoledronic acid did not change the proportion of M2 macrophages ($P>0.05$, Figure 2I). Based on the proportions of M1 and M2 macrophages in the tumors (Figure 2, H and I), we calculated that the M2/M1 macrophage ratio in the control group was 4.4, whereas IFNγ reduced the M2/M1 macrophage ratio to 1.1. Celecoxib reduced the M2/M1 macrophage ratio to 1.7, and the combination of the IFNγ and celecoxib reduced the M2/M1 macrophage ratio to 0.8. In contrast, zoledronic acid slightly increased the M2/M1 macrophage ratio to 4.8.

## IFNγ, celecoxib, and zoledronic acid decrease expression of MMP-2 and MMP-9

We did IHC staining of MMP-2 and MMP-9 in the tumor sections and quantified the staining using a two-score grading system.[27] We found that MMP-2 expression was significantly reduced by IFNγ alone, celecoxib alone, a combination of IFNγ and celecoxib, and zoledronic acid, compared to the control group (Figure 3, A–G, $P<0.01$). However, there was no statistically significant difference among the four drug-treatment groups ($P>0.05$). Similarly, we found that MMP-9 expression was significantly reduced by IFNγ alone, celecoxib alone, a combination of IFNγ and celecoxib, and zoledronic acid, compared to the control group (Figure 4, A–G, $P<0.05$ and $P<0.01$, respectively). Again, there was

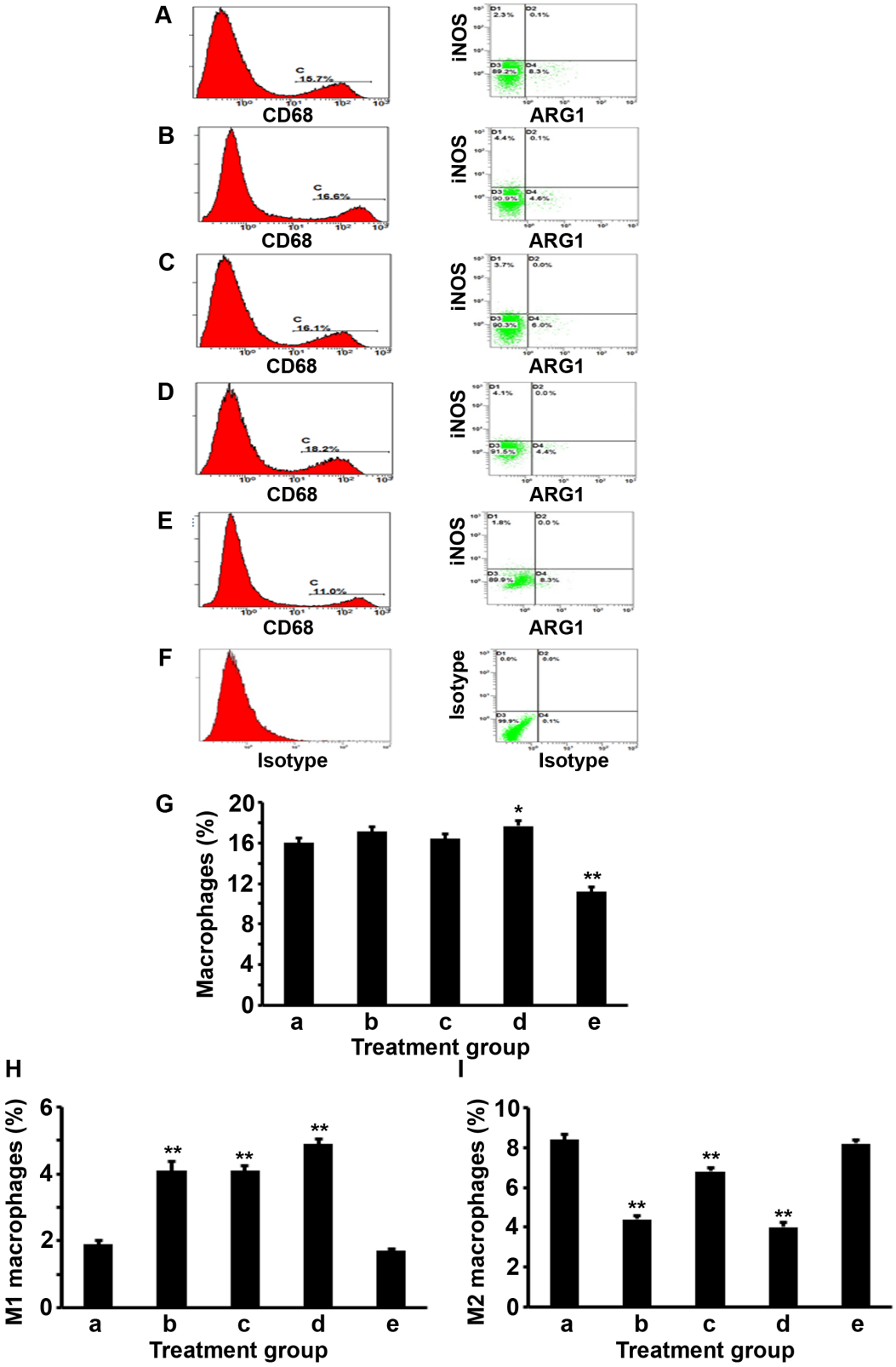



**Figure 2** IFNγ and celecoxib modulate the M2/M1 macrophage ratio in the tumors.

**Notes:** (**A**–**E**) Representative gatings of flow-cytometry analysis of $CD68^+$ macrophages (C in the histograms in the left panels), $CD68^+iNOS^+$ M1 macrophages (upper left window in the right panels), and $CD68^+ARG1^+$ M2 macrophages (lower right window in the right panels) from the mouse tumors. (**A**–**E**) Treatment groups a–e, ie, a, control; b, IFNγ; c, celecoxib; d, IFNγ + celecoxib; and e, zoledronic acid. (**F**) Representative gatings of flow-cytometry analysis using isotype control antibodies. (**G**–**I**) Percentages of macrophages, M1 macrophages, and M2 macrophages, respectively. Data represent means ± SEM (error bars). *$P<0.05$; **$P<0.01$.

**Abbreviations:** iNOS, inducible nitric oxide synthase; SEM, standard error of the mean; ARG, arginase.

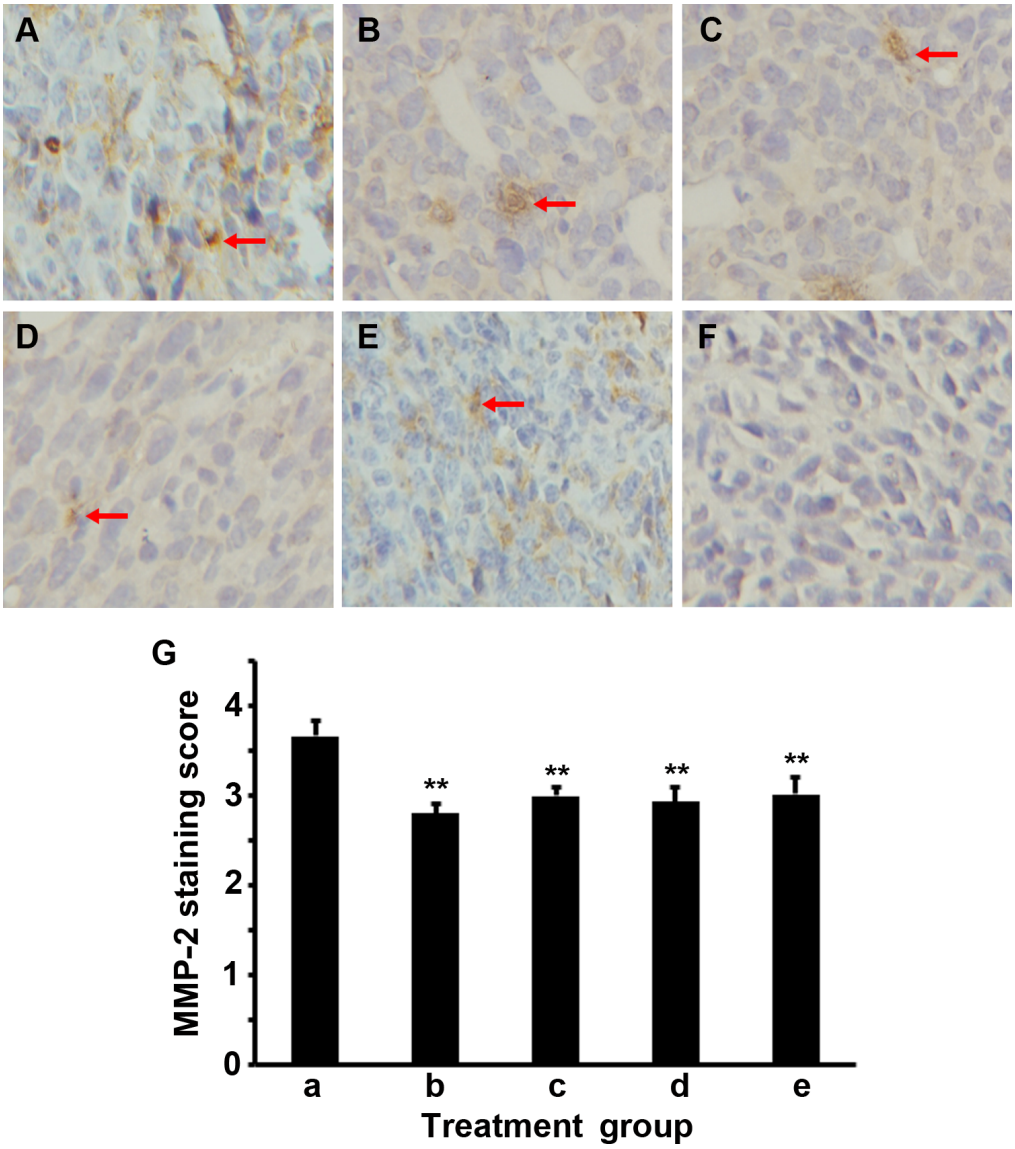



**Figure 3** IFNγ, celecoxib, and zoledronic acid decrease expression of MMP-2.
**Notes:** (**A**–**E**) Representative immunohistochemical staining of MMP-2 in the mouse tumors from groups a–e, ie, a, control; b, IFNγ; c, celecoxib; d, IFNγ + celecoxib; and e, zoledronic acid. Arrows indicate the positively stained cells. Original magnification 400×. (**F**) Negative control of staining. (**G**) Scores of immunohistochemical staining of MMP-2 in the mouse tumors. Data represent means ± SEM (error bars; n=15 tumors per group). $^{**}P<0.01$.
**Abbreviations:** MMP, matrix metalloproteinase; SEM, standard error of the mean.

no statistically significant difference among the four drug-treatment groups ($P>0.05$).

## IFNγ and celecoxib decrease VEGF expression and density of microvessels

We did IHC staining of VEGF in the tumor sections and quantified the staining using a two-score grading system.[27] We found that VEGF expression was significantly reduced by IFNγ alone, celecoxib alone, and a combination of IFNγ and celecoxib, compared to the control group (Figure 5, A–D, F, G; $P<0.01$). However, there was no statistically significant difference among these three drug-treatment groups ($P>0.05$). In contrast, zoledronic acid did not significantly change the expression of VEGF ($P>0.05$, Figure 5, E–G). We assessed the density of microvessels in the tumors by factor VIII staining according to a previous study.[28] We found that IFNγ alone, celecoxib alone, and a combination of IFNγ and celecoxib significantly decreased the density of microvessels compared to the control group (Figure 6, A–D, F, G; $P<0.05$ and $P<0.01$, respectively). The density of microvessels was significantly lower in the combined-treatment group than the IFNγ-alone group ($P<0.05$), but not significantly different from the celecoxib-alone group ($P>0.05$). In contrast, zoledronic acid did not significantly

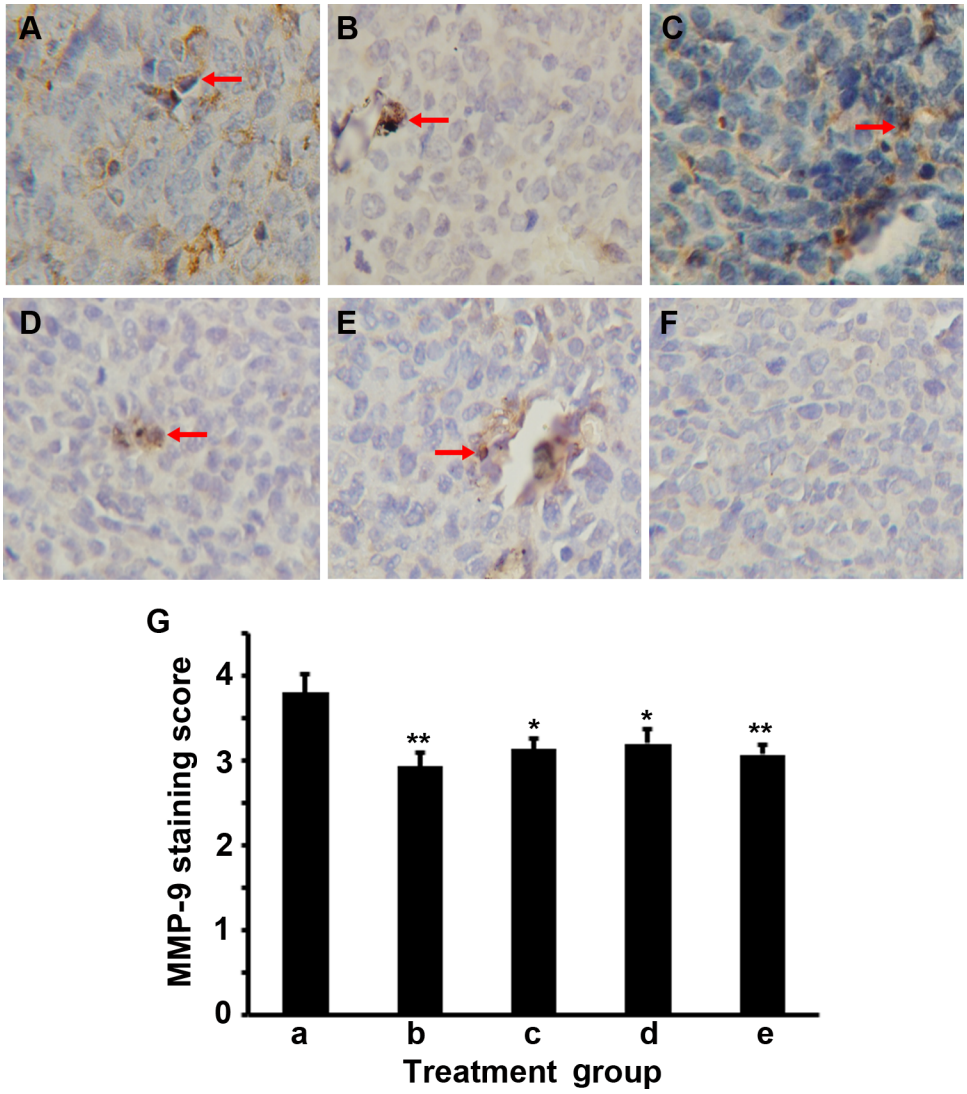



**Figure 4** IFNγ, celecoxib, and zoledronic acid decrease expression of MMP-9.
**Notes:** (**A**–**E**) Representative immunohistochemical staining of MMP-9 in the mouse tumors from groups a–e, ie, a, control; b, IFNγ; c, celecoxib; d, IFNγ + celecoxib; and e, zoledronic acid. Arrows indicate the positively stained cells. Original magnification 400×. (**F**) Negative control of staining. (**G**) Scores of immunohistochemical staining of MMP-9 in the mouse tumors. Data represent means ± SEM (error bars; n=15 tumors per group). *$P<0.05$; **$P<0.01$.
**Abbreviations:** MMP, matrix metalloproteinase; SEM, standard error of the mean.

change the density of microvessels in the tumors ($P>0.05$, Figure 6, E–G).

## Discussion

In the lung-tumor microenvironment, M2 macrophages usually outnumber M1 macrophages, creating a protumor immune microenvironment. Other cancers also present an M2-dominant tumor microenvironment, including prostate cancer and ovarian cancer.[29–31] Since M1 macrophages inhibit tumor growth while M2 macrophages promote tumor growth by expressing VEGF and MMPs,[11] it is intriguing to investigate if enhancing M1 macrophage differentiation and inhibiting M2 macrophage differentiation would affect tumor growth.

In the present study, we tested IFNγ, a well-known inducer of M1 macrophage differentiation,[20,21] and celecoxib, a COX-2 inhibitor.[22] We speculated that celecoxib could inhibit COX-2 and reduce $PGE_2$ production, thus inhibiting M2 macrophage differentiation, based on our previous study showing that $PGE_2$ facilitates M2 macrophage differentiation.[19] We found that IFNγ and celecoxib, either used alone or in combination, consistently inhibited lung-tumor growth in two independent experiments. IFNγ or celecoxib alone did not change the percentage of total macrophages, but their combination slightly increased the percentage of total macrophages. What was remarkable was that both IFNγ alone and celecoxib alone significantly increased the

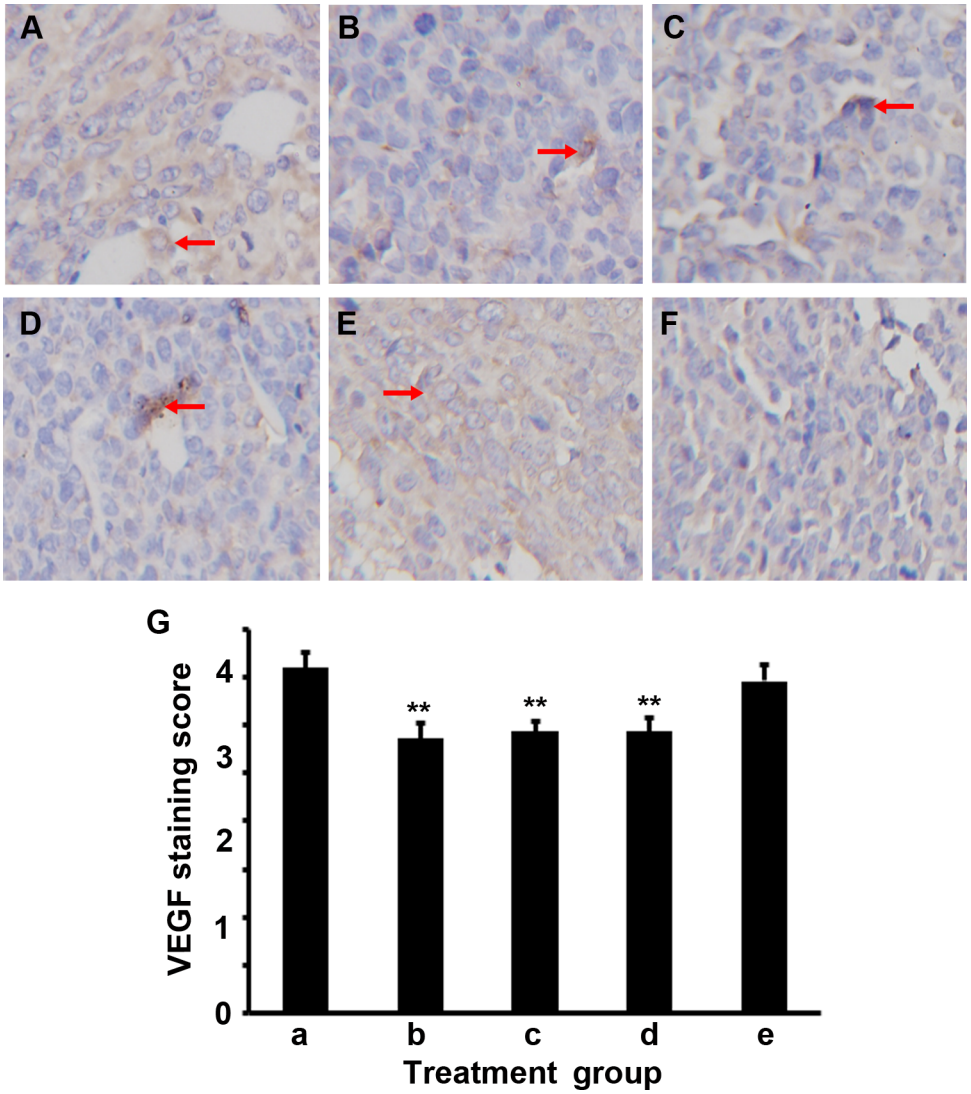



**Figure 5** IFNγ and celecoxib decrease expression of VEGF.
**Notes:** (**A**–**E**) Representative immunohistochemical staining of VEGF in the mouse tumors from groups a–e, ie, a, control; b, IFNγ; c, celecoxib; d, IFNγ + celecoxib; and e, zoledronic acid. Arrows indicate the positively stained cells. Original magnification 400×. (**F**) Negative control of staining. (**G**) Scores of immunohistochemical staining of VEGF in the mouse tumors. Data represent means ± SEM (error bars; n=15 tumors per group). $^{**}P<0.01$.
**Abbreviation:** SEM, standard error of the mean.

percentage of M1 macrophages, but decreased the percentage of M2 macrophages in the tumors. Therefore, the M2/M1 macrophage ratio was reduced to 1.1 and 1.7 by IFNγ alone and celecoxib alone, respectively. In contrast, the M2/M1 macrophage ratio in the control group was 4.4, which is four times and 2.6 times of those in the IFNγ-alone and celecoxib-alone groups, respectively. These results suggest that IFNγ and celecoxib indeed can modulate the M2/M1 macrophage ratio in the lung-tumor microenvironment. However, we only observed a slight further reduction of the M2/M1 macrophage ratio to 0.8 by the combination of IFNγ and celecoxib. This is because the combined treatment did not reduce M2 macrophages further than IFNγ alone, although the combined treatment increased the M1 percentage significantly more than IFNγ alone or celecoxib alone. Therefore, the synergy between IFNγ and celecoxib in modulating the M2/M1 macrophage ratio is not obvious, which is consistent with the lack of synergy in inhibition of tumor growth. Furthermore, IFNγ alone, celecoxib alone, and their combination reduced the expression of MMP-2, MMP-9, and VEGF to similar levels, which is another piece of evidence showing the lack of synergy between IFNγ and celecoxib. The density of microvessels in the tumors was also decreased by IFNγ alone, celecoxib alone, and their combination, except that the decrease with the combined treatment was significantly more than the IFNγ-alone treatment. Taken together, these results suggest that IFNγ alone or celecoxib alone can reduce the M2/M1 macrophage ratio in the tumor microenvironment,

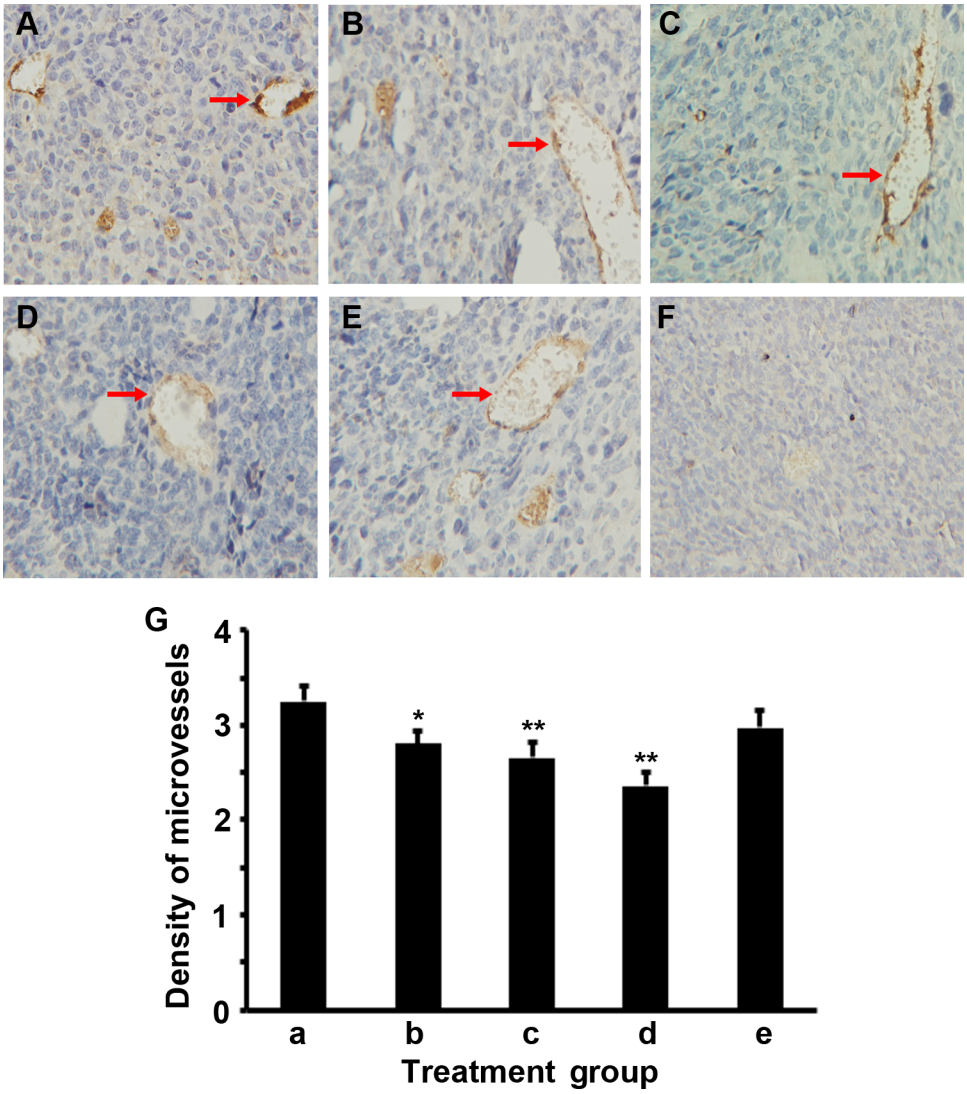



**Figure 6** IFNγ and celecoxib decrease the density of microvessels in the tumors.
**Notes:** (**A**–**E**) Representative immunohistochemical staining of factor VIII to show the microvessels in the mouse tumors from groups a–e, ie, a, control; b, IFNγ; c, celecoxib; d, IFNγ + celecoxib; and e, zoledronic acid. Arrows indicate the factor VIII-positive microvessels. Original magnification 200×. (**F**) Negative control of staining. (**G**) The density of microvessels in the mouse tumors. Data represent means ± SEM (error bars; n=15 tumors per group). *$P<0.05$; **$P<0.01$.
**Abbreviation:** SEM, standard error of the mean.

thus decreasing expression of MMP-2, MMP-9, and VEGF and associated angiogenesis, resulting in inhibition of mouse lung-tumor growth. IFNγ and celecoxib given at the current doses and schedules appear to have neither any synergy in modulating the M2/M1 macrophage ratio nor any synergy in inhibiting tumor growth.

It has been shown that TAM depletion reprograms the immunosuppressive tumor microenvironment and creates an antitumor immune microenvironment in breast cancer and liver cancer.[23,32] TAMs may be a therapeutic target in other tumors, such as prostate cancer, renal cell carcinoma, and osteosarcoma.[31,33,34] In addition, anti-EGFR antibody (cetuximab) may activate M2 macrophages, which might be the reason that addition of cetuximab to bevacizumab plus chemotherapy showed a negative outcome.[35] This finding implies that anti-TAM approaches may have potential in combinatory therapies. In this study, we tested if TAM depletion by zoledronic acid could affect tumor growth in our mouse lung cancer model. We did not find any inhibition of tumor growth in the first experiment, but we did see a 16% decrease in the tumor weight in the second experiment. The percentage of total macrophages was decreased in both experiments. We speculate that the discrepancy between the two experiments may be due to the difference in tumor growth. On average, the tumors in the first experiment grew much bigger than the second experiment. Although we implanted the same

number of cells in both experiments, it could be that the cell viability and cellular growth status were not the same, so the live cell number was fewer in the second experiment than the first experiment. Therefore, inhibition of tumor growth was more obvious in the second experiment by IFNγ alone, celecoxib alone, and a combination of IFNγ and celecoxib, as well as zoledronic acid. Although zoledronic acid reduced expression of MMP-2 and MMP-9, it did not affect VEGF expression or the density of microvessels in the tumors. This may partially explain the fact that in small tumors, zoledronic acid may have some effects, but in large tumors where more angiogenesis occurs, zoledronic acid becomes ineffective in treating subcutaneous tumors. It is worth pointing out that zoledronic acid has only been approved for treating multiple myeloma and cancer bone metastasis, as well as other bone-related diseases.[36] Based on our study, we are not optimistic about zoledronic acid's effects on lung tumors other than bone metastasis.

One limitation of the present study is that only a single dosage of each drug was tested. The doses and administration schedules were chosen based on previous reports.[37–39] It is reasonable to speculate that those doses may not necessarily be the optimal ones. Nevertheless, the positive results from the empirical doses used in this study are encouraging. Future studies are warranted to investigate the dose-dependent effects of IFNγ alone, celecoxib alone, and a combination of the optimal doses of IFNγ and celecoxib. The second limitation is that the treatments were given immediately after tumor inoculation. Any effects should be considered prophylactic in terms of preventing tumor growth, and the effects observed were minimal. The design of treatments after establishment of tumors and optimization to obtain more dramatic effects shall be considered in further studies. The third limitation of this study is that only CD68 in combination with iNOS and ARG1 were used for defining M1 and M2 macrophages, because the flow-cytometry instrument used was only able to show three colors. Ideally, a panel of six to eight markers (including F4/80) should be used. Finally, the association between macrophages and MMP-2, MMP-9, and VEGF is only suggestive, as other cells (tumor cells, fibroblasts, etc) may also express them.

In conclusion, this study provides the proof of principle that IFNγ and/or celecoxib treatment may inhibit lung-tumor growth through modulating the M2/M1 macrophage ratio in the tumor microenvironment, suggesting that IFNγ and celecoxib have potential to be further optimized in a new anticancer therapy.

## Acknowledgments

This work was partially supported by the National Natural Science Foundation of China (NSFC 81172236 – The mechanism of TAMs activation in lung cancer and a novel immunotherapy; NSFC 81372505 – The role of IL-17 in formation and progression of primary lung cancer and the underlying molecular mechanisms) and the Key Science and Technology Program of Sichuan Province, People's Republic of China (2009SZ0152 and 2011SZ0111) to LL. ZY was partially supported by two grants from the National Institute of General Medical Sciences (P20GM103518) and the National Cancer Institute (R01CA174714) of the National Institutes of Health, three grants from Department of Defense Health Program through the Prostate Cancer Research Program (W81XWH-14-1-0050, W81XWH-14-1-0149, and PC130118; the US Army Medical Research Acquisition Activity, 820 Chandler Street, Fort Detrick, MD 21702-5014 is the awarding and administering acquisition office), the Developmental Fund of Tulane Cancer Center (TCC), and Louisiana Cancer Research Consortium (LCRC) Fund. The content of this article is solely the responsibility of the authors, and does not necessarily represent the official views of the National Institutes of Health or the Department of Defense.

## Disclosure

The authors report no conflicts of interest in this work.

## References

1. Ledford H. Cancer treatment: the killer within. *Nature*. 2014; 508(7494):24–26.
2. Kantoff PW, Higano CS, Shore ND, et al. Sipuleucel-T immunotherapy for castration-resistant prostate cancer. *N Engl J Med*. 2010;363(5): 411–422.
3. Hodi FS, O'Day SJ, McDermott DF, et al. Improved survival with ipilimumab in patients with metastatic melanoma. *N Engl J Med*. 2010;363(8):711–723.
4. Harvey RD. Immunologic and clinical effects of targeting of PD-1 in lung cancer. *Clin Pharmacol Ther*. 2014;96(2):214–223.
5. Topalian SL, Hodi FS, Brahmer JR, et al. Safety, activity, and immune correlates of anti-PD-1 antibody in cancer. *N Engl J Med*. 2012;366(26): 2443–2454.
6. Brahmer JR, Tykodi SS, Chow LQ, et al. Safety and activity of anti-PD-L1 antibody in patients with advanced cancer. *N Engl J Med*. 2012;366(26):2455–2465.
7. Lipson EJ, Sharfman WH, Drake CG, et al. Durable cancer regression off-treatment and effective reinduction therapy with an anti-PD-1 antibody. *Clin Cancer Res*. 2013;19(2):462–468.
8. Witz IP, Levy-Nissenbaum O. The tumor microenvironment in the post-PAGET era. *Cancer Lett*. 2006;242(1):1–10.
9. Lewis CE, Pollard JW. Distinct role of macrophages in different tumor microenvironments. *Cancer Res*. 2006;66(2):605–612.
10. Mantovani A, Sica A, Locati M. New vistas on macrophage differentiation and activation. *Eur J Immunol*. 2007;37(1):14–16.
11. Mantovani A, Sica A, Locati M. Macrophage polarization comes of age. *Immunity*. 2005;23(4):344–346.

12. Baj-Krzyworzeka M, Szatanek R, Weglarczyk K, Baran J, Zembala M. Tumour-derived microvesicles modulate biological activity of human monocytes. *Immunol Lett*. 2007;113(2):76–82.
13. Mantovani A, Sozzani S, Locati M, Allavena P, Sica A. Macrophage polarization: tumor-associated macrophages as a paradigm for polarized M2 mononuclear phagocytes. *Trends Immunol*. 2002;23(11):549–555.
14. Martinez FO, Sica A, Mantovani A, Locati M. Macrophage activation and polarization. *Front Biosci*. 2008;13:453–461.
15. Gordon S. Alternative activation of macrophages. *Nat Rev Immunol*. 2003;3(1):23–35.
16. Mantovani A, Bottazzi B, Colotta F, Sozzani S, Ruco L. The origin and function of tumor-associated macrophages. *Immunol Today*. 1992;13(7):265–270.
17. Galdiero MR, Garlanda C, Jaillon S, Marone G, Mantovani A. Tumor associated macrophages and neutrophils in tumor progression. *J Cell Physiol*. 2013;228(7):1404–1412.
18. Ma J, Liu L, Che G, Yu N, Dai F, You Z. The M1 form of tumor-associated macrophages in non-small cell lung cancer is positively associated with survival time. *BMC Cancer*. 2010;10:112.
19. Liu L, Ge D, Ma L, et al. Interleukin-17 and prostaglandin E2 are involved in formation of an M2 macrophage-dominant microenvironment in lung cancer. *J Thorac Oncol*. 2012;7(7):1091–1100.
20. Davis MJ, Tsang TM, Qiu Y, et al. Macrophage M1/M2 polarization dynamically adapts to changes in cytokine microenvironments in *Cryptococcus neoformans* infection. *MBio*. 2013;4(3):e00264-13.
21. Sica A, Mantovani A. Macrophage plasticity and polarization: in vivo veritas. *J Clin Invest*. 2012;122(3):787–795.
22. Zhang H, Li Z, Wang K. Combining sorafenib with celecoxib synergistically inhibits tumor growth of non-small cell lung cancer cells in vitro and in vivo. *Oncol Rep*. 2014;31(4):1954–1960.
23. Zhang W, Zhu XD, Sun HC, et al. Depletion of tumor-associated macrophages enhances the effect of sorafenib in metastatic liver cancer models by antimetastatic and antiangiogenic effects. *Clin Cancer Res*. 2010;16(13):3420–3430.
24. Bertram JS, Janik P. Establishment of a cloned line of Lewis lung carcinoma cells adapted to cell culture. *Cancer Lett*. 1980;11(1):63–73.
25. Zhang Q, Liu S, Ge D, et al. Interleukin-17 promotes formation and growth of prostate adenocarcinoma in mouse models. *Cancer Res*. 2012;72(10):2589–2599.
26. Dai F, Liu L, Che G, et al. The number and microlocalization of tumor-associated immune cells are associated with patient's survival time in non-small cell lung cancer. *BMC Cancer*. 2010;10:220.
27. Rahman MA, Dhar DK, Yamaguchi E, et al. Coexpression of inducible nitric oxide synthase and COX-2 in hepatocellular carcinoma and surrounding liver: possible involvement of COX-2 in the angiogenesis of hepatitis C virus-positive cases. *Clin Cancer Res*. 2001;7(5):1325–1332.
28. Weidner N. Current pathologic methods for measuring intratumoral microvessel density within breast carcinoma and other solid tumors. *Breast Cancer Res Treat*. 1995;36(2):169–180.
29. Redente EF, Dwyer-Nield LD, Merrick DT, et al. Tumor progression stage and anatomical site regulate tumor-associated macrophage and bone marrow-derived monocyte polarization. *Am J Pathol*. 2010;176(6):2972–2985.
30. Zhang M, He Y, Sun X, et al. A high M1/M2 ratio of tumor-associated macrophages is associated with extended survival in ovarian cancer patients. *J Ovarian Res*. 2014;7(1):19.
31. Lanciotti M, Masieri L, Raspollini MR, et al. The role of M1 and M2 macrophages in prostate cancer in relation to extracapsular tumor extension and biochemical recurrence after radical prostatectomy. *Biomed Res Int*. 2014;2014:486798.
32. DeNardo DG, Brennan DJ, Rexhepaj E, et al. Leukocyte complexity predicts breast cancer survival and functionally regulates responses to chemotherapy. *Cancer Discov*. 2011;1(1):54–67.
33. Santoni M, Massari F, Amantini C, et al. Emerging role of tumor-associated macrophages as therapeutic targets in patients with metastatic renal cell carcinoma. *Cancer Immunol Immunother*. 2013;62(12):1757–1768.
34. Pahl JH, Kwappenberg KM, Varypataki EM, et al. Macrophages inhibit human osteosarcoma cell growth after activation with the bacterial cell wall derivative liposomal muramyl tripeptide in combination with interferon-γ. *J Exp Clin Cancer Res*. 2014;33:27.
35. Pander J, Heusinkveld M, van der Straaten T, et al. Activation of tumor-promoting type 2 macrophages by EGFR-targeting antibody cetuximab. *Clin Cancer Res*. 2011;17(17):5668–5673.
36. Ibrahim A, Scher N, Williams G, et al. Approval summary for zoledronic acid for treatment of multiple myeloma and cancer bone metastases. *Clin Cancer Res*. 2003;9(7):2394–2399.
37. Senzaki M, Ishida S, Yada A, et al. CS-706, a novel cyclooxygenase-2 selective inhibitor, prolonged the survival of tumor-bearing mice when treated alone or in combination with anti-tumor chemotherapeutic agents. *Int J Cancer*. 2008;122(6):1384–1390.
38. Curnis F, Gasparri A, Sacchi A, Cattaneo A, Magni F, Corti A. Targeted delivery of IFNγ to tumor vessels uncouples antitumor from counter-regulatory mechanisms. *Cancer Res*. 2005;65(7):2906–2913.
39. Hung TT, Chan J, Russell PJ, Power CA. Zoledronic acid preserves bone structure and increases survival but does not limit tumour incidence in a prostate cancer bone metastasis model. *PLoS One*. 2011;6(5):e19389.



**Drug Design, Development and Therapy** Dovepress

## Publish your work in this journal

Drug Design, Development and Therapy is an international, peer-reviewed open-access journal that spans the spectrum of drug design and development through to clinical applications. Clinical outcomes, patient safety, and programs for the development and effective, safe, and sustained use of medicines are a feature of the journal, which has also been accepted for indexing on PubMed Central. The manuscript management system is completely online and includes a very quick and fair peer-review system, which is all easy to use. Visit http://www.dovepress.com/testimonials.php to read real quotes from published authors.

**Submit your manuscript here:** http://www.dovepress.com/drug-design-development-and-therapy-journal

ISSN 0973 - 6042



# International Journal of Shoulder Surgery

Volume 8 Issue 3 Jul-Sep 2014

## Contents


- Decreased scapular notching with lateralization and inferior baseplate placement in reverse shoulder arthroplasty with high humeral inclination
- Short stem shoulder replacement
- Long-term functional results and isokinetic strength evaluation after arthroscopic tenotomy of the long head of biceps tendon
- Comparison of the cheese-wiring effects among three sutures used in rotator cuff repair
- Noncomminuted lateral end clavicle fractures associated with coracoclavicular ligament disruption: Technical considerations for optimal anatomic fixation and stability
- Scapular spine stress fractures: To fix or not to fix, our experience in a patient with bilateral fractures and review of the literature


PubMed

Online full text at
www.internationalshoulderjournal.org

Wolters Kluwer Health | Medknow

Original Article

Access this article online
Website: www.internationalshoulderjournal.org
DOI: 10.4103/0973-6042.140115
Quick Response Code:

# Comparison of the cheese-wiring effects among three sutures used in rotator cuff repair

Mark Lambrechts[1,2], Behrooz Nazari[3], Arash Dini[1], Michael J. O'Brien[1], Wendell M. R. Heard[1], Felix H. Savoie[1], Zongbing You[1,2,4]

## ABSTRACT

**Purpose:** The goal of this study was to compare the cheese-wiring effects of three sutures with different coefficients of friction.

**Materials and Methods:** Sixteen human cadaveric shoulders were dissected to expose the distal supraspinatus and infraspinatus muscle tendons. Three sutures were stitched through the tendons: #2 Orthocord™ suture (reference #223114, DePuy Mitek, Inc., Raynham, MA), #2 ETHIBOND* EXCEL Suture, and #2 FiberWire® suture (FiberWire®, Arthrex, Naples, FL). The sutures were pulled by cyclic axial forces from 10 to 70 N at 1 Hz for 1000 cycles through a MTS machine. The cut-through distance on the tendon was measured with a digital caliper.

**Results:** The cut-through distance in the supraspinatus tendons (mean ± standard deviation, $n$ = 12) were 2.9 ± 0.6 mm for #2 Orthocord™ suture, 3.2 ± 1.2 mm for #2 ETHIBOND* suture, and 4.2 ± 1.7 mm for #2 FiberWire® suture. The differences were statistically significant analyzing with analysis of variance ($P$ = 0.047) and two-tailed Student's $t$-test, which showed significance between Orthocord™ and FiberWire® sutures ($P$ = 0.026), but not significant between Orthocord™ and ETHIBOND* sutures ($P$ = 0.607) or between ETHIBOND* and FiberWire® sutures ($P$ = 0.103).

**Conclusion:** The cheese-wiring effect is less in the Orthocord™ suture than in the FiberWire® suture in human cadaveric supraspinatus tendons.

**Clinical Relevance:** Identification of sutures that cause high levels of tendon cheese-wiring after rotator cuff repair can lead to better suture selection.

**Key words:** Biomechanics, cadaver study, cheese-wiring, supraspinatus tendon, suture

[1]Department of Orthopaedic Surgery and Tulane Institute of Sports Medicine, Tulane University, School of Medicine, [2]Department of Structural and Cellular Biology, Tulane University School of Medicine, [4]Tulane Cancer Center, Louisiana Cancer Research Consortium, Tulane Center for Aging, Tulane Center for Stem Cell Research and Regenerative Medicine, Tulane University School of Medicine, New Orleans, LA 70112, USA, [3]Department of Orthopaedics, Tabriz Emam Reza Hospital, Tabriz, Iran

**Address for correspondence:**
Prof. Zongbing You,
1430 Tulane Ave SL 49, New Orleans, LA 70112, USA.
E-mail: zyou@tulane.edu

## INTRODUCTION

Rotator cuff tear is one of the most common injuries involving the shoulder. The tear most often involves the supraspinatus tendon. Without prompt treatment, the altered joint biomechanics can extend the tear to involve the infraspinatus tendon.[1,2] Repair of these injuries is based on individual patients with few protocols established to determine whether the patient best fits for steroid injection, physical therapy, or surgical intervention. However, surgery is generally recommended for all symptomatic patients younger than 60 with a full-thickness rotator cuff tear.[3] The expected outcome of surgery is a high fixation strength, but many variables can affect the success of surgery including the patient's age, tendon health, smoking, time from tear to surgery, arthroscopic technique, suture location, and suture selection.[4-7]

The choice of sutures has not been well studied. It has been reported that the suture location is a key factor in causing damage to the repaired tendons. Wieser *et al.*[8] found the ideal placement to be located in the center of the tendon just medial to the rotator cable. This finding is in contrast to Wang *et al.*[9] who found an ideal location of suture placement more medially at the muscle-tendon junction. Clearly, location of

Please cite this article as: Lambrechts M, Nazari B, Dini A, O'Brien MJ, Heard WM, Savoie FH, *et al.* Comparison of the cheese-wiring effects among three sutures used in rotator cuff repair. Int J Shoulder Surg 2014;8:81-5.

the placed sutures is important in minimizing postsurgical tendon damage, but the properties of the sutures should also be a consideration. Unfortunately, it is not easy to evaluate different sutures because different types of repair define surgical success differently. For example, rotator cuff repair requires suture stability under high load requirements, while flexor tendon repair requires minimal friction. Nevertheless, there are several well-recognized suture properties including the tensile strength, knot security, stiffness, and resistance to fraying.[10-15]

Coefficient of friction is an inherent property of the suture, which has not been well investigated. Silva *et al*.[16] found that #3-0 FiberWire® sutures (FiberWire®, Arthrex, Naples, FL) had a lower coefficient of friction (0.054) than #3-0 ETHIBOND* sutures (with a coefficient of friction of 0.076) (ETHIBOND* EXCEL, Ethicon, Somerville, NJ). We speculate that coefficient of friction may be an important factor in determining how easy the suture cuts through the tendon, that is, the cheese-wiring effect. Our hypothesis is that the sutures with lower coefficient of friction may be easier to cut-through the tendon than the sutures with higher coefficient of friction. The present study was conducted to test this hypothesis.

## MATERIALS AND METHODS

This study was conducted using human cadaveric supraspinatus and infraspinatus muscle tendons. Eight pairs of unembalmed human shoulders ($n = 16$) were obtained from donors through the Bureau of Anatomical Services, Louisiana State Department of Health and Hospitals. The average age of the donors was 77.1 ± 9.8 years of age. The use of these deidentified specimens was determined as "not human subjects study" by Tulane University Institutional Review Board (Project no. 206610-1). The specimens were stored at −20°C and thawed at room temperature prior to use. Only grossly intact tendons without obvious damage were used for the study. Twelve supraspinatus tendons ($n = 12$) were dissected out and detached distally from the greater tubercle of the humerus. The supraspinatus muscles remained attached to the scapula and the subscapularis and infraspinatus muscles remained undisturbed during testing of the supraspinatus tendons. After testing on the supraspinatus tendons, the infraspinatus tendons were dissected out and detached distally, while the infraspinatus muscle remained attached to the scapula. Only 5 infraspinatus tendons ($n = 5$) were not damaged and were used for testing. The three types of sutures used in this study were #2 FiberWire® suture (reference #AR-7200, Arthrex, Inc., Naples, FL), #2 ETHIBOND* EXCEL suture (reference #X519, Ethicon, Inc., Somerville, NJ), and #2 Orthocord™ suture (reference #223114, DePuy Mitek, Inc., Raynham, MA). FiberWire® suture is constructed of a multi-strand, long chain ultra-high molecular weight polyethylene (UHMWPE) core with a braided jacket of polyester and UHMWPE. ETHIBOND* suture is composed of a braided polyester core coated with polybutilate. Orthocord™ suture is made with a braided polyethylene core coated with a copolymer of caprolactone and glycolide.

### Biomechanical testing

We used a Bionix Servohydraulic Test System (MTS Systems Corporation, Eden Prairie, MN) for the mechanic tests. The scapula with the proximal attachment of supraspinatus (or infraspinatus) muscle was fixed to the sensor stage using a custom-made frame [Figure 1a]. A single pass-through suture loop was placed through the supraspinatus (or infraspinatus) tendon approximately 5 mm distal to the muscle-tendon junction [Figure 1b]. The other end of the suture loop was attached to the actuator [Figure 1a]. The specimen was kept moist at all times by spraying of phosphate buffered saline.

In our pilot study, two shoulders were used to determine the testing conditions. A force of 10 N was applied to preload the tendon and the suture for 1 min. No cutting through of the tendon was observed by any of the three sutures at 10 N loading. A mark line (start line) was made on the tendon with a marker pen. Then, a 10-50 N at 1 Hz for 1000 cycles of cyclic pulling load was applied to the suture. At the end of 1000 cycles, any cut-through of the tendon by the suture was recorded manually with a digital caliper [Figure 1c]. Then, the load was returned to 10 N for 1 min. Next, this step was repeated at 10-70 N at 1 Hz for 1000 cycles. Again, the cut-through distance was recorded. Finally, this step was repeated at 10-100 N at 1 Hz for 1000 cycles. However, at this load, all three sutures completely cut-through the tendon when the load was approximately 80-85 N. Therefore, we decided to test each suture by applying 10-70 N at 1 Hz for 1000 cycles.

Twelve supraspinatus muscle tendons were tested first, followed by testing five infraspinatus muscle tendons. The three sutures were tested on each tendon side-by-side, with approximately 5 mm inter-stitch distance. Each of the three sutures was stitched in an alternated order, so that the location of stitch

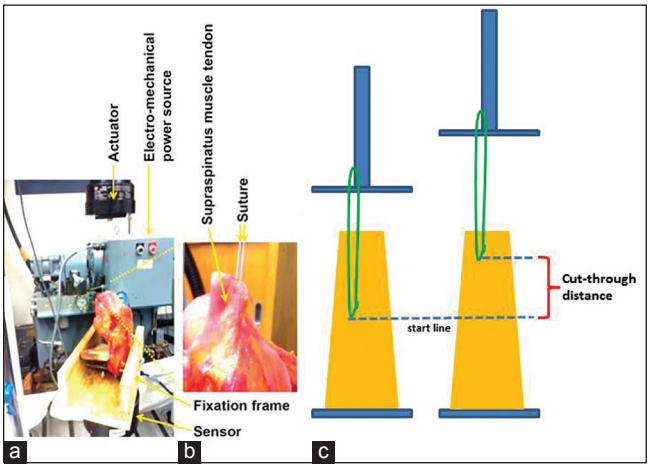



**Figure 1:** Illustration of how the mechanic testing was performed. (a) The specimen was fixed to the sensor of an MTS machine by a fixation frame; the suture was stitched through the supraspinatus muscle-tendon and connected to the actuator; and a computer (not shown) controlled the electro-mechanical power source to drive the actuator to provide uniaxial tensile force loading on the suture, and recorded the load and displacement through the testing time period. (b) A representative close-up picture is showing the tendon and suture. (c) An illustration of how the cut-through in the tendon was recorded

and order of testing were equally assigned to each suture. For example, on tendon #1, Orthocord™ suture was tested first, followed by ETHIBOND* suture and then FiberWire® suture. On tendon #2, the order of testing was ETHIBOND*, FiberWire®, and Orthocord™. On tendon #3, the order of testing was FiberWire®, Orthocord™, and ETHIBOND*. On tendons #4-12, the alternating order was repeated. The three investigators (M.L., B.N., and A.D.) who performed the tests were blinded to the sources of the sutures during testing.

### Measurement of the cut-through distance

After 1000 cycles of 10-70 N loading at 1 Hz were completed, the force was returned to 10 N. The cut-through distance [Figure 1c] was measured manually with a digital caliper. This cut-through distance is called displacement, which represents the cheese-wiring effect of the suture. The MTS machine also continuously recorded the axial displacement during the 1000 cycles, which was the change of distance between the sensor and actuator, including the cut-through distance and stretching of the muscle, tendon, and suture.

### Statistical analysis

The displacement and axial displacement were shown as means and standard deviations. The data was analyzed with analysis of variance (ANOVA) software provided by GraphPad Prism (GraphPad Software, Inc., La Jolla, CA) and using two-tailed Student's *t*-test. The significance was set at $P < 0.05$.

## RESULTS

We found that the axial displacement, as recorded by the MTS machine, was proportional to the cyclic load applied to each suture [Figure 2a-f]. In the tests of 12 supraspinatus tendons, the displacements (i.e., the cut-through distances on the tendons), as manually recorded with a digital caliper at the end of 1000 cycles of loading, were 2.9 ± 0.6 mm for #2 Orthocord™ suture, 3.2 ± 1.2 mm for #2 ETHIBOND* suture, and 4.2 ± 1.7 mm for #2 FiberWire® suture. Statistical significance existed using ANOVA ($P = 0.047$) and comparing Orthocord™ to FiberWire® sutures ($P = 0.026$), however, the difference was not statistically significant between ETHIBOND* and FiberWire® sutures ($P = 0.103$) or between Orthocord™ and ETHIBOND* sutures ($P = 0.607$) [Figure 3a]. The axial displacements, as recorded by the MTS machine from cycle 1 to 1000, were not statistically different among the three sutures [$P > 0.05$, Figure 3b]. However, the axial displacement from cycle 100 to 1000, while not significant with ANOVA, was clearly longer in FiberWire® suture than in Orthocord™ or ETHIBOND* sutures [Figure 3c]. The difference was statistically significant between Orthocord™ and FiberWire® sutures ($P = 0.022$) and between ETHIBOND* and FiberWire® sutures ($P = 0.011$), but there was no statistical significance between Orthocord™ and ETHIBOND* sutures ($P = 0.510$) [Figure 3d].

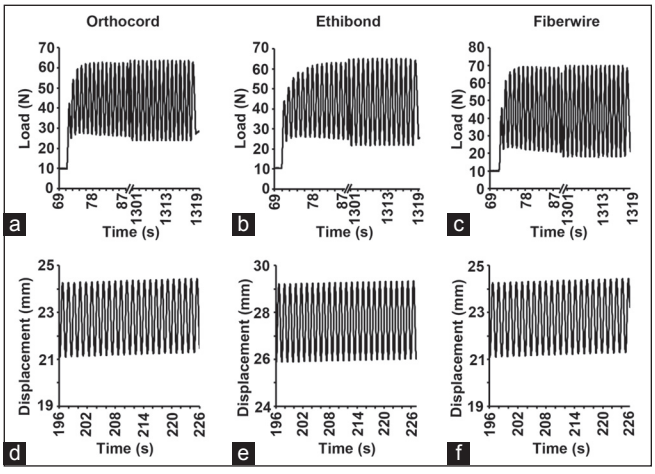



**Figure 2:** Representative recordings of uniaxial cyclic loading force over time (a-c) and axial displacement over time (d-f)

In the tests of 5 infraspinatus tendons, the displacements (i.e., the cut-through distances on the tendons), as manually recorded with a digital caliper at the end of 1000 cycles of loading, were 6.7 ± 2.0 mm for #2 Orthocord™ suture and 6.1 ± 0.6 mm for #2 ETHIBOND* suture, which was not statistically significant [$P = 0.612$, Figure 4a]. In contrast, #2 FiberWire® suture completely cut-through the infraspinatus tendon, which was >15 mm from start line to the distal end of the tendon. The axial displacements, as recorded by the MTS machine from cycle 1 to 1000, were not statistically different between Orthocord™ and ETHIBOND* sutures [$P > 0.05$, Figure 4b-c].

## DISCUSSION

This study found that #2 FiberWire® suture cuts through the supraspinatus tendon easier than #2 Orthocord™ suture under 1000 cycles of 10-70 N loading conditions. This finding was further supported by the tests with infraspinatus tendons, as #2 FiberWire® suture completely cut-through the tendon (>15 mm) whereas #2 Orthocord™ suture only cut-through <7 mm. Similarly, #2 ETHIBOND* suture only cut-through the infraspinatus tendons for approximately 6 mm. These findings suggest the #2 FiberWire® is more likely to cut-through the tendons than #2 Orthocord™ or ETHIBOND* suture. Although the difference is about 1 mm after 1000 cycles of loading at up to 70 N, the difference may be bigger at higher loads and/or more cycles.

It is worth pointing out that the overall axial displacements caused by the three sutures were of no difference [Figure 3b], which is contradictory to our manual measurement [Figure 3a]. We consider that this axial displacement, as recorded by the MTS machine, was the change of distance between the actuator and the sensor, including the cut-through by the suture and the stretched length of the muscle, tendon and suture. Thus, this axial displacement does not accurately reflect the cut-through by the suture at the beginning of the cyclic loading when the loading mainly stretched the muscle and tendon. This explanation is supported by our finding that the axial

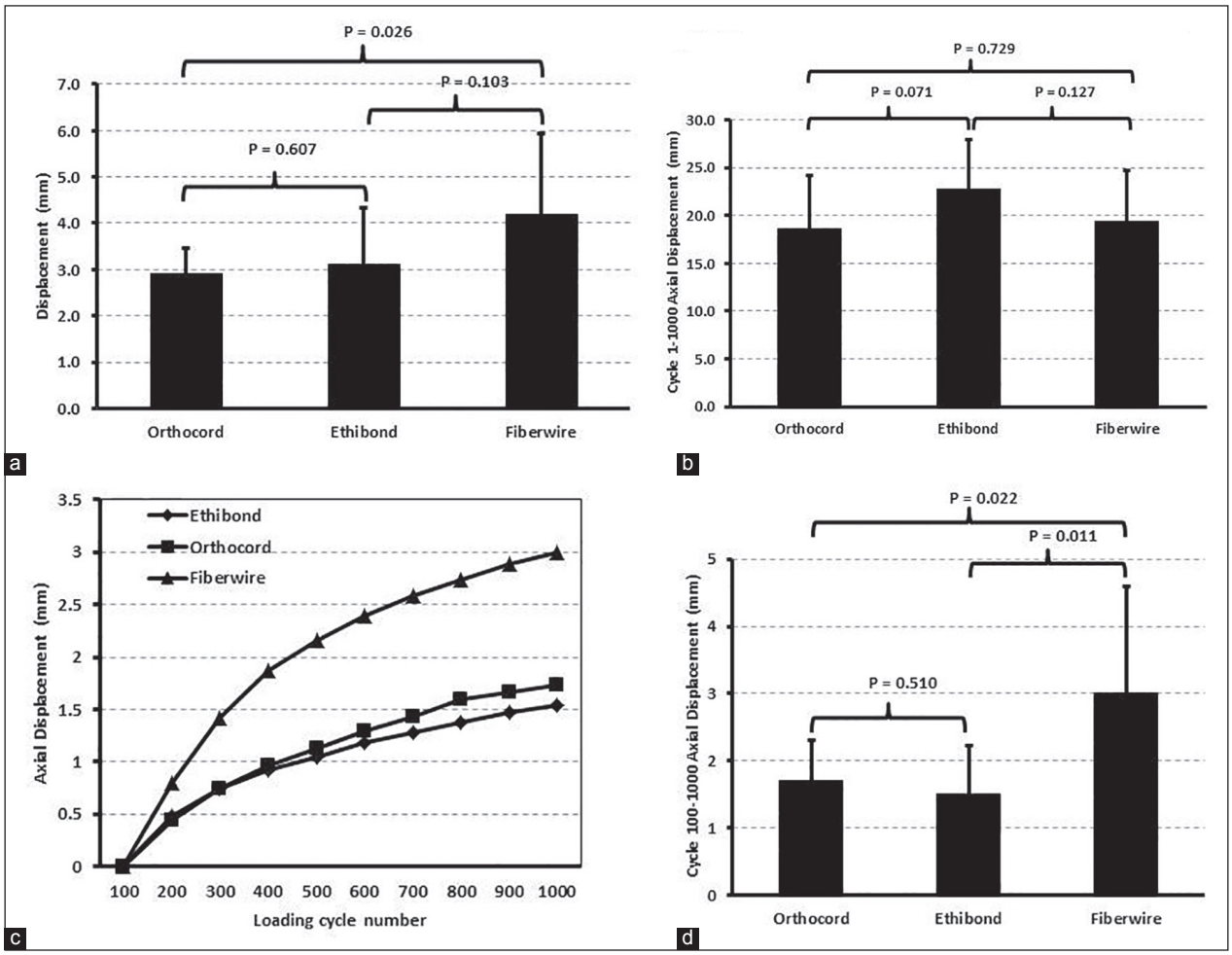



**Figure 3:** The displacements of sutures in the supraspinatus tendons recorded manually and automatically by the MTS machine. (a) The displacement (cut-through distance) of sutures measured manually with a digital caliper at the end of 1000 cycles of 10-70 N loading. (b) The overall axial displacements of sutures recorded by the MTS machine at the end of 1000 cycles of 10-70 N loading, which included the cut-through distance and the stretching of the muscle, tendon, and suture. (c) The axial displacements of sutures recorded by the MTS machine from 100 to 1000 cycles of 10-70 N loading. (d) The axial displacements of sutures at the end of 1000 cycles, recorded by the MTS machine from 100 to 1000 cycles of 10-70 N loading. The data represent means ± standard deviations (error bars, $n = 12$)

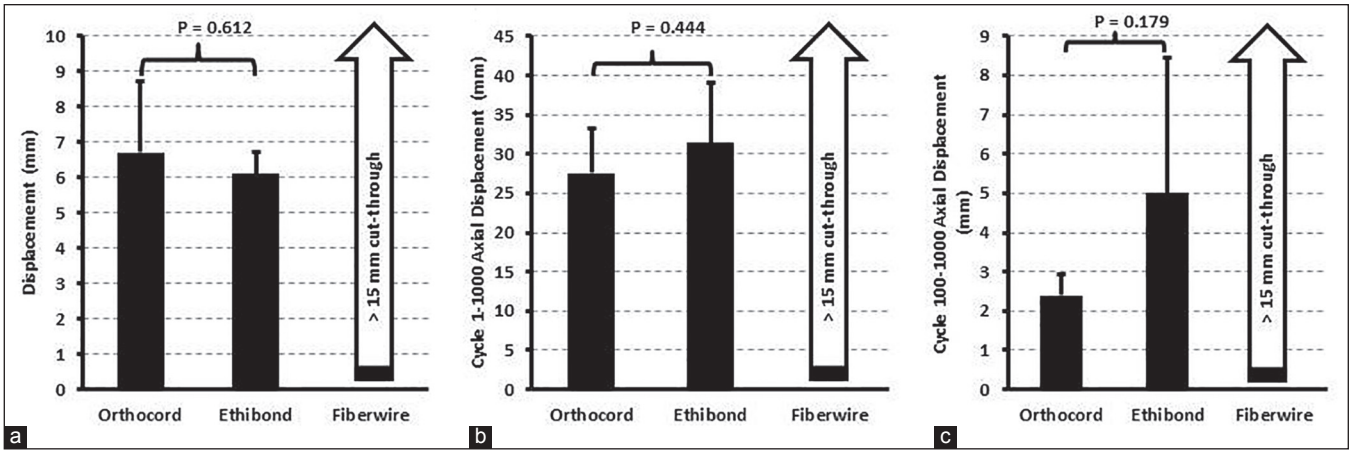



**Figure 4:** The displacements of sutures in the infraspinatus tendons recorded manually and automatically by the MTS machine. (a) The displacement (cut-through distance) of sutures measured manually with a digital caliper at the end of 1000 cycles of 10-70 N loading. (b) The overall axial displacements of sutures recorded by the MTS machine at the end of 1000 cycles of 10-70 N loading, which included the cut-through distance and the stretching of the muscle, tendon, and suture. (c) The axial displacements of sutures at the end of 1000 cycles, recorded by the MTS machine from 100 to 1000 cycles of 10-70 N loading. Of note, FiberWire® suture completely cut-through the infraspinatus tendons for a distance >15 mm. The data represent means ± standard deviations (error bars, $n = 5$)

displacements from cycles 100 to 1000 [Figure 3c-d] were consistent to our manual measurement [Figure 3a], because at this late stage the axial displacement mainly reflects the cut-through after the muscle and tendon had already been stretched by the initial pulling loads.

We speculate that the observed differences in the cut-through (or cheese-wiring effect) are due to the different coefficients of friction of sutures. It has been reported that #3-0 FiberWire® suture had a lower coefficient of friction than #3-0 ETHIBOND* suture.[16] This difference in friction may be caused by differences in material properties and the way how the strands are braided. FiberWire® suture is constructed of a multi-strand, long chain UHMWPE core with a braided jacket of polyester and UHMWPE. ETHIBOND* suture is composed of a braided polyester core coated with polybutilate. Orthocord™ suture is made with a braided polyethylene core coated with a copolymer of caprolactone and glycolide. Other physical properties of the sutures may also play a role. For example, it has been found that ETHIBOND* suture is considerably less stiff (13 ± 2 N/m) than FiberWire® suture (35 ± 6 N/m).[12] This indicates that the stiffer FiberWire® suture may be more likely to cut-through the tendons.

This study has some limitations since it was a laboratory study using human cadaveric tendons. First, no healing occurred in the cadaveric specimens. In live patients, healing may occur between the physical loads, so as to mitigate the cheese-wiring effect. Second, only a single pass-through stitch was tested. This could be meaningful in clinical situations where this type of suture method is used to restore the continuity of broken tendons. However, this finding may not be applicable to other suture methods such as mattress or figure of eight sutures. Finally, only 10-70 N cyclic loading was tested. This was due to a limitation caused by the cadaveric tendon quality where a load of 80-85 N led to complete cut-through of the tendons. It is possible that higher loads may be applied to fresh (or live) tendons.

## CONCLUSION

We found that #2 Orthocord™ and ETHIBOND* sutures cause less cheese-wiring effects than #2 FiberWire® suture in human cadaveric supraspinatus and infraspinatus tendons under 1000 cycles of 10-70 N cyclic pulling loads.

## ACKNOWLEDGMENTS

The authors thank Eric Morales and Dr. Erich Richter (Department of Neurosurgery, Louisiana State University-New Orleans) and Rita Richardson and Donna Watkins (Department of Orthopaedic Surgery, Tulane University) for their laboratory assistance. Z. You was partially supported by two grants from the National Institute of General Medical Sciences (P20GM103518) and the National Cancer Institute (R01CA174714) of the National Institutes of Health, three grants from Department of Defense Health Program through the Prostate Cancer Research Program (W81XWH-14-1-0050, W81XWH-14-1-0149, and PC130118; the U.S. Army Medical Research Acquisition Activity, 820 Chandler Street, Fort Detrick MD 21702-5014 is the awarding and administering acquisition office), the Developmental Fund of Tulane Cancer Center (TCC), and Louisiana Cancer Research Consortium (LCRC) Fund. The content of this article is solely the responsibility of the authors and does not necessarily represent the official views of the National Institutes of Health or the Department of Defense.

## REFERENCES

1. Jerosch J, Müller T, Castro WH. The incidence of rotator cuff rupture. An anatomic study. Acta Orthop Belg 1991;57:124-9.
2. Lee TQ. Current biomechanical concepts for rotator cuff repair. Clin Orthop Surg 2013;5:89-97.
3. Williams GR Jr, Rockwood CA Jr, Bigliani LU, Iannotti JP, Stanwood W. Rotator cuff tears: Why do we repair them? J Bone Joint Surg Am 2004;86-A:2764-76.
4. Chung SW, Kim JY, Kim MH, Kim SH, Oh JH. Arthroscopic repair of massive rotator cuff tears: Outcome and analysis of factors associated with healing failure or poor postoperative function. Am J Sports Med 2013;41:1674-83.
5. Favard L, Bacle G, Berhouet J. Rotator cuff repair. Joint Bone Spine 2007;74:551-7.
6. Kukkonen J, Kauko T, Virolainen P, Äärimaa V. Smoking and operative treatment of rotator cuff tear. Scand J Med Sci Sports 2014;24:400-3.
7. Mukovozov I, Byun S, Farrokhyar F, Wong I. Time to surgery in acute rotator cufftear: A systematic review. Bone Joint Res 2013;2:122-8.
8. Wieser K, Rahm S, Farshad M, Ek ET, Gerber C, Meyer DC. Stitch positioning influences the suture hold in supraspinatus tendon repair. Knee Surg Sports Traumatol Arthrosc 2013;21:1587-92.
9. Wang VM, Wang FC, McNickle AG, Friel NA, Yanke AB, Chubinskaya S, *et al*. Medial versus lateral supraspinatus tendon properties: Implications for double-row rotator cuff repair. Am J Sports Med 2010;38:2456-63.
10. Ilahi OA, Younas SA, Ho DM, Noble PC. Security of knots tied with ethibond, fiberwire, orthocord, or ultrabraid. Am J Sports Med 2008;36:2407-14.
11. Mahar AT, Moezzi DM, Serra-Hsu F, Pedowitz RA. Comparison and performance characteristics of 3 different knots when tied with 2 suture materials used for shoulder arthroscopy. Arthroscopy 2006;22:614.e1-2.
12. Najibi S, Banglmeier R, Matta J, Tannast M. Material properties of common suture materials in orthopaedic surgery. Iowa Orthop J 2010;30:84-8.
13. Swan KG Jr, Baldini T, McCarty EC. Arthroscopic suture material and knot type: An updated biomechanical analysis. Am J Sports Med 2009;37:1578-85.
14. Wright PB, Budoff JE, Yeh ML, Kelm ZS, Luo ZP. Strength of damaged suture: An *in vitro* study. Arthroscopy 2006;22:1270-1275.e3.
15. Wüst DM, Meyer DC, Favre P, Gerber C. Mechanical and handling properties of braided polyblend polyethylene sutures in comparison to braided polyester and monofilament polydioxanone sutures. Arthroscopy 2006;22:1146-53.
16. Silva JM, Zhao C, An KN, Zobitz ME, Amadio PC. Gliding resistance and strength of composite sutures in human flexor digitorum profundus tendon repair: An *in vitro* biomechanical study. J Hand Surg Am 2009;34:87-92.

**Source of Support and Conflict of Interests:** This work was partially supported by a grant provided by DePuy Mitek, Inc., to Tulane University (No. 551206, to Z.Y., F.H.S., and M.J.O.). F.H.S. is an unpaid consultant of DePuy Mitek, Inc., Smith & Nephew plc, and Rotation Medical and Biomet Sports Medicine, as well as a board member of the Arthroscopy Association of North America Education Foundation and of the Trustees for Arthroscopy.

frontiers in ONCOLOGY

ORIGINAL RESEARCH ARTICLE
published: 01 December 2014
doi: 10.3389/fonc.2014.00343

# AZD5363 inhibits inflammatory synergy between interleukin-17 and insulin/insulin-like growth factor 1

**Chong Chen[1,2], Qiuyang Zhang[1,2], Sen Liu[1,2], Mark Lambrechts[1,2], Yine Qu[1,2,3] and Zongbing You[1,2]***

[1] Department of Structural and Cellular Biology, Tulane Cancer Center and Louisiana Cancer Research Consortium, Tulane Center for Stem Cell Research and Regenerative Medicine, Tulane Center for Aging, Tulane University School of Medicine, New Orleans, LA, USA
[2] Department of Orthopaedic Surgery, Tulane Cancer Center and Louisiana Cancer Research Consortium, Tulane Center for Stem Cell Research and Regenerative Medicine, Tulane Center for Aging, Tulane University School of Medicine, New Orleans, LA, USA
[3] Department of Histology and Embryology, Hebei United University School of Basic Medicine, Tangshan, Hebei Province, China

**Edited by:**
*Gyu Seog Choi, Kyungpook National University Medical Center, South Korea*

**Reviewed by:**
*Jennifer Wu, Medical University of South Carolina, USA*
*Chang-Deng Hu, Purdue University, USA*

***Correspondence:**
*Zongbing You, Department of Structural and Cellular Biology, Tulane University School of Medicine, 1430 Tulane Avenue Mailbox 8649, New Orleans, LA 70112, USA*
*e-mail: zyou@tulane.edu*

In the United States, one-third of population is affected by obesity and almost 29 million people are suffering from type 2 diabetes. Obese people have elevated serum levels of insulin, insulin-like growth factor 1 (IGF1), and interleukin-17 (IL-17). Insulin and IGF1 are known to enhance IL-17-induced expression of inflammatory cytokines and chemokines, which may contribute to the chronic inflammatory status observed in obese people. We have previously demonstrated that insulin/IGF1 signaling pathway crosstalks with IL-17-activated nuclear factor-κB pathway through inhibiting glycogen synthase kinase 3β (GSK3β) activity. However, it is unclear whether GSK3α also plays a role and whether this crosstalk can be manipulated by AZD5363, a novel pan-Akt inhibitor that has been shown to increase glycogen synthase kinase 3 activity through reducing phosphorylation of GSK3α and GSK3β. In this study, we investigated IL-17-induced expression of C-X-C motif ligand 1 (*Cxcl1*), C-C motif ligand 20 (*Ccl20*), and interleukin-6 (*Il-6*) in wild-type, GSK3α$^{-/-}$, and GSK3β$^{-/-}$ mouse embryonic fibroblast cells as well as in mouse prostate tissues by real-time quantitative PCR. We examined the proteins involved in the signaling pathways by Western blot analysis. We found that insulin and IGF1 enhanced IL-17-induced expression of *Cxcl1*, *Ccl20*, and *Il-6*, which was associated with increased phosphorylation of GSK3α and GSK3β in the presence of insulin and IGF1. AZD5363 inhibited the synergy between IL-17 and insulin/IGF1 through reducing phosphorylation of GSK3α and GSK3β by inhibiting Akt function. These findings imply that the cooperative crosstalk of IL-17 and insulin/IGF1 in initiating inflammatory responses may be alleviated by AZD5363.

**Keywords: IL-17, insulin, IGF1, inflammation, prostate cancer, obesity**

## INTRODUCTION

Interleukin-17 (IL-17 or IL-17A) is an inflammatory cytokine (1). It can activate nuclear factor-κB (NF-κB) activator 1 (Act1) through similar expression to fibroblast growth factor genes, IL-17 receptors, and Toll–IL-1R (SEFIR) domains, upon its binding to a heterodimer of IL-17RA/IL-17RC receptor complex (2–6). Act1, as an E3 ubiquitin ligase, activates tumor necrosis factor receptor-associated factor 6 (TRAF6) through lysine-63-linked ubiquitination (7). The polyubiquitinated TRAF6 triggers transforming growth factor-β-activated kinase 1 (TAK1) and subsequently IκB kinase (IKK) complex, which in turn leads to activation of NF-κB pathway that induces transcription of a variety of cytokines, chemokines, and growth factor, e.g., C-X-C motif ligand 1 (Cxcl1) and IL-6 (8–10). Several studies have demonstrated that IL-17 stabilizes downstream *Cxcl1* mRNA through an inducible kinase IKKi-dependent Act1–TRAF2–TRAF5 complex, which ligands with splicing factor 2 [SF2, also named alternative splicing factor (ASF)] and prevents SF2/ASF-mediated mRNA degradation (11, 12).

Insulin is a hormone produced by the pancreas β cells, and its abnormal high concentration (hyperinsulinemia) may circulate in the body of people with obesity and type 2 diabetes mellitus with insulin resistance. Under hyperinsulinemic conditions, the liver produces insulin-like growth factor 1 (IGF1) (13). Two types of insulin receptors (IR-A and IR-B) can bind to either insulin or IGF1. IGF1 can also bind to a heterodimer of IR and IGF1 receptor (IGF1R). Upon binding with the receptors, insulin (or IGF1) leads to autophosphorylation of the β subunit of IR or IGF1R (14), which in turn recruits insulin receptor substrates-1 (IRS-1)

**Abbreviations:** Act1, NF-κB activator 1; ASF, alternative splicing factor; CCL2, C-C motif ligand 2; Ccl20, C-C motif ligand 20; CCL7, C-C motif ligand 7; cDNA, complementary deoxyribonucleic acid; C/EBPβ, CAAT enhancer binding protein β; Cxcl1, C-X-C motif ligand 1; CXCL5, C-X-C motif ligand 5; DMEM, Dulbecco's modified eagle's medium; Gapdh, glyceraldehyde-3-phosphate dehydrogenase; GSK, glycogen synthase kinase; IGF1, insulin-like growth factor 1; IGF1R, insulin-like growth factor 1 receptor; IKK, IκB kinase; IL-6, interleukin-6; IL-17, interleukin-17; IL-17R, interleukin-17 receptor; IR, insulin receptor; IRS, insulin receptor substrates; MEF, mouse embryonic fibroblast; mTORC2, mTor complex 2; NF-κB, nuclear factor-κB; PDK1, protein kinase 1; PH, pleckstrin homology; PI3K, phosphatidylinositol 3-kinase; SF2, splicing factor 2; SEFIR, similar expression to fibroblast growth factor genes, IL-17 receptors, and Toll–IL-1R; TAK1, transforming growth factor-β-activated kinase 1; TRAF6, tumor necrosis factor receptor-associated factor 6.

to IRS4, and then phosphatidylinositol 3-kinase (PI3K)/Akt pathway is activated (8). One of the major substrates of Akt is glycogen synthase kinase 3β (GSK3β) (8, 15). Previous studies have shown that insulin inactivates GSK3β by inducing phosphorylation at serine 9 mainly via Akt signaling pathway (15, 16).

Glycogen synthase kinase 3 includes two type of isoforms GSK3α and GSK3β, which are ubiquitously expressed in all cells and capable of phosphorylating more than 50 substrates (17). One of the substrates, CAAT enhancer binding protein β (C/EBPβ), is also induced by IL-17 (3, 9, 18). C/EBPβ transcription factor is essential for transcription of IL-17 downstream target genes such as IL-6 and 24p3/lipocalin 2 (19). Phosphorylation of C/EBPβ inhibits expression of IL-17 downstream target genes, thus GSK3β negatively regulates IL-17 signaling through phosphorylation of C/EBPβ (20). Indeed, inhibition of glycogen synthase kinase 3 (GSK3) activity by GSK3 inhibitor can enhance IL-17-induced expression of IL-6, 24p3/lipocalin 2, CXCL5, C-C motif ligand 2 (CCL2), CCL7, and NF-κB inhibitor zeta, whereas, overexpression of GSK3β can inhibit IL-17-induced IL-6 promoter and 24p3 promoter activities in a mouse stromal ST2 cell line (21). Therefore, GSK3β functions as an intrinsic negative regulator of IL-17-mediated inflammatory responses (21). Our previous study has shown that GSK3β inhibition by phosphorylation or gene knockout enhanced IL-17-induced expression of inflammatory cytokines and chemokines (8).

AZD5363 [(*S*)-4-amino-*N*-[1-(4-chlorophenyl)-3-hydroxypropyl]-1-(7*H*-pyrrolo [2, 3-d] pyrimidin-4-yl) piperidine-4-carboxamide] is a pan-Akt inhibitor that is currently being investigated in phase I clinical trials for cancer therapy (22, 23). Akt is a serine/threonine protein kinase, also known as protein kinase B (PKB), which regulates a variety of cellular process including cell proliferation, cell survival, and glucose and fatty acid metabolism (24–26). Because Akt signaling network is the key pro-tumor network in human cancers, it is a target in development of new therapies (27). The active form of Akt is phosphorylated Akt (P-Akt), which may occur at threonine 308 (Thr308) residue phosphorylated by 3-phosphoinositide dependent protein kinase 1 (PDK1), or at serine 473 (Ser 473) residue phosphorylated by mTor complex 2 (mTORC2) (28–30). Given that GSK3 is a downstream substrate of Akt, we hypothesized that inhibition of Akt by AZD5363 might inhibit the synergistic effects between IL-17 and insulin/IGF1. In this study, we tested this hypothesis.

## MATERIALS AND METHODS

### CELLS AND TISSUE CULTURE

Mouse embryonic fibroblast cells (wild-type, GSK3$\alpha^{-/-}$, or GSk3$\beta^{-/-}$ gene knockout) (31) were maintained in a 37°C, 5% $CO_2$ humidified incubator. All of these cell lines express IL-17 receptors A and C (data not shown). Dulbecco's Modified Eagle's Medium (DMEM; Mediatech, Inc., Manassas, VA, USA) with 10% fetal bovine serum (FBS; Mediatech, Inc.) and 1% penicillin/streptomycin was used as the growth medium. Mouse prostate tissues were dissected from 7 to 9-week-old male mice euthanized by $CO_2$ asphyxiation. The prostate tissues were washed three times with phosphate-buffered saline (PBS), cut into 1–2 $mm^3$ cubes, and kept in 60-mm cell culture dishes in serum-free DMEM in the incubator. The animal study was approved by the Animal Care and Use Committee of Tulane University.

### TREATMENT OF CELLS AND TISSUES

Mouse embryonic fibroblast cells were seeded into 60-mm cell culture dishes with $0.5 \times 10^6$ cells/dish. After 24 h incubation, the cells were incubated with serum-free DMEM for 20 h, and then treated with IL-17 (R&D Systems, Inc., Minneapolis, MN, USA), insulin, IGF1 (Sigma Aldrich, Inc., St Louis, MO, USA), and/or AZD5363 (Selleck Chemicals, Inc., Houston, TX, USA). The harvested mouse prostate tissues immersed in serum-free DMEM were incubated for 20 h before any treatments. The treatment for cells and tissues included: (1) control with vehicle; (2) AZD5363 at 2 μM for 3 h; (3) insulin at 50 ng/ml for 2.5 h; (4) IGF1 at 50 ng/ml for 2.5 h; (5) IL-17 at 20 ng/ml for 2 h; (6) insulin + IL-17 at the same doses but adding insulin 0.5 h before addition of IL-17; (7) IGF1 + IL-17 at the same doses but adding IGF1 0.5 h before addition of IL-17; (8) AZD5363 + Insulin + IL-17 at the same doses but adding AZD5363 1 h and insulin 0.5 h before addition of IL-17; and (9) AZD5363 + IGF1 + IL-17 at the same doses but adding AZD5363 1 h and IGF1 0.5 h before addition of IL-17.

### REAL-TIME QUANTITATIVE REVERSE TRANSCRIPTASE PCR

Following treatments, mouse embryonic fibroblast (MEF) cells or mouse prostate tissues were collected in lysis buffer. Mouse prostate tissues were homogenized with Fisher Scientific™ Model 505 sonic dismembrator. Total RNAs of MEF cells or mouse prostate tissues were isolated by using RNeasy Kit (QIAGEN, Valencia, CA, USA) according to the manufacturer's instructions. Genomic DNA contamination of each sample was avoided by using DNase I digestion. RNA was reversed to cDNA by using iScript™ cDNA synthesis kit (Bio-rad Laboratories, Hercules, CA, USA). Mouse glyceraldehyde-3-phosphate dehydrogenase (*Gapdh*), *Cxcl1*, *Ccl20*, and *Il-6* primers were obtained from Eurofins (Huntsville, AL, USA). The PCR primers specific for each gene were as follows: *Cxcl1* forward: 5′-CACCCAAACCGAAGTCATAG-3′, reverse: 5′-AAGCCAGCGTTCACCAGA-3′; *Ccl20* forward: 5′-AACTGGGTGAAAAGGGCTGT-3′, reverse: 5′-GTCCAATTCCATCCCAAAAA-3′; *Il-6* forward: 5′-CTACCCCAATTTCCAATGCT-3′, reverse: 5′-ACCACAGTGAGGAATGTCCA-3′; *Gapdh* forward: 5′-TGCACCACCAACTGCTTAG-3′, reverse: 5′-GGATGCAGGGATGATGTTC-3′. Quantitative real-time PCR (qRT-PCR) was conducted using iQ5® iCycler and iQ™ SYBR Green Supermix (Bio-Rad Laboratories) following the manufacturer's protocols. The result of each group was normalized to its own *Gapdh* level by using the formula ΔCt (Cycle threshold) = Ct of target gene − Ct of *Gapdh*. The fold change of mRNA level of each treatment group was calculated as: ΔΔCt = ΔCt of target gene in the treatment group − ΔCt of target gene in control group, and fold change = $2^{-\Delta\Delta Ct}$.

### WESTERN BLOT ANALYSIS

Following the treatment of cells or tissues, proteins were extracted by using RIPA lysis buffer, which contains 50 mM sodium fluoride, 0.5% Igepal CA-630 (NP-40), 10 mM sodium phosphate, 150 mM sodium chloride, 25 mM Tris (pH 8.0), 1 mM phenylmethylsulfonyl fluoride, 2 mM ethylenediaminetetraacetic

acid (EDTA), and 1.2 mM sodium vanadate. Protein concentration was assessed by using Bio-Rad Protein Assay Dye Reagent Concentrate (Bio-Rad Laboratories, Hercules, CA, USA) and BioTek ELx800 microplate reader (BioTek, Winooski, VT, USA). Eighty microgram of protein of each group was loaded to 10% SDS-polyacrylamide gel electrophoresis and transferred to polyvinylidene difluoride membrane. Membrane blocking was done using 5% non-fat dry milk in TBST buffer (25 mM Tris-HCl, 125 mM sodium chloride, and 0.1% Tween 20). Primary antibody was incubated with the membrane at 4°C overnight. The membrane was washed three times with TBST, and incubated with IRDye® 800CW- or IRDye® 680RD-conjugated secondary antibodies (LI-COR Biosciences, Lincoln, NE, USA) at room temperature for 1 h. The membrane was scanned by Odyssey Infrared Imager (LI-COR Biosciences) for visualization. The antibodies used included: rabbit anti-P-Akt (S473), rabbit anti-Akt, rabbit anti-P-GSK3α (S21), rabbit anti-GSK3α, rabbit anti-P-GSK3β (S9), and rabbit anti-GSK3β antibodies were purchased from Cell Signaling Technology, Danvers, MA, USA. Mouse anti-GAPDH antibody was purchased from Millipore, Billerica, MA, USA.

### STATISTICAL ANALYSIS

The data were presented as mean ± SD of triplicate experiments ($n = 3$). Statistical significance was determined by one-way ANOVA and Tukey's tests. All of the analyses were performed using GraphPad Prism® 5.0 (GraphPad Software, La Jolla, CA, USA).

## RESULTS

In the wild-type MEF cells, insulin or IGF1 alone treatment led to increased levels of P-Akt, P-GSK3α, and P-GSK3β (**Figures 1A,B**). When AZD5363 treatment was added, the levels of P-Akt were further increased. On the contrary, AZD5363 treatment reduced the levels of P-GSK3α and P-GSK3β (**Figures 1A,B**). In the GSK3α$^{-/-}$ MEF cells (**Figures 1C,D**) and GSK3β$^{-/-}$ MEF cells (**Figures 1E,F**), insulin or IGF1 alone treatment increased the levels of P-Akt, and subsequently the levels of P-GSK3β and P-GSK3α in GSK3α$^{-/-}$ and GSK3β$^{-/-}$ MEF cells, respectively. AZD5363 treatment led to a further increase of P-Akt compared to insulin or IGF1 alone treatment in both GSK3α$^{-/-}$ and GSK3β$^{-/-}$ MEF cells. However, AZD5363 treatment reduced the levels of P-GSK3β and P-GSK3α in GSK3α$^{-/-}$ and GSK3β$^{-/-}$ MEF cells, respectively, in comparison to insulin or IGF1 alone treatment.

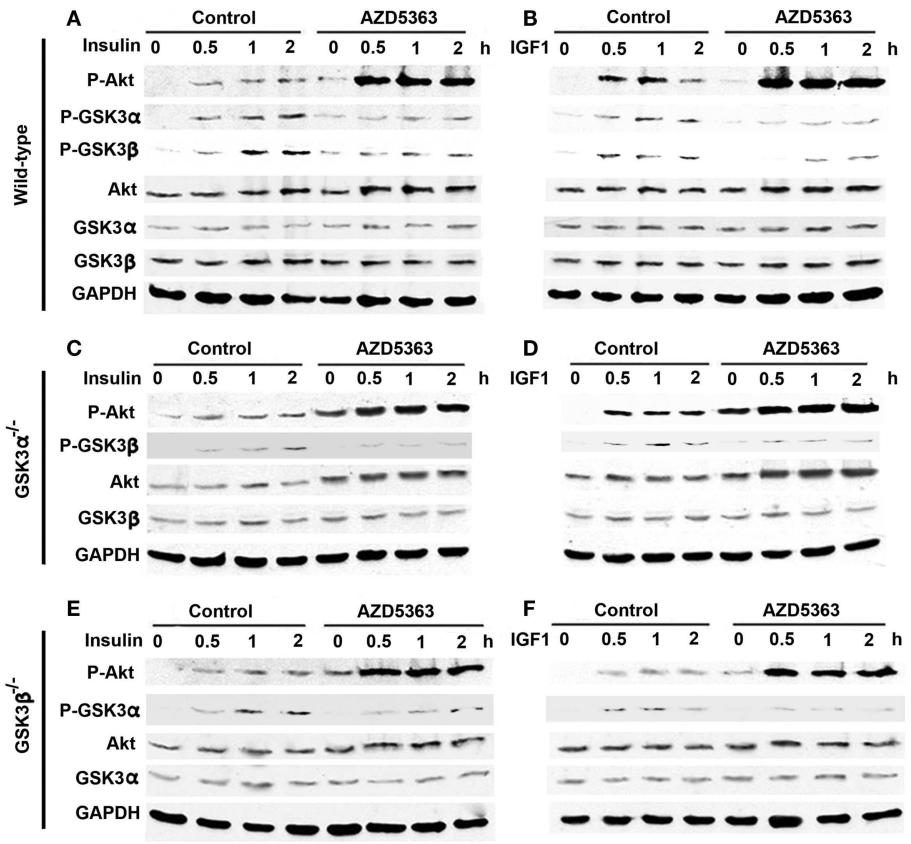



**FIGURE 1 | Effects of AZD5363 on insulin/IGF1 signaling pathways**. **(A)** Effects of insulin with or without AZD5363 on wild-type MEF cells; **(B)** Effects of IGF1 with or without AZD5363 on wild-type MEF cells; **(C)** Effects of insulin with or without AZD5363 on GSK3α$^{-/-}$ MEF cells; **(D)** Effects of IGF1 with or without AZD5363 on GSK3α$^{-/-}$ MEF cells; **(E)** Effects of insulin with or without AZD5363 on GSK3β$^{-/-}$ MEF cells; **(F)** Effects of IGF1 with or without AZD5363 on GSK3β$^{-/-}$ MEF cells. The concentrations of insulin and IGF1 were 50 ng/ml and the concentration of AZD5363 was 2 μM. The levels of phosphorylated and unphosphorylated Akt, GSK3α, and GSK3β were shown by western blot analysis. Equal loading of proteins was confirmed by reprobing GAPDH.

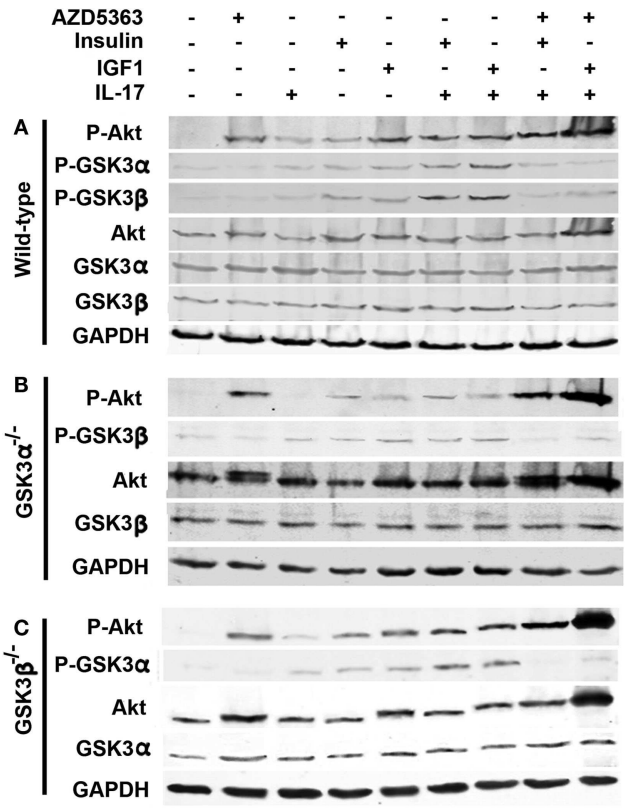



**FIGURE 2 | Effects of AZD5363 on IL-17 and insulin/IGF1 signaling pathways in wild-type MEF cells (A), GSK3α$^{-/-}$ MEF cells (B), and GSK3β$^{-/-}$ MEF cells (C)**. Cells were treated with 20 ng/ml IL-17, 50 ng/ml insulin, 50 ng/ml IGF1, and 2 μM AZD5363, either alone or in combination for 2 h. The levels of phosphorylated and unphosphorylated Akt, GSK3α, and GSK3β were shown by western blot analysis. Equal loading of proteins was confirmed by reprobing GAPDH.

As shown in **Figure 2A**, IL-17, insulin or IGF1 alone treatment only slightly increased the levels of P-Akt, P-GSK3α, and P-GSK3β in wild-type MEF cells, compared to control group. A combination of insulin and IL-17, or IGF1 and IL-17, further increased the levels of P-Akt, P-GSK3α, and P-GSK3β. When AZD5363 treatment was added to the combined treatment groups, the levels of P-GSK3α and P-GSK3β were dramatically reduced, though the levels of P-Akt were further increased. In GSK3α$^{-/-}$ and GSK3β$^{-/-}$ MEF cells, similar changes were observed, except that only GSK3β (**Figure 2B**) or GSK3α (**Figure 2C**) was present due to knockout of the other GSK3 isoform.

Because AZD5363 treatment decreased the levels of P-GSK3α and P-GSK3β that might affect IL-17-induced gene expression (8), we checked the mRNA levels of *Cxcl1* and *Ccl20* in wild-type, GSK3α$^{-/-}$ and GSK3β$^{-/-}$ MEF cells after the treatment as described above. In the wild-type MEF cells, IL-17 or insulin alone treatment increased *Cxcl1* mRNA levels by $2.0 \pm 0.4$ or $1.6 \pm 0.8$-fold, compared to control group (**Figure 3A**). *Cxcl1* mRNA level was increased by $4.6 \pm 0.6$-fold in the insulin and IL-17 combined treatment group, which was statistically significant compared to insulin or IL-17 alone treatment group ($p < 0.05$). Addition of AZD5363 to this combined treatment group reduced *Cxcl1* mRNA level to $1.8 \pm 0.1$-fold, which was significantly less than the insulin and IL-17 combined treatment group (**Figure 3A**, $p < 0.05$). Similarly, *Ccl20* mRNA levels were increased by $2.0 \pm 0.5$ and $1.6 \pm 0.3$-fold in IL-17 or insulin alone treated group, respectively. A combination of insulin and IL-17 treatment increased *Ccl20* mRNA level by $3.0 \pm 0.8$-fold, which was significantly higher than either IL-17 or insulin alone treatment. In contrast, addition of AZD5363 to the combined treatment reduced *Ccl20* mRNA level almost to the basal level of $1.1 \pm 0.3$-fold, which was significantly lower than the insulin and IL-17 combined treatment group (**Figure 3A**, $p < 0.05$). As shown in **Figure 3B**, IGF1 and IL-17 also synergistically induced *Cxcl1* and *Ccl20* mRNA expression, which was inhibited by addition of AZD5363. In GSK3α$^{-/-}$ (**Figures 3C,D**) and GSK3β$^{-/-}$ (**Figures 3E,F**) MEF cells, IL-17 alone treatment dramatically increased the levels of *Cxcl1* and *Ccl20* mRNA. In contrast to wild-type MEF cells, combination of insulin or IGF1 with IL-17 did not further increase levels of *Cxcl1* and *Ccl20* mRNA, compared to IL-17 alone treatment (**Figures 3C–F**). Furthermore, addition of AZD5363 to the combined treatment did not reduce the elevated mRNA levels of *Cxcl1* or *Ccl20* (**Figures 3C–F**).

In order to assess if our findings in the studies of cell lines are relevant to the *in vivo* organ tissues, we did similar experiments using *ex vivo* cultured mouse prostate tissues. As shown in **Figure 4A**, increased levels of P-Akt, P-GSK3α, and P-GSK3β were observed in mouse prostate tissues treated with insulin alone, IGF1 alone, a combination of insulin and IL-17, and a combination of IGF1 and IL-17, compared to the control group. However, addition of AZD5363 to the combined treatment groups reduced the levels of P-GSK3α and P-GSK3β, compared to the combined treatment groups. The changes in the signaling proteins were associated with the changes in the mRNA levels of *Cxcl1*, *Ccl20*, and *Il-6*. As shown in **Figure 4B**, a combination of insulin and IL-17 treatment significantly increased the mRNA levels of *Cxcl1*, *Ccl20*, and *Il-6*, compared to insulin or IL-17 alone treatment ($p < 0.05$). Similarly, a combination of IGF1 and IL-17 treatment showed the same effects (**Figure 4C**). However, when AZD5363 was added to the combined treatment groups, the induction of mRNA levels of *Cxcl1*, *Ccl20*, and *Il-6* was significantly reduced, compared to the combined treatment groups without AZD5363 (**Figures 4B,C**).

## DISCUSSION

Inflammation has been shown to be a driving force behind a variety of cancer types (32–34). IL-17 is an inflammatory cytokine that stimulates leukocytes, fibroblasts, epithelial cells, and endothelial cells to release inflammatory signals that can further fire up inflammation (1). We have previously demonstrated that IL-17 promotes formation and growth of prostate cancer in a mouse model (35, 36). Recently, we showed that insulin and IGF1 enhance IL-17-induced expression of inflammatory cytokines and chemokines (8). The crosstalk between insulin/IGF1 signaling pathway and IL-17 signaling pathway is mediated by GSK3β, as GSK3β knockout blocks the crosstalk. In the present study, we found that GSK3α

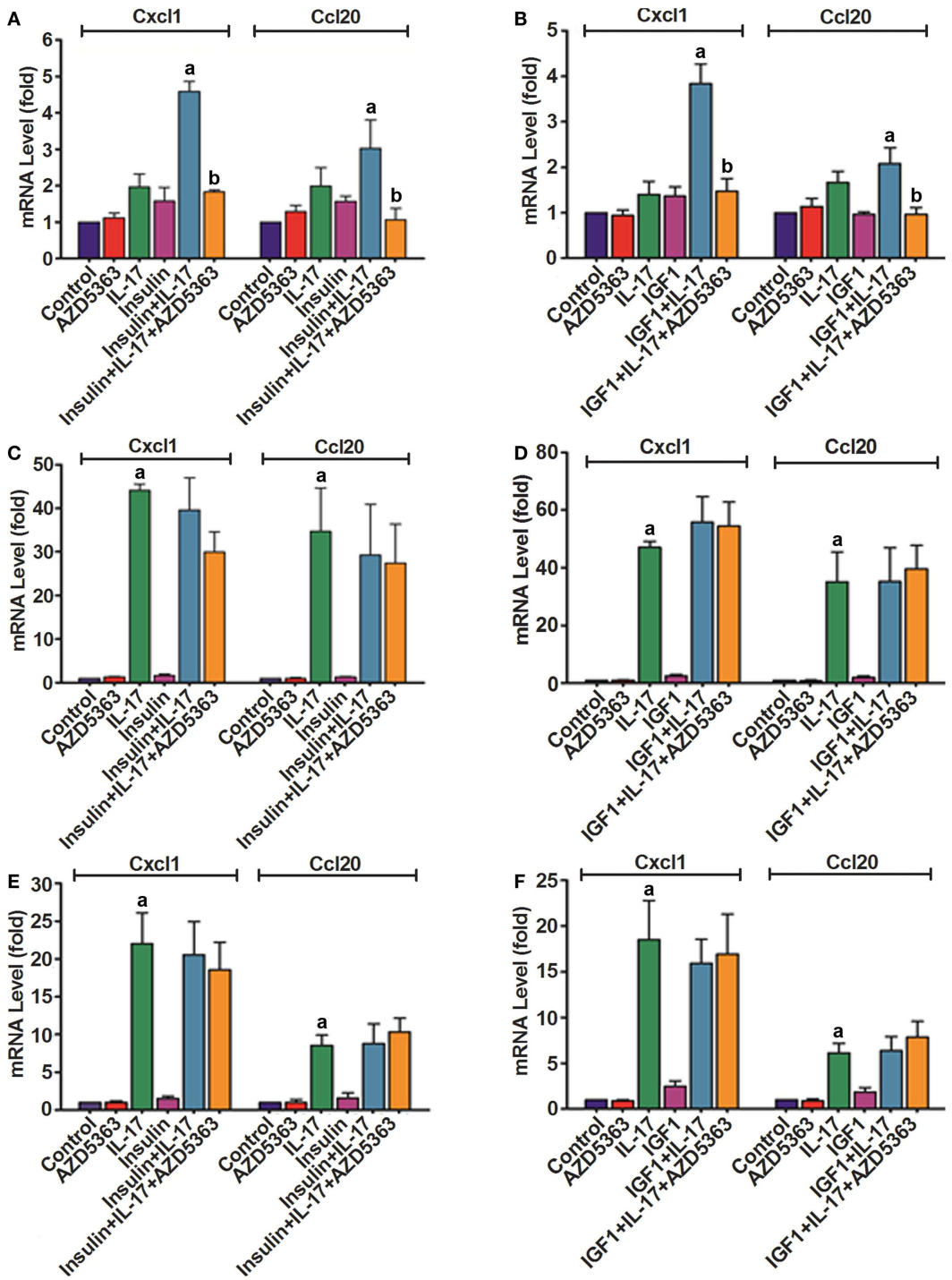



**FIGURE 3 | Expression of *Cxcl1* and *Ccl20* mRNAs in wild-type MEF cells (A,B), GSK3α$^{-/-}$ MEF cells (C,D), and GSK3β$^{-/-}$ MEF cells (E,F)**. Cells were treated with 20 ng/ml IL-17, 50 ng/ml insulin, 50 ng/ml IGF1, and 2 μM AZD5363, either alone or in combination for 2 h. The levels of *Cxcl1* and *Ccl20* mRNAs were determined using real-time PCR. Data represent mean ± SD of triplicate experiments ($n = 3$). a, $p < 0.05$ Compared to IL-17 alone or insulin/IGF1 alone; b, $p < 0.05$ compared to the combination of IL-17 and insulin or IGF1.

knockout also blocks the crosstalk between insulin/IGF1 and IL-17 pathways. In fact, knockout of either GSK3α or GSK3β appears to relieve the repressive function of GSK3 on IL-17-induced gene expression, as IL-17 can induce gene expression to the levels significantly higher than in the wild-type MEFs where IL-17 can usually induce gene expression to very modest levels. These findings

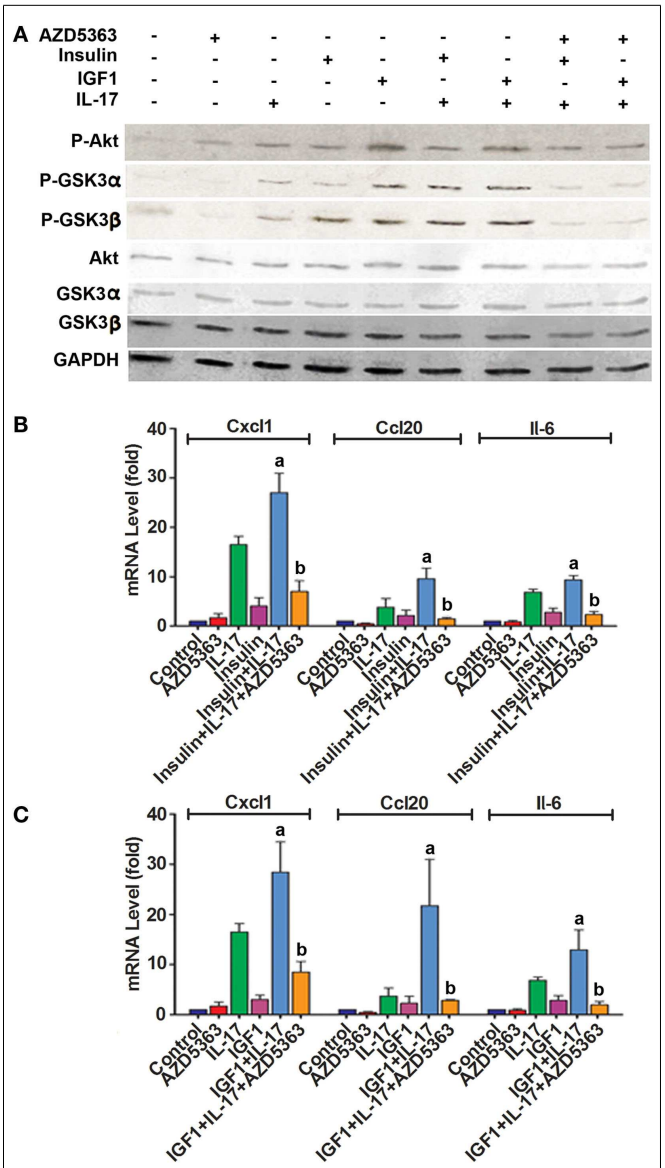



**FIGURE 4 | Effects of AZD5363 on IL-17 and insulin/IGF1 signaling pathways and expression of *Cxcl1* and *Ccl20* mRNAs in mouse prostate tissues**. Mouse prostate tissues were cultured *ex vivo* and treated with 20 ng/ml IL-17, 50 ng/ml insulin, 50 ng/ml IGF1, and 2 μM AZD5363, either alone or in combination for 2 h. **(A)** The levels of phosphorylated and unphosphorylated Akt, GSK3α and GSK3β were shown by western blot analysis. Equal loading of proteins was confirmed by reprobing GAPDH. **(B,C)** The levels of *Cxcl1* and *Ccl20* mRNAs were determined using real-time PCR. Data represent mean ± SD of triplicate experiments ($n = 3$). a, $p < 0.05$ Compared to IL-17 alone or insulin/IGF1 alone; b, $p < 0.05$ compared to the combination of IL-17 and insulin or IGF1.

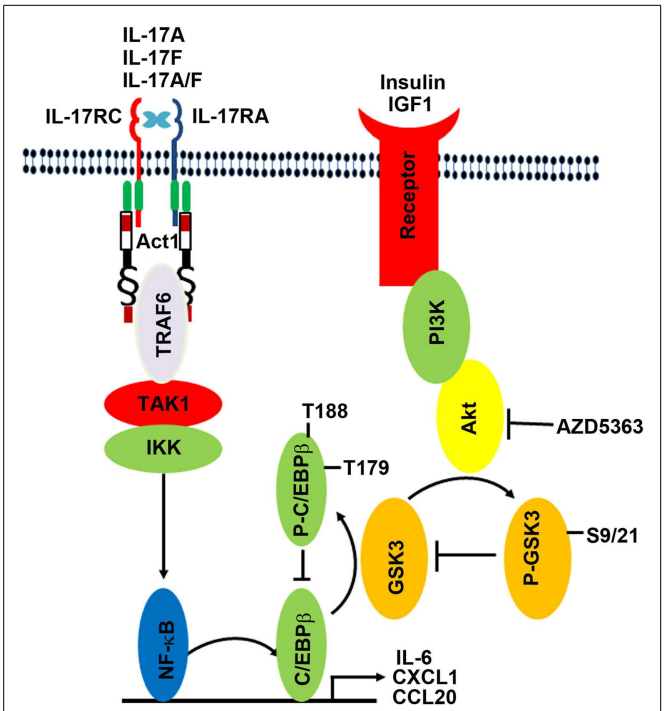



**FIGURE 5 | Illustration of the proposed crosstalk between insulin/IGF1 and IL-17 signaling pathways**. IL-17 acts through the IL-17RA:IL-17RC receptor complex to activate Act1–TRAF6–TAK1–IKK signaling cascade, thus activating NF-κB transcription factor and subsequently activating C/EBPβ transcription factors. NF-κB and C/EBPβ transcription factors are required for initiation of transcription of the downstream target genes such as *IL-6*, *Cxcl1*, and *Ccl20*. Insulin and IGF1 bind to their receptors and activate PI3K/Akt pathway; Akt phosphorylates GSK3B at serine 9 and GSK3A at serine 21 to inhibit GSK3 activity; GSK3 phosphorylates C/EBPβ at threonine 179 after a priming phosphorylation at threonine 188 by ERK1/2, thus inhibiting C/EBPβ's transcription function. Therefore, insulin/IGF1 signaling is linked with IL-17 signaling by GSK3 and C/EBPβ. AZD5363 inhibits Akt activation, thus enhancing GSK3 activity and subsequently diminishing IL-17-induced gene expression by inhibiting C/EBPβ function.

suggest that both GSK3α and GSK3β isoforms are required to be present, in order to repress IL-17-induced gene expression. Lithium chloride is an inhibitor to both GSK3α and GSK3β isoforms, which has been shown to increase IL-17-induced gene expression in two previous studies (8, 20). The exact molecular mechanisms underlying the crosstalk are yet to be determined, though a previous study suggested that it might be phosphorylation of C/EBPβ by GSK3, which inhibits the transcription function of C/EBPβ (21). As shown in **Figure 5**, IL-17 acts through the IL-17RA:IL-17RC receptor complex to activate Act1–TRAF6–TAK1–IKK signaling cascade, thus activating NF-κB transcription factor and subsequently activating C/EBPβ transcription factors. NF-κB and C/EBPβ transcription factors are required for initiation of transcription of the downstream target genes such as *IL-6*, *Cxcl1*, and *Ccl20*. Insulin and IGF1 bind to their receptors and activate PI3K/Akt pathway; Akt phosphorylates GSK3B at serine 9 and GSK3A at serine 21 to inhibit GSK3 activity; GSK3 phosphorylates C/EBPβ at threonine 179 after a priming phosphorylation at threonine 188 by ERK1/2, thus inhibiting C/EBPβ's transcription function. Therefore, insulin/IGF1 signaling is linked with IL-17 signaling by GSK3 and C/EBPβ. AZD5363 inhibits Akt activation, thus enhancing GSK3 activity and subsequently diminishing IL-17-induced gene expression by inhibiting C/EBPβ function.

Manipulation of the crosstalk between insulin/IGF1 and IL-17 is potentially significant in obese population. It has been reported

that serum and tissue levels of IL-17 are increased in obese mice (37, 38) and humans (39). Interestingly, serum levels of insulin and IGF1 are also increased in obese population, which together with IL-17, may be the underlying cause of the chronic inflammatory state with increased serum levels of inflammatory mediators TNFα and IL-6 (8, 40). Obesity has been associated with increased risks of breast cancer, endometrial cancer, esophageal adenocarcinoma, pancreas cancer, colorectal cancer, renal cancer, thyroid cancer, gallbladder cancer, and prostate cancer (41–49). Chronic inflammation in obesity is suspected as one of the possible mechanisms underlying the increased cancer risk. In our previous study, we found that melatonin can block the crosstalk between insulin/IGF1 and IL-17 through inhibition of Akt function (8). In the present study, we found that AZD5363, a pan-Akt inhibitor, can do the same. AZD5363 reduced phosphorylation of GSK3α at serine 21 and GSK3β at serine 9, thus increasing the enzyme activities of GSK3α and GSK3β, and subsequently represses IL-17-induced gene expression. Preclinical studies have shown that AZD5363 may be effective in inhibiting tumor growth (27), yet it remains to be determined whether AZD5363 may alter the inflammatory microenvironment in the tumors and how this contributes to the anti-tumor function of AZD5363.

Interestingly, we observed that AZD5363, a pan-Akt inhibitor, increased the P-Akt levels in wild-type, GSK3α$^{-/-}$ and GSK3β$^{-/-}$ MEF cells. In general, phosphorylated Akt is the activated form of Akt (30). However, it has been reported that several Akt inhibitors elevate the levels of P-Akt. The mechanism behind this may be that suppression of S6K (p70S6K) activity stabilizes IRS-1 and increases IRS-1 adapter protein levels, which in turn induces Akt activity (50–54). Another possible cause of the hyperphosphorylation is that the Akt inhibitor sensitizes the pleckstrin homology (PH) domain to bind basal levels of PIP3 to facilitate membrane localization and induce conformational change of Akt to become more susceptible to kinase phosphorylation or less susceptible to phosphatase dephosphorylation (55). Of note, the increase of P-Akt and total Akt was less obvious in the mouse prostate tissues, compared to the MEFs upon AZD5363 treatment. We speculate that this might be due to that the prostate glandular tissues responded differently from the MEFs. But the exact reason is not clear.

In summary, this study indicates that insulin and IGF1 can enhance IL-17-induced inflammatory responses through suppression of GSK3 function by phosphorylation of GSK3α and GSK3β. AZD5363 inhibits Akt function and thus inhibits the synergy between IL-17 and insulin/IGF1 through enhancing GSK3 function by reducing phosphorylation of GSK3α and GSK3β. These findings imply that the cooperative crosstalk of IL-17 and insulin/IGF1 in initiating inflammatory responses may be alleviated by AZD5363.

## AUTHOR CONTRIBUTIONS

Chong Chen performed the experiments, analyzed the data, and prepared the manuscript. Qiuyang Zhang, Mark Lambrechts, Sen Liu, and Yine Qu participated in the experiments and analysis of data. Zongbing You conceived and designed the work, analyzed the data, and prepared the manuscript. All authors critically revised the manuscript, approved the final version, and agreed to be accountable for all aspects of the manuscript.

## ACKNOWLEDGMENTS

The authors thank Dr. James R. Woodgett (Mount Sinai Hospital and the Samuel Lunenfeld Research Institute, Toronto, ON, Canada M5G1X5) for providing the wild-type, GSK3α$^{-/-}$, and GSk3β$^{-/-}$ MEF cells. The core facilities of Tulane Cancer Center and Louisiana Cancer Research Consortium were used in this study. This work was supported in whole or in part by National Institutes of Health (P20GM103518 and R01CA174714), by Department of Defense Health Program through the Prostate Cancer Research Program (W81XWH-14-1-0050, W81XWH-14-1-0149, and W81XWH-14-1-0458; the U.S. Army Medical Research Acquisition Activity, 820 Chandler Street, Fort Detrick MD 21702-5014 is the awarding and administering acquisition office), and by the Developmental Fund of Tulane Cancer Center (TCC) and Louisiana Cancer Research Consortium (LCRC) Fund. The content of this article is solely the responsibility of the authors and does not necessarily represent the official views of the National Institutes of Health or the Department of Defense.

## REFERENCES

1. Kolls JK, Linden A. Interleukin-17 family members and inflammation. *Immunity* (2004) **21**(4):467–76. doi:10.1016/j.immuni.2004.08.018
2. Novatchkova M, Leibbrandt A, Werzowa J, Neubuser A, Eisenhaber F. The STIR-domain superfamily in signal transduction, development and immunity. *Trends Biochem Sci* (2003) **28**(5):226–9. doi:10.1016/S0968-0004(03)00067-7
3. Chang SH, Park H, Dong C. Act1 adaptor protein is an immediate and essential signaling component of interleukin-17 receptor. *J Biol Chem* (2006) **281**(47):35603–7. doi:10.1074/jbc.C600256200
4. Qian Y, Liu C, Hartupee J, Altuntas CZ, Gulen MF, Jane-Wit D, et al. The adaptor Act1 is required for interleukin 17-dependent signaling associated with autoimmune and inflammatory disease. *Nat Immunol* (2007) **8**(3):247–56. doi:10.1038/ni1439
5. Maitra A, Shen F, Hanel W, Mossman K, Tocker J, Swart D, et al. Distinct functional motifs within the IL-17 receptor regulate signal transduction and target gene expression. *Proc Natl Acad Sci U S A* (2007) **104**(18):7506–11. doi:10.1073/pnas.0611589104
6. Ho AW, Shen F, Conti HR, Patel N, Childs EE, Peterson AC, et al. IL-17RC is required for immune signaling via an extended SEF/IL-17R signaling domain in the cytoplasmic tail. *J Immunol* (2010) **185**(2):1063–70. doi:10.4049/jimmunol.0903739
7. Liu C, Qian W, Qian Y, Giltiay NV, Lu Y, Swaidani S, et al. Act1, a U-box E3 ubiquitin ligase for IL-17 signaling. *Sci Signal* (2009) **2**(92):ra63. doi:10.1126/scisignal.2000382
8. Ge D, Dauchy RT, Liu S, Zhang Q, Mao L, Dauchy EM, et al. Insulin and IGF1 enhance IL-17-induced chemokine expression through a GSK3B-dependent mechanism: a new target for melatonin's anti-inflammatory action. *J Pineal Res* (2013) **55**(4):377–87. doi:10.1111/jpi.12084
9. Zhu S, Pan W, Song X, Liu Y, Shao X, Tang Y, et al. The microRNA miR-23b suppresses IL-17-associated autoimmune inflammation by targeting TAB2, TAB3 and IKK-alpha. *Nat Med* (2012) **18**(7):1077–86. doi:10.1038/nm.2815
10. Hwang SY, Kim JY, Kim KW, Park MK, Moon Y, Kim WU, et al. IL-17 induces production of IL-6 and IL-8 in rheumatoid arthritis synovial fibroblasts via NF-kappaB- and PI3-kinase/Akt-dependent pathways. *Arthritis Res Ther* (2004) **6**(2):R120–8. doi:10.1186/ar1038
11. Bulek K, Liu C, Swaidani S, Wang L, Page RC, Gulen MF, et al. The inducible kinase IKKi is required for IL-17-dependent signaling associated with neutrophilia and pulmonary inflammation. *Nat Immunol* (2011) **12**(9):844–52. doi:10.1038/ni.2080
12. Sun D, Novotny M, Bulek K, Liu C, Li X, Hamilton T. Treatment with IL-17 prolongs the half-life of chemokine CXCL1 mRNA via the adaptor TRAF5 and

the splicing-regulatory factor SF2 (ASF). *Nat Immunol* (2011) **12**(9):853–60. doi:10.1038/ni.2081
13. Baxter RC, Bryson JM, Turtle JR. Somatogenic receptors of rat liver: regulation by insulin. *Endocrinology* (1980) **107**(4):1176–81. doi:10.1210/endo-107-4-1176
14. Gallagher EJ, LeRoith D. The proliferating role of insulin and insulin-like growth factors in cancer. *Trends Endocrinol Metab* (2010) **21**(10):610–8. doi:10.1016/j.tem.2010.06.007
15. Cross DA, Alessi DR, Cohen P, Andjelkovich M, Hemmings BA. Inhibition of glycogen synthase kinase-3 by insulin mediated by protein kinase B. *Nature* (1995) **378**(6559):785–9. doi:10.1038/378785a0
16. Cross DA, Alessi DR, Vandenheede JR, McDowell HE, Hundal HS, Cohen P. The inhibition of glycogen synthase kinase-3 by insulin or insulin-like growth factor 1 in the rat skeletal muscle cell line L6 is blocked by wortmannin, but not by rapamycin: evidence that wortmannin blocks activation of the mitogen-activated protein kinase pathway in L6 cells between Ras and Raf. *Biochem J* (1994) **303**(Pt 1):21–6.
17. Chiara F, Rasola A. GSK-3 and mitochondria in cancer cells. *Front Oncol* (2013) **3**:16. doi:10.3389/fonc.2013.00016
18. Ruddy MJ, Wong GC, Liu XK, Yamamoto H, Kasayama S, Kirkwood KL, et al. Functional cooperation between interleukin-17 and tumor necrosis factor-alpha is mediated by CCAAT/enhancer-binding protein family members. *J Biol Chem* (2004) **279**(4):2559–67. doi:10.1074/jbc.M308809200
19. Shen F, Hu Z, Goswami J, Gaffen SL. Identification of common transcriptional regulatory elements in interleukin-17 target genes. *J Biol Chem* (2006) **281**(34):24138–48. doi:10.1074/jbc.M604597200
20. Shen F, Li N, Gade P, Kalvakolanu DV, Weibley T, Doble B, et al. IL-17 receptor signaling inhibits C/EBPbeta by sequential phosphorylation of the regulatory 2 domain. *Sci Signal* (2009) **2**(59):ra8. doi:10.1126/scisignal.2000066
21. Demarchi F, Bertoli C, Sandy P, Schneider C. Glycogen synthase kinase-3 beta regulates NF-kappa B1/p105 stability. *J Biol Chem* (2003) **278**(41):39583–90. doi:10.1074/jbc.M305676200
22. Toren P, Kim S, Cordonnier T, Crafter C, Davies BR, Fazli L, et al. Combination AZD5363 with enzalutamide significantly delays enzalutamide-resistant prostate cancer in preclinical models. *Eur Urol* (2014). doi:10.1016/j.eururo.2014.08.006
23. Lamoureux F, Thomas C, Crafter C, Kumano M, Zhang F, Davies BR, et al. Blocked autophagy using lysosomotropic agents sensitizes resistant prostate tumor cells to the novel Akt inhibitor AZD5363. *Clin Cancer Res* (2013) **19**(4):833–44. doi:10.1158/1078-0432.CCR-12-3114
24. Yung HW, Charnock-Jones DS, Burton GJ. Regulation of AKT phosphorylation at Ser473 and Thr308 by endoplasmic reticulum stress modulates substrate specificity in a severity dependent manner. *PLoS One* (2011) **6**(3):e17894. doi:10.1371/journal.pone.0017894
25. Altomare DA, Testa JR. Perturbations of the AKT signaling pathway in human cancer. *Oncogene* (2005) **24**(50):7455–64. doi:10.1038/sj.onc.1209085
26. Bellacosa A, Kumar CC, Di Cristofano A, Testa JR. Activation of AKT kinases in cancer: implications for therapeutic targeting. *Adv Cancer Res* (2005) **94**:29–86. doi:10.1016/S0065-230X(05)94002-5
27. Davies BR, Greenwood H, Dudley P, Crafter C, Yu DH, Zhang J, et al. Preclinical pharmacology of AZD5363, an inhibitor of AKT: pharmacodynamics, antitumor activity, and correlation of monotherapy activity with genetic background. *Mol Cancer Ther* (2012) **11**(4):873–87. doi:10.1158/1535-7163.MCT-11-0824-T
28. Alessi DR, Andjelkovic M, Caudwell B, Cron P, Morrice N, Cohen P, et al. Mechanism of activation of protein kinase B by insulin and IGF-1. *EMBO J* (1996) **15**(23):6541–51.
29. Alessi DR, James SR, Downes CP, Holmes AB, Gaffney PR, Reese CB, et al. Characterization of a 3-phosphoinositide-dependent protein kinase which phosphorylates and activates protein kinase B alpha. *Curr Biol* (1997) **7**(4):261–9. doi:10.1016/S0960-9822(06)00122-9
30. Sarbassov DD, Guertin DA, Ali SM, Sabatini DM. Phosphorylation and regulation of Akt/PKB by the rictor-mTOR complex. *Science* (2005) **307**(5712):1098–101. doi:10.1126/science.1106148
31. Hoeflich KP, Luo J, Rubie EA, Tsao MS, Jin O, Woodgett JR. Requirement for glycogen synthase kinase-3beta in cell survival and NF-kappaB activation. *Nature* (2000) **406**(6791):86–90. doi:10.1038/35017574
32. Chen C, Khismatullin DB. Lipopolysaccharide induces the interactions of breast cancer and endothelial cells via activated monocytes. *Cancer Lett* (2014) **345**(1):75–84. doi:10.1016/j.canlet.2013.11.022
33. Couzin-Frankel J. Inflammation bares a dark side. *Science* (2010) **330**(6011):1621. doi:10.1126/science.330.6011.1621
34. Coussens LM, Werb Z. Inflammation and cancer. *Nature* (2002) **420**(6917):860–7. doi:10.1038/nature01322
35. Zhang Q, Liu S, Ge D, Xue Y, Xiong Z, Abdel-Mageed AB, et al. Interleukin-17 promotes formation and growth of prostate adenocarcinoma in mouse models. *Cancer Res* (2012) **72**(10):2589–99. doi:10.1158/0008-5472.CAN-11-3795
36. Zhang Q, Liu S, Xiong Z, Wang AR, Myers L, Melamed J, et al. Interleukin-17 promotes development of castration-resistant prostate cancer potentially through creating an immunotolerant and pro-angiogenic tumor microenvironment. *Prostate* (2014) **74**(8):869–79. doi:10.1002/pros.22805
37. Winer S, Paltser G, Chan Y, Tsui H, Engleman E, Winer D, et al. Obesity predisposes to Th17 bias. *Eur J Immunol* (2009) **39**(9):2629–35. doi:10.1002/eji.200838893
38. Pini M, Fantuzzi G. Enhanced production of IL-17A during zymosan-induced peritonitis in obese mice. *J Leukoc Biol* (2010) **87**(1):51–8. doi:10.1189/jlb.0309188
39. Sumarac-Dumanovic M, Stevanovic D, Ljubic A, Jorga J, Simic M, Stamenkovic-Pejkovic D, et al. Increased activity of interleukin-23/interleukin-17 proinflammatory axis in obese women. *Int J Obes (Lond)* (2009) **33**(1):151–6. doi:10.1038/ijo.2008.216
40. Cohen DH, LeRoith D. Obesity, type 2 diabetes, and cancer: the insulin and IGF connection. *Endocr Relat Cancer* (2012) **19**(5):F27–45. doi:10.1530/ERC-11-0374
41. Stephenson GD, Rose DP. Breast cancer and obesity: an update. *Nutr Cancer* (2003) **45**(1):1–16. doi:10.1207/S15327914NC4501_1
42. Kaaks R, Lukanova A, Kurzer MS. Obesity, endogenous hormones, and endometrial cancer risk: a synthetic review. *Cancer Epidemiol Biomarkers Prev* (2002) **11**(12):1531–43.
43. Chen Q, Zhuang H, Liu Y. The association between obesity factor and esophageal caner. *J Gastrointest Oncol* (2012) **3**(3):226–31. doi:10.3978/j.issn.2078-6891.2012.026
44. Bracci PM. Obesity and pancreatic cancer: overview of epidemiologic evidence and biologic mechanisms. *Mol Carcinog* (2012) **51**(1):53–63. doi:10.1002/mc.20778
45. Moghaddam AA, Woodward M, Huxley R. Obesity and risk of colorectal cancer: a meta-analysis of 31 studies with 70,000 events. *Cancer Epidemiol Biomarkers Prev* (2007) **16**(12):2533–47. doi:10.1158/1055-9965.EPI-07-0708
46. Chow WH, Gridley G, Fraumeni JF Jr, Jarvholm B. Obesity, hypertension, and the risk of kidney cancer in men. *N Engl J Med* (2000) **343**(18):1305–11. doi:10.1056/NEJM200011023431804
47. Kitahara CM, Platz EA, Freeman LE, Hsing AW, Linet MS, Park Y, et al. Obesity and thyroid cancer risk among U.S. men and women: a pooled analysis of five prospective studies. *Cancer Epidemiol Biomarkers Prev* (2011) **20**(3):464–72. doi:10.1158/1055-9965.EPI-10-1220
48. Larsson SC, Wolk A. Obesity and the risk of gallbladder cancer: a meta-analysis. *Br J Cancer* (2007) **96**(9):1457–61. doi:10.1038/sj.bjc.6603703
49. Amling CL, Riffenburgh RH, Sun L, Moul JW, Lance RS, Kusuda L, et al. Pathologic variables and recurrence rates as related to obesity and race in men with prostate cancer undergoing radical prostatectomy. *J Clin Oncol* (2004) **22**(3):439–45. doi:10.1200/JCO.2004.03.132
50. Shah OJ, Wang Z, Hunter T. Inappropriate activation of the TSC/Rheb/mTOR/S6K cassette induces IRS1/2 depletion, insulin resistance, and cell survival deficiencies. *Curr Biol* (2004) **14**(18):1650–6. doi:10.1016/j.cub.2004.08.026
51. Manning BD, Logsdon MN, Lipovsky AI, Abbott D, Kwiatkowski DJ, Cantley LC. Feedback inhibition of Akt signaling limits the growth of tumors lacking Tsc2. *Genes Dev* (2005) **19**(15):1773–8. doi:10.1101/gad.1314605
52. Um SH, Frigerio F, Watanabe M, Picard F, Joaquin M, Sticker M, et al. Absence of S6K1 protects against age- and diet-induced obesity while enhancing insulin sensitivity. *Nature* (2004) **431**(7005):200–5. doi:10.1038/nature02866
53. Harrington LS, Findlay GM, Gray A, Tolkacheva T, Wigfield S, Rebholz H, et al. The TSC1-2 tumor suppressor controls insulin-PI3K signaling via regulation of IRS proteins. *J Cell Biol* (2004) **166**(2):213–23. doi:10.1083/jcb.200403069
54. O'Reilly KE, Rojo F, She QB, Solit D, Mills GB, Smith D, et al. mTOR inhibition induces upstream receptor tyrosine kinase signaling and activates Akt. *Cancer Res* (2006) **66**(3):1500–8. doi:10.1158/0008-5472.CAN-05-2925

55. Okuzumi T, Fiedler D, Zhang C, Gray DC, Aizenstein B, Hoffman R, et al. Inhibitor hijacking of Akt activation. *Nat Chem Biol* (2009) **5**(7):484–93. doi:10.1038/nchembio.183

**Conflict of Interest Statement:** The authors declare that the research was conducted in the absence of any commercial or financial relationships that could be construed as a potential conflict of interest.

*Received: 22 September 2014; paper pending published: 04 November 2014; accepted: 17 November 2014; published online: 01 December 2014.*

*Citation: Chen C, Zhang Q, Liu S, Lambrechts M, Qu Y and You Z (2014) AZD5363 inhibits inflammatory synergy between interleukin-17 and insulin/insulin-like growth factor 1. Front. Oncol. **4**:343. doi: 10.3389/fonc.2014.00343*

*This article was submitted to Surgical Oncology, a section of the journal Frontiers in Oncology.*

*Copyright © 2014 Chen, Zhang, Liu, Lambrechts, Qu and You. This is an open-access article distributed under the terms of the Creative Commons Attribution License (CC BY). The use, distribution or reproduction in other forums is permitted, provided the original author(s) or licensor are credited and that the original publication in this journal is cited, in accordance with accepted academic practice. No use, distribution or reproduction is permitted which does not comply with these terms.*

# IL-17 and Insulin/IGF1 Enhance Adhesion of Prostate Cancer Cells to Vascular Endothelial Cells Through CD44-VCAM-1 Interaction

Chong Chen,[1] Qiuyang Zhang,[1] Sen Liu,[1] Keshab R. Parajuli,[1] Yine Qu,[1,2] Jiandong Mei,[1,3] Zhiquan Chen,[1,4] Hui Zhang,[1,5] Damir B. Khismatullin,[6,7] and Zongbing You[1,6,8,9,10]*

[1]*Department of Structural and Cellular Biology, Tulane University, New Orleans, Louisiana*
[2]*Department of Histology and Embryology, Hebei United University School of Basic Medicine, Tangshan, Hebei Province, China*
[3]*Department of Thoracic Surgery, West China Hospital/West China School of Medicine, Sichuan University, Chengdu, China*
[4]*Department of Cardiothoracic Surgery, the Affiliated Hospital of Hebei United University, Tangshan, Hebei Province, China*
[5]*Department of Gynecology, the Affiliated Hospital of Taishan Medical College, Taian City, Shandong Province, China*
[6]*Tulane Cancer Center, Louisiana Cancer Research Consortium, Tulane University, New Orleans, Louisiana*
[7]*Department of Biomedical Engineering, Tulane University, New Orleans, Louisiana*
[8]*Department of Orthopaedic Surgery, Tulane University, New Orleans, Louisiana*
[9]*Tulane Center for Stem Cell Research Regenerative Medicine, Tulane University, New Orleans, Louisiana*
[10]*Tulane Center for Aging, Tulane University, New Orleans, Louisiana*

**BACKGROUND.** Extravasation is a critical step in cancer metastasis, in which adhesion of intravascular cancer cells to the vascular endothelial cells is controlled by cell surface adhesion molecules. The role of interleukin-17 (IL-17), insulin, and insulin-like growth factor 1 (IGF1) in adhesion of prostate cancer cells to the vascular endothelial cells is unknown, which is the subject of the present study.

**METHODS.** Human umbilical vein endothelial cells (HUVECs) and human prostate cancer cell lines (PC-3, DU-145, LNCaP, and C4–2B) were analyzed for expression of vascular cell adhesion molecule 1 (VCAM-1), integrins, and cluster of differentiation 44 (CD44) using flow cytometry and Western blot analysis. The effects of IL-17, insulin, and IGF1 on VCAM-1 expression and adhesion of prostate cancer cells to HUVECs were examined. The interaction of VCAM-1 and CD44 was assessed using immunoprecipitation assays.

Grant sponsor: National Institute of General Medical Sciences; Grant number: P20GM103518; Grant sponsor: National Cancer Institute; Grant number: R01CA174714; Grant sponsor: Department of Defense; Grant numbers: W81XWH-14–1-0050; W81XWH-14–1-0149; W81XWH-14–1-0458; Grant sponsor: The Developmental Fund of Tulane Cancer Center (TCC); Grant sponsor: Louisiana Cancer Research Consortium (LCRC) Fund.

The content of this article is solely the responsibility of the authors and does not necessarily represent the official views of the National Institutes of Health or the Department of Defense.

*Correspondence to: Zongbing You, Department of Structural and Cellular Biology, Tulane University School of Medicine, 1430 Tulane Ave mailbox 8649, New Orleans, LA 70112.
E-mail: zyou@tulane.edu
Received 24 November 2014; Accepted 6 January 2015
DOI 10.1002/pros.22971
Published online 14 February 2015 in Wiley Online Library (wileyonlinelibrary.com).

© 2015 Wiley Periodicals, Inc.

**RESULTS.** Insulin and IGF1 acted with IL-17 to increase VCAM-1 expression in HUVECs. PC-3, DU-145, LNCaP, and C4–2B cells expressed β1 integrin but not α4 integrin. CD44 was expressed by PC-3 and DU-145 cells but not by LNCaP or C4–2B cells. When HUVECs were treated with IL-17, insulin or IGF1, particularly with a combination of IL-17 and insulin (or IGF1), adhesion of PC-3 and DU-145 cells to HUVECs was significantly increased. In contrast, adhesion of LNCaP and C4–2B cells to HUVECs was not affected by treatment of HUVECs with IL-17 and/or insulin/IGF1. CD44 expressed in PC-3 cells physically bound to VCAM-1 expressed in HUVECs.

**CONCLUSIONS.** CD44-VCAM-1 interaction mediates the adhesion between prostate cancer cells and HUVECs. IL-17 and insulin/IGF1 enhance adhesion of prostate cancer cells to vascular endothelial cells through increasing VCAM-1 expression in the vascular endothelial cells. These findings suggest that IL-17 may act with insulin/IGF1 to promote prostate cancer metastasis. *Prostate 75:883–895, 2015.* © 2015 Wiley Periodicals, Inc.

*KEY WORDS:* **prostate cancer metastasis; IL-17; insulin; IGF1; VCAM-1**

## INTRODUCTION

More than 90% of deaths from cancer are caused by the metastases instead of the primary tumors [1]. Cancer metastasis is a process in which the secondary tumor sites are formed at locations distant to the primary site, including steps of stromal invasion and intravasation at the primary site, circulation in blood and lymph vessels, and extravasation and tumor formation at the distant site [2]. The number of cancer cells entering the systemic circulation (i.e., intravasation) daily can reach up to $4 \times 10^6$ per gram of primary tumor [3]. With a large number of cancer cells circulating intravascularly, the interactions between cancer cells and vascular endothelial cells play a key role in hematogenous cancer metastases to the distant sites of the body [4]. Several previous studies have shown that inflammatory cytokines cause adhesion of cancer cells to the activated vascular endothelium through inducing expression of adhesion molecules on the endothelium [5–7]. Colorectal cancer cells were observed to adhere to the vascular endothelium through binding to vascular cell adhesion molecule 1 (VCAM-1) in the presence of E-selectin [8]. It has been shown that cancer cells with expression of integrin $\alpha_4\beta_1$ (also called very late antigen-4, VLA-4) favorably attached to bone marrow stromal cells that constitutively expressed VCAM-1, leading to bone metastasis [9]. Therefore, understanding the molecular mechanisms underlying the interactions between cancer cells and vascular endothelial cells is vital to our understanding of cancer cells extravasation during cancer metastasis.

Interleukin-17 (IL-17 or IL-17A) is an inflammatory cytokine [10]. When it binds to a heterodimer of IL-17RA/IL-17RC receptor complex, IL-17 is able to activate nuclear factor-κB (NF-κB) activator 1 (Act1) through SEFIR (similar expression to fibroblast growth factor genes, IL-17 receptors, and Toll-IL-1R) domains [11–15]. Activation of Act1 triggers lysine-63-linked ubiquitination of tumor necrosis factor receptor-associated factor 6 (TRAF6), leading to activation of transforming growth factor-β-activated kinase 1 (TAK1) and IκB kinase (IKK) complex, and finally resulting in activation of NF-κB pathway that induces transcription of a variety of cytokines, chemokines, and growth factor [16–19]. We have previously demonstrated that IL-17 promotes development of hormone-dependent and castration-resistant prostate cancer in mouse prostates [20,21]. However, the role of IL-17 in development of metastatic tumors has not been determined.

Insulin is a hormone produced by pancreas β cells. The abnormal high concentration of insulin (hyperinsulinemia) may circulate in the body of people with obesity and type 2 diabetes mellitus with insulin resistance. Insulin-like growth factor 1 (IGF1) is produced by liver when stimulated by insulin [22]. Two types of insulin receptors (IR-A and IR-B) can bind to either insulin or IGF1. The receptors of IGF1 also include a heterodimer of IR and IGF1 receptor (IGF1R). Both insulin and IGF1 have been found to induce VCAM-1 expression in the vascular endothelial cells [23,24]. IL-17 can also increase expression of adhesion molecules, including intercellular adhesion molecule-1 (ICAM-1), VCAM-1 and E-selectin in the endothelial cells [25,26]. It has been shown that insulin can augment tumor necrosis factor-α (TNF-α)-induced expression of VCAM-1 in the endothelial cells [27]. We have previously demonstrated that insulin and IGF1 can enhance IL-17-induced chemokine expression [17]. Therefore, we conducted the present study to investigate if insulin and IGF1 can enhance IL-17-induced VCAM-1 expression in human umbilical vein endothelial cells (HUVECs), and hence boost adhesion of prostate cancer cells to HUVECs.

## MATERIALS AND METHODS

### Cell Culture

Human umbilical vein endothelial cells (HUVECs) were obtained from Life Technologies (Grand Island, NY) and cultured in Medium 200 with Low Serum Growth Supplement and Gentamicin/Amphotericin B (Life Technologies). HUVECs of passages 5–9 were used in the experiments. Human prostate cancer cell lines PC-3, DU-145, and LNCaP were purchased from the American Type Culture Collection (Manassas, VA) and C4–2B cell line was a gift from Dr. Leland WK Chung (Cedars-Sinai Medical Center, Los Angeles, CA). PC-3 and DU-145 cells were cultured in Dulbecco's Modified Eagle's Medium (DMEM; Mediatech, Inc., Manassas, VA) with 10% fetal bovine serum (FBS; Mediatech, Inc.) and 1% penicillin/streptomycin. C4–2B cells were cultured in Roswell Park Memorial Institute (RPMI)-1640 medium (Thermo Fisher Scientific, Inc., Waltham, MA) with 10% FBS and 1% penicillin/streptomycin. LNCaP cells were cultured in T-medium (Life Technologies) with 5% FBS and 1% penicillin/streptomycin. The cells were cultured in a 5% $CO_2$ humidified incubator at 37°C.

### Western Blot Analysis

Proteins of HUVECs, PC-3, DU-145, LNCaP, and C4–2B cells were extracted using RIPA lysis buffer, which contains 50 mM sodium fluoride, 0.5% Igepal CA-630 (NP-40), 10 mM sodium phosphate, 150 mM sodium chloride, 25 mM Tris (pH 8.0), 1 mM phenylmethylsulfonyl fluoride, 2 mM ethylenediaminetetraacetic acid (EDTA), and 1.2 mM sodium vanadate. The concentration of protein was measured using Bio-Rad protein Assay Dye Reagent Concentrate (Bio-Rad Laboratories, Hercules, CA) and BioTek ELx800 microplate reader (BioTek, Winooski, VT). Approximately 80 μg of protein was loaded to 10% SDS-polyacrylamide gel electrophoresis and transferred to polyvinylidene difluoride membrane. 5% nonfat dry milk in TBST buffer (25 mM Tris-HCl, 125 mM sodium chloride and 0.1% Tween 20) was used to block the membrane. The membrane was incubated with primary antibodies at 4°C overnight, and then incubated with IRDye® 800CW- or IRDye® 680RD-conjugated secondary antibodies (LI-COR Biosciences, Lincoln, NE) at room temperature for 1 hr. The results were scanned with an Odyssey Infrared Imager (LI-COR Biosciences). For loading control, the membrane was re-probed for glyceraldehyde 3-phosphate dehydrogenase (GAPDH). The antibodies used included: rabbit anti-VCAM-1 and mouse anti-CD44 antibodies (Cell Signaling Technology, Danvers, MA), and mouse anti-GAPDH antibodies (Millipore, Billerica, MA).

### Static Adhesion Assays

Approximately $1 \times 10^5$ HUVECs were seeded in each well of the 96-well plates. Two days later when the cells reached about 95% confluence, they were treated with 20 ng/ml recombinant humanIL-17 (R&D Systems, Inc., Minneapolis, MN), 50 ng/ml recombinant human insulin, or 50 ng/ml recombinant human IGF1 (Sigma Aldrich, Inc., St. Louis, MO), or a combination of IL-17 and insulin (or IGF1), for 24 hr. Prostate cancer cells were stained with 0.8 μM calcein AM (Life Technologies) for 15 min at 37°C and then washed three times with complete medium, thus the stained live prostate cancer cells gave rise to intense green fluorescence. Next, prostate cancer cells ($0.5 \times 10^5$ cells in 100-μl complete medium) were added onto HUVECs in the 96-well plates and incubated for 15 min at 37°C. After incubation, each well was gently washed three times with phosphate-buffered saline (PBS) to remove non-adherent prostate cancer cells. The adherent prostate cancer cells were visualized and photomicrographs were taken using an inverted fluorescence microscope with a digital camera (LEICA DMIRB, Leica Microsystems Inc., Buffalo Grove, IL). The fluorescence intensity (representing the number of adherent prostate cancer cells) was measured with a microplate reader (FLUOstar Optima, BMG Labtech, Cary, NC) atexcitation/emission wavelengths of 495 nm/520 nm.

### Flow Cytometry Analysis and Fluorescence-Activated Cell Sorting (FACS)

HUVECs, PC-3, DU-145, LNCaP, and C4–2B cells were grown to confluence in 100-mm tissue culture dishes and harvested using an Enzyme-Free PBS-based Cell Dissociation Buffer (Life Technologies). Approximately $1 \times 10^6$ cells were suspended in 100-μl FACS buffer (2% bovine serum albumin and 0.1% sodium azide in PBS). Fluorescein isothiocyanate (FITC)-conjugated mouse IgG1 (as isotype control) and mouse anti-human VCAM-1 antibodies (Ancell, Bayport, MN) were added to HUVECs separately. Phycoerythrin (PE)-conjugated mouse IgG1 (as isotype control), mouse anti-human β1 integrin and α4 integrin antibodies (Ancell), and mouse anti-human CD44 antibodies (Cell Signaling Technology) were added to PC-3, DU-145, LNCaP, and C4–2B cells separately. The cells were incubated with the antibodies (1:50 dilution) on ice for 45 min, followed by washing with FACS buffer twice. Flow cytometry analysis was conducted using a BD LSRII analyzer and FACS was conducted using BD FACSAria (BD Biosciences, San Jose, CA).

### Immunoprecipitation (IP)

HUVECs were grown to 100% confluence in 100-mm dishes and then treated with 20 ng/ml IL-17 and 50 ng/ml IGF1 for 24 hr or treated with PBS as control. Approximately $3 \times 10^6$ PC-3 or LNCaP cells were plated onto the confluent HUVECs for 30 min at 37°C. Non-adherent cancer cells were washed off with PBS. Next, HUVECs and adherent cancer cells were lysed in RIPA buffer. In a parallel set of groups, HUVECs and adherent cancer cells were first fixed with 2% formaldehyde at room temperature for 10 min according to a previous study [28], in order to preserve the binding of molecules between HUVECs and adherent cancer cells. After quenching with ice-cold 1.25 M glycine, HUVECs and adherent cancer cells were lysed in RIPA buffer. Mouse anti-CD44 antibodies (1 μg) or mouse isotype IgG control antibodies (1 μg) were added to the protein extract and incubated at 4°C for 1 hr. Then, 10 μl of protein A Sepharose™ CL-4B beads (GE Healthcare, Waukesha, WI) was added for incubation at 4°C overnight. After three washes with PBS, the immunoprecipitated protein was released from the beads by boiling and analyzed for VCAM-1 and CD44 using Western blot analysis.

### Statistical Analysis

The results were presented as mean ± standard deviation (SD) of three independent experiments ($n = 3$). Two-way analysis of variance (ANOVA) and one-way ANOVA and Tukey's test were used to determine the statistical significance using GraphPad Prism® 5.0 (Graphpad Software, La Jolla, CA). $P < 0.05$ was considered as statistically significant.

## RESULTS

### Insulin and IGF1 Enhance IL-17-Induced VCAM-1 Expression

When treated with IL-17, insulin, or IGF1 alone for 24 hr, VCAM-1 expression was only slightly increased in HUVECs (Fig. 1A), however, a combination of IL-17 and insulin (or IGF1) dramatically increased VCAM-1 expression (Fig. 1A). Expression of ICAM-1 and E-selectin was not affected (data not shown). Induction of VCAM-1 expression in HUVECs by IL-17 or the combination of IL-17 and insulin/IGF1 reached a peak level at 24 hr (Fig. 1B). Extension of the treatment time to 48 hr did not further increase the levels of VCAM-1 expression (data not shown). Flow cytometry analysis showed that the combination of IL-17 and insulin/IGF1 increased VCAM-1 expression on the surfaces of HUVECs to the levels higher than IL-17 or insulin/IGF1 alone (Fig. 1C and D).

### Prostate Cancer Cells Differentially Express Integrins and CD44

The conventional ligand of VCAM-1 is very late antigen-4 (VLA-4), which is made up by α4 and β1 integrins. Flow cytometry analysis showed that PC-3, DU-145, LNCaP, and C4–2B cells expressed β1 integrin, but not α4 integrin (Fig. 2A). This finding indicates that there is no intact VLA-4 ligand in PC-3, DU-145, LNCaP, and C4–2B cells to bind to VCAM-1 expressed in HUVECs. PC-3, DU-145, LNCaP, and C4–2B cells did not express VCAM-1, nor did HUVECs express CD44 (data not shown). Since it has been reported that CD44 can physically interact with VCAM-1 [29], we assessed CD44 expression in the prostate cancer cells. Flow cytometry analysis showed that more than 95% of PC-3 and DU-145 cells expressed high levels of CD44 on the cell surfaces (Fig. 2B), whereas LNCaP and C4–2B cells did not express CD44 at any detectable levels (Fig. 2B). Western blot analysis confirmed the results from flow cytometry analysis (Fig. 2C).

### Combination of IL-17 and Insulin/IGF1 Treatment Enhances Adhesion of PC-3 and DU-145 Cells to HUVECs

In assays of static adhesion within 15 min of time, few PC-3 cells adhered to the untreated HUVECs (Fig. 3A and B, the control group). When HUVECs were treated with insulin, IGF1, and IL-17 alone for 24 hr prior to addition of PC-3 cells, there were slightly more PC-3 cells adhered to HUVECs, which was statistically insignificant (Fig. 3A). In contrast, when HUVECs were treated with a combination of IL-17 and insulin/IGF1 for 24 hr prior to addition of PC-3 cells, the number of PC-3 cells adhered to HUVECs was significantly increased compared to the control group or any group treated with IL-17 or insulin/IGF1 alone (Fig. 3A and B, $P < 0.05$). Similarly, the combination of IL-17 and insulin/IGF1 also significantly increased the adhesion of DU-145 cells to HUVECs (Fig. 3C and D, $P < 0.05$). In contrast, when HUVECs were treated with IL-17, insulin, and IGF1, either alone or in combination, there was no increase in adhesion between LNCaP cells and HUVECs (Fig. 3E and F) or between C4–2B cells and HUVECs (Fig. 3G and H).

### CD44-VCAM-1 Interaction Mediates the Adhesion Between Prostate Cancer Cells and HUVECs

DU-145 cells were sorted into $CD44^{bright}$ and $CD44^{dim}$ populations using FACS (Fig. 4A). When HUVECs were treated with the combination of IL-17

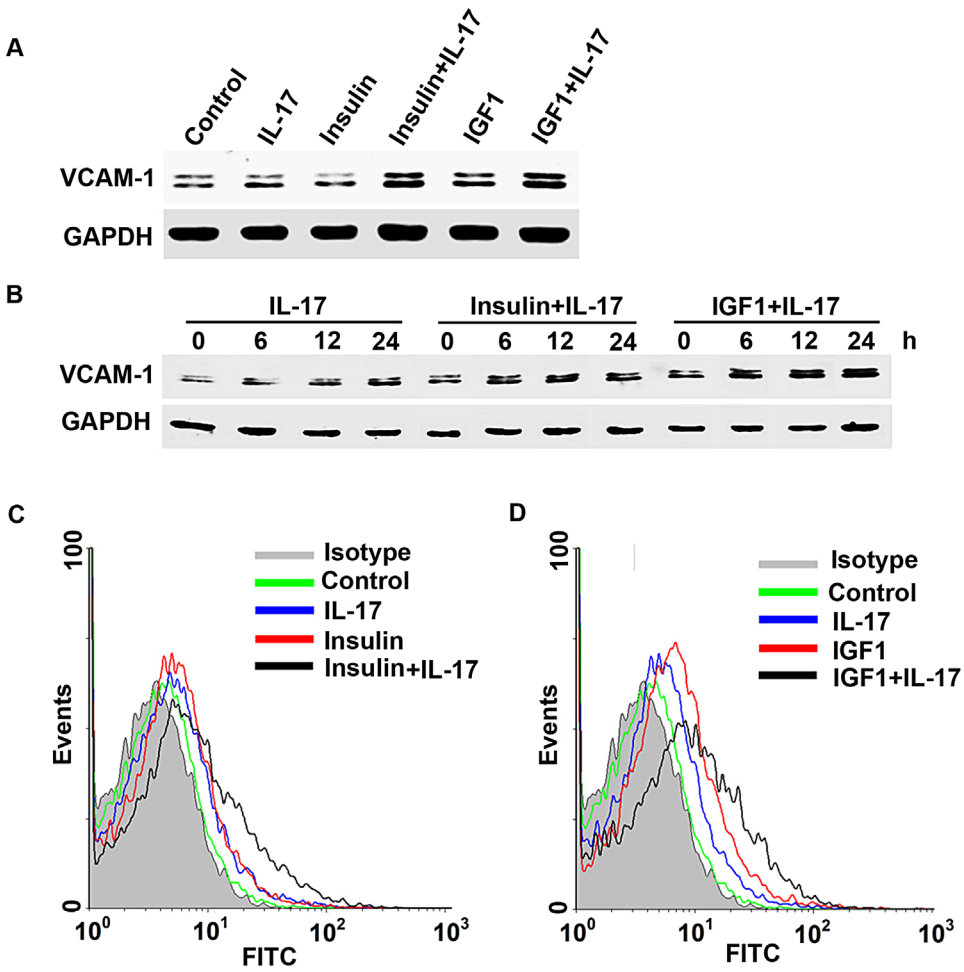



**Fig. 1.** VCAM-1 expression in HUVECs was induced by IL-17 and insulin/IGF1. **A**: Western blot analysis of VCAM-1 expression in HUVECs treated with IL-17, insulin, and IGF1, alone or in combination, for 24 hr. **B**: Western blot analysis of VCAM-1 expression in HUVECs treated with IL-17, insulin, and IGF1, alone or in combination, for 6, 12, and 24 hr. **C** and **D**: Flow cytometry analysis of VCAM-1 surface expression in HUVECs treated with IL-17, insulin, and IGF1, alone or in combination, for 24 hr.

and insulin/IGF1, there were significantly more $CD44^{bright}$ DU-145 cells adhered to HUVECs, compared to the unsorted DU-145 cells (Fig. 4B). However, the adhesion of $CD44^{dim}$ DU-145 cells to HUVECs was not increased by IL-17 and/or insulin/IGF1 treatment (Fig. 4B). Western blot analysis confirmed that $CD44^{bright}$ DU-145 cells expressed higher levels of CD44 than the unsorted DU-145 cells, whereas $CD44^{dim}$ DU-145 cells expressed little CD44 (Fig. 4C). Similarly, PC-3 cells were sorted into $CD44^{bright}$ and $CD44^{dim}$ populations using FACS (Fig. 5A). When HUVECs were treated with the combination of IL-17 and insulin/IGF1, there were significantly more $CD44^{bright}$ PC-3 cells adhered to HUVECs, compared to the HUVECs treated with IL-17 or insulin/IGF1 alone (Fig. 5B). However, there was no statistical difference between $CD44^{bright}$ and the unsorted PC-3 cells. In contrast, the adhesion of $CD44^{dim}$ PC-3 cells to HUVECs was not increased by IL-17 and/or insulin/IGF1 treatment (Fig. 5B). Since the adhesion between prostate cancer cells and HUVECs appeared to be dependent on expression of CD44 that has been shown to physically interact with VCAM-1 [29], we checked if CD44 binds to VCAM-1 when prostate cancer PC-3 cells adhered to HUVECs. We used three different negative controls: first, HUVECs alone control; as HUVECs expressed VCAM-1 but no CD44, anti-CD44 IP did not pull down VCAM-1 or CD44 (Fig. 6, lane 1); second, addition of LNCaP cells to HUVECs; as LNCaP cells expressed no CD44, anti-CD44 IP did not pull down VCAM-1 or CD44 (Fig. 6, lane 2); and third, IP with isotype IgG; as the non-specific IgG did not pull down CD44, VCAM-1 was not pulled down, either (Fig. 6, lanes 7–10). We initially used anti-CD44 antibodies to immunoprecipitate the CD44-VCAM-1

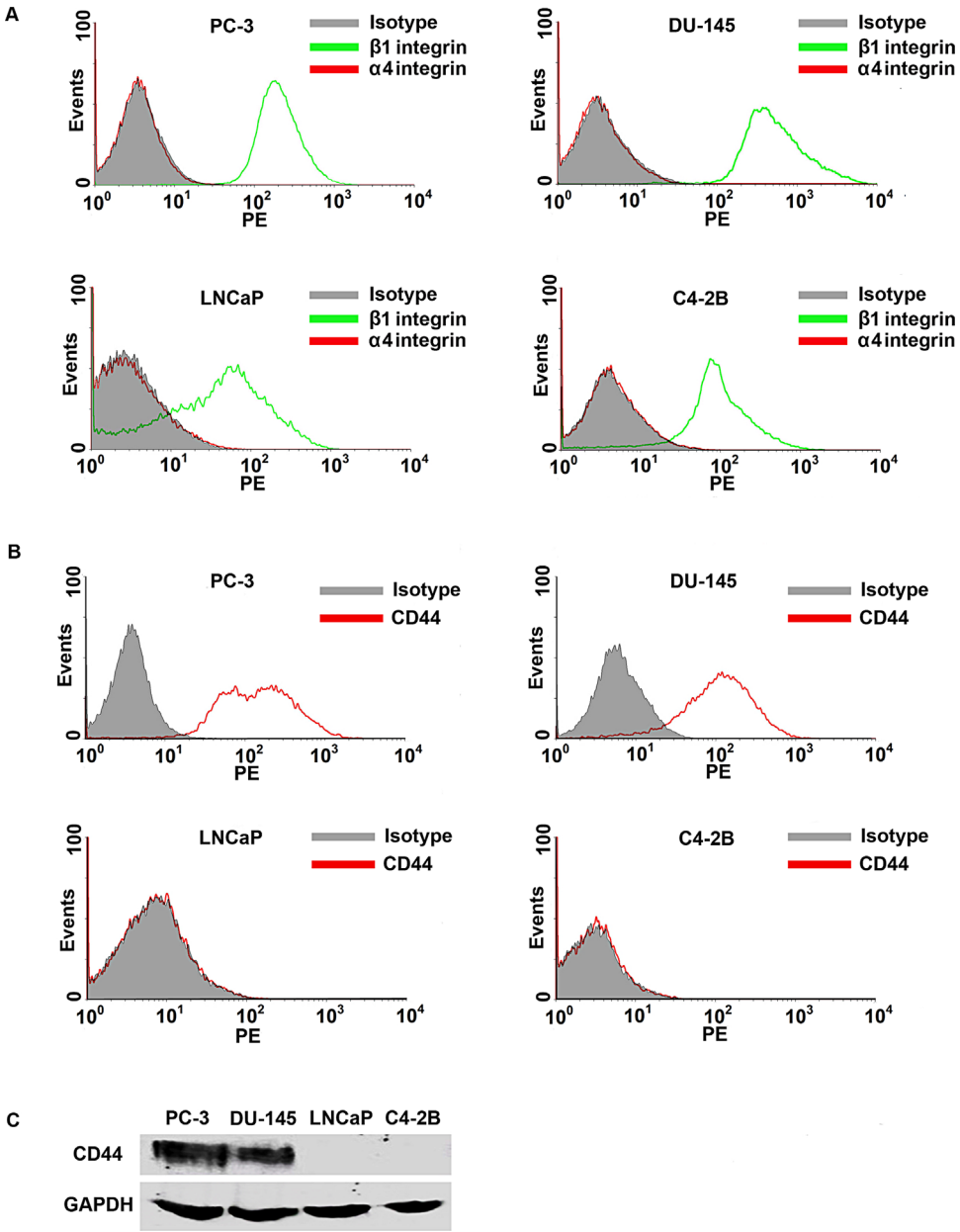



**Fig. 2.** Expression of adhesion molecules in prostate cancer cells. **A** and **B**: Flow cytometry analysis of $\alpha_4$ integrin, $\beta_1$ integrin, and CD44 expression in PC-3, DU-145, LNCaP, and C4–2B cells. **C**: Western blot analysis of CD44 expression in PC-3, DU-145, LNCaP, and C4–2B cells. Equal loading of proteins was confirmed by re-probing GAPDH.

complex when PC-3 cells were added onto HUVECs that were not treated (control group) or treated with IL-17 and IGF1 to increase VCAM-1 expression, without fixation using 2% formaldehyde. To our surprise, we did not pull down any VCAM-1 in either the control group or the IL-17 and IGF1 treated group, though CD44 was pulled down (Fig. 6, lanes 3–4). We suspected that the CD44-VCAM-1 interaction might be transient or weak, hence could not remain stable during the protein extraction procedure. Therefore, we adopted a previously reported technique to cross-link the protein interaction using 2% formaldehyde [28]. We found that anti-CD44 antibodies pulled down VCAM-1 in both the control and IL-17/IGF1 treated groups (Fig. 6, lanes 5–6). The amount of VCAM-1 protein pulled down was consistent to the levels of expression (Fig. 1A).

## DISCUSSION

It has been reported that IL-17 can activate NF-κB pathway [19], which is responsible for synthesis of

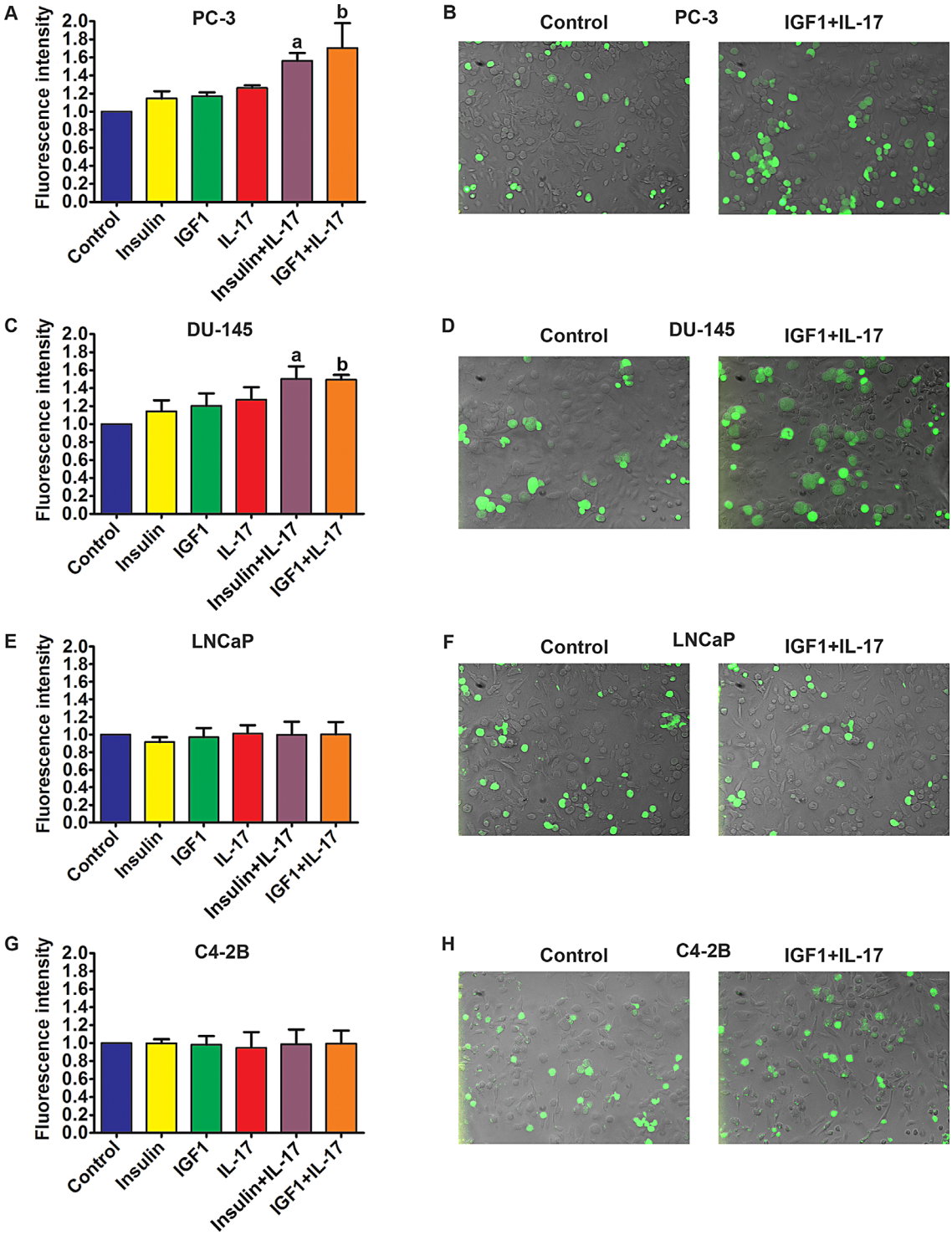



**Fig. 3.** Adhesion of prostate cancer cells to HUVECs. **A**, **C**, **E**, and **G**: Quantification of green fluorescence-labelled prostate cancer cells adhered to HUVECs within 15 min. HUVECs were treated with IL-17, insulin, and IGF1, alone or in combination, for 24 hr prior to addition of prostate cancer cells. Fluorescence intensity was proportional to the number of prostate cancer cells adhered to HUVECs. The fluorescence intensity of the control group was arbitrarily designated as "1," so the other groups were normalized with a formula: the fluorescence intensity of the treated group = the recorded fluorescence intensity of the treated group ÷ the recorded fluorescence intensity of the control group. Data represent means ± standard deviations of three independent experiments (n = 3). a, $P < 0.05$ compared to the control, insulin alone and IL-17 alone treatment groups; b, $P < 0.05$ compared to the control, IGF1 alone and IL-17 alone treatment groups. **B**, **D**, **F**, and **H**: representative photomicrographs of the adhered prostate cancer cells labelled with green fluorescence. HUVECs were not labelled and laid in the background beneath the green cells.

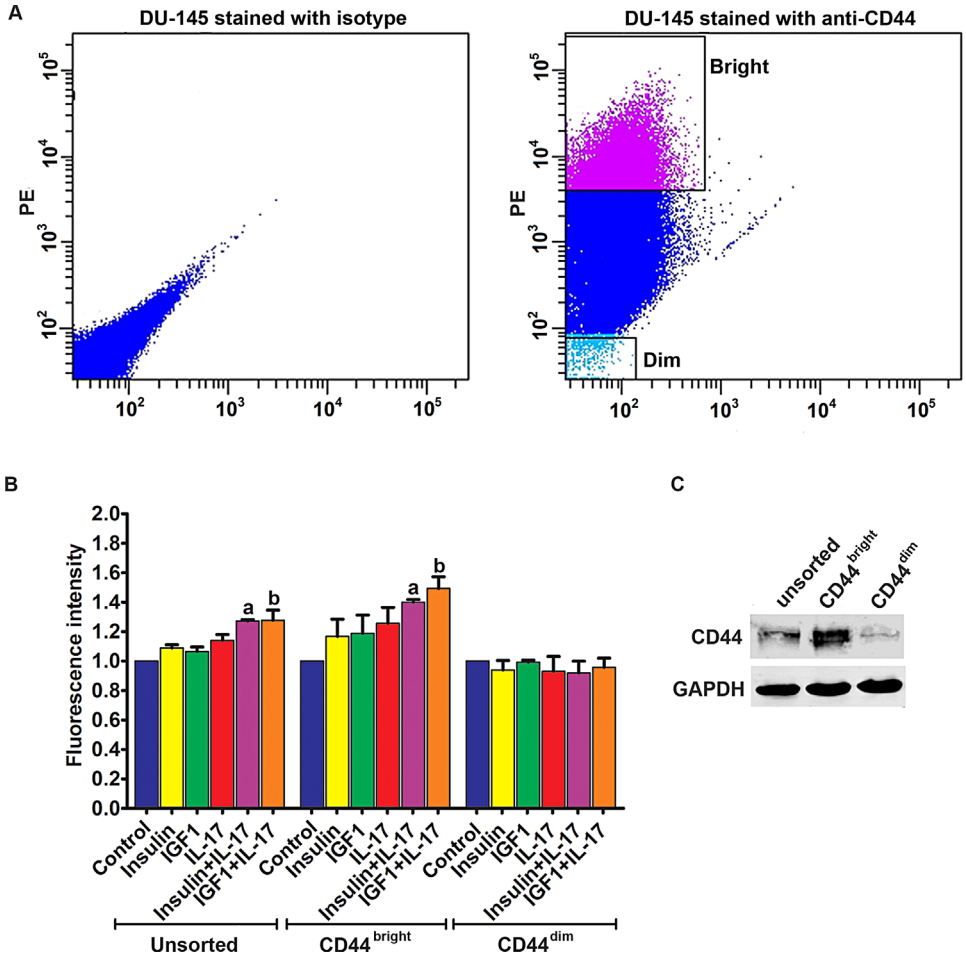



**Fig. 4.** Adhesion of the unsorted, CD44$^{bright}$, and CD44$^{dim}$ DU-145 cells to HUVECs. **A**: Left panel, flow cytometry analysis of DU-145 cells stained with isotype control IgG; right panel, a representative dot plot shows how CD44$^{bright}$ and CD44$^{dim}$ DU-145 cells were sorted using FACS. **B**: Quantification of green fluorescence-labelled prostate cancer cells adhered to HUVECs within 15 min. HUVECs were treated with IL-17, insulin, and IGF1, alone or in combination, for 24 hr prior to addition of prostate cancer cells. Fluorescence intensity was proportional to the number of prostate cancer cells adhered to HUVECs. The fluorescence intensity of the control group was arbitrarily designated as "1," so the other groups were normalized with a formula: the fluorescence intensity of the treated group = the recorded fluorescence intensity of the treated group ÷ the recorded fluorescence intensity of the control group. Data represent means ± standard deviations of three independent experiments (n = 3). In the unsorted DU-145 cells panel, a indicates $P < 0.05$ compared to the control, insulin alone and IL-17 alone treatment groups; b indicates $P < 0.05$ compared to the control, IGF1 alone and IL-17 alone treatment groups. In the CD44$^{bright}$ DU-145 cells panel, a and b indicate $P < 0.05$ compared to the corresponding single treatment and combined treatment groups within the CD44$^{bright}$ DU-145 cells panel, and between the CD44$^{bright}$ DU-145 cells panel and the unsorted DU-145 cells panel, as well as between the CD44$^{bright}$ DU-145 cells panel and the CD44$^{dim}$ DU-145 cells panel. **C**: Western blot analysis of CD44 expression in the unsorted, CD44$^{bright}$, and CD44$^{dim}$ DU-145 cells. Equal loading of proteins was confirmed by re-probing GAPDH.

VCAM-1 in the vascular endothelial cells [30]. In the present study, we showed that insulin and IGF1 were able to enhance IL-17-induced VCAM-1 expression in HUVECs. Of note, VCAM-1 is a glycoprotein with two different splice isoforms, namely, VCAM-1a (full-length with Mr ~ 90–95 kDa) and VCAM-1b (lacking exon 5 with Mr ~80–83 kDa) [31]. We observed that IL-17 single treatment slightly increased VCAM-1b but not VCAM-1a, while insulin single treatment slightly decreased VCAM-1a but slightly increased VCAM-1b, yet the combination of IL-17 and insulin treatment dramatically increased both VCAM-1a and VCAM-1b (Fig. 1A). The exact molecular mechanism that caused the different effects of IL-17 or insulin single treatment is not clear. Our previous study has demonstrated that insulin and IGF1 are able to enhance IL-17-induced expression of proinflammatory chemokines and cytokines [17]. We have shown that the underlying mechanism involves inhibition of glycogen synthase kinase 3 β (GSK3B) by

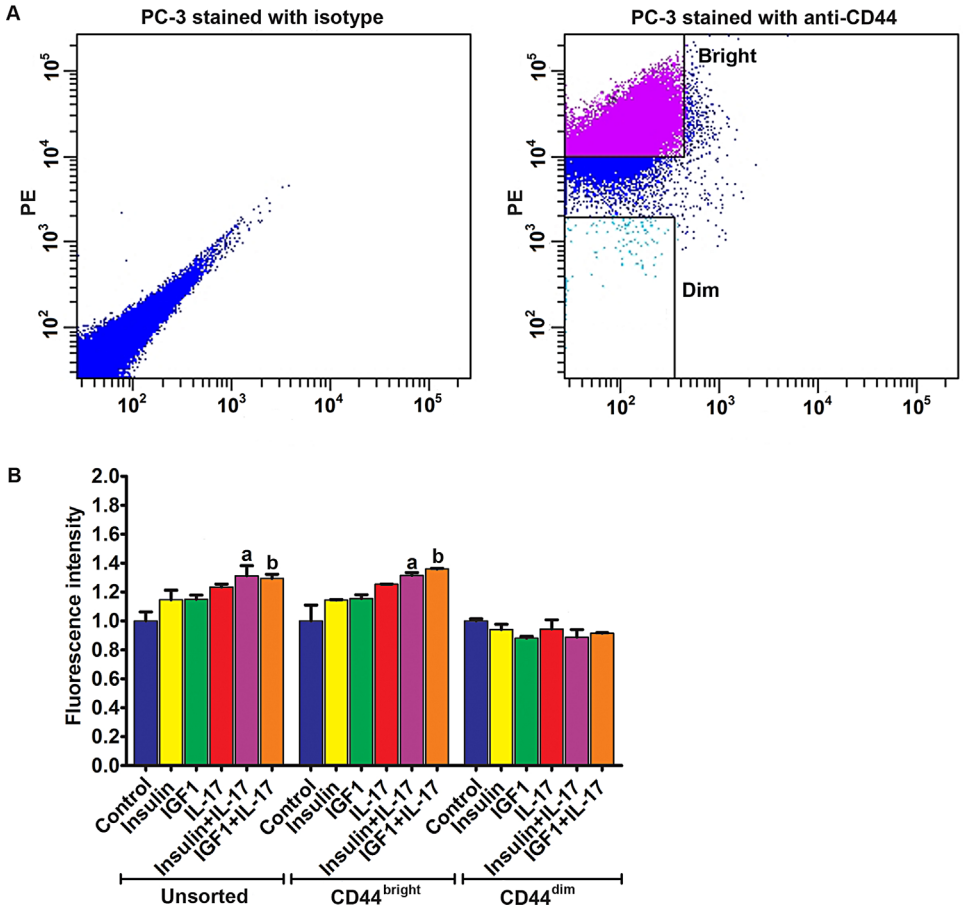



**Fig. 5.** Adhesion of the unsorted, CD44$^{bright}$, and CD44$^{dim}$ PC-3 cells to HUVECs. **A**: Left panel, flow cytometry analysis of PC-3 cells stained with isotype control IgG; right panel, a representative dot plot shows how CD44$^{bright}$ and CD44$^{dim}$ PC-3 cells were sorted using FACS. **B**: Quantification of green fluorescence-labelled prostate cancer cells adhered to HUVECs within 15 min. HUVECs were treated with IL-17, insulin, and IGF1, alone or in combination, for 24 hr prior to addition of prostate cancer cells. Fluorescence intensity was proportional to the number of prostate cancer cells adhered to HUVECs. The fluorescence intensity of the control group was arbitrarily designated as "1," so the other groups were normalized with a formula: the fluorescence intensity of the treated group = the recorded fluorescence intensity of the treated group ÷ the recorded fluorescence intensity of the control group. Data represent means ± standard deviations of three independent experiments (n = 3). In the unsorted PC-3 cells panel, a indicates $P < 0.05$ compared to the control, insulin alone and IL-17 alone treatment groups; b indicates $P < 0.05$ compared to the control, IGF1 alone and IL-17 alone treatment groups. In the CD44$^{bright}$ PC-3 cells panel, a and b indicate $P < 0.05$ compared to the corresponding single treatment and combined treatment groups within the CD44$^{bright}$ PC-3 cells panel, and between the CD44$^{bright}$ PC-3 cells panel and the CD44$^{dim}$ PC-3 cells panel.

Akt. Akt is activated by insulin and IGF1 through their receptor-activated phosphatidylinositol 3-kinase (PI3K). GSK3B phosphorylates CAAT enhancer binding protein β (C/EBPβ) and inhibits C/EBPβ's transcriptional function that is responsible for IL-17-induced gene expression [17,32]. Insulin and IGF1 can activate PI3K/Akt to phosphorylate GSK3B at serine 9 and inhibit GSK3B activity, and consequently increase C/EBPβ function to enhance IL-17-induced gene expression. Recently, we have demonstrated that insulin and IGF1 can also activate PI3K/Akt to phosphorylate GSK3A at serine 21 and inhibit GSK3A activity, and consequently enhance IL-17-induced gene expression [33]. We believe this mechanism may also be true for the enhanced expression of VCAM-1 in HUVECs treated with IL-17 and insulin/IGF1. IL-17 alone did not dramatically increase VCAM-1 expression to enhance adhesion because GSK3 negatively inhibits IL-17 signaling as demonstrated by previous studies [17,33,34]. In the presence of IGF1 or insulin, GSK3 function is inhibited by PI3K/Akt activated by IGF1 or insulin [17,33], thus VCAM-1 expression and subsequent adhesion are enhanced by IL-17. We have shown that the synergy between IL-17 and insulin/IGF1 can be blocked by melatonin that inhibits

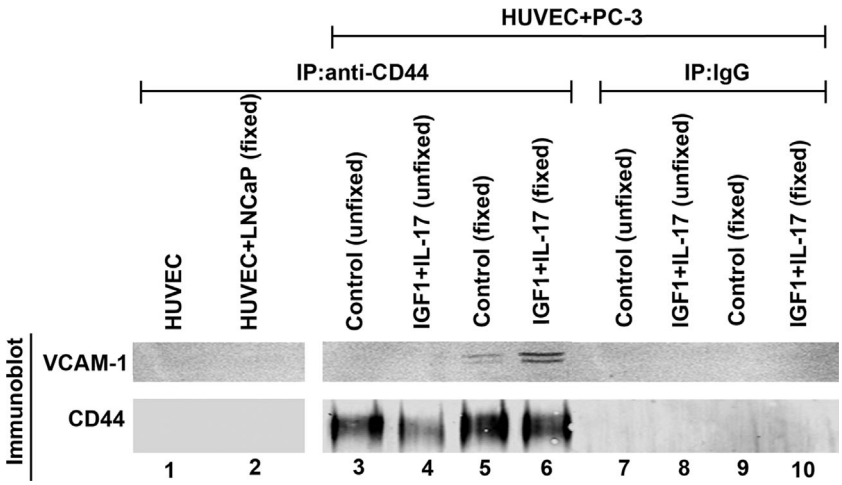



**Fig. 6.** CD44 expressed in prostate cancer cells binds to VCAM-1 expressed in HUVECs. Proteins were extracted from HUVECs alone and HUVECs with addition of LNCaP or PC-3 cells with or without cross-linking using 2% formaldehyde fixation. Immunoprecipitation (IP) was performed using isotype control mouse IgG or mouse anti-CD44 antibodies. Immunobot (Western blot) was performed using anti-VCAM-1 or anti-CD44 antibodies. Where indicated (including the HUVEC + LNCaP group), HUVECs were treated with IL-17 and IGF1 for 24 hr. Unfixed, adherent PC-3 cells and HUVECs were harvested for protein extraction without fixation. Fixed, adherent PC-3 cells and HUVECs were harvested for protein extraction after fixation with 2% formaldehyde for 10 min.

Akt [17] or by a new pan-Akt inhibitor AZD5363 [33]. Therefore, it is potentially possible to use melatonin or AZD5363 to manipulate the cross-talk between IL-17 andinsulin/IGF1 signaling pathways for preventive and therapeutic purposes.

VCAM-1 expression on the surface of endothelial cells contributes to leukocyte capture via binding to VLA-4 ($\alpha_4\beta_1$ integrin) expressed on the surface of leukocytes [35,36]. In the present study, we showed that the static adhesion of PC-3 and DU-145 cells to HUVECs was increased when HUVECs were treated with IL-17 and insulin/IGF1, which may be due to increased expression of VCAM-1 on the treated HUVECs. However, PC-3 and DU-145 cells did not express VLA-4, indicating that these prostate cancer cells cannot adhere to the endothelial cells through VLA-4-VCAM-1 interaction. It has been reported that VCAM-1 may bind to CD44 [4,29]. Therefore, we checked CD44 expression in the prostate cancer cells. We found that PC-3 and DU-145 cells expressed CD44 on their surface, whereas LNCaP and C4–2B cells did not express CD44. CD44 is a cell surface adhesion molecule and its main ligand is hyaluronic acid (HA) [37]. However, HA expression on HUVECs is usually not induced by inflammatory cytokines such as tumor necrosis factor-α (TNF-α), IL-1β, lipopolysaccharide, or interferon γ [38]. Thus, CD44-HA interaction may not be able to explain the increased adhesion of PC-3 and DU-145 cells to HUVECs. P-selectin, L-selectin, and E-selectin have been reported to bind to CD44 and facilitate capture of colon cancer cells and leukocytes on the vascular endothelial cells [39,40]. However, we did not detect any E-selectin expression in the HUVECs used in our study, thus E-selectin is unlikely to play any role in the adhesion of prostate cancer cells to HUVECs. We believe that the adhesion of prostate cancer cells to HUVECs is mediated through CD44-VCAM-1 interaction, based on the following evidence: first, only prostate cancer cells that express CD44 (PC-3 and DU-145 cells) adhered to HUVECs, particularly when VCAM-1 expression was enhanced by the treatment with IL-17 and insulin/IGF1, whereas the prostate cancer cells that do not express CD44 (LNCaP and C4–2B cells) did not adhere to HUVECs even after the treatment with IL-17 and insulin/IGF1; second, the sorted $CD44^{dim}$ populations of PC-3 and DU-145 cells no longer adhered to HUVECs, due to reduced or lack of CD44 expression; and third, CD44 expressed in PC-3 cells physically bound to VCAM-1 expressed in HUVECs under the static adhesion condition.

It is of significance to identify CD44-VCAM-1 interaction that mediates adhesion of prostate cancer cells to the vascular endothelial cells, as CD44 is usually expressed in the stem cell-like prostate and breast cancer cells that circulate intravascularly and eventually metastasize to distant organs [41–44]. Thus, prostate cancer stem cells may adhere to the vascular endothelium through CD44-VCAM-1 interaction. Previously, Draffin et al. have shown that CD44 is able to facilitate the adherence of metastatic prostate and breast cancer cells to bone marrow endothelial cells via binding to HA [45]. When CD44 expression was down-regulated by miR34-a, prostate

cancer regeneration and metastasis was inhibited [46]. In the present study, we provided evidence to support that CD44-VCAM-1 interaction may also contribute to the adhesion of prostate cancer cells to the vascular endothelium. Of particular interest, the adhesion is enhanced by IL-17 and insulin/IGF1 due to increased VCAM-1 expression in the vascular endothelial cells. This may be relevant to the increased risks of metastasis and mortality in obese men with prostate cancer. It has been found that obese men have a 3.6-fold increase in risk of prostate cancer metastasis and a 2.6-fold increased risk of prostate cancer-specific mortality, compared to prostate cancer patients with normal body mass index [47]. Another recent study found that overweight and obese men were threefold and fivefold more likely to develop metastases than normal weight men [48]. It is well known that obese people have increased serum levels of insulin and IGF1 [49] as well as IL-17 [50]. Thus, we speculate that, due to increased levels of IL-17 and insulin/IGF1, VCAM-1 expression is increased in the vascular endothelial cells in obese men with prostate cancer, which facilitates adhesion of the stem cell-like circulating tumor cells through CD44-VCAM-1 interaction and subsequently promotes extravasation and metastasis of prostate cancer. Further studies are required to validate this speculation.

## CONCLUSIONS

CD44-VCAM-1 interaction mediates the adhesion between prostate cancer cells and HUVECs. IL-17 and insulin/IGF1 enhance adhesion of prostate cancer cells to vascular endothelial cells through increasing VCAM-1 expression in the vascular endothelial cells. These findings suggest that IL-17 may act with insulin/IGF1 to promote prostate cancer metastasis.

## ACKNOWLEDGMENTS

The authors thank Mary Price from Tulane Cancer Center and Louisiana Cancer Research Consortium FACS Core for flow cytometry analysis. Jiandong Mei is a visiting scholar at Tulane University School of Medicine sponsored by the China Scholarship Council (201406240145).

## REFERENCES

1. Entschladen F, Drell TLt, Lang K, Joseph J, Zaenker KS. Tumour-cell migration, invasion, and metastasis: Navigation by neurotransmitters. Lancet Oncol 2004;5(4):254–258.
2. Orr FW, Wang HH, Lafrenie RM, Scherbarth S, Nance DM. Interactions between cancer cells and the endothelium in metastasis. J Pathol 2000;190(3):310–329.
3. Wong SY, Hynes RO. Lymphatic or hematogenous dissemination: How does a metastatic tumor cell decide. Cell Cycle 2006;5(8):812–817.
4. Miles FL, Pruitt FL, van Golen KL, Cooper CR. Stepping out of the flow: Capillary extravasation in cancer metastasis. Clin Exp Metastasis 2008;25(4):305–324.
5. Fidler IJ. The pathogenesis of cancer metastasis: The 'seed and soil' hypothesis revisited. Nat Rev Cancer 2003;3(6):453–458.
6. Scherbarth S, Orr FW. Intravital videomicroscopic evidence for regulation of metastasis by the hepatic microvasculature: Effects of interleukin-1alpha on metastasis and the location of B16F1 melanoma cell arrest. Cancer Res 1997;57(18): 4105–4110.
7. Huh SJ, Liang S, Sharma A, Dong C, Robertson GP. Transiently entrapped circulating tumor cells interact with neutrophils to facilitate lung metastasis development. Cancer Res 2010;70(14): 6071–6082.
8. Auguste P, Fallavollita L, Wang N, Burnier J, Bikfalvi A, Brodt P. The host inflammatory response promotes liver metastasis by increasing tumor cell arrest and extravasation. Am J Pathol 2007;170(5):1781–1792.
9. Matsuura N, Puzon-McLaughlin W, Irie A, Morikawa Y, Kakudo K, Takada Y. Induction of experimental bone metastasis in mice by transfection of integrin alpha 4 beta 1 into tumor cells. Am J Pathol 1996;148(1):55–61.
10. Kolls JK, Linden A. Interleukin-17 family members and inflammation. Immunity 2004;21(4):467–476.
11. Novatchkova M, Leibbrandt A, Werzowa J, Neubuser A, Eisenhaber F. The STIR-domain superfamily in signal transduction, development and immunity. Trends Biochem Sci 2003;28(5):226–229.
12. Chang SH, Park H, Dong C. Act1 adaptor protein is an immediate and essential signaling component of interleukin-17 receptor. J Biol Chem 2006;281(47):35603–35607.
13. Qian Y, Liu C, Hartupee J, Altuntas CZ, Gulen MF, Jane-Wit D, Xiao J, Lu Y, Giltiay N, Liu J, Kordula T, Zhang QW, Vallance B, Swaidani S, Aronica M, Tuohy VK, Hamilton T, Li X. The adaptor Act1 is required for interleukin 17-dependent signaling associated with autoimmune and inflammatory disease. Nat Immunol 2007;8(3):247–256.
14. Maitra A, Shen F, Hanel W, Mossman K, Tocker J, Swart D, Gaffen SL. Distinct functional motifs within the IL-17 receptor regulate signal transduction and target gene expression. Proc Natl Acad Sci U S A 2007;104(18):7506–7511.
15. Ho AW, Shen F, Conti HR, Patel N, Childs EE, Peterson AC, Hernandez-Santos N, Kolls JK, Kane LP, Ouyang W, Gaffen SL. IL-17RC is required for immune signaling via an extended SEF/IL-17R signaling domain in the cytoplasmic tail. J Immunol 2010;185(2):1063–1070.
16. Liu C, Qian W, Qian Y, Giltiay NV, Lu Y, Swaidani S, Misra S, Deng L, Chen ZJ, Li X. Act1 , a U-box E3 ubiquitin ligase for IL-17 signaling. Sci Signal 2009;2(92):63.
17. Ge D, Dauchy RT, Liu S, Zhang Q, Mao L, Dauchy EM, Blask DE, Hill SM, Rowan BG, Brainard GC, Hanifin JP, Cecil KS, Xiong Z, Myers L, You Z. Insulin and IGF1 enhance IL-17-induced chemokine expression through a GSK3B-dependent mechanism: a new target for melatonin's anti-inflammatory action. J Pineal Res 2013;55(4):377–387.
18. Zhu S, Pan W, Song X, Liu Y, Shao X, Tang Y, Liang D, He D, Wang H, Liu W, Shi Y, Harley JB, Shen N, Qian Y. The microRNA miR-23b suppresses IL-17-associated autoimmune

inflammation by targeting TAB2, TAB3 and IKK-alpha. Nat Med 2012;18(7):1077–1086.

19. Hwang SY, Kim JY, Kim KW, Park MK, Moon Y, Kim WU, Kim HY. IL-17 induces production of IL-6 and IL-8 in rheumatoid arthritis synovial fibroblasts via NF-kappaB- and PI3-kinase/Akt-dependent pathways. Arthritis Res Ther 2004;6(2):R120–R128.
20. Zhang Q, Liu S, Ge D, Xue Y, Xiong Z, Abdel-Mageed AB, Myers L, Hill SM, Rowan BG, Sartor O, Melamed J, Chen Z, You Z. Interleukin-17 promotes formation and growth of prostate adenocarcinoma in mouse models. Cancer Res 2012;72-(10):2589–2599.
21. Zhang Q, Liu S, Xiong Z, Wang AR, Myers L, Melamed J, Tang WW, You Z. Interleukin-17 promotes development of castration-resistant prostate cancer potentially through creating an immunotolerant and pro-angiogenic tumor microenvironment. Prostate 2014;74(8):869–879.
22. Baxter RC, Bryson JM, Turtle JR. Somatogenic receptors of rat liver: regulation by insulin. Endocrinology 1980;107(4):1176–1181.
23. Madonna R, Pandolfi A, Massaro M, Consoli A, De Caterina R. Insulin enhances vascular cell adhesion molecule-1 expression in human cultured endothelial cells through a pro-atherogenic pathway mediated by p38 mitogen-activated protein-kinase. Diabetologia 2004;47(3):532–536.
24. Balaram SK, Agrawal DK, Allen RT, Kuszynski CA, Edwards JD. Cell adhesion molecules and insulin-like growth factor-1 in vascular disease. J Vasc Surg 1997;25(5):866–876.
25. Roussel L, Houle F, Chan C, Yao Y, Berube J, Olivenstein R, Martin JG, Huot J, Hamid Q, Ferri L, Rousseau S. IL-17 promotes p38 MAPK-dependent endothelial activation enhancing neutrophil recruitment to sites of inflammation. J Immunol 2010;184(8):4531–4537.
26. Xing X, Yang J, Yang X, Wei Y, Zhu L, Gao D, Li M. IL-17A induces endothelial inflammation in systemic sclerosis via the ERK signaling pathway. PLoS ONE 2013;8(12):-e85032.
27. Mackesy DZ, Goalstone ML. Insulin augments tumor necrosis factor-alpha stimulated expression of vascular cell adhesion molecule-1 in vascular endothelial cells. J Inflamm (Lond) 2011;8:34.
28. Klockenbusch C, Kast J. Optimization of formaldehyde cross--linking for protein interaction analysis of non-tagged integrin beta1. J Biomed Biotechnol 2010;2010:927585.
29. Wang PC, Weng CC, Hou YS, Jian SF, Fang KT, Hou MF, Cheng KH. Activation of VCAM-1 and its associated molecule CD44 leads to increased malignant potential of breast cancer cells. Int J Mol Sci 2014;15(3):3560–3579.
30. Chen CC, Rosenbloom CL, Anderson DC, Manning AM. Selective inhibition of E-selectin, vascular cell adhesion molecule-1, and intercellular adhesion molecule-1 expression by inhibitors of I kappa B-alpha phosphorylation. J Immunol 1995;155(7):3538–3545.
31. Montes-Sanchez D, Ventura JL, Mitre I, Frias S, Michan L, Espejel-Nunez A, Vadillo-Ortega F, Zentella A. Glycosylated VCAM-1 isoforms revealed in 2D western blots of HUVECs treated with tumoral soluble factors of breast cancer cells. BMC Chem Biol 2009;9:7.
32. Ruddy MJ, Wong GC, Liu XK, Yamamoto H, Kasayama S, Kirkwood KL, Gaffen SL. Functional cooperation between interleukin-17 and tumor necrosis factor-alpha is mediated by CCAAT/enhancer-binding protein family members. J Biol Chem 2004;279(4):2559–2567.
33. Chen C, Zhang Q, Liu S, Lambrechts M, Qu Y, You Z. AZD5363 Inhibits Inflammatory Synergy between Interleukin-17 and Insulin/Insulin-Like Growth Factor 1. Front Oncol 2014;4:343.
34. Shen F, Li N, Gade P, Kalvakolanu DV, Weibley T, Doble B, Woodgett JR, Wood TD, Gaffen SL. IL-17 receptor signaling inhibits C/EBPbeta by sequential phosphorylation of the regulatory 2 domain. Sci Signal 2009;2(59):ra8.
35. Galkina E, Ley K. Immune and inflammatory mechanisms of atherosclerosis. Annu Rev Immunol 2009;27:165–197.
36. Alon R, Kassner PD, Carr MW, Finger EB, Hemler ME, Springer TA. The integrin VLA-4 supports tethering and rolling in flow on VCAM-1. J Cell Biol 1995;128(6):1243–1253.
37. Goodison S, Urquidi V, Tarin D. CD44 cell adhesion molecules. Mol Pathol 1999;52(4):189–196.
38. Mohamadzadeh M, DeGrendele H, Arizpe H, Estess P, Siegelman M. Proinflammatory stimuli regulate endothelial hyaluronan expression and CD44/HA-dependent primary adhesion. J Clin Invest 1998;101(1):97–108.
39. Thomas SN, Zhu F, Schnaar RL, Alves CS, Konstantopoulos K. Carcinoembryonic antigen and CD44 variant isoforms cooperate to mediate colon carcinoma cell adhesion to E- and L-selectin in shear flow. J Biol Chem 2008;283-(23):15647–15655.
40. Dimitroff CJ, Lee JY, Rafii S, Fuhlbrigge RC, Sackstein R. CD44 is a major E-selectin ligand on human hematopoietic progenitor cells. J Cell Biol 2001;153(6):1277–1286.
41. Al-Hajj M, Wicha MS, Benito-Hernandez A, Morrison SJ, Clarke MF. Prospective identification of tumorigenic breast cancer cells. Proc Natl Acad Sci U S A 2003;100(7):3983–3988.
42. Collins AT, Berry PA, Hyde C, Stower MJ, Maitland NJ. Prospective identification of tumorigenic prostate cancer stem cells. Cancer Res 2005;65(23):10946–10951.
43. Patrawala L, Calhoun T, Schneider-Broussard R, Li H, Bhatia B, Tang S, Reilly JG, Chandra D, Zhou J, Claypool K, Coghlan L, Tang DG. Highly purified CD44+ prostate cancer cells from xenograft human tumors are enriched in tumorigenic and metastatic progenitor cells. Oncogene 2006;25(12):1696–1708.
44. Hurt EM, Kawasaki BT, Klarmann GJ, Thomas SB, Farrar WL. CD44+ CD24(−) prostate cells are early cancer progenitor/stem cells that provide a model for patients with poor prognosis. Br J Cancer 2008;98(4):756–765.
45. Draffin JE, McFarlane S, Hill A, Johnston PG, Waugh DJ. CD44 potentiates the adherence of metastatic prostate and breast cancer cells to bone marrow endothelial cells. Cancer Res 2004;64(16):5702–5711.
46. Liu C, Kelnar K, Liu B, Chen X, Calhoun-Davis T, Li H, Patrawala L, Yan H, Jeter C, Honorio S, Wiggins JF, Bader AG, Fagin R, Brown D, Tang DG. The microRNA miR-34a inhibits prostate cancer stem cells and metastasis by directly repressing CD44. Nat Med 2011;17(2):211–215.
47. Gong Z, Agalliu I, Lin DW, Stanford JL, Kristal AR. Obesity is associated with increased risks of prostate cancer metastasis and death after initial cancer diagnosis in middle-aged men. Cancer 2007;109(6):1192–1202.
48. Keto CJ, Aronson WJ, Terris MK, Presti JC, Kane CJ, Amling CL, Freedland SJ. Obesity is associated with castration-resistant disease and metastasis in men treated with androgen depriva-

tion therapy after radical prostatectomy: Results from the SEARCH database. BJU Int 2012;110(4):492–498.

49. Cohen DH, LeRoith D. Obesity, type 2 diabetes, and cancer: The insulin and IGF connection. Endocr Relat Cancer 2012;19(5): F27–F45.

50. Sumarac-Dumanovic M, Stevanovic D, Ljubic A, Jorga J, Simic M, Stamenkovic-Pejkovic D, Starcevic V, Trajkovic V, Micic D. Increased activity of interleukin-23/interleukin-17 proinflammatory axis in obese women. Int J Obes (Lond) 2009;33(1): 151–156.




The Journal of Immunology

This information is current as of April 23, 2015.

# Estradiol Inhibits Th17 Cell Differentiation through Inhibition of *RORγT* Transcription by Recruiting the ER α/REA Complex to Estrogen Response Elements of the *RORγT* Promoter

Rong-Yi Chen, Yi-Ming Fan, Qiuyang Zhang, Sen Liu, Qingli Li, Guo-Lin Ke, Chen Li and Zongbing You

*J Immunol* 2015; 194:4019-4028; Prepublished online 13 March 2015;
doi: 10.4049/jimmunol.1400806
http://www.jimmunol.org/content/194/8/4019

**Supplementary Material** **http://www.jimmunol.org/content/suppl/2015/03/13/jimmunol.1400806.DCSupplemental.html**

**References** This article **cites 58 articles**, 26 of which you can access for free at:
http://www.jimmunol.org/content/194/8/4019.full#ref-list-1

**Subscriptions** Information about subscribing to *The Journal of Immunology* is online at:
http://jimmunol.org/subscriptions

**Permissions** Submit copyright permission requests at:
http://www.aai.org/ji/copyright.html

**Email Alerts** Receive free email-alerts when new articles cite this article. Sign up at:
http://jimmunol.org/cgi/alerts/etoc

*The Journal of Immunology* is published twice each month by
The American Association of Immunologists, Inc.,
9650 Rockville Pike, Bethesda, MD 20814-3994.
Copyright © 2015 by The American Association of Immunologists, Inc. All rights reserved.
Print ISSN: 0022-1767 Online ISSN: 1550-6606.

Downloaded from http://www.jimmunol.org/ at Tulane University Medical Center on April 23, 2015

# Estradiol Inhibits Th17 Cell Differentiation through Inhibition of *RORγT* Transcription by Recruiting the ERα/REA Complex to Estrogen Response Elements of the *RORγT* Promoter

**Rong-Yi Chen,*[,†,1] Yi-Ming Fan,*[,1] Qiuyang Zhang,[†] Sen Liu,[†] Qingli Li,[†,‡] Guo-Lin Ke,* Chen Li,* and Zongbing You[†,§,¶,‖,#]**

**The symptoms of vaginal candidiasis exacerbate in the second half of the menstrual cycle in premenopausal women when the serum estradiol level is elevated. Estradiol has been shown to inhibit Th17 differentiation and production of antifungal IL-17 cytokines. However, little is known about the mechanisms. In the present study, we used mouse splenocytes and found that estradiol inhibited Th17 differentiation through downregulation of *Rorγt* mRNA and protein expression. Estradiol activated estrogen receptor (ER)α to recruit repressor of estrogen receptor activity (REA) and form the ERα/REA complex. This complex bound to three estrogen response element (ERE) half-sites on the *Rorγt* promoter region to suppress *Rorγt* expression. Estradiol induced *Rea* mRNA and protein expression in mouse splenocytes. Using *Rea* small interfering RNA to knock down *Rea* expression enhanced *Rorγt* expression and Th17 differentiation. Alternatively, histone deacetylase 1 and 2 bound to the three ERE half-sites, independent of estradiol. Histone deacetylase inhibitor MS-275 dose- and time-dependently increased *Rorγt* expression and subsequently enhanced Th17 differentiation. In 15 healthy premenopausal women, high serum estradiol levels are correlated with low *RORγT* mRNA levels and high *REA* mRNA levels in the vaginal lavage. These results demonstrate that estradiol upregulates REA expression and recruits REA via ERα to the EREs on the *RORγT* promoter region, thus inhibiting *RORγT* expression and Th17 differentiation. This study suggests that the estradiol/ERα/REA axis may be a feasible target in the management of recurrent vaginal candidiasis.** *The Journal of Immunology*, **2015, 194: 4019–4028.**

Naive $CD4^+$ T cells differentiate into several effector subsets with distinct functions, including Th1, Th2, Th17, and regulatory T cells (Tregs) (1). Th17 differentiation has been intensively studied, yet the underlying molecular mechanisms have not been fully understood. Naive $CD4^+$ T cells are induced to differentiate into Th17 cells by a combination of TGF-β and IL-6 (2-4), TGF-β and IL-1β (5, 6), or TGF-β and IL-21 (7). IL-23 was originally found to stimulate IL-17 expression (8); however, later studies found that IL-23 is responsible for the survival and expansion of Th17 cells (2–4). Blockade of Th1 and/or Th2 differentiation (via anti–IFN-γ and/or anti–IL-4 Abs) can enhance Th17 differentiation (9, 10). The converging point of actions by these cytokines is a thymus-specific isoform of the retinoid acid receptor-related orphan receptor C (*RORC* or *RORgamma*), also called *RORγT* (11). RORγT is the key transcription factor that orchestrates Th17 differentiation and transcription of IL-17A and IL-17F (12). Another related orphan nuclear receptor RORα plays a partially redundant role with RORγT in promoting Th17 differentiation, and double deficiencies in *RORα* and *RORγT* globally impair Th17 generation and completely protect mice against experimental autoimmune encephalomyelitis (13). T cell–specific deficiency of *STAT3* impairs Th17 differentiation through decreasing RORγT expression and increasing expression of T-bet, a transcription factor responsible for Th1 differentiation, and Foxp3, a transcription factor responsible for Treg differentiation (14, 15). Recently, it has been shown that Th17 differentiation is regulated by a network of transcription factors, including RORγT, STAT3, BATF, IFN regulatory factor 4, c-Maf, and EP300 (16). The members of the regulatory network for Th17 differentiation are still expanding (17).

Th17 cells secrete IL-17A, IL-17F, IL-17A/F, IL-22, IL-21, and other cytokines and chemokines, which play important roles in host defense, autoimmunity, inflammation, and tumorigenesis (18, 19).

*Department of Dermatology, Affiliated Hospital of Guangdong Medical College, Zhanjiang, Guangdong 524001, China; [†]Department of Structural and Cellular Biology, Tulane University Health Sciences Center, New Orleans, LA 70112; and [‡]Department of Obstetrics and Gynecology, West China Second University Hospital, Sichuan University, Chengdu, Sichuan 610041, China; [§]Department of Orthopaedic Surgery, Tulane University Health Sciences Center, New Orleans, LA 70112; [¶]Tulane Cancer Center and Louisiana Cancer Research Consortium, Tulane University Health Sciences Center, New Orleans, LA 70112; [‖]Tulane Center for Aging, Tulane University Health Sciences Center, New Orleans, LA 70112; and [#]Tulane Center for Stem Cell Research and Regenerative Medicine, Tulane University Health Sciences Center, New Orleans, LA 70112

[1]R.-Y.C. and Y.-M.F. contributed equally to this work.

Received for publication March 28, 2014. Accepted for publication February 9, 2015.

This work was supported by National Natural Science Foundation of China Grant 81171512 (to Y.-M. F.) and by Affiliated Hospital of Guangdong Medical College Matching Fund 1100/B010002 (to R.-Y.C.). Z.Y. was partially supported by National Institute of General Medical Sciences Grant P20GM103518 and National Cancer Institute Grant R01CA174714 of the National Institutes of Health, Department of Defense Grants W81XWH-14-1-0050, W81XWH-14-1-0149, and W81XWH-14-1-0458, the Developmental Fund of Tulane Cancer Center, and by Louisiana Cancer Research Consortium funds. The content of this article is solely the responsibility of the authors and does not necessarily represent the official views of the National Institutes of Health or Department of Defense.

Address correspondence and reprint requests to Dr. Zongbing You or Dr. Yi-Ming Fan, Department of Structural and Cellular Biology, Tulane University School of Medicine, 1430 Tulane Avenue, Mailbox 8649, New Orleans, LA 70112 (Z.Y.) or Department of Dermatology, Affiliated Hospital of Guangdong Medical College, Zhanjiang, Guangdong 524001, China (Y.-M.F.). E-mail addresses: zyou@tulane.edu (Z.Y.) or ymfan1963@163.com (Y.-M.F.)

The online version of this article contains supplemental material.

Abbreviations used in this article: ChIP, chromatin immunoprecipitation; Ct, cycle threshold; E2, 17β-estradiol; ER, estrogen receptor; ERE, estrogen response element; HDAC, histone deacetylase; MAA, methoxyacetic acid; qPCR, quantitative PCR; qRT-PCR, real-time quantitative RT-PCR; REA, repressor of estrogen receptor activity; RORα, retinoid acid receptor–related orphan receptor α; RORγT, thymus-specific isoform of retinoid acid receptor–related orphan receptor C; siRNA, small interfering RNA; Treg, regulatory T cell.

Copyright © 2015 by The American Association of Immunologists, Inc. 0022-1767/15/$25.00



Downloaded from http://www.jimmunol.org/ at Tulane University Medical Center on April 23, 2015

IL-17–deficient mice are susceptible to bacterial infections (20–23) and oral candidiasis caused by the commensal fungus *Candida albicans* (24, 25). In humans, autosomal recessive deficiency in *IL-17RA* and autosomal-dominant deficiency of *IL-17F* lead to chronic mucocutaneous candidiasis disease, characterized by infections of the skin, nails, and oral and genital mucosae with *C. albicans* (26). IL-17 can recruit neutrophils and monocytes (27–30). IL-17 acts on neutrophils to enhance production of reactive oxygen species, which mediate killing of fungi (31). On the one hand, candida mannan of *C. albicans* may induce host IL-17 production to trigger antifungal activity (32–34). On the other hand, candidal 5-hydroxytryptophan metabolites inhibit host IL-17 production (35). When a balance is achieved, commensalism between *C. albicans* and the host is established. However, in many physiologic and pathologic conditions, the balance is interrupted, resulting in candidiasis.

In premenopausal women, serum estradiol level is at a high peak around ovulation, which slightly decreases after ovulation, but elevates to a low peak at the midluteal phase, and then returns to the basal level during menses (36). Coincidentally, colonization of *C. albicans* generally rises in the second half of the menstrual cycle when serum estradiol level is elevated, which is accompanied with exacerbated symptoms in patients with vaginal candidiasis (37). Therefore, we hypothesized that there might be a link between vaginal candidiasis and estradiol level. One clue for this link came from a recent report that estradiol deficiency increased Th17 cell population and serum IL-17 levels in ovariectomized mice, which could be prevented by administration of exogenous estradiol (38). The purified $CD4^+$ T cells expressed higher mRNA levels of *Rorγt*, *Rorα*, and *Stat3* in the ovariectomized mice, compared with the sham control mice. In contrast, *Foxp3* mRNA levels were lower in ovariectomized mice than in sham mice. Administration of exogenous estradiol to ovariectomized mice decreased *Rorγt* expression but increased *Foxp3* expression in $CD4^+$ T cells (38). These findings suggest that estradiol inhibits Th17 differentiation through downregulation of transcription factors, particularly RORγT. Another study further found that estrogen receptor (ER)α signaling in T cells inhibited Th1 and Th17 differentiation, as conditional knockout of *ERα* in T cells abolished estradiol-mediated experimental autoimmune encephalomyelitis protection (39). However, the mechanisms of how estradiol regulates *RORγT* expression are not known. In the present study, we report that estradiol acts on ERα to recruit repressor of ER activity (REA); binding of the ERα/REA complex to the estrogen response elements (EREs) of the *RORγT* promoter region suppresses *RORγT* expression, thus inhibiting Th17 differentiation.

## Materials and Methods

### *Animals*

Animal protocol was approved by the Animal Care and Use Committee of Tulane University, which was in compliance with the U.S. Department of Health and Human Services *Guide for the Care and Use of Laboratory Animals*. Six- to 8-wk-old mice of C57BL/6J or 129S4/SvJae*BALB/c genetic background were used. Our preliminary experiments found that the results were similar using either male or female mice of either genetic background, and thus this study was conducted with the pooled splenocytes from both male and female mice of the two genetic backgrounds.

### *Reagents*

17β-Estradiol (Tocris Bioscience) was dissolved as 50 mmol/l stock solutions in ethanol. Histone deacetylase (HDAC) inhibitor MS-275 ($C_{21}H_{20}N_4O_3$, Chemical Abstracts Service no. 209783-80-2, Sigma-Aldrich) was dissolved as 2.66 mmol/l stock solutions in DMSO. Cytokines (mouse IL-6, IL-23, and TGF-β1) and Abs (anti-mouse CD3ε, CD28, IL-4, and IFN-γ) for Th17 polarization of mouse naive T cells ($CD4^+CD62L^+$) were purchased from BioLegend. A mouse $CD4^+CD62L^+$ T cell isolation kit II, MidiMACS separator, and columns were purchased from Miltenyi Biotec.

### *Isolation of naive T cells from mouse splenocytes*

Lymphocyte suspension was prepared from fresh mouse spleens by gently grinding the spleens between two glass slides. The lymphocyte suspension was filtered through 70-μm cell strainers (BD Biosciences) to make a single-lymphocyte suspension. This lymphocyte suspension was further filtered through 30-μm pre-separation filters (Miltenyi Biotec). Then, $CD4^+CD62L^+$ naive T cells were isolated using a mouse $CD4^+CD62L^+$ T cell isolation kit II and MidiMACS separator, following the manufacturer's instructions. The collected cells were stained with anti–CD4-FITC and anti–CD62L-allophycocyanin Abs (Miltenyi Biotec) and analyzed with flow cytometry, which showed that the isolated lymphocytes were ≥92% positive for both CD4 and CD62L that were considered as naive T cells (40).

### *Th17 polarization*

Cell culture dishes (60 × 15 mm in size) were first coated with anti-mouse CD3ε (2 μg/ml) at 37°C for 2 h. After removing the Ab solution, the dishes were gently washed twice with PBS. Naive T cells at $2 \times 10^6$/ml were plated in the coated dishes in RPMI 1640 medium (phenol red–free, Invitrogen) containing 2 mM glutamine and 10% FBS (charcoal/dextran treated, catalog no. SH30068.03, HyClone Laboratories) in the presence of Th17 polarization medium consisting of anti-mouse CD28 (5 μg/ml), IL-6 (50 ng/ml), TGF-β1 (1 ng/ml), IL-23 (5 ng/ml), anti-mouse IL-4 (10 μg/ml), and anti-mouse IFN-γ (10 μg/ml). Where indicated, the cells were simultaneously treated without or with 1 nmol/l 17β-estradiol (E2), or with MS-275 at doses of 2.66, 26.6, and 266 nmol/l, or with methoxyacetic acid (MAA, an HDAC inhibitor; Sigma-Aldrich) at 2 mmol/l. Three days after the treatment, the cells were harvested for analysis.

### *Real-time quantitative RT-PCR*

Total RNA was isolated according to the instructions of an RNeasy Mini Kit (Qiagen) with on-membrane DNase I digestion to avoid genomic DNA contamination. cDNA was made from total RNA using an iScript cDNA synthesis kit (Bio-Rad Laboratories). The PCR primer sequences are shown in Table I. Real-time quantitative RT-PCR (qRT-PCR) was performed in triplicates with an iQ5 iCycler and iQ SYBR Green Supermix (Bio-Rad Laboratories) following the recommended protocols. Results were normalized to *Gapdh* levels using the formula Δcycle threshold (Ct) = Ct of target gene − Ct of *Gapdh*. The mRNA level of the control group (without Th17 polarization) was used as the baseline; therefore, ΔΔCt was calculated using the formula ΔΔCt = ΔCt of target gene − ΔCt of the baseline. The fold change of mRNA level was calculated as fold = $2^{-\Delta\Delta Ct}$.

### *Flow cytometry analysis*

The differentiated splenocytes were fixed with fixation buffer and stained with a mouse Th17/Treg phenotyping kit (BD Pharmingen) containing Abs against mouse CD4 conjugated with PerCP-Cy5.5, mouse IL-17A conjugated with PE, and mouse Foxp3 conjugated with Alexa Fluor 647. The staining procedures were performed according to the manufacturer's instructions. Approximately 10,000 cells were analyzed using BD FACSCanto II flow cytometry (BD Biosciences). The control cells were stained with isotype Abs conjugated with fluorophores and served as the control staining group to set up the gating. The Th17 population was defined as $CD4^+IL\text{-}17A^+$ and the Treg population was defined as $CD4^+Foxp3^+$.

### *Western blot analysis*

Proteins were extracted from the treated cells in RIPA lysis buffer (50 mM sodium fluoride, 0.5% Igepal CA-630 [Nonidet P-40], 10 mM sodium phosphate, 150 mM sodium chloride, 25 mM Tris [pH 8.0], 1 mM PMSF, 2 mM EDTA, 1.2 mM sodium vanadate) supplemented with protease inhibitor mixture (Sigma-Aldrich). An equal amount of proteins was subjected to 10% SDS-PAGE and transferred to polyvinylidene difluoride membranes. The membranes were blocked with 5% BSA in TBST buffer (25 mM Tris-HCl, 125 mM NaCl, 0.1% Tween 20) for 2 h and probed with the indicated primary Abs overnight and then IRDye 800CW– or IRDye 680–conjugated secondary Abs (LI-COR Biosciences) for 1 h. The results were visualized by using an Odyssey infrared imager (LI-COR Biosciences). For loading control, the membranes were stripped and probed for GAPDH. The Abs used are as follows: anti-RORγT (1:250 dilution, catalog no. 14-6988, eBioscience), anti-REA (1:500 dilution, catalog no. 07-234, Millipore), anti-STAT3 (1:1000 dilution, catalog no. 9139, Cell Signaling Technology), and anti-GAPDH (1:10,000 dilution, catalog no. MAB374, Millipore).

Downloaded from http://www.jimmunol.org/ at Tulane University Medical Center on April 23, 2015

### *Coimmunoprecipitation*

Mouse splenocytes were isolated by density gradient centrifugation with Ficoll-Paque Premium (GE Healthcare Life Sciences) following the manufacturer's instructions. The splenocytes were treated with or without 1 nmol/l E2 in RPMI 1640 medium for 45 min. Protein was extracted from the treated cells with RIPA buffer and divided into 500-μl aliquots (each containing ~500 μg protein). One microgram of the following Abs was added to the protein aliquots: chromatin immunoprecipitation (ChIP)–validated anti-ERα (catalog no. 17-603, Millipore), anti-REA, anti-HDAC1 (catalog no. 3601-100, BioVision), anti-HDAC2 (catalog no. 3602-100, BioVision), and normal rabbit IgG (catalog no. SC-2027, Santa Cruz Biotechnology) as negative control. After 1 h incubation at 4˚C, 20 μl 50% protein G agarose bead slurry was added for overnight incubation at 4˚C. The beads were washed three times with PBS and boiled in 20 μl SDS protein loading buffer. Then, the protein supernatants were subjected to 10% SDS-PAGE and analyzed as described in Western blot analysis.

### *ChIP*

Mouse splenocytes were treated with or without 1 nmol/l E2 in RPMI 1640 medium for 45 min. A ChIP assay was performed using an EZ-Magna ChIP G chromatin immunoprecipitation kit (catalog no. 17-409, Millipore) following the manufacturer's instructions. Briefly, the cells were cross-linked with 1% formaldehyde. After stopping the cross-linking reaction with 10× glycine solution, the cells were lysed and the lysates were sonicated to shear DNAs into 200- to 1000-bp fragments. Fifty microliters chromatin extract of each sample was added to 450 μl dilution buffer. Five microliters of the mixture was aliquoted as "input" and the rest was added with 1 μg Ab and 20 μl protein G magnetic beads for overnight incubation with rotation at 4˚C. The protein G magnetic beads were washed four times on the Magna GrIP rack (Millipore). Then, the beads were digested with proteinase K in 100 μl ChIP elution buffer at 62˚C for 2 h. Finally, DNA was purified for 32 cycles of PCR analysis and the products were run on 2% agarose gel electrophoresis and stained with ethidium bromide. Alternatively, quantitative PCR (qPCR) was performed using the purified DNA. Results were normalized to DNA inputs using the formula ΔCt (cycle threshold) = Ct of DNA from immunoprecipitate (IP) − Ct of DNA input. The ΔCt of IgG IP was used as the baseline; therefore, ΔΔCt was calculated using the formula ΔΔCt = ΔCt of anti-ERα IP − ΔCt of IgG IP. The fold change of ChIP results was calculated as fold = $2^{-\Delta\Delta Ct}$. The PCR and qPCR primer sequences are shown in Table I.

### *Small interfering RNA transfection*

Predesigned SMARTpool Accell mouse Phb2 small interfering RNA (siRNA, catalog no. E-040938-00-0020, product of GE Healthcare/Dharmacon, Lafayette, CO; purchased from Thermo Scientific) was used to target *Rea* (also named prohibitin 2, *Phb2*). An Accell nontargeting siRNA pool (catalog no. D-001910-10-20, product of GE Healthcare/Dharmacon; purchased from Thermo Scientific; contained four siRNAs that were designed with no homology to known human, mouse, or rat genes) was used as negative control. One μmol/l targeting or nontargeting siRNA was added to naive T cells for a 3-d incubation using Accell siRNA delivery media (Thermo Scientific) following the manufacturer's instructions. Then, the transfected cells were used in Th17 polarization as described above, followed by qRT-PCR and Western blot analysis.

### *Analysis of human specimens*

This human subject study was approved by the Institutional Review Board of the Affiliated Hospital of Guangdong Medical College. The procedures to obtain human specimens were in accordance with the *Ethical Principles for Medical Research Involving Human Subjects* as formulated in the World Medical Association Declaration of Helsinki (revised in 2008). Twenty-one healthy female volunteers (age 29–39 y) were recruited during their routine physical examination at the Affiliated Hospital of Guangdong Medical College. Informed consent was signed by each volunteer. The inclusion criteria were: 1) married; 2) with regular menstruation; 3) with normal vulva, vagina, and uterus on physical examination; and 4) with normal vaginal discharge under microscopic examination. The exclusion criteria were: 1) pregnant; 2) autoimmune diseases; 3) use of steroid hormones; 4) vaginal sexual intercourse, use of vaginal cream or vaginal suppositories, or vaginal lavage within 1 wk; 5) diabetes mellitus; 6) abnormal liver or renal function; or 7) systemic or local inflammatory diseases. Two millliliters vaginal lavage and 4 ml venous blood were collected from each volunteer. For vaginal lavage, 2 ml saline was used to rinse the vagina three times and finally collected at the posterior vaginal fornix. The vaginal lavage from six women was used to count the number of epithelial and

Table I. Nucleotide sequences of each PCR primer pair

| Species | Gene | Primer | Nucleotide Sequence (5′ to 3′) |
|---|---|---|---|
| Mouse | | | |
| qRT-PCR | | | |
| | *Il17a* | Sense | CAGGGAGAGCTTCATCTGTGT |
| | | Antisense | GCTGAGCTTTGAGGGATGAT |
| | *Il17f* | Sense | CCCAGGAAGACATACTTAGAAGAAA |
| | | Antisense | CAACAGTAGCAAAGACTTGACCA |
| | *Rorc* (*Rorγt*) | Sense | GCTGAGGAAGTGGGAAAGTC |
| | | Antisense | GAAAGCAGGAGCAATGGAAGT |
| | *Rora* | Sense | TCACCTCTCTGCTTGTTCTG |
| | | Antisense | GCTTCTTCCCCTACTGTTCCTT |
| | *Stat3* | Sense | AGGAATCGGCTATATTGCTGGT |
| | | Antisense | CACCTTGGATTGAGAGTCAAGAC |
| | *Foxp3* | Sense | GCAAGAGCTCTTGTCCATTGA |
| | | Antisense | CACCAGGAAAGACAGCAACC |
| | *Gapdh* | Sense | TGCACCACCAACTGCTTAG |
| | | Antisense | GGATGCAGGGATGATGTTC |
| ChIP PCR | | | |
| | *Rorγt primer 1* | Sense | ATCCCTCCAGTGGATCTGA |
| | | Antisense | GCCTTTGGAAACAAGACTGC |
| | *Rorγt primer 2* | Sense | GTGCATACCCTCAGCACCTT |
| | | Antisense | CTGTGGCTAGTGCACAGGAG |
| ChIP qPCR | | | |
| | *Rorγt primer 1* | Sense | GAGCTGAATCATTCCCAACA |
| | | Antisense | GCCTTTGGAAACAAGACTGC |
| | *Rorγt primer 2* | Sense | GGTTGCCCACCAATCTGT |
| | | Antisense | AGCTCAGGGAGGAGGGAT |
| Human | | | |
| qRT-PCR | | | |
| | *RORγT* | Sense | GTAACGCGGCCTACTCCTG |
| | | Antisense | GTCTTGACCACTGGTTCCTGT |
| | *REA* | Sense | AGGGTAAGAAATGAGCCTAGTCACC |
| | | Antisense | GGTAGGGCTGTGCTGGACC |
| | *GAPDH* | Sense | TGCACCACCAACTGCTTAGC |
| | | Antisense | GGCATGGACTGTGGTCATGAG |

Downloaded from http://www.jimmunol.org/ at Tulane University Medical Center on April 23, 2015

inflammatory cells after standard Giemsa stain, using a hematometer. The vaginal lavage from 15 women was centrifuged and the cell pellet was used for qRT-PCR analysis of *RORγT* and *REA* mRNA levels. The case with the lowest levels was used as the baseline, and the relative mRNA levels of other cases were calculated as described above. The PCR primer sequences are shown in Table I. Serum levels of estradiol were measured in the clinical laboratory using the routine chemiluminescent assay (Access estradiol reagent, catalog no. 33540, Beckman Coulter).

### *Statistical analysis*

All bar graphs are presented as mean ± SEM of three independent experiments ($n = 3$). One-way ANOVA was used to analyze the quantitative data. Pearson's correlation analysis was used to evaluate the correlations between the serum estradiol levels and vaginal *RORγT* or *REA* mRNA levels in human specimens. A $p$ value $<0.05$ was considered statistically significant.

## Results

### *Estradiol inhibits Th17 differentiation through downregulation of* Rorγt *expression*

Using a well-established protocol of Th17 differentiation (2–4) and qRT-PCR analysis (see primers in Table I), we found that naive T cells were induced to express *Il17a* and *Il17f* mRNAs, starting from 24 h with a peak at 72 h after induction with the Th17 polarization medium (Fig. 1A, 1B). Expression of both *Il17a* and *Il17f* was almost completely inhibited by addition of 1 nmol/l E2, a physiological concentration of E2 (41) (Fig. 1A, 1B). The key transcription factors *Rorγt* and *Rorα* mRNAs were induced by the Th17 polarization medium, starting from 24 h with a peak at 48 h (Fig. 1C, 1D). Addition of 1 nmol/l E2 to the Th17 polarization medium significantly downregulated *Rorγt* and *Rorα* mRNA levels (Fig. 1C, 1D, $p < 0.05$). In contrast, induction of *Stat3* mRNA expression by the Th17 polarization medium was not affected by addition of 1 nmol/l E2 (Fig. 1E). *Foxp3* mRNA expression was transiently induced by the Th17 polarization medium at 48 h, which was slightly enhanced by addition of 1 nmol/l E2 (Fig. 1F). We checked the protein expression of the transcription factors. We found that RORγT protein level was dramatically decreased by E2, whereas STAT3 protein level was not obviously affected by E2 (Fig. 1G). Furthermore, Th17 polarization increased Th17 cells to 8.5% of the assessed population, compared with 1.1% in the control treatment group, whereas E2 treatment group only had 3.2% Th17 cells (Fig. 2A–D). Alternatively, Th17 polarization slightly increased Tregs to 1.6%, compared with 0.5% in the control treatment group; however, E2 treatment further increased Tregs to 8.6% (Fig. 2E–H). These findings are consistent with the previous studies showing that estradiol binds to ERα and inhibits Th17 differentiation (38, 39).

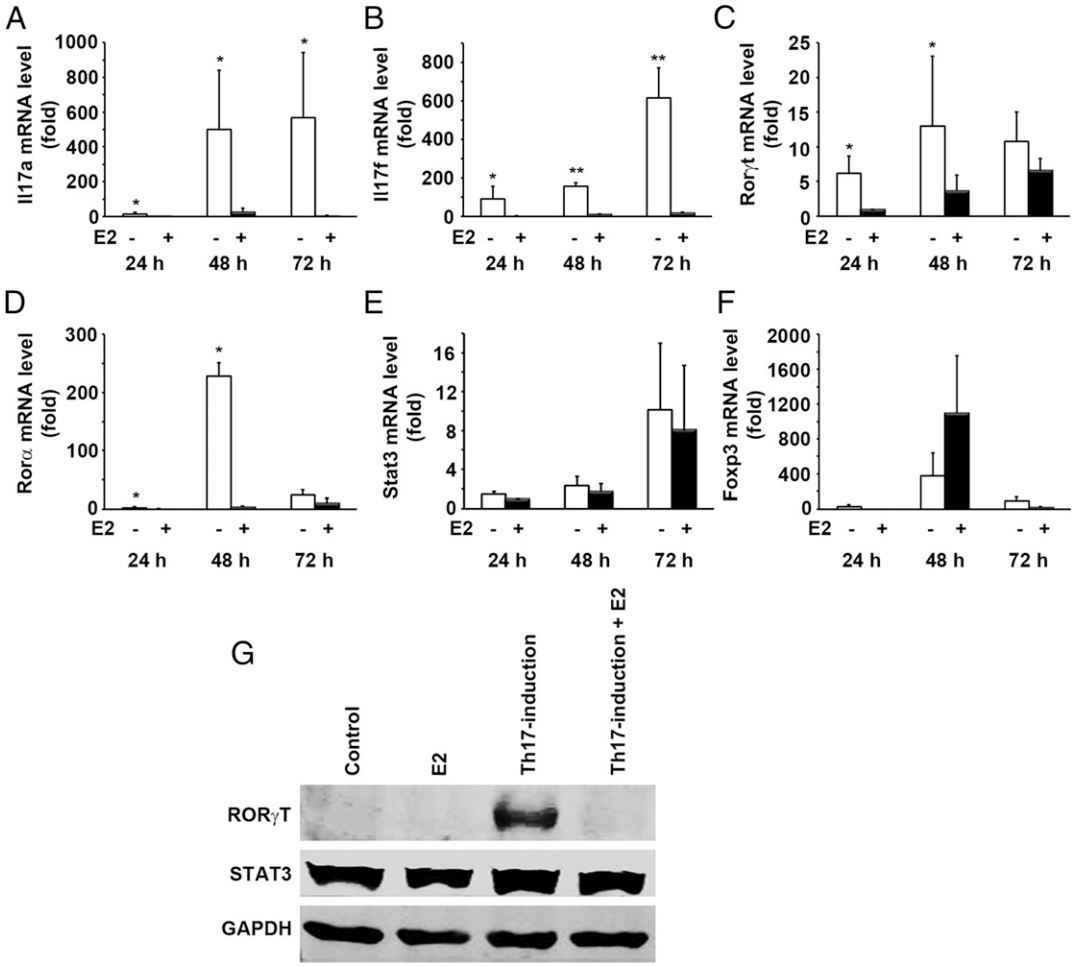



**FIGURE 1.** Estradiol inhibits Th17 differentiation through downregulation of *Rorγt* expression. $CD4^+CD62L^+$ naive T cells from mouse spleens were cultured in 2 μg/ml anti-CD3ε–coated dishes with 5 μg/ml anti-CD28, 50 ng/ml IL-6, 1 ng/ml TGF-β1, 5 ng/ml IL-23, 10 μg/ml anti–IL-4, and 10 μg/ml anti–IFN-γ, with or without 1 nmol/l E2. After 24, 48, and 72 h of differentiation, mRNA levels were measured by qRT-PCR. Data are means ± SEM ($n = 3$) of three independent experiments, with triplicates in each experimental group. $^*p < 0.05$, $^{**}p < 0.01$ compared with the corresponding E2-treated groups as determined by ANOVA. (**A**–**F**) mRNA levels of *Il17a*, *Il17f*, *Rorγt*, *Rorα*, *Stat3*, and *Foxp3*. (**G**) Protein level was analyzed by Western blot analysis, as shown in representative blots from one of three independent experiments. The membranes were probed for GAPDH as a loading control.

Downloaded from http://www.jimmunol.org/ at Tulane University Medical Center on April 23, 2015

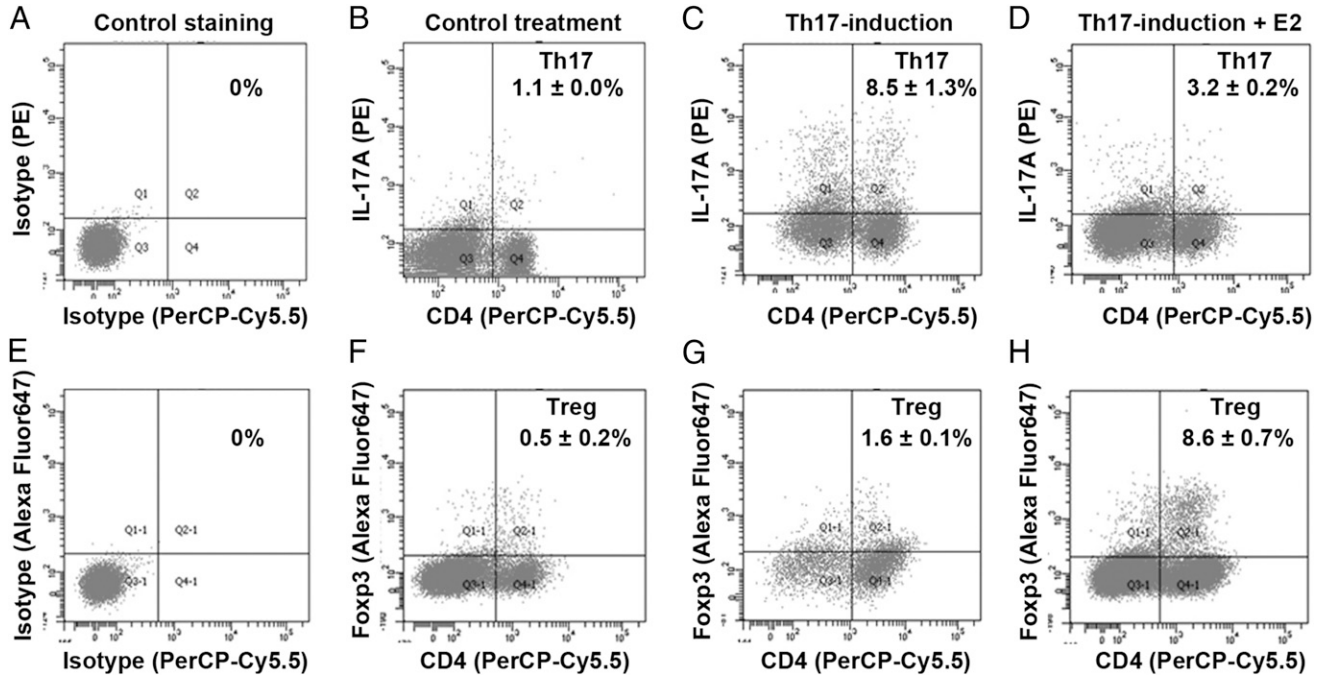



**FIGURE 2.** Estradiol reduces Th17 cells but increases Tregs. $CD4^+CD62L^+$ naive T cells from mouse spleens were cultured in 2 μg/ml anti-CD3ε–coated dishes with 5 μg/ml anti-CD28, 50 ng/ml IL-6, 1 ng/ml TGF-β1, 5 ng/ml IL-23, 10 μg/ml anti–IL-4, and 10 μg/ml anti–IFN-γ, with or without 1 nmol/l E2. After 3 d of differentiation, the cells were double stained for $CD4^+IL\text{-}17A^+$ Th17 and $CD4^+Foxp3^+$ Tregs using flow cytometry analysis. (**A**–**H**) Representative dot plots of two sets of independent flow cytometry analyses.

### *Mouse* Rorγt *gene promoter region contains three ERE half-sites*

Estradiol acts through ERα and ERβ. Because ERα has been shown to be responsible for inhibition of Th17 differentiation (39), our study focused on ERα. ERα is known to bind to the ERE sites of the promoter regions of the ERα target genes. The essential ERE is a 13-bp inverted repeat with the consensus sequence 5′-GGTCAnnnTGACC-3′ (42). Under certain conditions (such as when accompanied with another cofactor), ERα may also bind to the sequence with half of the 13-bp, so-called ERE half-site (43). We used the Transcription Element Search System (University of Pennsylvania) and analyzed a 2-kb (−1994 to +151) promoter region of mouse *Rorγt* gene (NC_00069.6). We found that there were three ERE half-sites located at 799 (named ERE1), 1618 (named ERE2), and 1653 bp (named ERE3) upstream to the *Rorγt* transcription start site (Supplemental Fig. 1). We designed two PCR primer sets to perform ChIP assays to determine whether ERα indeed binds to the ERE half-sites. Because ERE2 and ERE3 are only 31 bp apart and it is difficult to separate them in ChIP assays, they were covered by one PCR primer pair (Supplemental Fig. 1). We found that anti-ERα Ab did not pull down ERE1 in the absence of E2, but pulled down ERE1 in the presence of E2 (Fig. 3A, 3C). Similarly, anti-ERα Ab did not pull down ERE2/3 in the absence of E2, but pulled down ERE2/3 in the presence of E2 (Fig. 3B, 3D).

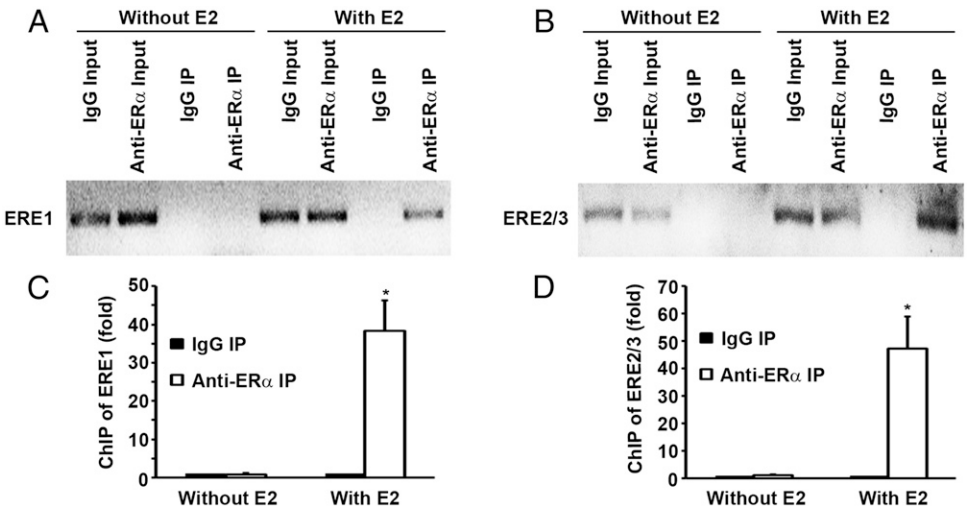



**FIGURE 3.** ERα binds to the three ERE half-sites (ERE1, ERE2, and ERE3) of mouse *Rorγt* gene promoter region. (**A** and **B**) Results of ChIP assays performed on mouse splenocytes treated with or without 1 nmol/l E2 for 45 min. Chromatin was immunoprecipitated (IP) with normal rabbit IgG or anti-ERα; PCR products were visualized on agarose gel stained with ethidium bromide. One representative of three independent experiments is shown. (**C** and **D**) Results of ChIP assays were measured by qPCR. Data are means ± SEM ($n = 3$) of three independent experiments. *$p < 0.01$ compared with the corresponding IgG IP groups as determined by ANOVA.

Downloaded from http://www.jimmunol.org/ at Tulane University Medical Center on April 23, 2015

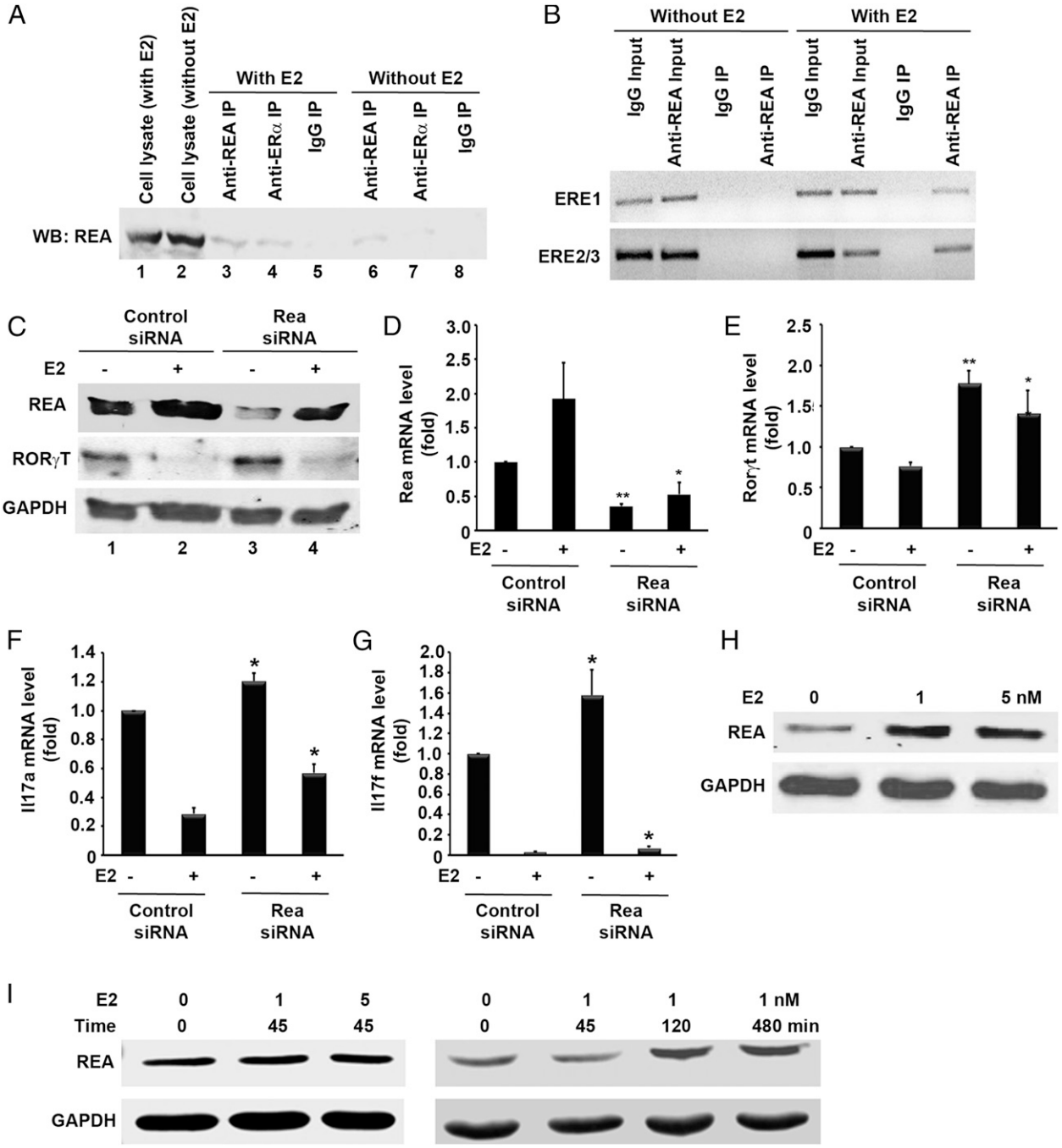



**FIGURE 4.** Estradiol activates ERα to recruit REA to inhibit *Rorγt* expression. (**A**) Results of coimmunoprecipitation assays performed on mouse splenocytes treated with or without 1 nmol/l E2 for 45 min. Protein was immunoprecipitated (IP) with normal rabbit IgG, anti-ERα, or anti-REA and analyzed by Western blot (WB) analysis. One representative of three independent experiments is shown. (**B**) Results of ChIP assays performed on mouse splenocytes treated with or without 1 nmol/l E2 for 45 min. One representative of three independent experiments is shown. (**C**–**G**) Mouse naive T cells were transfected with 1 μmol/l control or *Rea* siRNA for 3 d, followed by Th17 polarization for 3 d with or without 1 nmol/l E2. Protein level was analyzed by Western blot analysis, as shown in representative blots from one of three independent experiments (C); mRNA levels were measured by qRT-PCR (D–G), shown as mean ± SEM ($n = 3$) of three independent experiments, with triplicates in each experimental group. $*p < 0.05$, $**p < 0.01$ compared with the corresponding control siRNA-treated groups as determined by ANOVA. (**H** and **I**) Mouse splenocytes were treated with 0, 1, and 5 nmol/l E2 for 24 h (H) or 45, 120, or 480 min (I). Protein level was analyzed by Western blot analysis and one representative of three independent experiments is shown.

*ERα recruits REA to inhibit* Rorγt *expression*

Because we found that E2 inhibited *Rorγt* expression, we examined protein expression of several known corepressors of ERα in mouse splenocytes, including REA, nuclear receptor corepressor, silencing mediator of retinoid and thyroid hormone receptors, metastasis-associated 1, HDAC1, and HDAC2 (44). We found that only REA, HDAC1, and HDAC2 proteins were readily detectable in mouse splenocytes using Western blot analysis. Using coimmunoprecipitation assays, we found that anti-ERα Ab did not pull down REA in the absence of E2 (Fig. 4A, *lane 7*). In contrast, anti-ERα Ab pulled down REA in the presence of E2 (Fig. 4A, *lane 4*). Using ChIP assays, we found that anti-REA Ab did not pull down either ERE1 or ERE2/3 in the absence of E2, whereas it pulled down both ERE1 and ERE2/3 in the presence of E2 (Fig. 4B). To

Downloaded from http://www.jimmunol.org/ at Tulane University Medical Center on April 23, 2015

determine whether REA regulates *Rorγt* expression, we used a prevalidated commercial *Rea* siRNA to knock down REA protein expression in the absence of E2 (Fig. 4C, compare *lanes 1* and *3*) and in the presence of E2 (Fig. 4C, compare *lanes 2* and *4*). We found that a decrease of REA levels was accompanied with an increase of RORγT protein levels (Fig. 4C, compare *lanes 1* versus *3* and *lanes 2* versus *4*). We found that *Rea* siRNA decreased *Rea* mRNA levels in the absence and presence of E2 (Fig. 4D), which was accompanied with an increase in *Rorγt* mRNA levels (Fig. 4E). Subsequently, we found that *Il17a* and *Il17f* mRNA levels were also increased by *Rea* siRNA in both the absence and presence of E2, compared with the corresponding control siRNA groups (Fig. 4F, 4G). Because we observed that estradiol treatment increased *Rea* mRNA and protein levels in the presence of the control and *Rea* siRNAs (Fig. 4C, 4D), we examined the effects of estradiol on mouse splenocytes in the absence of any siRNAs to rule out any effects caused by the siRNAs. We found that REA protein expression was increased by E2 at 1 and 5 nmol/l after 24 h treatment (Fig. 4H). However, the levels of REA protein were not affected by E2 treatment at doses of either 1 or 5 nmol/l for 45 min; instead, REA expression was increased after 2 h treatment with 1 nmol/l E2 (Fig. 4I).

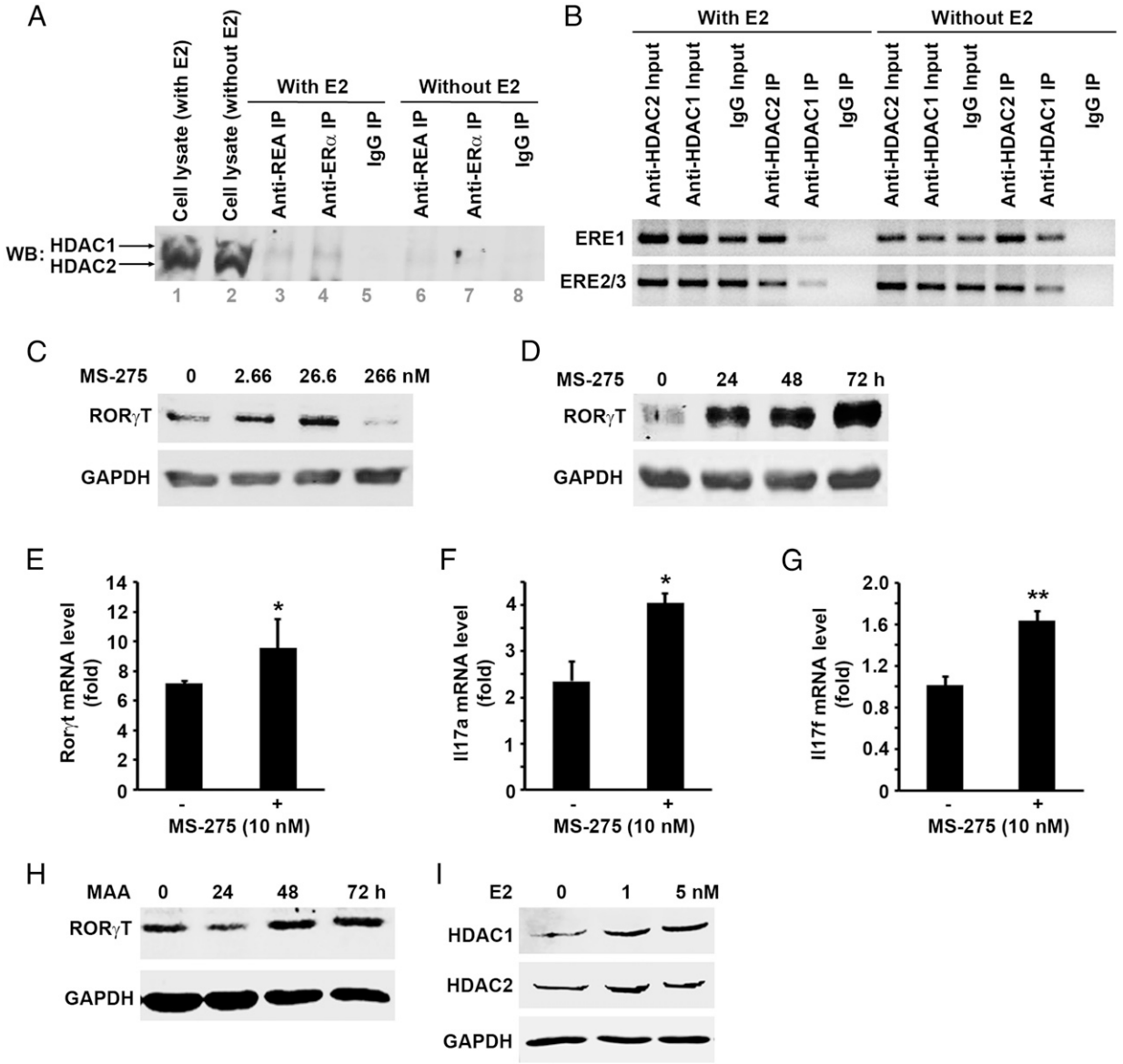



**FIGURE 5.** HDAC1 and HDAC2 constitutively bind to the EREs of *Rorγt* promoter region and inhibit *Rorγt* expression. (**A**) Results of coimmunoprecipitation assays performed on mouse splenocytes treated with or without 1 nmol/l E2 for 45 min. Protein was immunoprecipitated (IP) with normal rabbit IgG, anti-ERα, or anti-REA and analyzed by Western blot (WB) analysis. One representative of three independent experiments is shown. (**B**) Results of ChIP assays performed on mouse splenocytes treated with or without 1 nmol/l E2 for 45 min. One representative of three independent experiments is shown. (**C**) Mouse naive T cells were cultured in Th17 polarization medium in the presence of 0, 2.66, 26.6, and 266 nmol/l MS-275 for 24 h. Protein level was analyzed by Western blot analysis, and one of three independent experiments is shown. (**D**) Mouse naive T cells were cultured in Th17 polarization medium in the presence of 10 nmol/l MS-275 for 0, 24, 48, and 72 h. Protein level was analyzed by Western blot analysis and one of three independent experiments is shown. (**E**–**G**) Mouse naive T cells were cultured in Th17 polarization medium with or without 10 nmol/l MS-275 for 72 h. The mRNA levels were measured by qRT-PCR, shown as mean ± SEM ($n = 3$) of three independent experiments, with triplicates in each experimental group. $*p < 0.05$, $**p < 0.01$ as determined by ANOVA, compared with the corresponding groups without MS-275 treatment. (**H** and **I**) Mouse splenocytes were treated with 2 mM MAA for 0, 24, 48, and 72 h (H), or with 0, 1, and 5 nmol/l E2 for 24 h (I). Protein level was analyzed by Western blot analysis and one of three independent experiments is shown.

Downloaded from http://www.jimmunol.org/ at Tulane University Medical Center on April 23, 2015

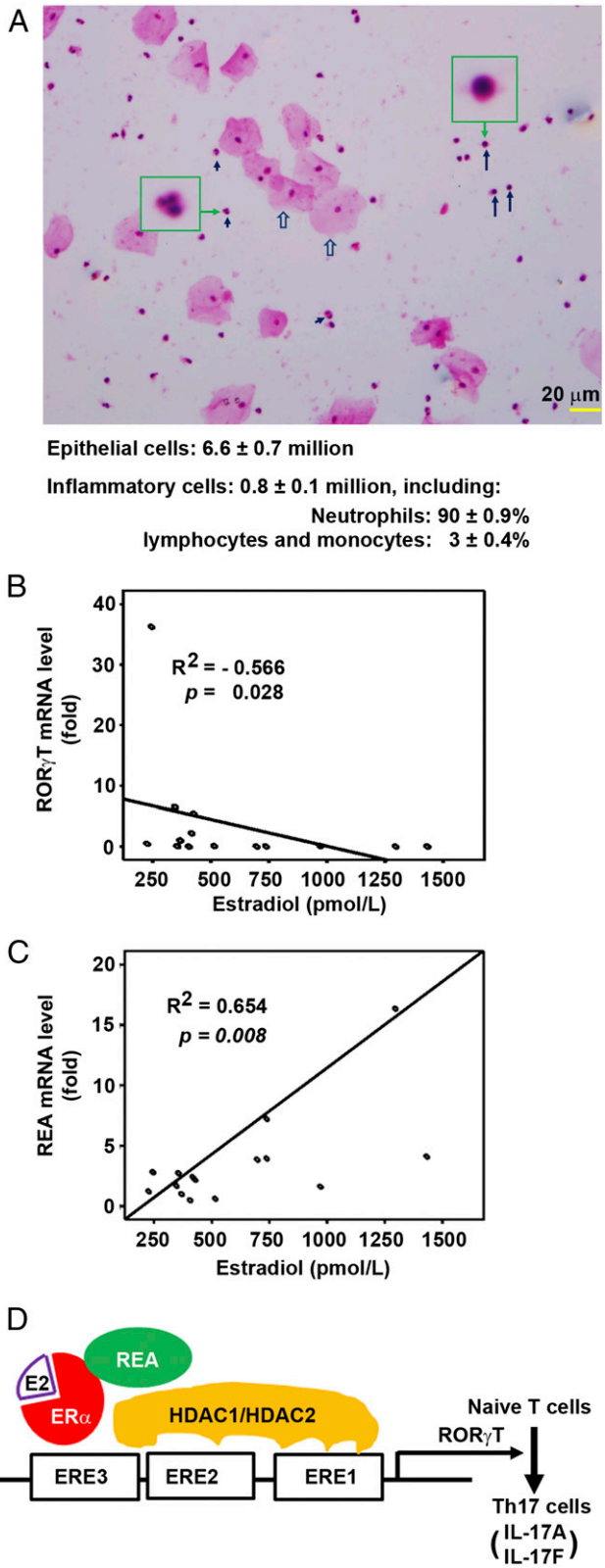



**FIGURE 6.** Human serum estradiol levels are correlated with *REA* and *RORγT* mRNA levels in the vaginal lavage. (**A**) Vaginal lavage from six healthy women was examined for the number of epithelial cells (open arrows) and inflammatory cells including neutrophils with segmented or banded nuclei (arrowheads) and lymphocytes/monocytes (arrows). The cells were stained with Giemsa stain. Original magnification ×250; the cells in the green boxes were enlarged 8-fold to show the morphology of the indicated cells. (**B** and **C**) Fifteen healthy women were examined for their serum E2 levels using routine chemiluminescent assays and *RORγT* and *REA* mRNA levels in the vaginal lavage using qRT-PCR. Scatter plots show the correlations between serum E2 levels and *RORγT* (or *REA*) mRNA levels using Pearson's correlation analysis. (**D**). Proposed model of how E2 inhibits Th17 differentiation. E2-induced ERα/REA complex binds to the EREs of the *RORγT* promoter region and suppresses *RORγT* transcription, resulting in decreased RORγT protein level and inhibition of Th17 differentiation and expression of IL-17A and IL-17F. HDAC1 and HDAC2 constitutively bind to the *RORγT* promoter region and inhibit *RORγT* transcription, independent of E2/ERα.

### *HDAC1 and HDAC2 constitutively bind to the EREs of* Rorγt *promoter region and inhibit* Rorγt *expression*

HDAC1 and HDAC2 have been shown to interact with REA in transcriptional repression (45). Using coimmunoprecipitation assays, we found that in the absence of E2, neither anti-REA or anti-ERα Abs pulled down HDAC1 or HDAC2 (Fig. 5A, *lanes 6* and *7*). In the presence of E2, both anti-REA and anti-ERα Abs pulled down a faint band corresponding to HDAC1 (Fig. 5A, *lanes 3* and *4*). Using ChIP assays, we found that both anti-HDAC1 and anti-HDAC2 Abs pulled down ERE1 and ERE2/3 in the absence and presence of E2 (Fig. 5B). We then tested whether HDAC inhibitor MS-275 (46) could affect RORγT protein expression in mouse splenocytes. We found that MS-275 increased RORγT protein expression at 2.66 and 26.6 nmol/l, whereas it decreased RORγT protein expression at 266 nmol/l after 24 h treatment (Fig. 5C). A low dose (10 nmol/l) of MS-275 increased RORγT protein expression furthermore after 48 and 72 h treatment (Fig. 5D). MS-275 also significantly increased *Rorγt* mRNA levels (Fig. 5E, $p < 0.05$). Additionally, MS-275 significantly increased *Il17a* and *Il17f* mRNA levels (Fig. 5F, 5G, $p < 0.05$ or 0.01, respectively). MAA is an HDAC inhibitor that inhibits HDAC1, HDAC2, and HDAC3 (47, 48). RORγT protein expression was also increased by treatment with 2 mM MAA after 48 and 72 h treatment (Fig. 5H). Additionally, E2 also slightly increased expression of HDAC1 and HDAC2 proteins after 24 h treatment (Fig. 5I).

### *Human serum estradiol levels are correlated with* REA *and* RORγT *mRNA levels in the vaginal lavage*

To determine whether the effects of estradiol on Th17 differentiation in the culture dishes are relevant to human physiologic conditions, we collected vaginal lavage from 21 healthy women. In each vaginal lavage of six healthy women, there were 6.6 ± 0.7 (mean ± SEM, $n = 6$) million epithelial cells and 0.8 ± 0.1 million inflammatory cells (Fig. 6A). Among the inflammatory cells, 90 ± 0.9% of them were neutrophils and 3 ± 0.4% of them were lymphocytes and monocytes (Fig. 6A). We measured the serum estradiol levels and *RORγT* and *REA* mRNA levels in the vaginal lavage in 15 healthy women. We found that the serum estradiol levels were inversely correlated with *RORγT* mRNA levels (Fig. 6B, $p < 0.05$). In contrast, the serum estradiol levels were positively correlated with *REA* mRNA levels (Fig. 6C, $p < 0.01$).

## Discussion

Although estradiol has been shown to inhibit *RORγT* expression in an ERα-dependent manner (38, 39), little is known about how E2/ERα act to inhibit *RORγT* expression. In this study, we demonstrate that E2 inhibits *RORγT* expression through recruitment of ERα/REA complex to the three ERE half-sites on the *RORγT* promoter region. ERα only binds to ERE1 and ERE2/3 in the presence of E2 (Fig. 3A, 3B). ERα only forms a complex with REA in the presence of E2 (Fig. 4A), and REA only binds to ERE1 and ERE2/3 in the presence of E2 (Fig. 4B). These results suggest that the E2-induced ERα/REA complex binds to the EREs

Downloaded from http://www.jimmunol.org/ at Tulane University Medical Center on April 23, 2015

of the *RORγT* promoter region and suppresses *RORγT* transcription, resulting in decreased RORγT protein level and inhibition of Th17 differentiation as evidenced by reduced numbers of Th17 cells (Fig. 2C, 2D) and decreased expression of IL-17A and IL-17F (summarized in Fig. 6D). REA selectively represses the transcriptional activity of the ER, but not other steroid and nonsteroid nuclear receptors (49–52). ERα–REA interaction is required for E2-mediated repression of B cell translocation gene 2 (53). We found that E2 upregulates *Rea* mRNA and protein expression (Fig. 4C, 4D, 4H, 4I). Knockdown of *Rea* expression by *Rea* siRNA can increase *Rorγt* expression and subsequently increase *Il17a* and *Il17f* expression. However, because E2 upregulates *Rea* expression, *Rea* siRNA is less effective in reducing REA levels in the presence of E2, compared with in the absence of E2 (Fig. 4C, 4E). Nevertheless, to our knowledge, this is the first study showing that E2 upregulates REA expression, in addition to inducing ERα/REA complex formation. Of note, in the control siRNA group, E2 treatment dramatically increased *Rea* and decreased *Il17* expression, but less so in reducing *Rorγt* mRNA expression (Fig. 4E), although RORγT protein level was dramatically decreased (Fig. 4C, *lanes 1* versus *2*). We are not sure about what caused the difference between *Rorγt* mRNA and protein levels.

Alternatively, we found that HDAC1 and HDAC2 bind to ERE1 and ERE2/3 in the presence and absence of E2 (Fig. 5B), which suggests that HDAC1 and HDAC2 constitutively bind to the RORγT promoter region, independent of estradiol. However, we did observe that at least HDAC1 forms a weak interaction with ERα and REA in the presence of E2 (Fig. 5A, *lanes 3* and *4*). A previous report showed that REA interacts with HDAC1 and HDAC2 in a ligand-independent manner using GST fusion proteins (45). We cannot rule out the possibility that E2 is required to translocate ERα/REA to the proximity of HDAC1/2 in the nucleus, thereby they may form a corepressor complex in inhibition of *RORγT* expression (Fig. 6D). This becomes more likely as expression of HDAC1 and HDAC2 is increased by E2 after 24 h treatment (Fig. 5I). We found that an HDAC inhibitor MS-275 upregulates *RORγT* expression in a dose- and time-dependent manner (Fig. 5C, 5D). MS-275 selectively inhibits HDAC1, HDAC2, and HDAC3 (46, 54, 55). We found that at low doses (up to 26.6 nmol/l), MS-275 upregulates RORγT expression; however, at a high dose (266 nmol/l), MS-275 decreases RORγT expression (Fig. 5C), which may be due to MS-275's toxicities, as we observed obvious lymphocyte death at this high dose (data not shown). MAA also inhibits HDAC1, HDAC2, and HDAC3 (47, 48), and thus MAA also increased RORγT expression, although at a later time point compared with MS-275 (Fig. 5H versus Fig. 5D). Our findings suggest that HDAC inhibitors may promote Th17 differentiation through enhancing RORγT expression, which warrants further investigation to test whether this is valid in animals.

The clinical relevance of this study is demonstrated by the correlation of serum estradiol levels and *RORγT* and *REA* mRNA levels in the vaginal lavage of 15 healthy women. We found that high levels of serum estradiol are correlated with low levels of *RORγT* mRNA but with high levels of *REA* mRNA (Fig. 6B, 6C). These human in vivo data are consistent with our in vitro results showing that E2 upregulates *Rea* to inhibit *Rorγt* transcription. Whether this mechanism is true in humans requires further investigation in human clinical trials using pharmacologic manipulations of E2 levels and/or REA levels. Serum E2 levels in premenopausal women fluctuate with elevated levels in the second half of the regular menstrual cycle (36). Given the findings from this study, it is reasonably to speculate that the elevated E2 levels inhibit *RORγT* transcription, thus inhibiting Th17 differentiation. Indeed, we observed that serum E2 levels were inversely correlated with vaginal *IL-17A* mRNA levels ($R^2 = -0.377$), but the correlation was not statistically significant ($p = 0.166$), which may be due to the small number of specimens. Other investigators have shown that across the menstrual cycle in healthy reproductive-aged women, serum E2 levels are inversely associated with the urine levels of IL-1β, IL-6, and IL-8 (56), which are IL-17 downstream target genes. Clinically, the symptoms of vaginal candidiasis are often exacerbated in the second half of the menstrual cycle when colonization of *C. albicans* rises (37), which may be related to the decrease in Th17 differentiation and reduction of IL-17 levels, as IL-17 has important antifungal activities (32–34). Whereas our present study focused on estradiol, other studies have demonstrated that progesterone may also inhibit Th17 differentiation (57, 58). Given that progesterone levels are also elevated in the second half of the menstrual cycle (36), we think that the elevated serum levels of E2 and progesterone may be responsible for the inhibition of Th17 differentiation and exacerbation of vaginal candidiasis in the second half of the menstrual cycle.

In conclusion, the present study demonstrates that estradiol acts on ERα to recruit REA and form ERα/REA complex; binding of the ERα/REA complex to the EREs of the *RORγT* promoter region suppresses *RORγT* expression, thus inhibiting Th17 differentiation. Additionally, HDAC1 and HDAC2 constitutively bind to the *RORγT* promoter region and suppress *RORγT* expression.

## Acknowledgments

This study used the core facilities of Tulane Cancer Center and Louisiana Cancer Research Consortium. We thank the clinical laboratory of the Affiliated Hospital of Guangdong Medical College for assistance in counting the cells in the vaginal lavage.

## Disclosures

The authors have no financial conflicts of interest.

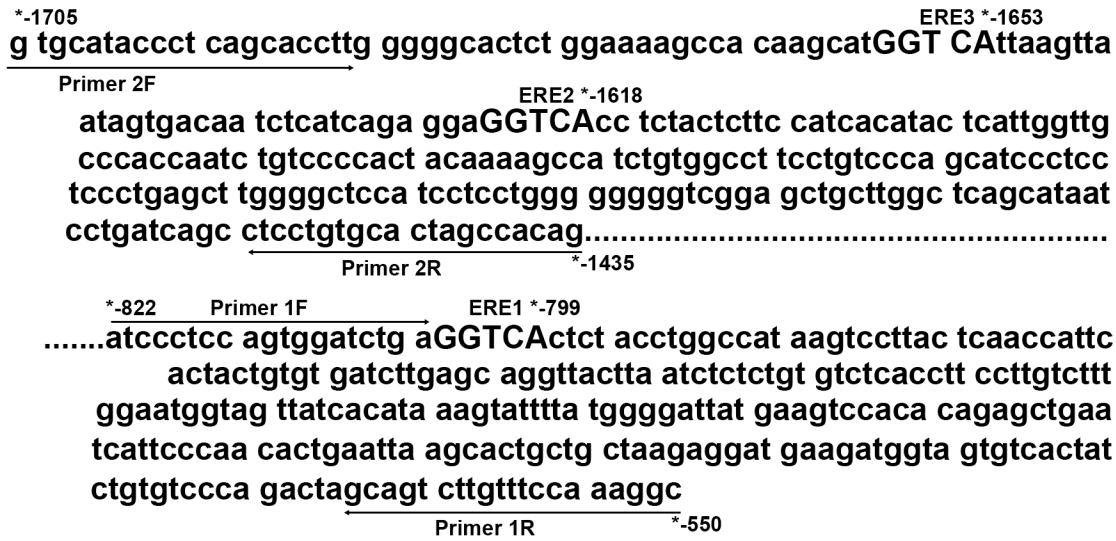
## References

1. Ouyang, W., J. K. Kolls, and Y. Zheng. 2008. The biological functions of T helper 17 cell effector cytokines in inflammation. *Immunity* 28: 454–467.
2. Veldhoen, M., R. J. Hocking, C. J. Atkins, R. M. Locksley, and B. Stockinger. 2006. TGFβ in the context of an inflammatory cytokine milieu supports de novo differentiation of IL-17-producing T cells. *Immunity* 24: 179–189.
3. Mangan, P. R., L. E. Harrington, D. B. O'Quinn, W. S. Helms, D. C. Bullard, C. O. Elson, R. D. Hatton, S. M. Wahl, T. R. Schoeb, and C. T. Weaver. 2006. Transforming growth factor-β induces development of the $T_H17$ lineage. *Nature* 441: 231–234.
4. Bettelli, E., Y. Carrier, W. Gao, T. Korn, T. B. Strom, M. Oukka, H. L. Weiner, and V. K. Kuchroo. 2006. Reciprocal developmental pathways for the generation of pathogenic effector $T_H17$ and regulatory T cells. *Nature* 441: 235–238.
5. Acosta-Rodriguez, E. V., G. Napolitani, A. Lanzavecchia, and F. Sallusto. 2007. Interleukins 1β and 6 but not transforming growth factor-β are essential for the differentiation of interleukin 17-producing human T helper cells. *Nat. Immunol.* 8: 942–949.
6. Chung, Y., S. H. Chang, G. J. Martinez, X. O. Yang, R. Nurieva, H. S. Kang, L. Ma, S. S. Watowich, A. M. Jetten, Q. Tian, and C. Dong. 2009. Critical regulation of early Th17 cell differentiation by interleukin-1 signaling. *Immunity* 30: 576–587.
7. Korn, T., E. Bettelli, W. Gao, A. Awasthi, A. Jäger, T. B. Strom, M. Oukka, and V. K. Kuchroo. 2007. IL-21 initiates an alternative pathway to induce proinflammatory $T_H17$ cells. *Nature* 448: 484–487.
8. Aggarwal, S., N. Ghilardi, M. H. Xie, F. J. de Sauvage, and A. L. Gurney. 2003. Interleukin-23 promotes a distinct CD4 T cell activation state characterized by the production of interleukin-17. *J. Biol. Chem.* 278: 1910–1914.
9. Park, H., Z. Li, X. O. Yang, S. H. Chang, R. Nurieva, Y. H. Wang, Y. Wang, L. Hood, Z. Zhu, Q. Tian, and C. Dong. 2005. A distinct lineage of CD4 T cells regulates tissue inflammation by producing interleukin 17. *Nat. Immunol.* 6: 1133–1141.
10. Harrington, L. E., R. D. Hatton, P. R. Mangan, H. Turner, T. L. Murphy, K. M. Murphy, and C. T. Weaver. 2005. Interleukin 17-producing $CD4^+$ effector T cells develop via a lineage distinct from the T helper type 1 and 2 lineages. *Nat. Immunol.* 6: 1123–1132.
11. Villey, I., R. de Chasseval, and J. P. de Villartay. 1999. RORγT, a thymus-specific isoform of the orphan nuclear receptor RORγ/TOR, is up-regulated by signaling through the pre-T cell receptor and binds to the TEA promoter. *Eur. J. Immunol.* 29: 4072–4080.

Downloaded from http://www.jimmunol.org/ at Tulane University Medical Center on April 23, 2015

12. Ivanov, I. I., B. S. McKenzie, L. Zhou, C. E. Tadokoro, A. Lepelley, J. J. Lafaille, D. J. Cua, and D. R. Littman. 2006. The orphan nuclear receptor RORγt directs the differentiation program of proinflammatory IL-17$^+$ T helper cells. *Cell* 126: 1121–1133.
13. Yang, X. O., B. P. Pappu, R. Nurieva, A. Akimzhanov, H. S. Kang, Y. Chung, L. Ma, B. Shah, A. D. Panopoulos, K. S. Schluns, et al. 2008. T helper 17 lineage differentiation is programmed by orphan nuclear receptors RORα and RORγ. *Immunity* 28: 29–39.
14. Yang, X. O., A. D. Panopoulos, R. Nurieva, S. H. Chang, D. Wang, S. S. Watowich, and C. Dong. 2007. STAT3 regulates cytokine-mediated generation of inflammatory helper T cells. *J. Biol. Chem.* 282: 9358–9363.
15. Harris, T. J., J. F. Grosso, H. R. Yen, H. Xin, M. Kortylewski, E. Albesiano, E. L. Hipkiss, D. Getnet, M. V. Goldberg, C. H. Maris, et al. 2007. Cutting edge: an in vivo requirement for STAT3 signaling in $T_H17$ development and $T_H17$-dependent autoimmunity. *J. Immunol.* 179: 4313–4317.
16. Ciofani, M., A. Madar, C. Galan, M. Sellars, K. Mace, F. Pauli, A. Agarwal, W. Huang, C. N. Parkurst, M. Muratet, et al. 2012. A validated regulatory network for Th17 cell specification. *Cell* 151: 289–303.
17. Kurebayashi, Y., S. Nagai, A. Ikejiri, and S. Koyasu. 2013. Recent advances in understanding the molecular mechanisms of the development and function of Th17 cells. *Genes Cells* 18: 247–265.
18. Onishi, R. M., and S. L. Gaffen. 2010. Interleukin-17 and its target genes: mechanisms of interleukin-17 function in disease. *Immunology* 129: 311–321.
19. Song, X., and Y. Qian. 2013. IL-17 family cytokines mediated signaling in the pathogenesis of inflammatory diseases. *Cell. Signal.* 25: 2335–2347.
20. Ishigame, H., S. Kakuta, T. Nagai, M. Kadoki, A. Nambu, Y. Komiyama, N. Fujikado, Y. Tanahashi, A. Akitsu, H. Kotaki, et al. 2009. Differential roles of interleukin-17A and -17F in host defense against mucoepithelial bacterial infection and allergic responses. *Immunity* 30: 108–119.
21. Aujla, S. J., Y. R. Chan, M. Zheng, M. Fei, D. J. Askew, D. A. Pociask, T. A. Reinhart, F. McAllister, J. Edeal, K. Gaus, et al. 2008. IL-22 mediates mucosal host defense against Gram-negative bacterial pneumonia. *Nat. Med.* 14: 275–281.
22. Kreindler, J. L., C. A. Bertrand, R. J. Lee, T. Karasic, S. Aujla, J. M. Pilewski, R. A. Frizzell, and J. K. Kolls. 2009. Interleukin-17A induces bicarbonate secretion in normal human bronchial epithelial cells. *Am. J. Physiol. Lung Cell. Mol. Physiol.* 296: L257–L266.
23. Nagata, T., L. McKinley, J. J. Peschon, J. F. Alcorn, S. J. Aujla, and J. K. Kolls. 2008. Requirement of IL-17RA in Con A induced hepatitis and negative regulation of IL-17 production in mouse T cells. *J. Immunol.* 181: 7473–7479.
24. Conti, H. R., F. Shen, N. Nayyar, E. Stocum, J. N. Sun, M. J. Lindemann, A. W. Ho, J. H. Hai, J. J. Yu, J. W. Jung, et al. 2009. Th17 cells and IL-17 receptor signaling are essential for mucosal host defense against oral candidiasis. *J. Exp. Med.* 206: 299–311.
25. Saijo, S., S. Ikeda, K. Yamabe, S. Kakuta, H. Ishigame, A. Akitsu, N. Fujikado, T. Kusaka, S. Kubo, S. H. Chung, et al. 2010. Dectin-2 recognition of α-mannans and induction of Th17 cell differentiation is essential for host defense against *Candida albicans*. *Immunity* 32: 681–691.
26. Puel, A., S. Cypowyj, J. Bustamante, J. F. Wright, L. Liu, H. K. Lim, M. Migaud, L. Israel, M. Chrabieh, M. Audry, et al. 2011. Chronic mucocutaneous candidiasis in humans with inborn errors of interleukin-17 immunity. *Science* 332: 65–68.
27. Hoshino, H., J. Lötvall, B. E. Skoogh, and A. Lindén. 1999. Neutrophil recruitment by interleukin-17 into rat airways in vivo. Role of tachykinins. *Am. J. Respir. Crit. Care Med.* 159: 1423–1428.
28. Liu, L., D. Ge, L. Ma, J. Mei, S. Liu, Q. Zhang, F. Ren, H. Liao, Q. Pu, T. Wang, and Z. You. 2012. Interleukin-17 and prostaglandin E2 are involved in formation of an M2 macrophage-dominant microenvironment in lung cancer. *J. Thorac. Oncol.* 7: 1091–1100.
29. Ye, P., F. H. Rodriguez, S. Kanaly, K. L. Stocking, J. Schurr, P. Schwarzenberger, P. Oliver, W. Huang, P. Zhang, J. Zhang, et al. 2001. Requirement of interleukin 17 receptor signaling for lung CXC chemokine and granulocyte colony-stimulating factor expression, neutrophil recruitment, and host defense. *J. Exp. Med.* 194: 519–527.
30. Laan, M., Z. H. Cui, H. Hoshino, J. Lötvall, M. Sjöstrand, D. C. Gruenert, B. E. Skoogh, and A. Lindén. 1999. Neutrophil recruitment by human IL-17 via C-X-C chemokine release in the airways. *J. Immunol.* 162: 2347–2352.
31. Taylor, P. R., S. Roy, S. M. Leal, Jr., Y. Sun, S. J. Howell, B. A. Cobb, X. Li, and E. Pearlman. 2014. Activation of neutrophils by autocrine IL-17A-IL-17RC interactions during fungal infection is regulated by IL-6, IL-23, RORγt and dectin-2. *Nat. Immunol.* 15: 143–151.
32. Robinson, M. J., F. Osorio, M. Rosas, R. P. Freitas, E. Schweighoffer, O. Gross, J. S. Verbeek, J. Ruland, V. Tybulewicz, G. D. Brown, et al. 2009. Dectin-2 is a Syk-coupled pattern recognition receptor crucial for Th17 responses to fungal infection. *J. Exp. Med.* 206: 2037–2051.
33. van de Veerdonk, F. L., R. J. Marijnissen, B. J. Kullberg, H. J. Koenen, S. C. Cheng, I. Joosten, W. B. van den Berg, D. L. Williams, J. W. van der Meer, L. A. Joosten, and M. G. Netea. 2009. The macrophage mannose receptor induces IL-17 in response to *Candida albicans*. *Cell Host Microbe* 5: 329–340.
34. LeibundGut-Landmann, S., O. Gross, M. J. Robinson, F. Osorio, E. C. Slack, S. V. Tsoni, E. Schweighoffer, V. Tybulewicz, G. D. Brown, J. Ruland, and C. Reis e Sousa. 2007. Syk- and CARD9-dependent coupling of innate immunity to the induction of T helper cells that produce interleukin 17. *Nat. Immunol.* 8: 630–638.
35. Cheng, S. C., F. van de Veerdonk, S. Smeekens, L. A. Joosten, J. W. van der Meer, B. J. Kullberg, and M. G. Netea. 2010. *Candida albicans* dampens host defense by downregulating IL-17 production. *J. Immunol.* 185: 2450–2457.
36. Ahrens, K. A., C. J. Vladutiu, S. L. Mumford, K. C. Schliep, N. J. Perkins, J. Wactawski-Wende, and E. F. Schisterman. 2014. The effect of physical activity across the menstrual cycle on reproductive function. *Ann. Epidemiol.* 24: 127–134.
37. Watson, C. J., D. Grando, S. M. Garland, S. Myers, C. K. Fairley, and M. Pirotta. 2012. Premenstrual vaginal colonization of *Candida* and symptoms of vaginitis. *J. Med. Microbiol.* 61: 1580–1583.
38. Tyagi, A. M., K. Srivastava, M. N. Mansoori, R. Trivedi, N. Chattopadhyay, and D. Singh. 2012. Estrogen deficiency induces the differentiation of IL-17 secreting Th17 cells: a new candidate in the pathogenesis of osteoporosis. *PLoS ONE* 7: e44552.
39. Lélu, K., S. Laffont, L. Delpy, P. E. Paulet, T. Périnat, S. A. Tschanz, L. Pelletier, B. Engelhardt, and J. C. Guéry. 2011. Estrogen receptor α signaling in T lymphocytes is required for estradiol-mediated inhibition of Th1 and Th17 cell differentiation and protection against experimental autoimmune encephalomyelitis. *J. Immunol.* 187: 2386–2393.
40. De Rosa, S. C., L. A. Herzenberg, L. A. Herzenberg, and M. Roederer. 2001. 11-Color, 13-parameter flow cytometry: identification of human naive T cells by phenotype, function, and T-cell receptor diversity. *Nat. Med.* 7: 245–248.
41. Teoh, H., S. W. Leung, and R. Y. Man. 1999. Short-term exposure to physiological levels of 17β-estradiol enhances endothelium-independent relaxation in porcine coronary artery. *Cardiovasc. Res.* 42: 224–231.
42. Driscoll, M. D., G. Sathya, M. Muyan, C. M. Klinge, R. Hilf, and R. A. Bambara. 1998. Sequence requirements for estrogen receptor binding to estrogen response elements. *J. Biol. Chem.* 273: 29321–29330.
43. Klinge, C. M. 2001. Estrogen receptor interaction with estrogen response elements. *Nucleic Acids Res.* 29: 2905–2919.
44. Mann, M., V. Cortez, and R. K. Vadlamudi. 2011. Epigenetics of estrogen receptor signaling: role in hormonal cancer progression and therapy. *Cancers (Basel)* 3: 1691–1707.
45. Kurtev, V., R. Margueron, K. Kroboth, E. Ogris, V. Cavailles, and C. Seiser. 2004. Transcriptional regulation by the repressor of estrogen receptor activity via recruitment of histone deacetylases. *J. Biol. Chem.* 279: 24834–24843.
46. Saito, A., T. Yamashita, Y. Mariko, Y. Nosaka, K. Tsuchiya, T. Ando, T. Suzuki, T. Tsuruo, and O. Nakanishi. 1999. A synthetic inhibitor of histone deacetylase, MS-27-275, with marked in vivo antitumor activity against human tumors. *Proc. Natl. Acad. Sci. USA* 96: 4592–4597.
47. Jansen, M. S., S. C. Nagel, P. J. Miranda, E. K. Lobenhofer, C. A. Afshari, and D. P. McDonnell. 2004. Short-chain fatty acids enhance nuclear receptor activity through mitogen-activated protein kinase activation and histone deacetylase inhibition. *Proc. Natl. Acad. Sci. USA* 101: 7199–7204.
48. Wade, M. G., A. Kawata, A. Williams, and C. Yauk. 2008. Methoxyacetic acid-induced spermatocyte death is associated with histone hyperacetylation in rats. *Biol. Reprod.* 78: 822–831.
49. Montano, M. M., K. Ekena, R. Delage-Mourroux, W. Chang, P. Martini, and B. S. Katzenellenbogen. 1999. An estrogen receptor-selective coregulator that potentiates the effectiveness of antiestrogens and represses the activity of estrogens. *Proc. Natl. Acad. Sci. USA* 96: 6947–6952.
50. Delage-Mourroux, R., P. G. Martini, I. Choi, D. M. Kraichely, J. Hoeksema, and B. S. Katzenellenbogen. 2000. Analysis of estrogen receptor interaction with a repressor of estrogen receptor activity (REA) and the regulation of estrogen receptor transcriptional activity by REA. *J. Biol. Chem.* 275: 35848–35856.
51. Park, S., Y. Zhao, S. Yoon, J. Xu, L. Liao, J. Lydon, F. DeMayo, B. W. O'Malley, and B. S. Katzenellenbogen. 2011. Repressor of estrogen receptor activity (REA) is essential for mammary gland morphogenesis and functional activities: studies in conditional knockout mice. *Endocrinology* 152: 4336–4349.
52. Park, S. E., J. Xu, A. Frolova, L. Liao, B. W. O'Malley, and B. S. Katzenellenbogen. 2005. Genetic deletion of the repressor of estrogen receptor activity (REA) enhances the response to estrogen in target tissues in vivo. *Mol. Cell. Biol.* 25: 1989–1999.
53. Karmakar, S., E. A. Foster, and C. L. Smith. 2009. Estradiol downregulation of the tumor suppressor gene BTG2 requires estrogen receptor-alpha and the REA corepressor. *Int. J. Cancer* 124: 1841–1851.
54. Cavasin, M. A., K. Demos-Davies, T. R. Horn, L. A. Walker, D. D. Lemon, N. Birdsey, M. C. Weiser-Evans, J. Harral, D. C. Irwin, A. Anwar, et al. 2012. Selective class I histone deacetylase inhibition suppresses hypoxia-induced cardiopulmonary remodeling through an antiproliferative mechanism. *Circ. Res.* 110: 739–748.
55. Dokmanovic, M., C. Clarke, and P. A. Marks. 2007. Histone deacetylase inhibitors: overview and perspectives. *Mol. Cancer Res.* 5: 981–989.
56. Whitcomb, B. W., S. L. Mumford, N. J. Perkins, J. Wactawski-Wende, E. R. Bertone-Johnson, K. E. Lynch, and E. F. Schisterman. 2014. Urinary cytokine and chemokine profiles across the menstrual cycle in healthy reproductive-aged women. *Fertil. Steril.* 101: 1383–1391.
57. Lee, J. H., B. Ulrich, J. Cho, J. Park, and C. H. Kim. 2011. Progesterone promotes differentiation of human cord blood fetal T cells into T regulatory cells but suppresses their differentiation into Th17 cells. *J. Immunol.* 187: 1778–1787.
58. Xu, L., B. Dong, H. Wang, Z. Zeng, W. Liu, N. Chen, J. Chen, J. Yang, D. Li, and Y. Duan. 2013. Progesterone suppresses Th17 cell responses, and enhances the development of regulatory T cells, through thymic stromal lymphopoietin-dependent mechanisms in experimental gonococcal genital tract infection. *Microbes Infect.* 15: 796–805.


Downloaded from http://www.jimmunol.org/ at Tulane University Medical Center on April 23, 2015




**Supplementary Figure 1.** Mouse Rorγt gene promoter region contains 3 ERE half-sites (ERE1, ERE2, and ERE3) identified in mouse Rorγt promoter region by the Transcription Element Search System (University of Pennsylvania) as shown in upper cases in the nucleotide sequence (reference#: NC_00069.6). The numbers indicate how many bp upstream to the Rorγt transcription start site. The ChIP PCR primer sequences are underlined.

Journal of Biological Methods | **2015** | Vol. 2(1) | e17
DOI: 10.14440/jbm.2015.63

REVIEW

# In vitro and in vivo model systems used in prostate cancer research

David Cunningham[1], Zongbing You[1,2,3,4,5*]

[1]Department of Structural & Cellular Biology, [2]Department of Orthopaedic Surgery, [3]Tulane Cancer Center and Louisiana Cancer Research Consortium, [4]Tulane Center for Stem Cell Research and Regenerative Medicine, [5]Tulane Center for Aging, Tulane University Health Sciences Center, New Orleans, LA, USA

*Corresponding author: Zongbing You, MD, PhD, Department of Structural & Cellular Biology, Tulane University School of Medicine, 1430 Tulane Ave Mailbox 8649, New Orleans, LA 70112, USA. Tel.: 504-988-0467; Fax: 504-988-1687; E-mail: zyou@tulane.edu.

Competing interests: The authors have declared that no competing interests exist.

Abbreviations used: AR, androgen receptor; ARBS, androgen receptor binding sites; ASIR, age standardized incidence rate; BPH, benign prostatic hyperplasia; CBP, Creb binding protein; EGF, epidermal growth factor; FGF, fibroblast growth factor; HA, hemagluttinin; HECD, E-cadherin; HPE, human prostatic epithelium; HPV, human papilloma virus; IVIS, in vivo imaging system; kD, kilodalton; LAPC, Los Angeles Prostate Cancer; LKB1, liver kinase B1; LPB, long probasin; mCRPC, metastatic castration-resistant prostate cancer; MMP, matrix metalloproteinase; mPIN, mouse prostatic intraepithelial neoplasia; NE, neuroendocrine; NSE, neuron specific enolase; PAP, prostatic acid phosphatase; PB/rPB, probasin; PCa, prostate cancer; PEG, polyethylene glycol; PIN, prostatic intraepithelial neoplasia; PhIP, 2-amino-1-methyl-6-phenylimidazo(4,5-b)pyridine; PSA, prostate specific antigen; PTEN, phosphatase and tensin homologue; Rb, retinoblastoma; ROS, reactive oxygen species; SRC, subrenal capsule; RGD, arginine-glycine-aspartate; STK11, serine/threonine kinase 11; SV40, simian virus 40; TMPRSS2-ERG, transmembrane protease, serine 2, ETS regulated gene; TGF-α, transforming growth fact α; TGF-β, transforming growth factor β; TRAMP, transgenic adenocarcinoma of the mouse prostate; WHO, World Health Organization; WT, wild type

Received April 27, 2015; Revision received May 18, 2015; Accepted May 18, 2015; Published June 4, 2015

**Abstract** New incidence of prostate cancer is a major public health issue in the Western world, and has been rising in other areas of the globe in recent years. In an effort to understanding the molecular pathogenesis of this disease, numerous cell models have been developed, arising mostly from patient biopsies. The introduction of the genetically engineered mouse in biomedical research has allowed the development of murine models that allow for the investigation of tumorigenic and metastatic processes. Current challenges to the field include lack of an animal model that faithfully recapitulates bone metastasis of prostate cancer.

**Keywords:** prostate cancer, cell lines, intratibial injection, mouse models, xenograft

## Introduction

The incidence of prostate cancer (PCa) is one of the most prevalent cancer diagnoses throughout the world, and is one of the most intensely studied problems in human disease. According to the American Cancer Society, in 2014 there were over 233,000 new cases of PCa diagnosed in the US, resulting in about 29,340 deaths [1]. As cancer is a disease of aging, prostate lesions occur infrequently before the age of 40, with the peak incidence occurring between the age of 70–74 [2]. According to the World Health Organization (WHO)'s International Agency for Research on Cancer, the cancer incidence on five continents indicates that the age standardized incidence rate (ASIR) of PCa among some Asian populations has increased from nearly three to over fifty fold in places such as Hong Kong and Shanghai [3].

The etiology of PCa has remained a puzzling issue. A strong correlation exists with age, with increased relative risk for individuals with a family history [4]. African-American men are at significantly higher incidence, with one recent study citing a 12% increase in the proportion of an African-American cohort with multiple positive biopsy cores compared to a White-American cohort [5]. Environmental risk factors, which have been quantified in adoption studies at 4.8%, include the consumption of long chain polyunsaturated fatty acids found in smoked or over-cooked fish, vitamin D deficiency in people with reduced tanning potential, and dietary factors such as intake of red meat [6-9]. Smoking may also put individuals at increased risk for PCa, and sexually transmitted diseases have been identified as a risk factor [10,11]. Inflammatory factors have been implicated in the development of PCa, such as bacterial toxins and exogenous carcinogens such as 2-amino-1-methyl-6-phenylimidazo(4,5-b)pyridine or PhIP [12,13].

There is a discussion in the field regarding the specificity of the prostate specific antigen (PSA) test as a useful prognostic indicator of potential metastatic castration resistant prostate cancer (mCRPC), with some saying that widespread epidemiological screening does not justify the modest decrease in cancer death [14-16]. In the new paradigm of "predict, prevent, and personalize" medicine, understanding the molecular phenotype and pathogenesis of disease will allow for more accurate and precise treatment of PCa

## In vitro model systems

By far the most useful *in vitro* model that we have of PCa is cell culture. The sheer number of cell lines that are available for study is expansive, due to the fact that PCa can arise from one of several cell sources in the prostate. In addition to the information contained in this review, a good cell line database is available from the British Columbia (BC) Cancer Agency [17]. A comprehensive and exhaustive two-part compendium of PCa cell lines is available from Sobel and Sadar [18,19]. All information is derived from the BC Cancer Agency Prostate Cancer Cell Line Database cited previously unless otherwise specified. A summary is available in **Table 1**.

### *DU-145*

Along with LNCaP and PC3 cells, DU-145 cells were once considered part of the triad that constituted the gold standard of PCa cell culture lines. DU-145 cells were first isolated from a brain metastatic prostate tumor in 1975 [20]. The isolation of this line represented an answer to the criticism of then existing cell lines MA 160 and EB 33, both of which represented cell isolated from admixtures of benign tumor or moderately differentiated adenocarcinoma. It is hormone independent and does not express androgen receptor (AR) mRNA/protein or PSA mRNA/protein. This observation has brought this cell line into disfavor among investigators. The vast majority of human prostate tumors express AR, so some would contend that this is a model that does not faithfully mimic human disease [21]. This is an important consideration, as the selection of this cell line for experimentation such as studies that seek to test the effect of hormone status would be futile on this model. In addition to absent AR, this line demonstrates a heterozygous P223L/V274F p53 expression pattern, changing its transcriptional program [22]. Phosphatase and tensin homolog (PTEN) expression is heterozygous [23]. This line contains marker chromosomes $M_1$, $M_2$, and $M_3$. Its karyotype ranges from 46 to 143 (modal of 64) with a metacentric Yq+ chromosome. This cell line's doubling time is established at 34 hours [24].

An important consideration in the selection of a PCa cell model is growth rate and behavior as a xenograft. DU-145 cells maintain phenotype and genotype when injected into mice and metastasize to a variety of organs, including spleen, lung, and liver [25,26]. Tumor growth in SCID mice has a 7-day latency with a biphasic growth rate of 5.5 for doubling in days 7–14 and 8.5 days for doubling after day 14 when placed without sponge material [27].

The response to growth factors is another important consideration to make when choosing a PCa cell line as growth factor independence via autocrine signaling has been defined as one of the hallmarks of cancer [28]. A substantial amount of work has been done on the effect of growth factors on this cell line. Of particular note is the increased expression of TGF-α and IGF-1 [29,30]. More information on the growth factors and growth factor receptor expression profile is available in **Table 1**.

Investigators have recently started to interrogate the role of energy metabolism in the role of PCa carcinogenesis. One of the main factors in energy metabolism is liver kinase B1 (LKB1, also referred to as serine/threonine kinase 11; STK11), an upstream kinase of Wnt/β-catenin and Hedgehog signaling pathway targets [31,32]. Recent work done on glucose deprivation and activation of AMP-activated protein kinase by vascular endothelial growth factor detected an absence of LKB1 in this cell line [33].

As a final note, one of the obvious goals of cancer treatment is to induce cancer cells into apoptosis and thus decreased tumor bulk. Pro- and anti-apoptotic proteins are delicately balanced in non-cancerous cells but can become deranged in cancer settings. An important consideration to make using DU-145 cells as an *in vitro* model system is the presence of the pro-apoptotic protein Bax. The expression of Bax in this cell line has been debatable. An older report by Shirahama et al. indicates the expression of Bax in this line [34], but the bulk of subsequent literature seems to indicate its absence [35-37]. It is recommended that Western blot analysis on this line's Bax expression be conducted prior to utilization as a research model.

### *PC3*

PC3 cells were isolated from a vertebral metastatic prostate tumor in 1979 in answer to the concern that few lines were available that were entirely composed of carcinoma cells [38]. This cell line is similar to DU-145 cells in that it is hormone insensitive and presents no AR or PSA mRNA/protein, bringing it into similarly marginal favor with some investigators. As a highly aneuploid line, its karyotype has a modal number of 58 with a doubling time of approximately 33 hours. Among the interesting observations made about this cell line is the expression of transferrin receptor and growth stimulation by treatment with bone marrow derived transferrin [39,40]. Autonomous growth can be attributed to high expression levels of TGF-α and EGF-R [41]. This has led some investigators to speculate that this is one factor that makes bone a hospitable metastatic site. It expresses aberrant p53 with a C deletion in codon 138 causing a nonsense codon at 169 (causing a loss of heterozygosity) and is PTEN deficient [42,43]. Little information is available on xenograft growth rates, but our experience with intratibial cancer cell inoculations suggests it is similar to DU-145 cells with latency of approximately one week and doubling times in the range of 4–5 days. Of important note to investigators working with PC3 cells is the recent observation that this line is more characteristic of neuroendocrine, or small cell, carcinoma rather than adenocarcinoma [44].

### *LNCaP*

As the lynchpin for numerous subsequent derivatives, LNCaP cells were first isolated from a human metastatic prostate adenocarcinoma found in a lymph node [45]. The original LNCaP cell line is androgen responsive with AR and PSA mRNA/protein expression. Of particular note, this cell line contains a T877A mutation in the AR coding sequence that gives it promiscuous binding affinity to a range of steroid compounds [46]. This slow growing cell line doubles every 60–72 hours (depending on serum concentration) and has a karyotype of 33 to 91 chromosomes (modal of 76–91). They are responsive to TGF-α, EGF and IGF-1, and express EGF/TGF-α-R, FGF-R, and IGF-1-R [47,48]. Of note is the expression of cytokeratins (CK) 8, 18, and 20, wild type (WT) p53 and PTEN inactivation [49-51]. Xenografting demonstrates a modest 50% success rate with a tumor doubling time of 86 hours when combined with a Matrigel™ formulation [18].

### *C4-2B*

These cells were isolated from a mouse vertebral metastasis in 1994 as a subline of LNCaP xenografts, a derivation of a previous cell line established by Wu et al [52]. The C4 line was generated using subcutaneous co-injection of LNCaP and human osteosarcoma MS cells. Mice were then castrated to drive the tumors into androgen independence, and subsequent tumor cells were cultured and termed C4. The C4 cells were then subcutaneously co-injected into a castrated mouse. Then, the tumor cells were cultured from the tumors formed and termed C4-2. These cells were then subcutaneously or orthotopically injected into castrated mice, with subsequent surveillance for metastasis. Several metastases were detected, with one metastasis spreading to the bone. These bone metastatic cancer cells were finally isolated and termed C4-2B [53]. The authors who initially isolated this line have noted that castrated mice have a higher incidence of bone metastasis than do intact mice. Karyotyping ranges from 61–90 chromosomes (modal of 83) in the C4 line with a doubling time of 48 hours for C4-2B specifically.

**Table 1. Common cell lines used in Prostate Cancer Research.**

| Name | Source | Metastasis in mice | Doubling time | PSA RNA | PSA protein | AR RNA | AR protein | Cytokeratin expression | Other markers | Karyotype | Reference |
|---|---|---|---|---|---|---|---|---|---|---|---|
| **Normal** | | | | | | | | | | | |
| pRNS-1-1 | radical prostatectomy | No | ~68 hours | No | No | Yes | Yes | 5, 8 | | 49–52, Monosomy 5, 16 | Lee, 1994 [84] |
| RWPE-1 | HPE cells from the peripheral zone | No | 120 hours | Yes | Yes | Yes | Yes | 8, 18 | | 45/51, Loss of 7q and 18 | Rhim, 1994 [75], Bello, 1997 [74] |
| BPH 1 | Epithelial cells from a transurethral specimen demonstrating BPH | No | ~35 hours | No | No | No | No | 8, 18 | Increased p53, PTEN, Bax, p21 | 71–79, modal of 76 | Hayward, 1994 [81] |
| PIN | | | | | | | | | | | |
| PIN Cells | Cultured from a human high grade PIN lesion | No (non-tumorigenic) | Not reported | Yes | Yes | Not reported | Not reported | 18, 34βE12 | IL10 receptor | Not reported | Stearns, 1999 [89] |
| **Hormone Naïve** | | | | | | | | | | | |
| RWPE-2 | v-Ki-ras transfection in RWPE-1 | Not metastatic; tumorigenic in mice | 58 hours | Yes | Yes | Yes | Yes | 8,18 | p53, Rb | Hyperdiploid | Bello, 1997 [74] |
| LNCaP | Lymph node | Yes; osteoblastic phenotype in bone metastasis | 28–60 hours | Yes | Yes | Yes | Yes | CK-8, 18, 20 | Vimentin, HECD 1, a-, b-, g-catenin, PAP, CBP | 33–91; highly aneuploid | Horoszewicz, 1980 [45] |
| LAPC-4 | Lymph node of androgen insensitive patient | Yes; osteolytic phenotype in bone metastasis | ~72 hours | Yes | Yes | Yes | Yes | 5, 8, and 18 | 2 p53 mutations (P72R and R175H) | 79–92, modal of 89 | Klein, 1997 [55] |
| LAPC-9 | Femoral metastasis in patient undergoing homone ablation therapy | Yes; osteoblastic phenotype in bone metastasis | Not reported | Yes | Yes | Yes | Yes | 5 | Ki-67 in the presence of androgens only | Not reported | Craft, 1999 [58] |
| VCaP | Vertebral metastasis | Yes; osteoblastic phenotype in bone metastasis | 120–144 hours | Yes | Yes | Yes | Yes | 8, 18 | PAP, Rb, p53, one copy of TMPRSS2-ERG gene fusion | Hypodiploid to hypertriploid | Korenchuk, 2001 [61] |
| MDA PCa 2a/2b | Two different areas of patient bone metastasis | Yes (both); osteoblastic phenotype in bone metastasis | 82–93 hours/42–73 hours | Yes | Yes | Yes | Yes | 5, 8, and 18 | WT p53, p21, Rb, and Bcl-2 | 49–94, modal of 63/44–92, modal of 47 | Navone, 1997 [70] |
| LuCaP | Lymph node (23.1, 23.8) and liver (23.12) metastasis in human patient | Yes; osteoblastic phenotype in bone metastasis | 11, 15, 21 days for 23.1, 23.8, 23.12 | Not reported | Yes | Not reported | Not reported | Not reported | 5-alpha reductase type 1 but not type 2 | 62–112 (modal of 78); adequate karyotype was difficult due to poor morphology | Ellis, 1996 [77] |

**Table 1 (continued). Common Cell Lines Used in Prostate Cancer Research.**

| Name | Source | Metastasis in mice | Doubling time | PSA RNA | PSA protein | AR RNA | AR protein | Cytokeratin expression | Other markers | Karyotype | Reference |
|---|---|---|---|---|---|---|---|---|---|---|---|
| **Castration Resistant** | | | | | | | | | | | |
| C4-2 | s.c. LNCaP tumor in nude mouse | Yes; osteoblastic phenotype in bone metastasis | ~48 hours | Yes | Yes | Yes | Yes | CK-8 | marker chromosome *m1* | 61–90, modal of 84 | Wu, 1994 [52] |
| C4-2B | Bone met LNCaP tumor in nude mouse | Yes; osteoblastic phenotype in bone metastasis | 48 hours | Yes | Yes | Yes | Yes | CK-8 | ABCG2 | 72–90, modal of 87, markers m1=i(7q), m2= der(11), t(11p+?) | Thalmann, 1994 [53] |
| 22Rv1 | CWR22R xenograft line | Yes; osteolytic phenotype in bone metastasis | 35–40 hours | Yes | Yes | Yes | Yes | 8, 18 | 45–56 kD cytoker-atins; AR splice variants | 50 | Sramkoski, 1999 [63] |
| ARCaP (aka MDA PCa 1) | Ascites aspirate from a patient with bone metastasis | Yes; osteolytic phenotype in bone metastasis | - | Yes | Yes | Yes | Yes | 8, 18 | EGF receptor, c-erb B2/neu, c-erb B3, bombesin, serotonin, NSE, c-met, neuro-physin, substance P, gelatinase A and stromelysin | near tetraploid | Zhau, 1996 [69] |
| PC-3 | Vertebral metas-tasis | Yes; osteolytic phenotype in bone metastasis | ~33 hours | No | No | No | No | 7, 8, 18, 19, HECD 1, | Transferrin receptor, TGF-α, EGF-R | aneuploid, modal of 58 | Kaighn, 1979 [38] |
| DU-145 | Brain metastasis | Yes; osteolytic phenotype in bone metastasis | ~34 hours | No | No | No | No | CK-8, -18 | TGF-α, IGF-1, EGF, bFGF IGF-I, TGF-β; EGF/ TGF-α-R, FGF-R, IGF-I-R, TGF-β-R | 46 - 143, modal of 64; M1, M2, M3, Yq+ | Stone, 1978 [20] |

They express AR and PSA mRNA/protein. These cells express low levels of p53 and are PTEN null [54]. This line consistently grows in either intact or castrated mice

***LAPC-4***

This cell line was introduced in 1997 and was the result of a series of subcutaneous xenografting experiments into SCID mice [55]. Explants from 6 of 8 Los Angeles prostate cancer (LAPC) patients were found to sustain growth very well in mice, doubling or tripling in volume. After several passages, several of the explants did not demonstrate detectable levels of human β-globin, and thus were deemed overrun by murine cells. This left only two explants, LAPC-3 and LAPC-4, as the sole survivors of the initial experiment. Of the two, LAPC-4 was the only cell line that retained its androgen dependence. Cytogenetics shows a range of 79–92 chromosomes (modal of 89) with loss of the Y chromosome. Doubling rate was calculated at around 72 hours. They are positive for AR/PSA mRNA/protein with P72R and R175H mutations in the p53 gene and express WT PTEN [56]. A mutation in the tumor protein 53 (TP53) gene causes an A175H mutation in p53. They can grow subcutaneously, orthotopically, or intratibially in mice [57]. Orthotopic inoculation tends to metastasize more frequently, while intratibial injection demonstrates an osteoblastic phenotype, mimicking frequent osteoblastic lesions found in humans

***LAPC 9***

These cells were first isolated from a femoral metastasis that formed in a patient undergoing androgen ablation therapy in 1999 [58]. Developed by the same group that isolated LAPC-4, it is a response to the need for an androgen sensitive counterpart. It is WT AR/PSA positive and will form tumors through subcutaneous injection in intact mice with as few as 10 cells. However, the investigators report that only a fraction of such injections will form tumors in castrated mice. A result of serial passaging in SCID mice, tumor-volume doubling time is approximately three weeks. These cells undergo growth arrest upon the removal of androgen but will retain sensitivity for up to 6 months post-removal. A very small subpopulation of cells was found to express cytokeratin 5 [59].

***VCaP***

These cells were first isolated in 2001, as the result of a vertebral metastatic lesion utilizing a procurement team designed to implement "warm" autopsies [60,61]. The cell line is positive for androgen sensitivity with wild-type AR mRNA/protein, and expresses PSA mRNA/protein, in addition to expressing prostatic acid phosphatase (PAP), retinoblastoma (Rb) and p53 (with an A248W mutation due to a mutation in TP53). Doubling time is 5 to 6 days and cytogenetics demonstrates a range of hypodiploid to hypertriploid genomes. PTEN remains intact in this cell line. These cells grow well in intact mice (doubling time of 10 days) as well as castrated mice (doubling time of 13 days) [18]. An important consideration to make in early PCa invasion is the role of the transmembrane protease, serine 2–ETS regulated gene (TMPRSS2-ERG) gene rearrangement. This translocation occurs when the 3' end of ERG (21q22.3), ETV1 (7p21.2), or ETV4 (17q21) is added to the 5' end of the androgen responsive TMPRSS2 gene, creating an androgen-responsive oncoprotein [62]. VCaP cell line is one of the few PCa cell lines to demonstrate at least one copy of this rearrangement.

***22Rv1***

22Rv1 is a cell line that is representative of prostate carcinoma introduced in 1999 [63]. This line was isolated from the xenograft CWR22R that was isolated from a patient with bone metastasis. 22Rv1 was developed by plating CWR22R on irradiated feeder cells, trypsinized, and isolated via CD44 staining. Two successive regrowths on feeder cells allowed for the isolation of this line. Doubling time ranges from 35–40 hours. Cytogenetic analysis reveals a hyperdiploid genome in early passages but will expand to a stable tetraploid state as passaging continues. It consistently demonstrates trisomy for chromosomes 7, 8, and 12. It is positive for AR mRNA/protein and PSA mRNA, but negative for PSA protein. It is responsive to EGF, but it is not inhibited by TGF-β. It expresses WT PTEN [64-66]. This model is of particular interest to investigators researching AR splice variants. Variants that activate in a ligand independent manner have been identified as one of the main players in hormone refractory tumor progression [67]. Two such variants have been identified as being expressed endogenously in 22Rv1, specifically a full length isoform with an exon 3 duplication and C terminal domain truncations with aberrant exon 2b expression [68].

***ARCaP***

ARCaP was first introduced by Zhau et al. in 1996 and is also referred to as MDA PCa 1 [69]. First isolated from the ascites fluid of a patient with metastatic disease, it is highly metastatic with hallmarks of adenocarcinoma expression patterns of low AR mRNA and PSA mRNA/protein, with additional markers suggesting selective neuroendocrine differentiation. It expresses a H847Y AR variant and a Q331R p53 variant. This line has a take (or engraftment) rate of 100% in intact or castrated nude mice. A surprising observation is that tumors grow three times faster in castrated mice than in intact mice. Treatment with steroid compounds *in vitro* inhibits growth as well. TP53 analysis reveals a loss of heterozygosity and an A196end mutation [18].

***MDA PCa 2a/2b***

These two cell lines were derived from a single patient with vertebral metastasis during late stage disease in 1997 [70]. These are one of the few cells lines that were isolated from an African-American patient. Coming from two different areas of the same lesion, they are both androgen sensitive and tumorigenic in mice, with the 2a form doubling in 82–93 hours and the 2b form doubling in 42–73 hours, depending on the passage number. Different growth rate indicates that these two lines are clones from different cells within the same lesion. The karyotypes are 49–92 (modal of 63) for 2a and 44–92 (modal of 47) for 2b. The 2a form has a higher incidence of chromosomal abnormalities with a tetraploid genome. The 2b form has unique genomic characteristics, demonstrating a near diploid karyotype during early passages but expands to near tetraploid at passage 36. This observable change indicates that these alterations are a product of *in vitro* passaging and not the result of a polyclonal population of cells derived from the patient sample. Both cell lines exhibit WT TP53, express AR mRNA/protein with 2 mutations in the ligand-binding domain of MDA PCa 2a (L701H and T877A), and express PSA mRNA/protein [71,72]. One dichotomizing factor between the 2a and 2b forms is the presence of Bax in only 2a. The take rate in mice is increased with the addition of Matrigel™. The 2b form grows faster than the 2a *in vivo*, although 2a is the only one of the two to form palpable intraprostatic tumors after 11 weeks. PTEN is intact [73]. When used in conjunction, this model is referred to as MDA

PCa 2 (two) a and 2b bone metastases model (TabBO).

***RWPE-2***

It is a genetically modified form of the human normal prostatic epithelium cell line RWPE-1 (discussed below). Ki-ras gene and human papilloma virus 18 (HPV) genome were introduced into the RWPE-1 line, making it tumorigenic [74,75]. It is positive for AR and PSA mRNA/protein, and is described as hormone sensitive but not hormone dependent. It will grow *in vitro* appreciably without androgens, but will increase proliferation in their presence. This line expresses cytokeratins 8 and 18 and has a 48–54 chromosome karyotype (modal of 51). A unique trait about this line is the nucleus stains very strongly for WT p53 and Rb. It responds very well to EGF treatment and is inhibited by TGF-β. An injection of one million cells subcutaneously will form undifferentiated tumors in nude mice with a latency of 3–4 weeks. Since it has been immortalized with HPV, it strongly expresses the viral protein E7. Of special consideration is the fact that HPV DNA is found in up to 90% of cervical, vulvar, penile, and perianal cancers [76]. This makes RWPE-2 an important model for studying the potential role of viral factors in the transformation of prostate epithelium into carcinomas.

***LuCaP***

Similar to MDA PCa 2a and 2b, LuCaP cells are the result of three successful xenografts from a single patient at autopsy. LuCaP 23.1 and 23.8 were isolated from lymph node metastases and 23.12 was isolated from a liver metastasis in response to the need for cell lines that faithfully model prostate carcinoma [77]. The patient was a 63 year old Caucasian and had undergone radiation, orchiectomy, and chemotherapy. The chromosome range is 62–112 (modal of 78). Retaining androgen sensitivity and responsiveness, these cells do not grow in culture but must be maintained in mouse hosts via serial transplantation [19]. Volume doubling time in mice is 11, 15, and 21 days for 23.1, 23.8, and 23.12, respectively.

## Non-tumor prostatic epithelial lines

***RWPE-1***

In comparison to the cancer cell lines discussed previously, non-tumorigenic human prostatic epithelium (HPE) cell lines are used as a way to contrast PCa pathogenesis. The most prevalent of this type of cell lines is RWPE-1. These cells were immortalized with human papilloma virus (HPV) 18 with subsequent isolation and propagation over 6–7 weeks [78,79]. This cell line is positive for AR/PSA mRNA/protein and is androgen sensitive, which was specifically developed to address the problem of normal prostatic epithelial growth and development [74]. It responds normally to EGF and TGF-β treatment and does not form tumors in mice. Benign prostatic hyperplasia (BPH) is an inflammatory condition that generates reactive oxygen species (ROS) and recent studies have tried to make a link connecting BPH to neoplasia [80]. BPH is a common condition among men in their sixth decade, with about 50% of that population demonstrating symptoms. RWPE-1 is therefore a good model to investigate the molecular mechanisms underlying the proliferation of benign prostatic epithelial cells.

***BPH1***

Hayward et al. isolated this cell line from benign prostatic hypertrophy or hyperplasia (BPH) tissues obtained through transurethral resection from a 68 year old patient undergoing the procedure for urinary obstruction consistent with BPH in 1994 [81]. Histologically benign, these cells were cultured out of the surgical specimen and immortalized, but not transformed, with the SV40 large T antigen. Karyotype analysis shows an aneuploid genome, with a range of 71–79 (modal of 76). Cells were viable but non-tumorigenic in mice. They are EGF, TGF-α, and FGF1/7 responsive, and are inhibited by FGF2 and TGF-β1/2 with androgen insensitivity. They are AR/PSA negative and WT p53 positive. It expresses PTEN, p21Cip1/Waf1, and Bax [82,83]. Doubling time is approximately 35 hours.

***pRNS-1-1***

This is another type of HPE cell introduced into the literature in 1994 [84]. This line has been immortalized, to at least 50 passages, with the pRSV-T plasmid, which contains an origin-defective SV40 genome and the rous sarcoma virus long terminal repeat (LTR) along with a neomycin resistance gene. It expresses cytokeratins 5 and 8, responds normally to typical growth signals (EGF, IGF, pituitary extract) and inhibitory signals (retinoic acid, TGF-β). However, investigation by Lee and colleagues seemed to indicate that these cells lost responsiveness to growth inhibitory signals such as TNF-α and vitamin D3, indicating the ability of this line to transform. This cell line has a karyotype of modal chromosome number of 49–52 with a doubling time of approximately 72 hours. PSA was detected in patient and early passage samples, but lost expression during later passages. An interesting observation made by Brinkmann and colleagues found these cells form normal prostatic glandular structures from cellular aggregates when treated with hepatocyte growth factor/scatter factor (HGF/SF) [85]. These aggregates would usually collapse after about a week in culture.

An important footnote in the story of pRNS-1-1 cells is the development of WPMY-1, isolated and developed by the same group and from the same prostate that gave us pRNS-1-1 [79]. This is a non-neoplastic stromal cell line that allows for the investigation of stromal/epithelial interactions in the development of PCa. Significant investigation is being conducted in the potential role that stromal cells play in the transition from hormone sensitive to castration resistant PCa [86].

***PIN***

No review of PCa cell lines would be complete without at least a mention of prostatic intraepithelial neoplasia (PIN). This is a condition that has been identified as a premalignant lesion in the development of PCa [87,88]. PIN cells are thus an important cell line for the investigation of oncogenic processes and molecules in a premalignant context. Developed and introduced into the literature in 1999 by Stearns and colleagues, this is a line isolated from an African-American patient [89]. The same HPV-18 construct used to immortalize RWPE-1 cells was also used to immortalize this cell line. The authors described this line in detail at passages 5 and 15, demonstrating PSA production via stimulation with DHT and dihydroxyepiandosterone at passage 5 but moving on to androgen insensitivity at passage 15. They also note that early passage cells expressed CK18 and 34βE12, but later passages lost detection of 34βE12. They indicated this as basal cell origin with no contribution from nearby cancer tissue. This group also looked at the role of interleukin-10 (IL-10), activin A, and inhibin (both members of the TGF-β superfamily) in this line's proliferative ability. They noted the ability of activin to stimulate growth even as TGF-β was able to reduce growth. Also noted is the ability of activin A to inhibit growth when present in culture media with IL-10. They also postulated that activin A blocks growth of these high grade PIN lesion cells by binding follistatin, thus preventing IL-10 growth stimulation. Xenograft studies revealed an inability of these cells to grow in mice.

## In vivo model systems

Since the initial use of the mouse model in biomedical research nearly a century ago, scientists have gone from techniques as simple as cross breeding in a desired trait to selectively manipulating the genome to induce a disease state. PCa understanding has benefitted tremendously from the use of these techniques, particularly through the use of the mouse models detailed below. The need for *in vivo* models was an outgrowth of the understanding that cancer cell lines in general (and prostate lines in particular) do not and cannot recapitulate the disease processes that occur in living tissues. Teasing apart molecular interactions and alterations in cancer cells is of incredible worth, but they do not take into account all of the cellular interactions that occur as a cell goes through the oncogenic and metastatic process. Before progressing to the main models of this review, it should be noted that rat and canine have been used for some important discoveries about spontaneous prostate lesions. They are not often favored by the PCa research community due either to inadequate genetic manipulation in case of rats or expensive price and pet affection in case of dogs. However, descriptions of these models can be found in the references [90,91]. Thus, mice have been the favored model organism in recapitulating various aspects of the disease process. Excellent reviews devoted solely to mouse models are available in the references [92,93]. Information provided in this section is summarized in **Table 2**.

### *Mouse surgery and xenograft models*

The most widely utilized tool in PCa research is the use of human PCa cell lines transplanted into mice, referred to as xenograft or xenotransplantation. There are three modes of xenograft employed today: subcutaneous, orthotopic, and under the subrenal capsule (SRC). Each has its own costs and benefits.

Subcutaneous xenograft models were developed first utilizing the insertion of patient prostatic tissue into the shoulder of nude mice in the late 1970s by Schröder and colleagues at Erasmus University Rotterdam. This gave us the first transplantable tumor cell line, PC-82 [94]. The advantages of this model system include easy accessibility and less demanding technical expertise, as well as the amount of tumor tissue that can be introduced. The take is reportedly very low, owing to poor vascularization of the dermal tissue. Take rates vary in the literature in recent years from as low as 3% to as high as 58% [95]. Additionally, low to moderately aggressive tumors do not seem to thrive very well in this type of environment, as only highly aggressive tumors seem to account for the majority of tumors recovered from nude mice [96].

Orthotopic xenograft models allow for the introduction of cancerous prostatic tissue into the mouse prostate. Stephenson et al. first introduced this model in 1992. In their initial study they very clearly concluded that the subcutaneous, or any ectopic, model does not reveal the metastatic potential of implanted human PCa tissue. Additionally, this work was expanded by An and colleagues to show a high degree of lung and lymph node metastasis, the first such demonstration published in the literature [97]. The obvious advantages of this model include the relevance of the interactions between the implanted tissue and the organ of origin, as bolstered by the evidence that metastatic potential is increased not only in orthotopically implanted prostatic tissue but also other organs as well [98]. The take rate for this procedure is in a much more favorable, reported at nearly 72% [96]. This model also offers the advantage of implanting a wider range of tumor aggression levels, allowing for the investigation of tumorigenic and metastatic processes. The main disadvantages to this type of procedure include the skill set that is required for conducting the surgery and the limited amount of tissue that can be introduced into the mouse prostate. Additionally, androgen ablation therapy prior to tissue introduction causes such a large amount of prostatic regression that it makes implementation of some experimental designs practically impossible.

**Table 2 . Common Mouse Models Used in Prostate Cancer Research.**

| Model | Genetic Alteration | Tumorigenic Time Course | Metastasis | Purpose | Reference |
|---|---|---|---|---|---|
| Pten | Cre recombinase to excise the coding sequence of Pten between two loxP sites | 6 weeks to PIN formation; 9–29 weeks for invasive carcinoma | Lymph nodes, lung | Defined time course through PIN lesions | Wang, 2003 [132] |
| TRAMP | SV40 large/small t antigen driven using a prostate specific promoter PB; can combine ARR2 with PB to drive SV40 or a host of other molecules | Mild hyperplasia in 8–12 weeks, metastatic disease starting at 18 weeks | Bone, lymph node, lung, adrenal gland, kidney | Fast time course to metastatic disease | Greenberg, 1995 [109], Gingrich, 1996 [110] |
| Hi Myc | ARR2-PB promoter to drive high expression of c-myc with androgen responsiveness | 3 months to PIN formation; 6 months to invasive cancer | None noted [145] | Defined time course; androgen sensitivity of promoter | Ellwood-Yen, 2003 [128] |
| Lo Myc | PB promoter to drive low expression of c-myc | 6–12 months for PIN; 12 months or more for invasive cancer | None noted [146] | Slower time course; allows for investigation of oncogenic/castration resistance drivers | Ellwood-Yen, 2003 [128] |
| LADY | LPB; -12kb/+28 region of the PB promoter used to solely drive expression of SV40 large T antigen | 10–15 weeks for dysplasia, 15–22 weeks for carcinoma in the 12T-7 (fast and slow) | Regional lymph nodes, liver, lung | Tumors demonstrate neuroendocrine differentiation [147] considered a late event in tumorigenesis | Kasper, 1998 [126] |
| MPAKT | -421/+28bp of PB driving the myr-HA-Akt1 construct | PIN lesions early in life; no invasive carcinoma detected up to 78 weeks | None reported | Study the transformation of prostatic epithelial cells | Majumder, 2003 [138] |

SRC xenografts are the most recent development in xenotransplantation. Initially introduced into the literature by Wang in 2005, they were able to successfully recover over 93% of tumors [96]. They note the caveat that there was a spread of recovery rates dependent on individual experience of the person performing the procedure, but this still illustrates that SRC grafting is a viable way to recover xenograft material. The authors postulate that this technique is so successful because of the high degree of vascularity to the tissue. It would be difficult to comment on the metastatic potential of this model, as searches on PubMed for the term "prostate cancer subrenal capsule" returns 31 hits. The majority of these publications are aimed at investigating the primary tumor itself and don't comment on metastatic potential, although some studies, which are described in the references, do conclude that the investigation of metastatic genes is possible with this technique [99-101]. Despite the disadvantage of not being the native tissue from which the implanted tumor arises, SRC xenografts offer some exciting possibilities when combined with using patient tissue as the graft material. Wang and colleagues have recently commented on the utility of this system, pointing to the fact that such a high degree of tumors can be recovered using the SRC grafts [102]. They suggested that this could impact basic research on PCa, identification of metastatic driver genes, and the ability to tailor clinical therapy to the patient's tumor biology [103-105]. Preclinical *in vivo* studies are difficult to translate to the bedside because of the homogeneity of cultured cell lines, which can be contrasted with the heterogeneity of different subpopulations of both cancer and stromal cells within a tumor mass. Next generation patient-derived PCa xenograft models allow the cancerous subpopulations of cells to express their dominance when transplanted into NOD/SCID mice, and therapy can be tested and tailored to the tumor biology depending on the tumor's growth response. One organization that has been developing this avenue of investigation is the Living Tumor Laboratory [106].

Relevant to the topic of xenograft procedures, the issue of bioengineered materials should be discussed. Substances such as Matrigel™, polyethylene glycol (PEG), collagen and sponge are often used in the creation of a cell suspension pre-procedure to allow a microenvironment hospitable for cancer cell growth. There is no question that these materials are useful in rendering a more faithful tumor microenvironment both in xenograft and 3-dimensional (3D) culture models. However, it is still being discussed in the field about the effect that these materials have on gene expression profiles and responsiveness to androgen. Work by Lang et al. seems to indicate that Matrigel™ induces morphological changes that may be indicative of gene expression profile changes [107]. More recent studies have indicated more finely tuned materials such as PEG hydrogels, containing arginine-glycine-aspartate (RGD) and matrix metalloproteinase (MMP) cleavage sites, provide a microenvironment that better recapitulates native tissue environment [108]. This consideration should be made particularly if hormone sensitivity or drug discovery studies are being conducted.

### *TRAMP*

Norman Greenberg and his group first developed this mouse in 1995 with subsequent description of metastatic disease in these animals by 28 weeks of age [109,110]. Spontaneously occurring prostate lesions were observed in limited types of animals; however, rats seem to form spontaneous adenocarcinoma on a regular basis [111,112]. Subsequent investigation showed that rat prostate contained a prostate specific promoter probasin (PB or rPB) that directed an androgen sensitive transcriptional program [113]. When considering the responsiveness of a mouse model to the development of PCa, the consideration and choice of promoter is absolutely essential and is the main distinguishing feature between different models. Greenberg and his group were able to drive the expression of the SV40 large T antigen using the upstream 426 bp 5' flanking region and 28 bp of the 5' untranslated region. Experimentation with chloramphenicol acetyl transferase and luciferase reporter assays demonstrated that the -426/+28 PB promoter contained two androgen receptor binding sites (ARBS) in the regions of -236 to -223 and -140 to -117, respectively, with the region containing both of these sites (-244 to -40) referred to as ARR [113]. The oncogenic effects of the SV40 protein are primarily interactions with the tumor suppressors p53 and Rb. The loss of both of these proteins has been implicated in the development and progression of prostate lesions [114-117]. Using the composite of two linked ARR regions, referred to as ARR2, the combination ARR2-PB construct has been used to investigate a wide range of molecules and their role in the initiation and progression of PCa. Such examples include the growth signaling molecule Ras, hepsin, the ubiquitin E3 ligase SCF (SKP2, an F box protein), and FGF8 [118-121]. Bigenic models have also been developed. Fibroblast growth factor 2 (FGF2) null mice have been crossed with TRAMP animals to investigate the role of that factor in tumor development, drawing upon observations of high expression of FGF2 in PC3 and DU-145 cells [122]. This model is generally regarded with very high utility, as the progression through PIN lesions to malignant disease is on a predictable time course that mimics human oncogenic milestones. However, the TRAMP model may not be the best suited for oncogenic studies. It is well purposed for studies of treatment and prevention. Recent studies of this model have shown that many tumors display neuroendocrine (NE) differentiation, suggesting that this model is likely a model of small cell carcinoma, rather than adenocarcinoma [123,124].

### *LADY*

One of the more insidious aspects of PCa is the fact that several cell types can contribute to the initiation or sustenance of a tumor. The typical prostate tissue architecture is composed of stroma, basal and luminal cells. However, in the consideration of the molecular and cellular mechanisms to account for castration resistance, scientists and physicians made the discovery that the nervous system makes a contribution to prostate tissue architecture in the form of NE cells. NE cells are thought to be paracrine signaling cells that control the growth of prostatic epithelium [125], and due to their lack of androgen receptor are thought to be a driver in castration resistance. The work of two groups led to the development of a mouse model that faithfully recapitulated the progression of prostatic intraepithelial neoplasia all the way to malignant disease [126,127]. The genetic modifications of the LADY model are similar to the TRAMP model, with a larger 12 kb region of the rPB promoter (referred to as the LPB) situated upstream of the sole SV40 large T antigen. The LADY model also has the distinction of containing the d1 2005 deletion mutation in the small t antigen, eliminating its expression. It was for the purpose of investigating the role of neuroendocrine differentiation that the LADY model was developed, and Masumori et al. were able to successfully demonstrate the presence of neuroendocrine differentiation in metastatic lesions [127].

### *Hi/Lo-Myc mouse*

Sawyers and colleagues published their work on using two constructs based on using the PB promoter to drive prostate specific expression of c-Myc oncogene. One construct, designated Lo-myc, uses the PB promoter alone to drive c-Myc expression. The other, designated Hi-myc, uses PB coupled with a sequence of the ARR2 promoter, both

of which lie upstream of the human c-Myc gene to drive progression from mouse prostatic intraepithelial neoplasia (mPIN) to invasive adenocarcinoma [128]. An important distinction between these two models is the androgen responsiveness of the Hi-myc model. The ARR2 is androgen responsive, which has the implication of reversing mPIN by silencing expression of the transgene in mice 3 months post-castration and causing regression, but not elimination, of prostate tumors in mice out to 5 months post-castration. The Lo-myc model displays no such responsiveness [128].

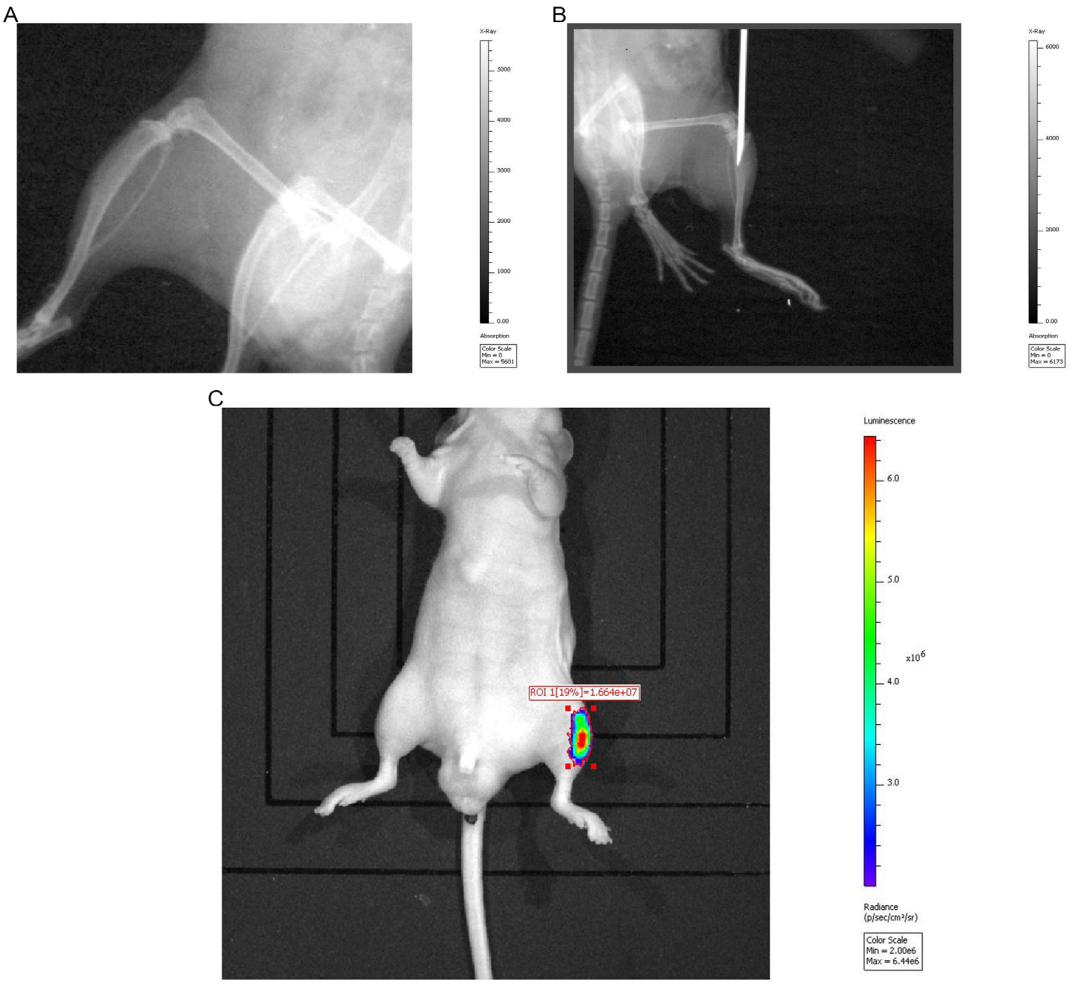



**Figure 1. Intratibial cancer cell injection mouse model. A.** X-ray image taken of a normal mouse tibia pre-procedure on the contralateral side with the radiolucent bone marrow cavity visible on the proximal end of the bone. **B.** X-ray image of a mouse tibia with a 21-gauge needle inserted into the proximal bone marrow cavity. **C.** Results of successful injection of PC3 cells expressing luciferase (and an injection of D-luciferin) using an IVIS (IVIS® Illumina XRMS Series III, PerkinElmer, Waltham, MA, USA).

***Pten knockout***

PTEN ablation has been shown to be an early event in PCa initiation and progression [129], and new technologies have allowed for this molecule to be knocked out in a mouse model. Briefly, it was discovered that Cre recombinase, a nuclease in the bacteriophage P1, recognized conserved sequences called loxP sites and excised any genetic information encoded between two of these sites [130]. Thus, mouse embryos can be engineered to have loxP sites flanking a gene of interest (a "floxed" gene). When Cre and a floxed gene are present in the same organism, the Cre will excise the floxed gene using loxP recognition, either in a constitutive manner or inducible manner through the use of estrogen compounds. A valuable tool in the investigation of PCa has been the Pten null mouse [131]. The value of this model is that the animal demonstrates the range of conditions seen in human subjects, progressing through low grade PIN to invasive carcinoma and metastasis in only 12 weeks [132]. There is also the benefit of Cre expression being predominantly tissue specific with highest expression seen in the lateral prostate [132]. The Pten knockout model has been successfully used to ascertain the contributions that IL-17 makes to the tumor microenvironment in a Pten and IL-17 receptor C double knockout model [133,134]. Additional bigenic models have also been developed using the Pten knockout background. Cross breeding between Pten heterozygotes and TRAMP, Nkx3.1, and p27Kip1 are all currently being implemented in experimentation [135-137].

***MPAKT***

The mouse prostate Akt (MPAKT) model was developed to study the role of protein kinase B (Akt) in the transformation of prostate epithelial cells [138]. The alteration to this animal's genome is the introduction of the coding sequence for Akt1 along with a myristolation sequence (myr) and a hemagluttinin (HA) epitope for proper targeting of the protein to the inner leaflet of the cell membrane. These elements are combined to create the PB-myr-HA-Akt1 construct [139]. PIN lesions were described via immunohistochemical (IHC) analysis early on in the mouse's life, but no invasive carcinoma was detected in any animals even after 78 weeks. The authors who originally developed this model think that there are more oncogenic factors at play in the transformation of prostate epithelium than just constitutive activation of the Akt

pathway. One interesting observation is the similarity of MPAKT and haploinsufficient Pten PIN lesions.

***Metastatic models***

Several important models for studying PCa metastasis are currently available. In an effort to model the bone metastatic tumor growth, the intratibial injection model was developed. PCa cells can be suspended in phosphate-buffered saline or Matrigel™ and directly injected into the tibias of genetically manipulated or WT mice. Imaging technologies can be applied to track changes in bone lesions and morphology of the tissue itself [140]. In vivo imaging system (IVIS) technologies have recently been implemented to track lesion growth, taking advantage of stable luciferase expression in PCa cell lines. An example of whole mouse *in vivo* imaging can be found in **Figure 1**.

Tail vein cancer cell injection is another method of assessing the role of different molecules in metastasis. The interactions between circulating tumor cells and the endothelium are extremely important factors in this process, and tail vein injections allow the delivery of a bolus of cancer cells into the bloodstream in a tolerable volume [141]. An excellent example of the utility of this model can be found in the recent publication by LeBeau and colleagues [142].

The other option for introducing cancer cells into the bloodstream is the use of intracardiac injection. Campbell and colleagues have introduced a good description of the protocol with accompanying visual documentation [140]. Jenkins et al. have combined the strategies of intracardiac inoculation of genetically altered PC-3M-luc-C6 cells to track propagation of metastasis [143].

## Conclusions

When juxtaposed with the depth and breadth of characterization of breast cancer, the field of PCa research has been lagging behind in the understanding of how molecular phenotype affects clinical parameters and prognosis. Markers commonly used to diagnose this disease, such as PSA, have been met with opposition to its continued widespread use. Significant molecules in the initiation and progression of PCa, specifically AR, have yet to be fully elucidated in terms of their contribution to castration resistance. It is for this reason that investigation needs to continue, specifically to better understand the drivers behind oncogenesis, how this affects clinical course, and to provide therapeutic targets. The techniques and models described herein are essential tools for bolstering that understanding. Perhaps the biggest challenge in the field is developing an animal model that faithfully recapitulates bone metastasis. Due to the high degree of morbidity and mortality that is associated with this type of tumor progression, an animal model that reliably seeds tumor cells from prostate to bone would be of substantial value, both clinically and scientifically [144]. Such a model would allow for investigation of circulating tumor cell/bone matrix interactions and potential therapeutic targets for metastatic prevention. As a final note, a thorough investigation of cell lines reveals few *in vitro* models being isolated from African-American men that are widely available to the research community. Due to the increased incidence of PCa in this population, we would be remiss if not making a concerted effort to correct this oversight.

## Acknowledgements

The authors thank the members of the You Laboratory for their support in generating animal data, particularly Drs. Qiuyang Zhang, Keshab R. Parajuli, Sen Liu, and Jiandong Mei. D. C. would like to acknowledge Keith Pickett at the Matas Library for training in Endnote. Z.Y. was supported in whole or in part by Department of Defense Health Program (W81XWH-14-1-0050, W81XWH-14-1-0149, W81XWH-14-1-0458, and OR140380; the U.S. Army Medical Research Acquisition Activity, 820 Chandler Street, Fort Detrick MD 21702-5014 is the awarding and administering acquisition office) and by National Institutes of Health (R01CA174714 and P20GM103518). The content of this article is solely the responsibility of the authors and does not necessarily represent the official views of the National Institutes of Health or the Department of Defense.

## References

1. American C (2014) Prostate Cancer: Detailed Guide. Cited November 21. Available from http://www.cancer.org/cancer/prostatecancer/detailedguide/prostate-cancer-key-statistics 2. Lesko SM, Rosenberg L, Shapiro S (1996) Family history and prostate cancer risk. Am J Epidemiol 144: 1996-144.
2. Lesko SM, Rosenberg L, Shapiro S (1996) Family history and prostate cancer risk. Am J Epidemiol 144: 1041-1047. PMID: 8942435
3. Cullen J, Elsamanoudi S, Brassell SA, Chen Y, Colombo M, et al. (2012) The burden of prostate cancer in Asian nations. J Carcinog 11: 7. doi: 10.4103/1477-3163.94025. PMID: 22529743
4. Albright F, Stephenson RA, Agarwal N, Teerlink CC, Lowrance WT, et al. (2014) Prostate cancer risk prediction based on complete prostate cancer family history. Prostate 75: 390-398. doi: 10.1002/pros.22925. PMID: 25408531
5. Ha YS, Salmasi A, Karellas M, Singer EA, Kim JH, et al. (2013) Increased incidence of pathologically nonorgan confined prostate cancer in African-American men eligible for active surveillance. Urology 81: 831-5. doi: 10.1016/j.urology.2012.12.046. PMID: 23465143
6. Sundquist K, Sundquist J, Ji J (2015) Contribution of shared environmental factors to familial aggregation of common cancers: an adoption study in Sweden. Eur J Cancer Prev 24: 162-164. doi: 10.1097/CEJ.0000000000000101. PMID: 25415834
7. Dybkowska E, Swiderski F, Waszkiewicz-Robak B (2014) Fish intake and risk of prostate cancer. Postepy Hig Med Dosw 68: 1199-205.
8. Beyene D, Daremipouran M, Apprey V, Williams R, Ricks-Santi L, et al. (2014) Use of Tanning Potential as a Predictor for Prostate Cancer Risk in African-American Men. In Vivo 28: 1181-7. PMID: 25398820
9. Wright JL, Neuhouser ML, Lin DW, Kwon EM, Feng Z, et al. (2011) AMACR polymorphisms, dietary intake of red meat and dairy and prostate cancer risk. Prostate 71: 498-506. doi: 10.1002/pros.21267. PMID: 20945498
10. Shahabi A, Corral R, Catsburg C, Joshi AD, Kim A, et al. (2014) Tobacco smoking, polymorphisms in carcinogen metabolism enzyme genes, and risk of localized and advanced prostate cancer: results from the California Collaborative Prostate Cancer Study. Cancer Med 3: 1644-1655. doi: 10.1002/cam4.334. PMID: 25355624
11. Caini S, Gandini S, Dudas M, Bremer V, Severi E, et al. (2014) Sexually transmitted infections and prostate cancer risk: a systematic review and meta-analysis. Cancer Epidemiol 38: 329-338. doi: 10.1016/j.canep.2014.06.002. PMID: 24986642
12. Sfanos KS, De Marzo AM (2012) Prostate cancer and inflammation: the evidence. Histopathology 60: 199-215. doi: 10.1111/j.1365-2559.2011.04033.x. PMID: 22212087
13. Nakai Y, Nelson WG, De Marzo AM (2007) The dietary charred meat carcinogen 2-amino-1-methyl-6-phenylimidazo[4,5-b]pyridine acts as both a tumor initiator and promoter in the rat ventral prostate. Cancer Res 67: 1378-1384. doi: 10.1158/0008-5472.CAN-06-1336. PMID: 17264317
14. Blanker MH, Noordzij MAA (2014) [Prostate cancer screening benefit very low, even after 13 years]. Ned Tijdschr Geneeskd 158: PMID: 25492737
15. Duffy MJ (2014) PSA in screening for prostate cancer: more good than harm or more harm than good? Adv Clin Chem. 2014;66:1-23. Adv Clin Chem 66: 1-23. PMID: 25344984
16. Thakur V, Talwar M, Singh PP (2014) Low free to total PSA ratio is not a good discriminator of chronic prostatitis and prostate cancer: An Indian experience. Indian J Cancer 51: 335-7.
17. Cell L, Cell L. BC Cancer Agency (2001) Cited November 21, 2014. Available from http://capcelllines.ca.
18. Sobel RE, Sadar MD (2005) Cell lines used in prostate cancer research: a compendium of old and new lines--part 1. J Urol 173: 342-359. doi: 10.1097/01.

ju.0000141580.30910.57. PMID: 15643172

19. Sobel RE, Sadar MD (2005) Cell lines used in prostate cancer research: a compendium of old and new lines--part 2. J Urol 173: 360-372. doi: 10.1097/01.ju.0000149989.01263.dc. PMID: 15643173
20. Stone KR, Mickey DD, Wunderli H, Mickey GH, Paulson DF (1978) Isolation of a human prostate carcinoma cell line (DU 145). Int J Cancer 21: 274-281. PMID: 631930
21. Heinlein CA, Chang C (2004) Androgen receptor in prostate cancer. Endocr Rev 25: 276-308. doi: 10.1210/er.2002-0032. PMID: 15082523
22. Bajgelman MC, Strauss BE (2006) The DU145 human prostate carcinoma cell line harbors a temperature-sensitive allele of p53. Prostate 66: 1455-1462. doi: 10.1002/pros.20462. PMID: 16741917
23. Fraser M, Zhao H, Luoto KR, Lundin C, Coackley C, et al. (2011) PTEN deletion in prostate cancer cells does not associate with loss of RAD51 function: implications for radiotherapy and chemotherapy. Clin Cancer Res 18: 1015-1027. doi: 10.1158/1078-0432.CCR-11-2189. PMID: 22114138
24. Webber MM, Bello D, Quader S (1997) Immortalized and tumorigenic adult human prostatic epithelial cell lines: characteristics and applications Part 2. Tumorigenic cell lines. Prostate 30: 58-64. PMID: 9018337
25. Mickey DD, Stone KR, Wunderli H, Mickey GH, Vollmer RT, et al. (1977) Heterotransplantation of a human prostatic adenocarcinoma cell line in nude mice. Cancer Res 37: 4049-4058. PMID: 908039
26. Bastide C, Bagnis C, Mannoni P, Hassoun J, Bladou F (2002) A Nod Scid mouse model to study human prostate cancer. Prostate Cancer Prostatic Dis 5: 311-315. doi: 10.1038/sj.pcan.4500606. PMID: 12627217
27. Billström A, Lecander I, Dagnaes-Hansen F, Dahllöf B, Stenram U, et al. (1995) Differential expression of uPA in an aggressive (DU 145) and a nonaggressive (1013L) human prostate cancer xenograft. Prostate 26: 94-104. PMID: 7531848
28. Hanahan D, Weinberg RA (2011) Hallmarks of cancer: the next generation. Cell 144: 646-74. doi: 10.1016/j.cell.2011.02.013. PMID: 21376230
29. Carruba G, Leake RE, Rinaldi F, Chalmers D, Comito L, et al. (1994) Steroid-growth factor interaction in human prostate cancer. 1. Short-term effects of transforming growth factors on growth of human prostate cancer cells. Steroids 59: 412-420. PMID: 7974525
30. Pietrzkowski Z, Mulholland G, Gomella L, Jameson BA, Wernicke D, et al. (1993) Inhibition of growth of prostatic cancer cell lines by peptide analogues of insulin-like growth factor 1. Cancer Res 53: 1102-1106. PMID: 8439954
31. Green JBA (2004) Lkb1 and GSK3-beta: kinases at the center and poles of the action. Cell Cycle 3: 12-14. PMID: 14657655
32. Xu P, Cai F, Liu X, Guo L (2014) LKB1 suppresses proliferation and invasion of prostate cancer through hedgehog signaling pathway. Int J Clin Exp Pathol 7: 8480-8488. PMID: 25674212
33. Yun H, Lee M, Kim SS, Ha J (2005) Glucose deprivation increases mRNA stability of vascular endothelial growth factor through activation of AMP-activated protein kinase in DU145 prostate carcinoma. J Biol Chem 280: 9963-72. doi: 10.1074/jbc.M412994200. PMID: 15640157
34. Shirahama T, Sakakura C, Sweeney EA, Ozawa M, Takemoto M, et al. (1997) Sphingosine induces apoptosis in androgen-independent human prostatic carcinoma DU-145 cells by suppression of bcl-X(L) gene expression. FEBS Lett 407: 97-100. PMID: 9141489
35. Nutt LK, Chandra J, Pataer A, Fang B, Roth JA, et al. (2002) Bax-mediated Ca2+ mobilization promotes cytochrome c release during apoptosis. J Biol Chem 277: 20301-20308. doi: 10.1074/jbc.M201604200. PMID: 11909872
36. von Haefen C, Wieder T, Gillissen B, Stärck L, Graupner V, et al. (2002) Ceramide induces mitochondrial activation and apoptosis via a Bax-dependent pathway in human carcinoma cells. Oncogene 21: 4009-4019. doi: 10.1038/sj.onc.1205497. PMID: 12037683
37. Marcelli M, Marani M, Li X, Sturgis L, Haidacher SJ, et al. (2000) Heterogeneous apoptotic responses of prostate cancer cell lines identify an association between sensitivity to staurosporine-induced apoptosis, expression of Bcl-2 family members, and caspase activation. Prostate 42: 260-273. PMID: 10679755
38. Kaighn ME, Narayan KS, Ohnuki Y, Lechner JF, Jones LW (1979) Establishment and characterization of a human prostatic carcinoma cell line (PC-3). Invest Urol 17: 16-23. PMID: 447482
39. Keer HN, Kozlowski JM, Tsai YC, Lee C, McEwan RN, et al. (1990) Elevated transferrin receptor content in human prostate cancer cell lines assessed *in vitro* and *in vivo*. J Urol 143: 381-385. PMID: 1688956
40. Rossi MC, Zetter BR (1992) Selective stimulation of prostatic carcinoma cell proliferation by transferrin. Proc Natl Acad Sci U S A 89: 6197-6201. PMID: 1631108
41. KZ. Ching (1993) Ramsey E, Pettigrew N, D'Cunha R, Jason M, Dodd JG (1993) Expression of mRNA for epidermal growth factor, transforming growth factor-alpha and their receptor in human prostate tissue and cell lines. Mol Cell Biochem. 1993;126(2):151-8. Mol Cell Biochem 126: 151-8. PMID: 7508078
42. van Bokhoven A, Varella-Garcia M, Korch C, Hessels D, Miller GJ (2001) Widely used prostate carcinoma cell lines share common origins. Prostate 47: 36-51. doi: 10.1002/pros.1045. PMID: 11304728
43. Barlaam B, Cosulich S, Degorce S, Fitzek M, Green S, et al. (2015) Discovery of (R)-8-(1-(3,5-difluorophenylamino)ethyl)-N,N-dimethyl-2-morpholino-4-oxo-4H-chromene-6-carboxamide (AZD8186): a potent and selective inhibitor of PI3Kβ and PI3Kδ for the treatment of PTEN-deficient cancers. J Med Chem 58: 943-962. doi: 10.1021/jm501629p. PMID: 25514658
44. Tai S, Sun Y, Squires JM, Zhang H, Oh WK, et al. (2011) PC3 is a cell line characteristic of prostatic small cell carcinoma. Prostate 71: 1668-1679. doi: 10.1002/pros.21383. PMID: 21432867
45. Horoszewicz JS, Leong SS, Chu TM, Wajsman ZL, Friedman M, et al. (1980) The LNCaP cell line--a new model for studies on human prostatic carcinoma. Prog Clin Biol Res 37: 115-132. PMID: 7384082
46. Veldscholte J, Ris-Stalpers C, Kuiper GG, Jenster G, Berrevoets C, et al. (1990) A mutation in the ligand binding domain of the androgen receptor of human LNCaP cells affects steroid binding characteristics and response to anti-androgens. Biochem Biophys Res Commun 173: 534-540. PMID: 2260966
47. Connolly JM, Rose DP (1990) Production of epidermal growth factor and transforming growth factor-alpha by the androgen-responsive LNCaP human prostate cancer cell line. Prostate 16: 209-218. PMID: 2330326
48. Nakamoto T, Chang CS, Li AK, Chodak GW (1992) Basic fibroblast growth factor in human prostate cancer cells. Cancer Res 52: 571-577. PMID: 1732045
49. Carroll AG, Voeller HJ, Sugars L, Gelmann EP (1993) p53 oncogene mutations in three human prostate cancer cell lines. Prostate 23: 123-134. PMID: 8104329
50. Isaacs WB, Carter BS, Ewing CM (1991) Wild-type p53 suppresses growth of human prostate cancer cells containing mutant p53 alleles. Cancer Res 51: 4716-4720. PMID: 1873816
51. Carson JP, Kulik G, Weber MJ (1999) Antiapoptotic signaling in LNCaP prostate cancer cells: a survival signaling pathway independent of phosphatidylinositol 3'-kinase and Akt/protein kinase B. Cancer Res 59: 1449-1453. PMID: 10197612
52. Wu HC, Hsieh JT, Gleave ME, Brown NM, Pathak S, et al. (1994) Derivation of androgen-independent human LNCaP prostatic cancer cell sublines: role of bone stromal cells. Int J Cancer 57: 406-412. PMID: 8169003
53. Thalmann GN, Anezinis PE, Chang SM, Zhau HE, Kim EE, et al. (1994) Androgen-independent cancer progression and bone metastasis in the LNCaP model of human prostate cancer. Cancer Res 54: 2577-2581. PMID: 8168083
54. Conley-LaComb MK, Saliganan A, Kandagatla P, Chen YQ, Cher ML, et al. (2013) PTEN loss mediated Akt activation promotes prostate tumor growth and metastasis via CXCL12/CXCR4 signaling. Mol Cancer 12: 85. doi: 10.1186/1476-4598-12-85. PMID: 23902739
55. Klein KA, Reiter RE, Redula J, Moradi H, Zhu XL, et al. (1997) Progression of metastatic human prostate cancer to androgen independence in immunodeficient SCID mice. Nat Med 3: 402-408. PMID: 9095173
56. Neshat MS, Mellinghoff IK, Tran C, Stiles B, Thomas G, et al. (2001) Enhanced sensitivity of PTEN-deficient tumors to inhibition of FRAP/mTOR. Proc Natl Acad Sci U S A 98: 10314-10319. doi: 10.1073/pnas.171076798. PMID: 11504908
57. Sawyers C, Sawyers C (2001) Xenograft Models and the Molecular Biology of Human Prostate Cancer. In: Xenograft Models and the Molecular Biology of Human Prostate Cancer. In, , Chung, LWK, Isaacs WB, Simons JW (editors). Prostate Cancer, , Biology, Genetics, and the New Therapeutics , editors. In: Chung, LWK, Isaacs WB, Simons JW (editors). Prostate Cancer: Biology, Genetics, and the New Therapeutics. New York City: Humana Press. pp 163-174; 2001. p. 163-174
58. Craft N, Chhor C, Tran C, Belldegrun A, DeKernion J, et al. (1999) Evidence for clonal outgrowth of androgen-independent prostate cancer cells from androgen-dependent tumors through a two-step process. Cancer Res 59: 5030-5036. PMID: 10519419
59. Silvers CR, Williams K, Salamone L, Huang J, Jordan CT, et al. (2010) A novel *in vitro* assay of tumor-initiating cells in xenograft prostate tumors. Prostate 70: 1379-1387. doi: 10.1002/pros.21171. PMID: 20687210
60. Rubin MA, Putzi M, Mucci N, Smith DC, Wojno K, et al. (2000) Rapid ("warm") autopsy study for procurement of metastatic prostate cancer. Clin Cancer Res 6: 1038-1045. PMID: 10741732

61. Korenchuk S, Lehr JE, MClean L, Lee YG, Whitney S, et al. (2001) VCaP, a cell-based model system of human prostate cancer. In Vivo 15: 163-8. PMID: 11317522
62. Mertz KD, Setlur SR, Dhanasekaran SM, Demichelis F, Perner S, et al. (2007) Molecular characterization of TMPRSS2-ERG gene fusion in the NCI-H660 prostate cancer cell line: a new perspective for an old model. Neoplasia 9: 200-6. PMID: 17401460
63. Sramkoski RM, Pretlow TG, Giaconia JM, Pretlow TP, Schwartz S, et al. (1999) A new human prostate carcinoma cell line, 22Rv1. In Vitro Cell Dev Biol Anim 35: 403-9. doi: 10.1007/s11626-999-0115-4. PMID: 10462204
64. Chlenski A, Nakashiro K, Ketels KV, Korovaitseva GI, Oyasu R (2001) Androgen receptor expression in androgen-independent prostate cancer cell lines. Prostate 47: 66-75. doi: 10.1002/pros.1048. PMID: 11304731
65. Tepper CG, Boucher DL, Ryan PE, Ma AH, Xia L, et al. (2002) Characterization of a novel androgen receptor mutation in a relapsed CWR22 prostate cancer xenograft and cell line. Cancer Res 62: 6606-14. PMID: 12438256
66. Tan J, Sharief Y, Hamil KG, Gregory CW, Zang DY, et al. (1997) Dehydroepiandrosterone activates mutant androgen receptors expressed in the androgen-dependent human prostate cancer xenograft CWR22 and LNCaP cells. Mol Endocrinol 11: 450-459. doi: 10.1210/mend.11.4.9906. PMID: 9092797
67. Li Y, Alsagabi M, Fan D, Bova GS, Tewfik AH, et al. (2011) Intragenic rearrangement and altered RNA splicing of the androgen receptor in a cell-based model of prostate cancer progression. Cancer Res 71: 2108-2117. doi: 10.1158/0008-5472.CAN-10-1998. PMID: 21248069
68. Dehm SM, Schmidt LJ, Heemers HV, Vessella RL, Tindall DJ (2008) Splicing of a novel androgen receptor exon generates a constitutively active androgen receptor that mediates prostate cancer therapy resistance. Cancer Res 68: 5469-5477. doi: 10.1158/0008-5472.CAN-08-0594. PMID: 18593950
69. Zhau HY, Chang SM, Chen BQ, Wang Y, Zhang H, et al. (1996) Androgen-repressed phenotype in human prostate cancer. Proc Natl Acad Sci U S A 93: 15152-15157. PMID: 8986779
70. Navone NM, Olive M, Ozen M, Davis R, Troncoso P, et al. (1997) Establishment of two human prostate cancer cell lines derived from a single bone metastasis. Clin Cancer Res. 1997;3(12 Pt 3: 1-2493. PMID: 9815652
71. Navone NM, Rodriquez-Vargas MC, Benedict WF, Troncoso P, McDonnell TJ, et al. (2000) TabBO: a model reflecting common molecular features of androgen-independent prostate cancer. Clin Cancer Res 6: 1190-1197. PMID: 10741751
72. Zhao XY, Boyle B, Krishnan AV, Navone NM, Peehl DM, et al. (1999) Two mutations identified in the androgen receptor of the new human prostate cancer cell line MDA PCa 2a. J Urol 162: 2192-2199. PMID: 10569618
73. Alimonti A, Nardella C, Chen Z, Clohessy JG, Carracedo A, et al. (2010) A novel type of cellular senescence that can be enhanced in mouse models and human tumor xenografts to suppress prostate tumorigenesis. J Clin Invest 120: 681-693. doi: 10.1172/JCI40535. PMID: 20197621
74. Bello D, Webber MM, Kleinman HK, Wartinger DD, Rhim JS (1997) Androgen responsive adult human prostatic epithelial cell lines immortalized by human papillomavirus 18. Carcinogenesis 18: 1215-1223. PMID: 9214605
75. Rhim JS, Webber MM, Bello D, Lee MS, Arnstein P, et al. (1994) Stepwise immortalization and transformation of adult human prostate epithelial cells by a combination of HPV-18 and v-Ki-ras. Proc Natl Acad Sci U S A 91: 11874-11878. PMID: 7991549
76. Woodworth CD, Waggoner S, Barnes W, Stoler MH, DiPaolo JA (1990) Human cervical and foreskin epithelial cells immortalized by human papillomavirus DNAs exhibit dysplastic differentiation *in vivo*. Cancer Res 50: 3709-3715. PMID: 1692766
77. Ellis WJ, Vessella RL, Buhler KR, Bladou F, True LD, et al. (1996) Characterization of a novel androgen-sensitive, prostate-specific antigen-producing prostatic carcinoma xenograft: LuCaP 23. Clin Cancer Res 2: 1039-1048. PMID: 9816265
78. Webber MM (1979) Normal and benign human prostatic epithelium in culture. I. Isolation. In Vitro 15: 967-982. PMID: 94033
79. Webber MM, Trakul N, Thraves PS, Bello-DeOcampo D, Chu WW, et al. (1999) A human prostatic stromal myofibroblast cell line WPMY-1: a model for stromal-epithelial interactions in prostatic neoplasia. Carcinogenesis 20: 1185-92. PMID: 10383888
80. Kosova F, Temeltaş G, Arı Z, Lekili M (2013) Possible relations between oxidative damage and apoptosis in benign prostate hyperplasia and prostate cancer patients. Tumour Biol 35: 4295-4299. doi: 10.1007/s13277-013-1560-y. PMID: 24375255
81. Hayward SW, Dahiya R, Cunha GR, Bartek J, Deshpande N, et al. (1995) Establishment and characterization of an immortalized but non-transformed human prostate epithelial cell line: BPH-1. In Vitro Cell Dev Biol Anim 31: 14-24. doi: 10.1007/BF02631333. PMID: 7535634
82. Jerde TJ, Wu Z, Theodorescu D, Bushman W (2011) Regulation of phosphatase homologue of tensin protein expression by bone morphogenetic proteins in prostate epithelial cells. Prostate 71: 791-800. doi: 10.1002/pros.21295. PMID: 21456062
83. Myzak MC, Hardin K, Wang R, Dashwood RH, Ho E (2005) Sulforaphane inhibits histone deacetylase activity in BPH-1, LnCaP and PC-3 prostate epithelial cells. Carcinogenesis 27: 811-819. doi: 10.1093/carcin/bgi265. PMID: 16280330
84. Lee M, Garkovenko E, Yun J, Weijerman P, Peehl D, et al. (1994) Characterization of adult human prostatic epithelial-cells immortalized by polybrene-induced DNA transfection with a plasmid containing an origin-defective sv40-genome. Int J Oncol 4: 821-830. PMID: 21566988
85. Brinkmann V, Foroutan H, Sachs M, Weidner KM, Birchmeier W (1995) Hepatocyte growth factor/scatter factor induces a variety of tissue-specific morphogenic programs in epithelial cells. J Cell Biol. 1995;131(6 Pt 131: 1-1573. PMID: 8522613
86. Chung LW, Huang WC, Sung SY, Wu D, Odero-Marah V, et al. (2006) Stromal-epithelial interaction in prostate cancer progression. Clin Genitourin Cancer 5: 162-70. doi: 10.3816/CGC.2006.n.034. PMID: 17026806
87. Abate-Shen C, Shen MM (2000) Molecular genetics of prostate cancer. Genes Dev 14: 2410-2434. PMID: 11018010
88. Weinberg DS, Weidner N (1993) Concordance of DNA content between prostatic intraepithelial neoplasia and concomitant invasive carcinoma. Evidence that prostatic intraepithelial neoplasia is a precursor of invasive prostatic carcinoma. Arch Pathol Lab Med 117: 1132-1137. PMID: 8239935
89. Wang M, Liu A, Garcia FU, Rhim JS, Stearns ME (1999) Growth of HPV-18 immortalized human prostatic intraepithelial neoplasia cell lines. Influence of IL-10, follistatin, activin-A, and DHT. Int J Oncol 14: 1185-1195. PMID: 10339677
90. Dunning WF (1963) Prostate Cancer in the Rat. Natl Cancer Inst Monogr 12: 351-69. PMID: 14073009
91. Bigio A, Bigio A (2012) Canine prostatic carcinoma. In: . Compend Contin Educ Vet. 2012;34(10):E1-5; 2012 PMID: 23532757
92. Kasper S (2005) Survey of genetically engineered mouse models for prostate cancer: analyzing the molecular basis of prostate cancer development, progression, and metastasis. J Cell Biochem 94: 279-297. doi: 10.1002/jcb.20339. PMID: 15565647
93. Parisotto M, Metzger D (2013) Genetically engineered mouse models of prostate cancer. Mol Oncol 7: 190-205. doi: 10.1016/j.molonc.2013.02.005. PMID: 23481269
94. Hoehn W, Schroeder FH, Reimann JF, Joebsis AC, Hermanek P (1980) Human prostatic adenocarcinoma: some characteristics of a serially transplantable line in nude mice (PC 82). Prostate 1: 95-104. PMID: 7279800
95. van Weerden WM, Romijn JC (2000) Use of nude mouse xenograft models in prostate cancer research. Prostate 43: 263-271. PMID: 10861745
96. Wang Y, Revelo MP, Sudilovsky D, Cao M, Chen WG, et al. (2005) Development and characterization of efficient xenograft models for benign and malignant human prostate tissue. Prostate 64: 149-159. doi: 10.1002/pros.20225. PMID: 15678503
97. Stephenson RA, Dinney CP, Gohji K, Ordóñez NG, Killion JJ, et al. (1992) Metastatic model for human prostate cancer using orthotopic implantation in nude mice. J Natl Cancer Inst 84: 951-957. PMID: 1378502
98. An Z, Wang X, Geller J, Moossa AR, Hoffman RM (1998) Surgical orthotopic implantation allows high lung and lymph node metastatic expression of human prostate carcinoma cell line PC-3 in nude mice. Prostate 34: 169-174. PMID: 9492844
99. Giavazzi R, Campbell DE, Jessup JM, Cleary K, Fidler IJ (1986) Metastatic behavior of tumor cells isolated from primary and metastatic human colorectal carcinomas implanted into different sites in nude mice. Cancer Res. 1986;46(4 Pt 46: 2-1928. PMID: 3948174
100. Gohji K, Nakajima M, Dinney C, Fan D, Pathak S, et al. (1993) The importance of orthotopic implantation to the isolation and biological characterization of a metastatic human clear cell renal-carcinoma in nude-mice. Int J Oncol 2: 23-32. PMID: 21573511
101. Naito S, von Eschenbach AC, Giavazzi R, Fidler IJ (1986) Growth and metastasis of tumor cells isolated from a human renal cell carcinoma implanted into different organs of nude mice. Cancer Res 46: 4109-4115. PMID: 3731078

102. Watahiki A, Wang Y, Morris J, Dennis K, O'Dwyer HM, et al. (2011) MicroRNAs associated with metastatic prostate cancer. PLoS One 6: doi: 10.1371/journal.pone.0024950. PMID: 21980368
103. Xie N, Cheng H, Lin D, Liu L, Yang O, et al. (2015) The expression of glucocorticoid receptor is negatively regulated by active androgen receptor signaling in prostate tumors. Int J Cancer 136: 2015-136. doi: 10.1002/ijc.29147. PMID: 25138562
104. Lin D, Watahiki A, Bayani J, Zhang F, Liu L, et al. (2008) ASAP1, a gene at 8q24, is associated with prostate cancer metastasis. Cancer Res 68: 4352-4359. doi: 10.1158/0008-5472.CAN-07-5237. PMID: 18519696
105. Lin D, Xue H, Wang Y, Wu R, Watahiki A, et al. (2014) Next generation patient-derived prostate cancer xenograft models. Asian J Androl 16: 407-12. doi: 10.4103/1008-682X.125394. PMID: 24589467
106. Living Tumour Laboratory. (2009) The Prostate Center at Vancouver General Hospital, British Columbia Cancer Research Center. Cited November 21, 2014. Available from http://www.livingtumorlab.com/index.html.
107. Lang SH, Sharrard RM, Stark M, Villette JM, Maitland NJ (2001) Prostate epithelial cell lines form spheroids with evidence of glandular differentiation in three-dimensional Matrigel cultures. Br J Cancer 85: 590-9. doi: 10.1054/bjoc.2001.1967. PMID: 11506501
108. Sieh S, Taubenberger AV, Rizzi SC, Sadowski M, Lehman ML, et al. (2012) Phenotypic characterization of prostate cancer LNCaP cells cultured within a bioengineered microenvironment. PLoS One 7: doi: 10.1371/journal.pone.0040217. PMID: 22957009
109. Greenberg NM, DeMayo F, Finegold MJ, Medina D, Tilley WD, et al. (1995) Prostate cancer in a transgenic mouse. Proc Natl Acad Sci U S A 92: 3439-3443. PMID: 7724580
110. Gingrich JR, Barrios RJ, Morton RA, Boyce BF, DeMayo FJ, et al. (1996) Metastatic prostate cancer in a transgenic mouse. Cancer Res 56: 4096-4102. PMID: 8797572
111. Pollard M (1973) Spontaneous prostate adenocarcinomas in aged germfree Wistar rats. J Natl Cancer Inst 51: 1235-1241. PMID: 4745857
112. Wilson EM, Viskochil DH, Bartlett RJ, Lea OA, Noyes CM, et al. (1981) Model systems for studies on androgen-dependent gene expression in the rat prostate. Prog Clin Biol Res 75A: 351-380. PMID: 6175980
113. Rennie PS, Bruchovsky N, Leco KJ, Sheppard PC, McQueen SA, et al. (1993) Characterization of two cis-acting DNA elements involved in the androgen regulation of the probasin gene. Mol Endocrinol 7: 23-36. doi: 10.1210/mend.7.1.8446105. PMID: 8446105
114. DeCaprio JA, Ludlow JW, Figge J, Shew JY, Huang CM, et al. (1988) SV40 large tumor antigen forms a specific complex with the product of the retinoblastoma susceptibility gene. Cell 54: 275-283. PMID: 2839300
115. Gannon JV, Lane DP (1987) p53 and DNA polymerase alpha compete for binding to SV40 T antigen. Nature 329: 456-8. doi: 10.1038/329456a0. PMID: 3309672
116. Bookstein R, Rio P, Madreperla SA, Hong F, Allred C, et al. (1990) Promoter deletion and loss of retinoblastoma gene expression in human prostate carcinoma. Proc Natl Acad Sci U S A 87: 7762-7766. PMID: 2217208
117. Fan K, Dao DD, Schutz M, Fink LM (1994) Loss of heterozygosity and overexpression of p53 gene in human primary prostatic adenocarcinoma. Diagn Mol Pathol 3: 265-270. PMID: 7866637
118. Scherl A, Li J, Cardiff RD, Schreiber-Agus N (2004) Prostatic intraepithelial neoplasia and intestinal metaplasia in prostates of probasin-RAS transgenic mice. Prostate 59: 448-459. doi: 10.1002/pros.20020. PMID: 15065094
119. Song Z, Wu X, Powell WC, Cardiff RD, Cohen MB, et al. (2002) Fibroblast growth factor 8 isoform B overexpression in prostate epithelium: a new mouse model for prostatic intraepithelial neoplasia. Cancer Res 62: 5096-5105. PMID: 12208767
120. Shim EH, Johnson L, Noh HL, Kim YJ, Sun H, et al. (2003) Expression of the F-box protein SKP2 induces hyperplasia, dysplasia, and low-grade carcinoma in the mouse prostate. Cancer Res 63: 1583-8. PMID: 12670908
121. Klezovitch O, Chevillet J, Mirosevich J, Roberts RL, Matusik RJ, et al. (2004) Hepsin promotes prostate cancer progression and metastasis. Cancer Cell 6: 185-95. doi: 10.1016/j.ccr.2004.07.008. PMID: 15324701
122. Polnaszek N, Kwabi-Addo B, Peterson LE, Ozen M, Greenberg NM, et al. (2003) Fibroblast growth factor 2 promotes tumor progression in an autochthonous mouse model of prostate cancer. Cancer Res 63: 5754-5760. PMID: 14522896
123. Chiaverotti T, Couto SS, Donjacour A, Mao JH, Nagase H, et al. (2008) Dissociation of epithelial and neuroendocrine carcinoma lineages in the transgenic adenocarcinoma of mouse prostate model of prostate cancer. Am J Pathol 172: 236-46. doi: 10.2353/ajpath.2008.070602. PMID: 18156212
124. di Sant'Agnese PA (1992) Neuroendocrine differentiation in carcinoma of the prostate. Diagnostic, prognostic, and therapeutic implications. Cancer 70: 254-268. PMID: 1350941
125. Terry S, Beltran H (2014) The many faces of neuroendocrine differentiation in prostate cancer progression. Front Oncol 4: 60. doi: 10.3389/fonc.2014.00060. PMID: 24724054
126. Kasper S, Sheppard PC, Yan Y, Pettigrew N, Borowsky AD, et al. (1998) Development, progression, and androgen-dependence of prostate tumors in probasin-large T antigen transgenic mice: a model for prostate cancer. Lab Invest 78: PMID: 9645768
127. Masumori N, Thomas TZ, Chaurand P, Case T, Paul M, et al. (2001) A probasin-large T antigen transgenic mouse line develops prostate adenocarcinoma and neuroendocrine carcinoma with metastatic potential. Cancer Res 61: 2239-2249. PMID: 11280793
128. Ellwood-Yen K, Graeber TG, Wongvipat J, Iruela-Arispe ML, Zhang J, et al. (2003) Myc-driven murine prostate cancer shares molecular features with human prostate tumors. Cancer Cell 4: 223-238. PMID: 14522256
129. Ciuffreda L, Falcone I, Incani UC, Del Curatolo A, Conciatori F, et al. (2014) PTEN expression and function in adult cancer stem cells and prospects for therapeutic targeting. Adv Biol Regul 56: 66-80. doi: 10.1016/j.jbior.2014.07.002. PMID: 25088603
130. Abremski K, Hoess R (1984) Bacteriophage P1 site-specific recombination. Purification and properties of the Cre recombinase protein. J Biol Chem 259: 1509-1514. PMID: 6319400
131. Kwak MK, Johnson DT, Zhu C, Lee SH, Ye D, et al. (2013) Conditional deletion of the Pten gene in the mouse prostate induces prostatic intraepithelial neoplasms at early ages but a slow progression to prostate tumors. PLoS One 8: doi: 10.1371/journal.pone.0053476. PMID: 23308230
132. Wang S, Gao J, Lei Q, Rozengurt N, Pritchard C, et al. (2003) Prostate-specific deletion of the murine Pten tumor suppressor gene leads to metastatic prostate cancer. Cancer Cell 4: 209-221. PMID: 14522255
133. Li Q, Liu L, Zhang Q, Liu S, Ge D, et al. (2014) Interleukin-17 Indirectly Promotes M2 Macrophage Differentiation through Stimulation of COX-2/PGE2 Pathway in the Cancer Cells. Cancer Res Treat 46: 297-306. doi: 10.4143/crt.2014.46.3.297. PMID: 25038765
134. Zhang Q, Liu S, Xiong Z, Wang AR, Myers L, et al. (2014) Interleukin-17 promotes development of castration-resistant prostate cancer potentially through creating an immunotolerant and pro-angiogenic tumor microenvironment. Prostate 74: 869-79. doi: 10.1002/pros.22805. PMID: 24691769
135. Kwabi-Addo B, Giri D, Schmidt K, Podsypanina K, Parsons R, et al. (2001) Haploinsufficiency of the Pten tumor suppressor gene promotes prostate cancer progression. Proc Natl Acad Sci U S A 98: 11563-11568. doi: 10.1073/pnas.201167798. PMID: 11553783
136. Kim MJ, Cardiff RD, Desai N, Banach-Petrosky WA, Parsons R, et al. (2002) Cooperativity of Nkx3.1 and Pten loss of function in a mouse model of prostate carcinogenesis. Proc Natl Acad Sci U S A 99: 2884-2889. doi: 10.1073/pnas.042688999. PMID: 11854455
137. Di Cristofano A, De Acetis M, Koff A, Cordon-Cardo C, Pandolfi PP (2001) Pten and p27KIP1 cooperate in prostate cancer tumor suppression in the mouse. Nat Genet 27: 222-224. doi: 10.1038/84879. PMID: 11175795
138. Majumder PK, Yeh JJ, George DJ, Febbo PG, Kum J, et al. (2003) Prostate intraepithelial neoplasia induced by prostate restricted Akt activation: the MPAKT model. Proc Natl Acad Sci U S A 100: 7841-7846. doi: 10.1073/pnas.1232229100. PMID: 12799464
139. Ramaswamy S, Nakamura N, Vazquez F, Batt DB, Perera S, et al. (1999) Regulation of G1 progression by the PTEN tumor suppressor protein is linked to inhibition of the phosphatidylinositol 3-kinase/Akt pathway. Proc Natl Acad Sci U S A 96: 2110-2115. PMID: 10051603
140. Campbell JP, Merkel AR, Masood-Campbell SK, Elefteriou F, Sterling JA (2012) Models of bone metastasis. J Vis Exp : 2012-67. doi: 10.3791/4260. PMID: 22972196
141. Vlodavsky I, Vlodavsky I (2001) Tail vein assay of cancer metastasis. In: Curr Protoc Cell Biol. Curr Protoc Cell Biol. 2001;Chapter 19:Unit 19.2; 2001
142. LeBeau AM, Sevillano N, Markham K, Winter MB, Murphy ST, et al. (2015) Imaging active urokinase plasminogen activator in prostate cancer. Cancer Res 75: 1225-1235. doi: 10.1158/0008-5472.CAN-14-2185. PMID: 25672980
143. Jenkins DE, Yu S, Hornig YS, Purchio T, Contag PR (2003) In vivo monitoring of tumor relapse and metastasis using bioluminescent PC-3M-luc-C6 cells in murine models of human prostate cancer. Clin Exp Metastasis 20: 745-756.

PMID: 14713108

144. Rucci N, Sanità P, Delle Monache S, Alesse E, Angelucci A (2014) Molecular pathogenesis of bone metastases in breast cancer: Proven and emerging therapeutic targets. World J Clin Oncol 5: 335-347. doi: 10.5306/wjco.v5.i3.335. PMID: 25114849

145. Nandana S, Ellwood-Yen K, Sawyers C, Wills M, Weidow B, et al. (2010) Hepsin cooperates with MYC in the progression of adenocarcinoma in a prostate cancer mouse model. Prostate 70: 591-600. doi: 10.1002/pros.21093. PMID: 19938013

146. Valkenburg KC, Williams BO (2011) Mouse models of prostate cancer. Prostate Cancer 2011: 895238. doi: 10.1155/2011/895238. PMID: 22111002

147. Abate-Shen C, Shen MM (2002) Mouse models of prostate carcinogenesis. Trends Genet 18: PMID: 120479

**MONOMETHYL AURISTATIN E PHOSPHATE: A MODIFIED MONOMETHYL AURISTATIN E WITH POTENTIAL ANTI-TUMOR ACTIVITY**

Cunningham D, Parajuli K, Zhang C, Wang G, Zhang Q, Liu S, Mei J, You Z
Department of Structural and Cellular Biology, Tulane University School of Medicine
Department of Orthopedics, Tulane University School of Medicine
Louisiana Cancer Research Center
RCMI, Xavier University College of Pharmacy

Metastasis to bone in patients with prostate, breast and lung cancers presents a very high degree of morbidity and mortality. Seventy to ninety percent of terminal prostate cancer patients present with bone metastasis, with rates of 70% and 45-70% in breast and lung cancer patients, respectively. With few viable treatment options, this delineates a clear need for targeted therapy. Monomethyl auristatin E (MMAE) is a synthetic derivative of dolastatin 10, a peptide that causes cell cycle arrest by stabilizing tubulin dimers, initially isolated from mollusks. While too toxic to be used as a chemotherapeutic alone, work by cancer immunologists have used MMAE conjugated to monocloncal antibodies directed against cancer cell surface markers to increase MMAE's efficacy and limit its side effects. We chemically modified MMAE to monomethyl auristatin E phosphate (MMAEp) to target bone metastasis because the phosphate moiety led to enrichment of the drug in the bone through binding to calcium ions in the bone matrix. Our data indicate that MMAEp is less toxic than its parent MMAE compound at low dosage, but with equal toxicity at high dosage. Preliminary data showed that MMAEp preferentially binds to the bone. In vivo study is currently underway using a mouse intra-tibial cancer cell injection model.

This work was partially supported by Department of Defense Health Program through the Prostate Cancer Research Program (W81XWH-14-1-0050, W81XWH-14-1-0149, and W81XWH-14-1-0458), by National Institutes of Health (P20GM103518, R01CA174714, and 2G12MD007595), and by the Developmental Fund of Tulane Cancer Center (TCC) and Louisiana Cancer Research Consortium (LCRC) Fund. The content is solely the responsibility of the authors and does not necessarily represent the official views of the National Institutes of Health or the Department of Defense.

**2014 SBUR Fall Symposium, Nov 13-16, 2014, Dallas, TX.**

# Methoxyacetic Acid Inhibits Prostate Cancer Cell Growth

Keshab R. Parajuli, Qiuyang Zhang, Sen Liu, Neil K. Patel, and Zongbing You

Departments of Structural & Cellular Biology and Orthopaedic Surgery, Tulane Cancer Center and Louisiana Cancer Research Consortium, Tulane Center for Stem Cell Research and Regenerative Medicine, and Tulane Center for Aging, Tulane University School of Medicine, New Orleans, Louisiana 70112

Background: Methoxyacetic acid (MAA) is a primary metabolite of ester phthalates that are used in production of consumer and pharmaceutical products. Environmental exposure to MAA causes embryo abnormalities in pregnant women and spermatocyte death in men through inhibition of histone deacetylases (HDACs). MAA's effects on solid tumors have never been investigated. The objective of this in-vitro study was to determine MAA's effects on prostate cancer cells.

Methods: Two immortalized human normal prostatic epithelial cell lines (RWPE-1 and pRNS-1-1) and four human prostate cancer cell lines (LNCaP, C4-2B, PC-3, and DU-145) were examined for their cell viability, apoptosis, cell cycle arrest, and gene expression after treatment with MAA at different concentrations and time points, using flow cytometry, Western blot, real-time PCR, and chromatin immunoprecipitation analyses.

Results: MAA time- and dose-dependently inhibited prostate cancer cell growth through induction of apoptosis and cell cycle arrest at G1 phase. Prostate cancer cell lines were more sensitive to MAA than normal prostatic epithelial cell lines. MAA-induced apoptosis was due to down-regulation of the anti-apoptotic gene baculoviral inhibitor of apoptosis protein repeat containing 2 (BIRC2, also named cIAP1), leading to activation of caspases 7 and 3, thus triggering off the downstream apoptotic events. MAA-induced cell cycle arrest (mainly G1 arrest) was due to up-regulation of p21 expression at the early time and down-regulation of cyclin-dependent kinase 4 (CDK4) and CDK2 expression at the late time. MAA up-regulates p21 expression through inhibition of HDAC activities, independent of p53/p63/p73.

Conclusions: These results suggest that MAA may be a potential therapeutic drug for the treatment of prostate cancer.

# METHOXYACETIC ACID SUPPRESSES PROSTATE CANCER CELL GROWTH BY INDUCING GROWTH ARREST AND APOPTOSIS

Parajuli KR*, Jhang Q*, Liu S*, Patel NK*, You Z*

*Department of Structural & Cellular Biology, Tulane University, New Orleans, LA.

Methoxyacetic acid (MAA) is a primary metabolite of ester phthalates that are used in production of consumer products and pharmaceutical products. MAA causes embryo malformation and spermatocyte death through inhibition of histone deacetylases (HDACs). Little is known about MAA's effects on cancer cells. In this study, two immortalized human normal prostatic epithelial cells (RWPE-1 and pRNS-1-1) and four human prostate cancer cell lines (LNCaP, C4-2B, PC3, and DU-145) were treated with at different doses (5, 10, and 20 mM) and for different time periods (12, 24, 48, and 72 hours). Cell viability, apoptosis, and cell cycle analysis were perform using flow cytometry and chemical assays. Gene expression and binding to DNA were assessed using real-time PCR, Western blot, and chromatin immunoprecipitation analyses. Here we report that MAA can dose-dependently inhibit prostate cancer cell growth through induction of apoptosis and cell cycle arrest at G1 phase. MAA-induced apoptosis is due to down-regulation of the anti-apoptotic gene baculoviral inhibitor of apoptosis protein repeat containing 2 (BIRC2, also named cIAP1), leading to activation of caspases 7 and 3, thus triggering off the downstream apoptotic events. MAA-induced cell cycle arrest (mainly G1 arrest) is due to up-regulation of p21 expression at the early time and down-regulation of cyclin-dependent kinase 4 (CDK4) and CDK2 expression at the late time. MAA up-regulates p21 expression through inhibition of HDAC activities, independent of p53/p63/p73. These results suggest that MAA may be a potential therapeutic drug for the treatment of prostate cancer.

This work was supported by Department of Defense Health Program and National Institutes of Health.

2015 Metabolism and Cancer, American Association of Cancer Research, June 7-10, 2015, Hyatt Regency Bellevue, Bellevue, WA.

# Aminomethylphosphonic acid inhibits human prostate xenograft tumor growth through interfering glycine synthesis in the cancer cells.

Keshab R. Parajuli, Qiuyang Zhang, Sen Liu, and Zongbing You

Rapidly proliferating cancer cells consume more glycine than rapidly proliferating normal cells, which offers an opportunity to target glycine metabolism in the cancer cells while avoiding causing severe side effects in the normal cells. Two-thirds of glycine consumed is synthesized intracellularly, e.g., through conversion of serine into glycine by serine hydroxymethyltransferase (SHMT). Aminomethylphosphonic acid (AMPA, C3H3NO5P) is an analog to glycine, which inhibits SHMT enzyme activity, thus blocking conversion of serine into glycine. Our previous in-vitro studies have shown that AMPA inhibited cell growth in six cancer cell lines (including four human prostate cancer cell lines PC-3, DU-145, LNCaP, and C4-2B), while had little effects on two human normal immortalized prostatic epithelial cell lines (RWPE-1 and pRNS-1-1). The purpose of the present study was to determine if AMPA could inhibit PC-3 xenograft tumor growth in nude mice. PC-3-LacZ-luc cells (stably expressing LacZ and luciferase for staining and in-vivo imaging) were first implanted subcutaneously to form tumors. Then, the tumors were cut into 2-mm pieces and surgically implanted orthotopically in the prostates of 39 six-week-old athymic nude male mice that were castrated during the same surgery. One week later, the prostate tumor sizes were measured using D-luciferin and IVIS® Lumina XRMS imaging system (PerkinElmer, Inc.). The animals were randomized into three treatment groups: 1) saline as control (n = 14); 2) 400 mg/kg/day of AMPA (n= 10); and 3) 800 mg/kg/day of AMPA (n = 15). The treatment was administrated intraperitoneally once a day until animal death. Animal body weight measurement and in-vivo imaging were performed once every 5 to 7 days. Upon animal death, tumors were harvested and weighed. Pathologic examination, immunohistochemical staining, and Western blot analyses were performed using the tumors. We found that the tumor size rapidly increased in the control group, whereas the tumor size increased only slightly in the two AMPA-treated groups ($p < 0.05$). Animal survival time was significantly longer in the AMPA-treated groups than the control group ($p < 0.05$) and the high-dose group had slightly longer survival time than the low-dose group ($p = 0.087$). The average final tumor weight was significantly less in the high-dose group than the control group ($p < 0.05$). The levels of cellular inhibitor of apoptosis protein 1 (C-IAP1) and cyclin D1 were dramatically reduced in the tumors from the two AMPA-treated groups compared to the control group. We also observed that the two AMPA-treated groups had much less intra-abdominal metastases compared to the control group. Further in-vitro studies found that AMPA inhibited migration and invasion of PC-3 cells using Transwell assays. In conclusion, we found that AMPA inhibits human prostate xenograft tumor growth through inducing apoptosis and inhibiting cellular proliferation, which suggests that AMPA may be developed into a new treatment for prostate cancer.

# MMP-7 PROMOTES THE INVASION AND PROGRESSION OF PROSTATE ADENOCARCINOMA IN MOUSE MODELS

Zhang Q*, Liu S*, Parajuli K*, Yine Qu*, Jiandong Mei*, Zhiquan Chen*, Hui Zhang*, and You Z*

*Department of Structural & Cellular Biology; Tulane Cancer Center; Tulane University School of Medicine, New Orleans, LA.

The matrix metalloproteinase 7 (MMP-7) is the smallest known secreted MMP (a family of 24 extracellular enzymes originally characterized by an ability to degrade components of the ECM) that frequently overexpressed in human cancer tissues and has been associated with cancer initiation and progression. The precise mechanisms of MMP-7 involve in tumorigenesis in prostate remain unclear, including the in vivo relevant activation mechanism of pro-MMP-7 and the substrates responsible for the tumor-promoting activity of MMP-7. We took a genetic approach to explore its role and mechanisms in prostate cancers by interbreeding MMP-7-deficient mice with mice that are conditionally mutant for PTEN, one established preclinical model for prostate cancer. Mice that were MMP-7-deficient (*MMP-7*$^{-/-}$) displayed prostates that were smaller than mice that maintained MMP-7 expression (*MMP-7*$^{+/+}$ or *MMP-7*$^{+/-}$). In addition, *MMP-7*$^{-/-}$ mice developed a reduced number of invasive prostate adenocarcinomas with lower rates of cellular proliferation and higher apoptosis than *MMP-7*$^{+/+}$ or *MMP-7*$^{+/-}$ mice. Moreover, the expression of matrix molecules (laminin-332, β4-integrin) and nonmatrix molecules (E-cadherin, β-catenin, Cox2, Cyclin D1, ErbB4, IGFBP-3, and CTGF etc.) were all reduced in *MMP-7*$^{-/-}$ mice, and the epithelial-to-mesenchymal (EMT) related genes (snail, slug, zeb1/2, vimentin) were increased in *MMP-7*$^{+/+}$ or *MMP-7*$^{+/-}$ mice. Taken together, our results suggested that MMP-7 promotes the invasion and progression of prostate adenocarcinoma, and that an MMP-7-E-canherin-β-catenin-EMT signaling axis is required for prostate cancer invasion and progression.

This work was supported by National Institute of General Medical Sciences; Grant number: P20GM103518; and National Cancer Institute; Grant number: R01CA174714; Grant sponsor: Department of Defense; Grant numbers: W81XWH-14-1-0050, W81XWH-14-1-0149, and W81XWH-14-1-0458; Grant sponsor: The Developmental Fund of Tulane Cancer Center (TCC) and Louisiana Cancer Research Consortium (LCRC) Fund.

## Acknowledgement Receipt

The USPTO has received your submission at **18:34:43** Eastern Time on **24-MAR-2015** by Deposit Account: 030937.

$ **130** fee paid by e-Filer via *RAM* with Confirmation Number: 5114.

You have also pre-authorized the following payments from your USPTO Deposit Account:

Charge any Additional Fees required under 37 C.F.R. Section 1.16 (National application filing, search, and examination fees)
Charge any Additional Fees required under 37 C.F.R. Section 1.17 (Patent application and reexamination processing fees)
Charge any Additional Fees required under 37 C.F.R. Section 1.19 (Document supply fees)
Charge any Additional Fees required under 37 C.F.R. Section 1.20 (Post Issuance fees)
Charge any Additional Fees required under 37 C.F.R. Section 1.21 (Miscellaneous fees and charges)

## eFiled Application Information

| | |
|---|---|
| EFS ID | 21867552 |
| Application Number | 62137691 |
| Confirmation Number | 8023 |
| Title | Monomethyl auristatin E phosphate as a treatment for cancer and other diseases |
| First Named Inventor | Zongbing You |
| Customer Number or Correspondence Address | 30238 |
| Filed By | Raymond Gerard Areaux/Jonette Brown |
| Attorney Docket Number | 20013 |
| Filing Date | |
| Receipt Date | 24-MAR-2015 |
| Application Type | Provisional |

## Application Details

| Submitted Files | Page Count | Document Description | File Size | Warnings |
|---|---|---|---|---|
| TM551_provisional_final.pdf | 16 | | 3958195 bytes | PASS |

| Document Description | Page Start | Page End |
|---|---|---|
| Specification | 1 | 5 |
| Abstract | 6 | 6 |
| Claims | 7 | 9 |
| Drawings-other than black and white line drawings | 10 | 16 |

| | | | | |
|---|---|---|---|---|
| ProvisionalSB_TM551_20013.pdf | 3 | Provisional Cover Sheet (SB16) | 2007131 bytes | PASS |
| fee-info.pdf | 2 | Fee Worksheet (SB06) | 29689 bytes | PASS |

This Acknowledgement Receipt evidences receipt on the noted date by the USPTO of the indicated documents, characterized by the applicant, and including page counts, where applicable. It serves as evidence of receipt similar to a Post Card, as described in MPEP 503.

New Applications Under 35 U.S.C. 111

If a new application is being filed and the application includes the necessary components for a filing date (see 37 CFR 1.53(b)-(d) and MPEP 506), a Filing Receipt (37 CFR 1.54) will be issued in due course and the date shown on this Acknowledgement Receipt will establish the filing date of the application.

National Stage of an International Application under 35 U.S.C. 371

If a timely submission to enter the national stage of an international application is compliant with the conditions of 35 U.S.C. 371 and other applicable requirements a Form PCT/DO/EO/903 indicating acceptance of the application as a national stage submission under 35 U.S.C. 371 will be issued in addition to the Filing Receipt, in due course.

New International Application Filed with the USPTO as a Receiving Office

If a new international application is being filed and the international application includes the necessary components for an international filing date (see PCT Article 11 and MPEP 1810), a Notification of the International Application Number and of the International Filing Date (Form PCT/RO/105) will be issued in due course, subject to prescriptions concerning national security, and the date shown on this Acknowledgement Receipt will establish the international filing date of the application.

*If you need help:*

- *To ask questions about Patent e-Filing, or to suggest improvements to the online system, or report technical problems, please call the Patent Electronic Business Center at (866) 217-9197 (toll free) or send email to EBC@uspto.gov.*
- *Send general questions about USPTO programs to the USPTO Contact Center (UCC) .*
- *For general questions regarding a petition, or requirements for filing a petition, contact the Office of Petitions Help Desk at 1 800-786-9199.*

# Electronic Acknowledgement Receipt

| | |
|---|---|
| **EFS ID:** | 21867552 |
| **Application Number:** | 62137691 |
| **International Application Number:** | |
| **Confirmation Number:** | 8023 |
| **Title of Invention:** | Monomethyl auristatin E phosphate as a treatment for cancer and other diseases |
| **First Named Inventor/Applicant Name:** | Zongbing You |
| **Customer Number:** | 30238 |
| **Filer:** | Raymond Gerard Areaux/Jonette Brown |
| **Filer Authorized By:** | Raymond Gerard Areaux |
| **Attorney Docket Number:** | 20013 |
| **Receipt Date:** | 24-MAR-2015 |
| **Filing Date:** | |
| **Time Stamp:** | 18:34:43 |
| **Application Type:** | Provisional |

## Payment information:

| | |
|---|---|
| Submitted with Payment | yes |
| Payment Type | Credit Card |
| Payment was successfully received in RAM | $130 |
| RAM confirmation Number | 5114 |
| Deposit Account | 030937 |
| Authorized User | ANDERSON, MAGGIE |

The Director of the USPTO is hereby authorized to charge indicated fees and credit any overpayment as follows:

Charge any Additional Fees required under 37 C.F.R. Section 1.16 (National application filing, search, and examination fees)

Charge any Additional Fees required under 37 C.F.R. Section 1.17 (Patent application and reexamination processing fees)

Charge any Additional Fees required under 37 C.F.R. Section 1.19 (Document supply fees)

Charge any Additional Fees required under 37 C.F.R. Section 1.20 (Post Issuance fees)

Charge any Additional Fees required under 37 C.F.R. Section 1.21 (Miscellaneous fees and charges)

## File Listing:

| Document Number | Document Description | File Name | File Size(Bytes)/ Message Digest | Multi Part /.zip | Pages (if appl.) |
|---|---|---|---|---|---|
| 1 | | TM551_provisional_final.pdf | 3958195<br>0428a9e039884f160bc593a930bbf3aa2ec8f501 | yes | 16 |

| Multipart Description/PDF files in .zip description | | |
|---|---|---|
| **Document Description** | **Start** | **End** |
| Specification | 1 | 5 |
| Abstract | 6 | 6 |
| Claims | 7 | 9 |
| Drawings-other than black and white line drawings | 10 | 16 |

**Warnings:**

**Information:**

| | | | | | |
|---|---|---|---|---|---|
| 2 | Provisional Cover Sheet (SB16) | ProvisionalSB_TM551_20013.pdf | 2007131<br>4b6f4e656304321ba56f1efbe0655da92cf95f4c | no | 3 |

**Warnings:**

**Information:**

| | | | | | |
|---|---|---|---|---|---|
| 3 | Fee Worksheet (SB06) | fee-info.pdf | 29689<br>dd195a5b80d2b5a198fc7692ca47b5e35274e0ba | no | 2 |

**Warnings:**

**Information:**

| | |
|---|---|
| **Total Files Size (in bytes):** | 5995015 |

**This Acknowledgement Receipt evidences receipt on the noted date by the USPTO of the indicated documents, characterized by the applicant, and including page counts, where applicable. It serves as evidence of receipt similar to a Post Card, as described in MPEP 503.**

**New Applications Under 35 U.S.C. 111**

**If a new application is being filed and the application includes the necessary components for a filing date (see 37 CFR 1.53(b)-(d) and MPEP 506), a Filing Receipt (37 CFR 1.54) will be issued in due course and the date shown on this Acknowledgement Receipt will establish the filing date of the application.**

**National Stage of an International Application under 35 U.S.C. 371**

**If a timely submission to enter the national stage of an international application is compliant with the conditions of 35 U.S.C. 371 and other applicable requirements a Form PCT/DO/EO/903 indicating acceptance of the application as a national stage submission under 35 U.S.C. 371 will be issued in addition to the Filing Receipt, in due course.**

**New International Application Filed with the USPTO as a Receiving Office**

**If a new international application is being filed and the international application includes the necessary components for an international filing date (see PCT Article 11 and MPEP 1810), a Notification of the International Application Number and of the International Filing Date (Form PCT/RO/105) will be issued in due course, subject to prescriptions concerning national security, and the date shown on this Acknowledgement Receipt will establish the international filing date of the application.**

Monomethyl auristatin E phosphate as a treatment for cancer and other diseases

TITLE OF THE INVENTION

Monomethyl auristatin E phosphate as a treatment for cancer and other diseases

INVENTORS

Zongbing You, a citizen of the People's Republic of China, of New Orleans, Louisiana

CROSS-REFERENCES TO RELATED APPLICATIONS

STATEMENT REGARDING FEDERALLY SPONSORED RESEARCH

This invention was made with U.S. Government support under Grant Number W81XWH-14-1-0149 awarded by the Department of Defense. The government has certain rights in this invention.

BACKGROUND OF THE INVENTION

FIELD OF THE INVENTION

[0001] The present invention relates to a novel compound to treat a disease, including but not limited to cancer, and methods of use thereof.

DESCRIPTION OF RELATED ART

[0002] Metastasis to bone in patients with prostate, breast, and lung cancers presents a very high degree of morbidity and mortality. Seventy to ninety percent of terminal prostate cancer patients present with bone metastasis, with rates of 70% and 45-70% in breast and lung cancer patients, respectively. With few viable treatment options, this delineates a clear need for targeted therapy.

[0003] Monomethyl auristatin E (MMAE) is a synthetic derivative of dolastatin 10, a chemical that causes cell cycle arrest by stabilizing tubulin dimers, initially isolated from mollusks. While it is too toxic to be used as a chemotherapeutic alone, cancer immunologists have used

Monomethyl auristatin E phosphate as a treatment for cancer and other diseases

MMAE conjugated to monoclonal antibodies directed against cancer cell surface markers to increase MMAE's efficacy and limit its side effects.

[0004] The present invention discloses a novel chemically-modified compound derived from MMAE, monomethyl auristatin E phosphate (MMAEp), to target bone metastasis. The phosphate moiety leads to enrichment of MMAEp in the bone through binding to calcium ions in the bone matrix. MMAEp is less toxic than its parent, MMAE, at low dosages but has equal toxicity to it at high dosages. Data presented here demonstrates that MMAEp preferentially binds to the bone and kills cancer cells.

## BRIEF SUMMARY OF THE INVENTION

[0005] The present invention provides a novel compound that is an improvement over the parental chemical, MMAE, for treating a disease.

[0006] In accordance with this discovery, it is an object of the invention to provide a novel compound that kills cancer cells while being less toxic to the rest of the body than MMAE.

[0007] It is an additional object of this invention to provide a cytotoxic compound that more efficiently enriches in the bone than MMAE.

[0008] It is an additional object of this invention to provide a novel method of treating cancers, including bone cancers.

[0009] Other objects and advantages of this invention will become readily apparent from the ensuing description.

## DETAILED DESCRIPTION

[0010] Detailed descriptions of one or more preferred embodiments are provided herein. It is to be understood, however, that the present invention may be embodied in various forms.

Therefore, specific details disclosed herein are not to be interpreted as limiting, but rather as a basis for the claims and as a representative basis for teaching one skilled in the art to employ the present invention in any appropriate manner.

[0011] Wherever any of the phrases "for example," "such as," "including" and the like are used herein, the phrase "and without limitation" is understood to follow unless explicitly stated otherwise. Similarly "an example," "exemplary" and the like are understood to be non-limiting.

[0012] The term "substantially" allows for deviations from the descriptor that do not negatively impact the intended purpose. Descriptive terms are understood to be modified by the term "substantially" even if the word "substantially" is not explicitly recited. Therefore, for example, the phrase "wherein the lever extends vertically" means "wherein the lever extends substantially vertically" so long as a precise vertical arrangement is not necessary for the lever to perform its function.

[0013] The terms "comprising" and "including" and "having" and "involving" (and similarly "comprises", "includes," "has," and "involves") and the like are used interchangeably and have the same meaning. Specifically, each of the terms is defined consistent with the common United States patent law definition of "comprising" and is therefore interpreted to be an open term meaning "at least the following," and is also interpreted not to exclude additional features, limitations, aspects, etc. Thus, for example, "a process involving steps a, b, and c" means that the process includes at least steps a, b and c. Wherever the terms "a" or "an" are used, "one or more" is understood, unless such interpretation is nonsensical in context.

[0014] In one embodiment, the present invention provides a novel compound to treat a disease by killing diseased cells in the body.

[0015] In a preferred embodiment, the present invention provides a novel compound that more efficiently and safely treats bone cancers. The novel compound, MMAEp, is an improvement

over MMAE, a currently-used anti-cancer agent, because it can be administered in low dosages in the bloodstream so as not to cause damage to other parts of the body, but can also concentrate in the bone in sufficient quantities to kill metastatic bone cancer cells. The novel compound binds to calcium ions in the bone matrix allowing the chemical to enrich in the bone and effectively target metastatic cancer cells in the bone.

[0016] In another embodiment, the present invention provides a compound that is able to target cancer cells, including but not limited to, prostate cancer, breast cancer, and lung cancer cells.

EXPERIMENTAL VERIFICATION

[0017] The following figures detail the findings related to an experiment performed on mice to determine the toxicity and anti-cancer properties of MMAEp as compared to MMAE.

[0018] Figure 1 shows the chemical structures of (A) dolastatin 10, (B) monomethyl auristatin E (MMAE), and (C) monomethyl auristatin E phosphate (MMAEp). Monomethyl auristatin E (MMAE) is a synthetic derivative of dolastatin 10, a chemical that causes cell cycle arrest by stabilizing tubulin dimers, initially isolated from mollusks. The addition of phosphate (MMAEp) enriches in bone to target cancer bone metastases because the phosphate moiety leads to enrichment of the drug in the bone through binding to calcium ions in the bone matrix.

[0019] Figure 2 shows *in vitro* data of representative initial high dose treatment of PC3 and C4-2B cells with MMAE and MMAEp. Both MMAE and MMAEp have similar toxicity profiles at higher dosing based on μg/ml concentration. This corresponds to a dose range of 60 nM to 1400 nM. Data shows that MMAEp is less toxic than its parent, MMAE, at low dosages, but is equally toxic to MMAE at high dosages.

[0020] Figure 3 shows *in vitro* half maximal inhibitory concentration (IC50) values. (A) Linear regression analysis of MMAE data points returned values of 2.43 nM for PC3 cells and 1.65 nM for C4-2B cells (Mean ± SE, n = 3). (B) Linear regression analysis of MMAEp data points returned values of 47.28 nM for PC3 cells and 48.17 nM for C4-2B cells (Mean ± SE, n = 3).

[0021] Figure 4 shows *in vivo* data from a mouse intra-tibial cancer cell injection model. For the study, PC3-Luciferase-LacZ cells were injected through the proximal epiphyseal plate of the tibia. Imaging began two weeks post inoculation; day number refers to start of treatment. Representative longitudinal luminescence *in vivo* imaging system (IVIS) images of the (A) control group, (B) MMAE treatment group (1mg/kg body weight), and (C) MMAEp treatment group (1mg/kg body weight) are shown.

[0022] Figure 5 shows representative longitudinal x-ray *in vivo* imaging system (IVIS) images from the mouse intra-tibial cancer cell injection model.

[0023] Figure 6 shows a drug treatment survival analysis comparing the control, MMAE treatment, and MMAEp treatment groups. Survival was significantly lower in the MMAE treatment group. T1/T2/T3/T4 indicate drug treatments. Mantel-Cox analysis indicates curves are significantly different (**, p=0.0046).

[0024] Figure 7 shows the measurements of tumor change from *in vivo* testing. (A) Longitudinal tracking of changes in cohort tumor ROI luminescence. Statistical analysis revealed no significant difference in tumor luminescence at any time point. (B) Longitudinal tracking of cohort body weight. No significant differences were present. (C) Comparison of endpoint masses between control and MMAEp treatment groups. Mass determined by subtracting the mass of the untreated contralateral tibia from the treated cancerous mass. (D) Comparison of endpoint tumor volumes. Excised tumors were measured along x/y/z planes and grouped into treatment groups for comparison.

Monomethyl auristatin E phosphate as a treatment for cancer and other diseases

ABSTRACT

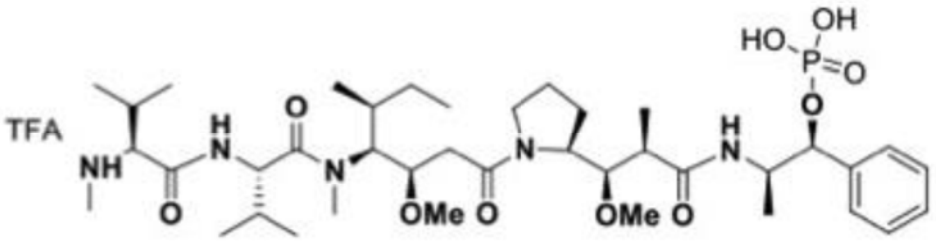
The present invention discloses a novel chemically-modified compound derived from monomethyl auristatin E (MMAE) to treat diseases including but not limited to bone metastasis. The novel compound is less toxic than its parent, MMAE, at low dosages but has equal toxicity to MMAE at high dosages.

Monomethyl auristatin E phosphate as a treatment for cancer and other diseases

EXEMPLARY CLAIMS

What is claimed is:

1. A compound that has the form:




2. A method of treating a disease comprising
    a. administering to a subject a therapeutically effective amount of a composition comprising said compound; and
    b. determining that the development of the disease has been prevented, minimized, or reversed.

3. The method of claim 2, wherein said composition further comprises one or more adjuvants.

4. The method of claim 2, wherein said composition is in a form of a product for oral delivery, said product from being selected from a group consisting of a concentrate, a dried powder, a liquid, a capsule, a pellet, or a pill.

5. The method of claim 2, wherein said composition is in a form of a product for parenteral administration including intravenous, intradermal, intramuscular, and subcutaneous administration.

6. The method of claim 2, wherein said composition further comprises at least one carrier, at least one binder, at least one diluent, at least one excipient, or mixtures thereof.

7. The method of claim 2, wherein the disease is a cancer.

8. The method of claim 2, wherein the cancer is a bone cancer.

9. A method for killing or inhibiting the proliferation of tumor cells or cancer cells comprising treating tumor cells or cancer cells with a compound of claim 1, or a pharmaceutically acceptable salt or solvate thereof, in an amount effective to kill or inhibit the proliferation of the tumor cells or cancer cells.

10. A method for treating cancer in a patient comprising administering to the patient a compound of claim 1, or a pharmaceutically acceptable salt or solvate thereof, wherein the compound is administered in an amount effective to treat cancer.

11. The method of claim 2, further comprising administering an effective amount of a chemotherapeutic agent.

12. A pharmaceutical composition comprising a compound of claim 1 or a pharmaceutically acceptable salt thereof and a pharmaceutically acceptable carrier.

13. A pharmaceutical composition comprising a combination of compounds of claim 1 or pharmaceutically acceptable salts thereof and a pharmaceutically acceptable carrier.

14. The pharmaceutical composition of claim 12 or 13, further comprising a therapeutically effective amount of chemotherapeutic agent selected from the group consisting of a tubulin-forming inhibitor, a topoisomerase inhibitor, and a DNA binder.

15. The method of any one of claims 2 through 11, wherein the compound is in a formulation comprising a pharmaceutically acceptable carrier.

16. The method of claim 2, wherein the subject is a mammal.

17. The method of claim 2, wherein the subject is a human.

**Figure 1**

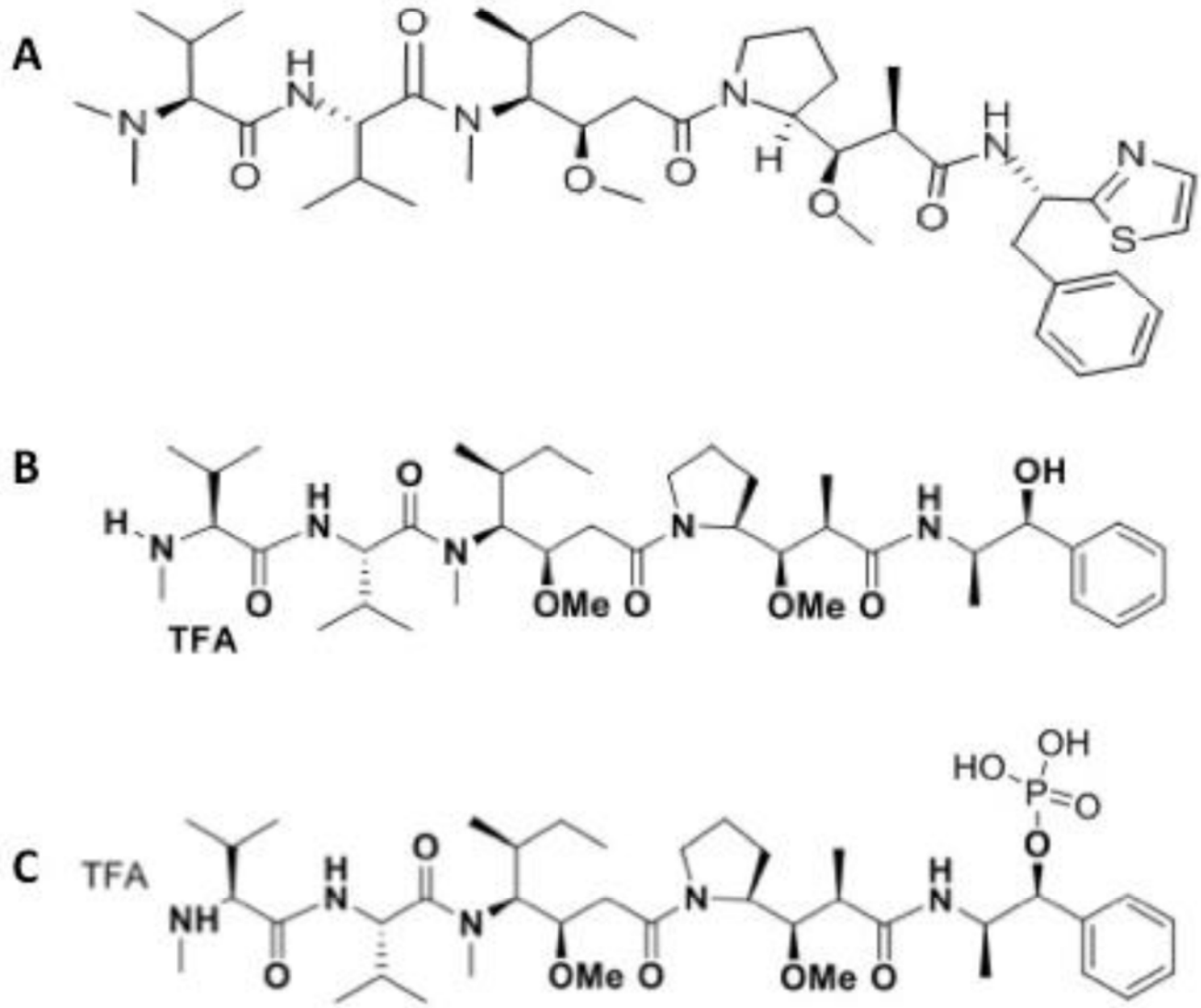


**Figure 2**

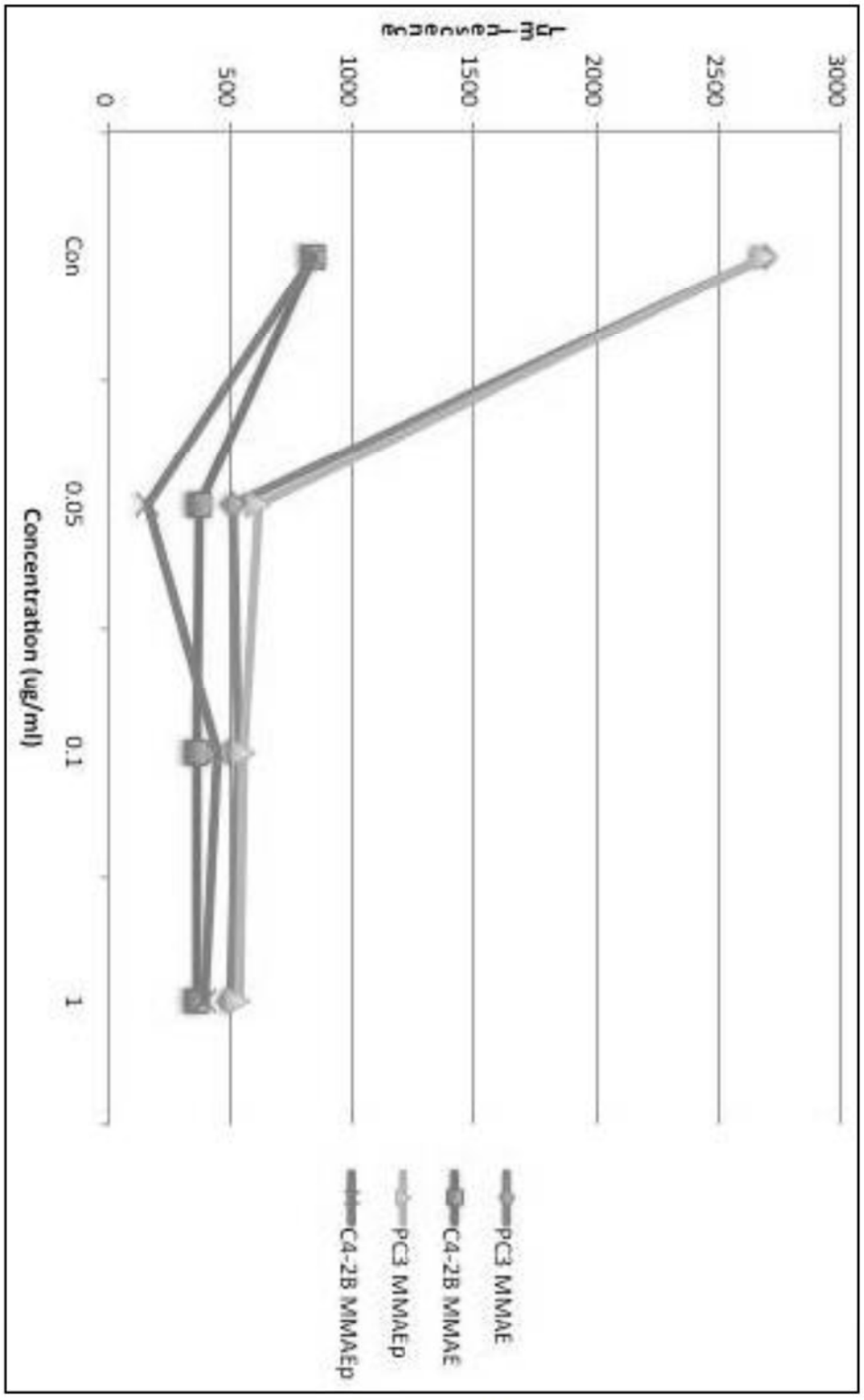

3000
2500
2000
1500
1000
500
0
Con
0.05
0.1
1
Concentration (ug/ml)
PC3 MMAE
C4-2B MMAE
PC3 MMAEp
C4-2B MMAEp

**Figure 3**

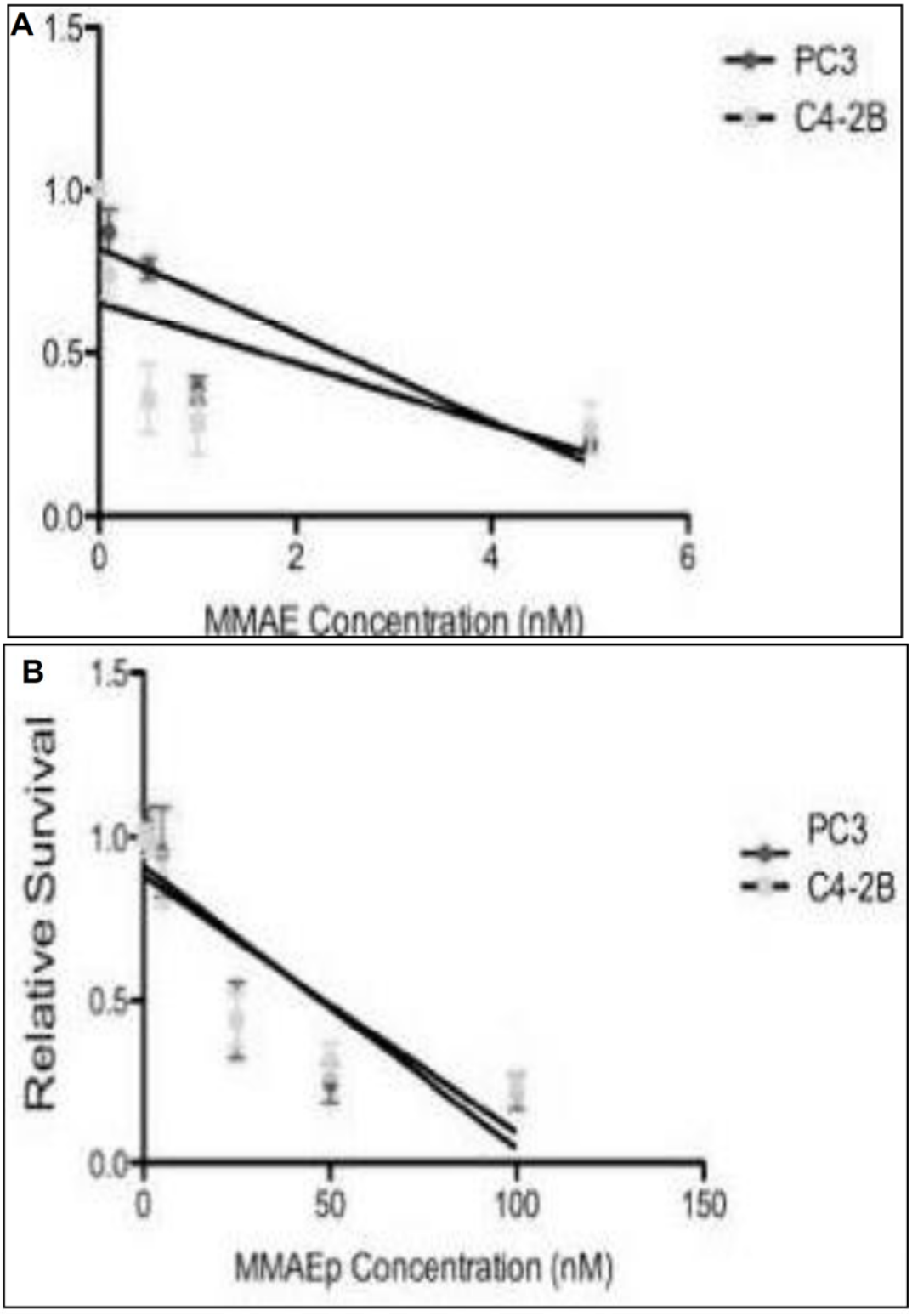

A
1.5
1.0
0.5
0.0
0
2
4
6
MMAE Concentration (nM)
PC3
C4-2B
B
Relative Survival
1.5
1.0
0.5
0.0
0
50
100
150
MMAEp Concentration (nM)
PC3
C4-2B

**Figure 4**

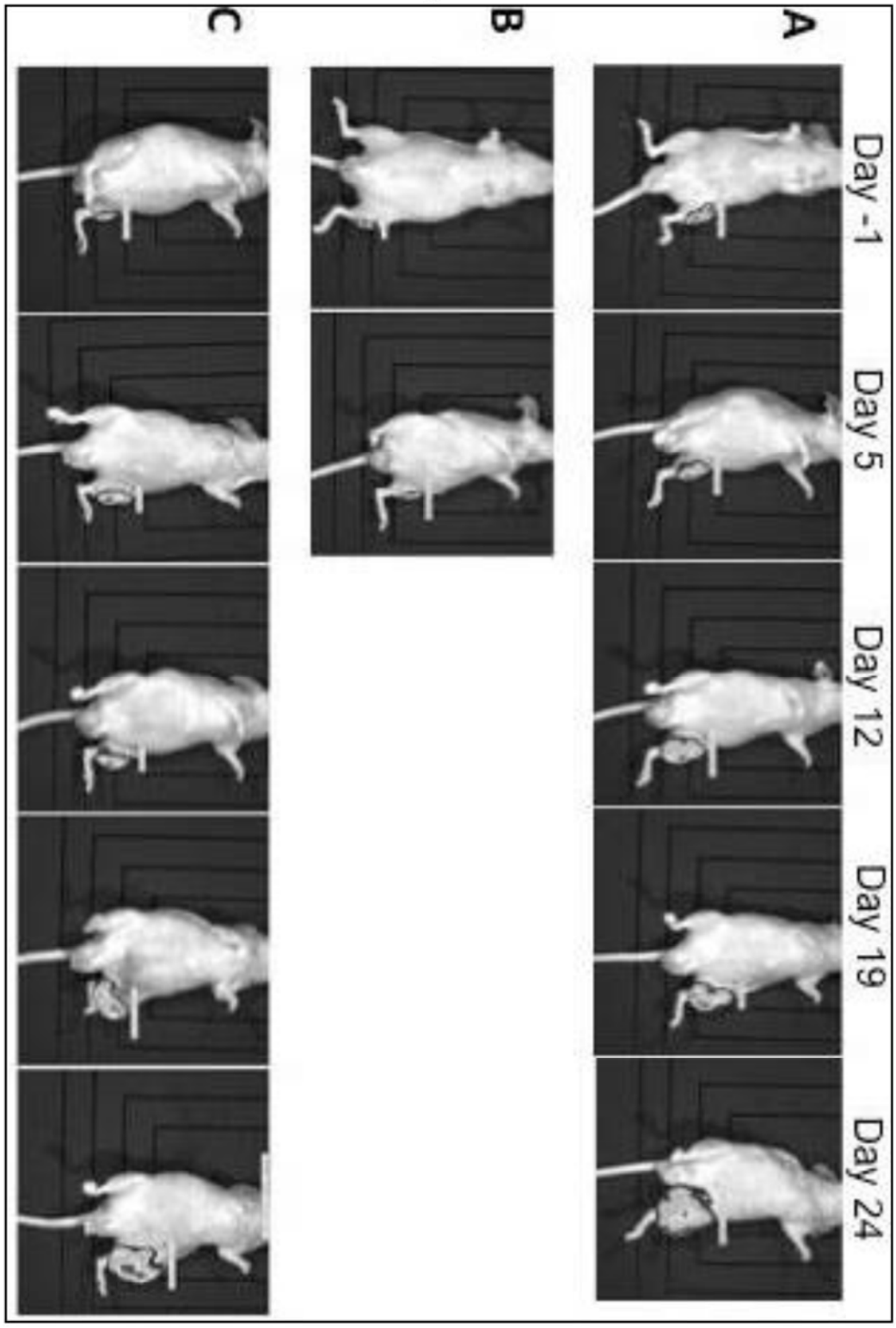


**Figure 5**

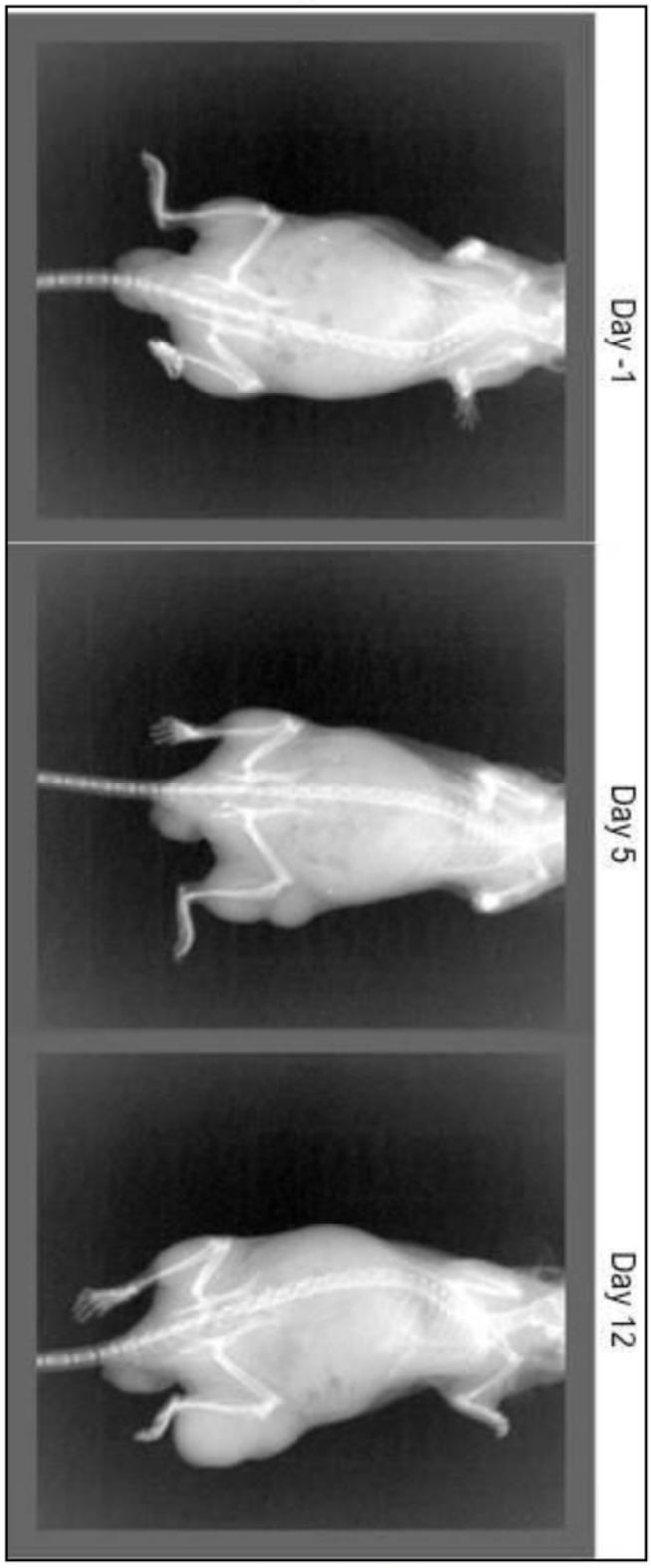


**Figure 6**

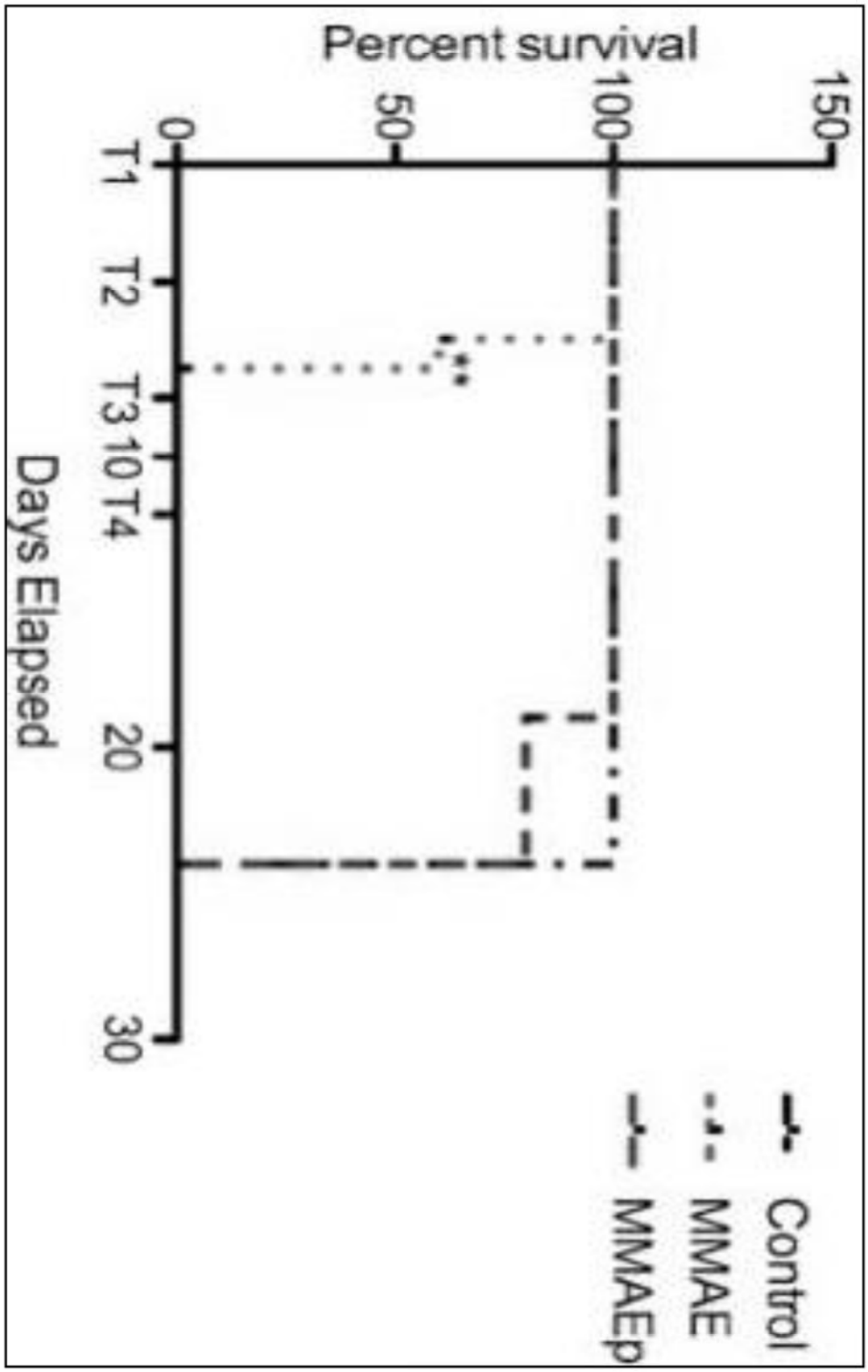
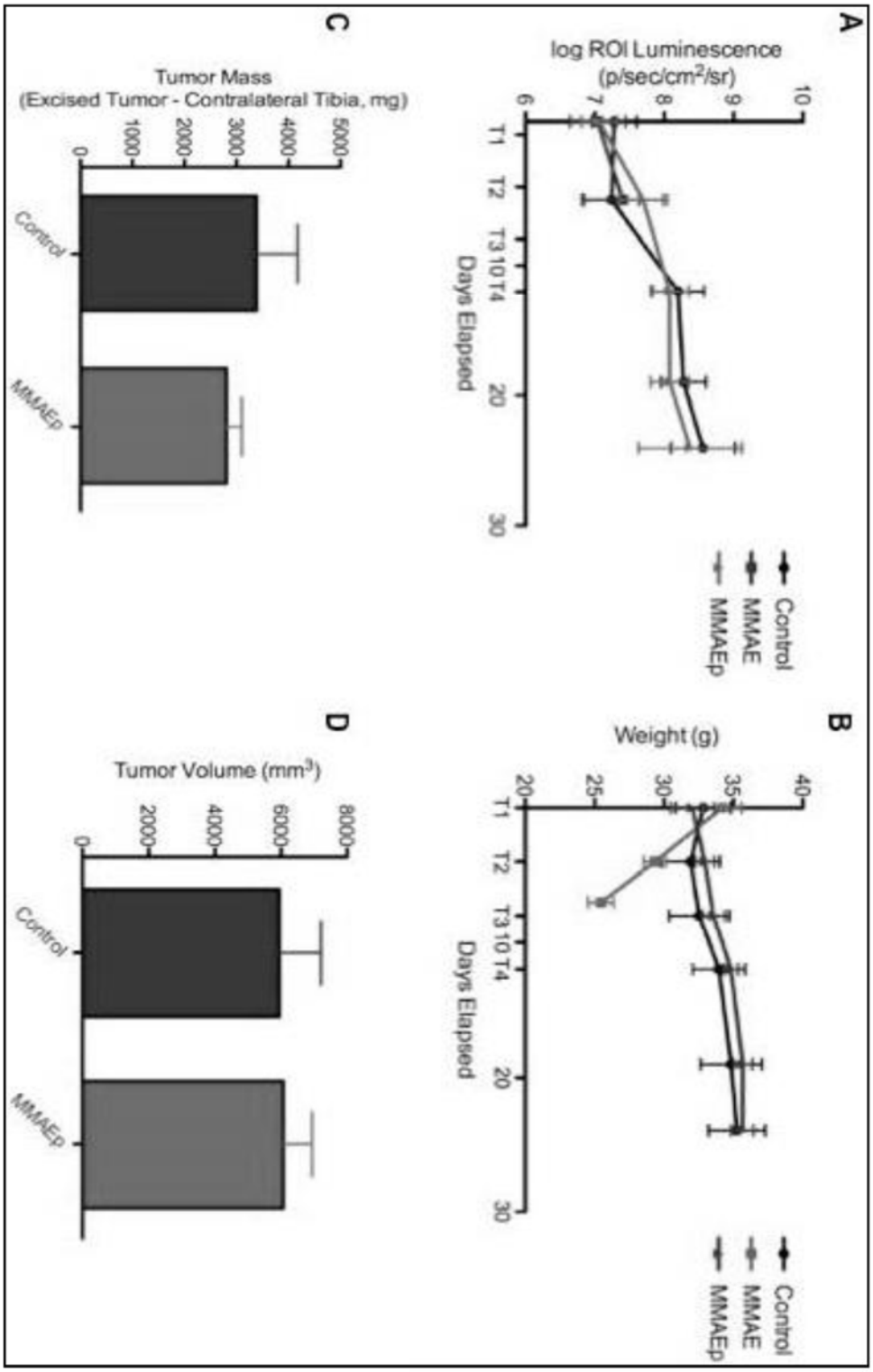

Percent survival
0
50
100
150
T1
T2
T3
10
T4
20
30
Days Elapsed
Control
MMAE
MMAEp

**Figure 7**


A
log ROI Luminescence
(p/sec/cm²/sr)
6
7
8
9
10
T1
T2
T3
10
T4
20
30
Days Elapsed
Control
MMAE
MMAEp
B
Weight (g)
20
25
30
35
40
T1
T2
T3
10
T4
20
30
Days Elapsed
Control
MMAE
MMAEp
C
Tumor Mass
(Excised Tumor - Contralateral Tibia, mg)
0
1000
2000
3000
4000
5000
Control
MMAEp
D
Tumor Volume (mm³)
0
2000
4000
6000
8000
Control
MMAEp